2020

THE EFFECT OF DELAY AND SEQUENCE ON BLASTING FRAGMENTATION RESULTS

Tristan Worsey
University of Kentucky, tpwo222@g.uky.edu
Author ORCID Identifier:
https://orcid.org/0000-0002-8601-3843
Digital Object Identifier: https://doi.org/10.13023/etd.2020.439

STUDENT AGREEMENT:

I represent that my thesis or dissertation and abstract are my original work. Proper attribution has been given to all outside sources. I understand that I am solely responsible for obtaining any needed copyright permissions. I have obtained needed written permission statement(s) from the owner(s) of each third-party copyrighted matter to be included in my work, allowing electronic distribution (if such use is not permitted by the fair use doctrine) which will be submitted to UKnowledge as Additional File.

I hereby grant to The University of Kentucky and its agents the irrevocable, non-exclusive, and royalty-free license to archive and make accessible my work in whole or in part in all forms of media, now or hereafter known. I agree that the document mentioned above may be made available immediately for worldwide access unless an embargo applies.

I retain all other ownership rights to the copyright of my work. I also retain the right to use in future works (such as articles or books) all or part of my work. I understand that I am free to register the copyright to my work.

REVIEW, APPROVAL AND ACCEPTANCE

The document mentioned above has been reviewed and accepted by the student's advisor, on behalf of the advisory committee, and by the Director of Graduate Studies (DGS), on behalf of the program; we verify that this is the final, approved version of the student's thesis including all changes required by the advisory committee. The undersigned agree to abide by the statements above.

Tristan Worsey, Student

Dr. Jhon Jairo Silva-Castro, Major Professor

Dr. Zach Agioutantis, Director of Graduate Studies

THE EFFECT OF DELAY AND SEQUENCE ON BLASTING FRAGMENTATION RESULTS

DISSERTATION

A dissertation submitted in partial fulfillment of the
requirements for the degree of Doctor of Philosophy in the
College of Engineering
at the University of Kentucky

By
Tristan Paul Worsey
Lexington, Kentucky
Director: Dr. Jhon Jairo Silva-Castro, Associate Professor of Mining Engineering
Lexington, Kentucky
2020

https://orcid.org/0000-0002-8601-3843

ABSTRACT OF DISSERTATION

THE EFFECT OF DELAY AND SEQUENCE ON BLASTING FRAGMENTATION RESULTS

Blasters use the delay between charges and the firing sequence of the explosive charges to help reduce vibrations and achieve the desired fragmentation. Although delay and sequence are recognized as very important for vibrations and fragmentation, only vibration models consider timing as a variable in the prediction tool, without any known model for fragmentation prediction based on the delay sequence. Of the few fragmentation models available, very few take delay into account and do not give guidance on row delay and/or sequence selections. With the invention of electronic detonators in 1984, there are new avenues to explore with sequence and timing. Currently, blasters shoot using a trial and error approach when deciding on what timing to use to optimize fragmentation to the operations' needs. Experience and trial and error are usually the deciding factors on what delay is selected to get certain fragmentation.

Delay sequence and its influences on fragmentation is the focus of this dissertation. Current fragmentation models look at what is the delay timing between holes. Rarely do they look at the delay timing of the whole shot. Current models also look at a general fragmentation for the shot based on some design parameters. With timing, it is important to look at fragmentation on a hole-by-hole basis. Dynamic confinement (a concept developed in this research) changes drastically with timing. Dynamic confinement is the level of void space in front of a hole that changes with time due to explosives energy and gravity. Changes in dynamic confinement produce important changes in the final fragmentation of the shot. Given the relation between dynamic confinement and timing, it is suggested that the fragmentation be looked on charge by charge and not just design or average for one hole, in contrast to current fragmentation models.

In this research, a conceptual model was created using the proposed dynamic confinement theory to include row timing into fragmentation models. The dissertation looks at previous fragmentation models, the theory behind dynamic confinement, the Worsey-Silva model, and some full-scale testing for validation.

KEYWORDS: Delay Sequence, Fragmentation, Dynamic Confinement, Fragmentation Model, Blasting, Blast Timing

Tristan Paul Worsey

11/18/2020

Date

THE EFFECT OF DELAY AND SEQUENCE ON BLASTING FRAGMENTATION RESULTS

By

Tristan Paul Worsey

Dr. Jhon Jairo Silva-Castro
Director of Dissertation

Dr. Zach Agioutantis
Director of Graduate Studies

11/18/2020
Date

ACKNOWLEDGMENTS

Thank you to Dr. Jhon Silva for believing in me and supporting me through my Ph.D. Without your support, I would not have finished my Ph.D.

Thank you to Sefton Grell, Stephen Chisholm, and the CRH Ogden Point operation. Very rarely do you find an operation that is willing to let one experiment on blast timing. If it were not for an open-minded operation, this research would not be possible.

I would like to thank Russel Lamont, Nathan Rouse, and Dyno Nobel for being supportive during my dissertation writing period. Without the leeway from work, I would not have been able to finish in time.

Thank you to John Morgan, Nathan Rouse, and RESPEC for being supportive of conducting the research for the dissertation and allowing me to attend school while working full time.

I would like to thank my committee members Dr. Sebastian Bryson, Dr. Kyle Perry, Dr. Braden Lusk, and Dr. Kimberly Anderson for taking their time to be on my Ph.D. committee.

Lastly, I would like to thank my parents Gill and Paul Worsey and my family for helping me through life and lending a helping hand when I needed it. Without their wisdom and support I would have never gone this far in life.

TABLE OF CONTENTS

LIST OF TABLES

LIST OF FIGURES

CHAPTER 1. INTRODUCTION

Chapter 1 provides background information about the fragmentation process and why the sequence of the detonation of charges is important. The different fragmentation models currently available and the variables included in those methodologies will be discussed in this chapter.

1.1 Objectives

The objectives of the dissertation were to explore the influences of regular rhythmic timing on fragmentation, develop a methodology for determining fragmentation from changing the sequences of regular rhythmic timing, and explore whether or not the timing with the lowest vibrations is also the timing with the smallest fragmentation. To achieve the objectives of the dissertation an extensive literature review was conducted on fragmentation models, full scale field tests were conducted to determine the change in fragmentation and vibrations, and equations were derived to alter fragmentation from changing sequence when using regular rhythmic timing.

1.2 Background

The background section will cover the literature review about the different methodologies for prediction of fragmentation.

Fragmentation is the goal when it comes to rock blasting. Drilling and blasting are done so that rock can be mechanically moved and processed. The quest for optimum fragmentation plagues every drill and blast engineer out there. The 18th Edition of ISEE Blasters Handbook outlines some basic blasting objectives shown in Table 1.2.1 (ISEE, 2011).

Table 1.2.1 Basic blasting objectives (ISEE 2011)

Basic Blasting Objectives	
Objective	Operation
Specific fragmentation size distribution	Mining and quarrying
Future handling ease	• Stripping • Excavations where the broken rock is not the final product • Breaking oversize material
Stable final wall of surface	Final boundary walls or surfaces

Specific fragmentation size distribution, future handling ease, and stable final wall of surface all to some degree have something to do with the fracturing and fragmentation process. Since fragmentation is at the core of basic blasting objectives, it has been a topic of interest to researchers for quite some time.

Although fragmentation has been the goal all along, it was not until recently that researchers started to predict it based on blast design parameters. Ouchterlony et al. stated, "Blast fragmentation and fragmentation modeling are relatively young disciplines that are sparingly reported in blasting textbooks, e.g. (Langefors & Kihlstrom, 1963), (Olofsson, 1988), (Persson & Holmberg, 1994), (Hustrulid, 1999) and even the recent one by (Zhang, 2016)" (Ouchterlony & Sanchidrian, 2019).

Early fragmentation work included doing screening to separate different rock sizes from a representative rock sample and then taking a couple of the different percent passing sizes to predict a fragmentation curve. Percent passing is the percentage of material that passes through a screen of that size. If a bucket of rock was dumped into a screen that had an opening of 4 in. by 4 in. and only 80 percent of the material size passed through, then the 80 percent passing size would be 4 inches. Percent passing size can be expressed by mass or by volume. One of the first and simplest methods to come up with a fragmentation

curve is shown in equation 1.2.1 (Gates, 1915), (Gaudin, 1926), (Schuhmann, 1940), (Ouchterlony & Sanchidrian, 2019). Each author built on previous equations to the next, and the last author changed the equations to match the terms of typically used fragmentation models today.

$$P_{GGS}(x) = ax^n = \left({}^{x}/_{x_{100}}\right)^n = 0.5\left({}^{x}/_{x_{50}}\right)^n$$

Equation 1.2.1

Where:

$P_{GGS}(x)$ is a power function that is typically referred to as GGS
x is the screen size
x_{100} is the largest fragment size
x_{50} is the median fragmentation size
n is a uniformity index
a is a constant to help fit the data

Equation 1.2.1 determines what percent mass is left between the two screen sizes. Using data from a screening analysis, it is possible to use this equation to plot a fragmentation curve. The created curve from equation 1.2.1 is plotting the mass percent of material caught in each screen and not the percentage that is passing through the screen. An example fragmentation curve that would be associated with equation 1.2.1 is shown in Figure 1.2.1 below (Gaudin, 1926). The percent of a given material sample passing through the screen is typically how fragmentation is displayed today and is often referred to as a cumulative distribution function.

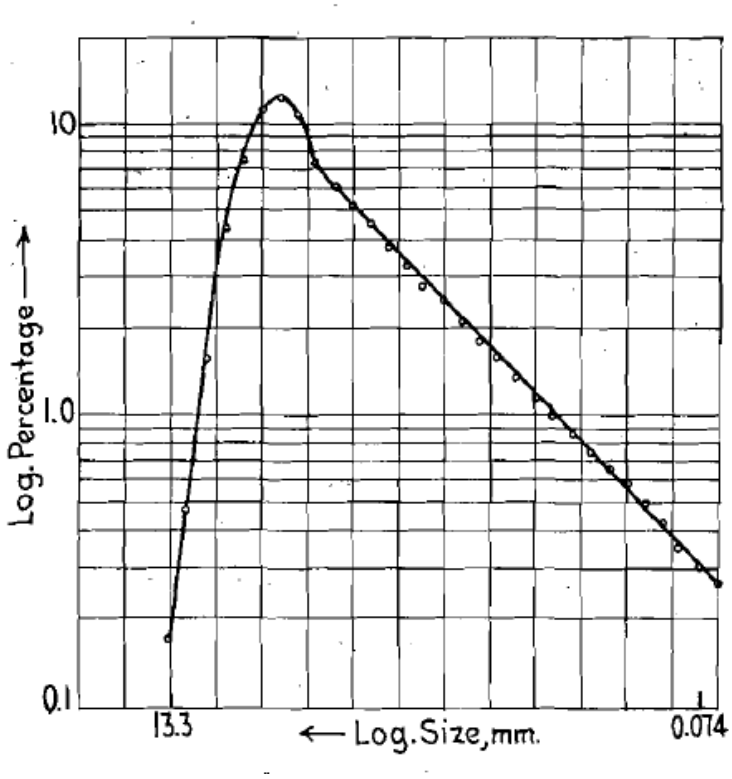

Figure 1.2.1 Example fragmentation curve for equation 1.1.1 (Gaudin, 1926)

The uniformity index in Equation 1.2.1 is determined by determining the line's slope connecting points B and C in Figure 1.2.2 from the screening data set (Gaudin, 1926).

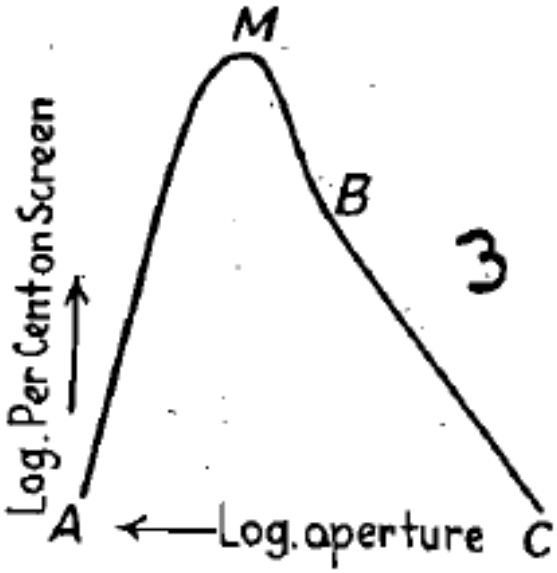

Figure 1.2.2 Size-Curve of Roll Products (Gaudin, 1926)

The primary purpose of an equation to estimate the fragmentation curve was to reduce the number of required measurements in the screening data. Screening data requires manual labor, and the data collected is used to optimize crushing and grinding equipment. To save time and money, fewer screens were used, and the B to C fragmentation curve was estimated with Equation 1.2.1.

Research then began investigating ways to estimate the full fragmentation curve to lessen the manual labor from the screening process and estimate data outside their screening equipment capacity. Multiple fragmentation distribution curve equations have been developed and are listed below with references.

- Rosin-Rammler /Rosin-Rammler-Sperling-Bennett - (Rosin & Rammler E, 1933), (Rosin & Rammler, 1933), (Bennett, 1936)
- Weibull - (Weibull, 1951), (Weibull, 1939)
- Gilvarry - (Gilvarry, 1961)
- Gilvarry-Berstrom - (Gilvarry & Bergstrom, 1961)

- Gaudin-Meloy - (Gaudin & Meloy, 1962)
- Grady-Kipp - (Grady & Kipp, 1985), (Grady & Kipp, 1987)
- Grady - (Grady, 1990)
- Swebrec Function - (Ouchterlony, 2003), (Ouchterlony, 2005), (Ouchterlony, 2005), (Ouchterlony F. , Olsson, Nyberg, Andersson, & Gustavsson, 2006)

The two main distribution curves used in rock blasting fragmentation models are the Rosin-Rammler-Sperling-Bennett and the Swebrec functions. The Rosin-Rammler-Sperling-Bennettt function is more known as the Rosin-Rammler function (Ouchterlony & Sanchidrian, 2019). The Rosin-Rammler function does a good job of estimating fragmentation between P40 and P90 but does not accurately estimate finer material and coarser material. Most of the research around fragmentation curves up until now has been done to correct the curve for fine and coarse material. The Swebrec function helps correct the problems of the Rosin-Rammler function and is widely used today to estimate the fragmentation curve based on maximum fragmentation size and 50 percent passing fragmentation size. Figure 1.2.3 shows how the Rosin-Rammler and Swebrec functions match up to collected fragmentation data (Ouchterlony & Sanchidrian, 2019).

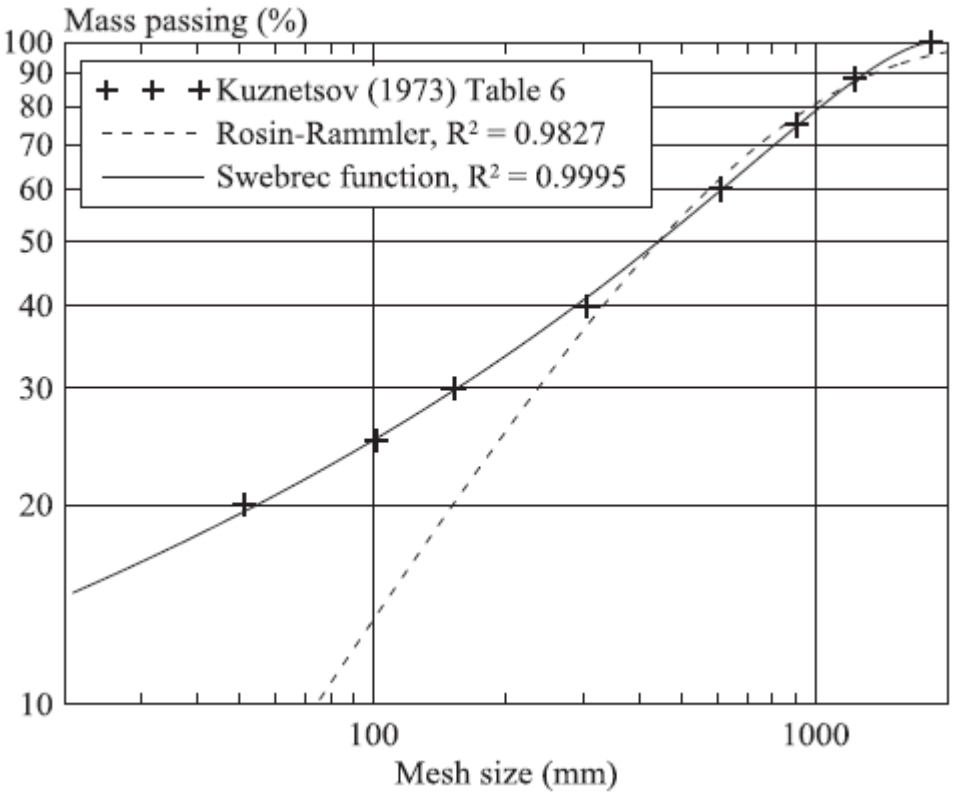

Figure 1.2.3 Fragmentation curve showing Rosin-Rammler and Swebrec curves with fragmentation data (Ouchterlony & Sanchidrian, 2019)

With easy ways to determine fragmentation curves, researchers now had a way to describe a muck pile to determine the downstream benefits. Some of these benefits include lower crushing and grinding costs, higher mill throughput, faster production rates out of material handling machines, higher extraction recoveries, lower maintenance costs with material handling equipment, and higher availability of material handling equipment.

Operations that blast would also use this information to select equipment to move and process the rock fragments. Fragmentation studies are starting to become more and more popular in the pre-feasibility reports of greenfield mines. There are now two (2) goals for being able to predict fragmentation. The first goal and what fragmentation models are built for is to optimize the current mine's fragmentation for total mining costs by

determining which parameters need to be changed to get the most value. The second goal is to determine the typical fragmentation for a greenfield site using the budgeted drill and blast design to select equipment and/or determine recovery. The second goal is problematic since most models need to be calibrated with site blasting to be accurate, but it is still a common practice of the industry.

Gkikizas did a good job of showing past research that linked fragmentation size to reduced costs downstream (Gkikizas, 2016). The first item shown in Gkikizas's theses is work done by Eloranta in Table 1.2.2 (Eloranta, 1997).

Table 1.2.2 Energy consumption by unit operation (Eloranta, 1997)

Unit Operation	Cost		
	kWh/t	$/kWh	$/t
Blasting	0.43	0.38	0.16
Crushing	3.24	0.07	0.23
Grinding	17.82	0.07	1.25

Table 1.2.2 shows blasting has the highest cost per unit of energy but the lowest cost per ton of material. The cost difference means there is an optimization that needs to be done with blasting to reduce crushing and grinding costs. To determine how the fragmentation influences the energy required in the crushing and grinding process Bond's third law of comminution was developed, listed in Eloranta's and Hustruild's literature (Eloranta, 1997), (Hustrulid, 1999). Bond's third law of comminution is listed below. (Kanchibotla, Valery, & Morell, 1999)

$$W = W_i\left(\frac{1}{\sqrt{P_{80}}} - \frac{1}{\sqrt{F_{80}}}\right)$$

Equation 1.2.2

Where:

W = The energy required in KWh/t

W_i = Work Index, characteristic of the rock in KWh/t

P_{80} = Product diameter (80% passing size) in µm

F_{80} = Feed diameter (80% passing size) in µm

Equation 1.2.2 brings fragmentation from rock blasting into how much energy is required for the mill to break the rock into the size for optimum extraction or final product size. This concept is known as the drill to mill approach. Equations that take fragmentation and show the downstream benefits are not important for fragmentation models themselves, but it gives background on why it is an important topic and why certain fragmentation values are used over others. In the example of Equation 1.2.2, the 80 percent passing size is of interest. Equation 1.2.2 explains why so many metal extraction processing facilities are interested in the 80 percent passing size and not the 50, 60, and so on.

Now that we can generate a fragmentation distribution and link the fragmentation distribution to downstream benefits, demand has risen for the ability to predict fragmentation instead of just measuring fragmentation. One of the first fragmentation models to predict the needed parameters to develop the fragmentation curve was done by Koshelev et al. in 1971 (Ouchterlony & Sanchidrian, 2019). Koshelev et al. equations can be seen below (Koshelev, Kuznetsov, Sofronov, & Chernikov, 1971).

$$x_c \approx \langle x \rangle \approx 10Q^{1/6}(V_0/Q)^{0.8}$$

Equation 1.2.3

Where:

x_c = Fragmentation value used in the Rosin-Rammler curve

$\langle x \rangle$ = Average/mean fragmentation value, not 50% passing in m

Q = TNT explosives in the blasthole in kg

V_0 = Blasted volume of a blasthole in m^3

Equation 1.2.3 now lets us change the blast design and see what happens to fragmentation curves without doing any testing and collecting fragmentation data. The equation was determined by collecting field data and running a statical analysis to determine the line's equation that best fits the data set. The model only has two (2) variables, which are weight of explosives and volume of rock blasted. If you increase the weight of the explosives, mean fragmentation size will decrease. If you increase the volume, mean fragmentation size with increase. Those two concepts are widely accepted in the industry, but when it comes to fine-tuning, more variables come to play. It is required to be careful not to confuse the mean fragmentation size as the 50 percent passing size as Ouchterlony et al. have found a common mistake in the literature (Ouchterlony & Sanchidrian, 2019).

Equation 1.2.3 may seem simple, but it was the starting block to coming up with fragmentation size without blasting. There are currently several models out there that build upon the basic principles of equation 1.1.3. A comprehensive list of fragmentation models through time have been published by Ouchterlony et al. and are listed below with references (Ouchterlony & Sanchidrian, 2019).

- Koshelev - (Koshelev, Kuznetsov, Sofronov, & Chernikov, 1971)
- Kuznetsov - (Kuznetsov, 1973)
- Protodyakonov - (Protodyakonov, 1962)
- SveDeFo - (Lundborg, 1971), (Larsson, 1974), (Holmberg, 1981)
- Kuz-Ram - (Cunningham, 1983)
- Lilly - (Lilly, 1986)

- Stag - (Stagg, Rholl, Otterness, & Smith, 1990)
- Otterness - (Otterness, Stagg, Rholl, & Smith, 1991)
- Chu-Kat - (Chung & Katsabanis, 2000)
- JKMRC - (Djordjevic, 1999), (Kanchibotla, Valery, & Morell, 1999), (Thornton, Kanchibotla, & Esterle, 2001)
- Esen - (Esen, Onederra, & Bilgin, 2003)
- Extended Kuz-Ram - (Cunningham, 2005)
- Ouch-Sanch - (Ouchterlony & Sanchidrian, 2019)

As research advanced, more variables were included in the fragment size prediction models, and a way to account for fines caused by borehole crushing was introduced. Some of the variables include explosives weight, powder factor, relative weight strength of explosives, burden, spacing, hole depth, stemming length, geology, and delay. The most common model seen in the literature today is the extended Kuz-Ram model utilizing the Swebrec fragmentation curve function. Fragmentation models will be discussed in more detail in Chapter 2.

1.3 General identification of variables of the problem

Rock fragmentation has many variables that need to be considered to properly model fragmentation. So many variables need to be accounted for that Dr. Worsey states, "One would need a company full of engineers with computers, like Google, to be able to accurately model the fragmentation process" (Worsey, 2020). The 18th Edition of the ISEE Blasters' Handbook breaks up the variables for fragmentation into four (4) different categories listed below (ISEE, 2011).

1. Explosives properties

    a. Chapman-Jouget (C-J) pressure
    b. Detonation velocity
    c. Density
2. Intact rock properties
    a. Young's modulus
    b. Poisson's ratio
    c. Uniaxial compressive strength
    d. Density
    e. Porosity
3. Rock fabric
    a. Joint/fracture spacing
    b. Join/fracture orientation
4. Blast pattern design
    a. Borehole depth
    b. Borehole Diameter
    c. Stemming
    d. Length
    e. Burden
    f. Spacing

ISEE's list of parameters that influence the blast fragmentation includes 16 different variables, and this list is not all-inclusive. Some of the other variables explained in the literature include the items below. If both lists are combined and shared it with the fragmentation researching community, there would still be variables needed to completely model the fragmentation process.

1. Delay timing
2. Stress wave velocity
3. Borehole inclination
4. Tensile strength

5. Dynamic tensile and compressive strength
6. Fracture toughness
7. Levels of water saturation
8. Gas pressure
9. Rock grain size

To simplify the discussion in this research, the parameters are going to be grouped into the following categories: explosives, rock information, blast design geometry, and delay timing. Delay timing and blast design geometry would normally be lumped together in a category called blast design, but due to the focus of the dissertation being on delay timing, it was separated out.

Explosives are the reason the fragmentation process begins. Without explosives, there would be no fragmentation. Most of the fragmentation models explained in Ouchterlony et al. utilize the weight of the explosive' charge and its relative weight strength (Ouchterlony & Sanchidrian, 2019). The early fragmentation models, such as the Kuz-Ram, were all built on empirical data sets that had a certain explosive that was used in the data set. To account for all the different explosives used in the world, relative weight strength was developed.

Weight strength (WS) is defined as "the energy output (heat of detonation) of an explosive material per unit of weight" (ISEE, 2011). Absolute weight strength (AWS) is defined as "the measure of explosives energy per unit weight" (ISEE, 2011). The difference between the two is AWS is theoretical, and WS would be the value if one could measure the energy output of a detonation. Relative Weight Strength (RWS) is defined as "the ratio of the absolute weight strength of an explosive to the absolute weight strength of ANFO" (ISEE, 2011). Although ISEE explains RWS as a ratio of an explosives compared

to ANFO, it does not have to be just ANFO. Early research typically did a RWS using TNT as the base explosives to relate other explosives to. RWS typically uses ANFO today because of its wide use in the explosives industry. The equation to determine relative weight strength can be seen below.

$$RWS_e = \frac{AWS_e}{AWS_x}$$

Equation 1.3.1

Where:

RWS_e = Relative weight strength of an explosives
AWS_e = Absolute weight strength of an explosives (cal/g)
AWS_x = Absolute weight strength of a reference explosives (cal/g)

Using relative weight strength as a parameter helped researchers use fragmentation prediction equations from one data set using a certain explosive and translate it over to an operation using a different explosive. Because different explosives have different detonation characteristics, it is not possible to use the explosives' weight alone when comparing the fragmentation of two different explosives. Utilizing weight and RWS helps capture the energy used in the fragmentation process. Weight and RWS values are also easy to obtain, making it practical to use in fragmentation models.

Explosives weight and relative weight strength do not capture all the explosives' parameters that are important for fragmentation. Weight and RWS does capture most of the fragmentation process from explosives in a simple form, excluding predicting fines. Fines predicting models require additional information to determine the amount of

fracturing around the borehole. Explosives parameters needed for fines include blasthole pressure, explosives density, and velocity of detonation.

Rock information is an important part of predicting the fragmentation when changing location and geologic formations at the same mine. Geology is one of the most difficult parameters that plagues fragmentation researchers. Geology influences fragmentation the most out of all the parameters and randomly changes throughout the world. Fragmentation models utilize a local geology and/or concrete block data set to develop a model, and then the model gets utilized in an area of completely different geology. Different geology will change the fragmentation mechanics. If a model is not accounting for geology, it can only be used in the geology that the model was formulated. Greenfield sites typically do not have localized blast fragmentation data, so this poses a problem with using fragmentation models without considering geology. Researchers have tried to fix this problem with some success.

The vast differences in geology worldwide are one big reason why computer modeling of fragmentation is not utilized by operations today. There are too many geologic cases to build a model that works everywhere it is needed to work. With greenfield sites, general estimation of fragmentation is what is currently possible, so simple fragmentation equations are acceptable for this process. Current fragmentation models that consider geology can also be used to get ideas on what to test to increase fragmentation at the mine.

To explain the influences of geology one must first explain the fracturing process in a homogenous material. The fracturing process starts with the pressure exerted onto the rock due to the explosive's detonation. The shock wave from the explosives travels through the rock, causing radial fracturing to grow due to the stress being higher than the

rock's dynamic strength. After the shock wave passes, the gas pressure builds up in the borehole and extends the cracks formed by the shockwave and applies a stress field. If there is a free face nearby, the fractures extend to the free face, and the rock fragments are pushed into motion by the gas pressure. In the case of a free face and prior to the movement, the shock wave reflects at the free face causing tension and spalling on the material if the dynamic tensile strength is exceeded.

Fracture growth is slower than the shock wave's speed and can be estimated to be around $1/3^{rd}$ the speed of the shock wave (Worsey, 2020). In a homogenous material, cracks will grow in the grain boundaries due to stress concentration in the material's weakest part. In homogeneous material, radial fractures will grow the same distance in all directions. Some of the neighboring fractures will have been stunted due to stress fields caused by slightly faster-growing cracks expanding. Figure 1.3.1 shows the cracks generated in a polyester resin (homogeneous material) (Worsey, 1981). The figure shows tightly spaced fractures of similar length with a handful of cracks extending outwards. The extended cracks can be explained by the resin not being perfectly homogenous and that the fracturing process is somewhat random.

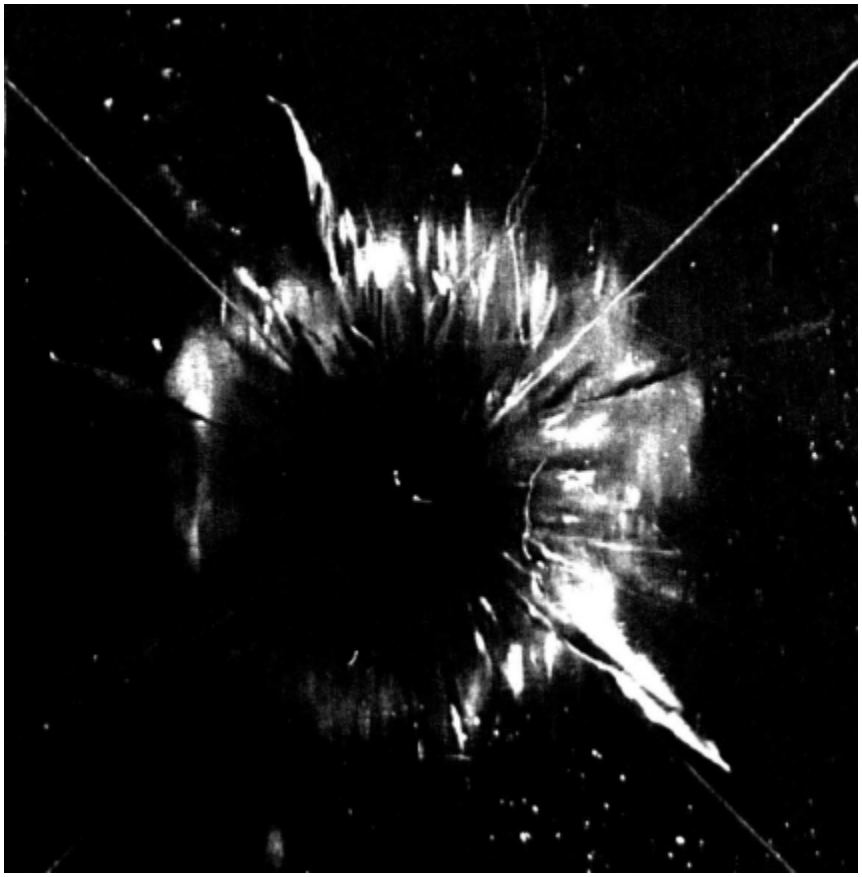

Figure 1.3.1 Fracturing around a detonated shot hole in polyester resin (Worsey, 1981)

In homogenous material, the strength properties are fundamental when it comes to fracturing. A typical strength value used in the mining industry is uniaxial compressive strength (UCS). This value is usually needed for processing and geotechnical engineering, so it is a value readily available at most mines. The problem with using this value is that it is not the stress conditions of blasting (Scott & Onederra, 2015). UCS is loading of a cylindrical core sample from the top and bottom with all surfaces on the sides being free faces. In blasting, the stress source comes within, and the load rate is dynamic instead of quasi-static. Using the UCS value is a problem when conducting mechanistic models but is acceptable for empirical models if it's just providing a strength index (Scott & Onederra, 2015).

Fleetwood helps explain the relationship of confinement and loading rate by saying "Once radial confining pressure is added to a rock specimen, as in triaxial testing procedures, the sample strength can increase dramatically. Sample strength also increases as the rate at which the load is applied increases." (Fleetwood, Villaescusa, & Li, 2009). Blasting is more confined and a faster loading rate than UCS testing. The rock cracks in tension, so tensile strength would be a better strength value, but it is not readily available like UCS, due to tensile strength testing being more expensive. Dynamic strength testing would also be better values, but it also is expensive and not commonly done by rock testing facilities. Therefore, most fragmentation models use UCS as a strength index. The tensile strength can be related to UCS as well and is typically 1/10 of the UCS on average.

Unfortunately for the fragmentation researchers, geology is not homogenous. Even homogenous like rock is not as homogeneous as a polyester resin. As soon as planes of weakness enter the equation, the fracturing process is complicated. Shock wave stress will overcome a plane of weakness in the rock mass before the rest of the rock, causing the cracks to grow in planes of weakness faster than the rest of the rock. The separation of the faster-growing crack applies a compressive stress field to neighboring cracks stunting their growth. Figure 1.3.2 illustrates how cracks cause compression on the surrounding rock as they expand (Perkins & Krech, 1968). The fractures will close if they do not reach a free face and will not be visible due the stress field still acting on the cracks after the blast. In that case, the acoustic sounding of the material can be used to identify the cracks. In the resin case, the material was opaque, and shining a light showed the cracks.

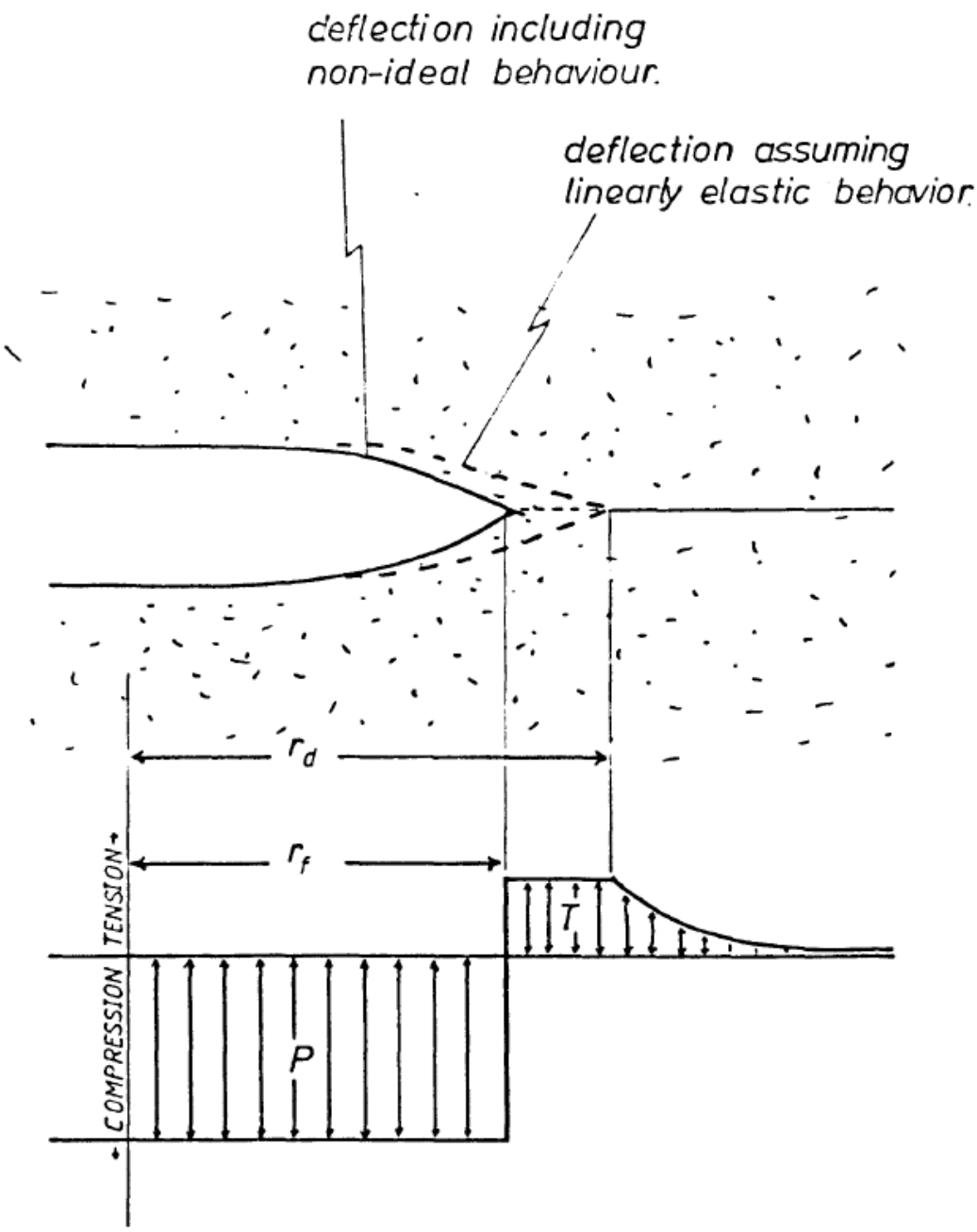

Figure 1.3.2 Fracture with damaged region stresses in the plane of the crack (Perkins & Krech, 1968)

Since the stress concentrates on the weakest part of the rock mass, any joints or plane of weaknesses will fracture, leaving the rest of the rock intact. If a rock mass has heavy jointing, one will find when the rock mass is blasted that all the rock pieces in the

muck pile should be of similar size as the joints' spacing. If the rock mass has widely spaced jointing, fractures will appear where the explosive was placed, additional to the joints of the rock mass. If explosives are not placed inside each boulder created by the joint sets, then the blasted pile will have large rock pieces similar to the joint spacing. This is because when the stress wave from the explosives reaches a plane of weakness, fracturing will occur on the weakness planes faster than the rest of the rock and inhibit new cracks from forming.

Pre-splitting is a common practice in the blasting industry to protect a final rock wall from nearby blasting. The pre-split causes a fracture plane that stops radial fractures from nearby blasts and interrupts the transmission of vibrational waves. Joints act like natural pre-splits, therefore stunting the growth of radial fractures from the blasthole. Characterizing the rock mass is a very important variable for determining fragmentation due to blasting. Types of discontinuities with a rock mass include faults, joints, bedding planes, foliation, and healed fractures (Scott & Onederra, 2015). Scott explains that geotechnical engineers are more concerned with structures that make the rock slope fail or the mine drift to fail, so they are not as concerned will all discontinuities in the rock mass (Scott & Onederra, 2015). Mine rock mass data is usually collected for geotechnical engineering purposes, and not all structures are included.

Mine operations commonly record the Rock Quality Designation (RQD), which is the core's length that has cracks spaced 4 inches or longer divided by the total length of the core. This value is useful when determining blast fragmentation of a rock mass, but only takes cracks that are spaced 4 inches apart into account. A piece of core could have fractures spaced 5 inches for the whole length of the core and have a RQD value of 100

percent, and a solid piece of core with not fractures could have a RQD value of 100 percent. Other rock mass characteristics are needed to successfully determine blast fragmentation. Measuring the spacing of all discontinuities and directions is the best approach but is very time consuming and typically not done.

Density and porosity are other rock values that are important when it comes to blasting. Scott explains that the density influences the rock's inertia, which will affect how the rock will move when explosive force is applied (Scott & Onederra, 2015). High porosity influences the density measurement, so sealed and unsealed core densities are needed. High porosity can cause the rock to respond slowly to explosive gas and have less movement (Scott & Onederra, 2015).

Rock stiffness is another important variable that is typically accounted for by calculating the Young's modulus and Poisson's ratio. While conducting UCS testing Young's modulus and Poisson's ratio can also be determined, making these values typically available. As indicated before, one problem is that Young's modulus and Poisson's ratio does change with the rate of strain, so dynamic values are best (Scott & Onederra, 2015).

Rock properties are usually included in fragmentation models as factors that take a couple of the properties discussed above to influence the final fragmentation. Scott does a good job of showing how rock mass factors are used for each fragmentation model shown in Figure 1.3.3 and Figure 1.3.4 (Scott & Onederra, 2015). One thing to note is that the empirical models have easy to obtain rock mass information and mechanistic models have the true property required that are hard to obtain. Hard to obtain dynamic rock mass values

are typically why computer modeling is less effective. Also, not much is known about dynamic rock mass values during a blast due to rock blasting's destructive nature.

Model	Basis	Rock mass description
Kuznetsov (1973)	Relationship derived from experimental data between the explosive charge and volume of rock broken by each blasthole and the particle size, for which 50 per cent of the muck pile by weight is finer.	A rock factor was included in the formula for the mean fragment size based on allocating: • 7 for medium rocks • 10 for hard, highly fissured rocks • 13 for very hard, weakly fissured rocks.
Cunningham (1983)	Consistent with work by Holmberg (1974), Cunningham extended the output of Kuznetov's model by describing the full fragment size distribution by fitting this to a Rosin Rammler curve.	Maintained Kuznetsov rock factor.
Lilly (1986)	Lilly developed a 'blastability index' that Cunningham (1987) incorporated into the Kuz-Ram model to replace Kuznetsov's simple rock factor. Lilly's work was based on conditions encountered in open pit iron ore mines.	Lilly's blastability index was based on a series of ratings based on the field observation of the rock mass character (friable, blocky or massive), joint plane spacing, joint plane orientation, strength and density.
Cunningham (1987)	Cunningham extended the inputs to the Kuz-Ram model to derive the shape factor for the Rosin Rammler fragment size distribution curve from basic blast geometry inputs.	Cunningham replaced Kuznetzov's rock factor with Lilly's blasting index.
JKMRC Mine to Mill Kanchibotla, Valery and Morrell (1999); Djordjevic (1999); Scott *et al* (1998)	A number of model developments were driven by projects during the 1990s exploring the impact of blasting on downstream processing. These focused on improving the description of the fine end of the fragmentation curve and required a departure from the Rosin Rammler size distribution to represent a higher proportion of fines. This was accounted for by merging two size distribution curves – one for the coarse end and one for the fine end.	Rock strength (unconfined compressive strength and tensile strength), Young's modulus, rock density, rock quality designation, fracture frequency.
Ouchterlony *et al* (2006)	A different curve (the Swebrec function) was proposed to describe the full fragment size distribution to replace the Rosin Rammler equation in the Kuz-Ram model. The Swebrec function has been successfully fitted to detailed sieved size distributions from carefully managed field experiments and confirms the increase in fines compared with the Rosin Rammler curve.	Ouchterlony applied the new size distribution curve to the 1987 Kuz-Ram model but also explored definitions for the top fragment size based on fracture spacing and blast geometry.
Scott and Onederra (2015)	A highly modified Kuz-Ram model has been successfully been applied in consulting assignments dealing with blasts in a wide range of rock types and blasting situations. Each of the three Swebrec parameters required to define the full size distribution are estimated by the model.	A rock factor is defined based on rock strength, fracture frequency and density. Statistical distributions of these data are utilised.

Figure 1.3.3 Kuz-Ram based empirical models (Scott & Onederra, 2015)

Model	Basis	Rock mass description
Kutter and Fairhurst (1971)	Griffith theory used to estimate crack extension from stress loading.	Dynamic compressive and tensile strength. The stress attenuation component required, density, Young's modulus, Poisson's ratio, P and S wave velocities.
Harries and Hengst (1977); Paine, Harries and Cunningham (1987)	Estimated the number and extent of radial cracks formed around a blasthole in response to tensile strain. This approach was extended by others and formed the basis of the ICI SABREX model.	Rock stiffness parameters including Young's modulus and density.
Margolin and Adams (1983)	Crack formation modelled under dynamic strain.	Fracture mechanics parameters to evaluate the activation of cracks.
McHugh (1983)	Predicted the extension of cracks from the effects of gas pressure.	Distribution of fractures, tensile breakage parameters
Ryu and Pariseau (1986)	Two-dimensional distinct element numerical model of block fragmentation in a jointed rock mass during the late or throw stage of a blast after wave effects have subsided.	Description of rock mass structural characteristics (block forming macro-discontinuities). Parameters include normal stiffness, shear stiffness, friction coefficient, friction angle, tensile strength of intact rock and rock density.
Minchinton and Lynch (1996); Dare-Bryan, Wade and Randall (2001)	A finite element / discrete element hybrid that can perform both two-dimensional and three-dimensional analysis of stress, fracturing and in-flight block interaction of the blasting process. Evolved from the integration of the mechanistic blasting model described by Minchinton and Lynch (1996).	Strain-rate-dependent rock fracture parameters.
Hybrid Stress Blasting Model Furtney, Cundall and Chitombo (2009); Onederra *et al* (2013)	A sophisticated blast modelling research tool that combines continuous and discontinuous numerical techniques to model detonation, dynamic wave propagation, rock fragmentation and muck pile formation.	Compressive and tensile strength, Young's modulus, damping coefficient, rock mass structural characteristics (joints dip and dip direction), joint strength indices.

Figure 1.3.4 Mechanistic models (Scott & Onederra, 2015)

Blast design geometry is another important consideration to rock blasting. If certain blast design geometry conditions are met, then the whole fragmentation process changes. Two common blast design geometry conditions referred to in the blasting industry are cratering and bench blasting.

Cratering is placing an explosive charge a certain distance from a free surface to get the explosives' optimal breakage. The confinement is typically higher, and the charge is more like a point charge than a cylinder (ISEE, 2011). The blast design geometry for cratering is completely different than the breaking mechanics of bench blasting. Figure 1.3.5 and Figure 1.3.6 show the blast geometry of cratering. Cratering is not the focus of this research and will not be discussed in detail. It is important to note that what breaking mechanism used in a blast drastically changes how the parameters influence the fragmentation. All fragmentation models should describe the breaking mechanism the model is for.

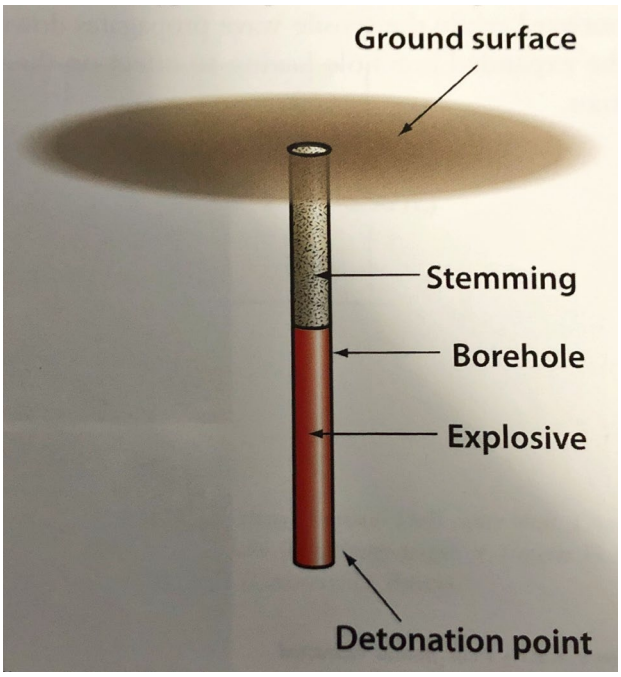

Figure 1.3.5 Cratering blast geometry (ISEE, 2011)

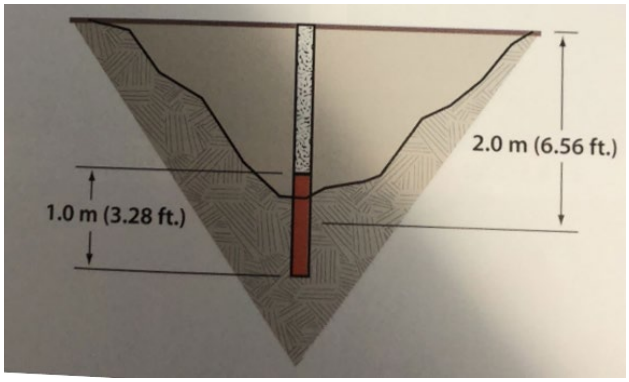

Figure 1.3.6 Area of fracturing from cratering (ISEE, 2011)

Bench blasting is the breaking mechanism for the fragmentation model in this dissertation and will focus on important blast design geometry parameters. A list of blast geometry design parameters is listed below that were included in various fragmentation models (Ouchterlony & Sanchidrian, 2019). Other variables were included but could be derived from just having the information below.

- Burden
- Spacing
- Hole depth
- Bench height
- Stemming length
- Hole diameter
- Hole inclination

One of the most comprehensive research done towards determining optimum blast geometry in bench blasting was Richard Ash's work at the Experimental Mine in Rolla, MO (Ash, 1968). Ash's work found that the above parameters were important for having a quality blast. This included the smallest fragmentation with minimal adverse effects of the blasting, such as airblast, ground vibrations, and fly rock. Some of the optimum parameters he found are as follows.

- Bench height/burden ratio – 4
- Hole diameter – bench height/(100 to 120)
- Powder Factor – 1 lb/cyd for quarry blasting
- Stemming height – 0.7 to 1.2 * burden
- Spacing – 1.2 to 1.4 * burden
- Sub-drill – 1/3 * burden

Ash's optimum parameters were designed so a blaster could go to a new operation and design a blast that performed while minimizing any bad side effects such as fly rock, airblast, and ground vibrations. There are likely cases outside of the guidelines that give better results, but the results might only be appropriate for mines with no neighbors etc. The guidelines were also given as a starting point. Once local site knowledge is gained, changing the parameters could potentially give better results due to the change in geologic

conditions from site to site. Ash's research was only on bench blasting and is a good base for ensuring bench blasting is the rock breaking mechanisms.

Ash's research shows that each variable in blasting geometry depends on the other, so only including one geometry variable alone will not fully capture what will happen with the fragmentation. Ash has explained why the more accurate fragmentation models consider all its geometry parameters.

Zang explains the relationship between break out angle and burden and spacing shown in Figure 1.3.7 and Figure 1.3.8 (Zhang, 2016). If one can measure the breakout angle, then the optimum spacing to burden relationship can be obtained by using equation 1.3.2. The equation was modified from the equation shown in Zhang's book (Zhang, 2016).

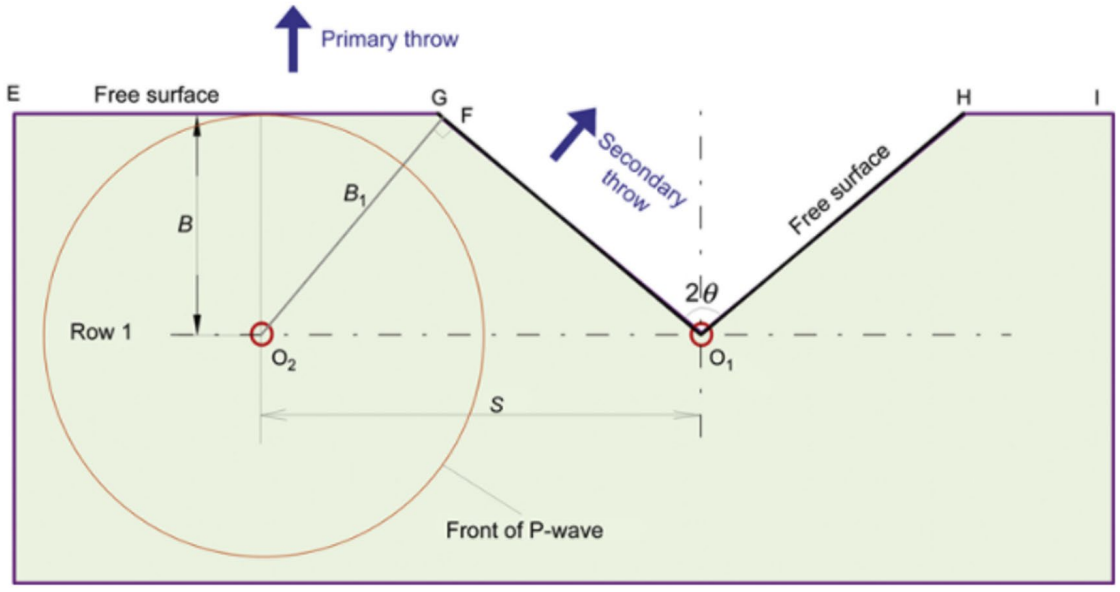

Figure 1.3.7 Conditions of p-wave and throw for a large spacing to burden relationship (Zhang, 2016)

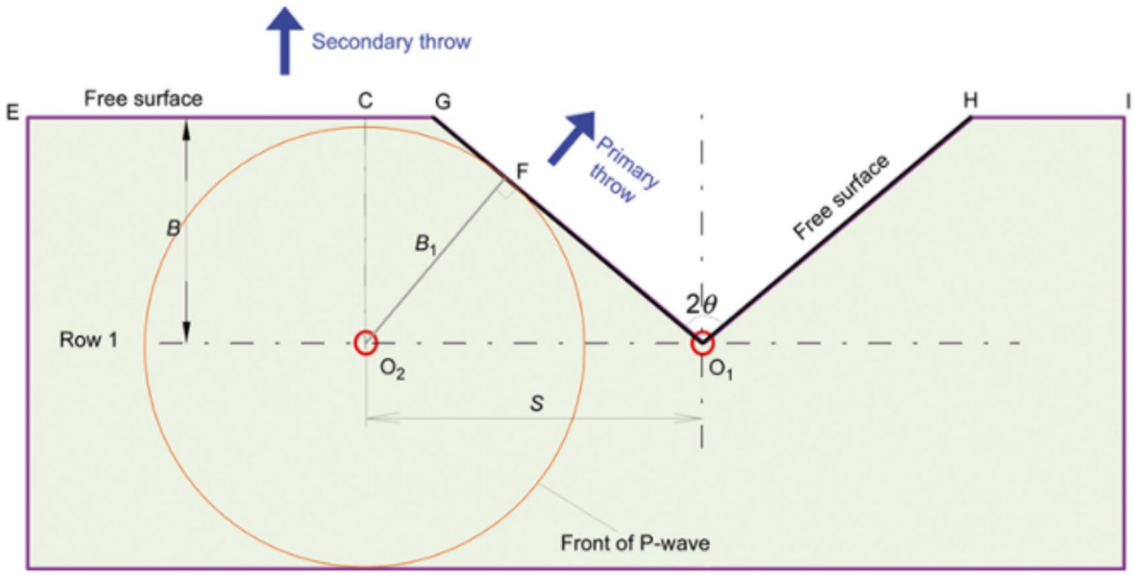

Figure 1.3.8 Conditions of p-wave and throw for a small spacing to burden relationship (Zhang, 2016)

$$S = \frac{B}{\sin\left(\frac{\pi}{2} - \theta\right)}$$

Equation 1.3.2

Where:

S = Spacing

B = Burden

θ = ½ of the measured breakout angle in radians

If equation 1.3.2 is followed, then B and B_1 will be equal, and the fracturing process will reach the free face at the same time. In conditions where B does not equal B_1, the fracturing process will dominate in the smaller variable's direction. Zang's equations helps to define what the spacing to burden relationship should be based on site specific measured breakout angle.

Timing is another variable that has just scratched the surface of fragmentation modeling and is very controversial in the literature. The first timing consideration in empirical models was induced in 2005 when Cunningham added a timing function to the Kuz-Ram model (Cunningham, 2005). Timing needed to be separated from blast design geometry because it is a variable that does not change the cost of the shot. Explosives, rock properties, and blast design have fragmentation with a single explosives charge. Timing influences on fragmentation require multiple charges or multiple holes to have an effect.

Timing has been proven to provide fragmentation differences in full-scale blasting. Literature that shows this includes (Hettinger, 2015), (Vanbrabant & Espinosa, 2006), and (Chiappetta, 2011). There has also been an extensive amount of small scale and medium scale tests that have proven that delay has an impact on fragmentation. Some of the small scale to medium-scale research that has been done includes (Gkikizas, 2016), (Johansson & Ouchterlony, 2013), and (Katsabanis & Omidi, 2015). All the research shows a change between delays, but there are two common concepts regarding timing and fragmentation. The first concept is that there is an optimum delay window after the shock wave has passed the next hole that gives the best fragmentation. The second is that there is an optimum delay window before the shock wave has passed the second hole. (Chiappetta, 2011) and (Vanbrabant & Espinosa, 2006) research supports optimum timings from the second concept. The rest of the research listed above supports the first concept.

Radial fracturing is associated with the shock wave as it passes through the rock medium. When two holes detonate, the shock waveform of one hole can interact with the second hole. This theory is commonly called “shock wave collision” or “stress wave

interaction". Zang describes the equations to determine optimal delay and when shock wave collision happens (Zhang, 2016). The basic equation below is typically how researchers report the optimal delay from the data (Zhang, 2016).

$$T_d = kB$$

Equation 1.3.3

Where:

T_d = Delay timing down the row in milliseconds
k = Constant that is typically expressed in ms/m and in the range of 3-5 ms/m
B = Burden in meters

Typical ranges for k are described as 3 to 5 ms/m according to Zang and 4 to 13.3 ms/m, according to Katsabanis et al. (Zhang, 2016), (Katsabanis & Omidi, 2015). Large scale testing was done in Georgia and found a delay of 4.8 ms/m was optimal (Hettinger, 2015). Other testing done by Stagg et al. found the optimum delay between the range of 3.3 to 26 ms/m (Stagg & Nutting, 1987). One can conclude from previous research that equation 1.2.3 has varying k factors for different conditions.

In order to have interacting stress waves from neighboring holes, the delay has to be less than equation 1.3.4 (Zhang, 2016). Figure 1.3.9 shows the parameters of equation 1.3.4 as they are happening in time. Zhang's equation below has variables that are difficult to measure. The P-wave velocity and length in the blast often require sacrificial sensors, and wires connected to the sensors are typically broken before the whole wave data is collected. The fragmentation radius of one hole is often difficult to determine since gas pressure after the shock wave has passed will extend the fractures. Johansson et al. determined that to have tensile wave interaction, a delay of 0.37 ms/m of burden is needed,

which is not found as an ideal delay from a fragmentation perspective in the majority of the literature (Johansson & Ouchterlony, 2013).

$$T_d < 2T_p + \frac{2S - R_{fg}}{c_p}$$

Equation 1.3.4

Where:

T_d = Delay time between holes

T_p = Length of stress wave caused by hole 1

S = Spacing

R_{fg} = Fragmentation radius of one hole

c_p = Velocity of the P-wave

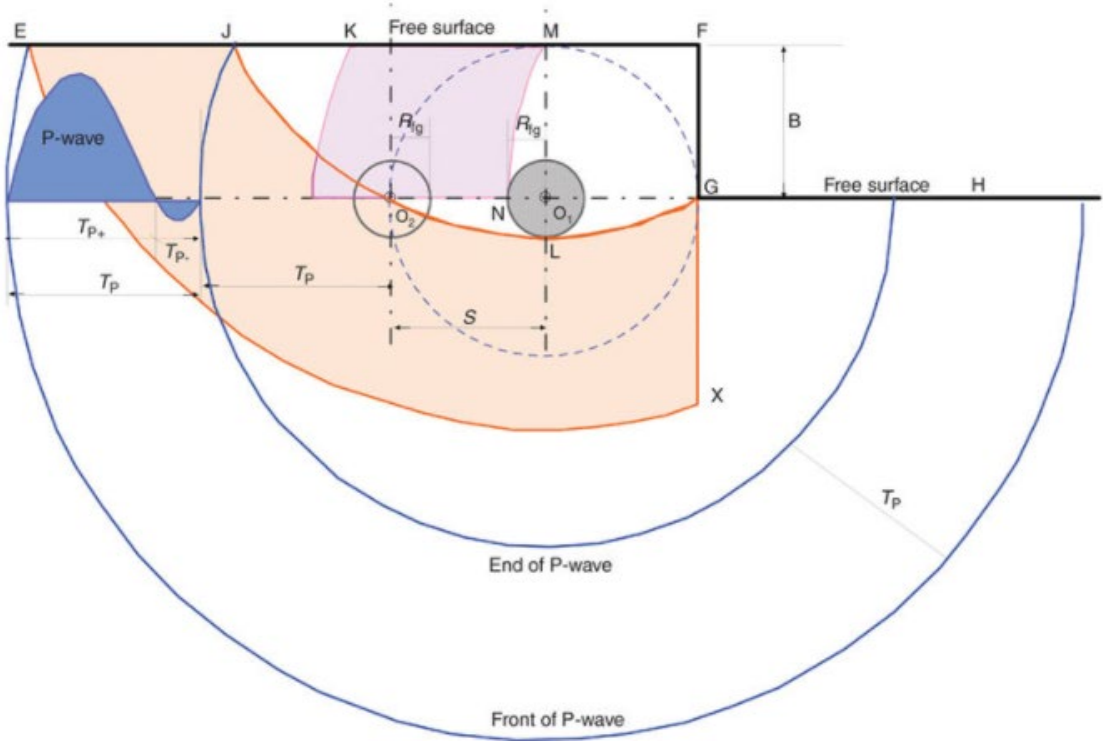

Figure 1.3.9 Example of stress wave travel when $t = 2T_p + \frac{S}{c_p}$ (Zhang, 2016)

According to the above literature, stress wave interaction due to the shock wave is not ideal for fragmentation. However, some cases have been documented where timing with stress wave interaction helped to get the desired fragmentation (Chiappetta, 2011) and (Vanbrabant & Espinosa, 2006). Those cases were in large metal mines with blast geometry that is not ideal for bench blasting. The drastic change in geometry is likely changing the fragmentation mechanics allowing for different delay timing being successful.

During the literature review for this research, no studies were found that showed the effect of row delay on fragmentation. The extended Kuz-Ram and the Ouch-Sanch models are the only two known fragmentation models that use delays that are based on empirical data. These models only look at delay down the row of a blast. There currently is not any known research that gives a fragmentation model that incorporates row delay.

1.4 Origin of the research and its significance

The origin of the research came from the advancement in detonators. The invention of accurate delay detonators did not come until 1984 when Tyler and Worsey filed the very first electronic detonator patent (United States of America Patent No. 4674047, 1984). Although electronics were invented in 1984, they were not widely used in the industry until the 2000s (Worsey, 2020). Worsey explained that the patent got in the way of commercial explosives manufactures developing their own electronic detonator until Tyler and Worsey allowed the patent to elapse in the early 1990s to advance the industry.

When electronic detonators first hit the market, they were very expensive and did not get major use until 2000 to 2010. Until electronic detonators became widely available, mines were using detonators with pyrotechnic delay elements. Pyrotechnic delay elements

had a wide range of detonator scatter. So much scatter that a 9 ms pyrotechnic delay cap could fire anywhere between 1.53 ms and 26.14 ms (Lusk, Hoffman, Mulligan, & Worsey, 2013). A blast with 3 meters of burden using 9 ms pyrotechnic delays on detonating cord as the hole initiator would fire anywhere from 0.51 ms/m of burden to 8.7 ms/m of burden.

Without accuracy and precision of the delay, only large timing changes could be done to influence the shot. Delaying shots to have stress overlap was not possible, and due to the scatter, the timing was usually picked to ensure holes fired in order. Utilizing delay in models would not have been helpful until 2000 to 2010 when electronic detonators were now starting to be widely used at mines. A 10 ms delay programmed into an electronic detonator could fire anytime between 9.816 ms and 10.201 ms (Lusk, Hoffman, & Wedding, 2011). A blast with 3 meters of burden using 10 ms electronic delay would fire anywhere from 3.272 ms/m to 3.4 ms/m. Electronics detonator accuracy and precision have now made it possible to start exploring influences due to delays that were not possible in the past.

Cunningham came up with the first model to incorporate delay in 2005, right when the electronic detonator started to become widely used. Since then, researchers have been exploring a wide range of delays and their influence on fragmentation. Although the timing is widely accepted to influence fragmentation, researchers have only been exploring delay down a row of holes typically referred to as “hole to hole” delay. Row delay has yet to be explored as a possible influencer in fragmentation.

Now that detonator accuracy and precision are to the nearest millisecond, signature hole waveform analysis became possible for controlling the level of blasting vibrations arriving at a nearby structure. Researchers began exploring how timing influenced wave

superposition and began finding optimal timing of the whole shot to minimize the vibrations' amplitude leaving the blast. This introduced the question: "Is the timing that is best for blasting vibration best for blasting fragmentation?". This question is currently not answered and was the reason for exploring the dissertation topic.

An approach that Dr. Silva uses to control blast vibrations is called "regular rhythmic timing (RRT)" (Silva-Castro, Lusk, Lee, & Jenks, 2016). Regular rhythmic timing standardizes the delay between successive charges. The difference between traditional timing and regular rhythmic timing can be seen in Figure 1.4.1 and Figure 1.4.2. Regular rhythmic timing has a pathway for the charges that match the charge sequence. Traditional timing has a different timing pathway than the charge sequence leading to variable delays between charges.

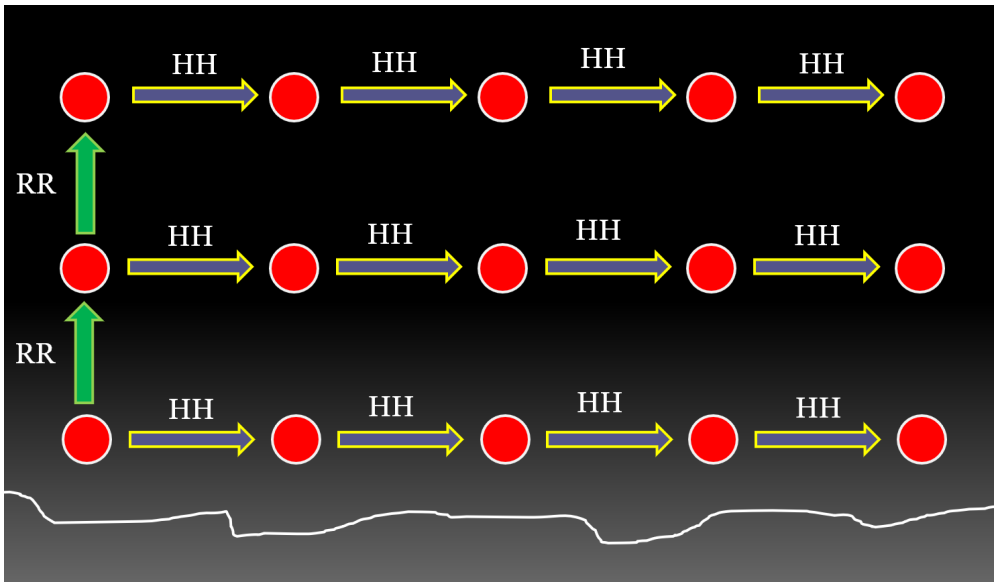

Figure 1.4.1 Traditional down the row and between row timing

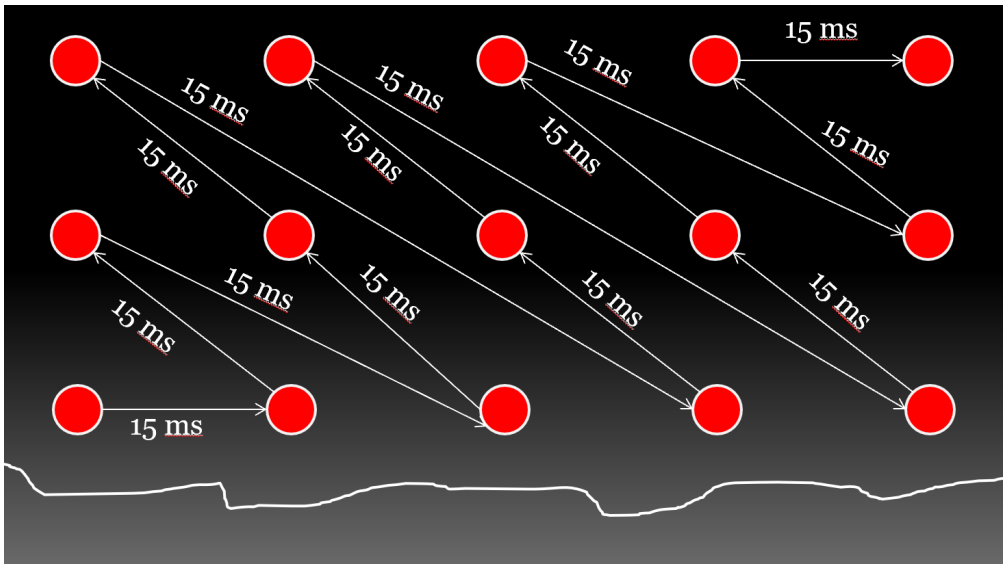

Figure 1.4.2 Regular rhythmic timing

Silva-Castro et al. developed regular rhythmic timing to eliminate the crowding caused by traditional down the row timing and timing between rows. Figure 1.4.3 shows the crowding effect of traditional timing when expanding the shot size (Silva-Castro, Lusk, Lee, & Jenks, 2016). Notice that as the detonators fire they get closer and closer together on the time scale on the right of the figure. The detonator firing timings also get closer together; the bigger the shot you have. Regular rhythmic timing gets rid of the above two problems and standardizes the timing between charges.

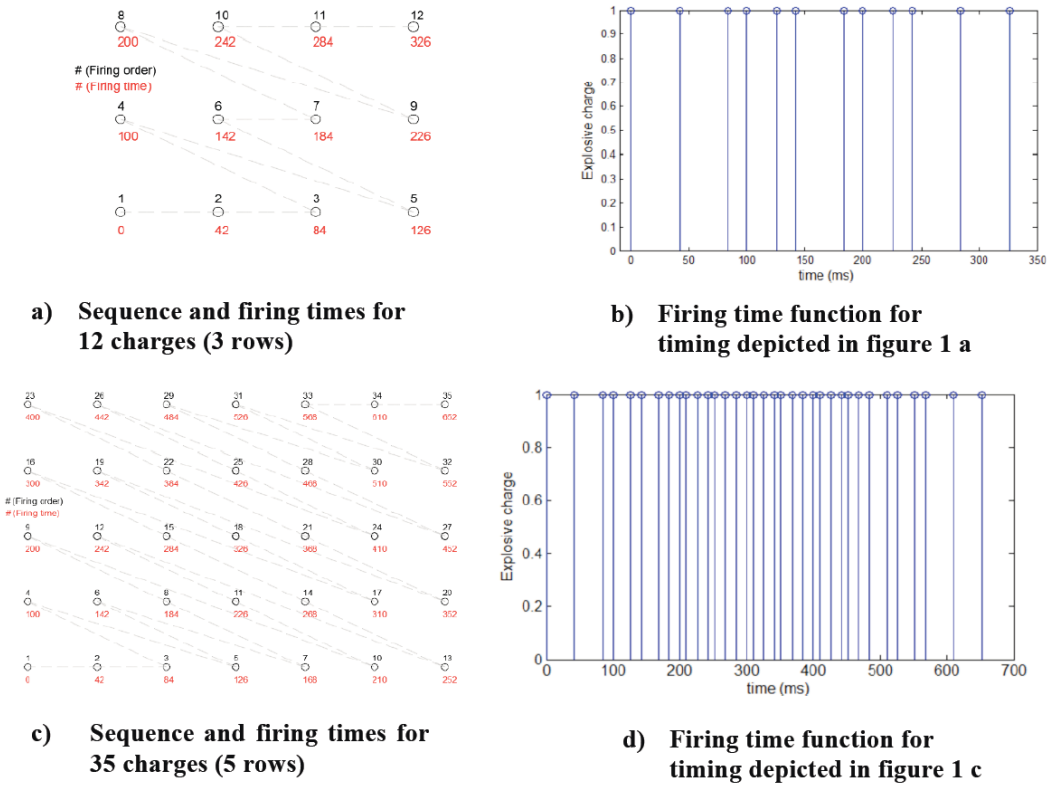

Figure 1.4.3 Sequence and firing time as a function of the number of charges (Silva-Castro, Lusk, Lee, & Jenks, 2016)

Regular rhythmic timing was able to reduce vibrations by roughly 6 percent just by eliminating the crowding (Silva-Castro, Lusk, Lee, & Jenks, 2016). The introduction of regular rhythmic timing to the vibration reduction world opened questions in the fragmentation world. Regular rhythmic timing adds delay timing to the whole shot. If you look at traditional timing versus regular rhythmic timing, it is not uncommon for the length of the shot to be 500 ms more for a regular rhythmic timing shot versus a traditional timing shot. The extended shot time of RRT had more time between neighboring holes than traditional timing.

The charge sequence becomes a more important factor because the timing path matches the charge sequence. In regular rhythmic timing you have a charge delay and a

charge sequence instead of a delay between rows and a delay between holes down a row. Signature hole analysis would determine the optimum delay between charges, but it did not give any guidance on the effect of the sequence on blast results such as fragmentation. To have industry acceptance of regular rhythmic timing, the impacts of charge sequence on blasting results needed to be explored.

Another important question identified during the literature review was that fragmentation models did not account for row delay. The timing between rows is typically longer than timing between holes down a row. The influence of long row delay is a question that is like the question of the influences of charge sequence when using regular rhythmic timing on blasting results.

1.5 Why the dissertation topic

Fragmentation and fracturing are two different terms when it comes to rock blasting. When measuring rock size after a blast, the measurement targets the fragmentation, but not the fracturing. Fracturing in blasting is the process in which explosive shock causes cracks in a rock mass. Fragmentation is the rock's size once it has reached its final state after the blasting process is finished.

When talking about the fracturing process, shock applied to the rock is important for determining how the cracks are initially formed. Once the crack has formed due to shock, the fracturing process ends, and the fragmentation process begins. Gas pressure created from the detonation of the explosives causes cracks to extend, disconnect, and move. Because there is a movement component in fragmentation, available space at the time of detonation becomes an important variable in the fragmentation process.

After the blasting process is complete, the final size of the rock is a combination of rock breakage due to explosives shock, gas pressure, and the ability to move. Adding timing to the equation will influence the ability to move drastically and should be considered when determining fragmentation size.

Due to the high velocities of explosives shock waves, fast timings are required to have shock interaction between explosive charges. Fragmentation models that use explosives shock and fracturing principles lead to faster timing to improve fragmentation. Fast timing does not give time for rock material to move. Therefore, fast timings are good for the fracturing process but not for the fragmentation process. There needs to be a variable to account for time in the fragmentation process, and delay sequence is one way to do it.

CHAPTER 2. FRAGMENTATION MODELS

This chapter describes all the literature available regarding the current fragmentation models. The most used fragmentation model today is the Kuz-Ram model with either the Rosin-Rammler model or the Swebrec fragmentation curves. Chapter two will go over the most relevant fragmentation models today and which model will be selected to use in the Wor-Sil modified fragmentation model.

2.1 Rosin-Rammler fragmentation curve

The Rosin-Rammler-Sperling-Bennett cumulative distribution function was developed in the 1930s from a combination of literature (Rosin & Rammler E, 1933), (Rosin & Rammler, 1933), (Bennett, 1936). The Rosin-Rammler-Sperling-Bennett curve is known as the Rosin-Rammler or RR distribution (Ouchterlony & Sanchidrian, 2019). The RR distribution was initially developed for coal processing but was adopted by the blasting industry since early blasting fragmentation models only predicted mean or 50 percent passing fragmentation size. Ouchterlony et al. show the RR distribution with terms that are common to today's fragmentation distribution functions in equation 2.1.1 below.

$$P_{RR}(x) = 1 - e^{-(x/x_c)^n} = 1 - e^{-ln2(x/x_{50})^n} = 1 - 2^{-(x/x_{50})^n} = 1 - 5^{-(x/x_{80})^n}$$

Equation 2.1.1

Where:

$P_{RR}(x)$ = to the percent passing of material size x

x = Material size in question

x_c = Characteristic size

x_{50} = 50% passing material size

x_{80} = 80% passing material size

n = Uniformity index from equation 1.1.1

An interesting note that Ouchterlony et al. point out about the RR function is that when the material size in question is less than the 50% passing size, the equation in a log-log graph is a straight line with the slope of n at the 63.2% passing size (Ouchterlony & Sanchidrian, 2019). This points to the RR function not appropriately estimating passing sizes below 50%. This fault is apparent in the literature when actual fragmentation curves are compared to estimated fragmentation curves, such as Figure 1.1.3 in Chapter 1.1. Ouchterlony et al. also point out that the RR function does not have a maximum size limit in the function, which is not the case with blasted material.

The RR function requires two (2) variables to estimate the cumulative fragmentation curve. The characteristic size, typically 50% passing size, and the uniformity index. Using this function will drastically reduce the amount of screening work done to determine a fragmentation distribution. It also allows for a prediction equation that solves only two(2) variables to come up with the total muck pile size distribution.

2.2 Julius Kruttschnitt Mineral Research Centre (JKMRC) fragmentation curve

The Julius Kruttschnitt Mineral Research Centre identified a need to change the RR function below a certain percent passing size and utilized equations to account for the fines from blasting (Djordjevic, 1999), (Kanchibotla, Valery, & Morell, 1999), (Thornton, Kanchibotla, & Esterle, 2001). Thornton et al. stated “it became apparent that the sieved run-of-mine (ROM) coal was much finer than that predicted from any incarnation of the Kuz-Ram model and an additional breakage step was required to account for the significant

breakage that undoubtedly occurs during handling" (Thornton, Kanchibotla, & Esterle, 2001). JKMRC called the change to the RR function the two-component model.

JKMRC determined that the splicing point of the RR function should be different between hard and soft (Australian coal and iron ore) rock. The hard rock's chosen splicing point was the 50% passing size, and soft rock was the 90% passing size. The splicing points are in question, and the selection of 50% passing and 90% passing is not discussed in the literature (Ouchterlony & Sanchidrian, 2019). It appears the splicing point of 90% likely comes from the problem with coal fines being generated in the material handling process as well as the blasted fines, while the splicing point of 50% comes from just the fines generated from blasting. The coal industry funded JKMRC research, so a large focus of the research is for blasting coal.

To estimate fines from blasting, the JKMRC team utilized equations from Jaeger et al. for estimating stress caused by gas pressure (Jaeger & Cook, 1979), (Thornton, Kanchibotla, & Esterle, 2001). Equation 2.2.1 is for quasi-static loading conditions, and it is assumed by Thornton et al. that this is the cause for the pressure caused by explosion gases. Thornton et al. then utilize equation 2.2.2 to determine the borehole pressure.

$$\sigma_x = P_b \left(\frac{r}{x}\right)^2$$

Equation 2.2.1

Where:

σ_x = Radial stress at a distance x (m) from the center of the blasthole (Pa)

r = Blasthole radius (m)

P_b = Borehole Pressure (Pa)

$$P_b = \frac{\rho_e {C_d}^2}{4}$$

Equation 2.2.2

Where:

P_b = Borehole Pressure (Pa)

C_d = Explosive velocity of detonation (m/s)

ρ_e = Explosive density (kg/m^3)

Equation 2.2.1 and Equation 2.2.2 are used to calculate the distance at which stress is equal to the material's compressive strength. Thornton et al. assume that material in this region will have a top size of 1 mm from excessive stress (Thornton, Kanchibotla, & Esterle, 2001). One millimeter particle size was chosen based on the run of mine size distribution data that Thorton et al. did not cite. The crushed zone volume is calculated by using the radius of the crushed zone and the volume of a cylinder. The volume blasted by the borehole is calculated by burden times spacing times height. The percent of 1 mm material from explosive gas pressure is estimated by dividing the volume of the 1 mm material by the blasthole volume.

Ouchterlony et al. have derived the final equations needed to calculate the distribution curve and are included below (Ouchterlony & Sanchidrian, 2019).

$$r_c = \frac{\emptyset_h}{2}\sqrt{P_h/\sigma_c}$$

Equation 2.2.3

Where:

r_c = crushed zone radius when stress is equal to uniaxial compressive strength (m)

$\emptyset_h$ = Hole diameter (m)

P_h = Bore hole pressure (Pa)

σ_c = Uniaxial compressive strength (m)

$$V_c = \pi\,(\emptyset_c^2 - \emptyset_h^2)/4$$

Equation 2.2.4

Where:

V_c = Volume of crushed rock per meter (m^3/m)

$\emptyset_c$ = Diameter of crushed rock

$\emptyset_h$ = Hole diameter

The fraction of "Fines" produced by one borehole is given by:

$$F_c = V_c/(BS)$$

Equation 2.2.5

Where:

F_c = fraction of 1 mm or less material of a blasted hole

B = Burden (m)

S = Spacing (m)

V_c = Volume of crushed rock per meter (m^3/m)

The uniformity index for the particle size fine fraction is given by:

$$n_{fines} = \ln\left[-\frac{\ln\,(1-F_c)}{\ln 2}\right]/\ln\,(\frac{1}{x_{50}})$$

Equation 2.2.6

Where:

n_{fines} = uniformity index for fines between 1 mm passing and 50% passing

F_c = fraction of 1 mm or less material of a blasted hole

x_{50} = 50% passing size (mm)

$for\ \frac{1}{x_{50}}, 1$ = assumed 1 mm top size of the crushed zone.

$for\ \frac{1}{x_{90}}$ replace ln2 with ln10

$$P(x) = \begin{cases} 1 - e^{-\ln 2(x/x_{50})^{n_{fines}}} & when\ x \leq x_{50} \\ 1 - e^{-\ln 2(x/x_{50})^{n_{coarse}}} & when\ x \geq x_{50} \end{cases}$$

Equation 2.2.7

Where:

$P(x)$ = Percent passing of size x

x = Material size of interest (mm)

x_{50} = 50% passing size (mm)

n_{fines} = Uniform index calculated by equation 2.2.6

n_{coarse} = Uniform index calculated screen data or calculated from the Kuz-Ram

$$P(x) = \begin{cases} 1 - e^{-\ln 10(x/x_{90})^{n_{fines}}} & when\ x \leq x_{90} \\ 1 - e^{-\ln 10(x/x_{90})^{n_{coarse}}} & when\ x \geq x_{90} \end{cases}$$

Equation 2.2.8

Where:

$P(x)$ = Percent passing of size x

x = Material size of interest (mm)

x_{90} = 90% passing size (mm)

n_{fines} = Uniform index calculated by equation 2.2.6 using ln10 and x_{90}

n_{coarse} = Uniform index calculated screen data or calculated from the Kuz-Ram

$$for\ soft\ rock, x_{50} = x_{90}/(\ln 10/\ln 2)^{1/n_{fines}}$$

Equation 2.2.9

Where:

x_{50} = 50% passing size (mm)

x_{90} = 90% passing size (mm)

n_{fines} = Uniform index calculated by equation 2.2.6 using ln10 and x_{90}

Figures 2.2.1 and Figure 2.2.2 illustrates a drawing showing all the terms and how the curve is spliced (Ouchterlony & Sanchidrian, 2019). The two-component model is used to help estimate fines from blasted material where the RR function fell short.

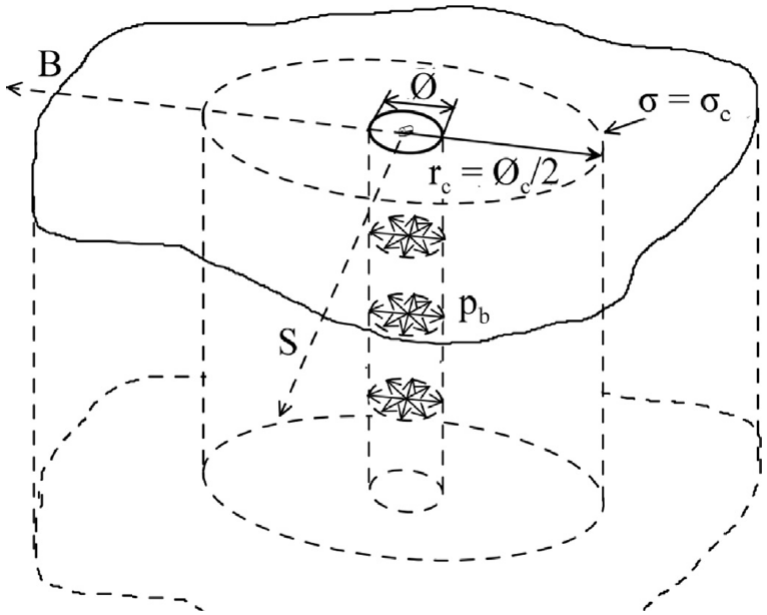

Figure 2.2.1 Variables of the crushed zone concept (Ouchterlony & Sanchidrian, 2019)

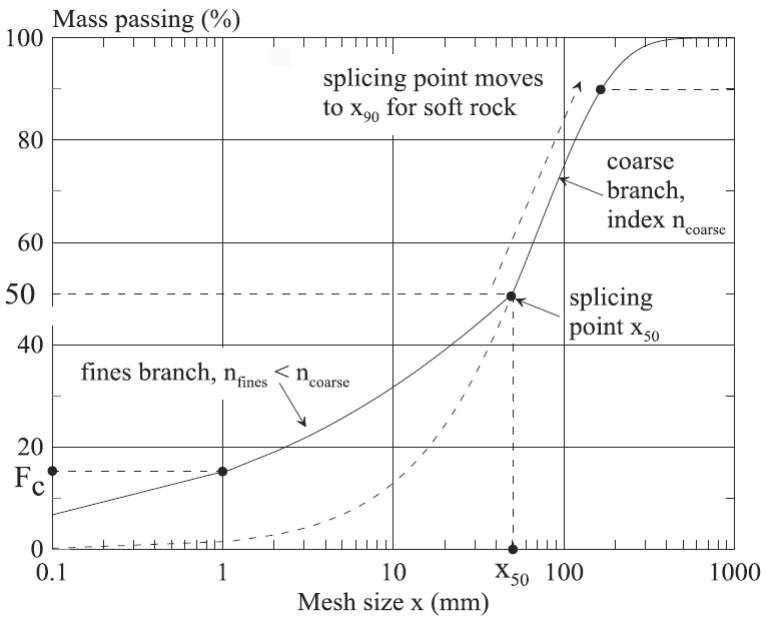

Figure 2.2.2 Two-component model splicing for soft rock (Ouchterlony & Sanchidrian, 2019)

2.3 Swebrec fragmentation curve

The European Union funded a project called “Less Fines” that shot a large number of rock and concrete samples and large scale blasts and manual screened all the data (Moser, 2005). Swedish Rock Engineering Research (SveBeFo) was involved in the “Less Fines” project and also did additional work with Montanuniversitaet Leoben (Ouchterlony & Sanchidrian, 2019). Analyzing the data from all the above projects gave birth to the Swebrec function (Ouchterlony F. , 2003), (Ouchterlony F. , 2005), (Ouchterlony & Moser, 2006).

The Swebrec function is a new distribution curve that now includes a maximum fragmentation size and a curve folding parameter that can be related to the uniformity index of the Kuz-Ram model (Ouchterlony F. , Olsson, Nyberg, Andersson, & Gustavsson, 2006). This function completely replaces the RR function to solve the fines and top size problems with one (1) equation. The Swebrec function is listed below (Ouchterlony F. ,

Olsson, Nyberg, Andersson, & Gustavsson, 2006). Since the curve folding parameter (b) can be related to the uniformity index (n) then the Kum-Ram model can still be used to calculate 50 percent passing size. The method does not have an equation for predicting maximum material size, but the curve can be estimated using partial screen data or photofragmentation analysis (Ouchterlony F. , Olsson, Nyberg, Andersson, & Gustavsson, 2006). If two different percent passing sizes are obtained, the maximum material size can be estimated. How the Swebrec curve fits in with full scale bench blasting data can be seen in Figure 2.3.1 below.

$$P(X) = \frac{1}{\left\{1+\left[\frac{\ln(\frac{x_{max}}{x})}{\ln(\frac{x_{max}}{x_{50}})}\right]^{b}\right\}}$$

Equation 2.3.1

Where:

$P(X)$ = Percent passing size of x

x = material size in question (mm)

x_{max} = Maximum material size (mm)

x_{50} = 50% passing size (mm)

b = Curve folding parameter

$$b \approx 0.5 * {x_{50}}^{0.25} * \ln(\frac{x_{max}}{x_{50}})$$

Equation 2.3.2

Where:

b = Curve folding parameter

x_{50} = 50% passing size (mm) (important size parameters are in millimeters)

x_{max} = Maximum material size (mm)

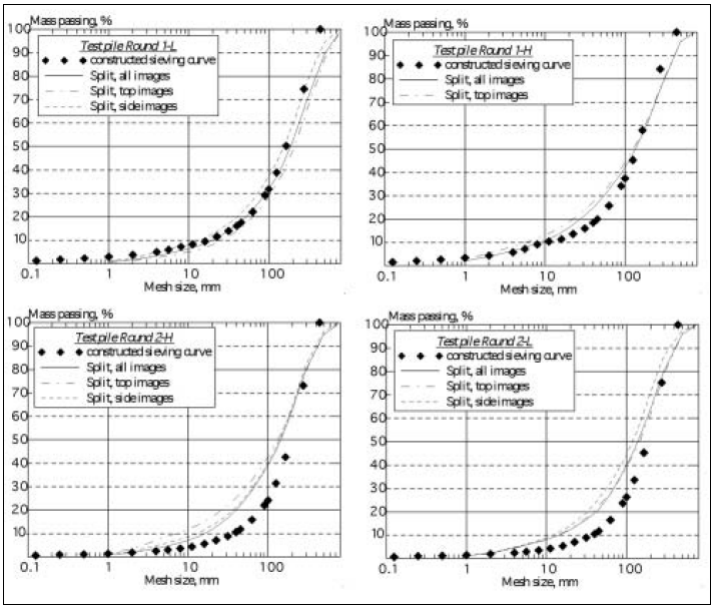

Figure 2.3.1 Screen and photofragmentation Swebrec curves compared to actual screen data curves (Ouchterlony F. , Olsson, Nyberg, Andersson, & Gustavsson, 2006)

Ouchterlony et al. list all the Swebrec equations, including the extended swebrec equation (Ouchterlony & Sanchidrian, 2019). The extended Swebrec equation was developed to capture percent passing sizes below 0.5 mm. Fine material at mines are typically not defined as the material below 0.5 mm, so this curve is only needed in special cases.

$$x_p/x_{max} = (x_{50}/x_{max})^{(1/P-1)^{-1/b}}$$

Equation 2.3.3

Where:

x_p = size of desired passing size (mm)

x_{max} = maximum material size (mm)

x_{50} = 50% passing size (mm)

P = percent passing size in fractional form

b = Curve folding parameter

$$if\ P_1 + P_2 = 1, P_2 < 0.5\ then\ b = \frac{\ln(1/P_2 - 1)}{\ln[\ln(x_{50}/x_{P2})/\ln(x_{P1}/x_{50})]},$$

$$\frac{1}{\ln\ (x_{max}/x_{50})} = \frac{1}{\ln\ (x_{50}/x_{P2})} - \frac{1}{\ln\ (x_{P1}/x_{50})}$$

Equation 2.3.4

Where:

P_1 = Known percent passing

P_2 = Second known percent passing less than 0.50

b = Curve folding parameter

x_{max} = maximum material size (mm)

x_{50} = 50% passing size (mm)

x_{P1} = Known material size (mm) corresponding with P_1

x_{P2} = Known material size (mm) corresponding with P_2

$$s_{50} = P'(x_{50}) = \frac{b}{4 * x_{50} * \ln\ (x_{max}/x_{50})}$$

Equation 2.3.5

Where:

s_{50} = slope of shape parameter 50% passing (mm^{-1})

$P'(x_{50})$ = slope of 50% passing size (mm^{-1})

b = Curve folding parameter

x_{max} = maximum material size (mm)

x_{50} = 50% passing size (mm)

$$P_{EXSwe} = \frac{1}{1 + a[\frac{\ln (x_{max}/x)}{\ln (x_{max}/x_{50})}]^b + (1-a)(\frac{x_{max}/x - 1}{x_{max}/x_{50} - 1})^c}$$

Equation 2.3.6

Where:

P_{EXSwe} = Percent pass on material size x

x = Material size of desired percent passing (mm)

b = Curve folding parameter

x_{max} = maximum material size (mm)

x_{50} = 50% passing size (mm)

a = adjusting factor

c = adjusting factor

Sanchidrian did a good job of taking a large amount of data from multiple sources and running an error comparison of many different fragmentation curves (Sanchidrian, 2015). Figure 2.3.2 shows all the data sets used in the Sanchidrian's analysis. Sanchidrian found that the extended Swebrec function performed the best. Most of the errors found in the research were at the coarse end (passing % > 80) and at the fine end (passing % < 20). Sanchidrian states, "Reasonable ranges of use for the Swebrec and the size-scaled Rosin-Rammler are thus 100>p>5 percent, or 80>p>2 percent" (Sanchidrian, 2015). Errors within these ranges can be expected to be around 15 percent. For the regular Rosin-Rammler function, Sanchidrian only advises using the function to estimate the range of 95>p>20 or 90>p>10 percent. Figure 2.3.3 and Figure 2.3.4 show how well each fragmentation function worked on the data set used in Sanchidrian et al. (Sanchidrian, Ouchterlony, Segarra, & moser, 2014).

Site	Rock	No. sets	Reference	n_p	x_{min} (mm)	x_{max} (mm)	p_{min} (%)
El Alto quarry, Spain	Limestone	1	Sanchidrián, Segarra and López (2006)	16	0.063	800	0.36
Mt. Coot-tha quarry, Australia	Hornfel	1	McKenzie (2003)	24	0.355	2000	2.75
Bårarp quarry, Sweden	Granite	7	Olsson and Bergqvist (2002)	19–20	0.075	500–1000	0.1–0.6
Kållered quarry, Sweden	Gneiss	6	Gynnemo (1997)	17	0.075	2000	0.34–0.49
Billingsryd quarry, Sweden	Dolerite	6	Gynnemo (1997)	18	0.074	2000	0.76–1.03
Rolla quarry, MO, USA	Dolomite	29	Otterness *et al* (1991)	6–8	9.525	228.6–457.2	7.9–20.6
Stewartville, MN, USA	Dolomitic limestone	20	Ash (1973), Dick, Fletcher and D'Andrea (1973)	7–8	4.7625	228.6–558.8	1.03–3.86
Guan Shan copper mine, China	Rhyoporphyry	8	Ma Bailing *et al* (1983)	11	100	1500	4.7–11.4
Rolla quarry, MO, USA	Dolomite	19	Stagg and Nutting (1987)	7–8	4.7625	304.8–609.6	2.8–7.4
Waterloo quarry, IA, USA	Limestone	7	Stagg, Rholl and Otterness (1989)	4–5	31.8–57.15	508	18.4
St Paul Park quarry, MN, USA	Dolomite	6	Stagg and Rholl (1987)	6	31.8	1000	22.1
Granite Falls quarry, MN, USA	Granitic gneiss	3	Stagg and Otterness (1995)	3	31.8	508	22.8
Manitowoc quarry, WI, USA	Dolomite	6	Stagg and Otterness (1995)	6	22.2	508	17.9

Key: n_p – no. of (size, passing) points; x_{max}, x_{min} – maximum and minimum size; p_{min} – minimum percentage passing.

Figure 2.3.2 Data set used to test fragmentation curve accuracy (Sanchidrian, 2015)

Function type	Name of $P_{CDF}(x)$	x domain	Number of parameters	Acronym	Equation No. in reference
Basic or semi-infinite functions	Weibull or RR	$[0, +\infty)$	2	WRR	(1)
	Grady	$[0, +\infty)$	2	GRA	(2)
	Lognormal	$[0, +\infty)$	2	LGN	(3)
	Log-logistic	$[0, +\infty)$	2	LGL	(4)
	Gilvarry	$[0, +\infty)$	3	GIL	(5)
Rescaled or transformed, finite-domain functions	Weibull or RR	$[0, x_{max}]$	3	TWRR	(1)+(6) or (7)
	Grady	$[0, x_{max}]$	3	TGRA	(2)+(6)
	Lognormal	$[0, x_{max}]$	3	TLGN	(3)+(6)
	Log-logistic	$[0, x_{max}]$	3	TLGL	(4)+(6)
	Swebrec	$[0, x_{max}]$	3	SWE	(8)
	Gilvarry	$[0, x_{max}]$	4	TGIL	(5)+(6)
Bi-component or extended functions	Weibull or RR	$[0, +\infty)$	5	BiWRR	(1)+(9)
	Grady	$[0, +\infty)$	5	BiGRA	(2)+(9)
	Lognormal	$[0, +\infty)$	5	BiLGN	(3)+(9) or (10)
	Log-logistic	$[0, +\infty)$	5	BiLGL	(4)+(9)
	Extended Swebrec	$[0, x_{max}]$	5	ExSWE	(11)
	Gilvarry	$[0, +\infty)$	7	BiGIL	(5)+(9)

Figure 2.3.3 Fragmentation size distribution models and their acronyms (Ouchterlony & Sanchidrian, 2019)

Medians of log-errors as estimators of the expected mean and maximum errors, expressed as relative errors in %.

Error type	Function	Number of parameters	Mean error (%)	Maximum error (%)
Coarse zone errors ($P = 80\%–100\%$)	ExSWE	5	4	8
	Rescaled functions with 3 parameters	3	6–7	10–15
	BiGIL	7	7	35
	BiWRR, BiGRA	5	7–9	58–92
Central zone errors ($P = 20\%–80\%$)	ExSWE	5	3	7
	BiWRR, BiGRA	5	3–4	8
	BiGIL	7	4	8
	Rescaled functions with 3 parameters	3	5–7	10–15
Fine zone errors ($P = 2\%–20\%$)	ExSWE, BiWRR	5	8	18–26
	BiGIL	7	8	25
	Bi-component functions with 5 parameters	5	10–16	31–34
	TWRR, SWE, TGRA	3	23–26	79–101
Very fine zone errors ($P = 0\%–2\%$)	ExSWE	5	35	67
	BiGIL	7	64	94
	BiWRR, BiGRA	5	39–93	127–163
	TWRR	3	171	302

Figure 2.3.4 Fragmentation size distribution model error by percent passing zone (Ouchterlony & Sanchidrian, 2019)

2.4 Kuz-Ram fragmentation prediction models

The Kuz-Ram was developed in the early 1980s by Claude Cunningham (Cunningham, 1983) and is the most used fragmentation model in the blasting industry. Cunningham later updated the Kuz-Ram model in 2005 (Cunningham, 2005). Cunningham adapted the early models from (Koshelev, Kuznetsov, Sofronov, & Chernikov, 1971) and (Kuznetsov, 1973) to predict the 50% passing material size. Cunningham utilized the Rosin-Rammler size distribution function to determine the rest of the distribution and determined an equation to determine the uniformity index. The Kuz-Ram was one of the first models not to require any previous fragmentation data to determine a full fragmentation distribution curve from blasting. The 1983 Kuz-Ram model equations are listed below.

$$x_{avg} = AQ^{\frac{1}{6}}\left(\frac{115}{E}\right)^{19/30}/q^{0.8}$$

Equation 2.4.1

Where:

x_{avg} = Average fragmentation size (cm) (Likely an error in the literature and was really supposed to be 50% passing size) (Ouchterlony & Sanchidrian, 2019)

A = Rock hardness factor that is 7 for medium-hard, 10 hard, highly fissured, and 13 very hard, weakly fissured (Protodyakonov, 1962)

Q = Weight of explosives in the borehole (kg)

E = Relative weight strength to ANFO

q = Powder factor (kg of explosives/m^3 of rock)

$$n = \left(2.2 - \frac{14B}{d}\right)\left(1 - \frac{W}{B}\right)[1 + (\frac{S}{B} - 1)/2]\frac{L}{H}$$

Equation 2.4.2

Where:

n = Uniformity index to be used in the RR fragmentation curve model

B = Burden (m)

d = Drill hole diameter (mm)

W = Standard drilling deviation (m)

L = Charge length above grade (m)

S = Spacing (m)

H= Bench height (m)

Most of the variables in the Kuz-Ram model are straight forward besides W and A in equations 2.4.1 and 2.4.2. Standard drilling deviation (W) is the standard deviation of where the drill hole bottom ends up versus the planned location. Rock hardness factor (A) is to help alter results due to different geology (Protodyakonov, 1962). Rock hardness factor is usually changed to make the data fit once the Kuz-Ram model is being used on an active blasting site. The recommended factors are to be used if no previous blast fragmentation data is known about the site in question.

Cunningham's Kuz-Ram model literature talks about the results of the equation 2.4.1 being the mean fragmentation. Spathis brings up the fact that mean is the average, not the 50% passing value, and one adjustment needs to be made to the equation (Spathis, 2004). Cunningham publishes an update to the Kuz-Ram model in 2005, utilizing the same equation with the notation of 50% passing instead of the mean (Cunningham, 2005). Equation 2.4.1, being 50% passing instead of the mean, is generally accepted as what Cunningham meant, but Ouchterlony et al. listed the following equation to fix the problem (Ouchterlony & Sanchidrian, 2019).

$$\frac{x_{50}}{\overline{x}} = g(n) = \frac{(\ln 2)^{1/n}}{\Gamma(1+\frac{1}{n})} < 1$$

Equation 2.4.3

Where:

x_{50} = 50% massing size (mm)
$\overline{x}$ = Average fragmentation size (mm)
n = Uniformity index
$\Gamma()$ = The mathematical gamma function

Cunningham updated his model in 1987 and improved upon the uniformity index, and replaced the rock hardness factor with Lilly's blastability index (Cunningham, 1987). Cunningham added bottom and column charge to the uniformity index equation to consider using two different types of explosives in one blasthole. Lilly came up with 5 different variables to determine the blastability index that includes rock mass description, joint plane

spacing, joint plane orientation, specific gravity influence, and hardness (Lilly, 1986). Adding Lilly's blastability index allowed engineers to take rock mass data collected by the mine and use it to predict fragmentation. The 1987 Kuz-Ram equation updates are below.

$$n = (2.2 - \frac{14B}{d})(1 - \frac{W}{B})(\sqrt{\frac{1 + \frac{S}{B}}{2}})\left(\frac{|L_b - L_c|}{L_{tot}} + 0.1\right)^{0.1}(\frac{L_{tot}}{H})$$

Equation 2.4.4

Where:

n = Uniformity index to be used in the RR fragmentation curve model

B = Burden (m)

d = Drill hole diameter (mm)

W = Standard drilling deviation (m)

L_{tot} = Total charge length (m)

L_b = Length of bottom explosives (m)

L_c = Length of top explosives (m)

S = Spacing (m)

H= Bench height (m)

$$A = 0.06 * (RMD + JF + RDI + HF)$$

Equation 2.4.5

Where:

RMD = Rock Mass Description – powdery/friable use 10, vertically jointed use JF, massive use 50

JF = Joint frequency = JPS+JPA

JPS = Vertical Joint Spacing – if spacing is 0.1 m use 10, 0.1 m to oversize use 20, and oversize to drilling pattern size use 50

JPA = Joint Plain Angle – if angle is dip out of face use 20, strike perpendicular to face use 30, and dip into face use 40

RDI = Density Influence = $25 * RD - 50$, RD == density (tonnes/m^3)

HF = Hardness Factor – if Young's modulus is less than 50GPa then use Y/3 and more than 50 GPa use UCS/5 (UCS in MPa)

Cunningham found that utilizing the 1987 Kuz-Ram over the 1983 Kuz-Ram fit the field data better. Figure 2.4.1 below shows collected fragmentation data versus the 1987 and 1983 Kuz-Ram predictions (Cunningham, 1987).

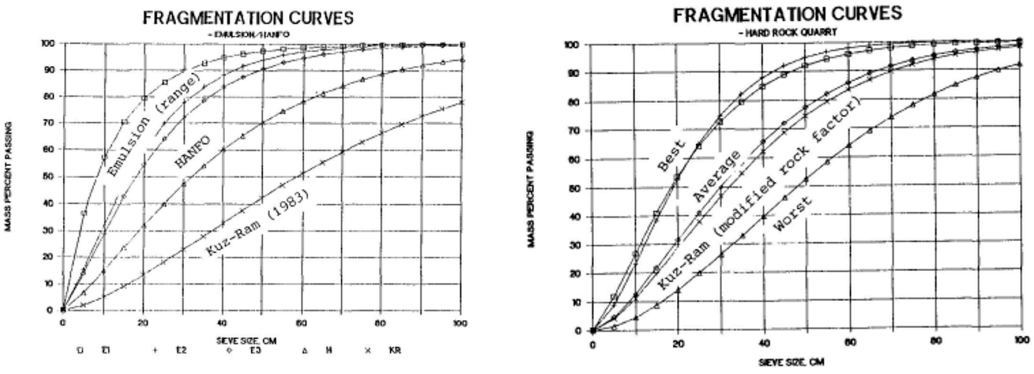

Figure 2.4.1 Photofragmentation results compared to the 1983 and 1987 Kuz-Ram predictions (Cunningham, 1987)

In 2005 Cunningham released the final version of the Kuz-Ram model that most blasting engineers use today (Cunningham, 2005). The Kuz-Ram model makes some updates to Lilly's blastability index, adds hole delay to the model, adds delay scatter to the model, effect of rock strength on uniformity, and helps explain some of the ratios' limits used. Ouchterlony et al. point out that Cunningham's 2005 literature has mistakes with the listed equations and leaves out terms that he talks about in the text, such as the rock factor

in the uniformity index equation (Ouchterlony & Sanchidrian, A Review of Development of Better Prediction Equations for Blast Fragmentation, 2019). In Cunningham's 2005 text, section 4.4 outlines adding rock factor to the uniformity index but does not include it in the final uniformity index equation (Cunningham, 2005). The equation below is the 2005 Kuz-Ram fragmentation model.

$$x_{50} = A_t A[Q^{\frac{1}{6}}\left(\frac{115}{E}\right)^{\frac{19}{30}} \Big/ q^{0.8}]\, C(A)$$

Equation 2.4.6

Where:

x_{50} = 50% passing material size (cm)

A = An alteration of Lilly's original blastability index shown in Equation 2.4.10

Q = Weight of explosives in the bore hole (kg)

E = Relative weight strength to ANFO

q = Powder factor (kg of explosives/m^3 of rock)

A_t = Delay Factor shown in equation 2.4.8

$C(A)$ = Site specific adjustment factor to fit the equation to collected fragmentation data – typically between 0.5 and 2

$$n = n_s * \left(\sqrt{2 - \frac{30B}{d}}\right) * \left(1 - \frac{W}{B}\right) * \left(\sqrt{\frac{1 + \frac{S}{B}}{2}}\right) * \left(\frac{L}{H}\right)^{0.3} * \left(\frac{A}{6}\right)^{0.3} * C(n)$$

Equation 2.4.7

Where:

n = Uniformity index to be used in the RR fragmentation curve model

B = Burden (m)

d = Drill hole diameter (mm)

W = Standard drilling deviation (m)

L = Charge length (m)

S = Spacing (m)

H= Bench height (m)

n_s = Delay scatter factor shown in equation 2.4.9

A = Rock factor calculated in equation 2.4.10

$C(n)$ = Site calibration to make equation 2.4.7 equal the uniformity index of collected fragmentation data

Cunningham introduced the influence of delay between holes in a row by assuming the original Kuz-Ram equation has the optimal fragmentation from delay and adjusts the 50% passing size higher if the delay increases on either side of the optimal delay (Cunningham, 2005). The use of the work done by Bergmann et al. was used to determine the optimal delay in terms of ms/m (Bergmann, Wu, & Edl, 1974). Bergmann et al. found the optimal delay between holes in a row to be 3 ms/m. The results of Bergmann et al. can be seen in Figure 2.4.2. The trend line in Figure 2.4.2 is the backbone of equation 2.4.8 that influences fragmentation based on the timing between holes down the row in the Kuz-Ram model. The trend line is built using spacing to burden ratios of 1 to 2 and likely is not valid for blast design geometry outside what was used in the experiment.

Bergmann et al. also collected p-wave velocity, and Cunningham used the optimal delay of 3 ms/m multiplied by the p wave velocity of 5.2 m/ms to come up with 15.6. T_{max} in Equation 2.4.8 below uses 15.6 to relate burden and site-specific p wave velocity to determine the optimal delay between holes in a row (Cunningham, 2005). The number

15.6 in T_{max} could be replaced with other data sets that measure optimal delay and p wave velocity.

$$A_t = \begin{cases} 0.66t^3 - 0.13t^2 - 1.58t + 2.1, when\ t \leq 1 \\ 0.9 + 0.1(t-1), when\ t > 1 \end{cases}$$

Equation 2.4.8

Where:

$t = \Delta T / T_{max}$

ΔT = Delay between holes in a row (ms)

T_{max}= Optimum benefit from delay between holes in a row = $15.6\, B/c_p$

B = Burden (m)

c_p = Compressional stress wave velocity (m/ms)

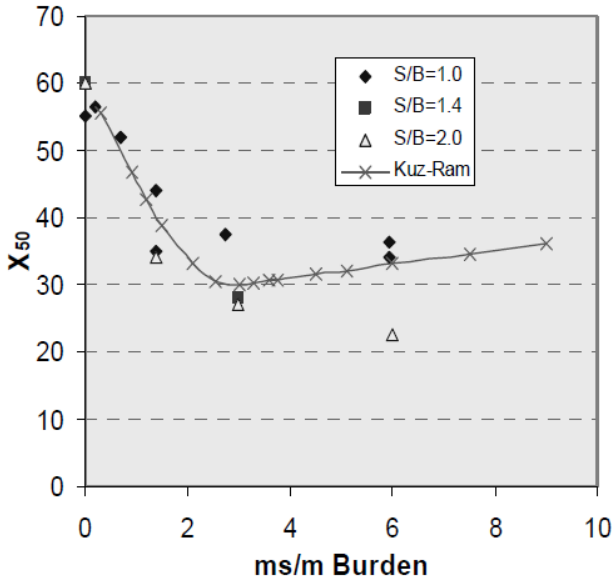

Figure 2.4.2 The influences of hole delay on fragmentation in granite (Cunningham, 2005)

The below equation is how Cunningham determined how cap scatter influences the uniformity index in equation 2.4.7 (Cunningham, 2005). The higher the detonator scatter, the less uniform the fragmentation distribution curve will be. The number 6 used to determine delay scatter ratio R_S is converting from a ratio between delay range and delay to delay standard deviation and delay (Cunningham, 2005).

$$n_s = 0.206 + \left(1 - \frac{R_S}{4}\right)^{0.8}$$

Equation 2.4.9

Where:

n_s = Delay scatter factor

R_S = Delay scatter ratio = $6\frac{S_t}{\Delta T}$

S_t = Standard deviation of delay scatter (ms)

ΔT = Delay between holes in a row (ms)

Cunningham changed the rock factor equation to the below equation (Cunningham, 2005). The joint frequency JF was dropped from the overall equation and only used in the RMD term. A new term called joint condition factor was added, and JPS and JPA were altered. JPS was changed by including a burden and spacing relationship and getting rid of the oversize term. JPA was changed by flipping the values for the orientation. Cunningham stated, "Dip here means a steep dip, > 30°. Out of face means that the extension of the join plane from the vertical face will be upwards. This is a change from the 1987 paper and is supported by Singh & Sastry (1987)" (Cunningham, 2005).

Cunningham failed to include the Singh & Sastry (1987) reference in the references section.

$$A = 0.06(RMD + RDI + HF)$$

Equation 2.4.10

Where:

RMD = Rock Mass Description – powdery/friable use 10, vertically jointed use JF, massive use 50

JF = Joint frequency = (JCF)(JPS)+JPA

JCF = Joint condition factor = tight joints use 1, relaxed joints use 1.5, and gouge-filled or open joints use 2

JPS = Vertical joint plane spacing factor – if spacing is less than 0.1 m use 10, 0.1 m to 0.3 m use 20, 0.3 m to $0.95\sqrt{BS}$ m use 80, and greater than size $\sqrt{BS}$ use 50

JPA = Joint Plain Angle – if angle is dip out of face use 40, strike perpendicular to face use 30, and dip into face use 20 – Dip is a steep dip greater than 30 degrees

RDI = Density Influence = $25 * RD - 50$, RD == density (tonnes/m^3)

HF = Hardness Factor – if Young's modulus is less than 50GPa then use Y/3 and more than 50 GPa use UCS/5 (UCS in MPa)

Cunningham's 2005 Kuz-Ram equation brought on the influence of delay and cap scatter to fragmentation modeling. The equation's existing parameters were refined, and limitations to the parameters were given. Cunningham never intended for the Kuz-Ram model to accurately predict fragmentation but more so to help understand what changing certain parameters to the blast would do to the blast's fragmentation. Cunningham stated, "It is a vehicle for exploring the expected behavior in terms of relative changes to fragmentation, and is, therefore, a useful way of refining understanding." (Cunningham,

2005). The 2005 Kuz-Ram equations are currently the main fragmentation prediction tool of the blasting industry.

2.5 Kuznetsov-Cunningham-Ouchterlony (KCO) fragmentation model

Ouchterlony modified Cunningham's Kuz-Ram model to fit the Swebrec fragmentation curve function in 2005 (Ouchterlony F. , 2005). The Swebrec function required 3 different variables and the Kuz-Ram only solved 50% passing fragmentation size. The other two variables included maximum fragmentation size and the shape parameter b. Ouchterlony determined a value for b by using the Kuz-Ram to find the uniformity index and 50% passing and determining the Rosin-Rommler slope at the 50% passing size, which was assumed to equal the slope of the Swebrec curve at the 50% passing size. The maximum fragmentation size was assumed to be in situ block size or burden or spacing. The equations are the same as the ones explained in the Swebrec and Kuz-Ram sections with the assumption that the slope of the Swebrec 50% passing point is equal to the slope of the RR function 50% passing point.

Ouchterlony refined his approach and later published final equations in 2015 (Ouchterlony F. , 2015) The KCO fragmentation model equations can be seen below. Equation 2.5.1 is a modified Kuz-Ram with an added 10 to make the units into mm instead of cm, and a powder factor exponent of 0.84 instead of 0.8. Quchterlony also adjusted the rock factor to be multiplied by 0.46 instead of 0.06. These changes were made to get the Kuz-Ram to fit Ouchterlony's data set. Equation 2.5.2 solves the problem of determining the maximum material size to utilize the Swebrec equation for fragmentation modeling and

not just on collected fragmentation data on-site. Figure 2.5.1 shows how the KCO fits with screened fragmentation data collected at Langasen (Ouchterlony & Sanchidrian, 2019).

$$x_{50} = \frac{10AQ^{1/6}\left(\frac{115}{E}\right)^{19/30}}{q^{\propto}}$$

Equation 2.5.1

Where:

x_{50} = 50% passing material size (mm)

A = Rock Factor in equation 2.4.10 but using 0.046 instead of 0.06

Q = Weight of explosives in the bore hole (kg)

E = Relative weight strength to ANFO

q = Powder factor (kg of explosives/m^3 of rock)

$\propto$ = Exponent that changes the relationship of powder factor to fragmentation size – KCO uses 0.84 instead of the 0.8 from the Kuz-Ram

$$s_{50} = \frac{b}{4x_{50}\ln\left(x_{max}/x_{50}\right)} \leftrightarrow {s_{50}x_{50}}^{0.75} = 0.2\left(\frac{0.0415}{B}\right)^{0.25}$$

Equation 2.5.2

Where:

s_{50} = slope of shape parameter 50% passing (mm^{-1})

b = Curve folding parameter, use 4.17

x_{max} = maximum material size (mm)

x_{50} = 50% passing size (mm)

B = Burden (m)

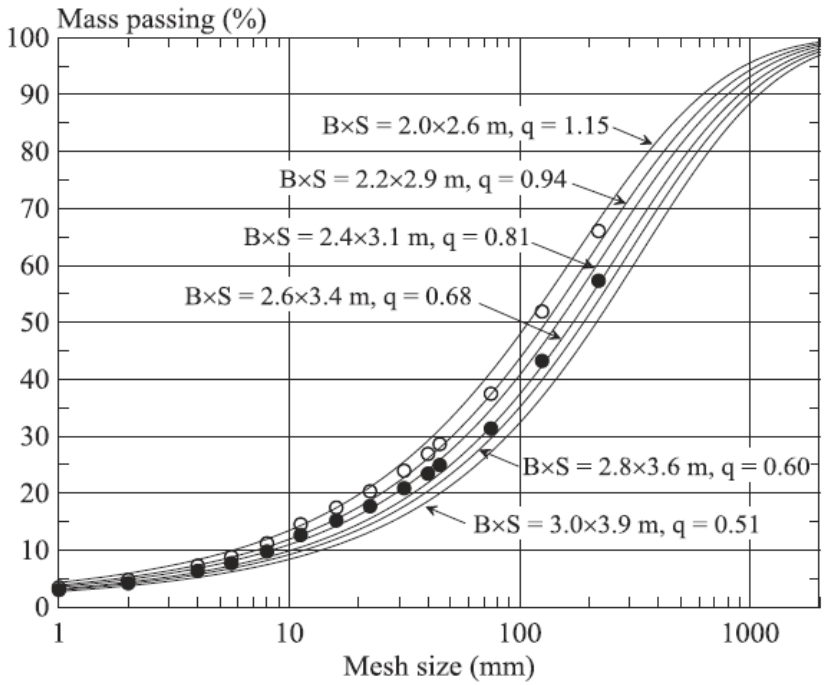

Figure 2.5.1 KCO fragmentation modeling versus screened data at Langasen (Ouchterlony & Sanchidrian, 2019)

The KCO model now makes it possible to utilize the Swebrec curve without the Rosin-Rammler curve but generalizes the folding parameter b for all blasts and does not include timing. Generalizing the folding parameter is likely not the case when the blast design geometry differs from Ouchterlony's data set. The KCO model also allows one to determine the maximum material size just by calculating the 50% passing size and knowing the Burden.

2.6 Fragmentation energy fan

The energy fan concept is currently being heavily discussed in recent fragmentation literature. The origin of the energy fans is unclear, but the concept is dated back to work done by the US Bureau of Mines in the 1990s. An energy fan is the log-log linear relationship between a certain percent passing material size and powder factor.

Researchers found that every passing percent material size regression fit all had a common focal point that leads to being able to extrapolate other percent passing values based on powder factor alone. Energy fans showed a clear trend that percent passing material size changed differently than other percent passing material sizes with powder factor (Ouchterlony, Sachidrian, & Moser, 2017).

Otterness et al. appear to be one of the first to publish data showing the energy fan, although they did not recognize the concept of an energy fan (Otterness, Stagg, Rholl, & Smith, 1991). Figure 2.6.1 is showing the Otterness et al. data set that leads to the concept of the energy fan. Figure 2.6.1 shows that there is a different relationship with the percent passing size with powder factor challenging the notion of utilizing distribution curves based on calculating the 50% passing size (Ouchterlony, Sachidrian, & Moser, 2017). Ouchterlony et al. seem to neglect the fact that the uniformity equation from the Kuz-Ram utilizes charge length, bench height, burden, and spacing to calculate the uniformity. Since powder factor is explosives over blast geometry, utilizing values from either explosives or geometry will help account for a powder factor change. Geometry is determined by bench height, burden, and spacing, and the length of charge is needed to determine the amount of explosives is in the hole. Since the uniformity equation of the Kuz-Ram utilizes explosives length and geometry, the model would be taking the energy fan concept into effect. The two areas the Kuz-ram model might not utilize the energy fan concept is when one changes hole diameter or explosives type/density.

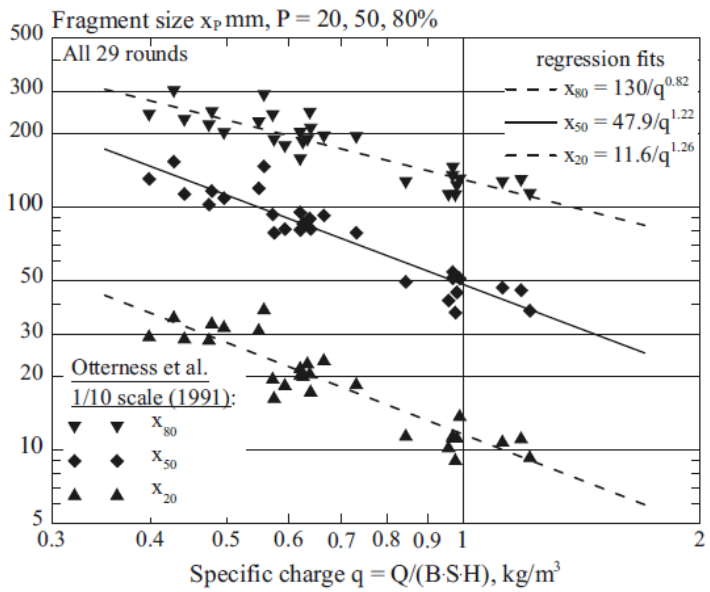

Figure 2.6.1 Percent passing fragmentation size versus powder factor from data from (Otterness, Stagg, Rholl, & Smith, 1991) (Ouchterlony, Sachidrian, & Moser, 2017)

Since the energy fan concept is extrapolating data between already collected fragmentation data, it is not an equation that will be used for the Wor-Sil equation. The concept is valid because it shows a method to take large data sets and test a variable such as timing to see if timing influences certain percent passing sizes differently. Figure 2.6.2 and equation 2.6.1 below show the energy fan concept (Ouchterlony, Sachidrian, & Moser, 2017).

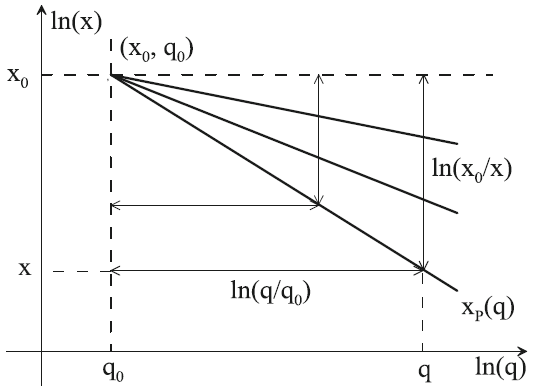

Figure 2.6.2 Fragmentation energy fan relating percent pass material size and powder factor (Ouchterlony, Sachidrian, & Moser, 2017)

$$\frac{x_p}{x_0} = \left(\frac{q_0}{q}\right)^{\alpha(P)} \; or \; \alpha(p) = \frac{\ln\left(x_p/x_0\right)}{\ln\left(q_0/q\right)} = \frac{\ln\left(x_0/x_p\right)}{\ln\left(q/q_0\right)}$$

Equation 2.6.1

Where:

x_p = Percent passing size at powder factor q (mm)

q = Powder factor associated with x_p (kg/m^3)

x_0= Percent passing size at the focal point of all the regression lines from the collected data (mm)

q_0 = Powder factor associated with x_0 (kg/m^3)

$\alpha(P)$ = monotonically decreasing function of the precent passing

2.7 Dimensionless fragmentation model (Ouch-Sanch)

The dimensionless fragmentation model (Ouch-Sanch) was developed to come up with a distribution-free fragmentation model that can predict any percent passing size since the energy fan showed that a change in powder factor changed the distribution (Ouchterlony, Sachidrian, & Moser, 2017). Ouchterlony et al. utilized the Kuz-Ram 50% passing size prediction concept and made a dimensionless equation instead of an empirical

equation. Sanchidrian et al. later expanded on the dimensionless fragmentation model to add timing and rock factors to develop the models' current form (Sanchidrian & Ouchterlony, 2017). The Ouch-Sanch model equations can be seen below.

$$\frac{x_p}{L_c} = k\left[\min\left(\frac{s_j}{L_j}, a_s\right) + a_0 j_0\right] {k_2}^h \left(\frac{\bar{\sigma}}{qe{L_c}^{\lambda}}\right)^K f_t(\Pi_t)$$

Equation 2.7.1

Where:

x_p = Material size of desired percent passing value

L_c = Characteristic size = $\sqrt{HS}$

k_2= Bench shape factor = $B\sqrt{HS}\cos\theta_i$

H = Bench Height

S = Spacing

B = Burden

θ_i= Drill hole angle to vertical

$\bar{\sigma}$ = Stored elastic energy at compressive failure = ${\sigma_c}^2/(2E)$

σ_c = Compressive strength

E = Young's modulus

q = Powder factor (kg/m^3)

e = Energy of explosives (Joule/kg) or (m^2/s^2)

k = Fitting parameter for fragment shape

K = Exponent fitting parameter for fragment shape

h = Additional exponent fitting parameter

λ= Additional exponent fitting parameter

$\min\left(\frac{s_j}{L_j}, a_s\right) + a_0 j_0$ = Joint correction factor (J_F) = $J_s + J_o$

J_s = Joint spacing term = $\min\left(\frac{s_j}{L_j}, a_s\right)$

J_o = Joint orientation term = $a_0 j_0$

s_j = Mean discontinuity spacing

L_j = Characteristic length

a_s = Limiting fitting parameter for $\frac{s_j}{L_j}$ for large joint spacings

j_0 = Lilly's blastability index normalized from 100 to 1 = 0.25 for horizontal, 0.5 for dipping out of the face, 0.75 for sub-vertical striking normal to the face, and 1 for dipping into the face or no visible jointing

a_0 = Fitting parameter for joint orientation

$f_t(\Pi_t)$ = Delay correction factor = $\delta_1 + (1 - \delta_1 - \delta_2 \Pi_t) e^{-\delta_3 \Pi_t}$

Π_t = 2005 Kuz-Ram delay factor = $c_p \Delta t / L_t$

c_p = p wave speed

Δt = Delay between holes in a row

L_t = Spacing, the 2005 Kuz-Ram delay factor used burden instead of spacing

Unfortunately, when a dimensionless equation is made from an empirical relationship, the terms in the equation loss their correlation to real data. For example, the relative weight strength of explosives is not what breaks the rock but correlates relative weight strength to fragmentation from an empirical data set. Correlating allows relative weight strength to capture what the explosives is doing to break the rock. Since there has not been any breakthroughs with collecting data during the fracturing process to fully explain what properties are fracturing and fragmenting the rock, explosives, and rock properties in relation to fragmentation are only theoretical.

The Ouch-Sanch model utilizes energy per unit mass instead of the relative weight strength ratio. A typical unit of energy per unit mass is calories per gram. Now the influencing factor on fragmentation is how many calories are in a gram of explosive, which does not correlate to fragmentation performance when comparing different materials. For

example, ANFO has an energy per unit mass of 880 cal/g, and smokeless gun powder has an energy per unit mass of 1235 cal/g (Hunsaker, 2019). A relationship between cal/g on fragmentation would mean that smokeless gun powder would have better fragmentation results for the same weight than ANFO would. Smokeless gun powder is currently only being used to break the rock in areas that explosives cannot be permitted for use and has poor fragmentation results compared to ANFO.

The Ouch-Sanch model relates the term by using 9 different fitting parameters to determine accurate fragmentation (Sanchidrian & Ouchterlony, 2017). The fitting parameters are to help determine what the fragmentation relationship is for each term on a large fragmentation data set. Each fitting term also has some relationship to the order in which the terms were fit (Sanchidrian & Ouchterlony, 2017). The fitting parameters are what determine what the fragmentation size will be for a given percent passing size. Sanchidrian et al. determined statistical fit curves for every fitting parameter utilizing the Less Fines and other project data, and the results can be shown in Figure 2.7.1 (Sanchidrian & Ouchterlony, 2017). The Ouch-Sanch model is excellent for predicting fragmentation at mines with a large fragmentation data set with rock mass data that covers a wide range of parameters. The model has not been widely tested and likely would not perform well at prediction fragmentation at sites that have blast design and rock conditions outside the bounds of the Less Fines project.

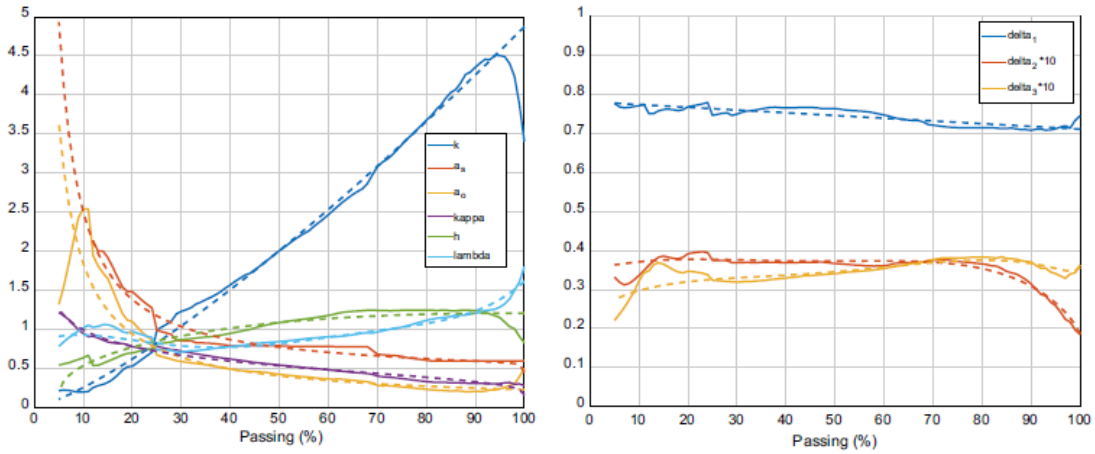

Figure 2.7.1 Relationship of Ouch-Sanch fitting parameters to percent passing size (Sanchidrian & Ouchterlony, 2017)

The Ouch-Sanch fragmentation model is a big step forward in the fragmentation modeling community, but it is also a very new concept. Ouchterlony et al. published the model's error using the Less Fines data set in 2019 comparing the Ouch-Sanch, Kuz-Ram, and the crushed zone/two-component model. The results can be seen in Figure 2.7.2 (Ouchterlony & Sanchidrian, 2019). Ouchterlony et al. state, "The average median expected error of the percentile size prediction for x_p-frag is about 20%, whereas the corresponding number for the Kuz-Ram model and the CZM is about 60%" (Ouchterlony & Sanchidrian, 2019). Ouchterlony et al.'s statement mean that the Ouch-Sanch fragmentation model can be fit into a large fragmentation data set better than the Kuz-Ram and crushed zone/two-component model. The error is also looking at the full range of % passing size and not the proven acceptable range of the Kuz-Ram model (Sanchidrian, 2015). The 9 different fitting variables make the Ouch-Sanch a complex model to try and use on greenfield sites without using the factors from the Less Fines data set.

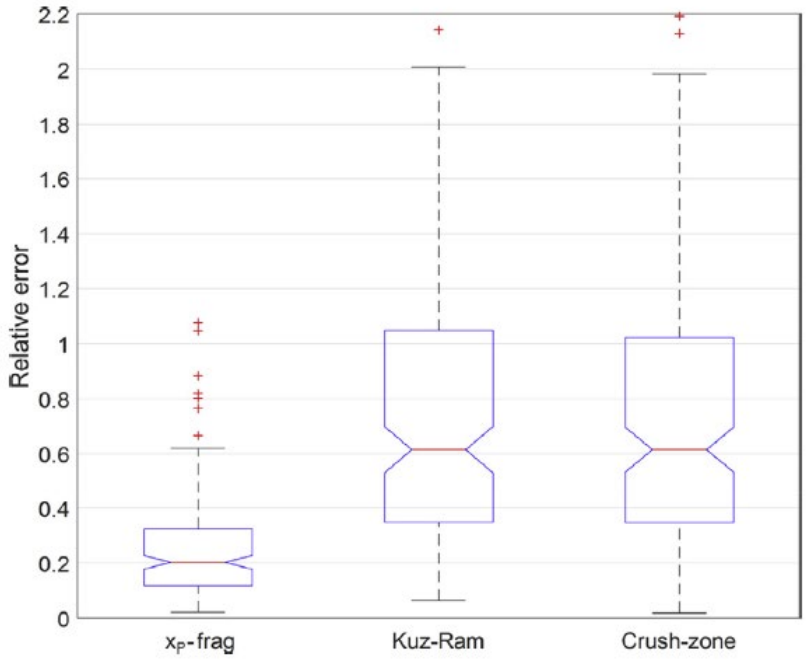

Figure 2.7.2 Boxplot of fragmentation model median total error for all percent passing sizes on the Less Fines data set (Ouchterlony & Sanchidrian, 2019)

The literature review had no indication that row delay or sequence was being considered when predicting fragmentation. Row delay is needed to be included in fragmentation modeling because row day is a big influencer on the confinement conditions of the blasthole when the blasthole fires in multiple row shots. Current methods for determining row delay are based on experience and there currently is not any methods to help guide blasters in selecting a row timing that will give the desired fragmentation outcomes.

2.8 Selected base fragmentation model for the Worsey-Silva model

The Worsey-Silva (Wor-Sil) model utilizes Silva's methodology for regular rhythmic timing and Worsey's methodology on utilizing dynamic confinement to adjust fragmentation. Chapter 4 explains the Wor-Sil model in more detail. The Wor-Sil model

is independent of any current fragmentation model. The model can be used in conjunction with any of the previous models.

A base fragmentation model is needed for the proof of concept. The decision has been made to utilize the 2005 Kuz-Ram fragmentation model with the Rosin-Rammler fragmentation curve as the base to the Wor-Sil model. The Ouch-Sanch fragmentation model could also be used, but the data set to validate the model does not have the required depth of information to define quality fitting parameters. The Kuz-Ram model is also currently the industry standard and providing a workflow for those models will help the Wor-Sil model gain industry acceptance.

The research data set utilized photofragmentation analysis to determine the fragmentation of the muck pile. Ouchterlony et al. showed that determining the fragmentation percent passing values between 20 and 80 percent with photofragmentation was acceptable (Ouchterlony & Sanchidrian, 2019). The Wor-Sil model will be used to estimate the fragmentation values between 20 and 80 percent passing.

Sanchidrian conducted a model error study on the Rosin-Rammler and the Swebrec distribution and found that the distributions are valid within a range of 5 to 100 and 2 to 80 percent passing size, respectively (Sanchidrian, 2015). The RR and Swebrec accuracy ranges fit well in the percent passing range that the photofragmentation data set is accurate for. Since the Kuz-Ram model utilizes the RR distribution, it is valid to use the Kuz-Ram model to predict the fragmentation between 20 and 80 percent passing sizes.

CHAPTER 3. STOCHASTIC APPROACH TO THE FRAGMENTATION PROBLEM

A stochastic approach to the fragmentation problem is needed due to all the randomness that happens in the process. The interaction of explosives with rock is a very random phenomenon mainly because not much is known about the detonation process and the non-homogeneous nature of the rocks. Variability is also present from operations executing the drilling and blasting plan. An operation with quality control will still have variances from the design that would influence the fragmentation. Chapter 3 introduces the principles of the Stochastic approach to the fragmentation problem.

3.1 Stochastic schemes

The Merriam-Webster dictionary defines stochastics as “involving a random variable” and “involving chance or probability” (Merriam-Webster. (n.d.), 2020). If the event being modeled has some sort of randomization and a probability of varying variables, using a stochastic approach will determine the most probable value and give confidence intervals for what the value will be.

Bench blasting has variables that change from hole to hole in the blast. Some of the variables that can change are the burden, spacing, charge weight, explosives density, hole depth, stemming heights, geology, primer placement, water, etc. Each change will influence the fragmentation of that hole. During the testing, many of these variables were measured to ensure consistency.

One example of how random a variable can be in a blast can be seen by looking at each hole's charge weights for test 1. The bulk truck’s scale had not been calibrated in some time, but it shows how variable the charge weight can be during the explosives

loading process. The average weight of explosives in the 69 holes was 415.8 lbs. The standard deviation of the weight was 18.5 lbs with minimum and maximum values of 330.7 and 451.9 lbs respectively. A 95 percent confidence interval would range from 411 to 420 lbs in a hole. The predicted 50 percent passing sizes, just considering the explosives weight variations, would change from 9.9 inches to 9.7 inches. A difference of 0.2 inches might not seem like much, but when you add all the variables that change in the shot, the average 50% passing size could vary by a couple of inches.

The most used probabilistic approach in the mining industry is the Monte Carlo simulation. The Monte Carlo simulation runs the simulation with randomly selected variables and conducts a prediction. The simulation is conducted as many times as needed to determine an average value. The more simulations used, the better the predicted average value becomes. The more simulations used also increases the amount of computing time needed to determine the average. The Monte Carlo simulation allows equations with random values to be solved in a defined time window (Silva-Castro, 2012).

The random variables can be determined by using discrete random variables. This method selects variables at random within a probabilistic range of values (Silva-Castro, 2012). Random variables will be weighed, so they are selected within a specific range of probability. If quality control measuring is being conducted on-site, average values and standard deviations can be obtained to influence the random variable generator.

In summary, the discrete random variables method is used to obtain a random value within a probabilistic range, and the Monte Carlo method is used to run the equation with the random values multiple times to determine a statistical average. The Monte Carlo simulation must be run enough times that the average value converges on an acceptable

amount of error. When using the Monte Carlo simulation on blast vibrations, the typical number of runs needed to have an acceptable error was 150 times (Silva-Castro, 2012).

3.2 Implementation of the stochastic approach to the fragmentation prediction

To implement the stochastic approach to the fragmentation prediction problem, the variables that need to be randomized need to be selected. Since the most used fragmentation model today is the Kuz-Ram model, the approach will utilize the variables from the Kuz-Ram model. The method can be used with any fragmentation prediction method by selecting the variables that vary in the field, randomize the variables, and conduct enough predictions to minimize error. Variables in the Kuz-Ram model include the following.

x_{50} = 50% passing material size (cm)

A = An alteration of Lilly's original blastability index shown in Equation 2.4.10

Q = Weight of explosives in the bore hole (kg)

E = Relative weight strength to ANFO

q = Powder factor (kg of explosives/m^3 of rock)

A_t = Delay Factor shown in equation 2.4.8

$C(A)$ = Site-specific adjustment factor to fit the equation to collected fragmentation data – typically between 0.5 and 2

n = Uniformity index to be used in the RR fragmentation curve model

B = Burden (m)

d = Drill hole diameter (mm)

W = Standard drilling deviation (m)

L = Charge length (m)

S = Spacing (m)

H= Bench height (m)

n_s = Delay scatter factor shown in equation 2.4.9

A = Rock factor calculated in equation 2.4.10

$C(n)$ = Site calibration to make equation 2.4.7 equal the uniformity index of collected fragmentation data

Each one of the above variables could be randomized to determine the average fragmentation. x_{50} to $C(A)$ would be variables for predicting the 50 percent passing size and n to $C(n)$ would be the variables for predicting the uniformity index.

The first step to the process would be to determine what variables to randomize. Determining which variables will change requires quality control data collection to determine the variability of the shot's above parameters. Quality control data collection would require measuring every variable for each hole and determining the average and the standard deviation. If the standard deviation is more than 5 percent of the average, use it in the discrete random variable process.

The next step is to run the prediction multiple times and compute the average and the standard deviation of all the runs for the 50 percent passing size and the uniformity index. The average predicted 50 percent passing size, and the average uniformity index will be what is used to determine the average cumulative distribution curve.

A confidence interval will be conducted on the 50% passing size and the uniformity index to determine an upper and lower bound fragmentation curve. The lower values for the confidence interval selected will be used to compute the low-value fragmentation curve, and the higher values for the confidence interval selected will be used to compute the high-value fragmentation curve. An example of what the result of a stochastic approach would look like can be seen below in Figure 3.2.1. Test 2 is fragmentation

results from the Ogden Point testing, and the average, lower 95%, and the upper 95% are using the 2005 Kuz-Ram fragmentation model with test 2's input parameters.

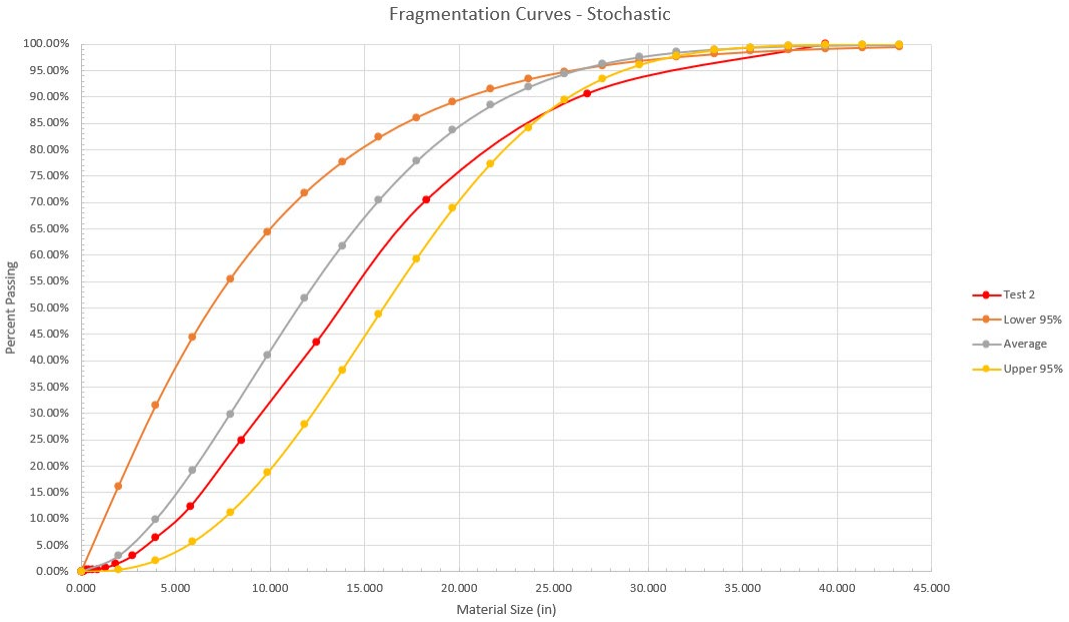

Figure 3.2.1 Stochastic fragmentation curves

Utilizing random variables and the Monte Carlo simulation will produce a range of fragmentation values within the confidence interval selected and an average percent passing size. Conducting the stochastic approach helps capture variability in the field to have accurate fragmentation predictions. The stochastic approach also opens the door to fragmentation improvements when implementing a quality control program on the drilling and blasting. One would be able to determine how tight control is needed with each parameter to have an acceptable variation in fragmentation.

CHAPTER 4. DYNAMIC CONFINEMENT APPROACH TO THE FRAGMENTATION PROBLEM

Confinement has been proven to be a very important factor when it comes to fragmentation from blasting. A blast will typically be designed to have as many free faces as possible. When looking at a blast with multiple rows, the shot's timing will influence how much confinement the inner rows will have. The following chapter explains dynamic confinement, a concept developed in this research, and how it can be used to optimize fragmentation.

4.1 Dynamic confinement

Dynamic confinement is considered the level of confinement a blasthole has when the hole is detonated. The confinement is dynamic because the confinement is only open during a time window, and it will close if the hole is not shot within that particular time window.

The initial free faces of the shot before detonation is the static confinement conditions of the shot. In surface blasting, there are typically five (5) static confinement conditions. Before the shot starts, the static confinement (in the horizontal plane) is only available to the holes next to the free face. Static confinement does not close with time. The benefits of static confinement for fragmentation are absolute. Absolute confinement means the space is available no matter when a charge is fired and is enough to not inhibit any of the movement from the blast. Figure 4.1.1 shows the five (5) typical static confinement conditions in surface bench blasting. Confinement scenarios 1 to 3 are the most common static confinement conditions in surface bench blasting.

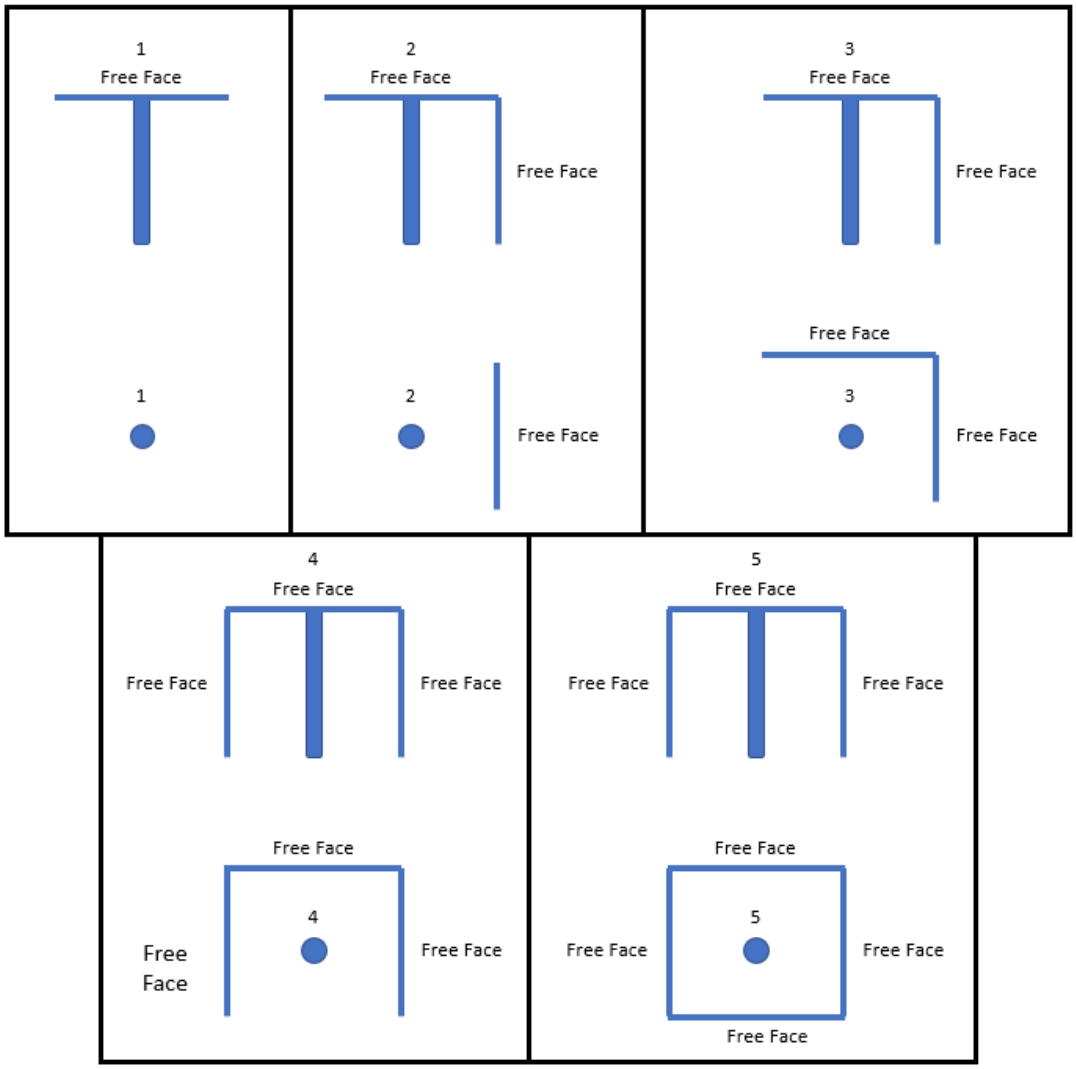

Figure 4.1.1 Side and a plane view of the five typical static confinement scenarios for surface bench blasting

Figure 4.1.2 is a multi-row shot with the static confinement scenario two (2) from Figure 4.1.1. As seen in this figure, the only two free faces available are the bench's surface and the free face in front of the first row (row 1). If the pattern in Figure 4.1.2 was fired, so all holes detonated at once, then the holes in row 1 would all have a two (2) free face confinement scenario, and the holes in row 2 and row 3 would have just one free face confinement scenario (the bench's surface). Johansson et al. found that decreasing

confinement creates a decrease in fragmentation size. Also, it showed the importance of a free face parallel to the drill holes (Johansson & Ouchterlony, 2013). Johansson's discovery is common knowledge in the blasting industry, but it proves the concept of less confinement decreases fragmentation size in a laboratory setting with tight control on the variables.

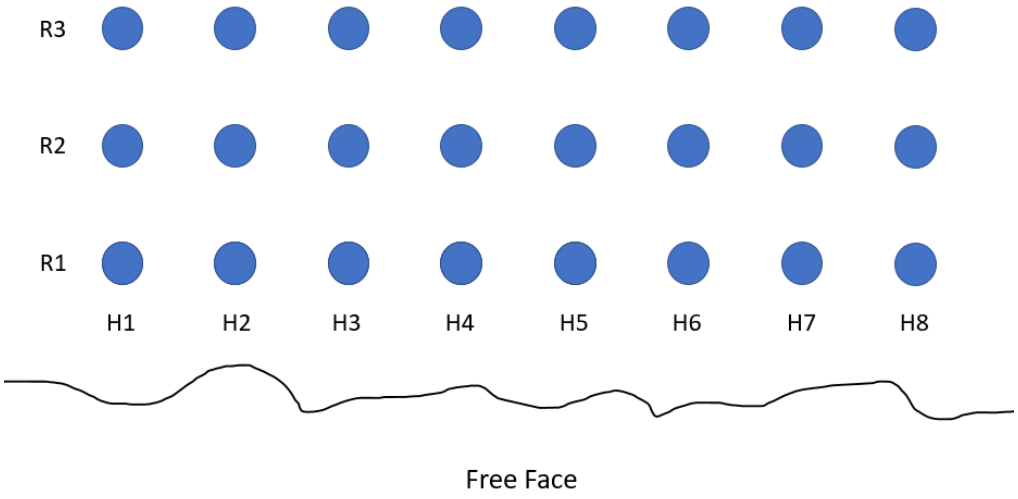

Figure 4.1.2 Plane view of a surface bench blast with only 2 degrees of freedom

Now look at the same example above and fire all holes in row 1 simultaneously, then shoot all holes in row 2 at some time after row 1 has detonated. The new scenario at the time of detonation of row 2 can be seen in Figure 4.1.3. A new free face has formed due to allowing time for row 1 to move out of the way of the face of row 2. Row 2 now has the same confinement conditions as row 1 had before the shot and gains fragmentation benefits of the additional free face. If row 3 was fired at the same time as row 2, then row 3 confinement condition would be only 1 free face instead of 2. The fragmentation from row 1 and 2 would be better than row 3. However, if row 3 was also delayed to fire

sometime after row 2, then row 3 would gain the fragmentation benefit of the extra free face.

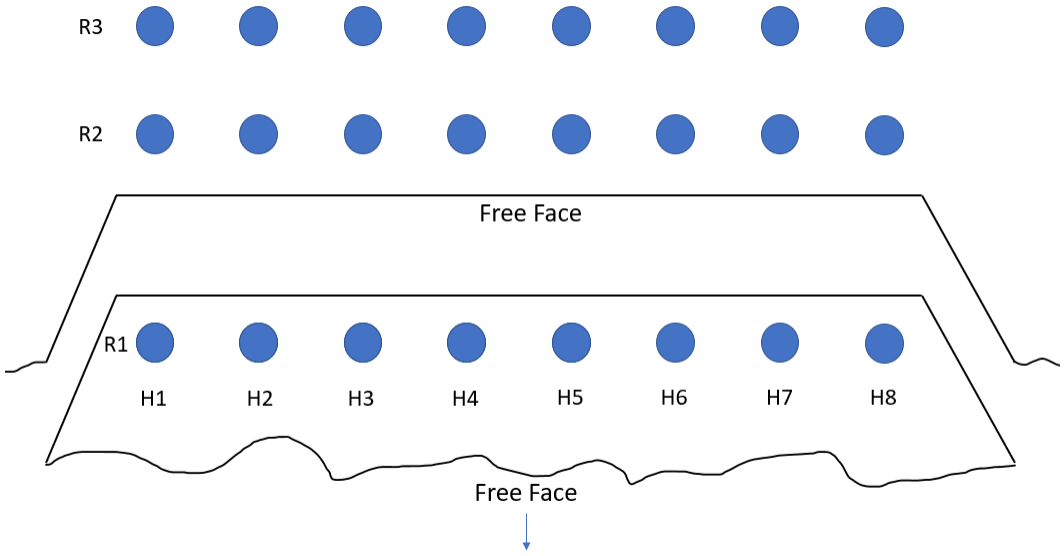

Figure 4.1.3 Plane view of a bench blast after row 1 has detonated, and at the time row 2 detonates with a time delay after row 1

The above figures illustrate how the confinement of a shot changes with the detonation time. The next question is, "how much space is needed for a free face to be effective?". Collecting the face velocity of the material after detonation would help to determine at what time a certain amount of space is created, but it does not determine how much space is needed for a free face to be beneficial. If the rock came out in one big "chunk" like Figure 4.1.3 and the second row has the same face velocity as the first, only a small amount of separation would be required to have the benefits of a free face.

However, the blasted rock from row 1 will not come out in one big "chunk". Row 1 material will be fractured and fragmented into smaller pieces and will start to move and

rotate. As the material moves and rotates, it creates void space in the moving rock mass, causing the volume to increase.

Having material swell is not a problem for row 1 because it has a static confinement condition with a free face that can accommodate the material's swelling. On the other hand, row 2's void space available for swelling is dependent on how much void space is created by the time between firing row 1 and row 2. This made the confinement conditions dynamic. The ISEE Blasters' Handbook defines swells, "a measure of the bulk volume increase of a blasted rock mass to its original in situ volume" (ISEE, 2011). The handbook also gives 30 percent as a typical value for material swell due to blasting. Now there is guidance on how to determine how much void space is needed to have a sufficient free face. This guidance is given by the minimum amount of time needed between rows for the row in front to be able to move out of the way for the next row. The time provides the extra space needed to accommodate the swelling of the next row.

Now that row delay time is needed to have an adequate dynamic free face (enough space) is known, the question of "why not just use an extreme amount of time to ensure there is enough space?" needs to be answered. The answer to that question is related to the fact that the void space created due to timing will eventually close because the material in the stemming zone will fall into the space due to gravity. Figure 4.1.4 shows the closing void space's concept due to gravity acting on the material in the stemming zone. At T1 the material starts to move away from the explosives charge in the directions of the free faces. At T2 the material in the stemming zone starts to fall due to gravity and the material in front of the explosives continues to move outward. T3 shows the void space is shrinking, and gases start to escape. T4 shows that there is still forward movement has the stemming

zone comes to rest. T5 is the final resting point of the muck pile. This behavior was recorded in the field tests developed for this research by observing the broken material of the stemming zone in the blastholes' location after the blast. Figure 4.1.5 shows this condition for one of the tests. The static confinement condition in Figure 4.1.5 is not as bad as fully confined, but there is a point in time during the dynamic confinement condition that would have a full free face as seen in Figure 4.1.4 for time T1 and T2. This point would be when the velocity of vertical upward movement of the stemming zone is zero. Gravity will then cause the stemming zone to fall back down closing the void space. Through testing at the Haile Gold Mine, it was determined that the time it took to reach zero upward velocity was 1000 ms and was drastically longer than it took to make the required void space due to face velocity. This is why this concept will not be utilized in the Wor-Sil methodology, but is something to keep in mind if using row delays longer than the maximum row delay calculated using the Wor-Sil methodology.

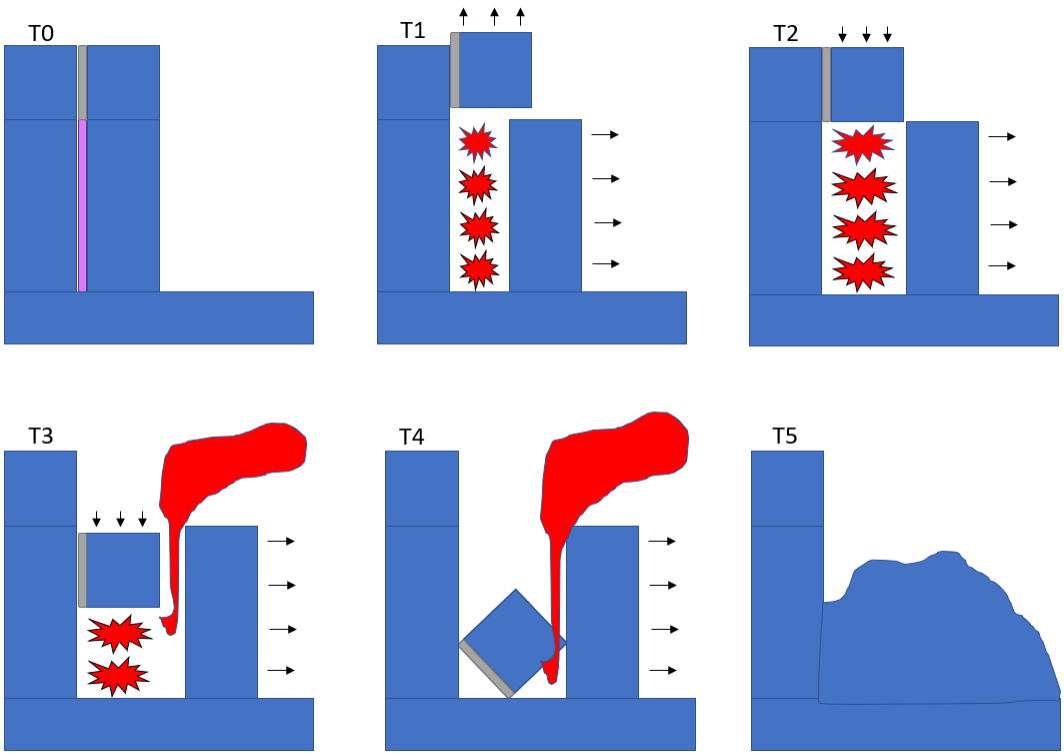

Figure 4.1.4 Side view of changing void space due to time after detonation

Figure 4.1.5 View of blast after all material movement has finished

The determination has been made that there is a certain time during the shot detonation process that produces the optimal amount of space available for the next row to shoot in. Why not just determine the time at which the stemming zone would start to close the dynamic void space? From conducting face velocity testing at the Haile Gold Mine, the time in which optimal void space was created was between 500 to 1000 ms using high-speed video to determine the apex of material's upward movement (Worsey T. , 2019). Suppose one determines the velocity of the upward movement of the stemming zone, and uses physics of a projectile. In that case, you can determine when the material in the stemming starts to close the void space. The blasting industry currently has issues with delay times longer than 120 ms due to the fear of rock shifting and separating undetonated explosives columns. The test at the Haile Gold Mine determined that 500 ms would be a reasonable time delay to separate production shots from trim shots when shooting the two shots together. However, the blaster on site refused to use 500 ms between shots and would only allow up to 120 ms.

Another question to solve is "if there is a time delay after the first hole in the first row fires that would cause adverse effects on the second row?". What about the shock wave? Johansson et al. determined the shock wave velocity in concrete to be around 10,000 ft/s (Johansson & Ouchterlony, 2013). With a burden of 16 ft, one would have to fire the 2^{nd}-row 1.6 ms after the first row to not to have shock interaction from the first row with the explosives of the second row. Row delays of 1.6 ms for typical surface blasting is not used. The justification above tells us why the industry is not concerned about the shock wave interfering with the second row's explosives.

What about the rock movement? Gkikizas found that material starts to detach and move at around 2.4 ms/ft of burden (Gkikizas, 2016). For the case of 16 ft of burden, the second row would need to be fired before 38.4 ms had passed. A row timing of 38.4 ms or less is not a common row timing used in bench blasting, but it can be found in large surface metal operations. The researcher worked at a previous operation, which used 17 or 25 ms between holes and 33 ms between rows. One big reason for doing this was minimizing cutoffs when utilizing a detonating cord as the initiation system, but another was because of the fear of the column shift. Since there is the possibility of burden detachment at 38.4 ms, this is a valid concern. Since there are at least two main different breaking mechanisms in blasting, one must investigate the blast geometry parameters to determine which breaking mechanism is being utilized. Below are the geometry parameters from the mine that used 33ms between rows.

- Burden – 16 ft
- Spacing – 18 ft
- Hole depth – 23 ft
- Stemming length – 16 ft
- Hole diameter – 7.875 in.
- Bench height – 20 ft
- PF – 0.5 lb/cyd

To be classified as a bench blast, Ash's thumb rules for geometry need to be satisfied. The terms below show what parameters would be needed to have bench blasting as the breaking mechanism. The blasting geometry did not meet the characteristics of bench blasting.

- Bench height/burden ratio – 4 > 20 ft/16 ft = 1.25

- Hole diameter – bench height/100-120 - 20/100*12 = 2.4 in. < 7.875 in.
- Powder Factor – 1 lb/cyd for quarry blasting > 0.5 lb/cyd
- Stemming height – 0.7 to 1.2 * burden – good range
- Spacing – 1.2 to 1.4 * burden – 16*1.2 = 19 ft > 18 ft

Since the blast geometry did not meet the requirements to have bench blasting as the rock's breaking mechanism, let us look at the cratering mechanism. ISEE defines cratering as "the fragmentation process of a single buried charge" (ISEE, 2011). Cratering only has one free face. ISEE also defines a cylindrical charge as a spherical charge when its charge length to hole diameter ratio is equal to or less than 8. The case above has a ratio of 10.6 and would only need 1.75 ft fewer explosives in the hole to satisfy the spherical charge requirements. The operation did not free face the shots, so the blast geometry represents a cratering fragmentation mechanism more than a bench blasting fragmentation mechanism.

Typical results from a crater shot can be seen in Figure 4.1.6 (ISEE, 2011). This mechanism matches the results of the blast geometry described above. The actual shot can be seen in Figure 4.1.7. One essential item to note during the cratering fragmentation mechanism is that fracturing and movement happen in all directions, and material shifting could be a problem with neighboring holes. If cratering is the method of fragmenting the rock, then any delay larger than 2.4 ms/ft risks having a column shift. Column shift would separate the explosives column, and when the neighboring hole fires, only a portion of the intended explosives would detonate. Less explosives firing would mean less fragmentation, but these cases also pose a safety risk of explosives left in the muck pile. Cratering fragmentation mechanism would be a case when the concept of dynamic confinement

should not be used and shows the importance of defining blast geometry for fragmentation models.

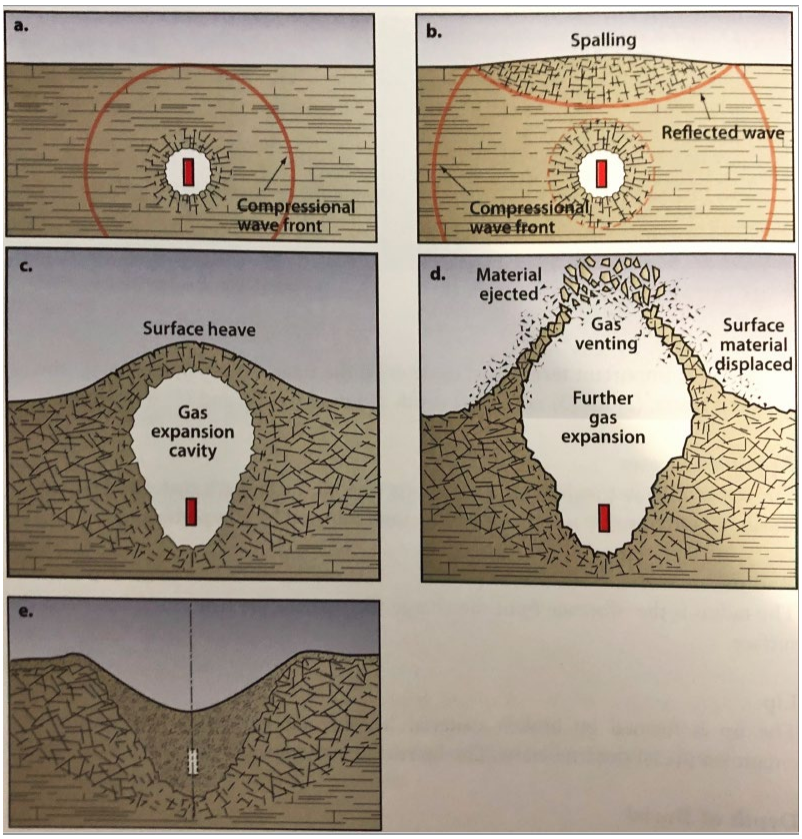

Figure 4.1.6 Cratering fragmentation mechanism (ISEE, 2011)

Figure 4.1.7 Example of cratering fragmentation mechanism

The cratering fragmentation mechanism needed to be explained because fragmentation models do not recognize different fragmentation mechanisms. It is possible that no one in the explosives industry recognizes that there are different fragmentation mechanisms because it was not discussed in the literature. Now let us look at the geometry of a blast that utilizes the bench blasting fragmentation mechanism. Figures 4.1.4 and 4.1.5 show blasting conditions that satisfy bench blasting fragmentation mechanism geometry. Notice how the material movement is in the direction of the free face, and material movement is not in the direction that would disturb a second row. The shock wave's initial fracturing process will travel in all directions, but the cracks growing in the direction without a free face will not separate. The reason is that the gas pressure will separate the fractures in the material that can move. Cracks that reach a free face will be able to move freely, and the gas will travel through the crack to reach equilibrium. During the process of gas escaping, the rock fractures will be thrown and rotated, adding to the fragmentation process. This concept is proven by the research done by Johansson et al. (Johansson & Ouchterlony, 2013). Johansson et al. were exploring the influences of fast timing on

fragmentation and not the bench blasting fragmentation process. However, their results prove the point of only getting facture separation in the free face's direction.

Johansson et al. set up an experiment in concrete blocks that had two (2) rows of five (5) holes (Johansson & Ouchterlony, 2013). The setup of the experiment can be seen in Figure 4.1.8. They shot experiments with a free face but shot the rows as separate experiments. They found that fragmentation was better for row 2 than it was for row 1. Fragmentation results of row 1 versus row 2 can be seen in Figure 4.1.9. The results prove that having pre-conditioned rock (pre fractured) from blasting yields better fragmentation. No column shift or separated cracks were observed during the experiment in the direction of the second row, and the free faces created by row 1 were relatively straight, and can be seen in Figure 4.1.9. Cracks not separating in directions without free faces are also confirmed with results from the Ogden Point testing seen in Figure 4.1.5 above.

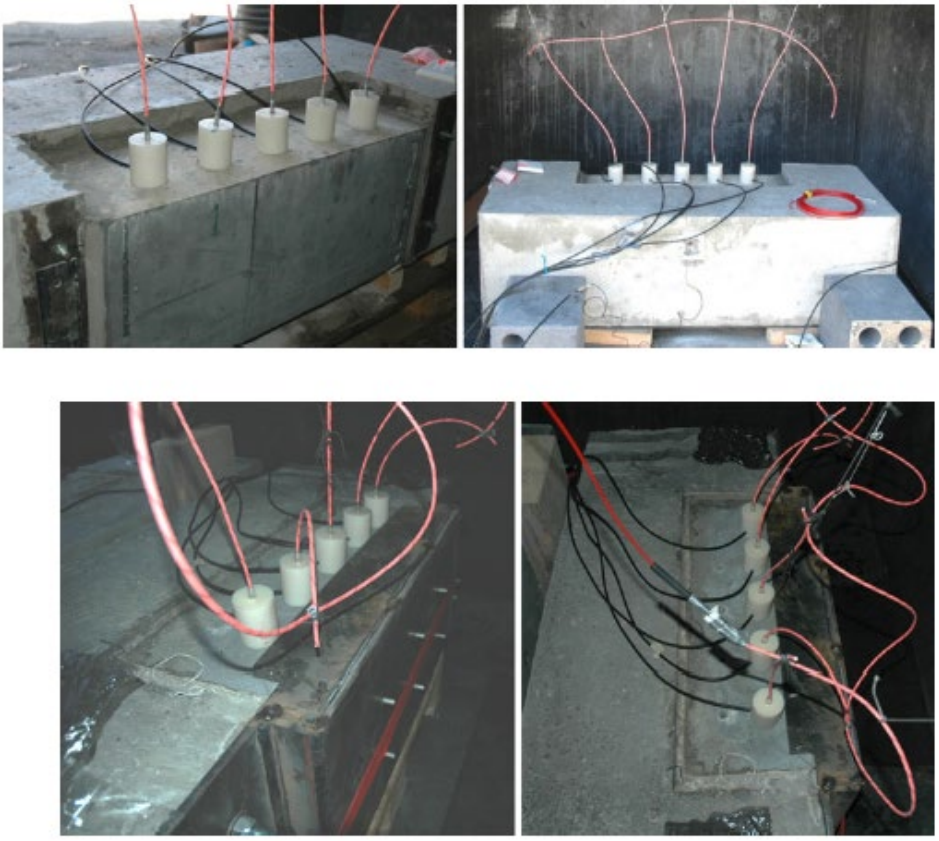

Figure 4.1.8 Johansson et al. experiment setup (Johansson & Ouchterlony, 2013)

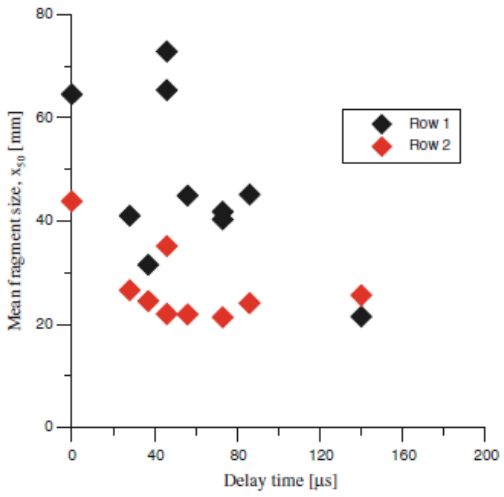

Figure 4.1.9 Johansson et al. fragmentation results (Johansson & Ouchterlony, 2013)

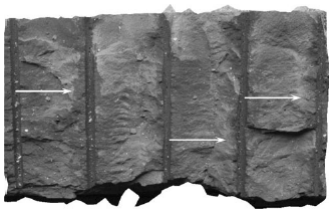

Figure 4.1.10 3D image of row 2's free face after shooting row 1 (Johansson & Ouchterlony, 2013)

Fractures will not be separated in directions without free faces when using bench blasting fragmentation mechanism geometry. Row delay slower than 2.4 ms/ft is an acceptable practice in conditions that utilize bench blasting fragmentation mechanism geometry and is required to have enough void space to allow uninhibited movement in the direction of the free face. The concept of dynamic confinement is possible when using the bench blasting fragmentation mechanism.

One area that does need to be explored is the elastic rebound of the rock mass. This could potentially be an issue when using long row timing in rock instead of concrete. Almost all rock masses have joints that have the potential to separate due to elastic rebound. This issue was not observed in the full-scale testing but is a reason only to utilize a row timing that is just enough to obtain the required dynamic confinement condition for optimal fragmentation.

4.2 Implementation of dynamic confinement to the fragmentation prediction

Section 4.2 explains the dynamic confinement approach to the fragmentation model and will be called the Worsey-Silva (Wor-Sil) model to follow the trend of fragmentation and vibration models.

The first step of the approach is to ensure the fragmentation mechanism is bench blasting. The Wor-Sil model adopts Ash's rules for quality blasting as the defining variables to have the bench blasting fragmentation mechanisms. Ash's rules are displayed below (Ash, 1968).

- Bench height/burden ratio – 4 or greater
- Hole diameter – bench height/100-120
- Powder factor – 1 lb/cyd to 2 lb/cyd
- Stemming height – 0.7 to 1.2 * burden
- Sub-drill – 1/3 * burden

Instead of using ash's rule for spacing to burden ratio, the Wor-Sil model will utilize Zhang's equation for determining optimum spacing to burden ratio with a field test to determine break out angle. Zhang's equation for determining optimal spacing to burden ratio is below (Zhang, 2016).

$$S = \frac{B}{\sin\left(\frac{\pi}{2} - \theta\right)}$$

Equation 4.2.1

Where:

S = Spacing

B = Burden

θ = ½ of the measured breakout angle in radians

A field test will be required to determine the breakout angle. The test involves shooting single holes to determine the breakout angle to calculate the spacing ratio using

the desired burden. 3D point cloud measurements will be taken to be able to estimate the breakout angle. Four angle tests are recommended in each formation blasting is being conducted in. If field tests are not possible, utilizing a breakout angle of 135 degrees is an acceptable average for bench blasting (ISEE, 2011). The workflow for the angle calibration is as follows, and an illustration can be seen in Figure 4.2.1.

1. Collect 3D point cloud data of pre-blast face and floor
2. Shoot 4 single holes in different places in the formation with the desired burden
3. Collect 3D point cloud data of blasted muck pile
4. Muck out fragmented material
5. Collect 3D point cloud data of the face and floor
6. Measure the angle between the newly generated rock surfaces for all 4 tests
7. Average the angle of all for tests
8. Use equation 4.2.1 to calculate spacing

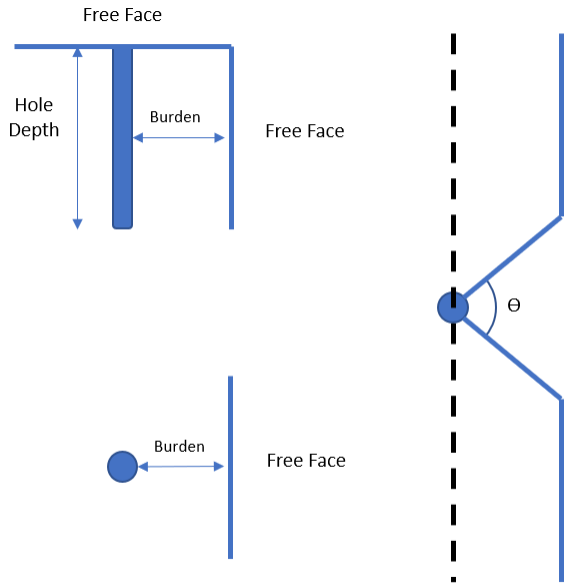

Figure 4.2.1 Break out angle calibration test

Another measurement that can be taken during the breakout angle calibration is face velocity. Utilizing a camera with 1000 frames per second or more will be needed for face velocity measurement. A reference grid will be needed in the frame to determine the distance in the video. A video camera with a fixed focal length can be used if the pixel length is determined at the distance of face movement. A time zero indicator will be needed to determine when the hole fires and can be an electronic detonator timed at the same time as the hole on the surface. Time zero to the first movement will be the rock response time, and the time between the start of the rock moving and the time the object is gone will be the time used to determine velocity called time velocity (s). Velocity will be the width of the scale object in feet divided by the time velocity in seconds to get face velocity in feet per second. Figure 4.2.2 shows the face velocity calibration set up. If measuring face velocity is not an option, estimating face velocity with equation 4.2.2 will suffice (DynoNobel, 1999).

$$FV = \frac{75}{\sqrt{PF}}$$

Equation 4.2.2

Where:

FV = Face velocity (ft/s)

PF = Powder factor (tons/lb)

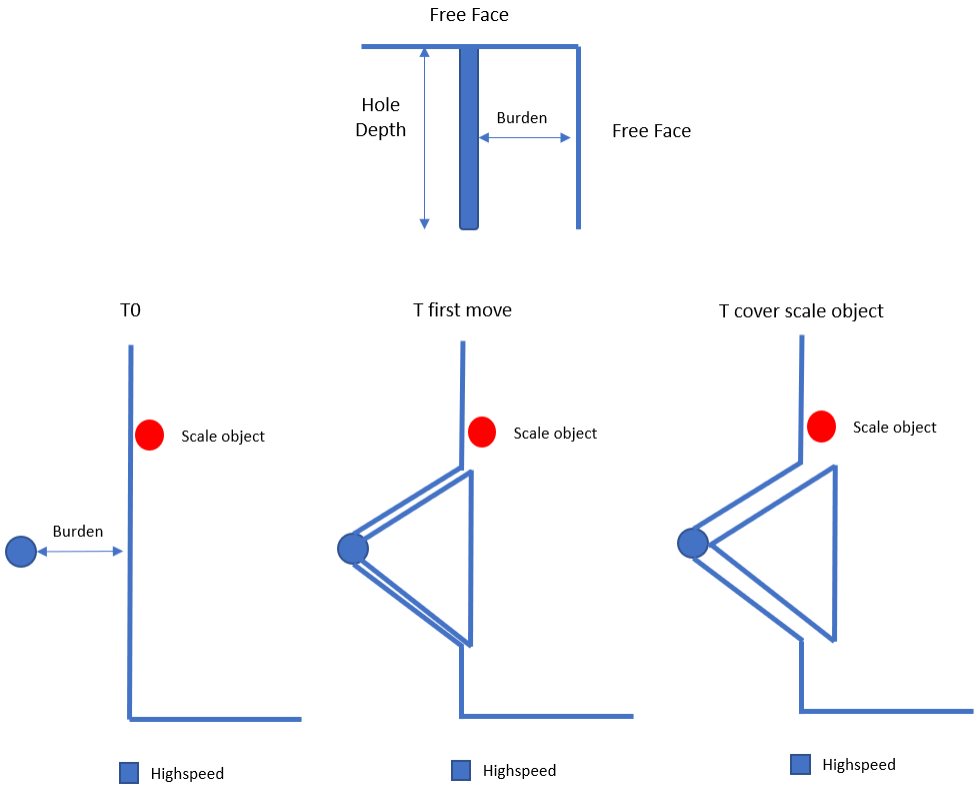

Figure 4.2.2 Face velocity calibration setup

A swell calibration will also be done on the single-hole tests. Utilizing the before and after blast geometry and after muck scans of the single hole tests will give in situ volume and blasted volume. The difference between blasted volume and in situ volume

divided by in situ volume will give the percent swell. If swell information cannot be determined, then use ISEE's average blasted swell value of 30 percent (ISEE, 2011).

After the single hole calibration is done, the next step will be to determine the optimum timing between rows. The optimum timing between rows will be when the material in front of the row has moved far enough to make the volume equal to the swell volume from one blasthole. The equation to determine optimum row delay is shown below. The below equation assumes that the area created by the face height and the spacing moves uniformly and is the reason that Zhang's spacing equation is needed. If the spacing to burden relationship is too large, then a crater is blown out of the face, and equation 4.2.3 is not accurate.

$$r_{max} = \frac{B * M_s}{V_F} * 1000$$

Equation 4.2.3

Where:

r_{max} = Optimum row delay (ms)
B = Burden (ft)
M_s = Material swell in fractional percent
V_F = Face velocity (ft/s)
1000 = Conversion from seconds to milliseconds

Deriving equation 4.2.3 can be seen below.

Step 1 – calculate the volume of one hole

$$Volume = B * S * H = B * \frac{\mathrm{B}}{\sin\left(90 - \frac{A}{2}\right)} * H$$

Step 2 – determine the swell volume

$$Swell\ Volume = Hole\ Volume * Swell = B * \frac{\mathrm{B}}{\sin\left(90 - \frac{A}{2}\right)} * H * M_s$$

Step 3 – determine linear distance material must move to provide void space

$$Distance = \frac{Swell\ Volume}{Spacing * Bench\ Height}$$

$$= B * \frac{\mathrm{B}}{\sin\left(90 - \frac{A}{2}\right)} * H * M_s * \frac{1}{H} * \frac{\sin\left(90 - \frac{A}{2}\right)}{B} = B * M_s$$

Step 4 – determine how long it takes for the muck to travel the linear distance

$$Row\ Delay = Linear\ Distance/Face\ Velocity = B * M_s/V_F = \Delta r$$

A minimum row delay needs to be determined for the model's calibration. This will likely be the minimum row delay the blaster in charge feels comfortable with. If the site is not at risk of fly rock with nearby neighbors, personnel, or equipment, then two (2) times the optimal hole delay down the row can be used as the minimum row delay.

A final calibration will be conducted utilizing two rows of 5 holes. A total of 6 shots will be conducted using the final calibration. For the first 3 shots, utilize the optimal delay between holes in a row that has already been determined. If hole delay has not been optimized, use the optimal delay ratio of 3 ms/m of the burden from Cunningham's literature (Cunningham, 2005). Also, for the first 3 shots, use the optimal row delay calculated from equation 4.2.3. Collect fragmentation data on all 3 shots and average the results. Repeat this process for the next 3 calibration shots but use the minimum row delay instead. The workflow of the calibration can be seen below and is illustrated in Figure 4.2.3.

1. Set up 6 shots with 2 rows of 5 holes with the standard blast design used on site

2. Shoot 3 shots with optimum row timing
3. Collect fragmentation data of each shot and average the data
4. Shoot 3 shots with minimum row timing
5. Collect fragmentation data of each shot and average the data
6. Make sure to record 20, 50, and 80 percent passing at a minimum

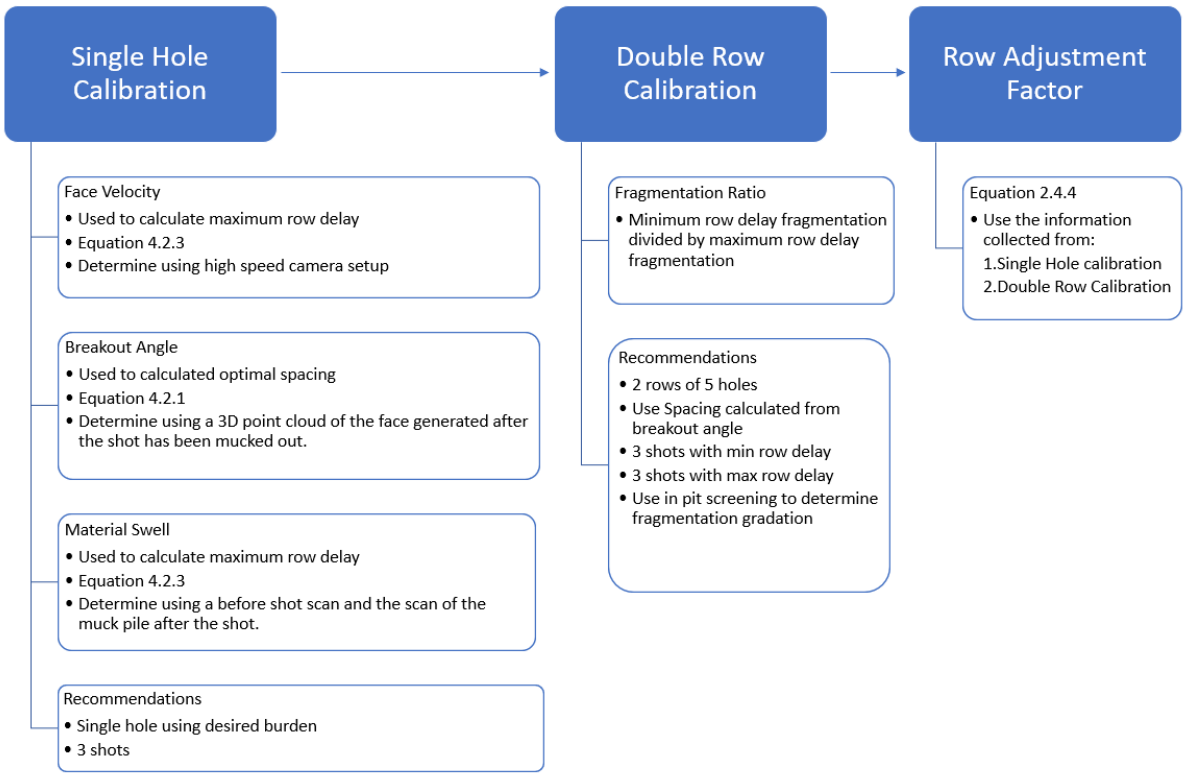

Figure 4.2.3 Wor-Sil row fragmentation methodology

The influence of delay has been discovered to affect the larger percent passing sizes, such as the 80% passing size more than the smaller percent passing sizes. Gkikizas proves this concept by looking at the influences of delay on different percent passing sizes (Gkikizas, 2016). Delay influences the large fragments instead of the smaller fragments because the large fragments come from the middle of the spacing, and small fragments come from the area closest to the borehole. Neighboring radial fracturing would only influence the area farthest away from the blasthole that was not previously fragmented, causing the next hole's top size to be smaller. The concept assumes the blastholes are spaced far enough away that the "borehole crushing diameter" is not equal to the spacing of the holes Figure.

4.2.4 shows Gikizas work that proves that delay influence decreases with smaller percent passing sizes (Gkikizas, 2016). Gikikizas work means that a fragmentation model looking at row delay should minimize the influence on the lower passing sizes.

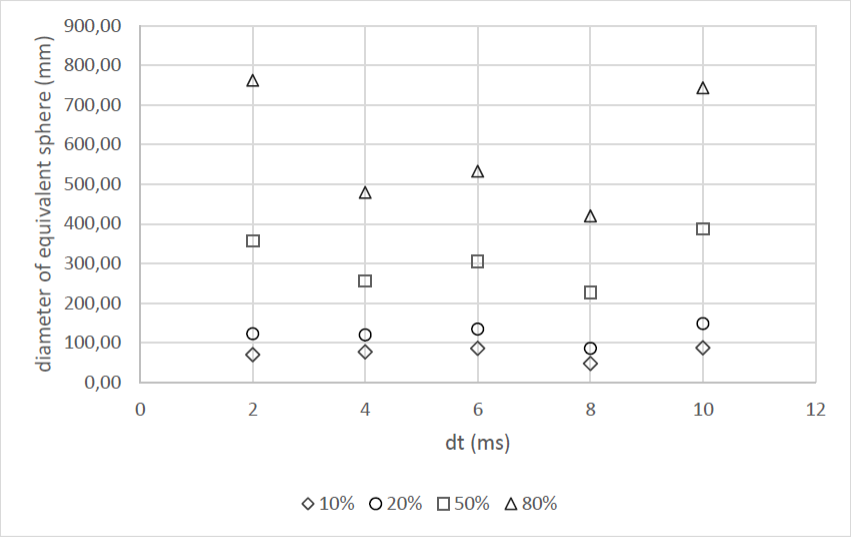

Figure 5.2: x_n versus delay time

Figure 4.2.4 Percent passing size compared to delay between holes in a row (Gkikizas, 2016)

Utilizing the fragmentation data from the site calibration, a row delay equation based on an equation of a line between two points will be used to alter the 80 percent passing size and the 50 percent passing size. The proposed row delay equation is below.

$$x_{r_x} = \frac{(x_{rmin} - x_{rmax})}{(r_{min} - r_{max})} * r_x + (x_{rmax} - \frac{(x_{rmin} - x_{rmax})}{(r_{min} - r_{max})} * r_{max})$$

Equation 4.2.4

Where:

x_{r_x} = Fragmentation size for a desired percent passing size due to row delay (in)

x_{rmin} = Fragmentation size of the desired percent passing size using minimum row delay (in)

x_{rmax} = Fragmentation size of the desired percent passing size using maximum row delay (in)

r_{min} = Minimum row delay (ms)

r_{max} = Maximum row delay (ms)

r_x = Row delay being used (ms) where $r_{min} < r_x < r_{max}$

Using the newly adjusted 50 and 80 percent passing sizes and using the average 20 percent passing size of the site data, run the Swebrec function or the Rosin-Rammler to complete the fragmentation curve. This step is not necessary if all the desired percent passing sizes were collected to determine the onsite fragmentation data. In the case that percent passing data was collected on all desired passing sizes, equation 4.2.4 can be run on all the collected passing sizes 50 percent and above.

If no site calibration is done, the following equation can be used to determine the influence of row delay on fragmentation. The equation is determining a row adjustment factor based on the equation of a line between the results of minimum row timing and maximum row timing. Equation 4.2.5 assumes the following: maximum row timing gives smaller fragmentation than the minimum row timing, the change in fragmentation due to row timing is a linear relationship, two times the hole delay is the minimum row delay to have a clear definition between the hole and the row timing, the optimal hole timing is used between holes down a row or sequence, and bench blasting geometry is used for the shot.

$$R_x = \frac{(R_{xmin/xmax} - 1)}{B * (\frac{2 * R_{ht}}{c_p} - \frac{M_s}{V_F})} * r_x + \left(1 - \frac{(R_{xmin/xmax} - 1)}{\left(\frac{2 * R_{ht}}{c_p} - \frac{M_s}{V_F}\right)} * \frac{M_s}{V_F}\right) =$$

$$= \frac{\left(\frac{x_{rmin}}{x_{rmax}} - 1\right)}{(r_{min} - r_{max})} * r_x + \left(1 - \frac{\left(\frac{x_{rmin}}{x_{rmax}} - 1\right)}{(r_{min} - r_{max})} * r_{max}\right)$$

Equation 4.2.5

Where:

R_x = Row timing adjustment factor for selected row timing

r_x = Selected row timing (ms) where $r_{min} < r_x < r_{max}$

$R_{xmin/xmax}$ = Material size ratio of minimum row delay and maximum row delay use 1.25 from Ogden Point research if not known

B = Burden (ft)

2 = Multiplication factor of optimum hole delay to find minimum row delay

R_{ht} = Optimum hole timing ratio = $c_p * t_{ms/ft}$, if not known use 15.6 from the 2005 Kuz-Ram

$t_{ms/ft}$ = optimal hole timing ratio determined from research expressed as ms/ft

c_p = P wave velocity (ft/ms)

M_s = Material swell in fractional percent

V_F = Face velocity (ft/ms)

$r_{min} = \frac{2 * R_{ht} * B}{c_p}$ = Minimum row delay or minimum allowed delay (ms)

$r_{max} = \frac{B * M_s}{V_F}$ = Maximum row delay (ms)

x_{rmin} = Fragmentation size of x passing size when using minimum row timing (in)

x_{rmax} = Fragmentation size of x passing size when using maximum row timing (in)

Once the row adjustment factor is determined, run the 2005 Kuz-Ram model to determine the 50 percent passing size and uniformity index. Adjust the 50 percent passing size using the row adjustment factor. Then run the Rosin-Rammler function to determine the rest of the fragmentation curve.

Another method that could be used involves the Swebrec function, but some errors were found in the literature, so it was not used in chapter 6. The Kuz-ram model can be run to determine first the 50 percent passing size, then the 20 and 80 percent passing size. The row adjustment factor will be used to adjust the size of the 50 and 80 percent passing size. Then the Swebrec function will be run on the adjusted 50 and 80 percent passing sizes and the 20 percent passing size. The work follow is below.

1. Determine row adjustment factor due to selected row timing
2. Use the 2005 Kuz-Ram model to determine the 50 percent passing size and uniformity index
3. Calculate the 20 and 80 percent passing sizes using the Rosin-Rammler Function.
4. Adjust the 50 and 80 percent passing sizes by multiplying by the row adjustment factor
5. Run the Swebrec function using the adjusted 50 and 80 percent passing sizes and the 20 percent passing size to determine final fragmentation curve due to row timing.

CHAPTER 5. FIELD TESTS

Chapter 5 explains the experiment setup and results. Large scale testing was conducted at the Ogden Point Quarry in Colborne, Ontario, Canada. Six full-scale tests were shot utilizing two different explosives contractors to explore the influences of charge sequence and timing on fragmentation.

5.1 Field test location

The field tests were located at the Ogden Point Quarry in Colborne, Ontario, Canada. The mine had three (3) production benches called level 1, level 2, and level 3. All tests were conducted on the level 3 bench. One face was selected to do all the testing to minimize geology influences on the tests. The mine plan had the quarry working in the north direction so the face on the north mining area was selected for all the tests. An overview of the testing area can be seen in Figure 5.1.1.

Figure 5.1.1 Level 3 field testing area

The mine in Canada was not an ideal location for the testing because the mine was a 12-hour drive from Lexington, KY and required moving large amounts of equipment over the border. The testing location was selected by finding the first location that would allow timing changes outside the operation's current blast timing, and the Ogden Point Quarry management was the first and only mine to agree. It is the perception in the blasting industry that blast vibrations, fly rock, and air blast are some of the risks associated with

changing the timing and are reasons why a quarry operation would not want to explore timing changes.

5.2 Field test setup

The field test utilized the current blast design of the operation. The design of the first test was to be used for all the tests. Unfortunately, mid-way through the testing, the blasting contractor lost the contract, and a new contractor finished the last three (3) tests. The change in contractor caused the testing plan to change to conducting the same three (3) tests with each contractor. The blast design for the field tests is shown in Table 5.2.1. The second contractor was instructed to use the design in table 5.2.1 as much as possible. The actual blast design for each contractor can be seen in Table 5.2.2. Contractor 1 completed tests 1 through 3, and Contractor 2 completed tests 4 through 6.

Table 5.2.1 Test design

Burden	13.5	ft
Spacing	15.7	ft
Stemming	7	ft
Stem Size	0.75	in
Hole Diameter	4	in
Explosives	Gassed Emulsion	
Rows	3	
Holes	69	
Explo Density	1.15	g/cc
Rock Density	2.65	g/cc
Bench Height	60	ft
Hole Depth	60	ft
Charge Weight	332	lbs/hole
Powder Factor	0.7	lbs/cyd

Table 5.2.2 Test design by contractor

	Contractor 1	Contractor 2	
Burden	13.5	13	ft
Spacing	15.7	15.5	ft
Stemming	7	7	ft
Stem Size	0.75	0.75	in
Hole Diameter	4	4	in
Explosives	Gassed Emulsion	Titan XL 1000 G	
Rows	3	3	
Holes	69	69	
Explo Density	1.15	1.15	g/cc
RWS	108	72	
Rock Density	2.65	2.65	g/cc
Bench Height	60	60	ft
Hole Depth	60	60	ft
Charge Weight	332	332	lbs/hole
Powder Factor	0.7	0.74	lbs/cyd

A signature hole analysis was conducted on level 3 and determined that the blastholes needed 15ms between delays to have the lowest vibrations, so 15 ms delay between holes was used for every test. The only variable that was to be changed in the tests was how the holes fired. The original testing matrix had several delay sequences, but due to the unexcepted contractor change, only three were tested by each contractor. The tested delay sequences can be seen in figure 5.2.1. Sequence A, D, and C were the order in which the delay sequences were tested. Sequence B was scrapped from the research once the contractor changed. Sequence A was selected to see the influences of extreme delay between rows. Sequence A was named “down the row” because the sequence path followed the rows. Sequence C was selected to see the influences of the short delay between rows. Sequence C was named “zigzag” because of the shape the sequence path

makes. Sequence D was selected to mimic a typical charge sequence used currently in the industry. Sequence D was named "traditional" because it represents the sequence currently being used.

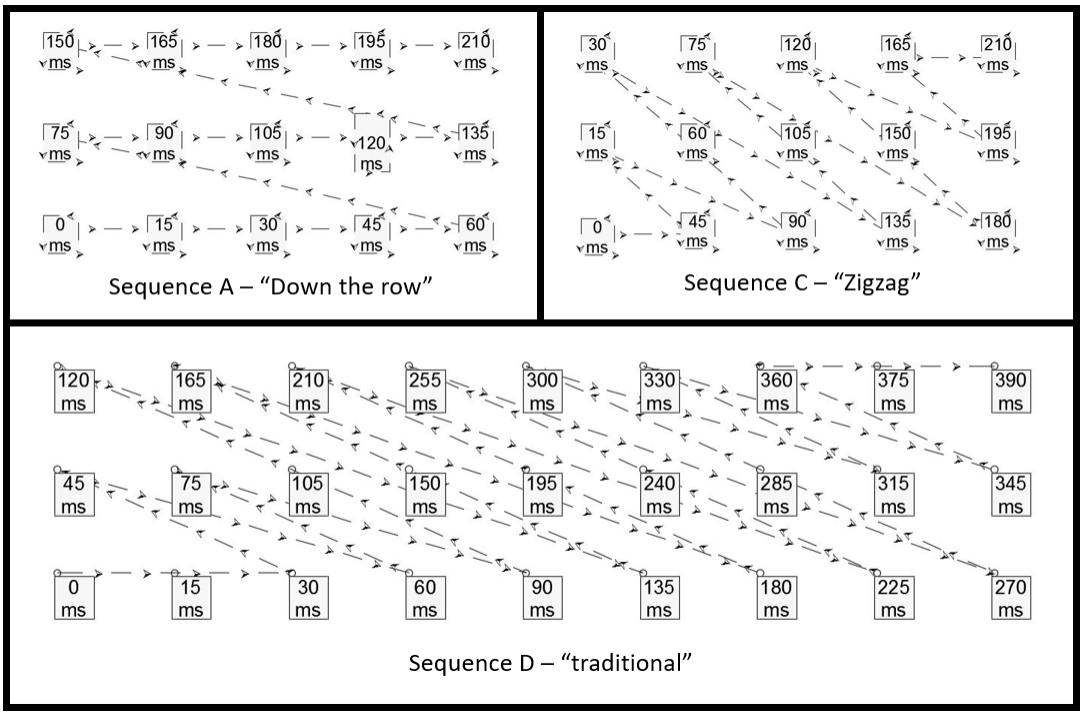

Figure 5.2.1 Types of delay sequences tested

The sequences in figure 5.2.1 were tested to determine if the sequence and row timing had any influence on fragmentation while keeping delay between charges constant. The delay between holes down a row is down the path of the sequence, and row delay is the time between the repeating sequences. There is a "run-up" and "run-down" period when the sequence is not uniform when utilizing regular rhythmic timing. The variable delay during the run-up and run-down are ignored for row delay calculation. Figure 5.2.2 shows the runup, uniform sequences, row delay, and the run down.

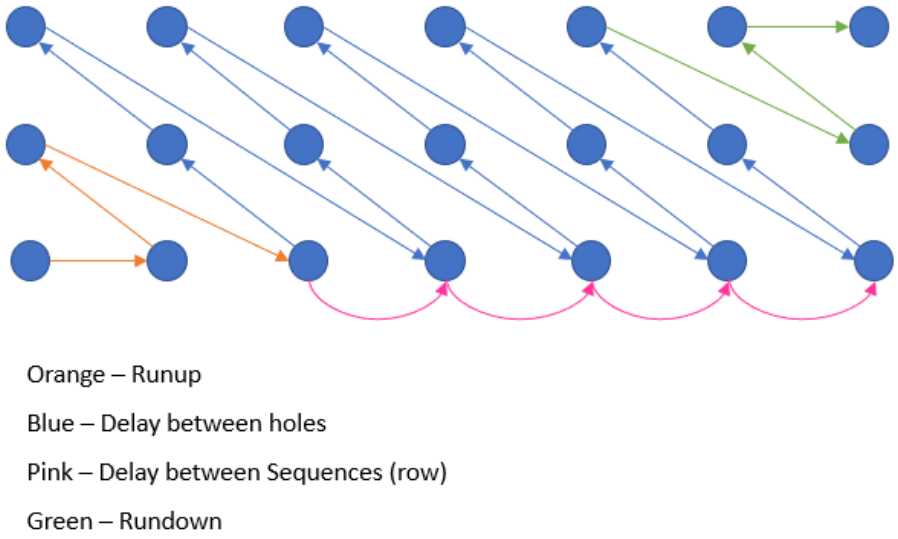

Figure 5.2.2 Regular rhythmic run-up and run-down

The data collected for each shot included fragmentation data, pictures, videos, and vibration data. Quality checks were also made to ensure each test represented the test design as much as possible. This involved being on the bench measuring drill holes, checking burden and spacings, measuring stemming heights, and being present for the loading of every hole. The order of the test can be seen below.

- Test 1 – Contractor 1 – sequence A – down the row
- Test 2 – Contractor 1 – sequence D – traditional
- Test 3 – Contractor 1 – sequence C – zigzag
- Test 4 – Contractor 2 – sequence A – down the row
- Test 5 – Contractor 2 – sequence D – traditional
- Test 6 – Contractor 2 – sequence C – zigzag

Being present for more than one week at the testing site was not possible, so the collection of fragmentation during the material excavation process was not considered. The fragmentation pictures were taken on the muck pile's surface. Collecting surface muck pile

pictures for fragmentation analysis is not the best practice, but unfortunately, there was no other choice.

Wipfrag was utilized to process the photofragmentation data. Photofragmentation software is typically not accurate at drawing boundaries around rock circles, so all boundaries were drawn by hand to increase the accuracy of the data. Figure 5.2.3 shows an example photo with boundaries drawn on the rocks. To determine the size of the rocks in the image, two-scale objects of approximately 8.2 inches in diameter were used. The use of two-scale objects was needed to determine the change in size due to varying rock pieces' varying distances to the camera. Four photos were randomly taken in separate locations in the muck pile. Photos were taken as far as safety would allow into the muck pile. The results of all four photos where combined by WipFrag to determine an average fragmentation distribution for the pile.

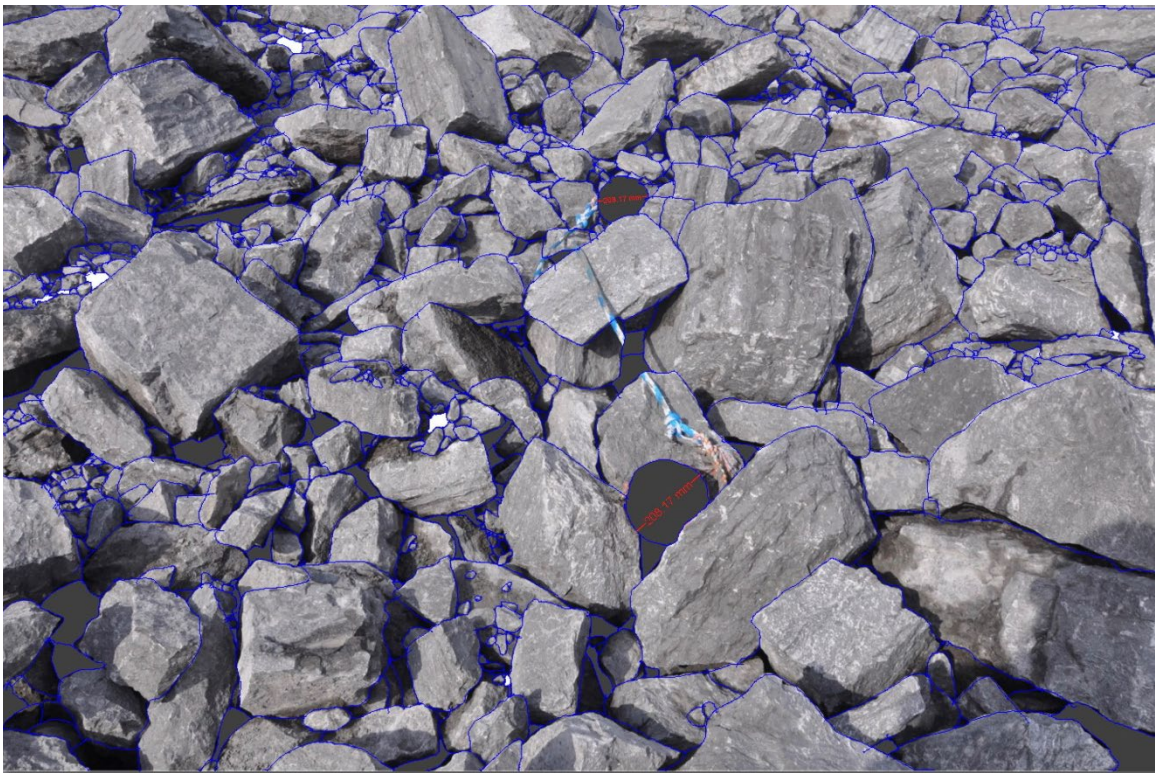

Figure 5.2.3 Hand drawn boundaries on fragmentation photo

A seismograph was set up 100 ft behind the initiating hole of tests 1, 2, and 3 to determine vibration data that can be compared between tests. The seismograph was moved to 328 ft behind the initiating hole for tests 4, 5, and 6 due to the decoupling of the seismograph at 100 ft. The distance was perpendicular to the free face. The seismograph model used was a NOMIS Mini Supergraph II. A standard triaxial geophone and microphone were used at 16,384 samples/second. New equipment was acquired during tests 4, 5, and 6, and accelerometers were also used. Shottrack Vib25 and Vib200 accelerometers were used with a sampling rate of 32,000 samples/second. Figure 5.2.4 shows the setup of the seismograph and accelerometers during test 4. The geophone of the Nomis seismograph was mounted onto a steel plate via the ground spike threads on the bottom of the sensor. The plate was mounted into the ground by using sleeve anchor bolts.

The Shottrack Vib units were not bolted into the ground; however, they were heavily sandbagged to control the decoupling of the sensors. The Shottrack information did not prove useful for the research so the data was not included.

Figure 5.2.4 Seismograph set up for test 4

A Phantom 4 pro drone and 2 action video cameras where used to shoot multiple angles of each test shot. The drone was positioned in front of the free face above the shot. The first camera was placed behind the shot on top of the bench, and the second camera was placed in front of the shot on the bench floor. Pictures were also taken throughout the whole process.

For test 5 only, swell data was collected using pre-blast and post-blast photogrammetry models. Strayos software was used to determine the volume of the in-situ rock, and the blasted rock by calculating the volume between the model's surface and the floor elevation.

A typical set up for the test blasts can be seen in Figure 5.2.5 below. The plan view shows the placement of the seismograph, burden, spacing, hole diameter, and the first hole to detonate. The side view shows the length of the stemming and explosives column.

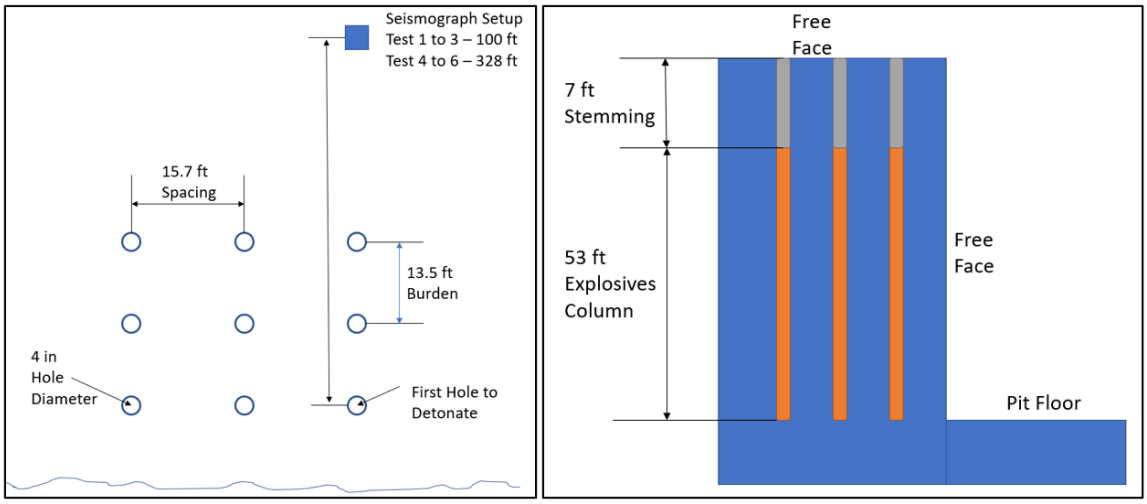

Figure 5.2.5 Plan and side view of the test plan design

5.3 Test data results

Chapter 5.3 shows the data collected from each test. The appendix has all the blast reports for each test.

5.3.1 Test 1

Test blast one was using contractor 1 and testing sequence A "down the row". Blast reports from all tests can be seen in the appendix. Test blast one was shot on September 12, 2017. Test one utilized 15 ms down the sequence and 300 ms between repeating sequences. Before shot and after shot results can be seen in Figure 5.3.1. No bad effects of the sequence were realized post-blast and after digging the shot rock. Bad effects of the blast would include misfired explosives, drastic increase in vibrations at neighbor's houses,

drastic increase in airblast at neighbor's house, not reaching grade, and/or poor production performance.

Figure 5.3.1 Test 1 before and after blast results

The Fragmentation results can be seen in Figure 5.3.2. Four fragmentation photos were taken in random places on the muck pile. Figure 5.3.2 shows the fragmentation for each photo and the cumulative fragmentation of all 4 photos.

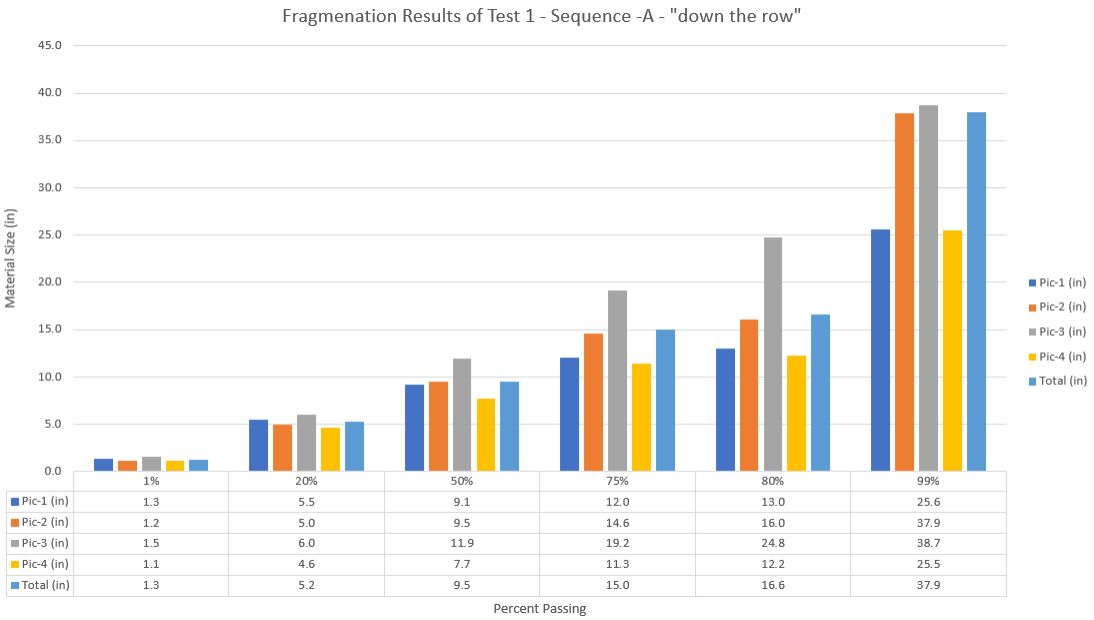

	1%	20%	50%	75%	80%	99%
Pic-1 (in)	1.3	5.5	9.1	12.0	13.0	25.6
Pic-2 (in)	1.2	5.0	9.5	14.6	16.0	37.9
Pic-3 (in)	1.5	6.0	11.9	19.2	24.8	38.7
Pic-4 (in)	1.1	4.6	7.7	11.3	12.2	25.5
Total (in)	1.3	5.2	9.5	15.0	16.6	37.9

Figure 5.3.2 Fragmentation results of test 1 – sequence A – “down the row.”

Vibration results can be seen in Figure 5.3.3. Vibration results on the transverse channel in Figure 5.3.3 appear to be oscillating around a moving axis. This is evidence that something affected the sensor. Some possible issues could be decoupling, interference due to the mounting plate, and the sensor is out of range of vibrations influencing the sensor. The peak particle velocity was 5.11 in/s, with a frequency of 41.3 Hz on the vertical channel.

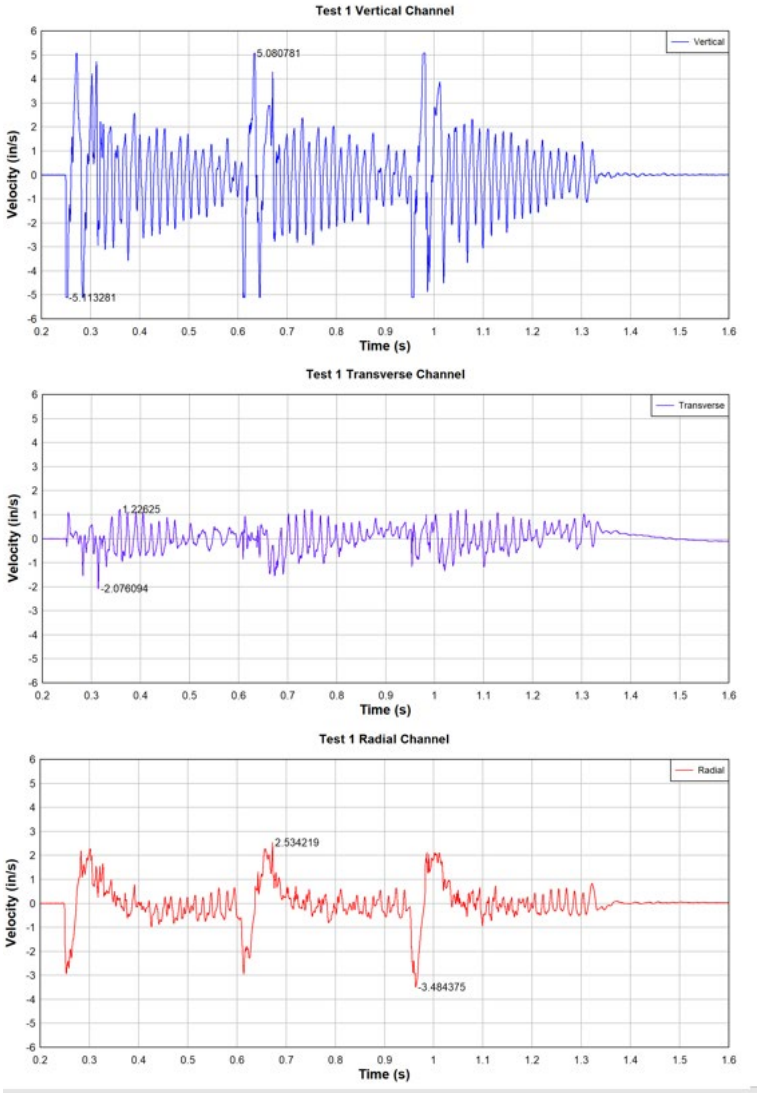

Figure 5.3.3 Test 1 vibration waveform

5.3.2 Test 2

Test blast 2 was using contractor 1 and testing sequence D "traditional". Blast report for test 2 can be seen in the appendix. Test blast 2 was shot on September 13, 2017. Test 2 utilized 15 ms down the sequence and 45 ms between repeating sequences. Before shot and after shot, results can be seen in Figure 5.3.4. No bad effects of the sequence were realized post-blast and after digging the shot rock.

Figure 5.3.4 Test 2 before and after blast results

The Fragmentation results can be seen in Figure 5.3.5. Four fragmentation photos were taken in random places on the muck pile. Figure 5.3.5 shows the fragmentation for each photo and the cumulative fragmentation of all 4 photos.

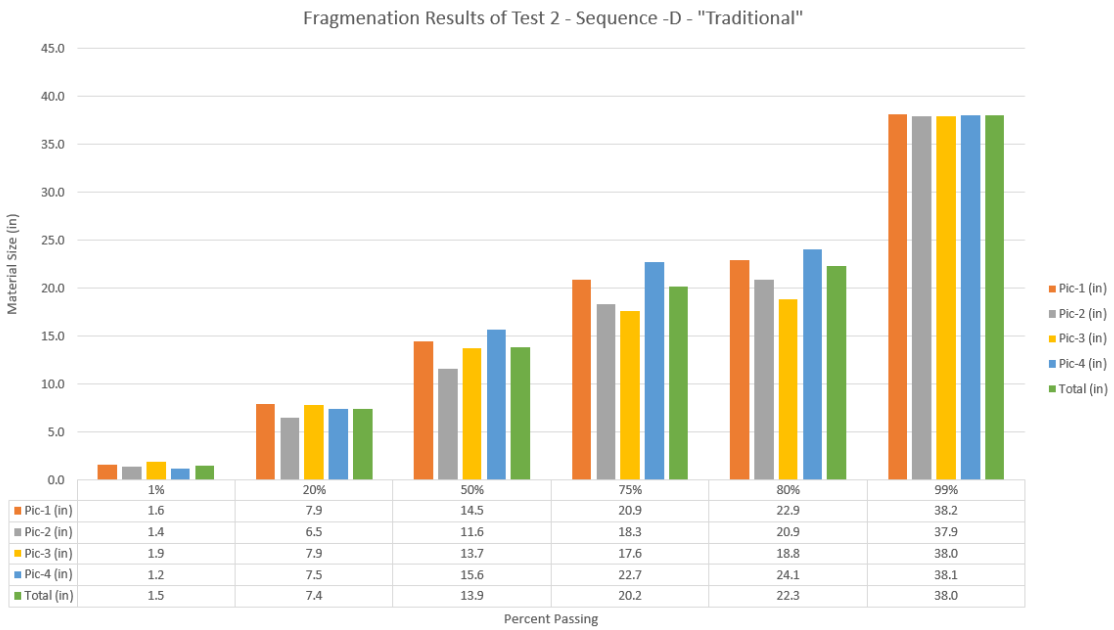

	1%	20%	50%	75%	80%	99%
Pic-1 (in)	1.6	7.9	14.5	20.9	22.9	38.2
Pic-2 (in)	1.4	6.5	11.6	18.3	20.9	37.9
Pic-3 (in)	1.9	7.9	13.7	17.6	18.8	38.0
Pic-4 (in)	1.2	7.5	15.6	22.7	24.1	38.1
Total (in)	1.5	7.4	13.9	20.2	22.3	38.0

Figure 5.3.5 Fragmentation results of test 2 – sequence D – “traditional”

Vibration results can be seen in Figure 5.3.6. Vibration results in Figure 5.3.6 appear to be oscillating around the zero axes. This is evidence that the vibration data is good. The peak particle velocity was 5.11 in/s, with a frequency of 73.8 Hz on the vertical channel.

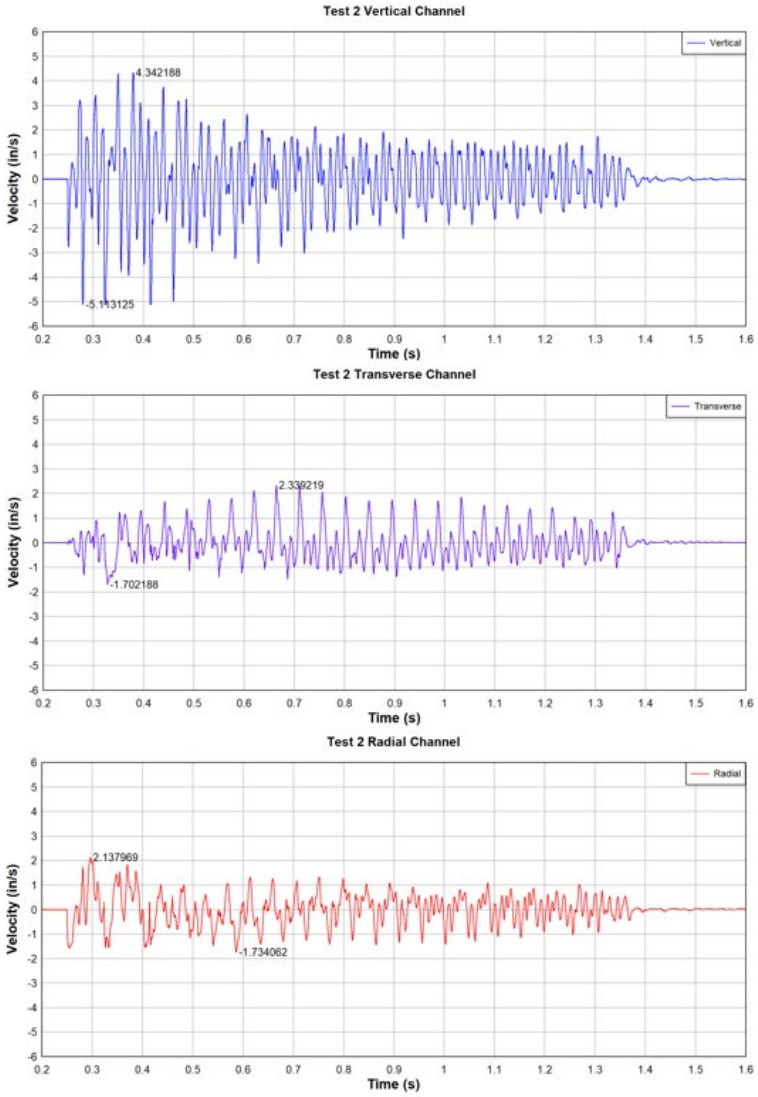

Figure 5.3.6 Test 2 vibration waveform

5.3.3 Test 3

Test blast 3 was using contractor 1 and tested sequence C "zigzag". The blast report for test 3 can be seen in the appendix. Test blast 3 was shot on November 27, 2017. Test 3 utilized 15 ms down the sequence and 45 ms between repeating sequences. The zigzag sequence is the same delay between repeating sequences as traditional with a sharper

initiation angle. Before shot and after shot, results can be seen in Figure 5.3.7. No bad effects of the sequence were realized post-blast and after digging the shot rock.

Figure 5.3.7 Test 3 before and after blast results

The Fragmentation results can be seen in Figure 5.3.8. Four fragmentation photos were taken in random places on the muck pile. Figure 5.3.8 shows the fragmentation for each photo and the cumulative fragmentation of all 4 photos.

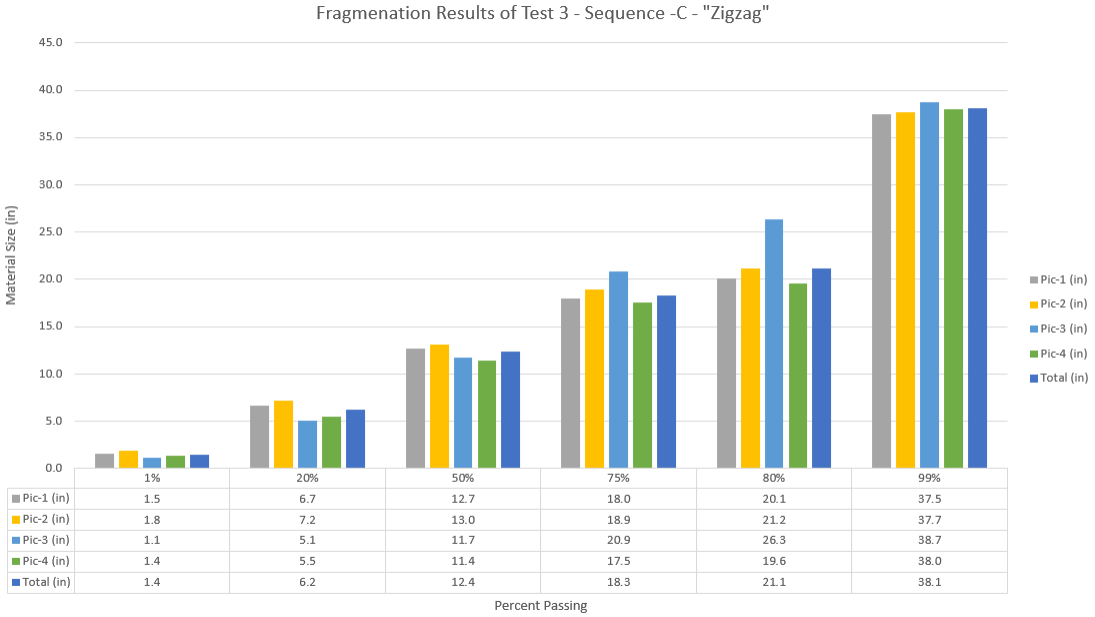

	1%	20%	50%	75%	80%	99%
Pic-1 (in)	1.5	6.7	12.7	18.0	20.1	37.5
Pic-2 (in)	1.8	7.2	13.0	18.9	21.2	37.7
Pic-3 (in)	1.1	5.1	11.7	20.9	26.3	38.7
Pic-4 (in)	1.4	5.5	11.4	17.5	19.6	38.0
Total (in)	1.4	6.2	12.4	18.3	21.1	38.1

Figure 5.3.8 Fragmentation results of test 3 – sequence C – “zigzag”

Vibration results can be seen in Figure 5.3.9. The peak particle velocity was 7.18 in/s, with a frequency of 73.1 Hz on the vertical channel.

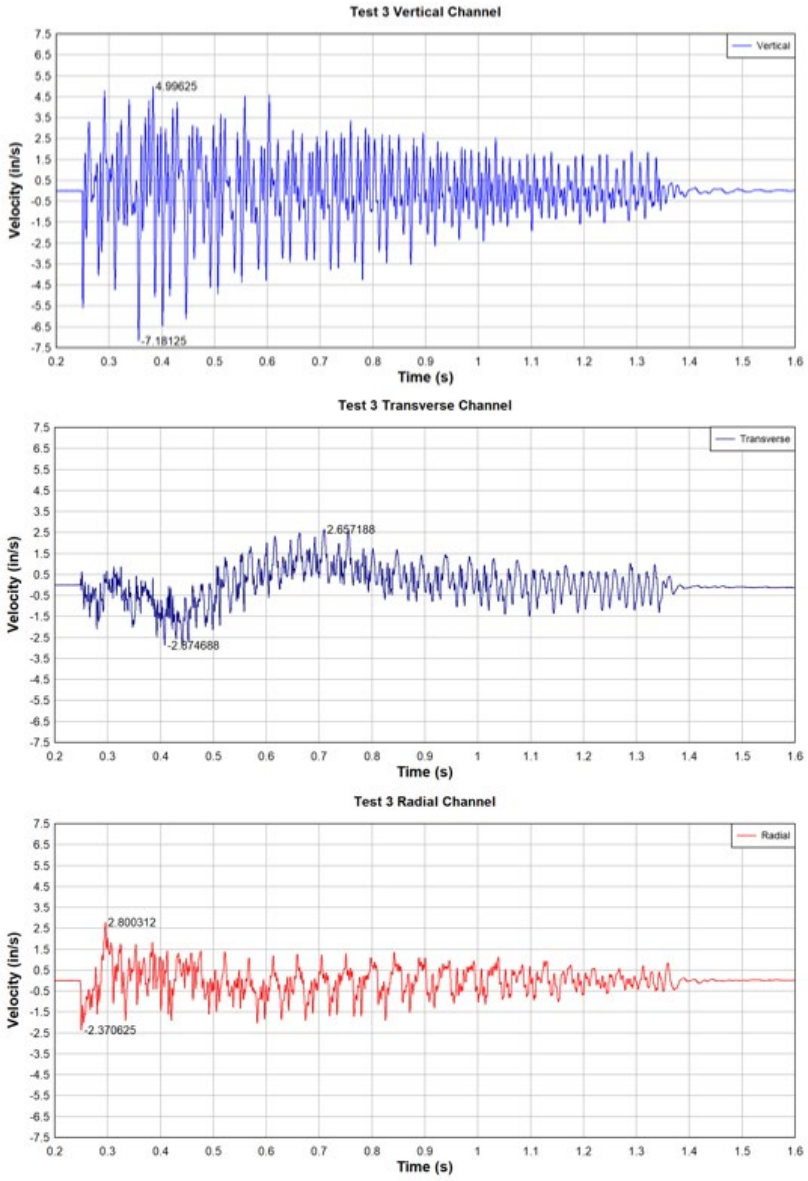

Figure 5.3.9 Test 3 vibration waveform

Test shot 1 and 2 had an extraneous sound to the blast when they were shot, so an air blast monitor was installed for test 3, 4, 5, and 6. Figure 5.3.10 shows the air overpressure in millibars.

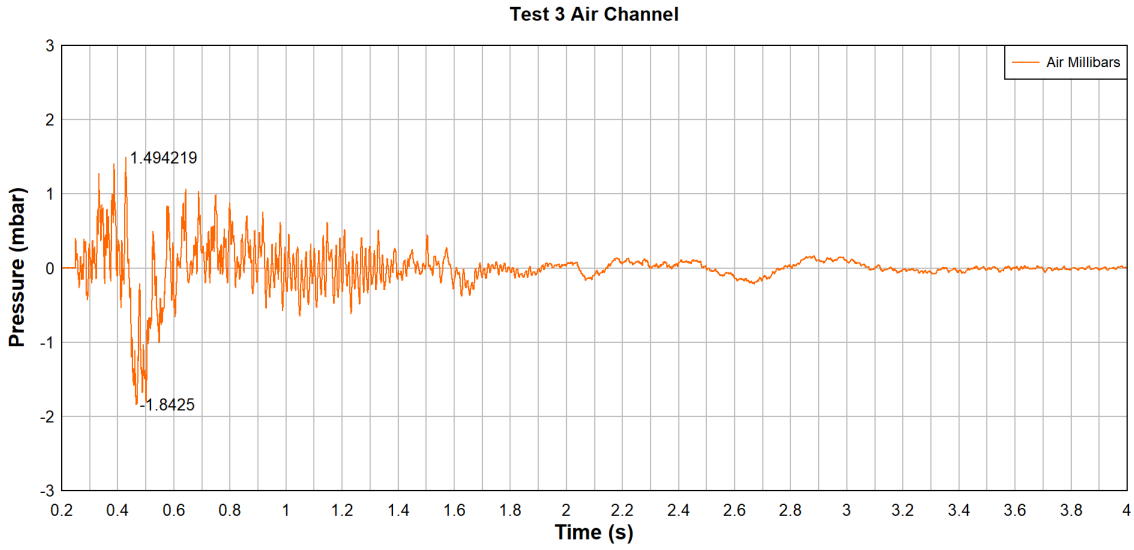

Figure 5.3.10 Test 3 air over pressure waveform

5.3.4 Test 4

Test blast 4 was using contractor 2 and testing sequence A “down the row”. Blast report for test 4 can be seen in the appendix. Test blast 4 was shot on April 29, 2018. Test 4 utilized 15 ms down the sequence and 315 ms between repeating sequences. Before shot and after shot, results can be seen in Figure 4.3.11. No bad effects of the sequence were realized post-blast and after digging the shot rock.

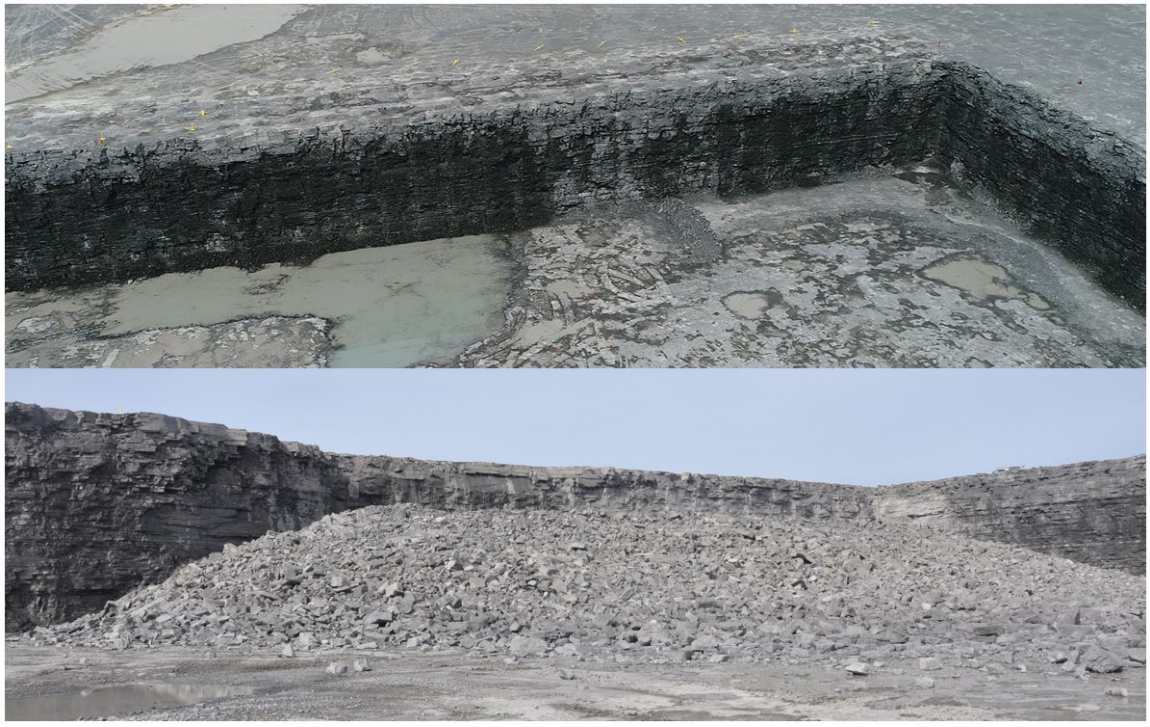

Figure 5.3.11 Test 4 before and after blast results

The Fragmentation results can be seen in Figure 5.3.12. Four fragmentation photos were taken in random places on the muck pile. Figure 5.3.12 shows the fragmentation for each photo and the cumulative fragmentation of all 4 photos.

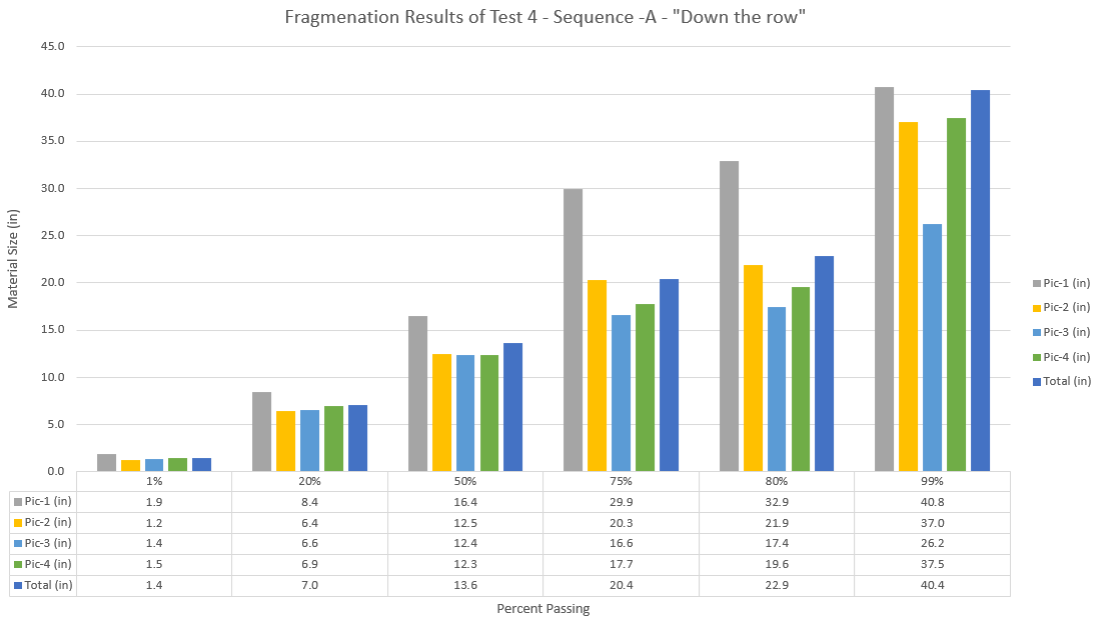

	1%	20%	50%	75%	80%	99%
Pic-1 (in)	1.9	8.4	16.4	29.9	32.9	40.8
Pic-2 (in)	1.2	6.4	12.5	20.3	21.9	37.0
Pic-3 (in)	1.4	6.6	12.4	16.6	17.4	26.2
Pic-4 (in)	1.5	6.9	12.3	17.7	19.6	37.5
Total (in)	1.4	7.0	13.6	20.4	22.9	40.4

Figure 5.3.12 Fragmentation results of test 4 – sequence A – “down the row”

Vibration results can be seen in Figure 5.3.13. The monitoring location for test 4 was moved 328 ft behind the initiating hole to help eliminate decoupling of the geophone. The peak particle velocity was 2.54 in/s, with a frequency of 86.2 Hz on the vertical channel.

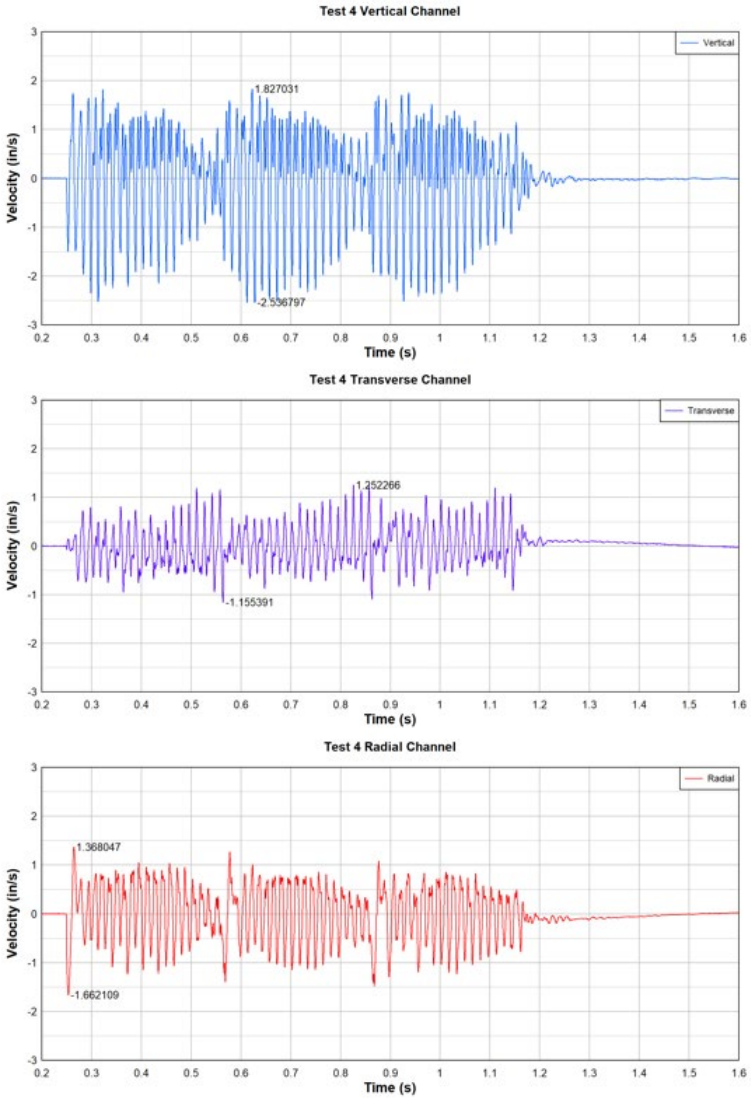

Figure 5.3.13 Test 4 vibration waveform

Figure 5.3.14 shows the air over pressure in millibars.

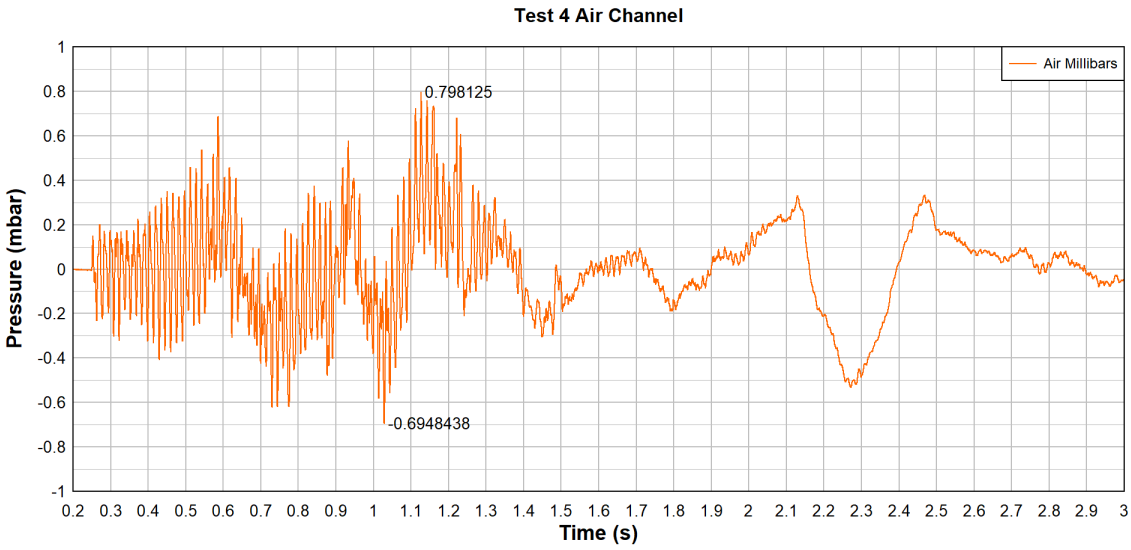

Figure 5.3.14 Test 4 air over pressure waveform

5.3.5 Test 5

Test blast 5 was done using contractor 2 and testing sequence D “traditional”. Blast report for test 5 can be seen in the appendix. Test blast 5 was shot on May 23, 2018. Test 5 utilized 15 ms down the sequence and 45 ms between repeating sequences. Before shot and after shot, results can be seen in Figure 4.3.15. No bad effects of the sequence were realized post-blast and after digging the shot rock.

Figure 5.3.15 Test 5 before and after blast results

The fragmentation results can be seen in Figure 5.3.16. Four fragmentation photos were taken in random places on the muck pile. Figure 5.3.16 shows the fragmentation for each photo and the cumulative fragmentation of all 4 photos.

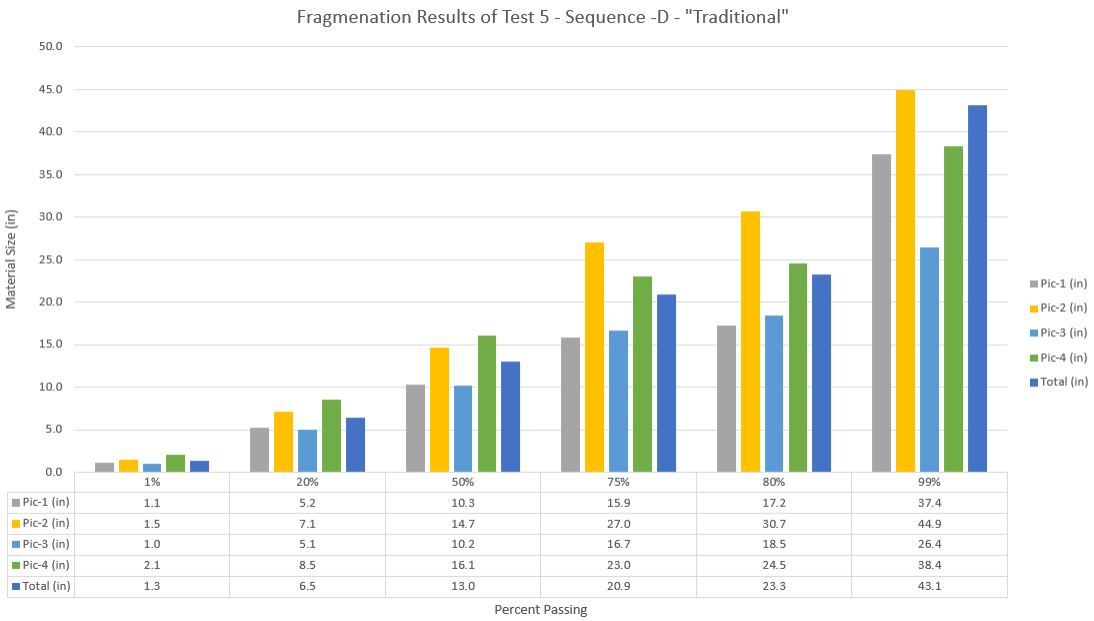

	1%	20%	50%	75%	80%	99%
Pic-1 (in)	1.1	5.2	10.3	15.9	17.2	37.4
Pic-2 (in)	1.5	7.1	14.7	27.0	30.7	44.9
Pic-3 (in)	1.0	5.1	10.2	16.7	18.5	26.4
Pic-4 (in)	2.1	8.5	16.1	23.0	24.5	38.4
Total (in)	1.3	6.5	13.0	20.9	23.3	43.1

Figure 5.3.16 Fragmentation results of test 5 – sequence D – “traditional”

Vibration results can be seen in Figure 5.3.17. The monitoring location for test 5 was moved to 328 ft behind the initiating hole to help eliminate bad vibration data. The peak particle velocity was 4.66 in/s, with a frequency of 66 Hz on the vertical channel.

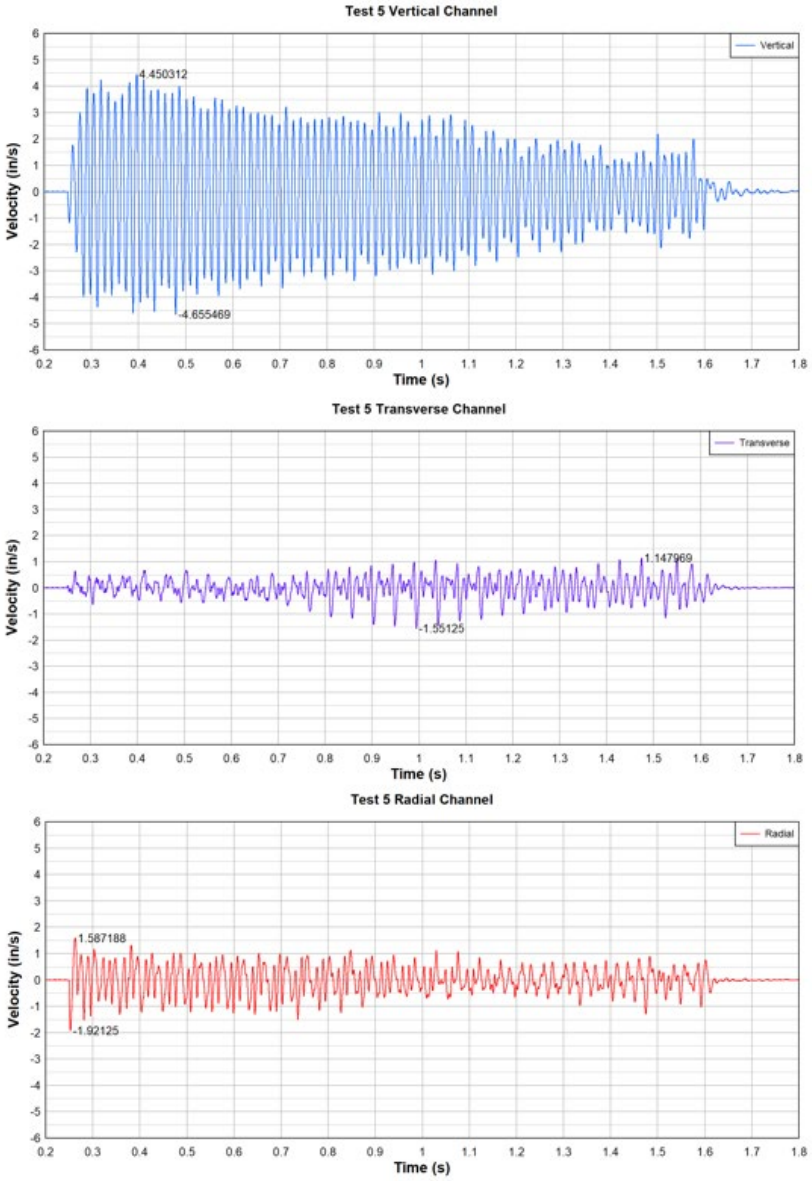

Figure 5.3.17 Test 5 vibration waveform

Figure 5.3.18 shows the air overpressure in millibars.

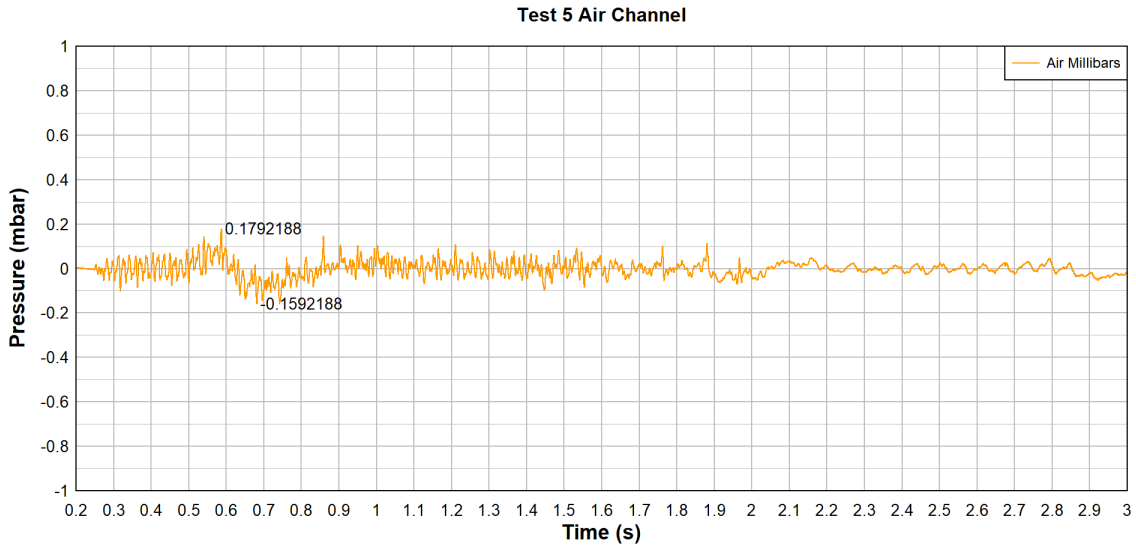

Figure 5.3.18 Test 5 air over pressure waveform

Test 5 had pre-blast and post-blast drone photogrammetry flights done to determine material swell. Strayos photogrammetry software was used to get the volume data. The bench floor elevation and the surface were used to determine volume. Table 5.3.1 shows the swell data.

Table 5.3.1 Test 5 swell data

In-Situ Volume	39379.32	cyd
Blasted Volume	59384.3	cyd
Added Volume	20004.98	cyd
% Swell	50.8	%

5.3.6 Test 6

Test blast 6 was done using contractor 2 and testing sequence C “zigzag”. Blast report for test 6 can be seen in the appendix. Test blast 6 was shot on May 24, 2018. Test

6 utilized 15 ms down the sequence and 45 ms between repeating sequences. Before shot and after shot results can be seen in Figure 4.3.19. No bad effects of the sequence were realized post blast and after digging the shot rock.

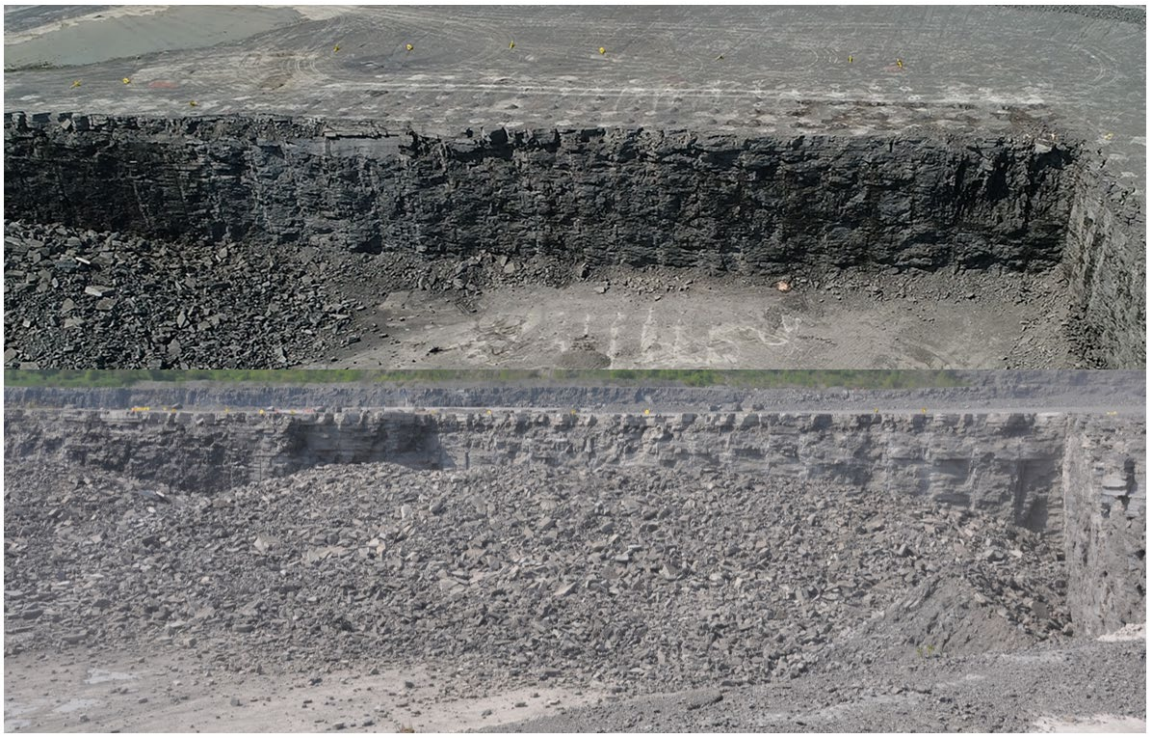

Figure 5.3.19 Test 6 before and after blast results

The fragmentation results can be seen in Figure 5.3.20. Four fragmentation photos were taken in random places on the muck pile. Figure 5.3.20 shows the fragmentation for each photo and the cumulative fragmentation of all 4 photos.

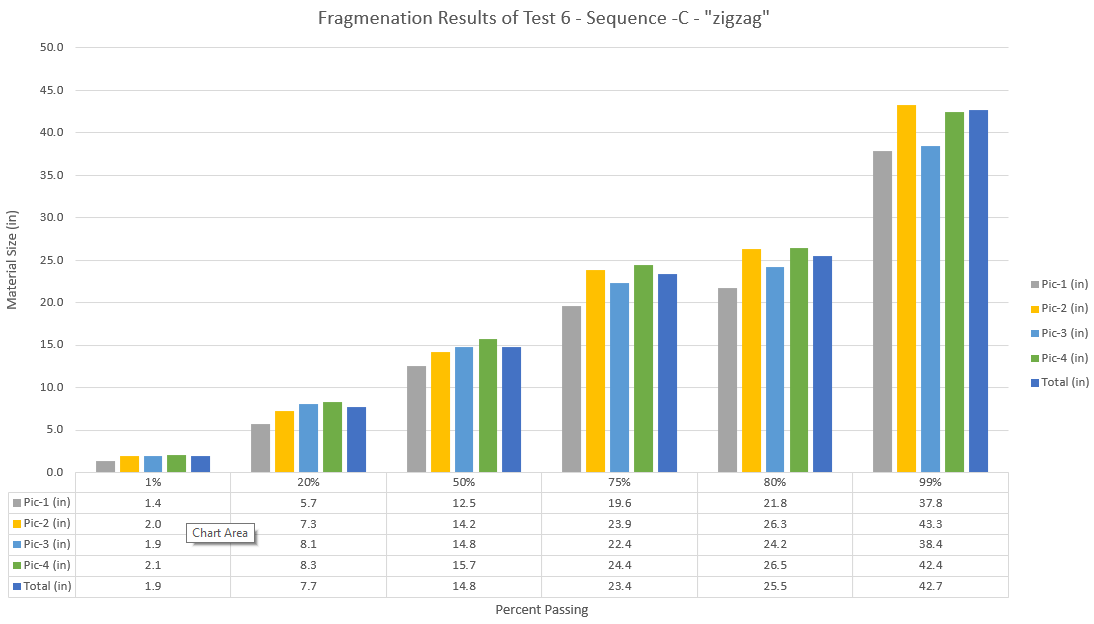

	1%	20%	50%	75%	80%	99%
Pic-1 (in)	1.4	5.7	12.5	19.6	21.8	37.8
Pic-2 (in)	2.0	7.3	14.2	23.9	26.3	43.3
Pic-3 (in)	1.9	8.1	14.8	22.4	24.2	38.4
Pic-4 (in)	2.1	8.3	15.7	24.4	26.5	42.4
Total (in)	1.9	7.7	14.8	23.4	25.5	42.7

Figure 5.3.20 Fragmentation results of test 6 – sequence C – “zigzag”

Vibration results can be seen in Figure 5.3.21. The monitoring location for test 6 was moved to 328 ft behind the initiating hole to help eliminate bad vibration data. The peak particle velocity was 2.05 in/s with a frequency of 59.3 Hz on the radial channel.

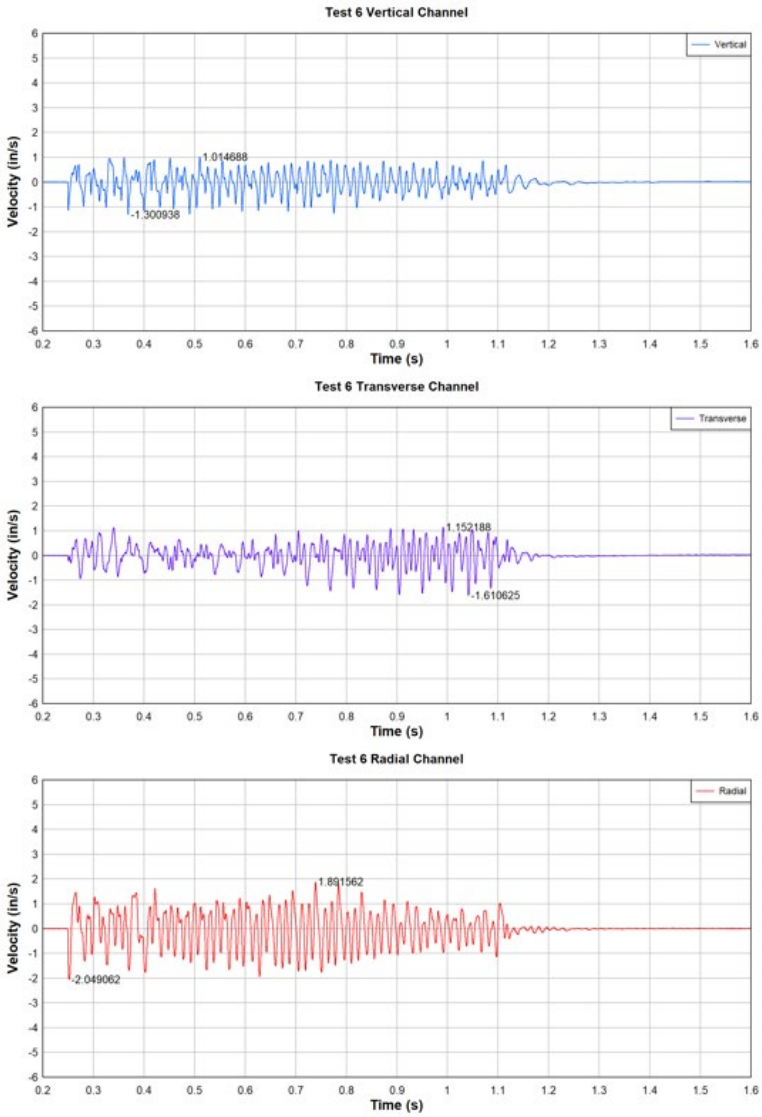

Figure 5.3.21 Test 6 vibration waveform

Figure 5.3.22 shows the air over pressure in millibars.

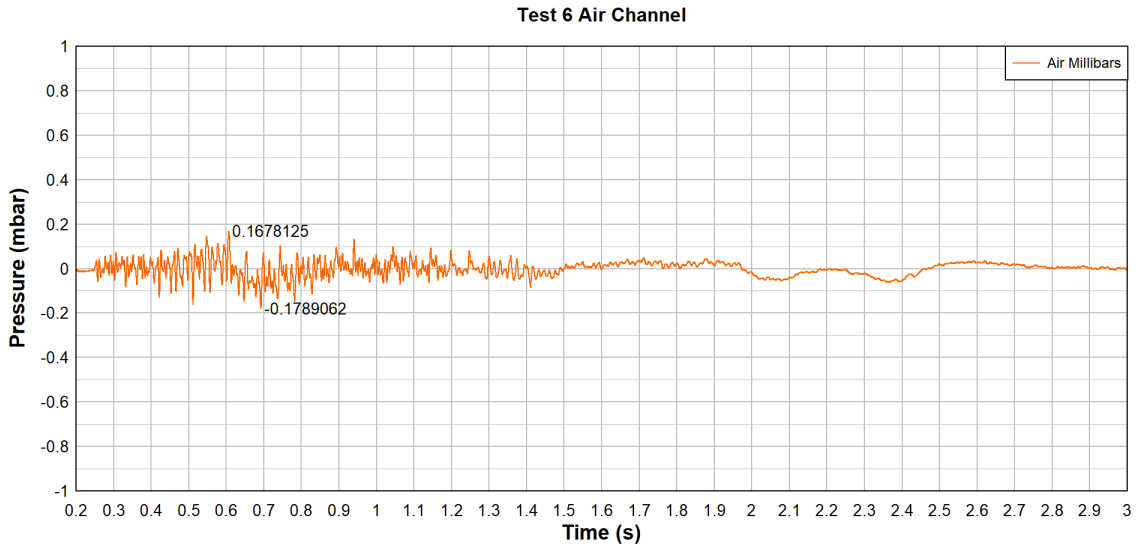

Figure 5.3.22 Test 6 air over pressure waveform

5.4 Field test results

Fragmentation was affected by row timing proved by the field tests done at Ogden Point. The type of explosives also affected how much of an influence row timing was. Figure 5.4.1 shows the fragmentation results side by side. Contractor 1 had the smallest fragmentation size for all three tests except for the lower sizes on test D. Sequence A "down the row" had the best fragmentation for contractor 1 and had the best fragmentation for the percent passing sizes greater than 50 percent for contactor 2. Test 4 sequence A had an outlier data point in the fragmentation that explains why the fragmentation differences between sequences for contractor 2 are tighter than expected. Figure 5.4.2 shows that outlier for test 4.

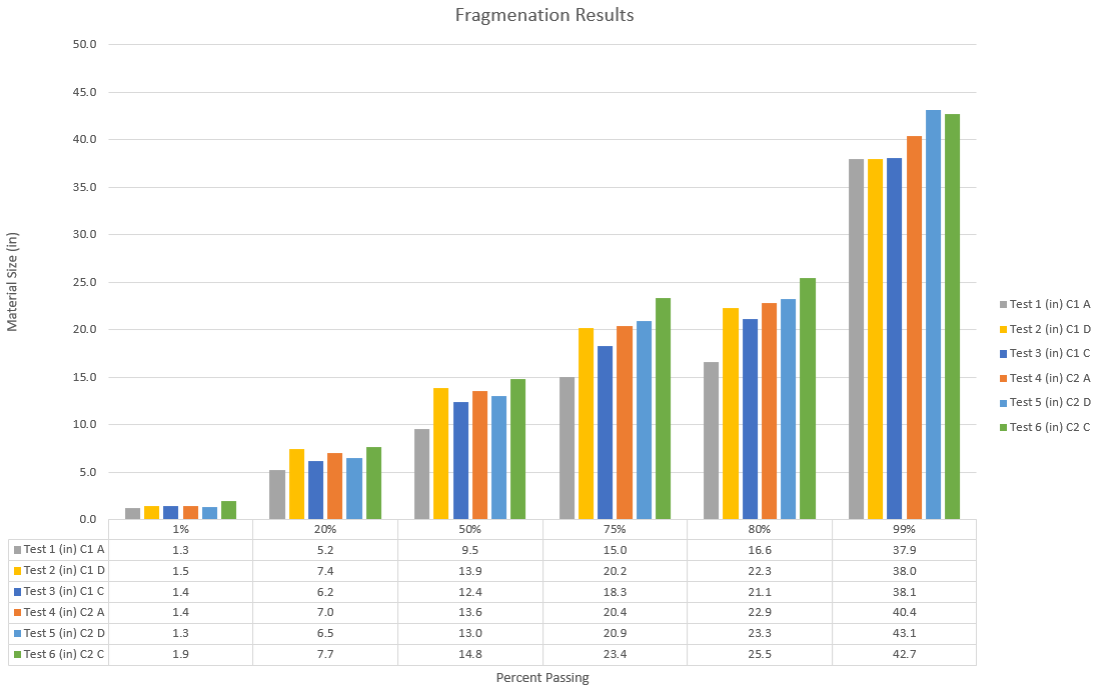

	1%	20%	50%	75%	80%	99%
Test 1 (in) C1 A	1.3	5.2	9.5	15.0	16.6	37.9
Test 2 (in) C1 D	1.5	7.4	13.9	20.2	22.3	38.0
Test 3 (in) C1 C	1.4	6.2	12.4	18.3	21.1	38.1
Test 4 (in) C2 A	1.4	7.0	13.6	20.4	22.9	40.4
Test 5 (in) C2 D	1.3	6.5	13.0	20.9	23.3	43.1
Test 6 (in) C2 C	1.9	7.7	14.8	23.4	25.5	42.7

Figure 5.4.1 Ogden Point testing fragmentation results

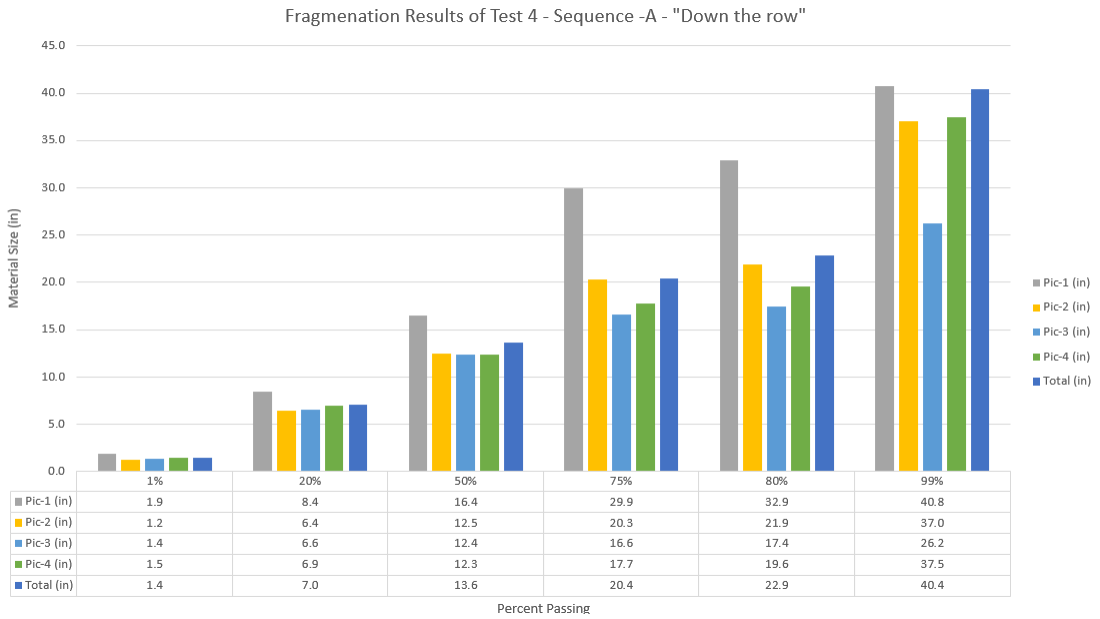

	1%	20%	50%	75%	80%	99%
Pic-1 (in)	1.9	8.4	16.4	29.9	32.9	40.8
Pic-2 (in)	1.2	6.4	12.5	20.3	21.9	37.0
Pic-3 (in)	1.4	6.6	12.4	16.6	17.4	26.2
Pic-4 (in)	1.5	6.9	12.3	17.7	19.6	37.5
Total (in)	1.4	7.0	13.6	20.4	22.9	40.4

Figure 5.4.2 Test 4 fragmentation

It was observed also that fragmentation was not influenced by row delay in the lower percent passing, which is supported by the literature. Figure 5.4.3 shows the changes

in percent passing due to row delay. Only percent passing sizes between 20 and 80 percent were shown in the figure since that range is the limit of photofragmentation. The main reasoning for less influence in the small percent passing sizes is because the smaller pieces are heavily dependent on the intense fracturing that happens close to the borehole. Fragmentation influences from delay are in the boundary zones of the radial fracturing, where the rock pieces will be the largest. If the burden and spacing are small enough that the intense fracturing zone touches the neighboring hole's intense fracturing zone, the delay would likely not have any influence on fragmentation.

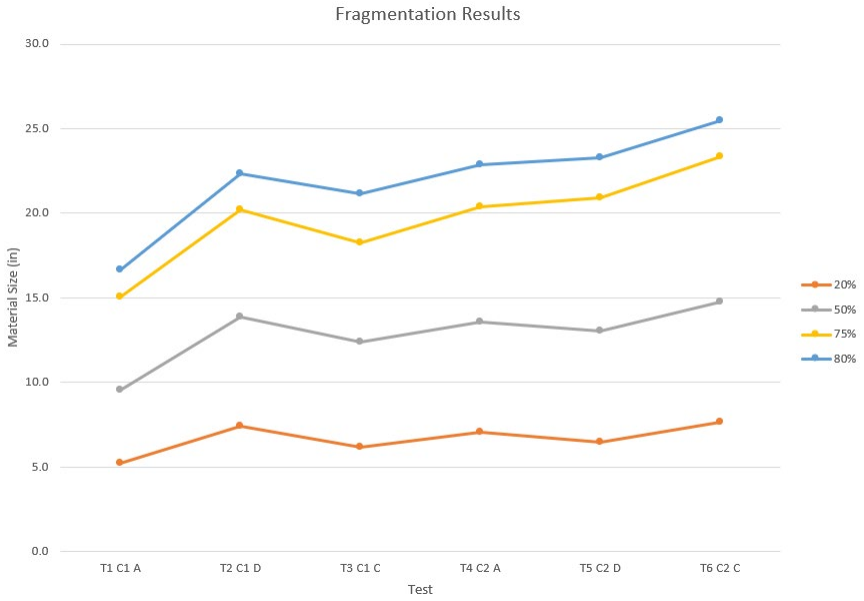

Figure 5.4.3 Fragmentation results from each passing size

The smallest fragmentation size was generated from sequence A which supports the Wor-Sil equation methodology. Allowing the material to be able to freely move allows for fractures to be extended farther and increase fragmentation from kinetic energy. Sources of fragmentation from kinetic energy include the collision of fragments in flight and collision with the bench floor. Material allowed to freely move in front of the hole

also minimizes the separating of fractures going back to the next row, allowing for radial fractures of the new row to propagate the furthest. A large row delay is needed to allow free movement. Figure 5.4.4 shows the fragmentation results due to row delay for contractor 1. Test 1 utilized a row timing of 300 ms, and test 2 and 3 utilized a row timing of 45 ms but using different sequences. Test 1 has smaller fragmentation and has an increased uniformity index. Figure 5.4.4 supports the need for long row timing. Test 2 and 3 utilize the same row timing but have different sequences. The change in fragmentation between test 2 and test 3 can be explained by variation in photofragmentation, geology or could be due to the spacing between the charges. Since there is no screen data to check the accuracy of the photofragmentation it is hard to say which one of the cases influenced the fragmentation difference between tests 2 and 3. An average ratio between the fragmentation of max and minimum row delay ended up being 1.25.

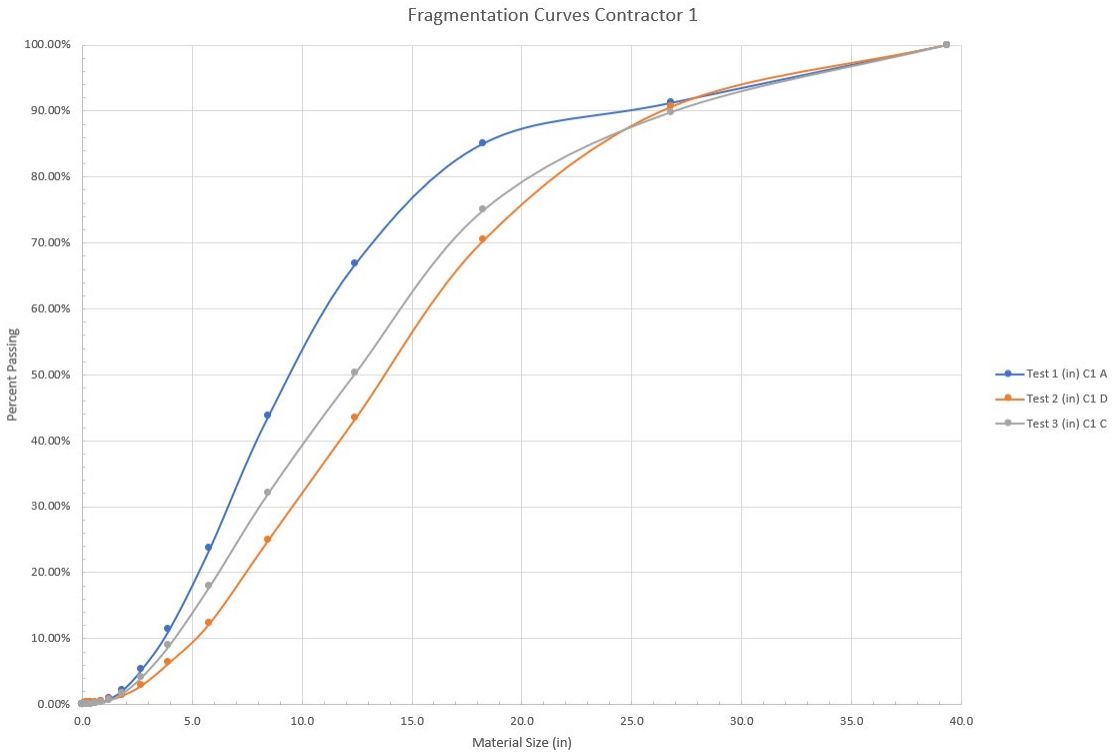

Figure 5.4.4 Contractor 1 fragmentation curves

Contractor 1 had better fragmentation than contractor 2 because contactor 1 used a gassed emulsion with higher relative weight strength (RWS) and mixed the emulsion with 30% AN prill. Contractor 1's RWS was 108 percent, and contractor 2's RWS was 72 percent. This explains why contractor 1 had better fragmentation than contractor 2. Figure 5.4.5 shows the fragmentation curves of test 1 and test 4. Although it is still unclear what property of explosives causes radial fracturing to increase, in general, higher RWS can be associated with increased radial fracturing. The higher RWS could have meant that radial fracturing interacted more between rows causing the fragmentation to be smaller.

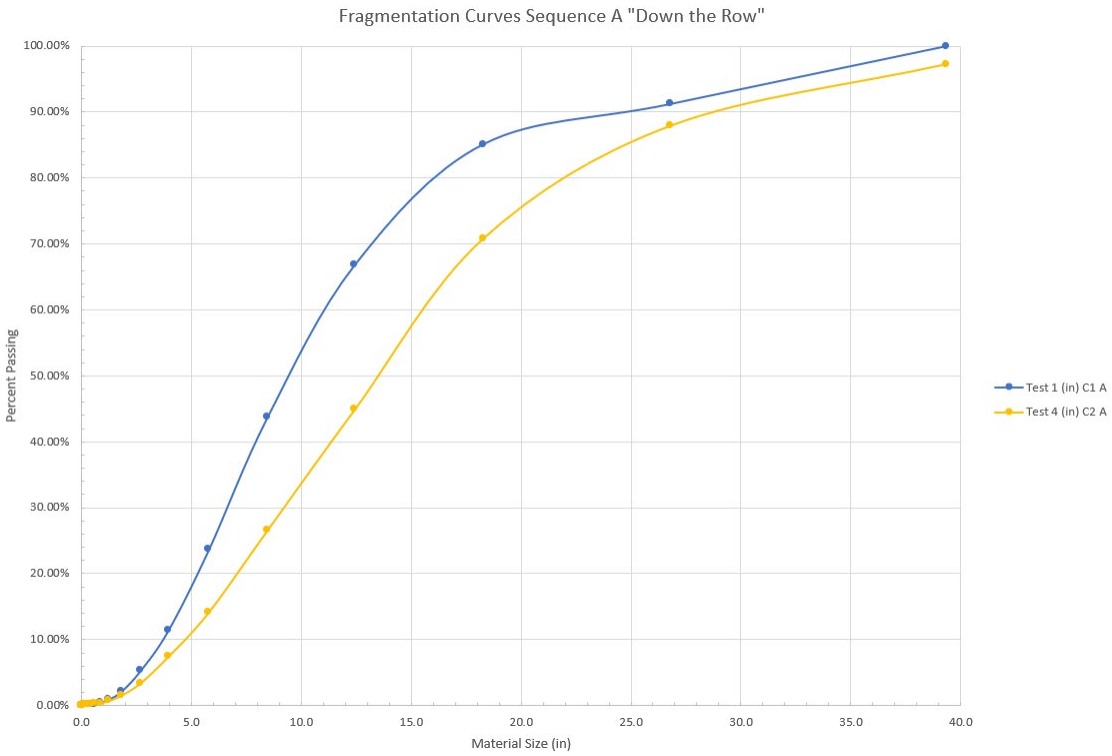

Figure 5.4.5 Fragmentation curves from sequence A “down the row”

Using a different explosive also changed the influence of delay timing. Contractor 1’s explosive resulted in an average standard deviation of 2.2 for percent passing fragmentation sizes 20 to 80 percent due to row delay. Contactor 1’s average standard deviation of the 80 percent passing fragmentation size was 3.0. Contractor 2’s explosives resulted in an average standard deviation of 1.1 for the percent passing sizes 20 to 80 percent due to row delay. Contractor 2’s average standard deviation of the 80 percent passing fragmentation size was 1.4. The trend is evidence that different types of explosives influence the effect of row delay. The difference is likely due to varying maximum fracture extents from different explosives and needs to be explored. The fragmentation data in test 4 was influenced by an outlier photo that could potentially miss lead the influences of row delay with different explosives. If photo 1 is taken out of the fragmentation analysis for

test 4 then the fragmentation sizes are decreased by roughly 2.2 inches in the 75 and 80 percent passing, the 50 percent passing size is the smallest out of all tests, and the 20 percent passing size is almost the same as test 5. Exploring the influence of explosives on fragmentation was out of the scope of the research. Figure 5.4.6 shows the fragmentation curves for each test for contractor 2.

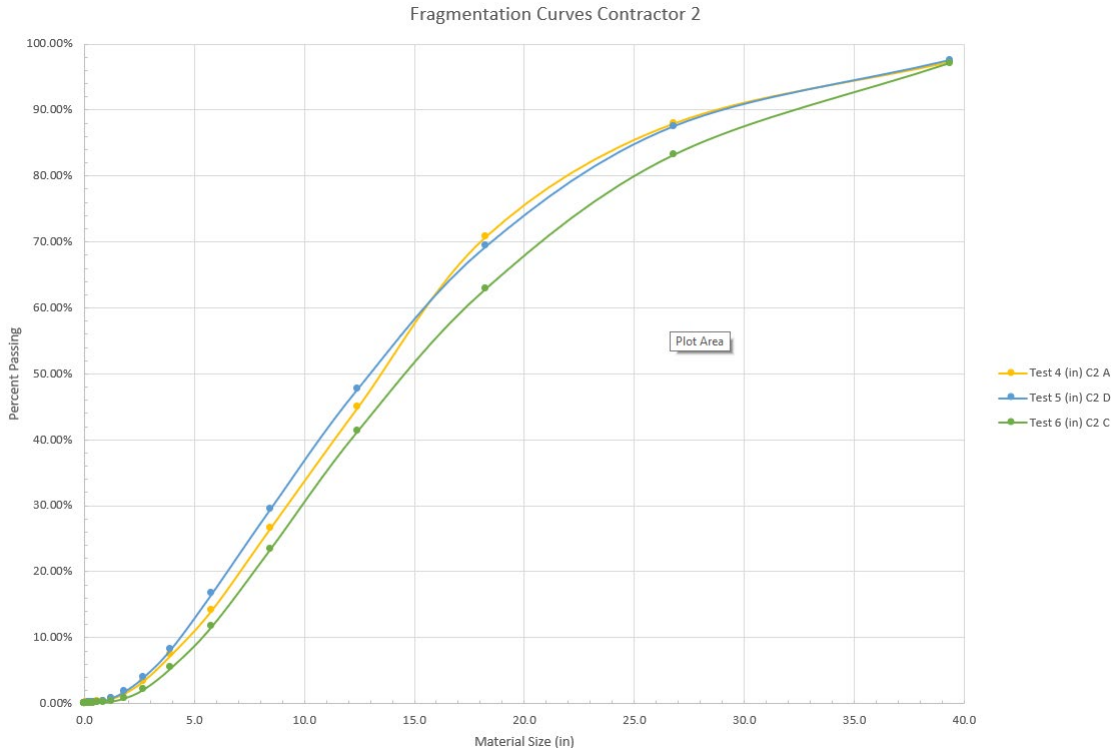

Figure 5.4.6 Fragmentation curves for contractor 2 testing

The vibration results that can be seen in chapter 5.3 and Table 5.4.1 were very interesting. Although the delay between charges was constant, the magnitude and shape of the waveform changed. Test 1 through 3 should be analyzed carefully because the data has some evidence of decoupling, or a malfunction of the sensor. Test 4 through 6 had the sensor 328 ft away instead of 100 ft and had quality data. The zigzag sequence, C, had the lowest vibrations for the vertical channel, and down the row sequence, A, had the lowest

vibrations for the radial and transverse channels. The zigzag sequence C had the lowest PPV. The lowest PPV did not yield the best fragmentation. An interesting note is that test 4 and 5 have very similar amplitudes in velocity in the radial and transverse channels but not the vertical channel.

Table 5.4.1 Vibration results from field tests

Test	R (in/s)	R (Hz)	T (in/s)	T(Hz)	V (in/s)	V (Hz)	Air (dBL)	Distance (ft)
T1 C1 A	3.484	13.0	2.076	61.5	5.113	41.3	N/A	100
T2 C1 D	2.138	35.1	2.339	35.1	5.113	73.8	N/A	100
T3 C1 C	2.800	22.3	2.875	6.7	7.181	73.1	139	100
T4 C2 A	1.662	41.3	1.252	78.0	2.537	86.2	132	328
T5 C2 D	1.921	55.3	1.551	55.7	4.656	66.6	119	328
T6 C2 C	2.049	59.3	1.611	78	1.301	73.1	119	328

Vibration results were collected to determine whether or not the timing that yielded the best fragmentation had the lowest vibrations. Since tests 4 and 5 had better fragmentation than test 6, the lowest vibrations test did not have the smallest fragmentation. The reason why signature hole analysis is not tied with fragmentation is that the vibration is optimized at a location outside of the blast. Vibration at one location over another has different timing to optimize the peak particle velocity. Practices that reduce the energy of the blast from leaving the breakage zone are what increase fragmentation and decrease vibrations. This concept needs to be explored more. Utilizing an array of seismographs

around the shot and varying distances is needed to analyze further and was out of the scope of this research.

Test 2 will be used to compare the model to the field tests because the photofragmentation data did not have any outliers and the row delay of 45 ms was short enough to show how fragmentation is influenced by row delay below the maximum calculated row delay.

CHAPTER 6. MODEL VS. FIELD TESTS

Chapter 6 will go over how well the Silva-Worsey row delay fragmentation methodology using a stochastic approach predicts the fragmentation curve of the collected fragmentation data. The stochastic approach will look at changing each variable in the Wor-Sil methodology to see what variables are important to randomize.

6.1 Field test compared to Wor-Sil calibration methodology

The field testing shown in chapter 5 did not follow the Wor-Sil calibration methodology because the field-testing led to the calibration methodology's determination. The field tests were set up to determine how the row delay and sequences affect fragmentation while keeping a single delay constant. Keeping a single delay between charges constant was to determine if the sequence with the best fragmentation also had the lowest vibrations. Analyzing the field tests' fragmentation data led to the concept of the void space created between the repeating sequences' delay. The delay between repeating sequences was created by which sequence was selected. Determining this void space was then correlated to the changes in fragmentation. The field tests also did not match Ash's bench blasting rules perfectly, but the geometry was closer to bench blasting than the geometry was to cratering.

6.2 Predicting test 2 with the Wor-Sil methodology

Cunningham's 2005 Kuz-Ram model was used to predict the blast's fragmentation without considering row delay. The Wor-Sil methodology is used to adjust the fragmentation due to row delay. The input variables for the Kuz-Ram model for the Ogden

Point Quarry test blast 2 can be seen in figure 6.2.1. The 2005 Kuz-Ram model utilizes hole timing but it does not utilize row timing.

Kuz-Ram Model Parameters		
Rock Type	Limestone	
Rock Specific Gravity	2.68	SG
Elastic Modulus	40	GPa
UCS	40	MPa
Explosives		
Density	1.15	SG
RWS	1.08	(% ANFO)
Nominal VOD	5200	m/s
Effective VOD	5200	m/s
Hole Timing		
Hole Delay	15	ms
SD Cap Scatter	0.1	
P-wave Velocity	4.8768	m/ms
Opt Delay Ratio	15.6	

Jointing		
Spacing	0.3	m
Dip	0	deg
Dip Direction	0	deg
In-situ block	1	m
Pattern Design		
Hole Diameter	101.6	mm
Charge Length	16.2	m
Burden	4.1	m
Spacing	4.8	m
Drill Accuracy SD	0.1	m
Bench Height	18.3	m
Face Dip Direction	0	deg

Figure 6.2.1 Kuz-Ram model input variables

The input variables used for the Wor-Sil model can be seen in figure 6.2.2. The variables will later be randomized to see the influence on the fragmentation prediction. The row delay of 45 ms was used since test 2 had 45 ms between repeating sequences. The size ratio of 1.25 was used because it was the average size ratio from the testing data. The swell factor was calculated based on before and after blast topo flights of test 5. The face velocity was calculated using the powder factor of test 2 and equation 4.2.2.

Row Timing		
Row Delay	45	ms
Size Ratio Min/Max	1.25	
Swell	0.5	
Face Velocity	0.01277	m/ms

Figure 6.2.2 Wor-Sil model input variables

The results of making the row delay adjustment to the Kuz-Ram equation can be seen in Figure 6.2.3. The Kuz-Ram model predicted smaller fragmentation than the data, and the Wor-Sil model predicted slightly larger fragmentation in the percent passing sizes greater than 35 percent. Table 6.2.1 shows the error of each model for the 50, 70, and 80 percent passing sizes. Utilizing the Wor-Sil model better describes the fragmentation of test 2 than the Kuz-Ram model only. The larger sizes' error is cut in half and shows that incorporating row delay in fragmentation models is essential.

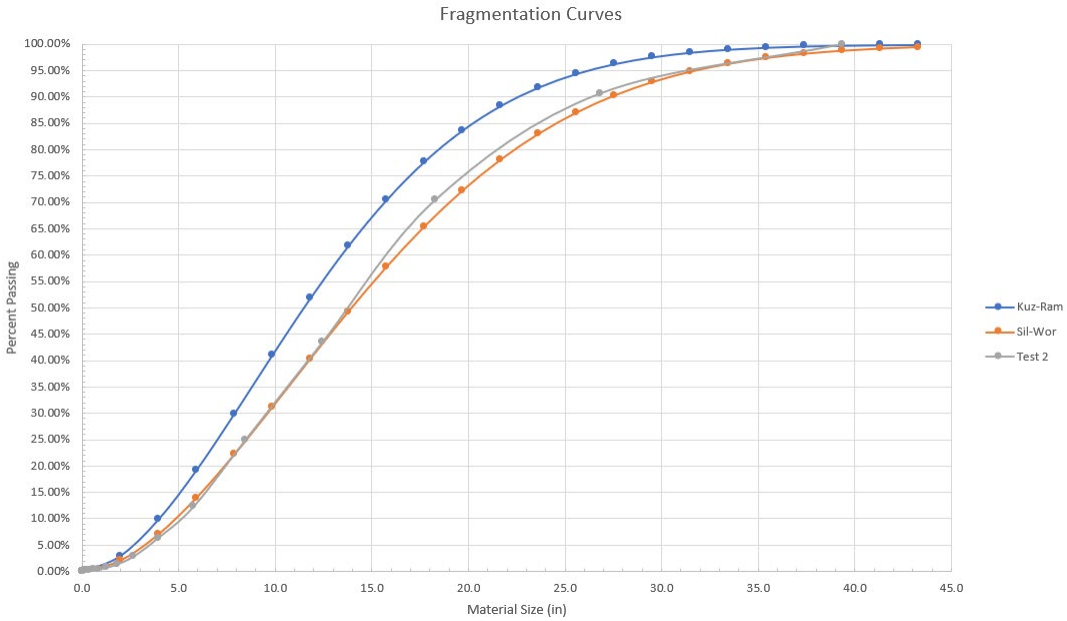

Figure 6.2.3 Fragmentation curves for Kuz-Ram, Wor-Sil, and Test 2

Table 6.2.1 Fragmentation model error

Percent Passing	50%	70%	80%
2005 Kuz-Ram Prediction (in)	11.5	15.5	18.3
Wor-Sil Prediction (in)	14.1	19.1	22.3
Test 2 (in)	13.7	18.0	21.2
2005 Kuz-Ram - Test 2 (in)	-2.2	-2.5	-2.9

Wor-Sill - Test 2 (in)	0.4	1.1	1.1
2005 Kuz-Ram Error	16.1%	13.9%	13.7%
Wor-Sil Error	2.9%	6.1%	5.2%

6.3 Influences of variable swell on Wor-Sil model

Swell was changed from 20 to 80 percent to determine the influence of swell on the Wor-Sil model. Figure 6.3.1 shows the influence of swell on the fragmentation curve. As swell gets bigger, the fragmentation size will increase for a constant row delay due to no longer having enough void space for the blasted material to swell into. This is because the swell determines what the maximum delay is needed to obtain maximum fragmentation. As swell is increased, so is the maximum delay, which increases the fragmentation factor for a constant row delay. A larger fragmentation factor will increase fragmentation size.

A smaller percent swell has a bigger impact on the fragmentation in 45 ms because small swells need less time between rows to obtain optimal fragmentation. As a row delay gets closer to the maximum delay, the fragmentation factor turns to 1 giving better fragmentation. A 20 percent swell has an optimal row delay of 64 ms, and an 80 percent swell has an optimal row delay of 257 ms. This shows that collecting swell information is very important for the model, and the standard deviation of swell can be used to obtain an average fragmentation curve for predictions.

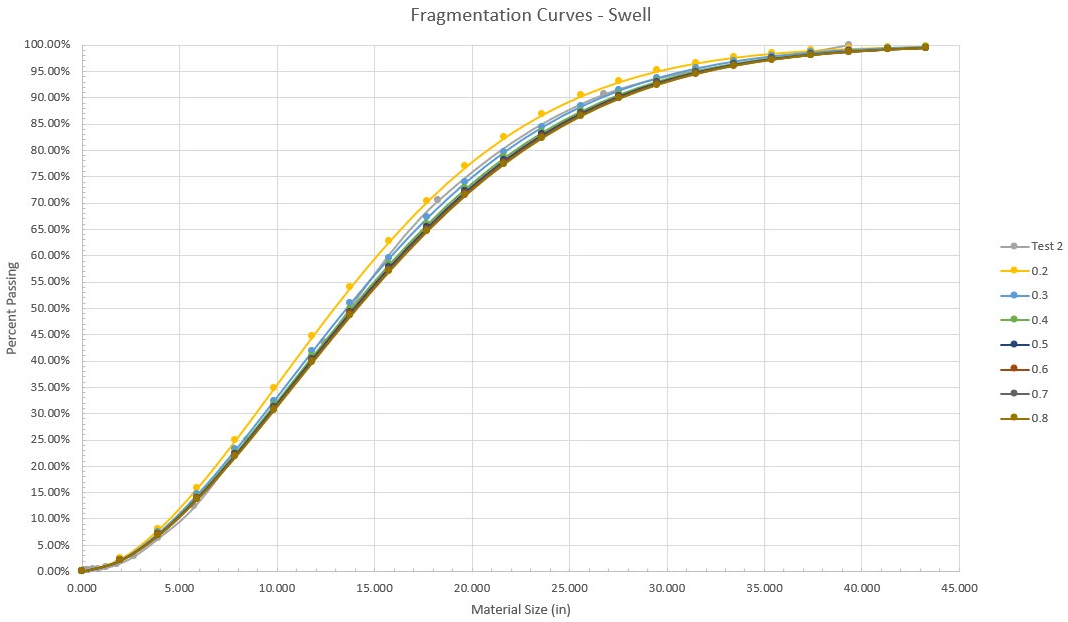

Figure 6.3.1 Influence of swell on the Wor-Sil model

6.4 Influences of variable face velocity on Wor-Sil model

The face velocity was adjusted from 20 to 120 ft/s to determine the influence of face velocity on the Wor-Sil model. As face velocity increases, the required time to develop adequate void space to blast into is also reduced. For a constant row delay, increasing face velocity will decrease the fragmentation size. Face velocity will vary in the field with varying burden, geology, and hole loading. These variables have some degree of scattering, so utilizing a stochastic approach would be beneficial for determining an average fragmentation curve.

The degree of scatter would depend on how good the quality control of the blast was. Velocity scatter would be 15 ft/s for powder factors varying from 1.5 to 2.5 tons of rock/lb of explosives. Conducting multiple face velocity tests on site will help determine adequate scatter for face velocities. When face velocities are fast, fast row times are appropriate, and when face velocities are slow, slow row times need to be utilized. The

current practice is to base row timing recommendations on ms/ft of burden, but determining the face velocity is a critical parameter to know whether a row delay is appropriate or not.

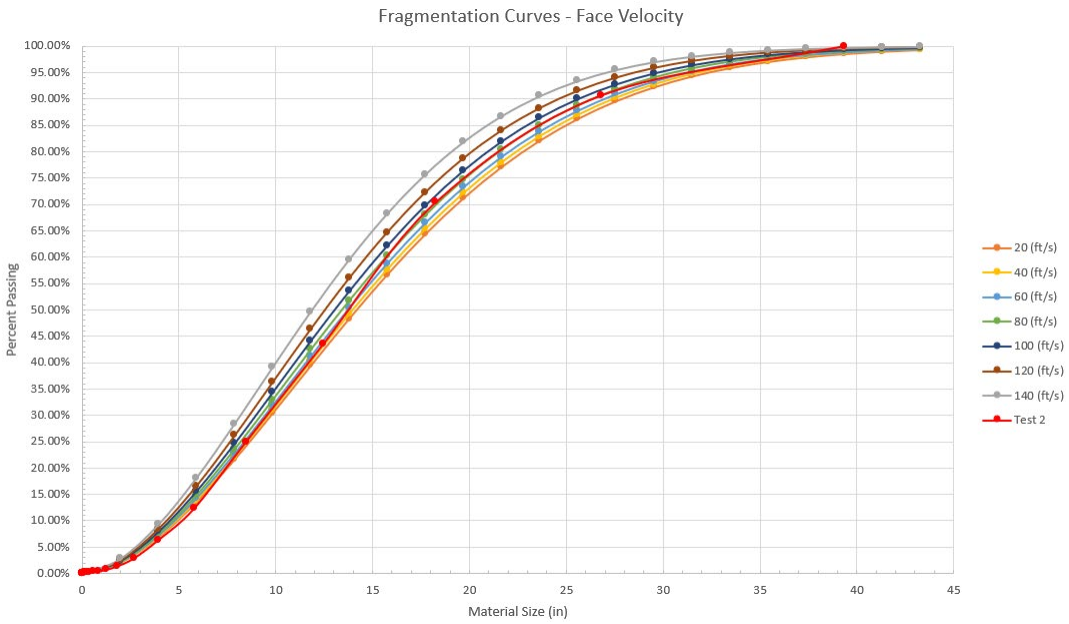

Figure 6.4.1 Influence of face velocity on the Wor-Sil model

6.5 Influence of burden on Wor-Sil model

To determine the influences of burden on the Wor-Sil model, the burden was adjusted from 10.5 to 16.5 ft. Figure 6.5.1 shows the influences of changing the burden with other variables constant. Burden did not significantly influence the fragmentation curve because it only slightly changes the maximum row delay needed for optimal fragmentation. A 14.5 ft burden has a maximum row delay of 173 ms, and a 16.5 ft burden has a maximum row delay of 197 ms. If the row delay used was closer to the maximum row delay instead of the minimum row delay, the influence of burden would be more important. A quarry with good quality control can typically have a burden tolerance of

plus or minus 1 ft. Surveying drill hole locations would help with determining a burden deviation.

The varying burden would be accounted for by varying face velocity to some extent. Although the change is small, the varying burden does add to the change in fragmentation. Using burden would help in a stochastic model to determine an average fragmentation curve.

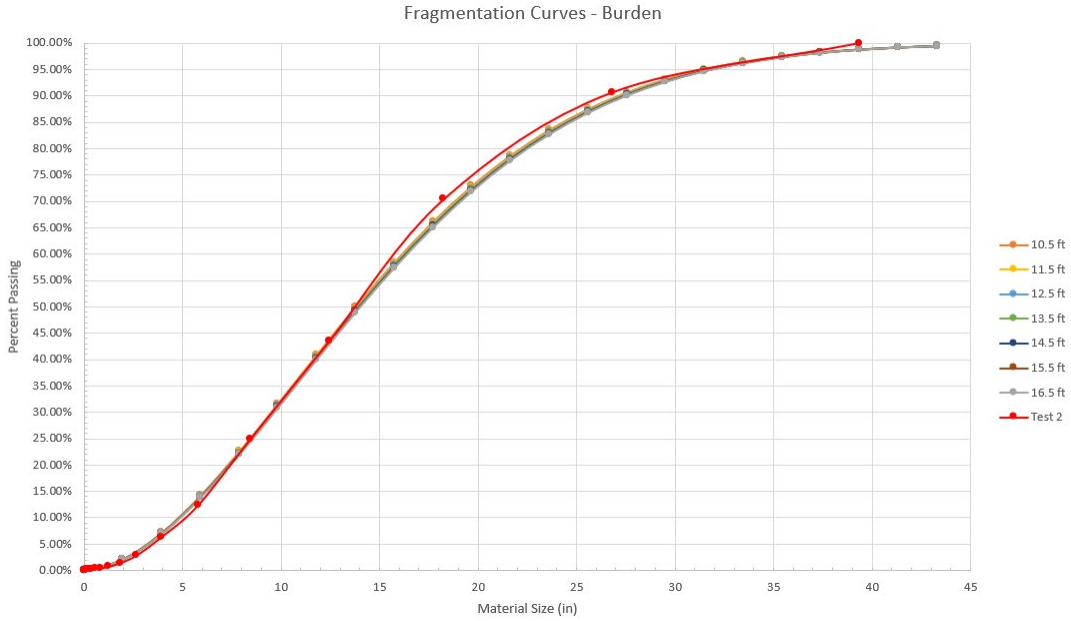

Figure 6.5.1 Influence of burden on the Wor-Sil model

6.6 Influence of size ratio on Wor-Sil model

To determine the influences of material size ratio on the Wor-Sil model, the ratio was adjusted from 1.1 to 1. 4. Figure 6.6.1 shows the influences of size ratio when keeping all the other parameters constant. The material size ratio appears to have the biggest influence on the fragmentation curves out of all the parameters. This is the case because the material size ratio is how the Wor-Sil model relates swell, face velocity, burden, and

row timing to fragmentation. The range of material size ratios from the Ogden Point fragmentation was 1.1 to 1.4, with the average being 1.25.

Using the material size ratio as the only random variable when using a stochastic approach to modeling fragmentation will be more influential than a burden, swell, and face velocity when using the Wor-Sil model. The other variables can be used but will not have as big of an effect on typical variations seen in the field.

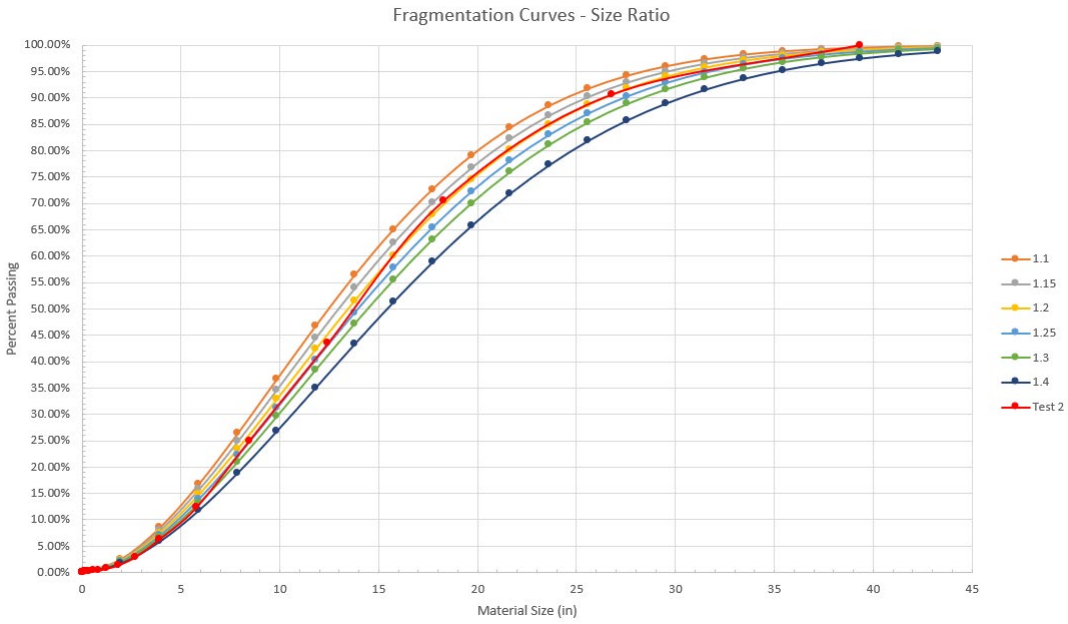

Figure 6.6.1 Influence of material size ratio on the Wor-Sil model

6.7 Influence of row time on Wor-Sil model

Row timing is the variable being changed to get the desired fragmentation results. Since electronic detonators have high precision and accuracy, there is no need to randomize the row timing. To show the influences of row timing on fragmentation for the current model, row times were varied from 45 to 165 ms while keeping all other parameters

constant. Figure 6.7.1 shows the results of varying row timing. If a longer row delay is used, fragmentation increases.

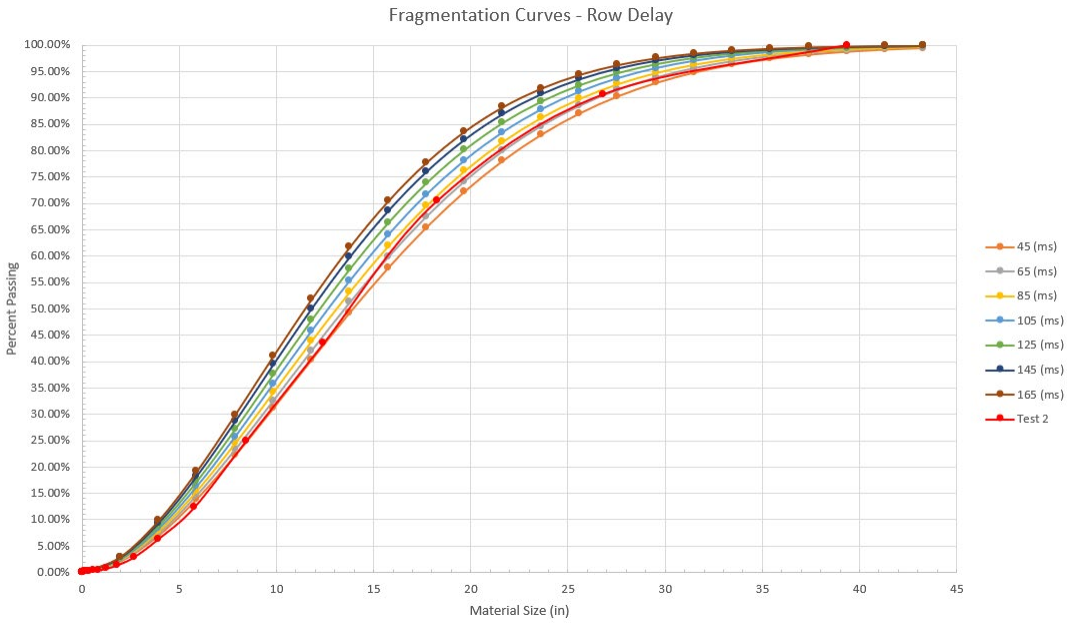

Figure 6.7.1 Influence of row timing on the Wor-Sil model

6.8 Calibrating Wor-Sil model

To calibrate the Wor-Sil model utilizing the 2005 Kuz-Ram model as the base model for predicting fragmentation, the Kuz-Ram model fragmentation curve must match the fragmentation data from the test with the maximum row timing. In the Ogden Point example, the Kuz-Ram model prediction would be calibrated to match the fragmentation of test 1. Test 1 had the most row timing and produced the smallest fragmentation.

The Kuz-Ram model has calibration factors built into the 50 percent passing equation and the uniformity index equation to help fit the model to the data while keeping the relationship of certain parameters in the model. An example of calibrating the model

can be seen in Figure 6.8.1. Conducting the calibration on the base model will end up calibrating the Wor-Sil model since using the optimal row delay will result in no change in fragmentation. The Wor-Sil model assumes that the base fragmentation size is the best possible fragmentation case and adjusts fragmentation for row timings that does not have ideal void space.

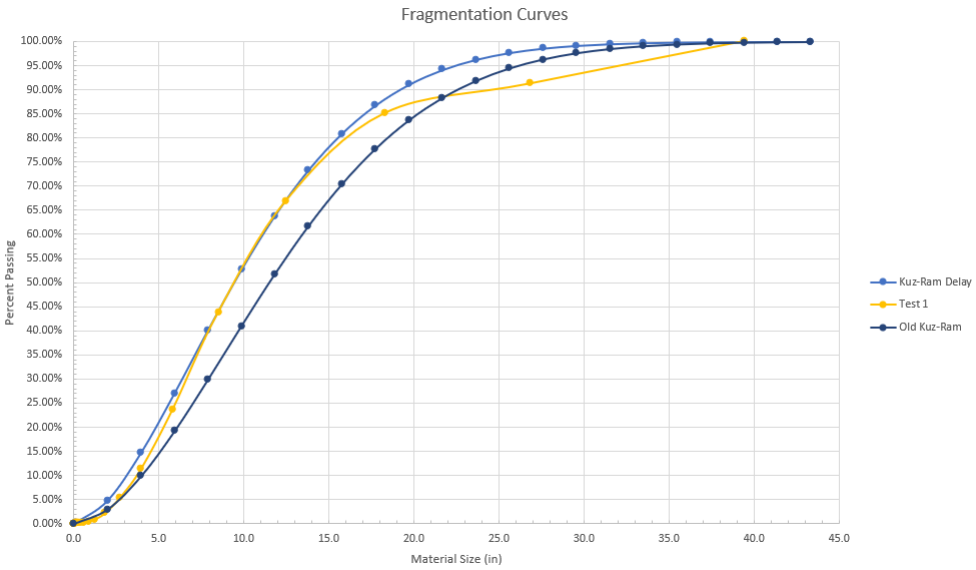

Figure 6.8.1 Calibrating 2005 Kuz-Ram with test 1

Once the 2005 Kuz-Ram has been adjusted, the Wor-Sil model can be used on the 50 percent passing size from the adjusted Kuz-Ram to determine the 50 percent passing size for the desired row timing. The Rosin-Rammler function is then used to determine the final Wor-Sil fragmentation curve. Figure 6.8.2 shows how the Wor-Sil model with a 45 ms row delay fits with test 2 and 3 after being calibrated. Using the calibration increases the accuracy of the prediction when predicting both tests 2 and 3. Test 2 and 3 both had a row delay of 45 ms. The calibrated model has an error of 7 and 6 percent for predicting test 2 and 3's 50 percent passing size, respectively.

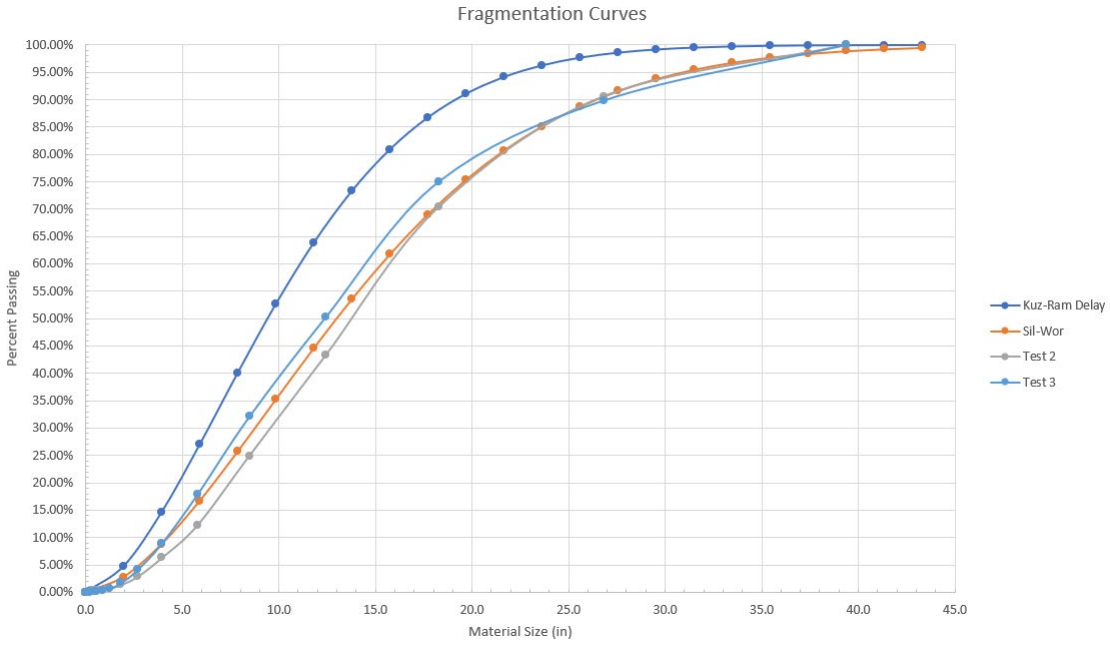

Figure 6.8.2 Calibrated Wor-Sil Model for tests 1, 2, and 3

6.9 Reason for row adjustment on fragmentation.

Current fragmentation models only take hole delay into account for determining fragmentation curves. The research from Ogden Point proves that the row delay influences fragmentation. With the Wor-Sil model, it is possible to select a row timing to generate a particle size distribution, according to the mine requirements.

The Ogden Point Quarry had a problem with the material breaking down into fines clogging up the material handling system causing the reduction of stockpile inventory due to funneling of draw points when wet. This led the quarry to optimize the fragmentation from the blast to reduce the fines downstream. The coarser the muck pile the Less Fines that were generated during the transportation process.

Utilizing the proposed methodology can help mines select row timing that gives them the outcomes they need to save money downstream. Some of the known reasons for needing a certain fragmentation include; a key material size being sold, ore recovery, material handling, reduction of operating costs, and etc.

CHAPTER 7. DISCUSSION, CONCLUSIONS AND FUTURE WORK RECOMMENDATIONS

Chapter 7 goes over the discussion of fragmentation models, conclusions, novel contributions, and future work of the research. Several conclusions can be made from the research.

7.1 Discussion

Fragmentation models are used to understand what changing parameters of the blast does on fragmentation to optimize operational cost and maximize product. Every operation has its own optimized fragmentation for costs and product. A site's optimized fragmentation changes with time as costs and key products change. Some operations need large fragments, small fragments, or fragment sizes somewhere in between. A gold operation doing a run of mine leach process to recovery gold needs smaller fragments to get the surface area on the rock surface to allow the chemicals to leach the gold out of the rock. A rock quarry with a market for riprap that is 3 feet in diameter for $47/ton or ¾" clean rock for $20/ton needs larger fragments to optimize profits.

Another reason fragmentation models are used are to predict the fragmentation of an operation that hasn't started mining yet. Knowing the typical fragmentation before operating helps that operation select equipment or determine the amount of recovery of the salable products. Prefeasibility studies for metal operations conduct fragmentation studies frequently. Being able to accurately predict fragmentation of a green field site allows that operation to not go over budget when the operation goes into production and selects the appropriate equipment for the fragmentation size. A gold mine using run of mine material in a heap leaching process, needs to know what the budgeted blasting costs will yield in

recovery. If fragmentation is wrong, then the operation could be over budget due to having to increase blasting cost or it could suffer in recovery. Both cases could lead the mine to be unprofitable.

Current fragmentation models are in some form all based on the Kuz-Ram model. The crushed zone model utilizes the Kuz-Ram model but fixes the smaller percent passing size due to intense fracturing close to the borehole. The KCO model utilizes the Kuz-ram model to predict the 50% passing size but uses the Swebrec fragmentation curve to define the fragmentation distribution. The Ouch-Sanch model utilizes the Kuz-ram model for relationships of blast parameters to fragmentation and then makes the Kuz-Ram equation dimensionless. Fragmentation modeling is a long history that has been seeking to solve the next variable in the fragmentation equation. Fragmentation modeling of blasting first started in the 1960s and is still a big topic today.

Models to date consider explosives, blast design geometry, geology, and hole timing. The fragmentation modeling process is very complicated. Not knowing what happens when fractures form when explosives detonates is a reason fragmentation modeling is complicated. Another reason that fragmentation modeling is complicated is because of changing geology. Geology and fracturing due to explosives detonating go hand in hand because fragmentation models need to incorporate rock and explosives properties that define the conditions during the fragmentation process. Take dynamic strength testing using a Split-Hopkinson bar for example. The dynamic strength is determined by wedging a small piece of core between two rods. Stress is applied by launching a rod into the rod in front of the core which then transmits the stress into the sample. With blasting, the sample is large and has a different confinement and loading

scenario than the Split-Hopkinson bar. Bench blasting has the stress come from within the rock and the source of the stress is in contact with the rock sample. Because the scenarios are very different you can only correlate Split-Hopkinson bar dynamic strength data to fragmentation with empirical data. This goes for all explosives and geologic properties that are used in fragmentation models. Mechanistic models will struggle to become useful until researchers are able to witness in real time how fractures form due to explosives in changing geology. Until then empirical models will be the most useful.

The above research identifies two main parameters that are currently lacking in empirical fragmentation modeling. Dynamic confinement and fragmentation mechanics are those two missing parameters. Free faces have been proven to provide better fragmentation than when not used. Hole timing is too quick to provide new free faces. The longer row timing parameter in the shot is where new free faces for shots with multiple rows are created. When blasted rock is fragmented it moves. Where the rock pieces are during time depend on the confinement conditions, gravity, and material velocity. When multiple row blasting is conducted this opens a new confinement condition called "dynamic confinement". Dynamic confinement is the amount of void space available at the time of detonation. Row timing is how dynamic confinement is changed during a shot. Since no current model utilizes row timing, there is no way to determine optimal row timing besides trial and error. The Worsey-Silva model determines the fragmentation changes due to dynamic confinement and can be used with any fragmentation model. The Wor-Sil model can be calibrated to be used on any site. Material swells when the rock is blasted and is the reason free faces are so important. Material needs to be able to move when explosive stress is applied to help in the fragmentation process and having void space for

the material swell allows for the rock to move. Utilizing burden, swell, and face velocity one can determine what row timing is required to obtain the necessary void space to have the smallest fragmentation or select the row timing that gets the desired fragmentation. When utilizing the Worsey-Silva model, fragmentation modeling was able to be improved by 6% over the 2005 Kuz-Ram model.

Fragmentation mechanism is currently not defined in the fragmentation modeling world. Fragmentation mechanisms change how fractures propagate and separate. Changes in confinement conditions and loading conditions changes the way fractures, caused from the explosive shock, extend and separate when the rock starts to move. The research introduces cratering and bench blasting as two common fragmentation mechanisms that should be considered differently when making fragmentation models. The Worsey-Silva model was developed for the bench blasting fragmentation mechanism and gives the geometry needed to have the right mechanism. More research needs to be done to incorporate row timing with the cratering fragmentation mechanism. Other fragmentation mechanisms need to be identified and models development for them. Areas that could possibly have different fragmentation mechanisms include construction and underground blasting.

The industry currently lacks large scale tests with varying row delays. There was no other literature looking at this on a full scale or as the main topic of research. Because of this no data sets were found that utilized the same set up between tests that varied row timing only. The research conducted above is a big contribution to the fragmentation community because it is one of a kind. It took a whole year to get 6 full tests completed so increasing this data set will be a lengthy process. It also seems that the current industry

is still researching hole delay and has yet to switch over to looking a row delay. The Wor-Sil model lacks a large data set to help define swell, face velocity, fragmentation ratio for varying sites. Future testing will be done conducting the calibration methodology developed in this research to determine equations to predict swell, face velocity, and fragmentation ratios for green field sites.

7.2 Conclusions

The following are conclusions of the research, current fragmentation models, and previous literature.

- Current fragmentation prediction models do not incorporate row delay when determining fragmentation curves.
- Row Delay is an important variable when determining fragmentation from bench blasting which is supported by the Ogden Point research which showed approximately a 6-inch difference in the 80 percent passing due to changing row delay.
- The Worsey-Silva methodology for predicting fragmentation, including row delay, improves the available fragmentation models that only include hole-delay. However, the limit of the proposed methodology is when utilizing a different fragmentation mechanism from bench blasting. In that case, the fragmentation due to row delay is unknown.
- Defining fragmentation mechanisms are important for fragmentation prediction models. Current fragmentation models do not include a fragmentation mechanism that the model is for. In this research, the influence of the row delay was included on bench blasting fragmentation mechanism models.
- Bench blasting and cratering are two common fragmentation mechanics in surface mining that need to be analyzed differently when modeling fragmentation.
- Using a stochastic approach to fragmentation modeling can help to include the variability of the field when conducting fragmentation predictions.

- The 2005 Kuz-Ram model is the most used fragmentation prediction model in the industry and is the base of other models available today.
- Photofragmentation methods for collecting fragmentation data are accurate for the percent passing size ranges of 20 to 80 percent. In the case of values outside the range using material screening is necessary to get accurate data.
- Cumulative distribution curves, such as the Rosin-Rammler and the Swebrec, are accurate for the percent passing size ranges of 5 to 80 percent.
- The timing used that is best for ground vibrations does not match the timing that is best for fragmentation. The principal reason is because vibration optimization uses timing to cancel vibration waves that have already left the blast at a certain point outside the fragmentation zone.
- Regular rhythmic timing (RRT) can be used without adverse effects on bench blasting. Adverse effects include undetonated explosives, extreme vibration, extreme air blast, not reaching floor grade, and changes in operation productivity.
- In a RRT scenario, the sequence determines the row delay of the shot.
- When using regular rhythmic timing, different sequences produce different vibrations and different fragmentation.
- The Silva-Worsey methodology can be used when using traditional and regular rhythmic timing.

7.3 Novel contributions

The following are novel contributions made from the conducted research and ideas formed from previous literature.

- Determining row delay is an important factor when predicting fragmentation.
- This research presents a methodology and equations to improve current fragmentation model to include row delay.
- Identifying that there are multiple fragmentation mechanics that determine what the fragmentation is from a blast.
- Recognizing that fragmentation models must define the fragmentation mechanics and the parameters to achieve the same mechanic for the model as the blast in question.

- Defining parameters to have the bench blasting fragmentation mechanism
- Regular rhythmic timing can be used in a bench blasting setting without any adverse effects of the blast, such as undetonated explosives, excessive airblast, excessive vibrations, toe, etc.
- Selecting a timing sequence is important when considering blast vibrations and fragmentation.
- Introduces stochastic approaches to the mining industry for fragmentation modeling.
- Illustrating and defining dynamic confinement.

7.4 Recommendations for future work

The following are recommendations for future work that were discovered during the literature review and research.

- Conducting more research on bench blasts to strengthen the relationship of row timing on fragmentation.
    - Compile a decade's worth of data investigating row delay and fragmentation that currently does not exist.
    - Determining a fitting relationship to the data set.
    - Collect fragmentation data using screening methods as well as photofragmentation methods.
- Investigate the relationship of blast design to swell to come up with a prediction equation for swell.
- Investigate the relationship of blast design to face velocity to come up with a prediction equation for velocity that utilizes more design parameters than powder factor.
- Determine fragmentation models for cratering and other fragmentation mechanisms.
- Identifying all the fragmentation mechanisms in the blasting industry for surface and underground.

- Investigate the influences of distances between charges on fragmentation when utilizing regular rhythmic timing.
- Fragmentation models currently use burden to determine how timing influences fragmentation. Investigating how the geometry of burden and spacing influence how timing influence fragmentation is needed.

APPENDIX

BLAST REPORTS

Blast Report

DFA / CRH (Ontario)

page 1

Quarry:	Ogden Point	Blast Number:	17-017
P.O. #:	4500940667	Orica Order #:	2237906
Blast Date:	2017-09-12	Blast Time:	2:31 PM

Blaster-in-charge: Kevin Myerscough (Print Name)

Blast Location: 3rd Bench, North Face, Middle (Bench / Face)

GPS Coordinates: 43.98780 °N Latitude (Centre of Blast) 77.87529 °W Longitude (Centre of Blast)

Wind from the: SW at 15 kph Temperature: 21 to 25 °C

Clear:		Rain:		Overcast:	
Partly Cloudy:	X	Snow:		Inversion:	

Ceiling: 30,000 ft

- Drilling Information -		Angle from Vertical			Nominal Bit Diameter:			
Primary Bit diam:	101.6 mm	0°	# Holes:	69	=	4,099.3 ft	(4	" diam)
Secondary Bit diam:	mm	0°	# Holes:		=	0.0 ft	(	" diam)
Tertiary Bit diam:	mm	0°	# Holes:		=	0.0 ft	(	" diam)

tonnes Blasted:	62,893	te		
Total tonnes per day:	63,198	te	OPBB40	Rate Code
Total Holes Loaded:	69	holes		
... including:	3	Dead Holes		
... and:		Helper Holes		
Helper Hole Collar:		ft avg		
# Rows Blasted:	3	rows		
- Pattern (Front Row)-				
Burden:	14.5	ft avg		
Spacing:	15.7	ft avg		
# Holes:	24	front row		
- Pattern (Main Body) -				
Burden:	13.5	ft avg		
Spacing:	15.7	ft avg		
# Holes:	45	main body		
Bench Height:	58.4	ft avg		
Sub-drill:	1.0	ft avg		
Hole Depth:	59.4	ft avg		
- Stone Decking -				
Front Row:		ft avg		
Main Body:		ft avg		
# Decks:		per blast		
- Collar Stemming -				
Front Row:	6.5	ft avg		
Main Body:	6.5	ft avg		
Material used:	3/4" clear			
- Charge Length -				
Front Row:	52.9	ft avg		
Main Body:	52.9	ft avg		
- Charge Weight -				
Front Row:	154.3	kg/hole		
Main Body:	154.3	kg/hole		
Max. per delay:	205.0	kg/delay		
SD () Equation:	177.4	kg/delay		
Total kg Loaded:	11,794	kg		
Rock Density:	2.65	g/cc = te/m³		

Theoretical PF (Based on a single hole)

Yield Powder Factor (kg Loaded / te Blasted)

Bulk Explosives:	in (kg)	out (kg)	kg	
CENTRA GOLD 70	34,000	22,320	11,680	
Packaged Explosives:	cs shipped	cs returned	kg	
E113 90X400	10	7	75	
Boosters:	kg / unit	# usec	kg	
PENTEX 8 (OR EQUIVALENT)	0.23	69	15.7	
PENTEX 12 (OR EQUIVALENT)	0.34	69	23.5	
total explosives weight in Blast (kg):			11,794	
Pkgd Prod (75 kg) % of Total kg:			0.6%	
Detonators:	case #'s	ms	# used	
UNITRONIC 600 6M	61554303-15		69	
UNITRONIC 600 20M	61478124-32		69	
Cord & Accessories:		U of M	# used	
HARNESS WIRE DUPLEX (6 PACK) 400M		units	1	
		units		
		units		

0.838 lb/yd³	Yield PF:	0.188 kg/te (actual)
0.691 lb/yd³	Front row:	0.155 kg/te (theoretical)
0.742 lb/yd³	Main Body:	0.166 kg/te (theoretical)
0.725 lb/yd³	"KPI" PF:	0.162 kg/te (theoretical)

Resource Deployment:

# of Blasts today (this Quarry)		1
# of Blasters (this Blast)		1
# of Helpers (this Blast)	Note Exception	2
# of MMU's (this Blast)		1

Services:

GPS LAYOUT	Enter hours	0.0
BULK TRUCK CHARGE	>/=10,000 kg	1
BLASTER HOURS	Enter Blaster hours	7.0
HELPER HOURS	Enter total Helper man-hours	13.0
SEISMOGRAPH RENTAL	Enter # Orica Seismographs	0
3D LASER PROFILE	Enter hours	0.0
BORETRACK	Enter hours	1.0
TECHNICAL BLAST DESIGN	(per day) Enter # of days	0.0

Cost Reduction Notes (this Blast) - change in Bit , B, S, Expl or IS from previous Blast:

ORICA
The Blasting Professionals™

Blast Report

OFA / DIV of CRH (Ontario

Quarry:	Ogden Point	Blast Number:	17-017
P.O. #:	4500940667	Orica Order #:	2237906
Blast Date:	2017-09-12	Blast Time:	2:31 PM

page 2

Blast Co-ordinates	Enter ° N Lat.	Enter ° W Long.	(N) Radians	(W) Radians
Mid Blast				
Front Row Corner	43.98778	77.87460	0.767732	1.359168
Back Row Corner	43.98782	77.87597	0.767732	1.359192
Average (Centre of Blast)	43.98780	77.87529	0.767732	1.359180

1st

Seismograph Co-ordinates	Enter ° N Lat.	Enter ° W Long.	(N) Radians	(W) Radians
1st Reading	43.98741	77.86949	0.767725	1.359079
2nd Reading				
Average	43.98741	77.86949	0.767725	1.359079
Distance (1st Seis. From Centre of Blast)	466.2	m		
Post Blast Data: ppV:	9.3	mm/s	Trigger set at: 2.0 mm/s	
frequency:	18.0	Hz	V / T / L : T (Vertical, Transverse or Longitudinal)	
air overpressure:	127.8	dB	Trigger set at: 115 dB	

North side of Main Gate

2nd

Seismograph Co-ordinates	Enter ° N Lat.	Enter ° W Long.	(N) Radians	(W) Radians
1st Reading	43.99522	77.86748	0.767861	1.359044
2nd Reading				
Average	43.99522	77.86748	0.767861	1.359044
Distance (2nd Seis. From Centre of Blast)	1035.9	m		
Post Blast Data: ppV:	DNT	mm/s	Trigger set at: 2.0 mm/s	
frequency:	DNT	Hz	V / T / L : ? (Vertical, Transverse or Longitudinal)	
air overpressure:	DNT	dB	Trigger set at: 115 dB	

C.P. Tracks, NE corner of property - Did Not Trigger

3rd

Seismograph Co-ordinates	Enter ° N Lat.	Enter ° W Long.	(N) Radians	(W) Radians
1st Reading				
2nd Reading				
Average	0.00000	0.00000	0.000000	0.000000
Distance (3rd Seis. From Centre of Blast)	0.0	m		
Post Blast Data: ppV:	0.0	mm/s	Trigger set at: 2.0 mm/s	
frequency:	0.0	Hz	V / T / L : ? (Vertical, Transverse or Longitudinal)	
air overpressure:	0.0	dB	Trigger set at: 115 dB	

Scaling Factor denotes the degree of Blast confinement.
The higher the SF, the more confined the Blast.
A Scaling Factor of 30 is commonly used in the Scaled Distance formula for Quarry Bench Blasting:

Enter a scaling Factor: 35 Quarry Bench Blast - narrow, multi-row Blast with 1 Free Face?

$$W = \frac{D^2}{35^2}$$

$$= \frac{(466.2)^2}{35^2} \text{ kg}$$

$$= \frac{217{,}342}{1{,}225} \text{ kg}$$

Maximum Indicated Charge Weight per Delay = 177 kg

Orica
Blaster-in-charge: Kevin Myerscough

jim bray

Signature required, indicating that
Blast Report is Complete & Accurate.

Date/Time	Vert at 2:31:50 PM September 12, 2017
Trigger Source	Geo: 2.000 mm/s, Mic: 122.0 dB(L)
Range	Geo: 254.0 mm/s
Record Time	10.0 sec at 1024 sps

Serial Number	BE12878 V 10.72-1.1 Minimate Blaster
Battery Level	6.4 Volts
Unit Calibration	December 28, 2016 by Instantel
File Name	N878H2BX.P20

Notes
Quarry: Ogden Point
Client: CRH
User Name: Orica Canada Inc.
Operater: Kevin Myerscough

Setup Location
Set up @ North side of Main Gate

Microphone	Linear Weighting
PSPL	127.8 dB(L) at 1.767 sec
ZC Freq	7.4 Hz
Channel Test	Passed (Freq = 20.1 Hz Amp = 486 mv)

	Tran	Vert	Long	
PPV	9.271	5.207	4.699	mm/s
ZC Freq	18	30	18	Hz
Time (Rel. to Trig)	0.462	0.018	0.642	sec
Peak Acceleration	0.106	0.106	0.080	g
Peak Displacement	0.066	0.026	0.042	mm
Sensor Check	Passed	Passed	Passed	
Frequency	7.3	7.8	7.3	Hz
Overswing Ratio	3.8	3.4	4.2	

Peak Vector Sum 9.730 mm/s at 0.462 sec

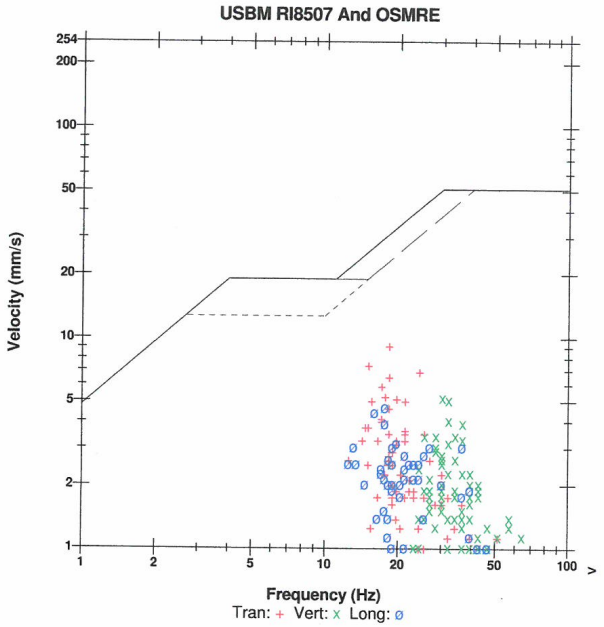

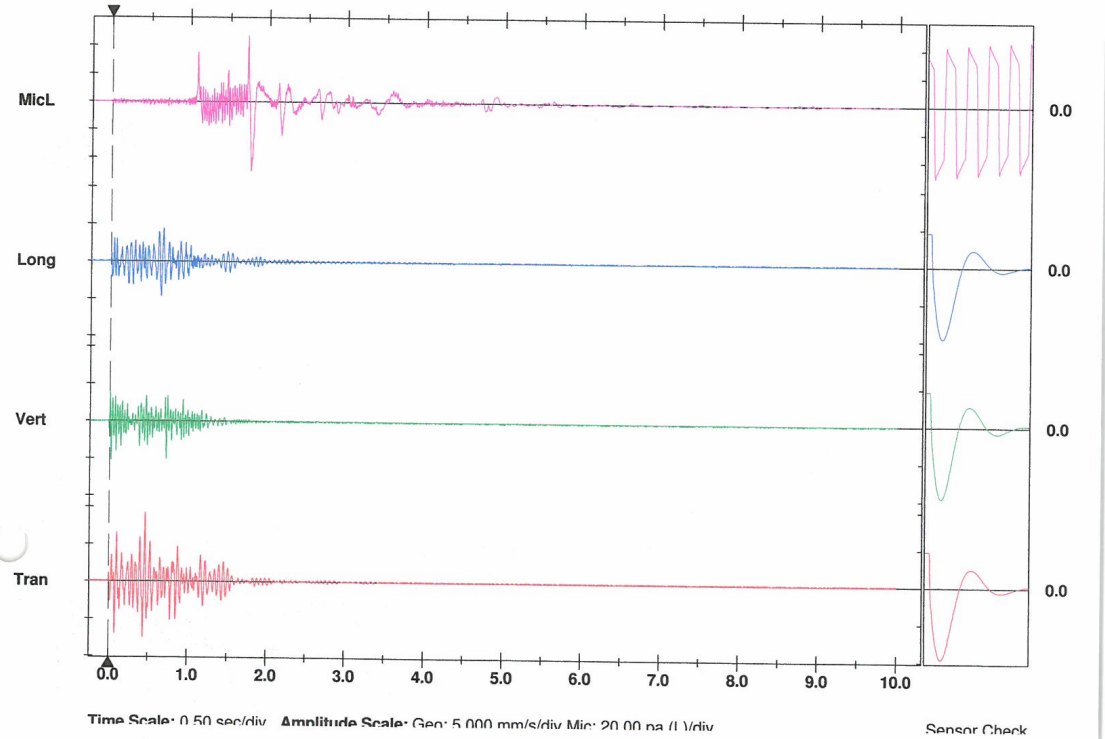

Date/Time Vert at 2:31:50 PM September 12, 2017
Trigger Source Geo: 2.000 mm/s, Mic: 122.0 dB(L)
Range Geo: 254.0 mm/s
Record Time 10.0 sec at 1024 sps

Serial Number BE12878 V 10.72-1.1 Minimate Blaster
Battery Level 6.4 Volts
Unit Calibration December 28, 2016 by Instantel
File Name N878H2BX.P20

Notes
Quarry: Ogden Point
Client: CRH
User Name: Orica Canada Inc.
Operater: Kevin Myerscough

Setup Location
Set up @ North side of Main Gate

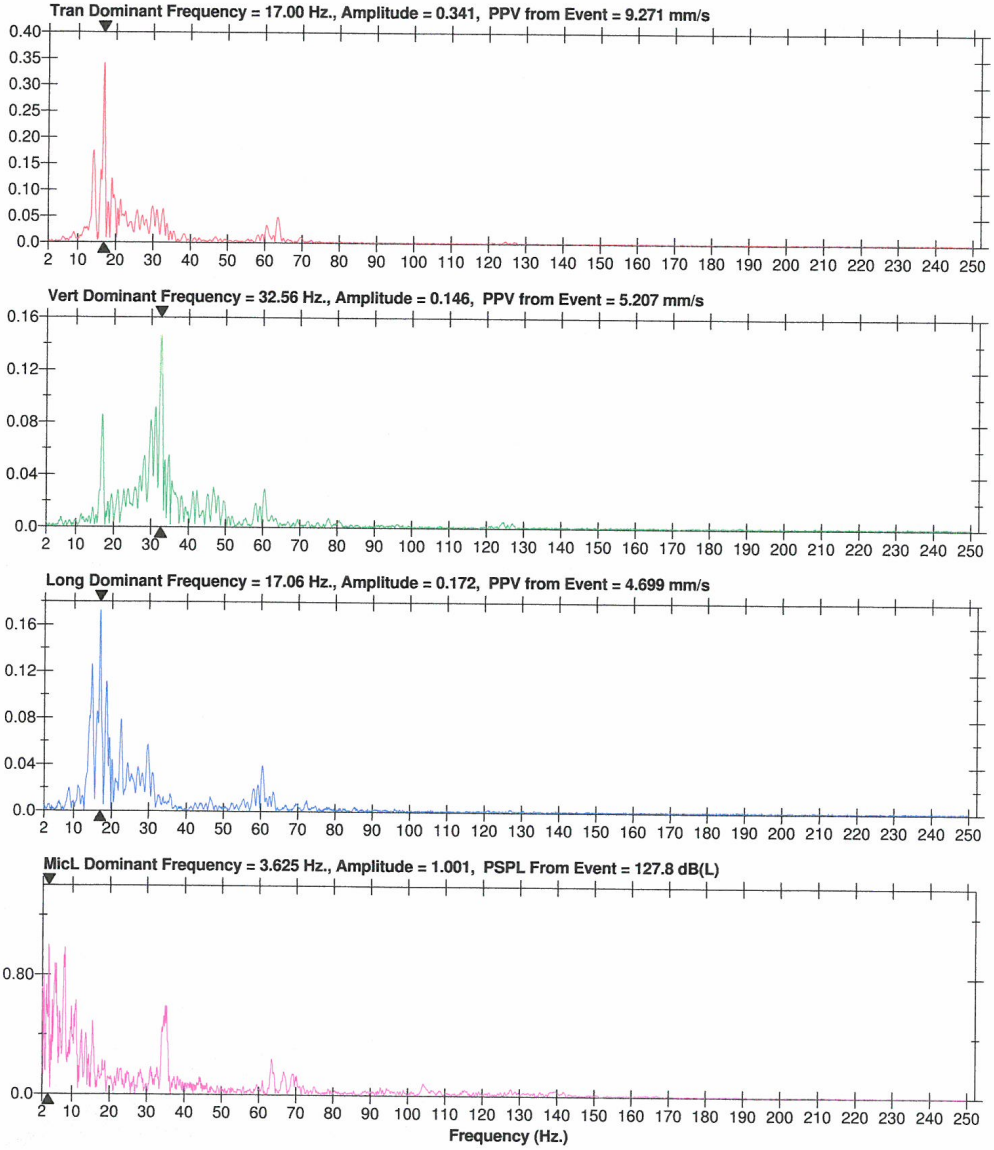

Event Report: Monitor Log - Micromate ISEE # UM6858-Compliance

Start Time	End Time	Status
----------	----------	SERIAL NUMBER: UM6858
Sep 12 /17 2:09:45 PM		Start Monitoring Waveform Geo: 2.00 in/s
Sep 12 /17 2:09:44 PM	Sep 12 /17 2:45:34 PM	No events recorded. (Keyboard Exit) Waveform Geo: 2.00 in/s

Ogden Point 17-017 Timing Diagram

3rd Bench, North Face, Middle
69 holes, 4" diameter, avg. depth is 59.41' including subdrill
14.5' x 15.7' front row, 13.5 x 15.7' second and third rows
Total footage is 4,099.5'
Face and body holes loaded to 6.5' collar with CG70 and E113 if required
15 ms between holes, 330 - 345 ms between rows, designed by Respec
2 initiation points per hole, 3 ms apart

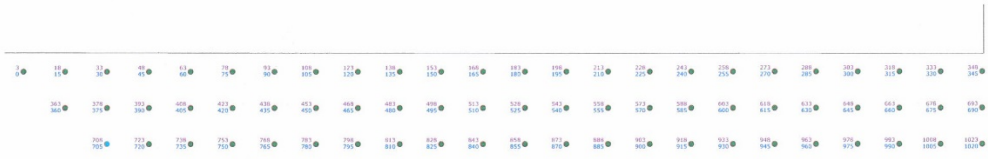

ORICA

Not to scale

SHOTPlus 5.6.4.3	12/09/2
Mine	Ogden Point
Location	3rd Bench, North Face, Middle
Title/author	Ogden Point 17-017, 3rd Bench, North/Mi
Filename	17-017 Timing.spf

Ogden Point 17-017 Bulk Load Sheet

3rd Bench, North Face, Middle
69 holes, 4" diameter, avg. depth is 59.41' including subdrill
14.5' x 15.7' front row, 13.5 x 15.7' second and third rows
Total footage is 4,099.5'

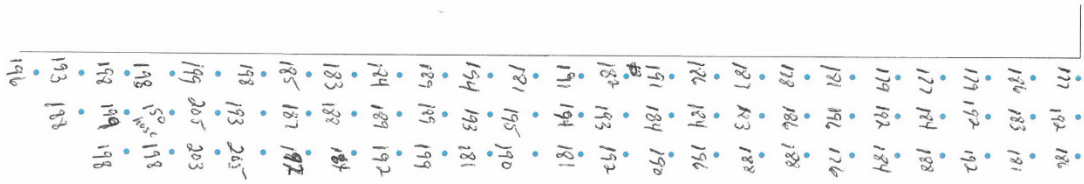

ORICA

Not to scale

SHOTPlus 5.6.4.3	11/09/2017
Mine	Ogden Point
Location	3rd Bench, North Face, Middle
Title/author	Ogden Point 17-017, 3rd Bench, North/Middle
Filename	17-017 Drill Plan.spf

ORICA
The Blasting Professionals™

Tie-in Verification

Quarry: Ogden Poir
Blast Number: 17-017
P.O. Number: 4500918309
Customer Name: DFA/CRH
Blast Date: 12-Sep-17

Tied in by: John Simpson (Print Name) Sign Off: _____ (Signature) Time: 11:00am

Logged by: Kevin Myerscough (Print Name) Sign Off: _____ (Signature) Time: 11:15am

Tie-in verified by: Kevin Myerscough (Print Name) Sign Off: _____ (Signature) Time: 11:30am

Inventory verified by: Andrew Rolston (Print Name) Sign Off: _____ (Signature) Time: 11:45am

Accessories Used in Blast:

____ m Handidet: __ / ____	ms	____ units	____ m Exel M	____ ms	____ units
____ m Handidet: __ / ____	ms	____ units	____ m Exel M	____ ms	____ units
____ m Handidet: __ / ____	ms	____ units	____ m Exel M	____ ms	____ units
____ m Connectadet:	____ ms	____ units	Lead-in Lines:		____ units
____ m Connectadet:	____ ms	____ units	Connecting Wire:		____ pails
____ m Connectadet:	____ ms	____ units	Electric MS:		____ units

Booster - 8 oz:	69	units	Other: E113 90x400 - 3 units
Booster - 12 oz:	69	units	____ units
Booster - 16 oz:	____	units	____ units
Booster - 16 oz Duo:	____	units	____ units

6	m UT600:	69	units	Harness Wire:	1 rolls
20	m UT600:	69	units		
____	m UT600:	____	units		
____	m UT600:	____	units		
____	m i-kon:	____	units	Harness Wire:	____ rolls
____	m i-kon:	____	units		
____	m i-kon:	____	units		
____	m i-kon:	____	units		

Blast Design

DFA / CRH (Ontario)

Quarry: Ogden Point
P.O. #: 4500918309
Design Date: 2017-09-08

Blast Number: 17-017
Orica Order #:

page 1

Blaster-in-charge: Kevin Myerscough (Print Name)

Blast Location: 3rd Bench, North Face, Middle (Bench / Face)
GPS Coordinates: 43.98780 °N Latitude (Centre of Blast) 77.87529 °W Longitude (Centre of Blast)

Design te Blasted: 62,893 te
Total Holes Loaded: 69 holes
... including: 3 Dead Holes
... and: 0 Helper Holes
Helper Hole Collar: 0.0 ft avg
Rows Blasted: 3 rows

- Drilling Information -

		mm	Angle from Vertical			=	Nominal Bit Diameter:
Primary Bit diam:	101.6	mm	0°	# Holes:	69	=	4,099.3 ft (4 " diam)
Secondary Bit diam:		mm	0°	# Holes:		=	0.0 ft (" diam)
Tertiary Bit diam:		mm	0°	# Holes:		=	0.0 ft (" diam)

- Design Pattern (Front Row)-
Burden: 14.5 ft avg
Spacing: 15.7 ft avg
Holes: 24 front row
- Design Pattern (Main Body) -
Burden: 13.5 ft avg
Spacing: 15.7 ft avg
Holes: 45 main body
Bench Height: 58.4 ft avg
Sub-drill: 1.0 ft avg
Hole Depth: 59.4 ft avg
- Design Stone Decking -
Front Row: ft avg
Main Body: ft avg
- Design Collar Stemming -
Front Row: 6.0 ft avg
Main Body: 6.0 ft avg
Material used: 3/4" clear

Bulk Expl. Required:

	kg
CENTRA GOLD 70	11,055

Pkgd Expl. Required:

		kg
E113 90X400	3	75

Boosters Required:

	kg/u	# used	kg
PENTEX 12 (OR EQUIVALENT)	0.34	69	23.5
PENTEX 8 (OR EQUIVALENT)	0.23	69	15.7

total explosives weight in Blast (kg): 11,169
Pkgd Prod (75 kg) % of Total kg: 0.7%

Detonators Required:

	ms	# req'd
UNITRONIC 600 20M	614781242-32	69
UNITRONIC 600 6M	615549365-15	69

Cord & Access. Req'd:

	U of M	# req'd
IRE DUPLEX (6 PACK) 400M	units	1
	units	
	units	

- Design Charge Length -
Front Row: 53.4 ft avg
Main Body: 53.4 ft avg
- Design Charge Weight -
Front Row: 155.7 kg/hole
Main Body: 155.7 kg/hole
Max Chge Wt / delay: 175 ~~[illegible]~~ kg/delay

Required kg Loaded: 11,169 kg
Rock Density: 2.65 g/cc = te/m³

- Design Powder Factor -
0.697 lb/yd³ Expected Yield PF: 0.178 kg/te (actual)
0.749 lb/yd³ Front row: 0.156 kg/te (theoretical)
0.732 lb/yd³ Main Body: 0.168 kg/te (theoretical)
"KPI" PF: 0.164 kg/te (theoretical)

Resource Deployment:

# of Blasts today (this Quarry)		1
# of Blasters (this Blast)		1
# of Helpers (this Blast)	Note Exception	2
# of MMU's (this Blast)		1

Services Req'd:

GPS LAYOUT	Enter hours	0.0
BULK TRUCK CHARGE	<2,000kg	
BLASTER HOURS	Enter Blaster hours	9.0
HELPER HOURS	Enter total Helper man-hours	14.0
SEISMOGRAPH RENTAL	Enter # Orica Seismographs	0
3D LASER PROFILE	Enter hours	0
BORETRACK	Enter hours	1
TECHNICAL BLAST DESIGN	(per day) Enter # of days	0.0

Cost Reduction Notes (this Blast) - change in Bit , B, S, Expl or IS from previous Blast:

ORICA
The Blasting Professionals™

Blast Design

DFA / DIV of CRH (Ontario)

Quarry: Ogden Point
P.O. #:
Blast Date: 12/09/2017

Blast Number: 17-017
Orica Order #:

page 2

Paste ShotPlus Diagram inside Rectangle:

Ogden Point 17-017
69 holes total, 4"
14.5'x15.7' front row
13.5'x15.7' body rows

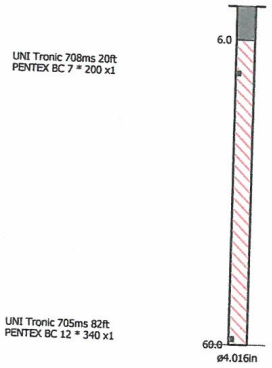

Orica
Blaster-in-charge: Kevin Myerscough

DFA / CRH
Quarry Manager:

Signature required, indicating sign off on Blast Design

Ogden Point 17-09-12 #17 3rd Bench, North Face, Middle

Design p2

Ogden Point 17-017 Drill Plan

3rd Bench, North Face, Middle
69 holes, 4" diameter, avg. depth is 59.41' including subdrill
14.5' x 15.7' front row, 13.5 x 15.7' second and third rows
Total footage is 4,099.5'

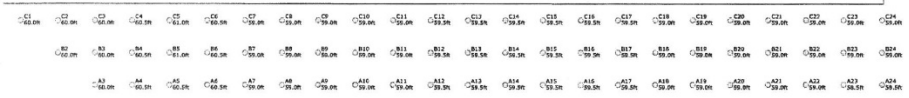

ORICA

Scale 1:500

SHOTPlus 5.6.4.3	23/08/201
Mine	Ogden Point
Location	3rd Bench, North Face, Middle
Title/author	Ogden Point 17-017, 3rd Bench, North/Middl
Filename	Ogden Point 17-017 Drill Plan.spf

23/08/2017

Driller's Log

ORICA

Mine	Ogden Point
Location	3rd Bench, North Face, Middle
Title	Ogden Point 17-017, 3rd Bench, North/Middle Fa Kevin Myerscough
Filename	Ogden Point 17-017 Drill Plan.spf
Comment	

Row ID	Hole ID	Design Angle	Design Depth	Measured Depth	Comments
B					
B	B2	0.0	60.0	59	
B	B3	0.0	60.0	59.5	
B	B4	0.0	60.5	60.1	
B	B5	0.0	61.0	61	
B	B6	0.0	60.5	59.4	Redrill
B	B7	0.0	59.0	57.9	Redrill
B	B8	0.0	59.0	56.5	Redrill
B	B9	0.0	59.0	57.9	Redrill
B	B10	0.0	59.0	58.3	
B	B11	0.0	59.0	57.8	Redrill
B	B12	0.0	59.5	59.2	
B	B13	0.0	59.5	59.9	
B	B14	0.0	59.5	58	
B	B15	0.0	59.5	59	
B	B16	0.0	59.5	58.2	Redrill
B	B17	0.0	59.5	59	
B	B18	0.0	59.0	58.8	
B	B19	0.0	59.0	58.3	
B	B20	0.0	59.0	58.1	
B	B21	0.0	59.0	56.7	Redrill
B	B22	0.0	59.0	58.7	
B	B23	0.0	59.0	59	
B	B24	0.0	59.0	59.5	

SHOTPlus 5 Plan

Blast Summary Data

Burden: 13.5ft	Spacing: 15.0ft	Subdrill: 1.0ft	Stemming: 7.0ft
1st row burden: 14.0ft	Hole Diameter: 4.0in	Number of holes: 66	Hole angle: 0.0°
Rock density: 2.65g/cc	Total drilled: 3910.6ft	Blasted tonnage: 62,445S/T	

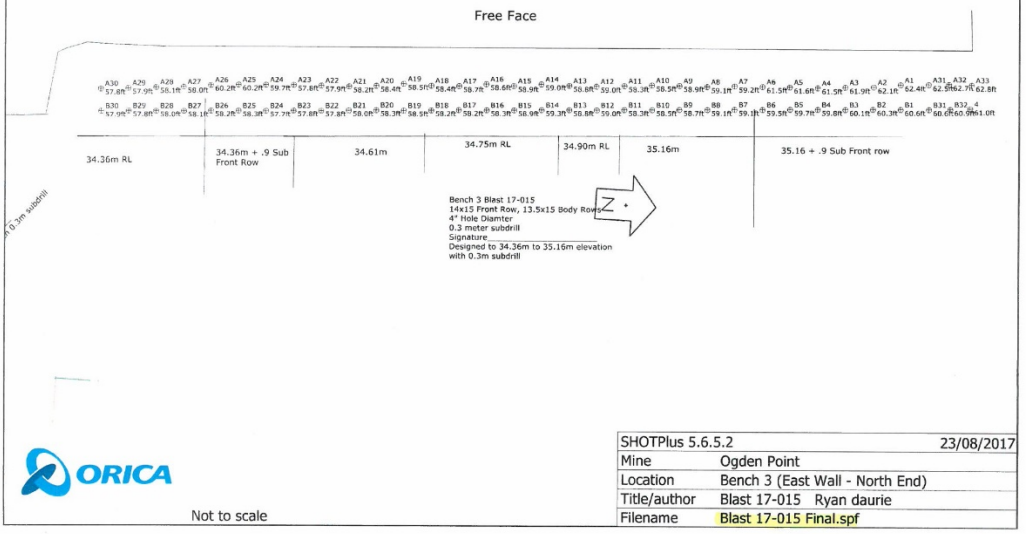

ORICA

Not to scale

SHOTPlus 5.6.5.2	23/08/2017
Mine	Ogden Point
Location	Bench 3 (East Wall - North End)
Title/author	Blast 17-015 Ryan daurie
Filename	Blast 17-015 Final.spf

23/08/2017

Driller's Log

ORICA

Mine	Ogden Point
Location	Bench 3 (East Wall - North End)
Title	Blast 17-015 Ryan daurie
Filename	Blast 17-015 Final.spf
Comment	

Row ID	Hole ID	Design Angle	Design Depth	Measured Depth	Comments
Indep.	B5	0.0	59.7		
Indep.	B6	0.0	59.5		
Indep.	B7	0.0	59.1		
Indep.	B8	0.0	59.1		
Indep.	B9	0.0	58.7		
Indep.	B10	0.0	58.5		
Indep.	B11	0.0	58.3		
Indep.	B12	0.0	59.0		
Indep.	B13	0.0	58.8		
Indep.	B14	0.0	59.3		
Indep.	B15	0.0	58.9		
Indep.	B16	0.0	58.3		
Indep.	B17	0.0	58.2		
Indep.	B18	0.0	58.2		
Indep.	B19	0.0	58.5		
Indep.	B20	0.0	58.3		
Indep.	B21	0.0	58.0		
Indep.	B22	0.0	57.8		
Indep.	B23	0.0	57.8		
Indep.	B24	0.0	57.7		
Indep.	B25	0.0	58.3		
Indep.	B26	0.0	58.2		
Indep.	B27	0.0	58.1		
Indep.	B28	0.0	58.0		
Indep.	B29	0.0	57.8		
Indep.	A31	0.0	62.5		
Indep.	A32	0.0	62.7		
Indep.	A33	0.0	62.8		
Indep.	4	0.0	61.0		
Indep.	B32	0.0	60.9		
Indep.	B31	0.0	60.6		

Blast Report

DFA / CRH (Ontario)

Quarry: Ogden Point | Blast Number: 17-020
P.O. #: 4500940667 | Orica Order #: 2238624
Blast Date: 2017-09-13 | Blast Time: 12:59 PM

page 1

Blaster-in-charge: Kevin Myerscough (Print Name)

Blast Location: Bench 3, North Face, East End (Bench / Face)
GPS Coordinates: 43.98783 °N Latitude (Centre of Blast) 77.87391 °W Longitude (Centre of Blast)

Wind from the: E at 5 kph Temperature: 16 to 20 °C

Clear:		Rain:	X	Overcast:	X
Partly Cloudy:	X	Snow:		Inversion:	Ceiling 30,000 ft

- Drilling Information -

			Angle from Vertical				Nominal Bit Diameter:
Primary Bit diam:	101.6	mm	0°	# Holes: 72	=	4,320.0 ft	(4 " diam)
Secondary Bit diam:		mm	0°	# Holes:	=	0.0 ft	(" diam)
Tertiary Bit diam:		mm	0°	# Holes:	=	0.0 ft	(" diam)

Bulk Explosives:

	in (kg)	out (kg)	kg
CENTRA GOLD 70	34,000	22,300	11,700

Packaged Explosives:

	cs shipped	cs returned	kg
E113 90X400	2	0	50
FORTEL PRO 75X400	10	3	175
FORTEL PRO 90X400	13	6	175

Boosters:

	kg / unit	# usec	kg
PENTEX 8 (OR EQUIVALENT)	0.23	72	16.3
PENTEX 12 (OR EQUIVALENT)	0.34	72	24.5

total explosives weight in Blast (kg): 12,141
Pkgd Prod (400 kg) % of Total kg: 3.3%

Detonators:

	case #'s	ms	# used
UNITRONIC 600 6M			72
UNITRONIC 600 20M			72

Cord & Accessories:

	U of M	# used
HARNESS WIRE DUPLEX (6 PACK) 400M	units	1
	units	
	units	

Resource Deployment:

# of Blasts today (this Quarry)		1
# of Blasters (this Blast)		1
# of Helpers (this Blast)	Note Exception	2
# of MMU's (this Blast)		1

Services:

GPS LAYOUT	Enter hours	0.0
BULK TRUCK CHARGE	>/=10,000 kg	1
BLASTER HOURS	Enter Blaster hours	9.5
HELPER HOURS	Enter total Helper man-hours	13.0
SEISMOGRAPH RENTAL	Enter # Orica Seismographs	0
3D LASER PROFILE	Enter hours	0.0
BORETRACK	Enter hours	0.0
TECHNICAL BLAST DESIGN	(per day) Enter # of days	0.0

tonnes Blasted:	69,301 te
Total tonnes per day:	69,301 te (OPBB40 Rate Code)
Total Holes Loaded:	72 holes
... including:	Dead Holes
... and:	Helper Holes
Helper Hole Collar:	ft avg
# Rows Blasted:	3 rows
- Pattern (Front Row)-	
Burden:	14.5 ft avg
Spacing:	15.7 ft avg
# Holes:	25 front row
- Pattern (Main Body) -	
Burden:	13.5 ft avg
Spacing:	15.7 ft avg
# Holes:	47 main body
Bench Height:	59.0 ft avg
Sub-drill:	1.0 ft avg
Hole Depth:	60.0 ft avg
- Stone Decking -	
Front Row:	ft avg
Main Body:	ft avg
# Decks:	per blast
- Collar Stemming -	
Front Row:	7.0 ft avg
Main Body:	7.0 ft avg
Material used:	3/4" clear
- Charge Length -	
Front Row:	53.0 ft avg
Main Body:	53.0 ft avg
- Charge Weight -	
Front Row:	154.5 kg/hole
Main Body:	154.5 kg/hole
Max. per delay:	204.0 kg/delay
SD () Equation:	141.4 kg/delay
Total kg Loaded:	12,141 kg
Rock Density:	2.65 g/cc = te/m³

Theoretical PF (Based on a single hole)

0.783 lb/yd³
0.685 lb/yd³
0.736 lb/yd³
0.719 lb/yd³

- Powder Factor -

Yield PF:	0.175	kg/te (actual)
Front row:	0.153	kg/te (theoretical)
Main Body:	0.165	kg/te (theoretical)
"KPI" PF:	0.161	kg/te (theoretical)

Yield Powder Factor (kg Loaded / te Blastec

Cost Reduction Notes (this Blast) - change in Bit , B, S, Expl or IS from previous Blast:

ORICA
The Blasting Professionals™

Blast Report

DFA / DIV of CRH (Ontario

Quarry:	Ogden Point	Blast Number:	17-020
P.O. #:	4500940667	Orica Order #:	2238624
Blast Date:	2017-09-13	Blast Time:	12:59 PM

page 2

Blast Co-ordinates	Enter ° N Lat.	Enter ° W Long.	(N) Radians	(W) Radians
Mid Blast				
Front Row Corner	43.98782	77.87318	0.767732	1.359143
Back Row Corner	43.98784	77.87463	0.767733	1.359169
Average (Centre of Blast)	43.98783	77.87391	0.767732	1.359156

1st

Seismograph Co-ordinates	Enter ° N Lat.	Enter ° W Long.	(N) Radians	(W) Radians
1st Reading	43.98741	77.86949	0.767725	1.359079
2nd Reading				
Average	43.98741	77.86949	0.767725	1.359079

Distance (1st Seis. From Centre of Blast)	356.7	m	
Post Blast Data: ppV:	7.1	mm/s	Trigger set at: 2.0 mm/s
frequency:	19.0	Hz	V / T / L : L (Vertical, Transverse or Longitudinal)
air overpressure:	124.3	dB	Trigger set at: 115 dB

North Side of Main Gate

2nd

Seismograph Co-ordinates	Enter ° N Lat.	Enter ° W Long.	(N) Radians	(W) Radians
1st Reading	43.99522	77.86748	0.767861	1.359044
2nd Reading				
Average	43.99522	77.86748	0.767861	1.359044

Distance (2nd Seis. From Centre of Blast)	970.4	m	
Post Blast Data: ppV:	DNT	mm/s	Trigger set at: 2.0 mm/s
frequency:	0.0	Hz	V / T / L : ? (Vertical, Transverse or Longitudinal)
air overpressure:	0.0	dB	Trigger set at: 115 dB

CP Tracks, NE corner of property - Did Not Trigger

3rd

Seismograph Co-ordinates	Enter ° N Lat.	Enter ° W Long.	(N) Radians	(W) Radians
1st Reading				
2nd Reading				
Average	0.00000	0.00000	0.000000	0.000000

Distance (3rd Seis. From Centre of Blast)	0.0	m	
Post Blast Data: ppV:	0.0	mm/s	Trigger set at: 2.0 mm/s
frequency:	0.0	Hz	V / T / L : ? (Vertical, Transverse or Longitudinal)
air overpressure:	0.0	dB	Trigger set at: 115 dB

Scaling Factor denotes the degree of Blast confinement.
The higher the SF, the more confined the Blast.
A Scaling Factor of 30 is commonly used in the Scaled Distance formula for Quarry Bench Blasting:

Enter a scaling Factor: 30 Quarry Bench Blasting - 2 Free Faces

$$W = \frac{D^2}{30^2}$$

$$= \frac{(356.7)^2}{30^2} \text{ kg}$$

$$= \frac{127{,}235}{900} \text{ kg}$$

Maximum Indicated Charge Weight per Delay = 141 kg

jim bray

Orica
Blaster-in-charge: Kevin Myerscough

Signature required, indicating that Blast Report is Complete & Accurate.

Event Report: Monitor Log - Micromate ISEE # UM6858-Compliance

Start Time	End Time	Status
----------	----------	SERIAL NUMBER: UM6858
Sep 13 /17 12:39:58 PM		Start Monitoring Waveform Geo: 2.00 in/s
Sep 13 /17 12:39:58 PM	Sep 13 /17 1:09:36 PM	No events recorded. (Keyboard Exit) Waveform Geo: 2.00 in/s

Date/Time	Vert at 12:59:48 PM September 13, 2017
Trigger Source	Geo: 2.000 mm/s, Mic: 122.0 dB(L)
Range	Geo: 254.0 mm/s
Record Time	10.0 sec at 1024 sps

Serial Number	BE12878 V 10.72-1.1 Minimate Blaster
Battery Level	6.4 Volts
Unit Calibration	December 28, 2016 by Instantel
File Name	N878H2DO.3O0

Notes
Quarry: Ogden Point
Client: CRH
User Name: Orica Canada Inc.
Operater: Kevin Myerscough

Setup Location
Set up @ North side of Main Gate

Microphone	Linear Weighting
PSPL	124.3 dB(L) at 1.076 sec
ZC Freq	9.1 Hz
Channel Test	Passed (Freq = 20.1 Hz Amp = 504 mv)

	Tran	Vert	Long	
PPV	6.731	6.858	7.112	mm/s
ZC Freq	51	39	19	Hz
Time (Rel. to Trig)	0.954	0.624	0.605	sec
Peak Acceleration	0.252	0.159	0.186	g
Peak Displacement	0.040	0.025	0.047	mm
Sensor Check	Passed	Passed	Passed	
Frequency	7.4	7.8	7.3	Hz
Overswing Ratio	3.8	3.4	4.2	

Peak Vector Sum 9.653 mm/s at 0.840 sec

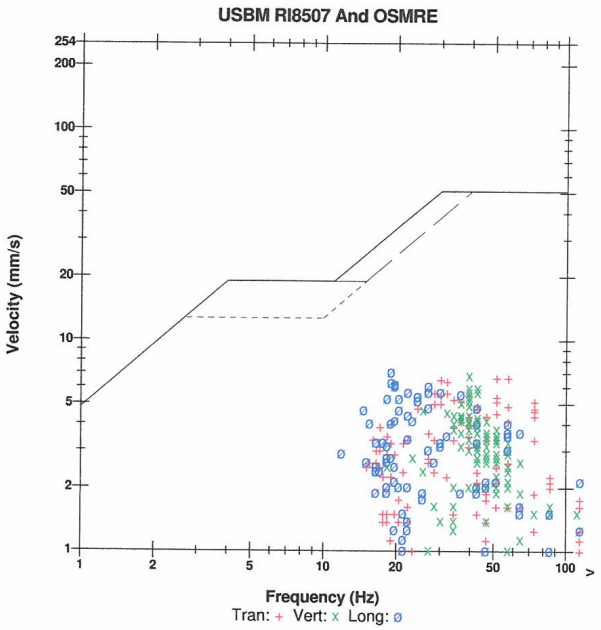

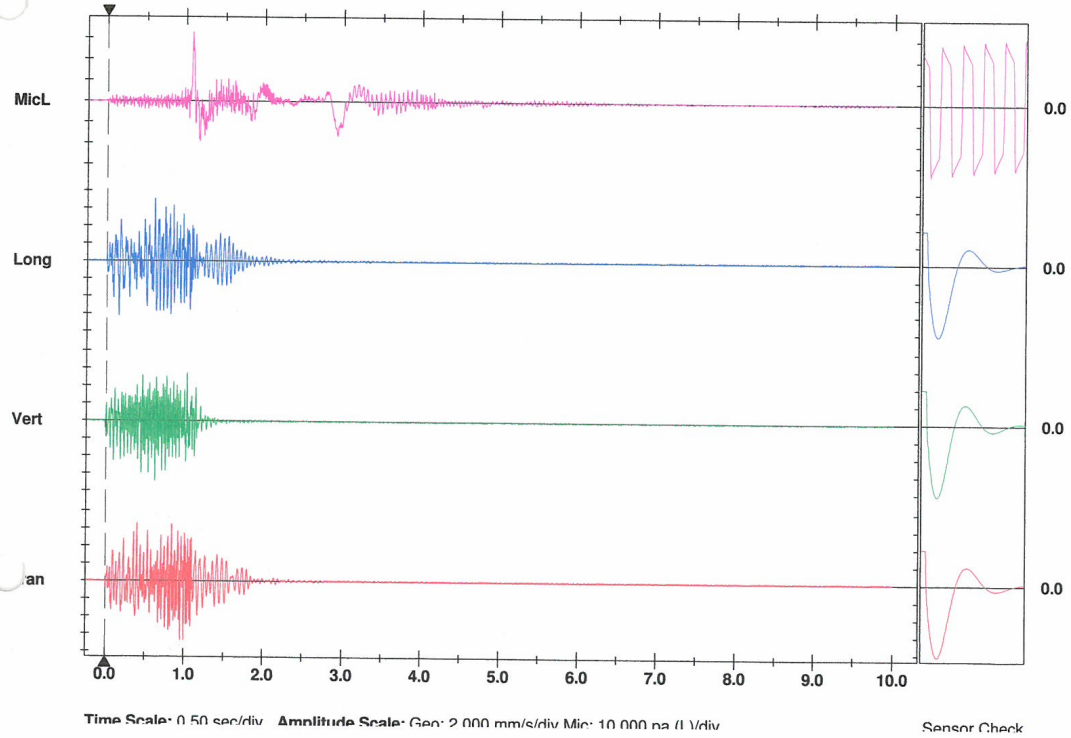

Date/Time Vert at 12:59:48 PM September 13, 2017
Trigger Source Geo: 2.000 mm/s, Mic: 122.0 dB(L)
Range Geo: 254.0 mm/s
Record Time 10.0 sec at 1024 sps

Serial Number BE12878 V 10.72-1.1 Minimate Blaster
Battery Level 6.4 Volts
Unit Calibration December 28, 2016 by Instantel
File Name N878H2DO.3O0

Notes
Quarry: Ogden Point
Client: CRH
User Name: Orica Canada Inc.
Operater: Kevin Myerscough

Setup Location
Set up @ North side of Main Gate

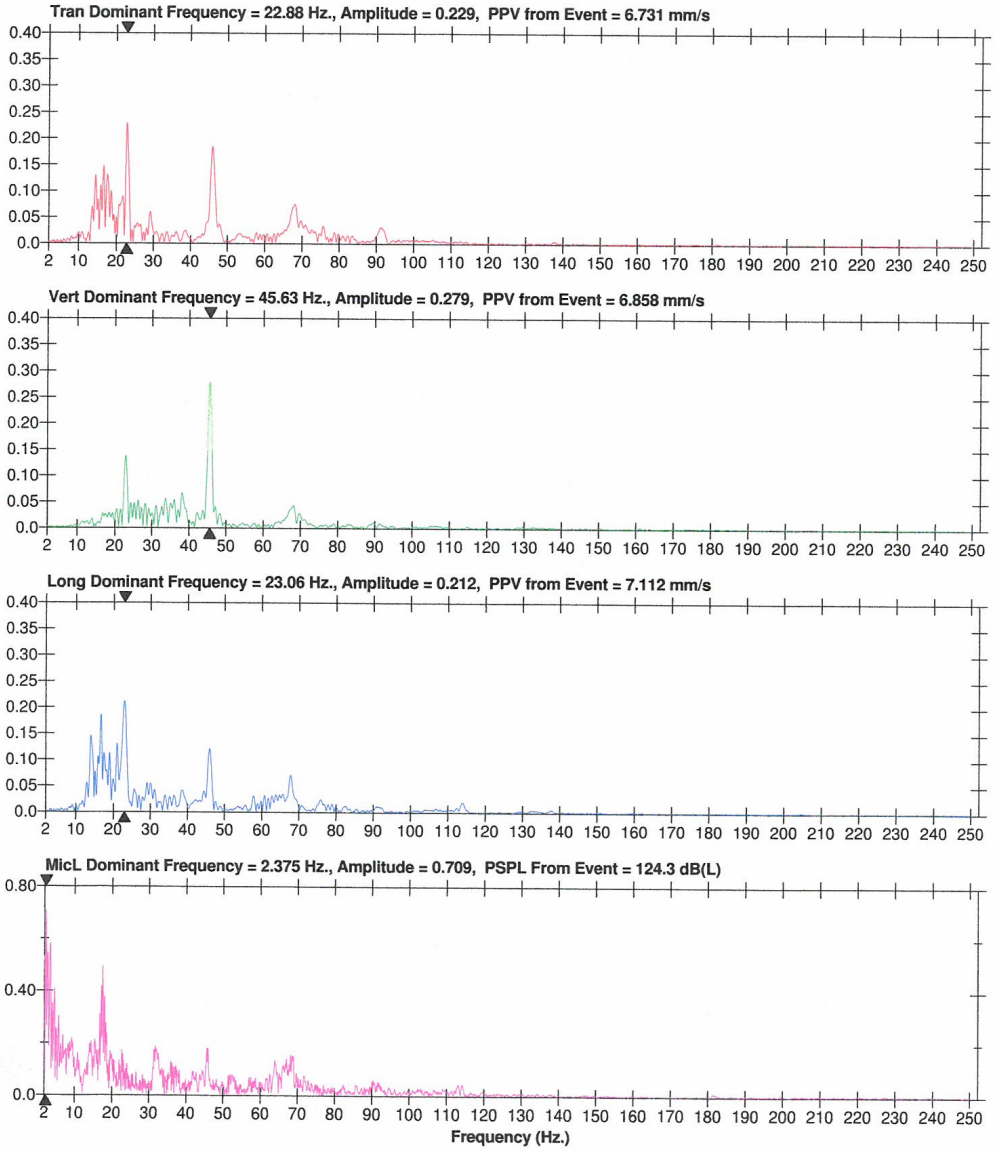

SHOTPlus 5 Plan

Ogden Point 17-020, 3rd Level - North Face, East End Timing Diagram

72 holes, 4" dia., avg. depth is 60' including subdrill
14.5' x 15.7' on front row, 13.5' x 15.7' on second and third rows
Total drilling is 4,321'
Face and body holes loaded to 6' collar with CG70 and E113 if required
Timing predetermined by Respec
2 initiation points per hole, 3 ms apart

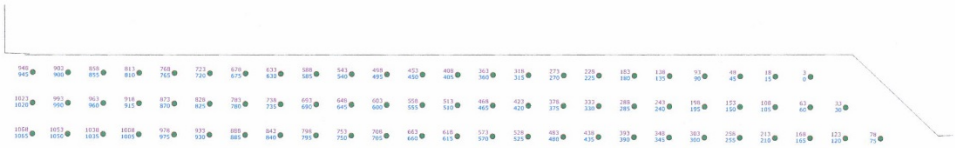

ORICA

Not to scale

SHOTPlus 5.6.4.3	13/09/2
Mine	Ogden Point
Location	3rd Level, North Face, East End
Title/author	Ogden Point 17-020 Kevin Myerscough
Filename	17-020 Bench 3 2017 [illegible]-13.spf

Ogden Point 17-020, 3rd Level - North Face, East End Bulk Load Sheet

72 holes, 4" dia., avg. depth is 60' including subdrill
14.5' x 15.7' on front row, 13.5' x 15.7' on second and third rows
Total drilling is 4,321'

These holes were originally planned to be part of this blast, however since this blast is being shot before 17-015, they will be added to that blast

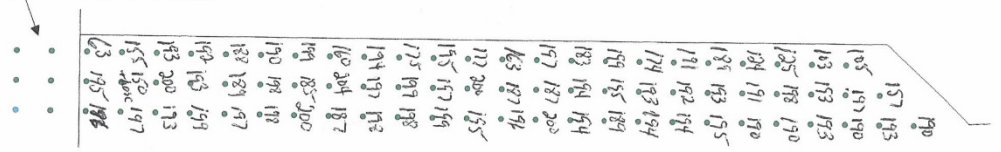

ORICA

Not to scale

SHOTPlus 5.6.4.3	12/09/2017
Mine	Ogden Point
Location	3rd Level, North Face, East End
Title/author	Ogden Point 17-020 Kevin Myerscough
Filename	17-020 Bench 3 Drill Plan.s

ORICA
The Blasting Professionals™

Tie-in Verification

Quarry: Ogden Poir
Blast Number: 17-020
P.O. Number: 4500940667
Customer Name: DFA/CRH
Blast Date: 13-Sep-17

Tied in by:	Brad Crook (Print Name)	Sign Off:	(Signature)	Time: 11:30am
Logged by:	Kevin Myerscough (Print Name)	Sign Off:	(Signature)	Time: 11:45am
Tie-in verified by:	Kevin Myerscough (Print Name)	Sign Off:	(Signature)	Time: 12:00pm
Inventory verified by:	Andrew Rolston (Print Name)	Sign Off:	(Signature)	Time: 12:15pm.

Accessories Used in Blast:

____ m Handidet: __ / ____ ms ____ units		____ m Exel MS ____ ms ____ units	
____ m Handidet: __ / ____ ms ____ units		____ m Exel MS ____ ms ____ units	
____ m Handidet: __ / ____ ms ____ units		____ m Exel MS ____ ms ____ units	
____ m Connectadet: ____ ms ____ units		Lead-in Lines: ____ units	
____ m Connectadet: ____ ms ____ units		Connecting Wire: ____ pails	
____ m Connectadet: ____ ms ____ units		Electric MS: ____ units	
Booster - 8 oz: 72 units		Other: E113 90x400- 9 units	
Booster - 12 oz: 72 units		E113 75x400- 7 units	
Booster - 16 oz: ____ units		____ units	
Booster - 16 oz Duo: ____ units		____ units	
6 m UT600: 72 units		Harness Wire: 1 rolls	
20 m UT600: 72 units			
____ m UT600: ____ units			
____ m UT600: ____ units			
____ m i-kon: ____ units		Harness Wire: ____ rolls	
____ m i-kon: ____ units			
____ m i-kon: ____ units			
____ m i-kon: ____ units			

Blast Design
DFA / CRH (Ontario)

Quarry: Ogden Point
P.O. #: 4500940667
Design Date: 2017-09-12

Blast Number: 17-020
Orica Order #:

page 1

Blaster-in-charge: Kevin Myerscough (Print Name)

Blast Location: Bench 3, North Face, East End (Bench / Face)
GPS Coordinates: enter data on p2 °N Latitude (Centre of Blast) enter data on p2 °W Longitude (Centre of Blast)

Design te Blasted:	69,301	te
Total Holes Loaded:	72	holes
... including:	0	Dead Holes
... and:	0	Helper Holes
Helper Hole Collar:	0.0	ft avg
# Rows Blasted:	3	rows

- Drilling Information -

		Angle from Vertical			Nominal Bit Diameter:
Primary Bit diam:	101.6 mm	0°	# Holes:	72	= 4,320.0 ft (4 " diam)
Secondary Bit diam:	mm	0°	# Holes:		= 0.0 ft (" diam)
Tertiary Bit diam:	mm	0°	# Holes:		= 0.0 ft (" diam)

- Design Pattern (Front Row)-

Burden:	14.5	ft avg
Spacing:	15.7	ft avg
# Holes:	25	front row

- Design Pattern (Main Body) -

Burden:	13.5	ft avg
Spacing:	15.7	ft avg
# Holes:	47	main body
Bench Height:	59.0	ft avg
Sub-drill:	1.0	ft avg
Hole Depth:	60.0	ft avg

- Design Stone Decking -

Front Row:		ft avg
Main Body:		ft avg

- Design Collar Stemming -

Front Row:	6.5	ft avg
Main Body:	6.5	ft avg
Material used:	3/4" clear	

Bulk Expl. Required:

		kg
CENTRA GOLD 70		12,150

Pkgd Expl. Required:

		kg
E113 90X400	6	150
E113 75X400	4	100

Boosters Required:

	kg/u	# used	kg
PENTEX 8 (OR EQUIVALENT)	0.23	72	16.3
PENTEX 12 (OR EQUIVALENT)	0.34	72	24.5

total explosives weight in Blast (kg):	12,441
Pkgd Prod (250 kg) % of Total kg:	2.0%

Detonators Required:

	ms	# req'd
UNITRONIC 600 6M		72
UNITRONIC 600 20M		72

Cord & Access. Req'd:

	U of M	# req'd
IRE DUPLEX (6 PACK) 400M	units	1
	units	
	units	

- Design Charge Length -

Front Row:	53.5 ft avg
Main Body:	53.5 ft avg

- Design Charge Weight -

Front Row:	156.0 kg/hole
Main Body:	156.0 kg/hole
Max Chge Wt / delay:	185.0 kg/delay

Required kg Loaded:	12,441	kg
Rock Density:	2.65	g/cc = te/m^3

- Design Powder Factor -

	Expected Yield PF:	0.180 kg/te (actual)
0.691 lb/yd^3	Front row:	0.155 kg/te (theoretical)
0.743 lb/yd^3	Main Body:	0.166 kg/te (theoretical)
0.726 lb/yd^3	"KPI" PF:	0.162 kg/te (theoretical)

Resource Deployment:

# of Blasts today (this Quarry)		1
# of Blasters (this Blast)		1
# of Helpers (this Blast)	Note Exception	2
# of MMU's (this Blast)		1

Services Req'd:

GPS LAYOUT	Enter hours	0.0
BULK TRUCK CHARGE	<2,000kg	
BLASTER HOURS	Enter Blaster hours	9.0
HELPER HOURS	Enter total Helper man-hours	14.0
SEISMOGRAPH RENTAL	Enter # Orica Seismographs	0
3D LASER PROFILE	Enter hours	0
BORETRACK	Enter hours	1
TECHNICAL BLAST DESIGN	(per day) Enter # of days	0.0

Cost Reduction Notes (this Blast) - change in Bit , B, S, Expl or IS from previous Blast:

ORICA
The Blasting Professionals™

Blast Design

DFA / DIV of CRH (Ontario)

Quarry:	Ogden Point	Blast Number:	ECTB1689
P.O. #:	4500940667	Orica Order #:	
Blast Date:	13/09/2017		

page 2

Paste ShotPlus Diagram inside Rectangle:

Bench 3, North Face, East End
72 holes, 4", 60' deep including subdrill
14.5'x15.7' front row
13.5'x15.7' body

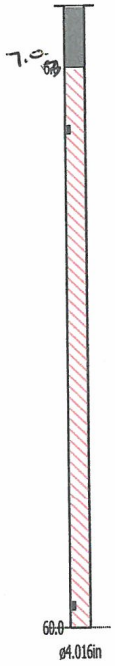

jim bray

Orica
Blaster-in-charge: Kevin Myerscough

DFA / CRH
Quarry Manager:

Signature required, indicating sign off on Blast Design.

17-020 Bench 3 2017-09-13 BBR

=~=~=~=~=~=~=~=~=~=~=~=~= PuTTY log 2017.09.13 14:35:11 =~=~=~=~=~=~=~=~=~=~=~=

\@{p\o|yxl

4

uni tronic600 BlastBox Report - SN: 1160   Version: 02.03

144 DETS IN BLAST.

NO GLOBALS

POS-	DET ID	DELAY	STATUS
1	451A490A	0	Ok
2	42180B15	3	Ok
3	451A4908	15	Ok
4	42180B27	18	Ok
5	451A4906	30	Ok
6	42180B14	33	Ok
7	451A4902	45	Ok
8	42180B13	48	Ok
9	451F5EC9	60	Ok
10	42180AEB	63	Ok
11	451A491E	75	Ok
12	42180AEC	78	Ok
13	451A4900	120	Ok
14	42180B37	123	Ok
15	45211FCA	165	Ok
16	42180B26	168	Ok
17	45211FCC	210	Ok
18	42180B17	213	Ok
19	451A4922	255	Ok
20	42180B16	258	Ok
21	451A490C	300	Ok
22	42180B01	303	Ok
23	451A4930	345	Ok
24	42180AED	348	Ok
25	45211FC0	390	Ok
26	42180B02	393	Ok
27	451A4924	435	Ok
28	42180B03	438	Ok
29	451A4912	480	Ok
30	42180AEE	483	Ok
31	451A4916	525	Ok
32	42180B04	528	Ok
33	451A4920	570	Ok
34	42180AEF	573	Ok
35	45211FD2	615	Ok
36	42180B05	618	Ok
37	452120FB	660	Ok
38	42180AF0	663	Ok
39	452120F3	705	Ok
40	42180B06	708	Ok
41	4521CBB0	750	Ok
42	42180B28	753	Ok
43	4521CB6A	795	Ok
44	42180B29	798	Ok
45	4521CBA2	840	Ok
46	42180B2D	843	Ok
47	4521CBB6	885	Ok
48	42180B18	888	Ok
49	45211FDA	930	Ok
50	42180B1A	933	Ok
51	4521CB8E	975	Ok
52	42180B2E	978	Ok
53	45211FDE	1005	Ok
54	42180B08	1008	Ok
55	45211FE0	1035	Ok
56	42180B31	1038	Ok
57	45211FD4	1050	Ok
58	42180B1D	1053	Ok
59	4521CB92	1065	Ok

60	42180B30	1068	Ok
61	45211FD8	1020	Ok
62	42180B1C	1023	Ok
63	45211FE6	990	Ok
64	42180B32	993	Ok
65	45211FE2	960	Ok
66	42180B0B	963	Ok
67	4521CB98	915	Ok
68	42180B2F	918	Ok
69	45211FD6	870	Ok
70	42180B09	873	Ok
71	45211FDC	825	Ok
72	42180B1B	828	Ok
73	4521CBB8	780	Ok
74	42180B19	783	Ok
75	4521CBAE	735	Ok
76	42180B2C	738	Ok
77	4521CBB2	690	Ok
78	42180B2A	693	Ok
79	4521CBAC	645	Ok
80	42180B2B	648	Ok
81	452120F7	600	Ok
82	42180B33	603	Ok
83	452120F9	555	Ok
84	42180B21	558	Ok
85	4521CB78	510	Ok
86	42180B35	513	Ok
87	4521CB7A	465	Ok
88	42180AFA	468	Ok
89	45211FD0	420	Ok
90	42180B25	423	Ok
91	45211FC2	375	Ok
92	42180AFD	378	Ok
93	451A4938	330	Ok
94	42180B10	333	Ok
95	451A491C	285	Ok
96	42180AFF	288	Ok
97	451A4936	240	Ok
98	42180B11	243	Ok
99	451A48FE	195	Ok
100	42180AE8	198	Ok
101	451A48FC	150	Ok
102	42180B00	153	Ok
103	45211FCE	105	Ok
104	42180AEA	108	Ok
105	451A48F8	90	Ok
106	42180AE9	93	Ok
107	451A4914	135	Ok
108	42180B12	138	Ok
109	451A4904	180	Ok
110	42180B24	183	Ok
111	451A491A	225	Ok
112	42180AFE	228	Ok
113	451B4326	270	Ok
114	42180B0F	273	Ok
115	451F5ECD	315	Ok
116	42180B36	318	Ok
117	451F5ECB	360	Ok
118	42180AFC	363	Ok
119	45211FEE	405	Ok
120	42180AFB	408	Ok
121	452120F5	450	Ok
122	42180B0E	453	Ok
123	452120FD	495	Ok
124	42180B23	498	Ok
125	4521CB7E	540	Ok
126	42180B22	543	Ok
127	45211FC4	585	Ok

```
128 42180AF9   588 Ok
129 45211FEC   630 Ok
130 42180B0D   633 Ok
131 4521CB80   675 Ok
132 42180B34   678 Ok
133 4521CB7C   720 Ok
134 42180B0C   723 Ok
135 45211FEA   765 Ok
136 42180AF8   768 Ok
137 45211FE4   810 Ok
138 42180B1F   813 Ok
139 45211FE8   855 Ok
140 42180B0A   858 Ok
141 45211FC6   900 Ok
142 42180B20   903 Ok
143 45211FC8   945 Ok
144 42180B1E   948 Ok

Dates are d/m/y h:m
Download    13/09/17 12:59
Blast ARMED 13/09/17 12:59
Blast FIRED 13/09/17 13:02
Current draw(mA): A:12  B:10

Orica Mining Services
```

Blast Report

DFA / CRH (Ontario)

Quarry:	Ogden Point	Blast Number:	17-028
P.O. #:	4500940667	Orica Order #:	2271639
Blast Date:	2017-11-27	Blast Time:	1:00pm

page 1

Blaster-in-charge: Kevin Myerscough (Print Name)

Blast Location: Bench 3 North Face, East End (Bench / Face)

GPS Coordinates: 43.98798 °N Latitude (Centre of Blast) 77.87381 °W Longitude (Centre of Blast)

Wind from the: NW at 10 kph Temperature: -1 to -5 °C

Clear:		Rain:	x	Overcast:	x
Partly Cloudy:	X	Snow:		Inversion:	

Ceiling: 30,000 ft

	tonnes Blasted:	69,162 te	
	Total tonnes per day:	69,162 te	OPBB40 (Rate Code)
	Total Holes Loaded:	72 holes	
	… including:		Dead Holes
	… and:		Helper Holes
	Helper Hole Collar:		ft avg
	# Rows Blasted:	3 rows	
	- Pattern (Front Row)-		
	Burden:	14.5 ft avg	
	Spacing:	15.7 ft avg	
	# Holes:	23 front row	
	- Pattern (Main Body) -		
	Burden:	13.5 ft avg	
	Spacing:	15.7 ft avg	
	# Holes:	49 main body	
	Bench Height:	59.0 ft avg	
	Sub-drill:	1.0 ft avg	
	Hole Depth:	60.0 ft avg	
	- Stone Decking -		
	Front Row:	ft avg	
	Main Body:	ft avg	
	# Decks:	per blast	
	- Collar Stemming -		
	Front Row:	7.0 ft avg	
	Main Body:	7.0 ft avg	
	Material used:	HL3	
	- Charge Length -		
	Front Row:	53.0 ft avg	
	Main Body:	53.0 ft avg	
	- Charge Weight -		
	Front Row:	154.5 kg/hole	
	Main Body:	154.5 kg/hole	
	Max. per delay:	240.0 kg/delay	
	SD () Equation:	134.3 kg/delay	
	Total kg Loaded:	12,316 kg	
	Rock Density:	2.65 g/cc = te/m³	

Theoretical PF (Based on a single hole) — Yield Powder Factor (kg Loaded / te Blasted)

- Powder Factor -

0.795 lb/yd³	Yield PF:	0.178 kg/te (actual)
0.685 lb/yd³	Front row:	0.153 kg/te (theoretical)
0.736 lb/yd³	Main Body:	0.165 kg/te (theoretical)
0.719 lb/yd³	"KPI" PF:	0.161 kg/te (theoretical)

- Drilling Information -

			Angle from Vertical			Nominal Bit Diameter:
Primary Bit diam:	101.6	mm	0°	# Holes: 72	=	4,320.0 ft (4 " diam)
Secondary Bit diam:		mm	0°	# Holes:	=	0.0 ft (" diam)
Tertiary Bit diam:		mm	0°	# Holes:	=	0.0 ft (" diam)

Bulk Explosives:

	in (kg)	out (kg)	kg
CENTRA GOLD 70	32,150	20,000	12,150

Packaged Explosives:

	cs shipped	cs returned	kg
FORTEL PRO 90X400	15	10	125

Boosters:

	kg / unit	# usec	kg
PENTEX 8 (OR EQUIVALENT)	0.23	72	16.3
PENTEX 12 (OR EQUIVALENT)	0.34	72	24.5

total explosives weight in Blast (kg): 12,316

Pkgd Prod (125 kg) % of Total kg: 1.0%

Detonators:

	case #'s	ms	# used
UNITRONIC 600 6M	61637652-15		72
UNITRONIC 600 20M	61618492-32		72

Cord & Accessories:

	U of M	# used
HARNESS WIRE DUPLEX (6 PACK) 400M	units	1
	units	
	units	

Resource Deployment:

# of Blasts today (this Quarry)		1
# of Blasters (this Blast)		1
# of Helpers (this Blast)	Note Exception	3
# of MMU's (this Blast)		1

Services:

GPS LAYOUT	Enter hours	0.0
BULK TRUCK CHARGE	>/=10,000 kg	1
BLASTER HOURS	Enter Blaster hours	7.5
HELPER HOURS	Enter total Helper man-hours	19.5
SEISMOGRAPH RENTAL	Enter # Orica Seismographs	0
3D LASER PROFILE	Enter hours	0.0
BORETRACK	Enter hours	0.0
TECHNICAL BLAST DESIGN	(per day) Enter # of days	0.0

Cost Reduction Notes (this Blast) - change In Bit , B, S, Expl or IS from previous Blast:

Timing designed by Tristan Worsey of Respec

ORICA
The Blasting Professionals™

Blast Report

DFA / DIV of CRH (Ontario

Quarry:	Ogden Point	Blast Number:	17-028
P.O. #:	4500940667	Orica Order #:	2271639
Blast Date:	2017-11-27	Blast Time:	1:00pm

page 2

Blast Co-ordinates	Enter ° N Lat.	Enter ° W Long.	(N) Radians	(W) Radians
Mid Blast				
Front Row Corner	43.98796	77.87309	0.767735	1.359142
Back Row Corner	43.98799	77.87453	0.767735	1.359167
Average (Centre of Blast)	43.98798	77.87381	0.767735	1.359154

1st

Seismograph Co-ordinates	Enter ° N Lat.	Enter ° W Long.	(N) Radians	(W) Radians
1st Reading	43.98742	77.86954	0.767725	1.359080
2nd Reading				
Average	43.98742	77.86954	0.767725	1.359080

Distance (1st Seis. From Centre of Blast)	347.6	m		
Post Blast Data: ppV:	8.0	mm/s	Trigger set at: 2.0	mm/s
frequency:	47.0	Hz	V / T / L : V	(Vertical, Transverse or Longitudinal)
air overpressure:	125.3	dB	Trigger set at: 115	dB

Set up at North side of Main Gate

2nd

Seismograph Co-ordinates	Enter ° N Lat.	Enter ° W Long.	(N) Radians	(W) Radians
1st Reading	43.98498	77.88936	0.767683	1.359426
2nd Reading				
Average	43.98498	77.88936	0.767683	1.359426

Distance (2nd Seis. From Centre of Blast)	1289.4	m		
Post Blast Data: ppV:	5.2	mm/s	Trigger set at: 2.0	mm/s
frequency:	43.0	Hz	V / T / L : T	(Vertical, Transverse or Longitudinal)
air overpressure:	106.1	dB	Trigger set at: 115	dB

Setup at CP Tracks, NE corner of property

3rd

Seismograph Co-ordinates	Enter ° N Lat.	Enter ° W Long.	(N) Radians	(W) Radians
1st Reading				
2nd Reading				
Average	0.00000	0.00000	0.000000	0.000000

Distance (3rd Seis. From Centre of Blast)	0.0	m		
Post Blast Data: ppV:	0.0	mm/s	Trigger set at: 2.0	mm/s
frequency:	0.0	Hz	V / T / L : ?	(Vertical, Transverse or Longitudinal)
air overpressure:	0.0	dB	Trigger set at: 115	dB

Scaling Factor denotes the degree of Blast confinement.
The higher the SF, the more confined the Blast.
A Scaling Factor of 30 is commonly used in the Scaled Distance formula for Quarry Bench Blasting:

Enter a scaling Factor: 30 Quarry Bench Blasting - 2 Free Faces

$$W = \frac{D^2}{30^2}$$

$$= \frac{(347.6)^2}{30^2} \text{ kg}$$

$$= \frac{120{,}826}{900} \text{ kg}$$

Maximum Indicated Charge Weight per Delay = 134 kg

jim bray

Orica
Blaster-in-charge: *Kevin Myerscough*

Signature required, indicating that Blast Report is Complete & Accurate.

Instantel

Event Report

Date/Time	Tran at 1:00:36 PM November 27, 2017
Trigger Source	Geo: 2.000 mm/s
Range	Geo: 254.0 mm/s
Record Time	5.0 sec at 1024 sps
Operator/Setup:	Operator/UM6858.mmb

Serial Number	UM6858 V 10-87 Micromate ISEE
Battery Level	3.8 Volts
Unit Calibration	December 22, 2016 by Instantel
File Name	UM6858_20171127130036.IDFW

Notes
Location: Ogden Point
Client: CRH
User Name: Kevin Myerscough
General: Orica Canada Inc.

Extended Notes
Setup at CP Tracks, NE corner of property

Microphone	Linear Weighting
PSPL	106.1 dB(L) at 2.647 sec
ZC Freq	4.4 Hz
Channel Test	Passed (Freq = 19.7 Hz Amp = 1629 mv)

	Tran	Vert	Long	
PPV	5.202	2.010	3.413	mm/s
ZC Freq	43	85	47	Hz
Time (Rel. to Trig)	0.362	0.187	0.429	sec
Peak Acceleration	0.268	0.205	0.219	g
Peak Displacement	0.020	0.006	0.017	mm
Sensor Check	Passed	Passed	Passed	
Frequency	7.1	7.5	7.3	Hz
Overswing Ratio	4.1	3.7	4.2	

Peak Vector Sum 5.504 mm/s at 0.362 sec

USBM RI8507 And OSMRE

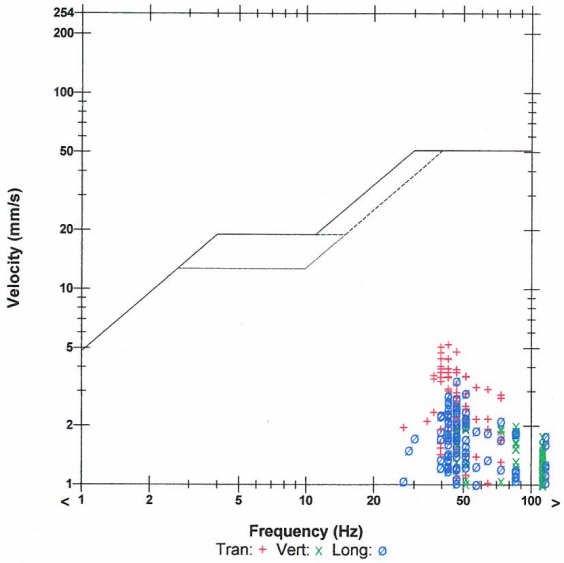

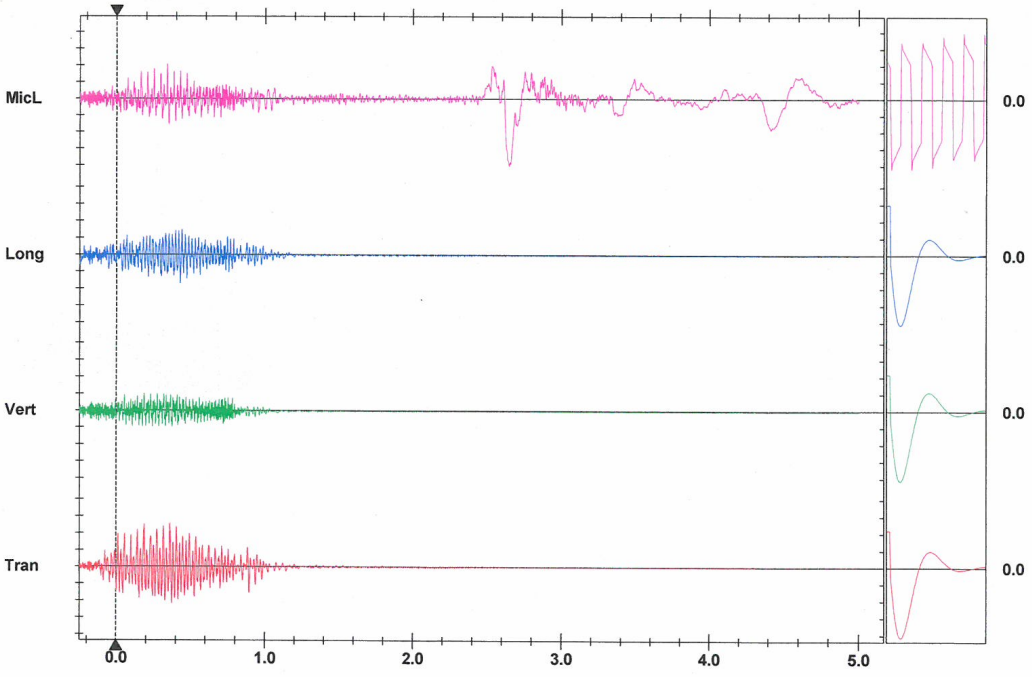

Instantel

FFT Report

Date/Time	Tran at 1:00:36 PM November 27, 2017	**Serial Number**	UM6858 V 10-87 Micromate ISEE
Trigger Source	Geo: 2.000 mm/s	**Battery Level**	3.8 Volts
Range	Geo: 254.0 mm/s	**Unit Calibration**	December 22, 2016 by Instantel
Record Time	5.0 sec at 1024 sps	**File Name**	UM6858_20171127130036.IDFW
Operator/Setup:	Operator/UM6858.mmb		

Notes
Location: Ogden Point
Client: CRH
User Name: Kevin Myerscough
General: Orica Canada Inc.

Extended Notes
Setup at CP Tracks, NE corner of property

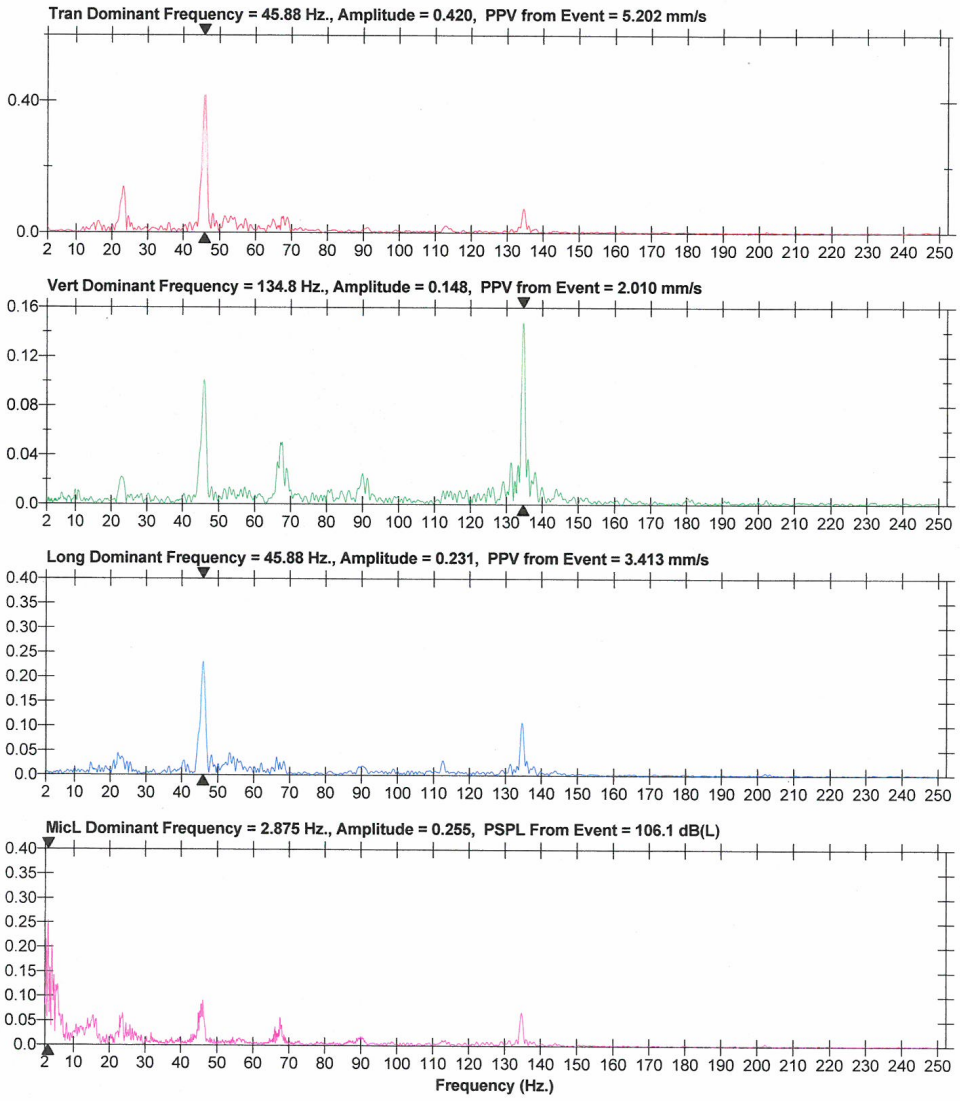

Instantel

Event Report

Date/Time Vert at 1:00:34 PM November 27, 2017
Trigger Source Geo: 2.000 mm/s, Mic: 122.0 dB(L)
Range Geo: 254.0 mm/s
Record Time 5.0 sec at 1024 sps

Serial Number BE12878 V 10.72-1.1 Minimate Blaster
Battery Level 6.3 Volts
Unit Calibration December 28, 2016 by Instantel
File Name N878H68K.4Y0

Notes
Quarry: Ogden Point
Client: CRH
User Name: Orica Canada Inc.
Operater: Kevin Myerscough

Setup Location
Set up @ North side of Main Gate

Microphone Linear Weighting
PSPL 125.3 dB(L) at 1.263 sec
ZC Freq 5.8 Hz
Channel Test Passed (Freq = 20.1 Hz Amp = 745 mv)

	Tran	Vert	Long	
PPV	5.334	8.001	5.842	mm/s
ZC Freq	51	47	47	Hz
Time (Rel. to Trig)	0.869	1.073	1.027	sec
Peak Acceleration	0.225	0.278	0.186	g
Peak Displacement	0.027	0.025	0.033	mm
Sensor Check	Passed	Passed	Passed	
Frequency	7.3	7.7	7.3	Hz
Overswing Ratio	4.0	3.6	4.4	

Peak Vector Sum 8.608 mm/s at 1.073 sec

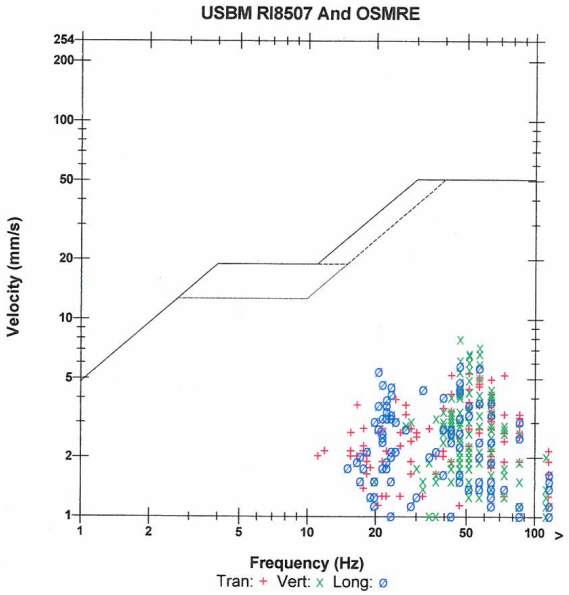

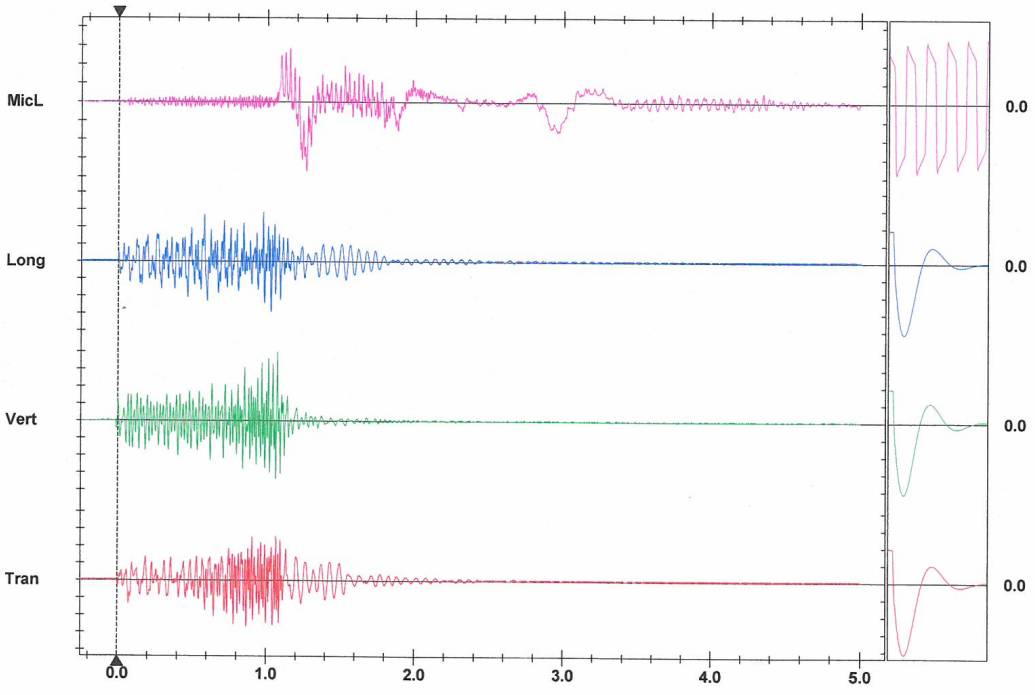

Instantel

FFT Report

Date/Time Vert at 1:00:34 PM November 27, 2017
Trigger Source Geo: 2.000 mm/s, Mic: 122.0 dB(L)
Range Geo: 254.0 mm/s
Record Time 5.0 sec at 1024 sps

Serial Number BE12878 V 10.72-1.1 Minimate Blaster
Battery Level 6.3 Volts
Unit Calibration December 28, 2016 by Instantel
File Name N878H68K.4Y0

Notes
Quarry: Ogden Point
Client: CRH
User Name: Orica Canada Inc.
Operater: Kevin Myerscough

Setup Location
Set up @ North side of Main Gate

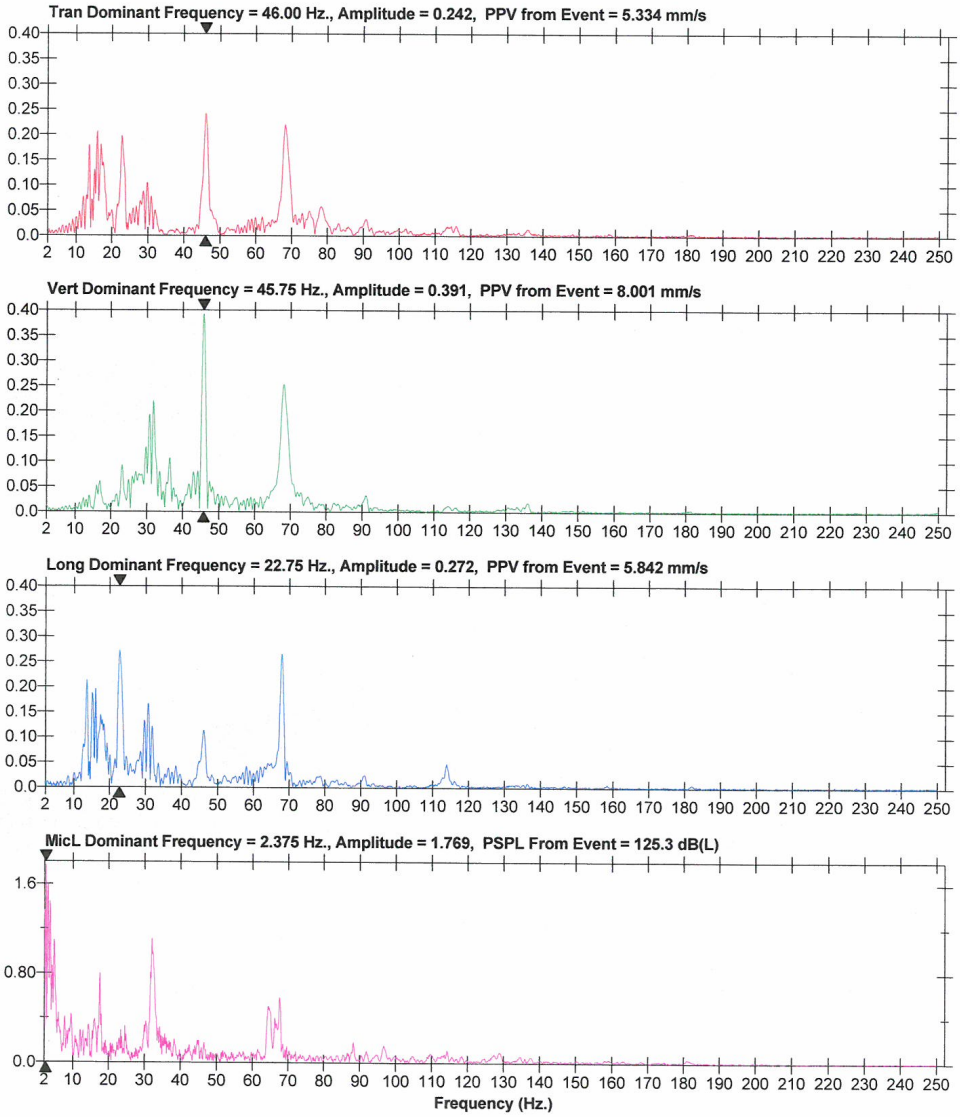

SHOTPlus 5 Plan

Ogden Point 17-028 Bench 3 North/East Face Timing Diagram

72 holes total, 4" diameter, 60' deep including subdrill
14.5' x 15.7' front row pattern
13.5' x 15.7' body rows pattern
45 ms between holes, 60 ms between rows
2 initiation points per hole, 4 ms apart
Body holes loaded to 7' collar with CG70
Face holes loaded to 7' collar with CG70 and Fortel Pro, depending on profile data

ORICA

Not to scale

SHOTPlus 5.6.4.3	26/11/2
Mine	Ogden Point
Location	Bench 3 North Face, East End
Title/author	Ogden Point 17-028 Kevin Myerscough
Filename	Ogden Point 2017-11-27 #28 Bench 3 No

Ogden Point 17-028 Bench 3 North/East Face Load Sheet

72 holes total, 4" diameter, 60' deep including subdrill
14.5' x 15.7' front row pattern
13.5' x 15.7' body rows pattern
Total drilling is 4,320'

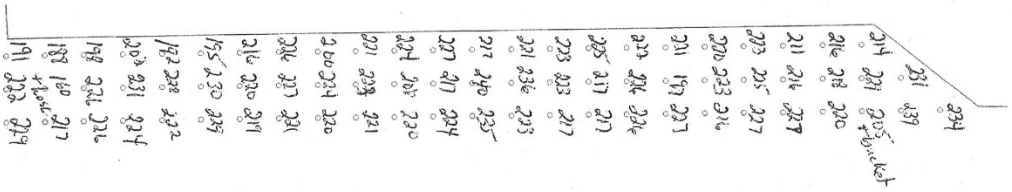

ORICA

Not to scale

SHOTPlus 5.6.4.3	24/11/201
Mine	Ogden Point
Location	Bench 3 North Face, East End
Title/author	Ogden Point 17-028 Kevin Myerscough
Filename	Ogden Point 17-028 ,Drill Plan.spf

ORICA
The Blasting Professionals™

Tie-in Verification

Quarry: Ogden Poir
Blast Number: 17-028
P.O. Number: 4500940667
Customer Name: DFA/CRH
Blast Date: 27-Nov-17

Tied in by:	John Simpson (Print Name)	Sign Off:	(Signature)	Time: 11:30am
Logged by:	Kevin Myerscough (Print Name)	Sign Off:	(Signature)	Time: 11:45am
Tie-in verified by:	Kevin Myerscough (Print Name)	Sign Off:	(Signature)	Time: 12:00pm
Inventory verified by:	Andrew Rolston (Print Name)	Sign Off:	(Signature)	Time: 12:15pm

Accessories Used in Blast:

____ m Handidet: __ / ____ ms ____ units		____ m Exel M: ____ ms ____ units	
____ m Handidet: __ / ____ ms ____ units		____ m Exel M: ____ ms ____ units	
____ m Handidet: __ / ____ ms ____ units		____ m Exel M: ____ ms ____ units	
____ m Connectadet: ____ ms ____ units		Lead-in Lines: ____ units	
____ m Connectadet: ____ ms ____ units		Connecting Wire: ____ pails	
____ m Connectadet: ____ ms ____ units		Electric MS: ____ units	
Booster - 8 oz: 72 units		Other: Fortel Pro-90x400- 5 units	
Booster - 12 oz: 72 units		____ units	
Booster - 16 oz: ____ units		____ units	
Booster - 16 oz Duo: ____ units		____ units	
20 m UT600: 72 units		Harness Wire: 1 rolls	
6 m UT600: 72 units			
____ m UT600: ____ units			
____ m UT600: ____ units			
____ m i-kon: ____ units		Harness Wire: ____ rolls	
____ m i-kon: ____ units			
____ m i-kon: ____ units			
____ m i-kon: ____ units			

Blast Design

DFA / CRH (Ontario)

Quarry: Ogden Point
P.O. #: 4500940667
Design Date: 2017-11-24

Blast Number: 17-028
Orica Order #:

page 1

Blaster-in-charge: Kevin Myerscough (Print Name)

Blast Location: Bench 3 North Face, East End (Bench / Face)
GPS Coordinates: enter data on p2 °N Latitude (Centre of Blast) enter data on p2 °W Longitude (Centre of Blast)

Design te Blasted:	69,162	te
Total Holes Loaded:	72	holes
... including:	0	Dead Holes
... and:	0	Helper Holes
Helper Hole Collar:	0.0	ft avg
# Rows Blasted:	3	rows

- Drilling Information -

			Angle from Vertical				Nominal Bit Diameter:
Primary Bit diam:	101.6	mm	0°	# Holes:	72	=	4,320.0 ft (4 " diam)
Secondary Bit diam:		mm	0°	# Holes:		=	0.0 ft (" diam)
Tertiary Bit diam:		mm	0°	# Holes:		=	0.0 ft (" diam)

- Design Pattern (Front Row)-

Burden:	14.5	ft avg
Spacing:	15.7	ft avg
# Holes:	23	front row

- Design Pattern (Main Body) -

Burden:	13.5	ft avg
Spacing:	15.7	ft avg
# Holes:	49	main body
Bench Height:	59.0	ft avg
Sub-drill:	1.0	ft avg
Hole Depth:	60.0	ft avg

- Design Stone Decking -

Front Row:		ft avg
Main Body:		ft avg

- Design Collar Stemming -

Front Row:	7.0	ft avg
Main Body:	7.0	ft avg
Material used:	HL3	

Bulk Expl. Required:

		kg
CENTRA GOLD 70		11,234

Pkgd Expl. Required:

		kg
FORTEL PRO 90X400	5	125

Boosters Required:

	kg/u	# used	kg
PENTEX 8 (OR EQUIVALENT)	0.23	72	16.3
PENTEX 12 (OR EQUIVALENT)	0.34	72	24.5

total explosives weight in Blast (kg):	11,400
Pkgd Prod (125 kg) % of Total kg:	1.1%

Detonators Required:

	ms	# req'd
UNITRONIC 600 6M	16376 52-15	72
UNITRONIC 600 20M	16184 1232	72

Cord & Access. Req'd:

	U of M	# req'd
IRE DUPLEX (6 PACK) 400M	units	1
	units	
	units	

- Design Charge Length -

Front Row:	53.0	ft avg
Main Body:	53.0	ft avg

- Design Charge Weight -

Front Row:	154.5	kg/hole
Main Body:	154.5	kg/hole
Max Chge Wt / delay:	160.0	kg/delay

Required kg Loaded:	11,400	kg
Rock Density:	2.65	g/cc = te/m³

- Design Powder Factor -

	Expected Yield PF:	0.165	kg/te (actual)
0.685 lb/yd³	Front row:	0.153	kg/te (theoretical)
0.736 lb/yd³	Main Body:	0.165	kg/te (theoretical)
0.719 lb/yd³	"KPI" PF:	0.161	kg/te (theoretical)

Resource Deployment:

# of Blasts today (this Quarry)		1
# of Blasters (this Blast)		1
# of Helpers (this Blast)	Note Exception	3
# of MMU's (this Blast)		1

Services Req'd:

GPS LAYOUT	Enter hours	0.0
BULK TRUCK CHARGE	<2,000kg	
BLASTER HOURS	Enter Blaster hours	9.0
HELPER HOURS	Enter total Helper man-hours	21.0
SEISMOGRAPH RENTAL	Enter # Orica Seismographs	0
3D LASER PROFILE	Enter hours	0
BORETRACK	Enter hours	0
TECHNICAL BLAST DESIGN	(per day) Enter # of days	0.0

Cost Reduction Notes (this Blast) - change in Bit , B, S, Expl or IS from previous Blast:

Timing designed by Tristan Worsey of Respec

ORICA
The Blasting Professionals™

Blast Design

DFA / DIV of CRH (Ontario)

Quarry:	Ogden Point	Blast Number:	17-028
P.O. #:	43063	Orica Order #:	
Blast Date:	27/11/2017		

page 2

Paste ShotPlus Diagram inside Rectangle:

Ogden Point 17-028 Bench 3 NE
72 holes, 4", 60' deep including subdrill
14.5' x 15.7' front row
13.5' x 15.7' body rows

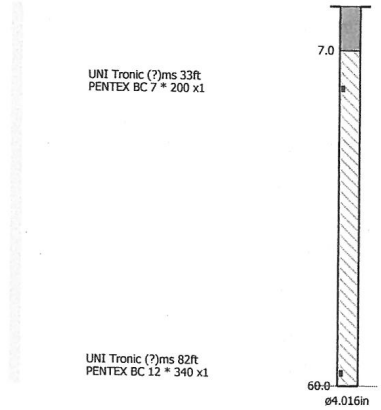

Orica
Blaster-in-charge: Kevin Myerscough

DFA / CRH
Quarry Manager: Casey Dack

Signature required, indicating sign off on Blast Design.

Dyno Nobel North America — BLAST REPORT

DYNO Dyno Nobel

SERVICE SITE LOCATION: Gamebridge ORDER NO.: 1110464

BLAST NUMBER: 2018-01 Level 3 BLAST TIME: 2:30 pm BLAST DATE: 04/29/2018

CUSTOMER: CRH CANADA GROUP INC. MINE: OGDEN POINT QUARRY ADDRESS: Colborne, ON

ROCK TYPE: Limestone ROCK SPECIFIC GRAVITY: 2.65 EXPECTED VIBRATION: 0.000 MMS

LOCATION OF BLAST

LOCATION OF BLAST IN MINE: North BENCH: Level 3

BLAST GPS POINTS: N 043.98805 & W -077.87308

WEATHER

WEATHER: Partly Cloudy CEILING: High TEMPERATURE: 9 C WIND DIRECTION & SPEED: Northwest 10 KPH

NEAREST NON-OWNED STRUCTURE

NAME: GPS Points: N & W

DISTANCE: (KM) DIRECTION: °

SEISMOGRAPH DATA

	LOCATION	DISTANCE	GPS POINTS	CALIBRATION DATE
1	N/A	N/A	N N/A & W N/A	N/A

	L (F)	T (F)	V (F)	AIR (db)	SEISMOGRAPH	SERIAL	OPERATOR
1	N/A N/A	N/A N/A	N/A N/A	N/A	N/A	N/A	N/A

BLAST DATA

		EXPLOSIVES SIZE, TYPE & WEIGHT		
NUMBER OF HOLES (EA)	60	SIZE	TYPE	WEIGHT
HOLE DIAMETER (CM)	10.16	BULK	TITAN XL 1000 G	9,362
HOLE DEPTH (M)	18.28	0.34 KG	SPARTAN 350	41
FACE HEIGHT (M)	18.28			
SUB DRILLING (M)	0			
AVG. STEM FACE HOLES (M)	2.13			
STEM OTHER HOLES (M)	2.13			
BURDEN FRONT ROW (M)	4.41			
BURDEN OTHER ROWS (M)	3.96			
SPACING FRONT ROW (M)	4.72			
SPACING OTHER ROWS (M)	4.72		TOTAL WEIGHT (KG):	9,403

DETONATORS USED IN BLAST: Electronic MATS USED: No STEM TYPE: CLEAN CRUSHED STONE TOTAL DRILL DEPTH: 1,097 (M

TYPE	MFG	DATE CODE	USED	TYPE	MFG	DATE CODE	USED
DIGISHOT 30 FT	Dyno Nobel Global	NA	57	DIGISHOT 80FT	Dyno Nobel Global	NA	63
DIGISHOT SURFACE WIRE	Dyno Nobel Global		1	SPARTAN 350	Dyno Nobel Global	NA	120

M3 IN SHOT: 21,316 SCALED DISTANCE FACTOR: 0 % OF ANFO: 0

TONNES IN SHOT: 56,487 HOLES/DELAY : 1 FUEL OIL % (BULK): 0

MAX KGS/DELAY: 0 MAXIMUM KGS/HOLE: 157

POWDER FACTOR (KGS/MT): 0.17 POWDER FACTOR (KGS/M3): 0.44

BLASTER'S NAME: Porco, Domenic BLASTER'S NUMBER & STATE: NA

BLASTER'S SIGNATURE: SITE SAFETY INSPECTION PERFORMED: Yes

NUMBER OF PERSONNEL ON SITE: 4

REMARKS : Bench was flat and in good condition. Face of the blast was clear of muck. No areas of weak burdens along the blast. The floor in front of the blast had some areas of pooling water. All of the holes were full of water but loaded well. No seams or voids in the rock. The hole size, pattern dimensions and timing were given to Dyno by Respec for testing of the fragmentation. Stemming material had some fines in it causing some clumping. Great fragmentation in the muck pile. Good seismograph readings.

START TIME	END TIME	TOTAL TIME	TRUCK NUMBERS
7:00 AM	12:00 PM	05:00	HT-0954

Dyno Nobel North America

CUSTOMER NAME: OGDEN POINT QUARRY
BENCH: Level 3
BLASTER'S NAME: Porco, Domenic

DIAGRAM

BLAST DATE: 04/29/2018
BLAST NUMBER: 2018-01 Level 3

DYNO
Dyno Nobel

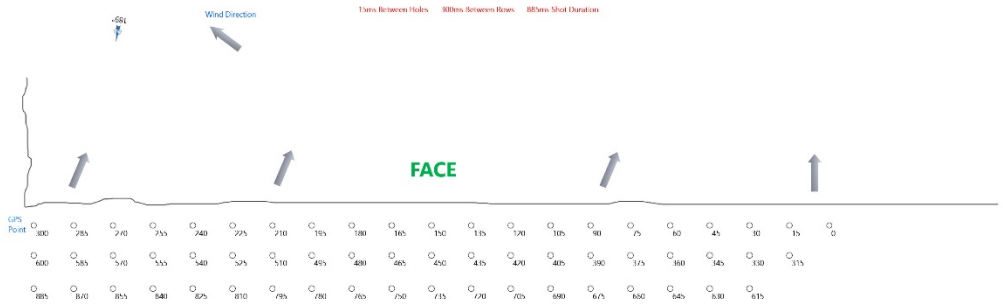

Dyno Nobel North America

CUSTOMER NAME: OGDEN POINT QUARRY

BLAST NUMBER: 2018-01 Level 3

BLAST DATE: 04/29/2018

BENCH: Level 3

BLASTER'S NAME: Porco, Domenic

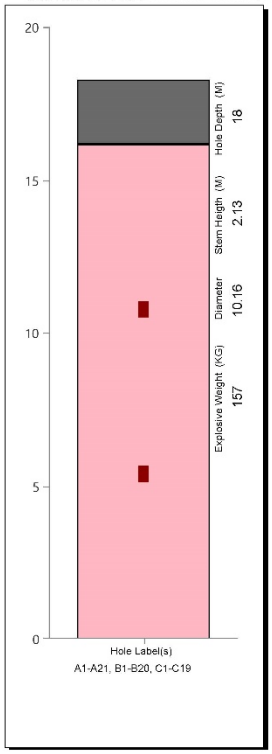

BULK REPORT

RESPONSIBLE PARTY INFORMATION

Date: APRIL 27/18 Time In: 7:00 A

Location: OGDEN POINT Time Out: 1:00 P

Customer: CRH Blaster In Charge: D PORCO

EXPLOSIVE LOADING

Type of Powder Delivered: TITAN 1000 (E) EM Temperature: 27°C

Pump Rate: 120 Water Rate: 1.9

Average Density: .92 Acid Delivered: 45

Prill Delivered: 6 Sodium Delivered: 67

Fuel Delivered: 1 % of Fuel in Anfo: 6

% of Anfo in Blend: 1 Average Depth: 60'

Hole Diameter: 4 Computer Total: 9362

Total Eulsion: 9072

DENSITY CUPS

Density Cup #	Time	Density	Density Cup #	Time	Density
1	8:30	.918	5		
2	9:00	.90	6		
3	10:00	.94	7		
4			8		

BLAST AREA/ACCESS

Access Road Condition: OK Stemming Out/ In Place: OK

Remarks: _____

Operator: TOMMY THOMPSON (sign) _____

Blaster in Charge D PORCO (sign) _____

Scale In: _____ 9362 kg Scale Out: _____

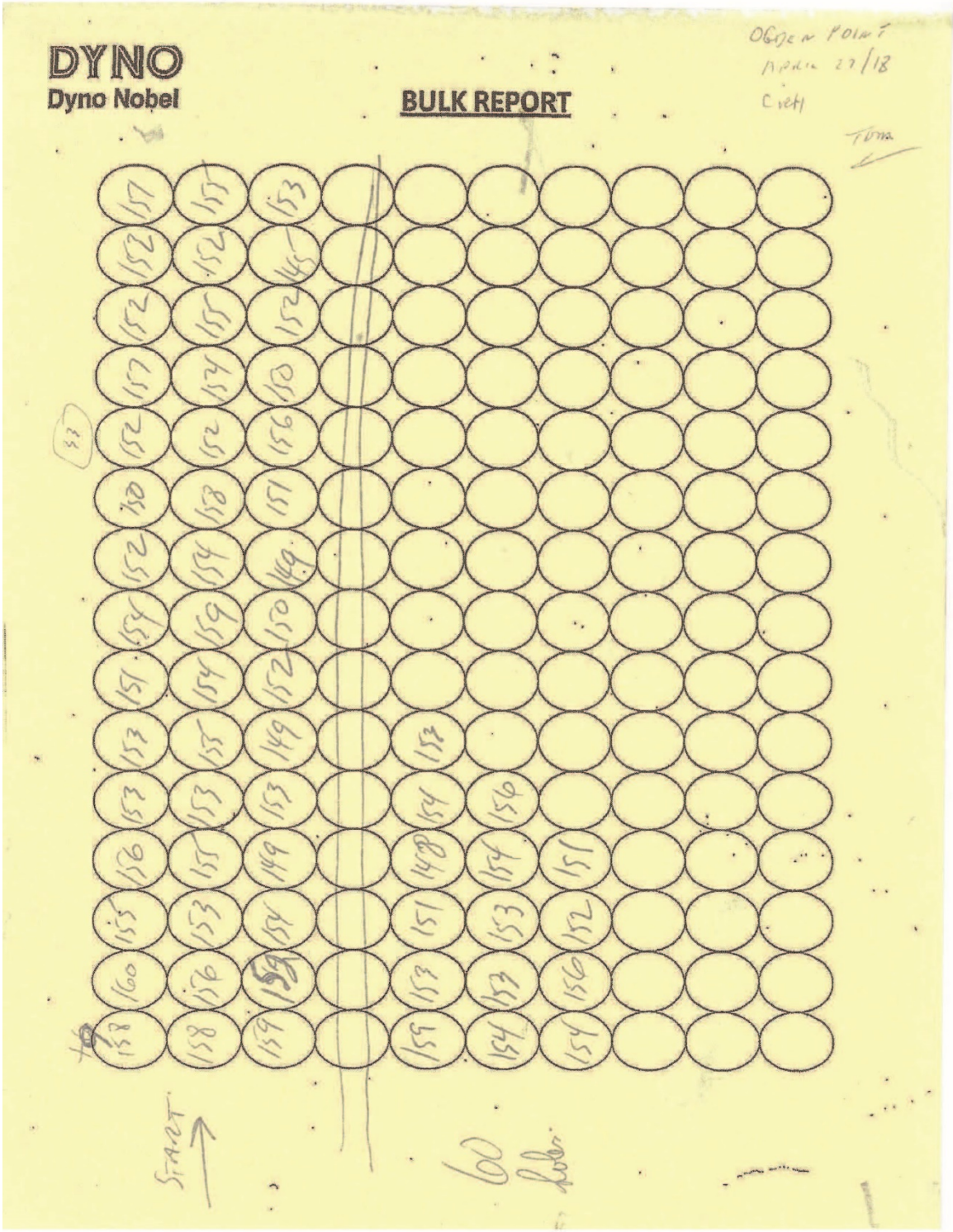
DYNO
Dyno Nobel
BULK REPORT
OGDEN POINT
APRIL 27/18
C vetl
Tuna
START


R1.28 59.9ft
R1.25 59.0ft
R2.25 59.3ft
R1.24 58.7ft
R2.24 59.3ft
R3.24 59.4ft
R1.23 58.6ft
R2.23 59.2ft
R3.23 59.5ft
R1.22 58.6ft
R2.22 59.4ft
R3.22 59.2ft
R1.21 58.9ft
R2.21 59.6ft
R3.21 59.0ft
R1.20 58.7ft
R2.20 59.2ft
R3.20 59.3ft
R1.19 59.1ft
R2.19 59.3ft
R3.19 59.4ft
R1.18 59.1ft
R2.18 59.5ft
R3.18 59.6ft
R1.17 59.1ft
R2.17 59.6ft
R3.17 59.7ft
R1.16 59.0ft
R2.16 59.5ft
R3.16 60.0ft
R1.15 59.1ft
R2.15 59.6ft
R3.15 60.1ft
R1.14 59.0ft
R2.14 59.6ft
R3.14 60.0ft
R1.13 59.3ft
R2.13 59.7ft
R3.13 60.4ft
R1.12 59.7ft
R2.12 60.3ft
R3.12 60.4ft
R1.11 59.9ft
R2.11 60.4ft
R3.11 60.6ft
R1.10 60.0ft
R2.10 60.4ft
R3.10 60.9ft
R1.9 60.1ft
R2.9 60.5ft
R3.9 60.9ft
R1.8 60.3ft
R2.8 60.7ft
R3.8 61.3ft
R1.7 60.6ft
R2.7 60.7ft
R3.7 61.9ft
R1.6 60.5ft
R2.6 61.0ft
R3.6 61.6ft
R1.5 60.7ft
R2.5 61.0ft
R3.5 61.7ft
R1.4 60.9ft
R2.4 61.2ft
R3.4 61.8ft
R1.3 61.0ft
R2.3 61.4ft
R3.3 62.1ft
R1.2 61.1ft
R2.2 61.5ft
R3.2 62.2ft
R1.1 61.4ft
R2.1 61.5ft
R3.1 62.2ft

DynoConsult

Drill log

DYNO Dyno Nobel

Reference		**Date:**	April 22, 2018
Client:	CRH Group Canada inc.	**Blast no.:**	Level 3 2018-01
Site:	Ogden Point Quarry, Colborne ON		

BLAST PARAMETERS				
Pattern	1st row	14' x 15.5'	other rows	13' x 15.5'
Number of holes	75			
Hole diameter	4 in			
Notes				

DRILLING INFORMATION					
Row ID	**Hole ID**	**Design angle**	**Design depth (ft)**	**Measured depth (ft)**	**Comments**
1	1	0	61.4		
1	2	0	61.1		
1	3	0	61.0		
1	4	0	60.9		
1	5	0	60.7		
1	6	0	60.5		
1	7	0	60.6		
1	8	0	60.3		
1	9	0	60.1		
1	10	0	60.0		
1	11	0	59.9		
1	12	0	59.7		
1	13	0	59.3		
1	14	0	59.0		
1	15	0	59.1		
1	16	0	59.0		
1	17	0	59.1		
1	18	0	59.1		
1	19	0	59.1		
1	20	0	58.7		
1	21	0	58.5		
1	22	0	58.6		
1	23	0	58.6		
1	24	0	58.7		
1	25	0	59.0		
1	26	0	58.9		
2	1	0	61.5		
2	2	0	61.5		
2	3	0	61.4		

SIGNATURES			
Driller		Date	
Blaster		Date	
Supervisor		Date	

DynoConsult

Drill log

DYNO Dyno Nobel

Reference		**Date:**	April 22, 2018
Client:	CRH Group Canada inc.	**Blast no.:**	Level 3 2018-01
Site:	Ogden Point Quarry, Colborne ON		

BLAST PARAMETERS				
Pattern	1st row	14' x 15.5'	other rows	13' x 15.5'
Number of holes	75			
Hole diameter	4 in			
Notes				

DRILLING INFORMATION					
Row ID	**Hole ID**	**Design angle**	**Design depth (ft)**	**Measured depth (ft)**	**Comments**
2	4	0	61.2		
2	5	0	61.0		
2	6	0	61.0		
2	7	0	60.7		
2	8	0	60.7		
2	9	0	60.5		
2	10	0	60.4		
2	11	0	60.4		
2	12	0	60.3		
2	13	0	59.7		
2	14	0	59.6		
2	15	0	59.5		
2	16	0	59.5		
2	17	0	59.8		
2	18	0	59.5		
2	19	0	59.3		
2	20	0	59.2		
2	21	0	59.6		
2	22	0	59.4		
2	23	0	59.2		
2	24	0	59.3		
2	25	0	59.3		
3	1	0	62.2		
3	2	0	62.2		
3	3	0	62.1		
3	4	0	61.8		
3	5	0	61.7		
3	6	0	61.6		
3	7	0	61.9		

SIGNATURES			
Driller		Date	
Blaster		Date	
Supervisor		Date	

DynoConsult

Drill log

DYNO Dyno Nobel

Reference		**Date:**	April 22, 2018
Client:	CRH Group Canada inc.	**Blast no.:**	Level 3 2018-01
Site:	Ogden Point Quarry, Colborne ON		

BLAST PARAMETERS				
Pattern	1st row	14' x 15.5'	other rows	13' x 15.5'
Number of holes	75			
Hole diameter	4 in			
Notes				

DRILLING INFORMATION

Row ID	Hole ID	Design angle	Design depth (ft)	Measured depth (ft)	Comments
3	8	0	61.3		
3	9	0	60.9		
3	10	0	60.9		
3	11	0	60.8		
3	12	0	60.4		
3	13	0	60.4		
3	14	0	60.0		
3	15	0	60.1		
3	16	0	60.0		
3	17	0	59.7		
3	18	0	59.5		
3	19	0	59.4		
3	20	0	59.3		
3	21	0	59.0		
3	22	0	59.2		
3	23	0	59.5		
3	24	0	59.4		

SIGNATURES			
Driller		Date	
Blaster		Date	
Supervisor		Date	

QuarryX

Blasting Engineer: Paul P. Kuznik, P. Eng.
Client: CRH Ogden Point
Site:CRH Ogden Point
Hole 1 of 25

Project: CRH Ogden Point P3 2018-01
Filename: OPC P3.qxd
Printed at: 2018-04-24 14:30:42
Scale: 1:150

DYNO Dyno Nobel

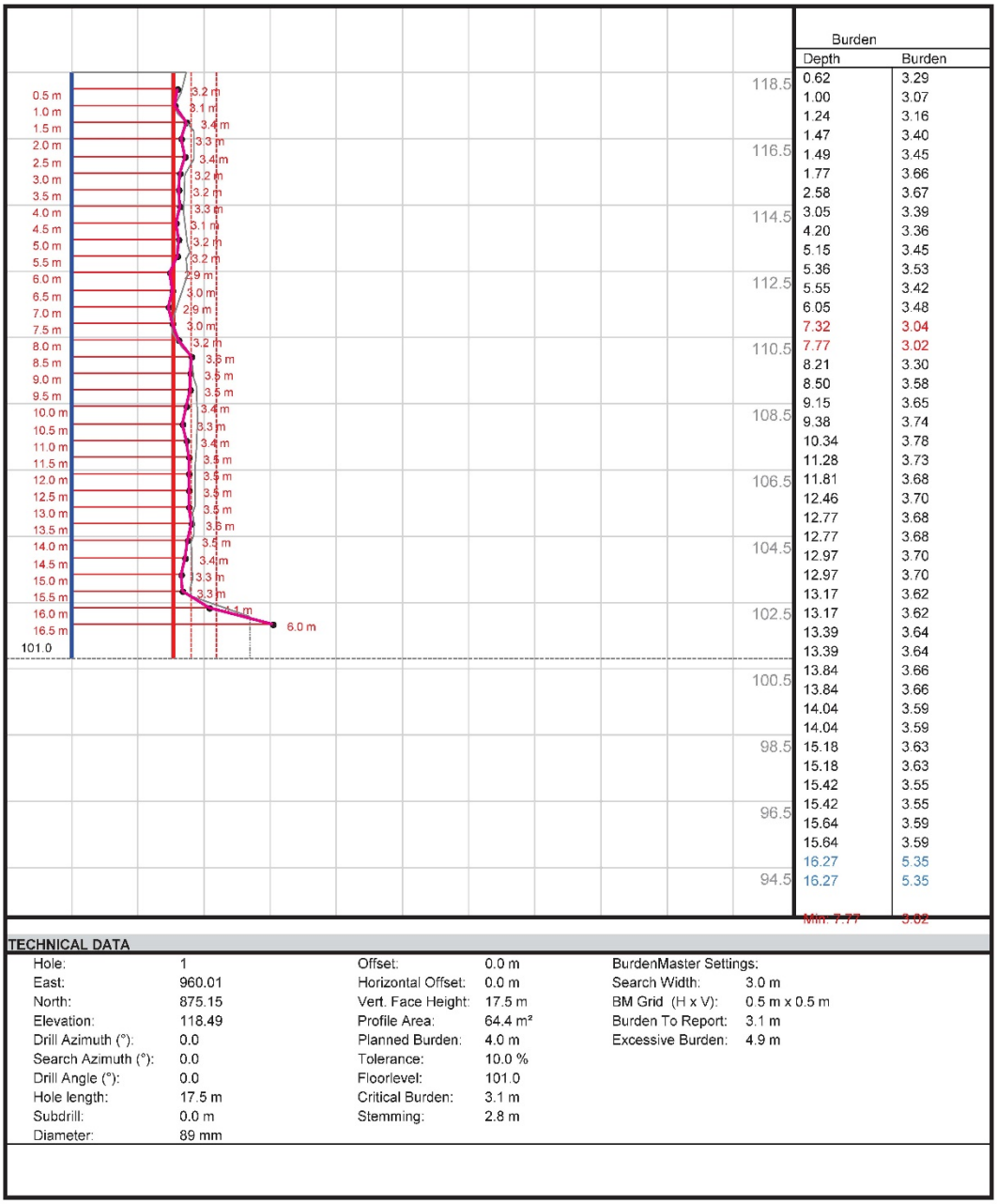

Burden	
Depth	Burden
0.62	3.29
1.00	3.07
1.24	3.16
1.47	3.40
1.49	3.45
1.77	3.66
2.58	3.67
3.05	3.39
4.20	3.36
5.15	3.45
5.36	3.53
5.55	3.42
6.05	3.48
7.32	3.04
7.77	3.02
8.21	3.30
8.50	3.58
9.15	3.65
9.38	3.74
10.34	3.78
11.28	3.73
11.81	3.68
12.46	3.70
12.77	3.68
12.77	3.68
12.97	3.70
12.97	3.70
13.17	3.62
13.17	3.62
13.39	3.64
13.39	3.64
13.84	3.66
13.84	3.66
14.04	3.59
14.04	3.59
15.18	3.63
15.18	3.63
15.42	3.55
15.42	3.55
15.64	3.59
15.64	3.59
16.27	5.35
16.27	5.35
Min: 7.77	3.02

TECHNICAL DATA

Hole:	1	Offset:	0.0 m	BurdenMaster Settings:	
East:	960.01	Horizontal Offset:	0.0 m	Search Width:	3.0 m
North:	875.15	Vert. Face Height:	17.5 m	BM Grid (H x V):	0.5 m x 0.5 m
Elevation:	118.49	Profile Area:	64.4 m²	Burden To Report:	3.1 m
Drill Azimuth (°):	0.0	Planned Burden:	4.0 m	Excessive Burden:	4.9 m
Search Azimuth (°):	0.0	Tolerance:	10.0 %		
Drill Angle (°):	0.0	Floorlevel:	101.0		
Hole length:	17.5 m	Critical Burden:	3.1 m		
Subdrill:	0.0 m	Stemming:	2.8 m		
Diameter:	89 mm				

QuarryX

Blasting Engineer: Paul P. Kuznik, P. Eng.
Client: CRH Ogden Point
Site:CRH Ogden Point
Hole 2 of 25

Project: CRH Ogden Point P3 2018-01
Filename: OPC P3.qxd
Printed at: 2018-04-24 14:30:43
Scale: 1:150

DYNO Dyno Nobel

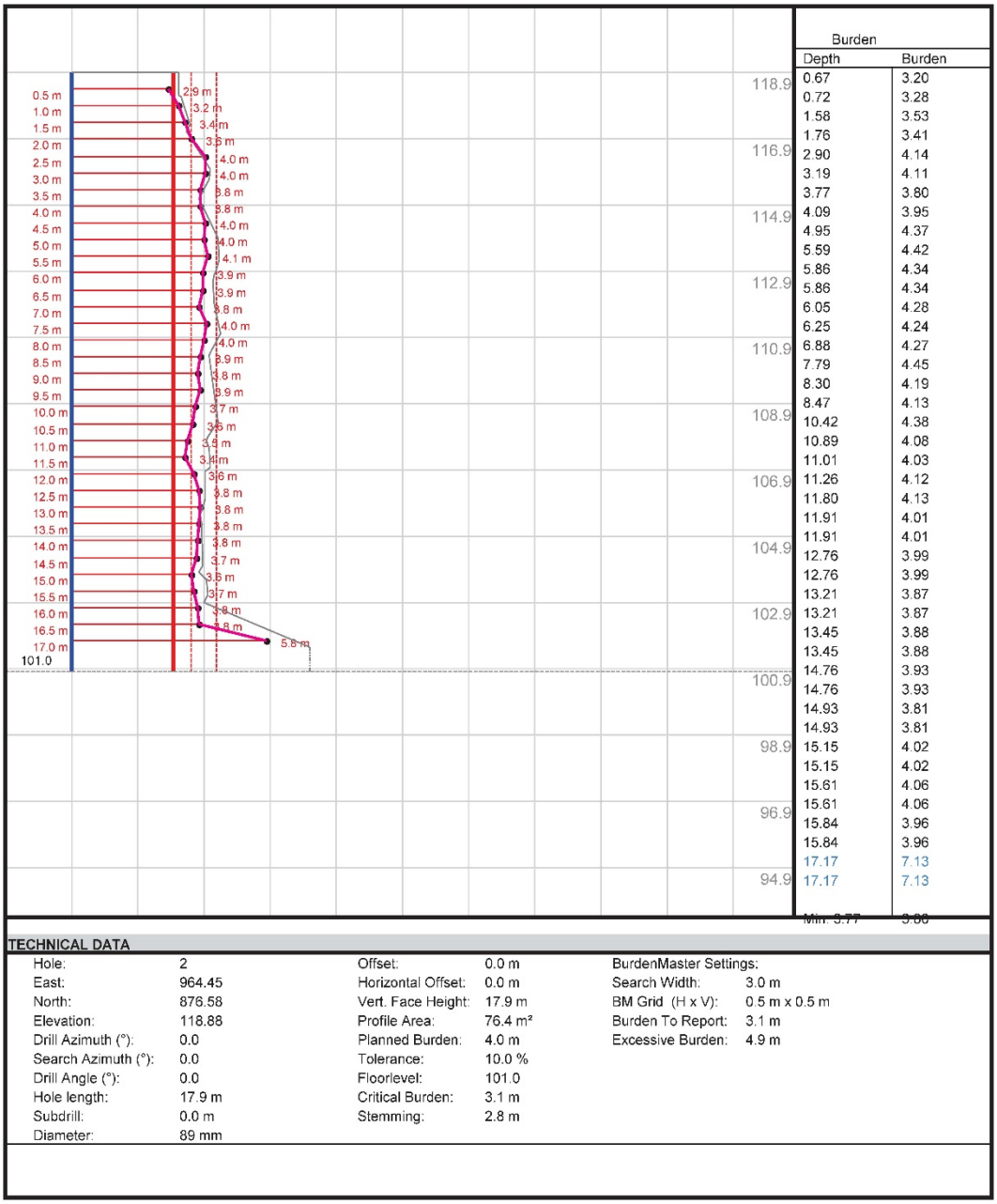

Burden	
Depth	Burden
0.67	3.20
0.72	3.28
1.58	3.53
1.76	3.41
2.90	4.14
3.19	4.11
3.77	3.80
4.09	3.95
4.95	4.37
5.59	4.42
5.86	4.34
5.86	4.34
6.05	4.28
6.25	4.24
6.88	4.27
7.79	4.45
8.30	4.19
8.47	4.13
10.42	4.38
10.89	4.08
11.01	4.03
11.26	4.12
11.80	4.13
11.91	4.01
11.91	4.01
12.76	3.99
12.76	3.99
13.21	3.87
13.21	3.87
13.45	3.88
13.45	3.88
14.76	3.93
14.76	3.93
14.93	3.81
14.93	3.81
15.15	4.02
15.15	4.02
15.61	4.06
15.61	4.06
15.84	3.96
15.84	3.96
17.17	7.13
17.17	7.13
Min: 3.77	3.80

TECHNICAL DATA

Hole:	2	Offset:	0.0 m	BurdenMaster Settings:	
East:	964.45	Horizontal Offset:	0.0 m	Search Width:	3.0 m
North:	876.58	Vert. Face Height:	17.9 m	BM Grid (H x V):	0.5 m x 0.5 m
Elevation:	118.88	Profile Area:	76.4 m²	Burden To Report:	3.1 m
Drill Azimuth (°):	0.0	Planned Burden:	4.0 m	Excessive Burden:	4.9 m
Search Azimuth (°):	0.0	Tolerance:	10.0 %		
Drill Angle (°):	0.0	Floorlevel:	101.0		
Hole length:	17.9 m	Critical Burden:	3.1 m		
Subdrill:	0.0 m	Stemming:	2.8 m		
Diameter:	89 mm				

QuarryX

Blasting Engineer: Paul P. Kuznik, P. Eng.
Client: CRH Ogden Point
Site:CRH Ogden Point
Hole 3 of 25

Project: CRH Ogden Point P3 2018-01
Filename: OPC P3.qxd
Printed at: 2018-04-24 14:30:43
Scale: 1:150

DYNO Dyno Nobel

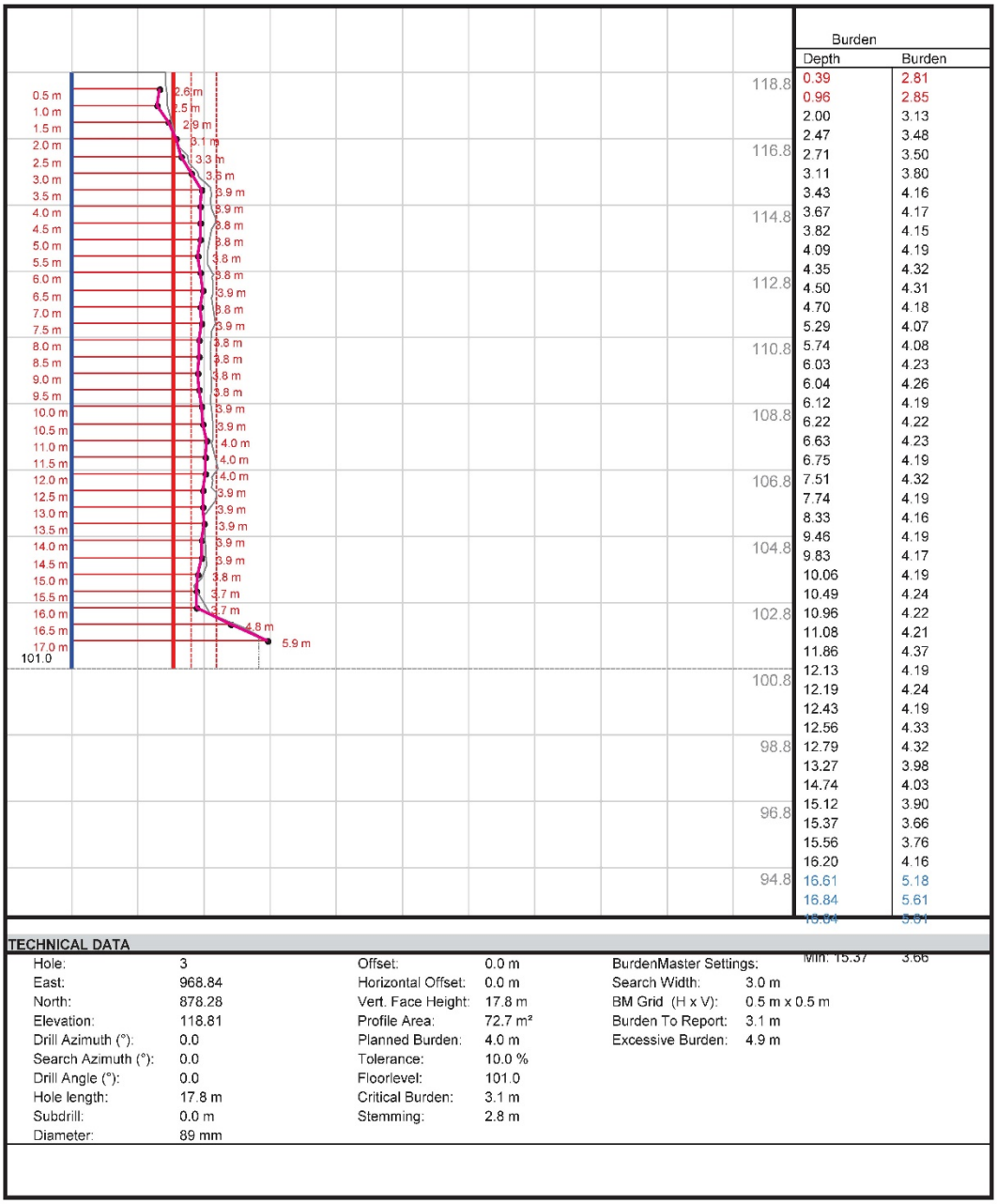

Burden	
Depth	Burden
0.39	2.81
0.96	2.85
2.00	3.13
2.47	3.48
2.71	3.50
3.11	3.80
3.43	4.16
3.67	4.17
3.82	4.15
4.09	4.19
4.35	4.32
4.50	4.31
4.70	4.18
5.29	4.07
5.74	4.08
6.03	4.23
6.04	4.26
6.12	4.19
6.22	4.22
6.63	4.23
6.75	4.19
7.51	4.32
7.74	4.19
8.33	4.16
9.46	4.19
9.83	4.17
10.06	4.19
10.49	4.24
10.96	4.22
11.08	4.21
11.86	4.37
12.13	4.19
12.19	4.24
12.43	4.19
12.56	4.33
12.79	4.32
13.27	3.98
14.74	4.03
15.12	3.90
15.37	3.66
15.56	3.76
16.20	4.16
16.61	5.18
16.84	5.61
Min: 15.37	3.66

TECHNICAL DATA

Hole:	3	Offset:	0.0 m	BurdenMaster Settings:	
East:	968.84	Horizontal Offset:	0.0 m	Search Width:	3.0 m
North:	878.28	Vert. Face Height:	17.8 m	BM Grid (H x V):	0.5 m x 0.5 m
Elevation:	118.81	Profile Area:	72.7 m²	Burden To Report:	3.1 m
Drill Azimuth (°):	0.0	Planned Burden:	4.0 m	Excessive Burden:	4.9 m
Search Azimuth (°):	0.0	Tolerance:	10.0 %		
Drill Angle (°):	0.0	Floorlevel:	101.0		
Hole length:	17.8 m	Critical Burden:	3.1 m		
Subdrill:	0.0 m	Stemming:	2.8 m		
Diameter:	89 mm				

QuarryX

Blasting Engineer: Paul P. Kuznik, P. Eng.
Client: CRH Ogden Point
Site:CRH Ogden Point
Hole 4 of 25

Project: CRH Ogden Point P3 2018-01
Filename: OPC P3.qxd
Printed at: 2018-04-24 14:30:44
Scale: 1:150

DYNO Dyno Nobel

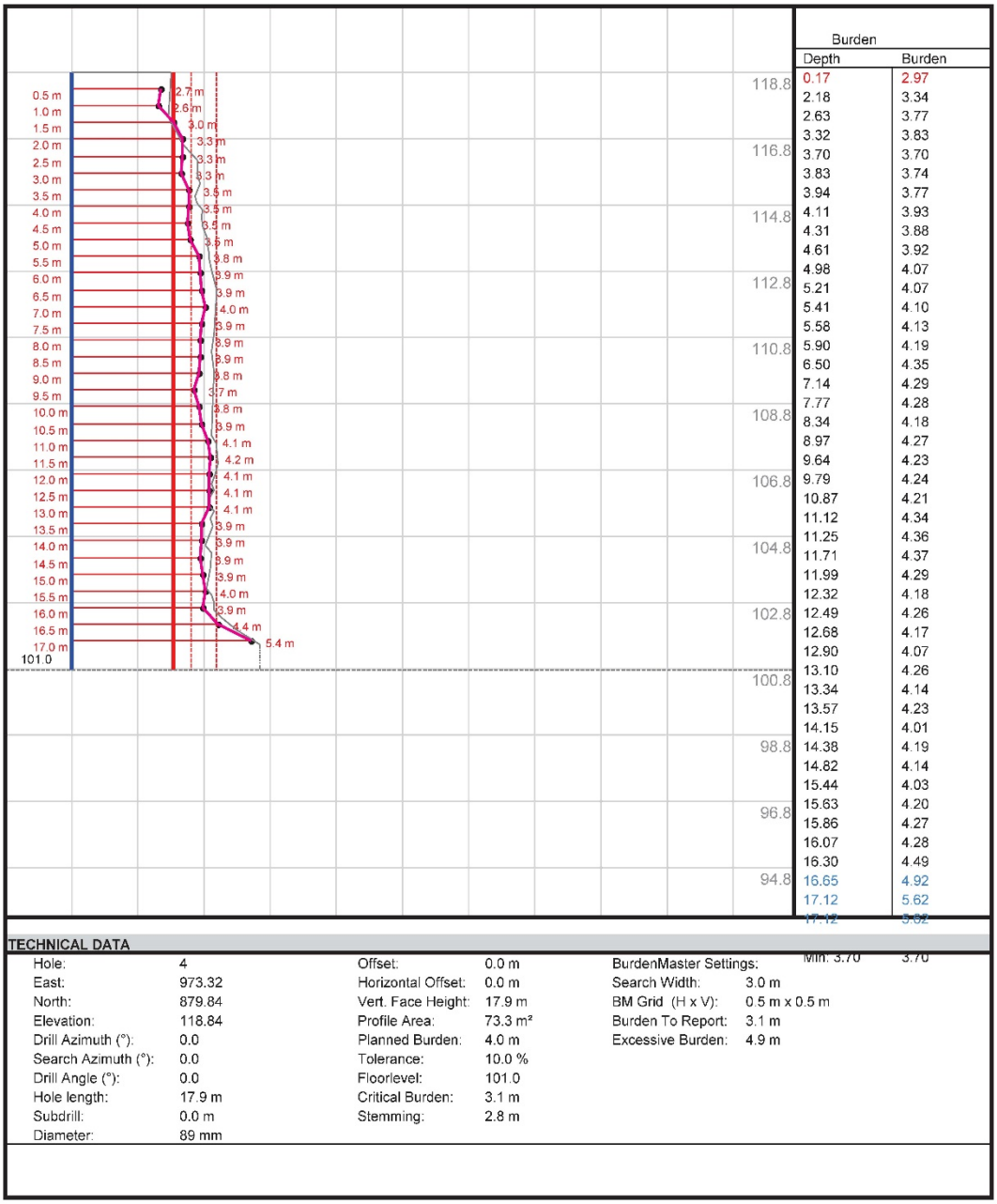

Burden	
Depth	Burden
0.17	2.97
2.18	3.34
2.63	3.77
3.32	3.83
3.70	3.70
3.83	3.74
3.94	3.77
4.11	3.93
4.31	3.88
4.61	3.92
4.98	4.07
5.21	4.07
5.41	4.10
5.58	4.13
5.90	4.19
6.50	4.35
7.14	4.29
7.77	4.28
8.34	4.18
8.97	4.27
9.64	4.23
9.79	4.24
10.87	4.21
11.12	4.34
11.25	4.36
11.71	4.37
11.99	4.29
12.32	4.18
12.49	4.26
12.68	4.17
12.90	4.07
13.10	4.26
13.34	4.14
13.57	4.23
14.15	4.01
14.38	4.19
14.82	4.14
15.44	4.03
15.63	4.20
15.86	4.27
16.07	4.28
16.30	4.49
16.65	4.92
17.12	5.62
Min: 3.70	3.70

TECHNICAL DATA

Hole:	4	Offset:	0.0 m	BurdenMaster Settings:	
East:	973.32	Horizontal Offset:	0.0 m	Search Width:	3.0 m
North:	879.84	Vert. Face Height:	17.9 m	BM Grid (H x V):	0.5 m x 0.5 m
Elevation:	118.84	Profile Area:	73.3 m²	Burden To Report:	3.1 m
Drill Azimuth (°):	0.0	Planned Burden:	4.0 m	Excessive Burden:	4.9 m
Search Azimuth (°):	0.0	Tolerance:	10.0 %		
Drill Angle (°):	0.0	Floorlevel:	101.0		
Hole length:	17.9 m	Critical Burden:	3.1 m		
Subdrill:	0.0 m	Stemming:	2.8 m		
Diameter:	89 mm				

QuarryX

Blasting Engineer: Paul P. Kuznik, P. Eng.
Client: CRH Ogden Point
Site:CRH Ogden Point
Hole 5 of 25

Project: CRH Ogden Point P3 2018-01
Filename: OPC P3.qxd
Printed at: 2018-04-24 14:30:45
Scale: 1:150

DYNO Dyno Nobel

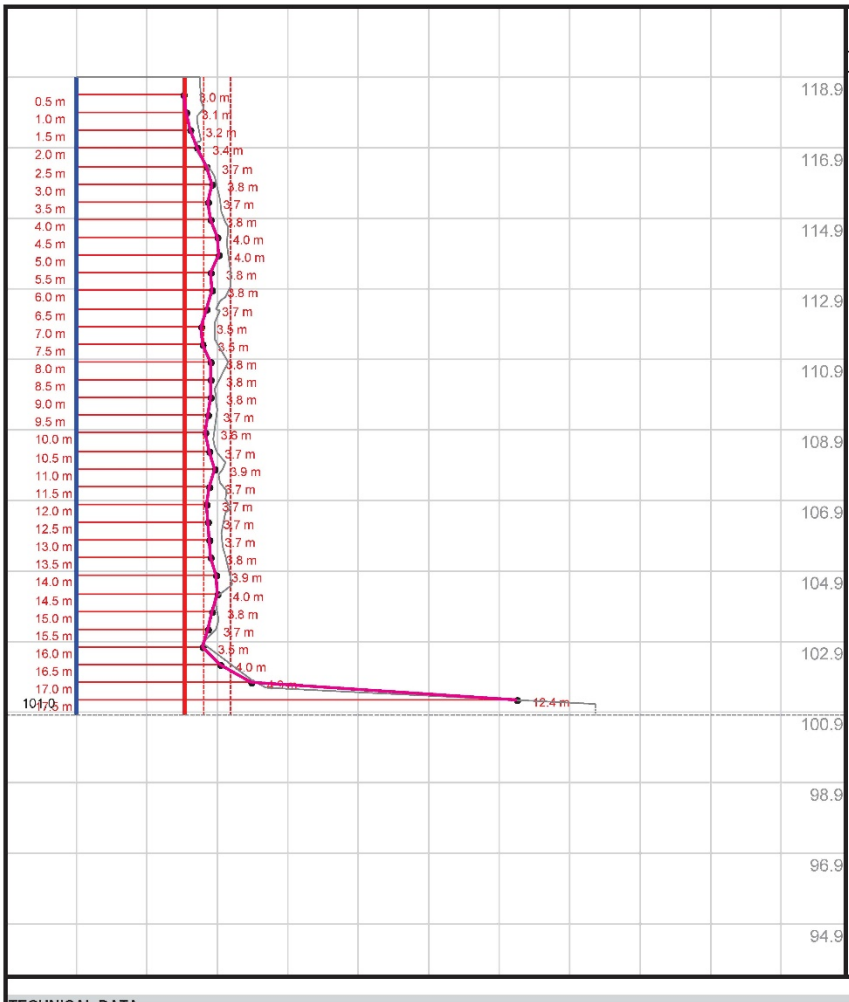

Burden

Depth	Burden
0.63	3.50
1.09	3.38
1.22	3.38
1.84	3.39
2.09	3.40
2.58	3.78
2.77	3.88
3.79	4.07
4.07	4.21
4.30	4.26
4.65	4.22
5.52	4.33
5.87	4.33
6.27	4.06
6.53	3.94
6.89	3.89
7.35	3.90
8.54	3.99
8.76	3.89
9.15	3.94
9.34	3.96
10.17	3.85
10.38	3.89
10.56	3.98
10.82	4.19
11.02	4.12
11.16	3.99
11.38	4.06
11.62	4.22
11.84	4.20
12.13	4.35
12.23	4.21
12.79	4.06
13.20	4.10
13.45	4.20
14.24	4.37
14.64	3.87
15.25	4.00
15.50	3.93
15.90	3.55
16.11	3.86
16.90	4.93
17.14	5.32
17.61	14.60
Min: 15.90	3.55

TECHNICAL DATA

Hole:	5	Offset:	0.0 m	BurdenMaster Settings:	
East:	977.81	Horizontal Offset:	0.0 m	Search Width:	3.0 m
North:	881.53	Vert. Face Height:	17.9 m	BM Grid (H x V):	0.5 m x 0.5 m
Elevation:	118.86	Profile Area:	77.7 m²	Burden To Report:	3.1 m
Drill Azimuth (°):	0.0	Planned Burden:	4.0 m	Excessive Burden:	4.9 m
Search Azimuth (°):	0.0	Tolerance:	10.0 %		
Drill Angle (°):	0.0	Floorlevel:	101.0		
Hole length:	17.9 m	Critical Burden:	3.1 m		
Subdrill:	0.0 m	Stemming:	2.8 m		
Diameter:	89 mm				

QuarryX

Blasting Engineer: Paul P. Kuznik, P. Eng.
Client: CRH Ogden Point
Site:CRH Ogden Point
Hole 6 of 25

Project: CRH Ogden Point P3 2018-01
Filename: OPC P3.qxd
Printed at: 2018-04-24 14:30:45
Scale: 1:150

DYNO Dyno Nobel

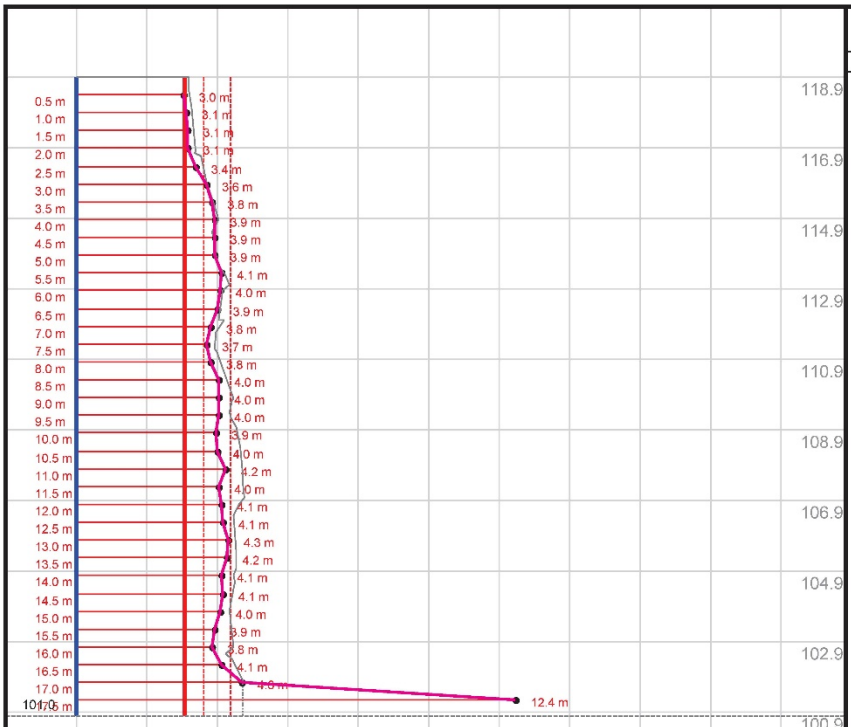

Burden	
Depth	Burden
0.37	3.15
2.09	3.36
2.13	3.33
2.92	3.67
3.51	3.83
4.35	3.79
4.59	3.90
5.22	3.96
5.58	4.18
5.98	4.10
6.81	4.00
7.17	3.94
7.60	3.89
7.98	4.03
9.02	4.43
9.40	4.31
9.58	4.36
10.41	4.61
11.23	4.69
11.47	4.69
11.81	4.74
12.29	4.41
13.35	4.50
13.80	4.49
13.80	4.49
13.98	4.44
13.98	4.44
14.18	4.47
14.18	4.47
14.36	4.41
14.36	4.41
14.99	4.32
14.99	4.32
15.98	4.42
15.98	4.42
16.18	4.21
16.18	4.21
16.36	4.38
16.36	4.38
16.96	4.69
16.96	4.69
Min: 2.92	3.67

TECHNICAL DATA

Hole:	6	Offset:	0.0 m	BurdenMaster Settings:	
East:	982.28	Horizontal Offset:	0.0 m	Search Width:	3.0 m
North:	883.25	Vert. Face Height:	18.0 m	BM Grid (H x V):	0.5 m x 0.5 m
Elevation:	118.92	Profile Area:	74.5 m²	Burden To Report:	3.1 m
Drill Azimuth (°):	0.0	Planned Burden:	4.0 m	Excessive Burden:	4.9 m
Search Azimuth (°):	0.0	Tolerance:	10.0 %		
Drill Angle (°):	0.0	Floorlevel:	101.0		
Hole length:	18.0 m	Critical Burden:	3.1 m		
Subdrill:	0.0 m	Stemming:	2.8 m		
Diameter:	89 mm				

QuarryX

Blasting Engineer: Paul P. Kuznik, P. Eng.
Client: CRH Ogden Point
Site:CRH Ogden Point
Hole 7 of 25

Project: CRH Ogden Point P3 2018-01
Filename: OPC P3.qxd
Printed at: 2018-04-24 14:30:46
Scale: 1:150

DYNO Dyno Nobel

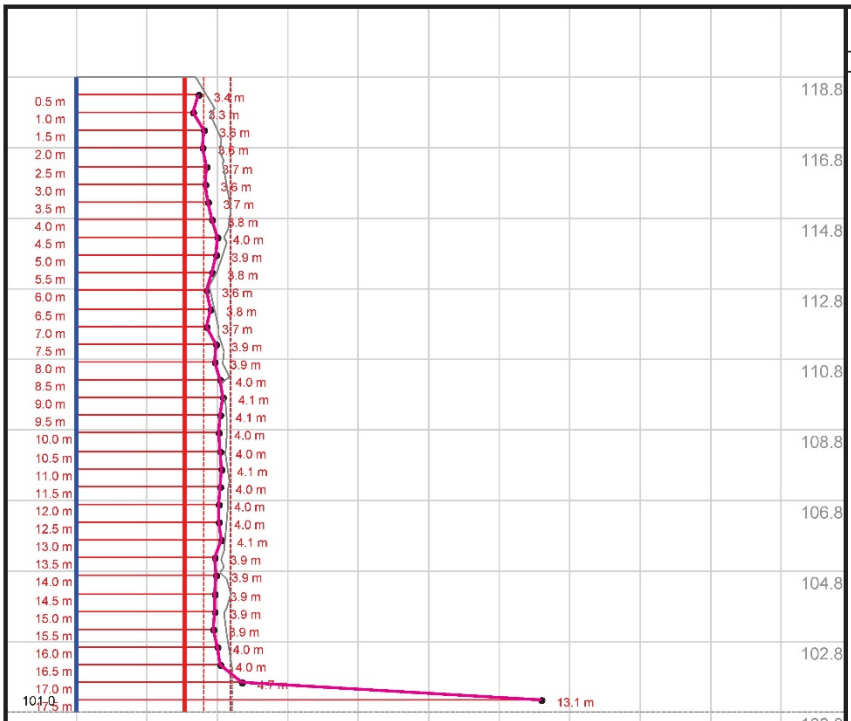

Burden	
Depth	Burden
0.86	3.89
1.08	3.76
1.49	3.95
1.75	4.09
2.10	4.05
2.35	4.17
2.38	4.10
3.70	4.34
4.27	4.27
4.51	4.14
4.64	4.22
5.33	4.00
5.46	3.98
5.85	3.75
7.06	3.99
7.24	4.02
7.68	4.14
8.04	4.12
8.42	4.32
8.62	4.06
8.82	4.12
9.04	4.14
9.10	4.18
9.59	4.22
9.83	4.22
10.05	4.25
10.59	4.20
11.34	4.29
11.55	4.28
11.98	4.27
13.29	4.17
13.52	4.06
13.56	4.08
13.74	4.14
13.91	4.03
14.11	4.24
14.50	4.34
14.91	4.23
15.07	4.14
15.07	4.14
15.67	4.25
15.67	4.25
16.63	4.40
16.63	4.40
Min: 5.85	3.75

TECHNICAL DATA

Hole:	7	Offset:	0.0 m	BurdenMaster Settings:	
East:	986.75	Horizontal Offset:	0.0 m	Search Width:	3.0 m
North:	884.76	Vert. Face Height:	17.8 m	BM Grid (H x V):	0.5 m x 0.5 m
Elevation:	118.8	Profile Area:	73.9 m²	Burden To Report:	3.1 m
Drill Azimuth (°):	0.0	Planned Burden:	4.0 m	Excessive Burden:	4.9 m
Search Azimuth (°):	0.0	Tolerance:	10.0 %		
Drill Angle (°):	0.0	Floorlevel:	101.0		
Hole length:	17.8 m	Critical Burden:	3.1 m		
Subdrill:	0.0 m	Stemming:	2.8 m		
Diameter:	89 mm				

QuarryX

Blasting Engineer: Paul P. Kuznik, P. Eng.
Client: CRH Ogden Point
Site:CRH Ogden Point
Hole 8 of 25

Project: CRH Ogden Point P3 2018-01
Filename: OPC P3.qxd
Printed at: 2018-04-24 14:30:46
Scale: 1:150

DYNO Dyno Nobel

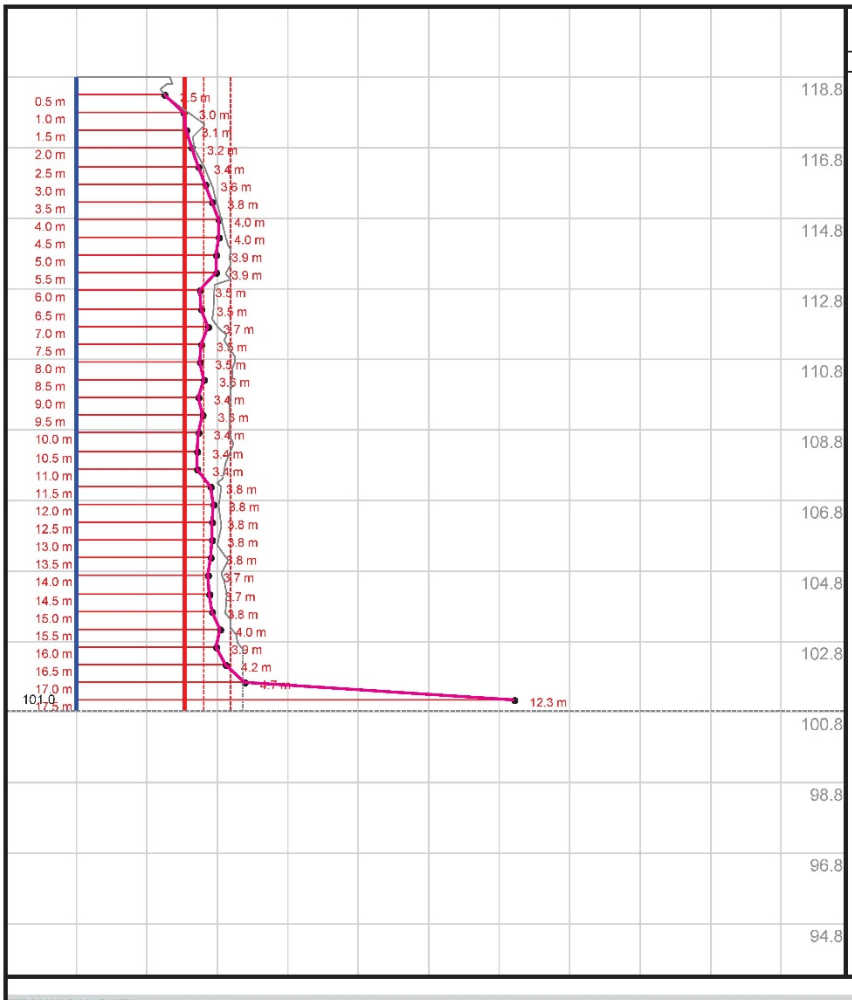

Burden	
Depth	Burden
0.19	2.69
0.36	2.36
0.57	2.55
1.66	3.29
2.01	3.31
2.65	3.67
3.14	3.84
3.71	4.02
4.46	4.18
4.85	4.36
5.08	4.31
5.53	4.18
5.68	4.33
6.66	3.83
6.77	3.81
7.04	4.01
7.23	4.22
7.40	4.17
7.85	4.46
7.99	4.47
8.19	4.37
8.42	4.38
9.22	4.29
9.38	4.31
9.93	4.29
10.15	4.36
10.28	4.40
10.85	4.20
11.26	4.10
11.39	3.96
11.49	4.09
12.03	3.99
12.61	4.09
13.14	3.95
13.55	4.26
13.93	4.08
14.12	4.16
14.51	4.23
15.06	4.21
15.26	4.34
15.49	4.33
15.66	4.50
15.87	4.55
16.06	4.68
[illegible]	[illegible]
Min: 6.77	3.81

TECHNICAL DATA

Hole:	8	Offset:	0.0 m	BurdenMaster Settings:	
East:	991.17	Horizontal Offset:	0.0 m	Search Width:	3.0 m
North:	886.52	Vert. Face Height:	17.8 m	BM Grid (H x V):	0.5 m x 0.5 m
Elevation:	118.76	Profile Area:	72.3 m²	Burden To Report:	3.1 m
Drill Azimuth (°):	0.0	Planned Burden:	4.0 m	Excessive Burden:	4.9 m
Search Azimuth (°):	0.0	Tolerance:	10.0 %		
Drill Angle (°):	0.0	Floorlevel:	101.0		
Hole length:	17.8 m	Critical Burden:	3.1 m		
Subdrill:	0.0 m	Stemming:	2.8 m		
Diameter:	89 mm				

QuarryX

Blasting Engineer: Paul P. Kuznik, P. Eng.
Client: CRH Ogden Point
Site:CRH Ogden Point
Hole 9 of 25

Project: CRH Ogden Point P3 2018-01
Filename: OPC P3.qxd
Printed at: 2018-04-24 14:30:47
Scale: 1:150

DYNO Dyno Nobel

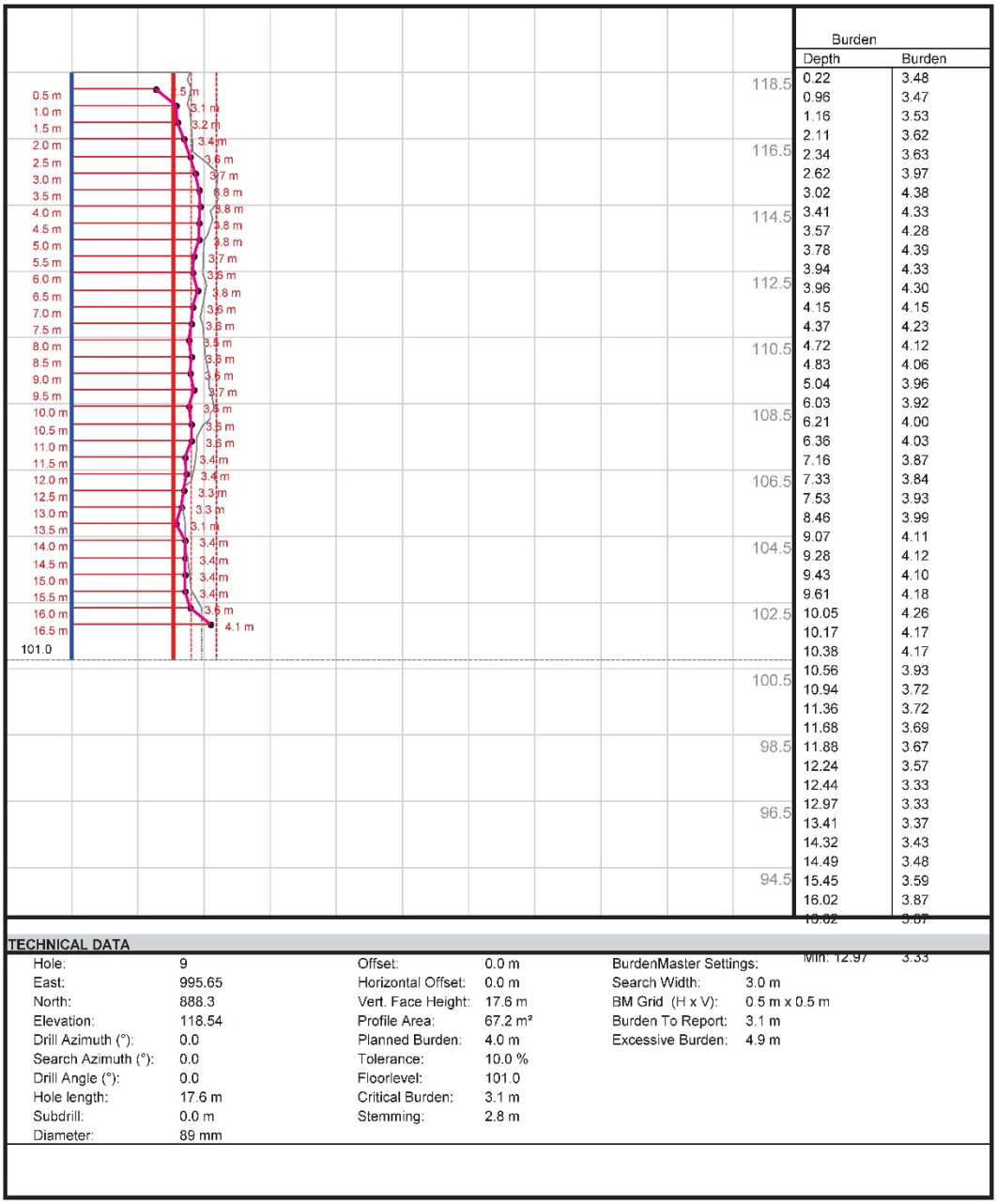

Burden	
Depth	Burden
0.22	3.48
0.96	3.47
1.16	3.53
2.11	3.62
2.34	3.63
2.62	3.97
3.02	4.38
3.41	4.33
3.57	4.28
3.78	4.39
3.94	4.33
3.96	4.30
4.15	4.15
4.37	4.23
4.72	4.12
4.83	4.06
5.04	3.96
6.03	3.92
6.21	4.00
6.36	4.03
7.16	3.87
7.33	3.84
7.53	3.93
8.46	3.99
9.07	4.11
9.28	4.12
9.43	4.10
9.61	4.18
10.05	4.26
10.17	4.17
10.38	4.17
10.56	3.93
10.94	3.72
11.36	3.72
11.68	3.69
11.88	3.67
12.24	3.57
12.44	3.33
12.97	3.33
13.41	3.37
14.32	3.43
14.49	3.48
15.45	3.59
16.02	3.87
[illegible]	[illegible]
Min: 12.97	3.33

TECHNICAL DATA

Hole:	9	Offset:	0.0 m	BurdenMaster Settings:	
East:	995.65	Horizontal Offset:	0.0 m	Search Width:	3.0 m
North:	888.3	Vert. Face Height:	17.6 m	BM Grid (H x V):	0.5 m x 0.5 m
Elevation:	118.54	Profile Area:	67.2 m²	Burden To Report:	3.1 m
Drill Azimuth (°):	0.0	Planned Burden:	4.0 m	Excessive Burden:	4.9 m
Search Azimuth (°):	0.0	Tolerance:	10.0 %		
Drill Angle (°):	0.0	Floorlevel:	101.0		
Hole length:	17.6 m	Critical Burden:	3.1 m		
Subdrill:	0.0 m	Stemming:	2.8 m		
Diameter:	89 mm				

QuarryX

Blasting Engineer: Paul P. Kuznik, P. Eng.
Client: CRH Ogden Point
Site:CRH Ogden Point
Hole 10 of 25

Project: CRH Ogden Point P3 2018-01
Filename: OPC P3.qxd
Printed at: 2018-04-24 14:30:47
Scale: 1:150

DYNO Dyno Nobel

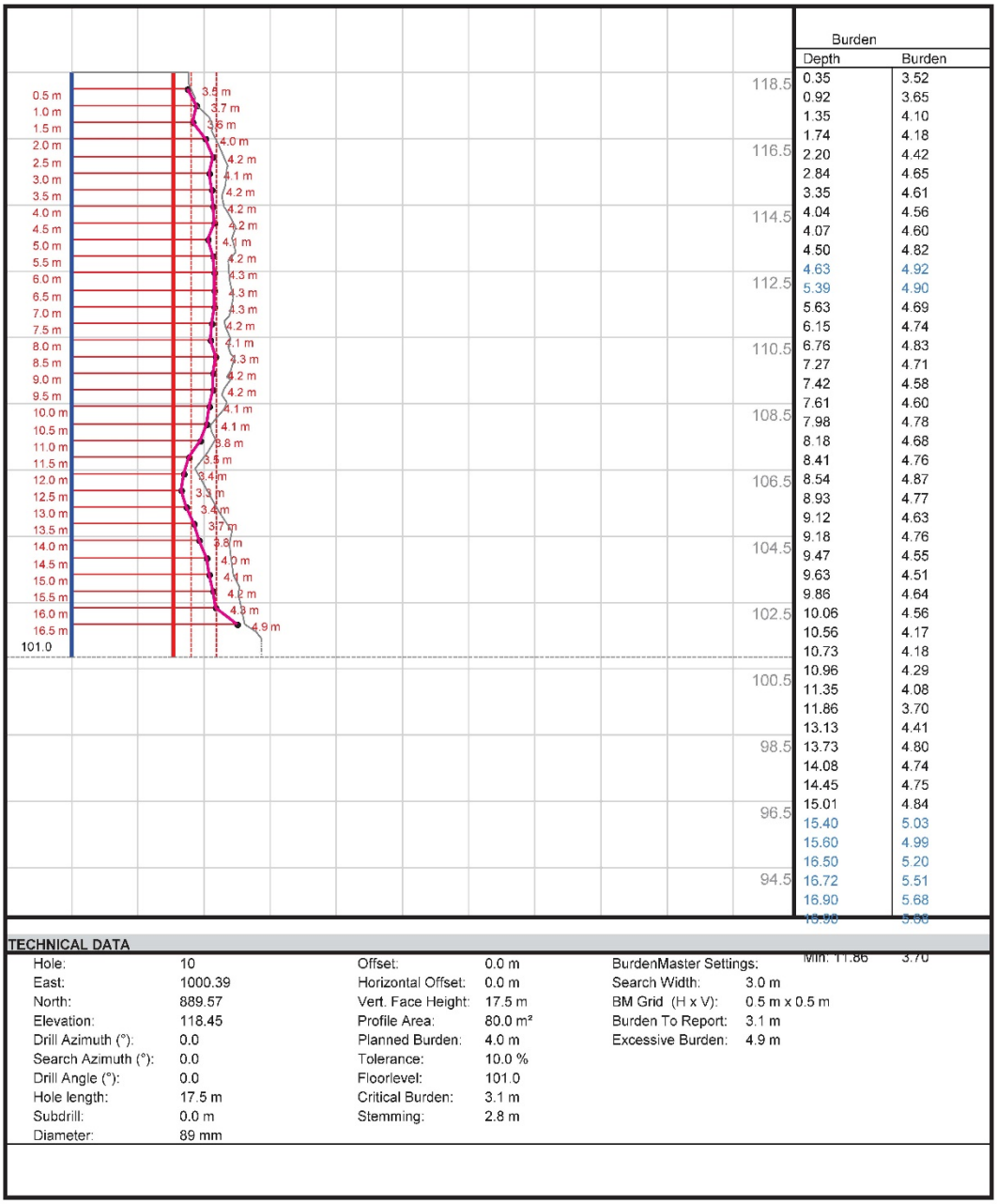

Burden	
Depth	Burden
0.35	3.52
0.92	3.65
1.35	4.10
1.74	4.18
2.20	4.42
2.84	4.65
3.35	4.61
4.04	4.56
4.07	4.60
4.50	4.82
4.63	4.92
5.39	4.90
5.63	4.69
6.15	4.74
6.76	4.83
7.27	4.71
7.42	4.58
7.61	4.60
7.98	4.78
8.18	4.68
8.41	4.76
8.54	4.87
8.93	4.77
9.12	4.63
9.18	4.76
9.47	4.55
9.63	4.51
9.86	4.64
10.06	4.56
10.56	4.17
10.73	4.18
10.96	4.29
11.35	4.08
11.86	3.70
13.13	4.41
13.73	4.80
14.08	4.74
14.45	4.75
15.01	4.84
15.40	5.03
15.60	4.99
16.50	5.20
16.72	5.51
16.90	5.68
[illegible]	[illegible]
Min: 11.86	3.70

TECHNICAL DATA

Hole:	10	Offset:	0.0 m	BurdenMaster Settings:	
East:	1000.39	Horizontal Offset:	0.0 m	Search Width:	3.0 m
North:	889.57	Vert. Face Height:	17.5 m	BM Grid (H x V):	0.5 m x 0.5 m
Elevation:	118.45	Profile Area:	80.0 m²	Burden To Report:	3.1 m
Drill Azimuth (°):	0.0	Planned Burden:	4.0 m	Excessive Burden:	4.9 m
Search Azimuth (°):	0.0	Tolerance:	10.0 %		
Drill Angle (°):	0.0	Floorlevel:	101.0		
Hole length:	17.5 m	Critical Burden:	3.1 m		
Subdrill:	0.0 m	Stemming:	2.8 m		
Diameter:	89 mm				

QuarryX

Blasting Engineer: Paul P. Kuznik, P. Eng.
Client: CRH Ogden Point
Site:CRH Ogden Point
Hole 11 of 25

Project: CRH Ogden Point P3 2018-01
Filename: OPC P3.qxd
Printed at: 2018-04-24 14:30:48
Scale: 1:150

DYNO Dyno Nobel

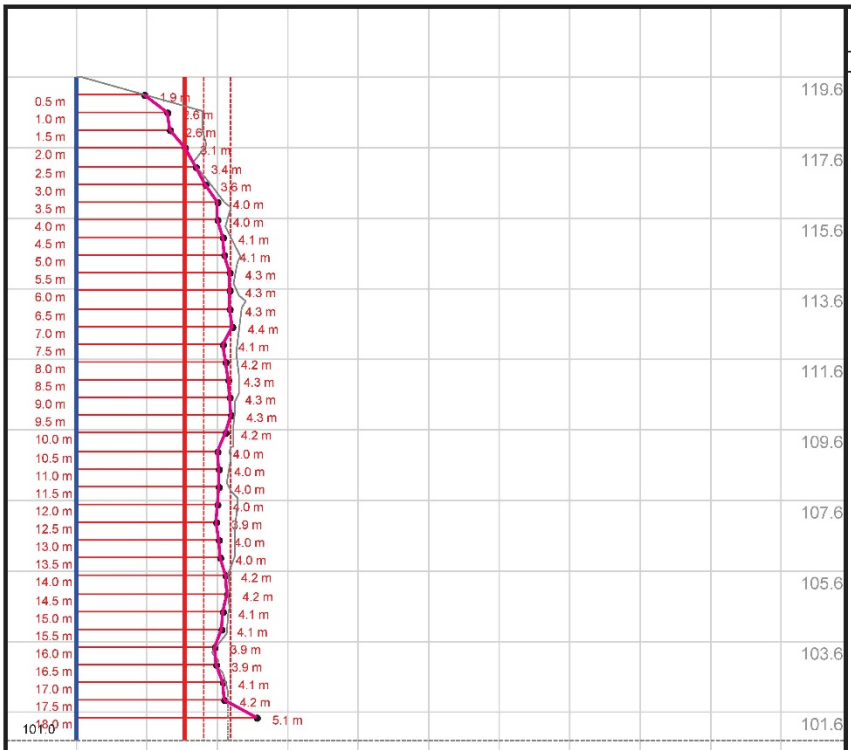

Burden	
Depth	Burden
0.97	3.53
1.91	3.68
2.40	3.27
3.04	3.81
3.51	4.16
4.19	4.21
5.02	4.61
5.20	4.55
5.37	4.50
5.77	4.44
6.14	4.58
6.27	4.77
6.48	4.63
7.73	4.48
8.37	4.58
8.53	4.56
8.70	4.58
8.88	4.57
9.09	4.45
9.42	4.44
9.77	4.43
10.35	4.43
10.40	4.35
10.51	4.31
10.70	4.35
11.40	4.24
11.61	4.35
11.82	4.53
11.97	4.52
12.70	4.45
13.44	4.45
13.95	4.25
14.32	4.31
14.57	4.28
14.90	4.32
15.08	4.25
15.61	4.21
15.83	4.07
16.15	3.83
16.38	4.00
16.54	3.92
16.74	4.11
17.09	4.24
17.29	4.27
[illegible]	[illegible]
Min: 2.87	3.68

TECHNICAL DATA

Hole:	11	Offset:	0.0 m	BurdenMaster Settings:	
East:	1003.9	Horizontal Offset:	0.0 m	Search Width:	3.0 m
North:	891.18	Vert. Face Height:	18.6 m	BM Grid (H x V):	0.5 m x 0.5 m
Elevation:	119.59	Profile Area:	77.1 m²	Burden To Report:	3.1 m
Drill Azimuth (°):	0.0	Planned Burden:	4.0 m	Excessive Burden:	4.9 m
Search Azimuth (°):	0.0	Tolerance:	10.0 %		
Drill Angle (°):	0.0	Floorlevel:	101.0		
Hole length:	18.6 m	Critical Burden:	3.1 m		
Subdrill:	0.0 m	Stemming:	2.8 m		
Diameter:	89 mm				

QuarryX

Blasting Engineer: Paul P. Kuznik, P. Eng.
Client: CRH Ogden Point
Site:CRH Ogden Point
Hole 13 of 25

Project: CRH Ogden Point P3 2018-01
Filename: OPC P3.qxd
Printed at: 2018-04-24 14:30:48
Scale: 1:150

DYNO Dyno Nobel

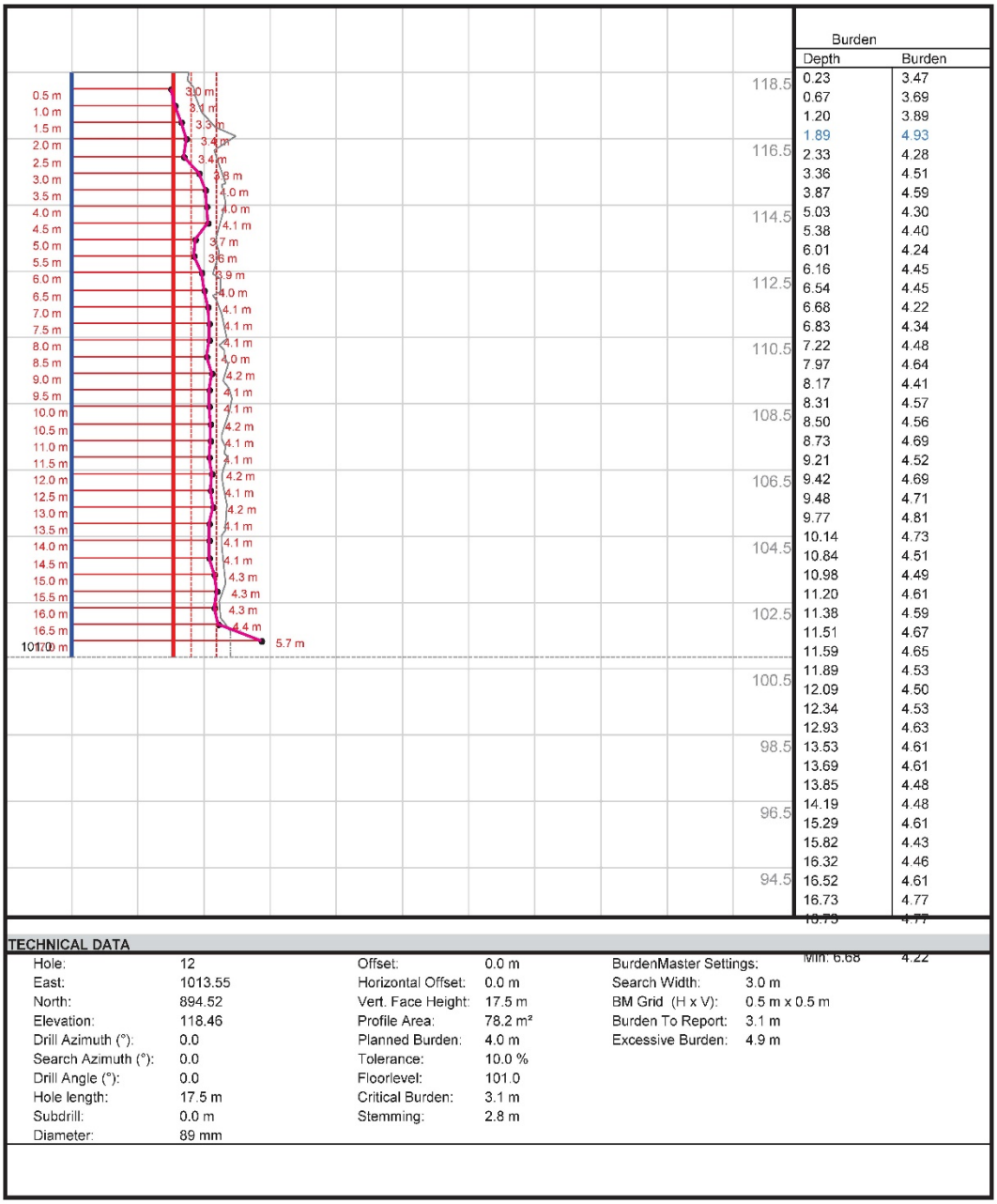

Burden	
Depth	Burden
0.23	3.47
0.67	3.69
1.20	3.89
1.89	4.93
2.33	4.28
3.36	4.51
3.87	4.59
5.03	4.30
5.38	4.40
6.01	4.24
6.16	4.45
6.54	4.45
6.68	4.22
6.83	4.34
7.22	4.48
7.97	4.64
8.17	4.41
8.31	4.57
8.50	4.56
8.73	4.69
9.21	4.52
9.42	4.69
9.48	4.71
9.77	4.81
10.14	4.73
10.84	4.51
10.98	4.49
11.20	4.61
11.38	4.59
11.51	4.67
11.59	4.65
11.89	4.53
12.09	4.50
12.34	4.53
12.93	4.63
13.53	4.61
13.69	4.61
13.85	4.48
14.19	4.48
15.29	4.61
15.82	4.43
16.32	4.46
16.52	4.61
16.73	4.77
Min: 6.68	4.22

TECHNICAL DATA

Hole:	12	Offset:	0.0 m	BurdenMaster Settings:	
East:	1013.55	Horizontal Offset:	0.0 m	Search Width:	3.0 m
North:	894.52	Vert. Face Height:	17.5 m	BM Grid (H x V):	0.5 m x 0.5 m
Elevation:	118.46	Profile Area:	78.2 m²	Burden To Report:	3.1 m
Drill Azimuth (°):	0.0	Planned Burden:	4.0 m	Excessive Burden:	4.9 m
Search Azimuth (°):	0.0	Tolerance:	10.0 %		
Drill Angle (°):	0.0	Floorlevel:	101.0		
Hole length:	17.5 m	Critical Burden:	3.1 m		
Subdrill:	0.0 m	Stemming:	2.8 m		
Diameter:	89 mm				

QuarryX

Blasting Engineer: Paul P. Kuznik, P. Eng.
Client: CRH Ogden Point
Site:CRH Ogden Point
Hole 14 of 25

Project: CRH Ogden Point P3 2018-01
Filename: OPC P3.qxd
Printed at: 2018-04-24 14:30:49
Scale: 1:150

DYNO Dyno Nobel

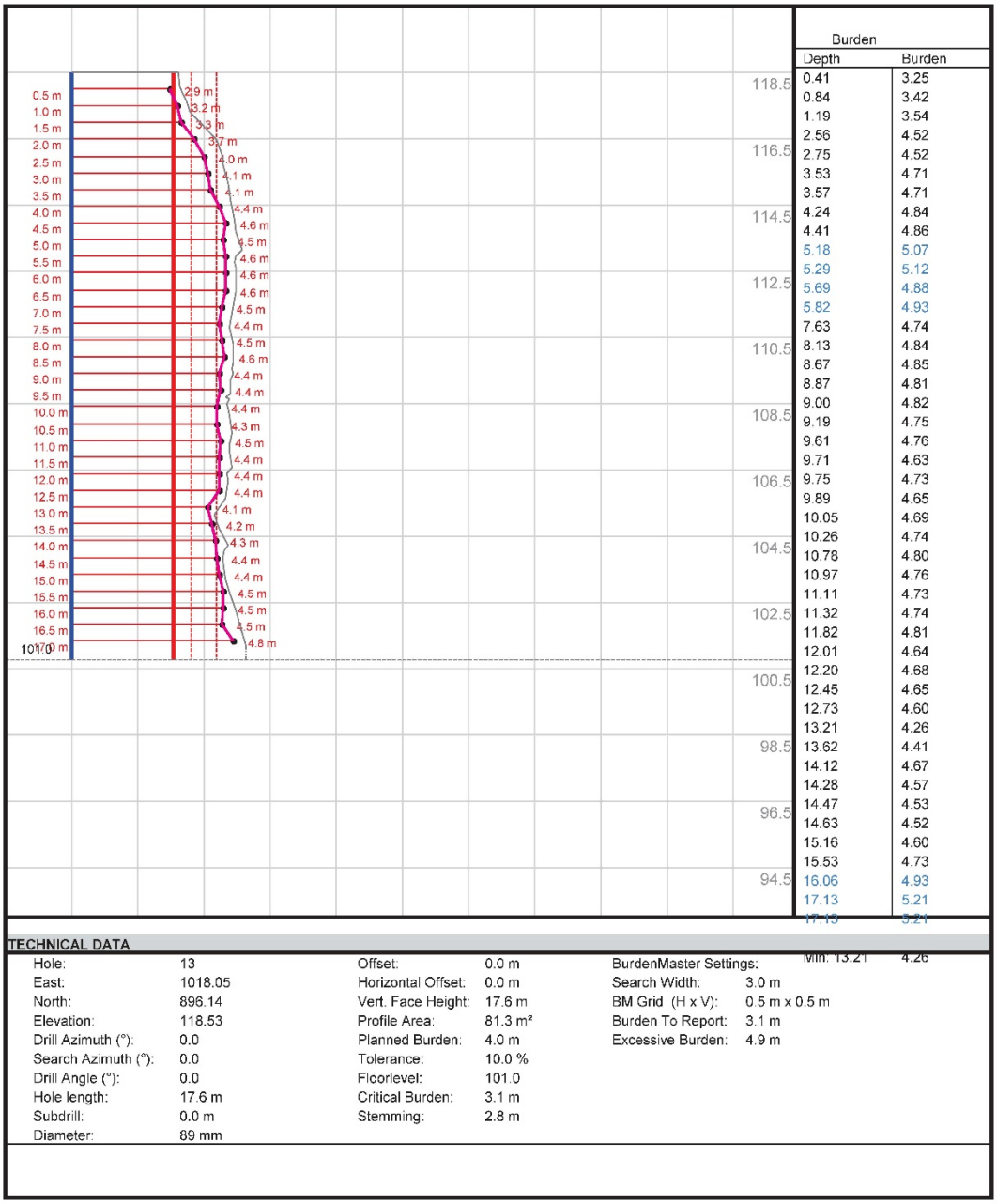

Burden	
Depth	Burden
0.41	3.25
0.84	3.42
1.19	3.54
2.56	4.52
2.75	4.52
3.53	4.71
3.57	4.71
4.24	4.84
4.41	4.86
5.18	5.07
5.29	5.12
5.69	4.88
5.82	4.93
7.63	4.74
8.13	4.84
8.67	4.85
8.87	4.81
9.00	4.82
9.19	4.75
9.61	4.76
9.71	4.63
9.75	4.73
9.89	4.65
10.05	4.69
10.26	4.74
10.78	4.80
10.97	4.76
11.11	4.73
11.32	4.74
11.82	4.81
12.01	4.64
12.20	4.68
12.45	4.65
12.73	4.60
13.21	4.26
13.62	4.41
14.12	4.67
14.28	4.57
14.47	4.53
14.63	4.52
15.16	4.60
15.53	4.73
16.06	4.93
17.13	5.21
[illegible]	[illegible]
Min: 13.21	4.26

TECHNICAL DATA

Hole:	13	Offset:	0.0 m	BurdenMaster Settings:	
East:	1018.05	Horizontal Offset:	0.0 m	Search Width:	3.0 m
North:	896.14	Vert. Face Height:	17.6 m	BM Grid (H x V):	0.5 m x 0.5 m
Elevation:	118.53	Profile Area:	81.3 m²	Burden To Report:	3.1 m
Drill Azimuth (°):	0.0	Planned Burden:	4.0 m	Excessive Burden:	4.9 m
Search Azimuth (°):	0.0	Tolerance:	10.0 %		
Drill Angle (°):	0.0	Floorlevel:	101.0		
Hole length:	17.6 m	Critical Burden:	3.1 m		
Subdrill:	0.0 m	Stemming:	2.8 m		
Diameter:	89 mm				

QuarryX

Blasting Engineer: Paul P. Kuznik, P. Eng.
Client: CRH Ogden Point
Site:CRH Ogden Point
Hole 15 of 25

Project: CRH Ogden Point P3 2018-01
Filename: OPC P3.qxd
Printed at: 2018-04-24 14:30:49
Scale: 1:150

DYNO Dyno Nobel

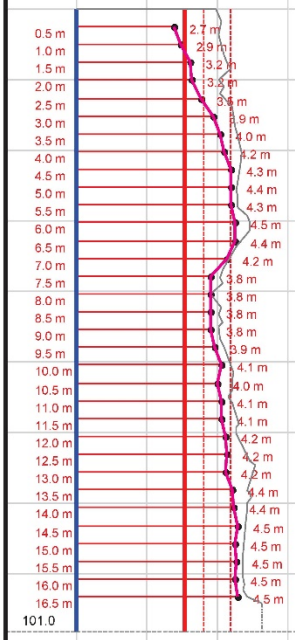

Burden

Depth	Burden
0.33	4.07
1.29	4.15
1.50	4.22
1.97	4.00
2.16	4.17
2.74	4.37
3.29	4.47
4.06	4.65
4.37	4.61
5.22	4.55
5.45	4.55
5.79	4.81
5.98	4.88
6.68	4.48
7.32	4.12
7.70	4.11
8.01	3.79
8.56	4.01
8.78	4.10
9.27	4.04
9.47	4.14
10.20	4.42
10.39	4.37
10.70	4.37
10.89	4.26
11.04	4.37
11.65	4.57
11.75	4.48
11.94	4.49
12.67	4.87
12.82	5.02
13.53	4.81
13.56	4.86
13.72	4.93
13.88	4.79
14.05	4.80
14.40	4.77
15.29	4.68
15.81	4.68
15.97	4.70
16.16	4.71
16.30	4.67
16.49	4.80
16.69	5.23
[illegible]	[illegible]
Min: 8.01	3.79

TECHNICAL DATA

Hole:	14	Offset:	0.0 m	BurdenMaster Settings:	
East:	1022.35	Horizontal Offset:	0.0 m	Search Width:	3.0 m
North:	897.76	Vert. Face Height:	17.5 m	BM Grid (H x V):	0.5 m x 0.5 m
Elevation:	118.44	Profile Area:	78.4 m²	Burden To Report:	3.1 m
Drill Azimuth (°):	0.0	Planned Burden:	4.0 m	Excessive Burden:	4.9 m
Search Azimuth (°):	0.0	Tolerance:	10.0 %		
Drill Angle (°):	0.0	Floorlevel:	101.0		
Hole length:	17.5 m	Critical Burden:	3.1 m		
Subdrill:	0.0 m	Stemming:	2.8 m		
Diameter:	89 mm				

QuarryX

Blasting Engineer: Paul P. Kuznik, P. Eng.
Client: CRH Ogden Point
Site:CRH Ogden Point
Hole 16 of 25

Project: CRH Ogden Point P3 2018-01
Filename: OPC P3.qxd
Printed at: 2018-04-24 14:30:50
Scale: 1:150

DYNO Dyno Nobel

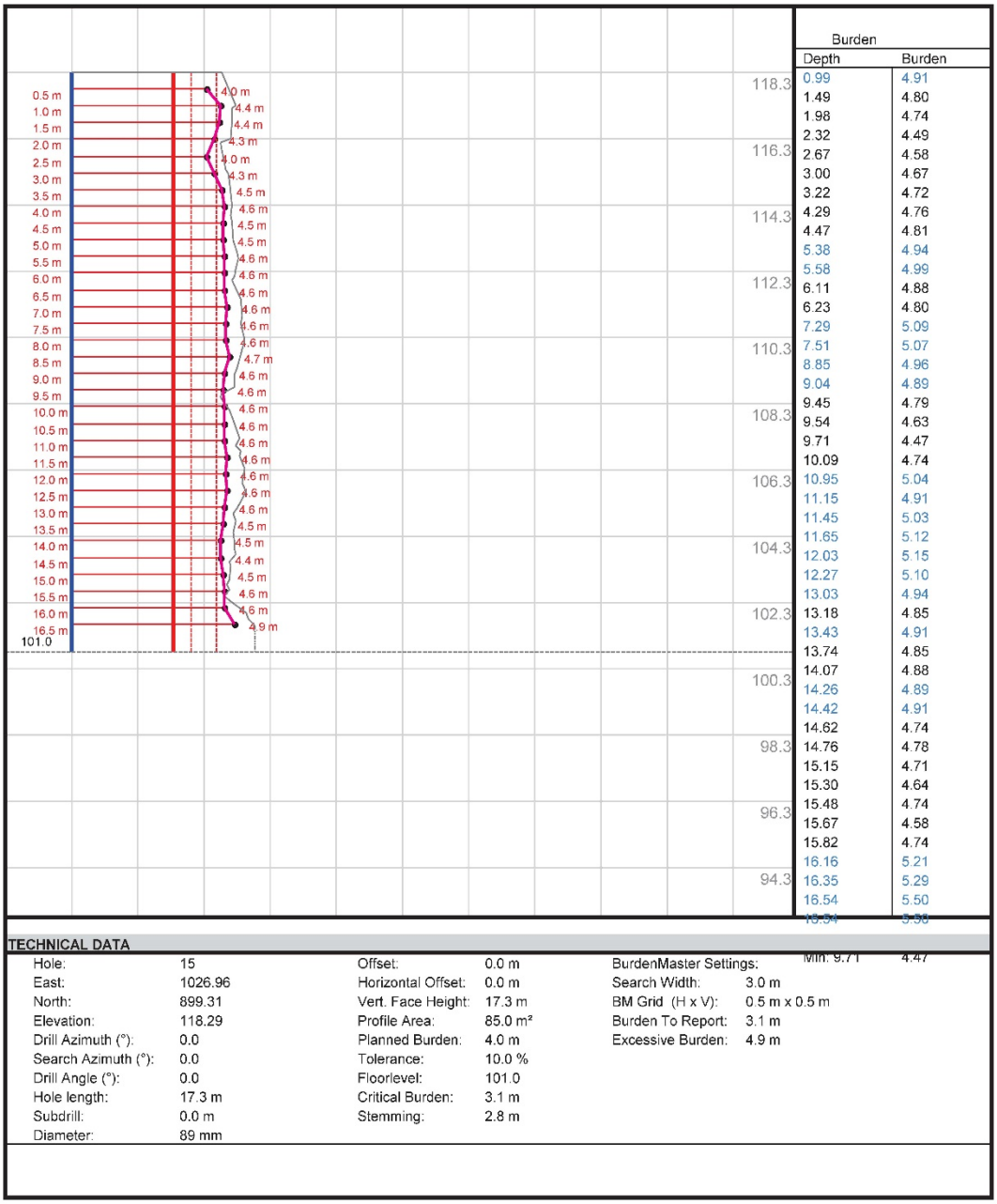

Burden	
Depth	Burden
0.99	4.91
1.49	4.80
1.98	4.74
2.32	4.49
2.67	4.58
3.00	4.67
3.22	4.72
4.29	4.76
4.47	4.81
5.38	4.94
5.58	4.99
6.11	4.88
6.23	4.80
7.29	5.09
7.51	5.07
8.85	4.96
9.04	4.89
9.45	4.79
9.54	4.63
9.71	4.47
10.09	4.74
10.95	5.04
11.15	4.91
11.45	5.03
11.65	5.12
12.03	5.15
12.27	5.10
13.03	4.94
13.18	4.85
13.43	4.91
13.74	4.85
14.07	4.88
14.26	4.89
14.42	4.91
14.62	4.74
14.76	4.78
15.15	4.71
15.30	4.64
15.48	4.74
15.67	4.58
15.82	4.74
16.16	5.21
16.35	5.29
16.54	5.50
[illegible]	[illegible]
Min: 9.71	4.47

TECHNICAL DATA

Hole:	15	Offset:	0.0 m	BurdenMaster Settings:	
East:	1026.96	Horizontal Offset:	0.0 m	Search Width:	3.0 m
North:	899.31	Vert. Face Height:	17.3 m	BM Grid (H x V):	0.5 m x 0.5 m
Elevation:	118.29	Profile Area:	85.0 m²	Burden To Report:	3.1 m
Drill Azimuth (°):	0.0	Planned Burden:	4.0 m	Excessive Burden:	4.9 m
Search Azimuth (°):	0.0	Tolerance:	10.0 %		
Drill Angle (°):	0.0	Floorlevel:	101.0		
Hole length:	17.3 m	Critical Burden:	3.1 m		
Subdrill:	0.0 m	Stemming:	2.8 m		
Diameter:	89 mm				

QuarryX

Blasting Engineer: Paul P. Kuznik, P. Eng.
Client: CRH Ogden Point
Site:CRH Ogden Point
Hole 17 of 25

Project: CRH Ogden Point P3 2018-01
Filename: OPC P3.qxd
Printed at: 2018-04-24 14:30:50
Scale: 1:150

DYNO Dyno Nobel

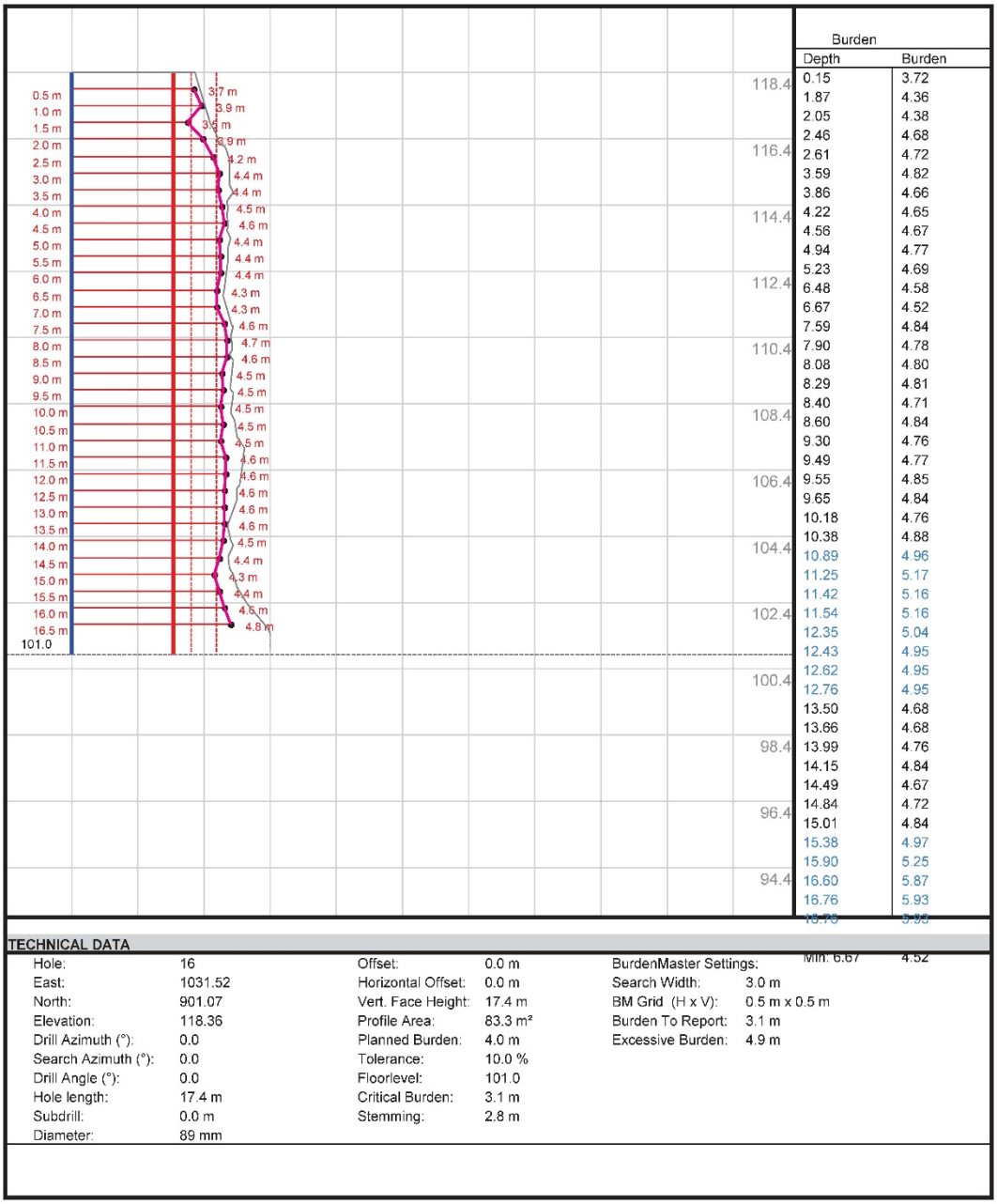

Burden	
Depth	Burden
0.15	3.72
1.87	4.36
2.05	4.38
2.46	4.68
2.61	4.72
3.59	4.82
3.86	4.66
4.22	4.65
4.56	4.67
4.94	4.77
5.23	4.69
6.48	4.58
6.67	4.52
7.59	4.84
7.90	4.78
8.08	4.80
8.29	4.81
8.40	4.71
8.60	4.84
9.30	4.76
9.49	4.77
9.55	4.85
9.65	4.84
10.18	4.76
10.38	4.88
10.89	4.96
11.25	5.17
11.42	5.16
11.54	5.16
12.35	5.04
12.43	4.95
12.62	4.95
12.76	4.95
13.50	4.68
13.66	4.68
13.99	4.76
14.15	4.84
14.49	4.67
14.84	4.72
15.01	4.84
15.38	4.97
15.90	5.25
16.60	5.87
16.76	5.93
[illegible]	[illegible]
Min: 6.67	4.52

TECHNICAL DATA

Hole:	16	Offset:	0.0 m	BurdenMaster Settings:	
East:	1031.52	Horizontal Offset:	0.0 m	Search Width:	3.0 m
North:	901.07	Vert. Face Height:	17.4 m	BM Grid (H x V):	0.5 m x 0.5 m
Elevation:	118.36	Profile Area:	83.3 m²	Burden To Report:	3.1 m
Drill Azimuth (°):	0.0	Planned Burden:	4.0 m	Excessive Burden:	4.9 m
Search Azimuth (°):	0.0	Tolerance:	10.0 %		
Drill Angle (°):	0.0	Floorlevel:	101.0		
Hole length:	17.4 m	Critical Burden:	3.1 m		
Subdrill:	0.0 m	Stemming:	2.8 m		
Diameter:	89 mm				

QuarryX

Blasting Engineer: Paul P. Kuznik, P. Eng.
Client: CRH Ogden Point
Site:CRH Ogden Point
Hole 18 of 25

Project: CRH Ogden Point P3 2018-01
Filename: OPC P3.qxd
Printed at: 2018-04-24 14:30:51
Scale: 1:150

DYNO Dyno Nobel

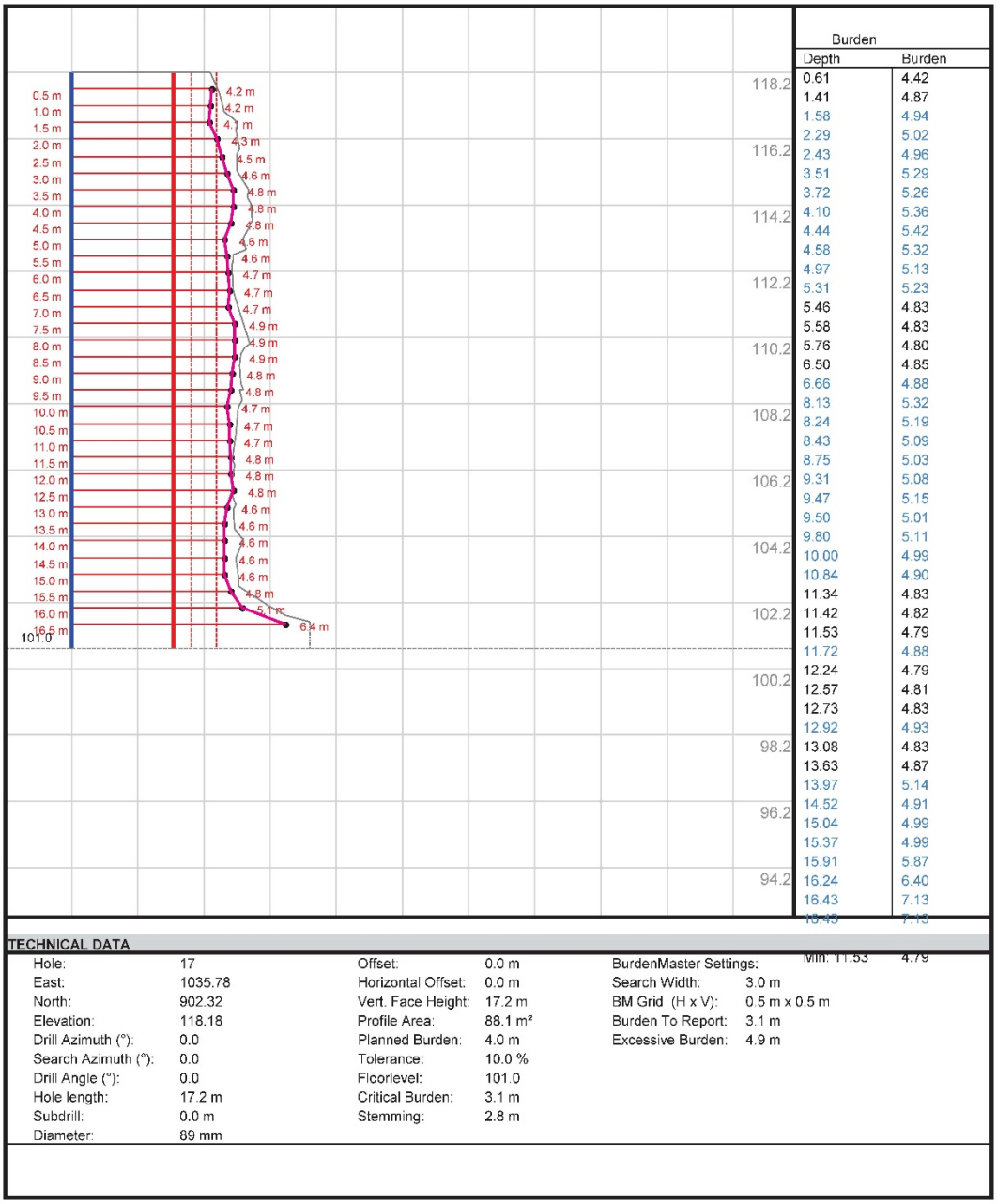

Burden

Depth	Burden
0.61	4.42
1.41	4.87
1.58	4.94
2.29	5.02
2.43	4.96
3.51	5.29
3.72	5.26
4.10	5.36
4.44	5.42
4.58	5.32
4.97	5.13
5.31	5.23
5.46	4.83
5.58	4.83
5.76	4.80
6.50	4.85
6.66	4.88
8.13	5.32
8.24	5.19
8.43	5.09
8.75	5.03
9.31	5.08
9.47	5.15
9.50	5.01
9.80	5.11
10.00	4.99
10.84	4.90
11.34	4.83
11.42	4.82
11.53	4.79
11.72	4.88
12.24	4.79
12.57	4.81
12.73	4.83
12.92	4.93
13.08	4.83
13.63	4.87
13.97	5.14
14.52	4.91
15.04	4.99
15.37	4.99
15.91	5.87
16.24	6.40
16.43	7.13
[illegible]	[illegible]
Min: 11.53	4.79

TECHNICAL DATA

Hole:	17	Offset:	0.0 m	BurdenMaster Settings:	
East:	1035.78	Horizontal Offset:	0.0 m	Search Width:	3.0 m
North:	902.32	Vert. Face Height:	17.2 m	BM Grid (H x V):	0.5 m x 0.5 m
Elevation:	118.18	Profile Area:	88.1 m²	Burden To Report:	3.1 m
Drill Azimuth (°):	0.0	Planned Burden:	4.0 m	Excessive Burden:	4.9 m
Search Azimuth (°):	0.0	Tolerance:	10.0 %		
Drill Angle (°):	0.0	Floorlevel:	101.0		
Hole length:	17.2 m	Critical Burden:	3.1 m		
Subdrill:	0.0 m	Stemming:	2.8 m		
Diameter:	89 mm				

QuarryX

Blasting Engineer: Paul P. Kuznik, P. Eng.
Client: CRH Ogden Point
Site:CRH Ogden Point
Hole 19 of 25

Project: CRH Ogden Point P3 2018-01
Filename: OPC P3.qxd
Printed at: 2018-04-24 14:30:51
Scale: 1:150

DYNO Dyno Nobel

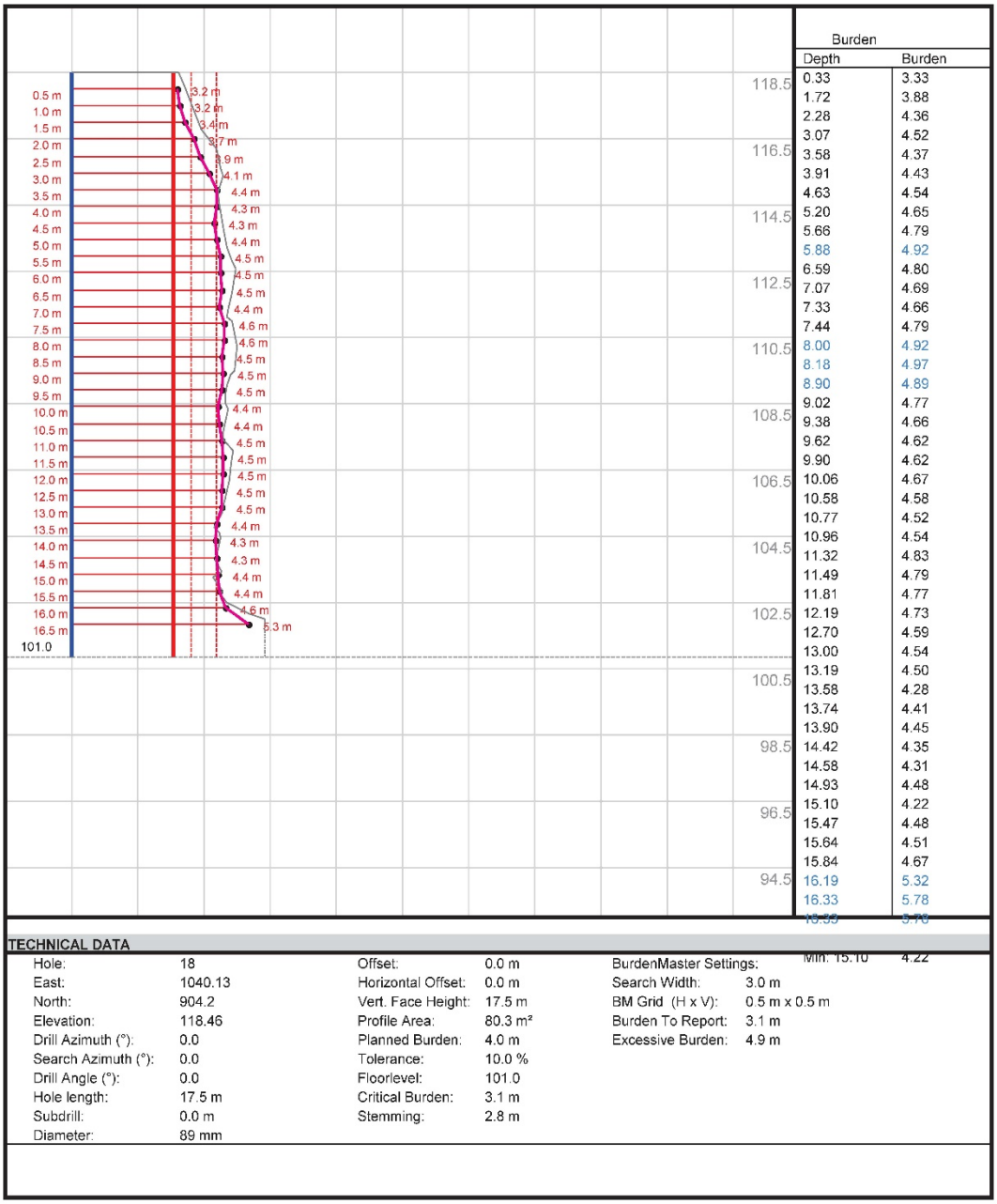

Burden	
Depth	Burden
0.33	3.33
1.72	3.88
2.28	4.36
3.07	4.52
3.58	4.37
3.91	4.43
4.63	4.54
5.20	4.65
5.66	4.79
5.88	4.92
6.59	4.80
7.07	4.69
7.33	4.66
7.44	4.79
8.00	4.92
8.18	4.97
8.90	4.89
9.02	4.77
9.38	4.66
9.62	4.62
9.90	4.62
10.06	4.67
10.58	4.58
10.77	4.52
10.96	4.54
11.32	4.83
11.49	4.79
11.81	4.77
12.19	4.73
12.70	4.59
13.00	4.54
13.19	4.50
13.58	4.28
13.74	4.41
13.90	4.45
14.42	4.35
14.58	4.31
14.93	4.48
15.10	4.22
15.47	4.48
15.64	4.51
15.84	4.67
16.19	5.32
16.33	5.78
[illegible]	[illegible]

Min: 15.10 4.22

TECHNICAL DATA

Hole:	18	Offset:	0.0 m	BurdenMaster Settings:	
East:	1040.13	Horizontal Offset:	0.0 m	Search Width:	3.0 m
North:	904.2	Vert. Face Height:	17.5 m	BM Grid (H x V):	0.5 m x 0.5 m
Elevation:	118.46	Profile Area:	80.3 m²	Burden To Report:	3.1 m
Drill Azimuth (°):	0.0	Planned Burden:	4.0 m	Excessive Burden:	4.9 m
Search Azimuth (°):	0.0	Tolerance:	10.0 %		
Drill Angle (°):	0.0	Floorlevel:	101.0		
Hole length:	17.5 m	Critical Burden:	3.1 m		
Subdrill:	0.0 m	Stemming:	2.8 m		
Diameter:	89 mm				

QuarryX

Blasting Engineer: Paul P. Kuznik, P. Eng.
Client: CRH Ogden Point
Site:CRH Ogden Point
Hole 20 of 25

Project: CRH Ogden Point P3 2018-01
Filename: OPC P3.qxd
Printed at: 2018-04-24 14:30:52
Scale: 1:150

DYNO Dyno Nobel

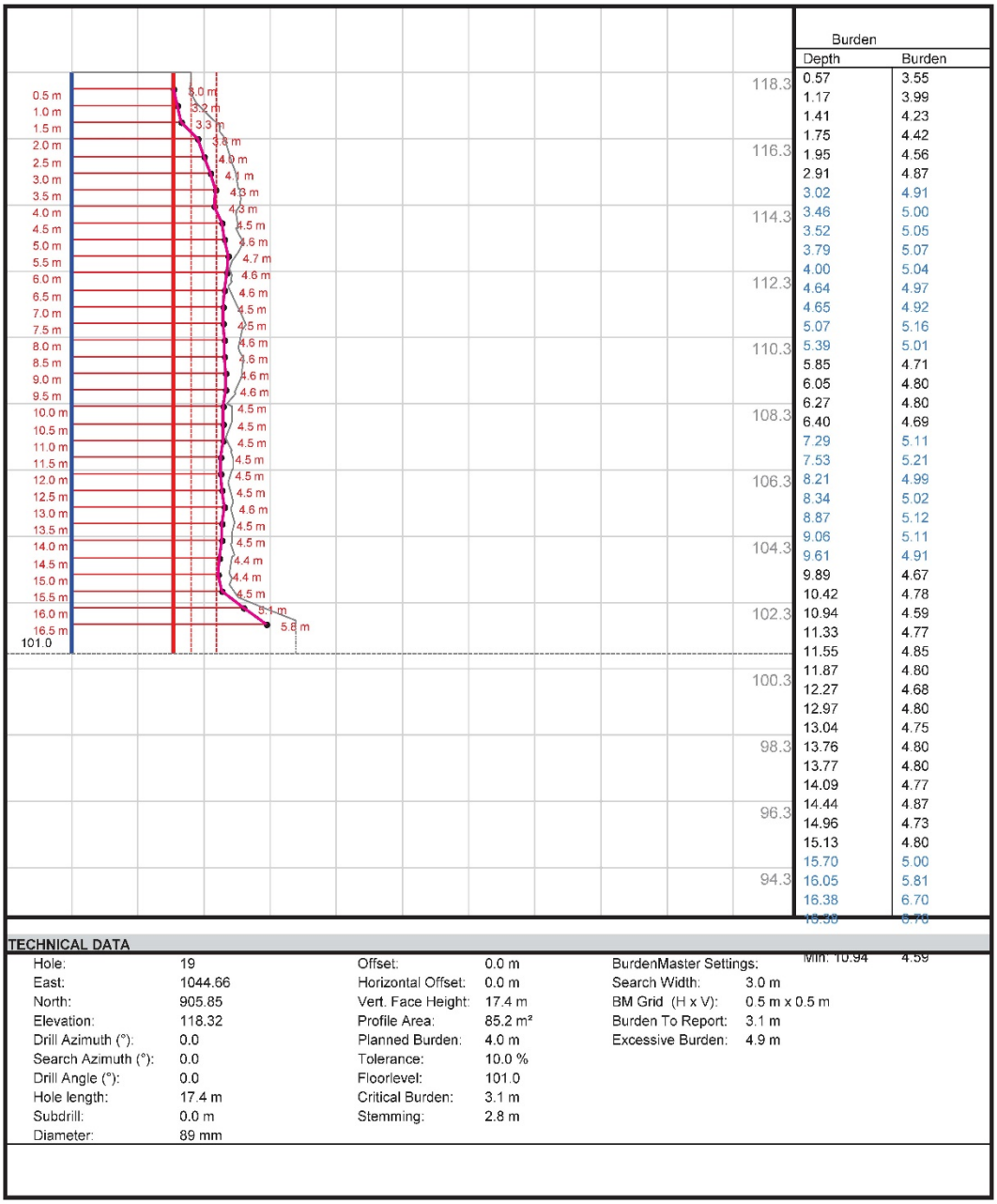

Burden	
Depth	Burden
0.57	3.55
1.17	3.99
1.41	4.23
1.75	4.42
1.95	4.56
2.91	4.87
3.02	4.91
3.46	5.00
3.52	5.05
3.79	5.07
4.00	5.04
4.64	4.97
4.65	4.92
5.07	5.16
5.39	5.01
5.85	4.71
6.05	4.80
6.27	4.80
6.40	4.69
7.29	5.11
7.53	5.21
8.21	4.99
8.34	5.02
8.87	5.12
9.06	5.11
9.61	4.91
9.89	4.67
10.42	4.78
10.94	4.59
11.33	4.77
11.55	4.85
11.87	4.80
12.27	4.68
12.97	4.80
13.04	4.75
13.76	4.80
13.77	4.80
14.09	4.77
14.44	4.87
14.96	4.73
15.13	4.80
15.70	5.00
16.05	5.81
16.38	6.70
16.50	6.78
Min: 10.94	4.59

TECHNICAL DATA

Hole:	19	Offset:	0.0 m	BurdenMaster Settings:	
East:	1044.66	Horizontal Offset:	0.0 m	Search Width:	3.0 m
North:	905.85	Vert. Face Height:	17.4 m	BM Grid (H x V):	0.5 m x 0.5 m
Elevation:	118.32	Profile Area:	85.2 m²	Burden To Report:	3.1 m
Drill Azimuth (°):	0.0	Planned Burden:	4.0 m	Excessive Burden:	4.9 m
Search Azimuth (°):	0.0	Tolerance:	10.0 %		
Drill Angle (°):	0.0	Floorlevel:	101.0		
Hole length:	17.4 m	Critical Burden:	3.1 m		
Subdrill:	0.0 m	Stemming:	2.8 m		
Diameter:	89 mm				

QuarryX

Blasting Engineer: Paul P. Kuznik, P. Eng.
Client: CRH Ogden Point
Site:CRH Ogden Point
Hole 21 of 25

Project: CRH Ogden Point P3 2018-01
Filename: OPC P3.qxd
Printed at: 2018-04-24 14:30:52
Scale: 1:150

DYNO Dyno Nobel

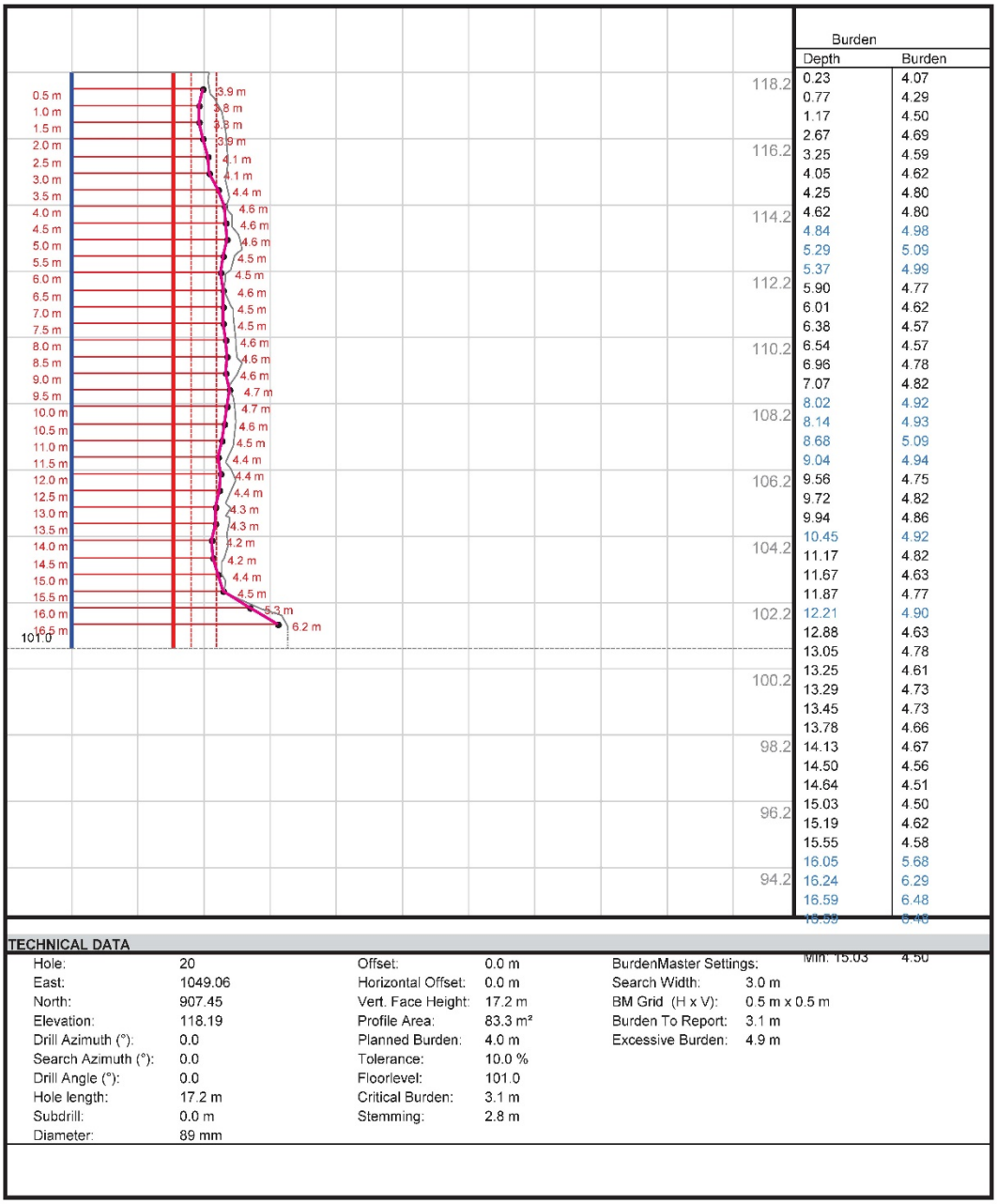

Burden	
Depth	Burden
0.23	4.07
0.77	4.29
1.17	4.50
2.67	4.69
3.25	4.59
4.05	4.62
4.25	4.80
4.62	4.80
4.84	4.98
5.29	5.09
5.37	4.99
5.90	4.77
6.01	4.62
6.38	4.57
6.54	4.57
6.96	4.78
7.07	4.82
8.02	4.92
8.14	4.93
8.68	5.09
9.04	4.94
9.56	4.75
9.72	4.82
9.94	4.86
10.45	4.92
11.17	4.82
11.67	4.63
11.87	4.77
12.21	4.90
12.88	4.63
13.05	4.78
13.25	4.61
13.29	4.73
13.45	4.73
13.78	4.66
14.13	4.67
14.50	4.56
14.64	4.51
15.03	4.50
15.19	4.62
15.55	4.58
16.05	5.68
16.24	6.29
16.59	6.48
[illegible]	[illegible]
Min: 15.03	4.50

TECHNICAL DATA

Hole:	20	Offset:	0.0 m	BurdenMaster Settings:	
East:	1049.06	Horizontal Offset:	0.0 m	Search Width:	3.0 m
North:	907.45	Vert. Face Height:	17.2 m	BM Grid (H x V):	0.5 m x 0.5 m
Elevation:	118.19	Profile Area:	83.3 m²	Burden To Report:	3.1 m
Drill Azimuth (°):	0.0	Planned Burden:	4.0 m	Excessive Burden:	4.9 m
Search Azimuth (°):	0.0	Tolerance:	10.0 %		
Drill Angle (°):	0.0	Floorlevel:	101.0		
Hole length:	17.2 m	Critical Burden:	3.1 m		
Subdrill:	0.0 m	Stemming:	2.8 m		
Diameter:	89 mm				

QuarryX

Blasting Engineer: Paul P. Kuznik, P. Eng.
Client: CRH Ogden Point
Site:CRH Ogden Point
Hole 22 of 25

Project: CRH Ogden Point P3 2018-01
Filename: OPC P3.qxd
Printed at: 2018-04-24 14:30:53
Scale: 1:150

DYNO Dyno Nobel

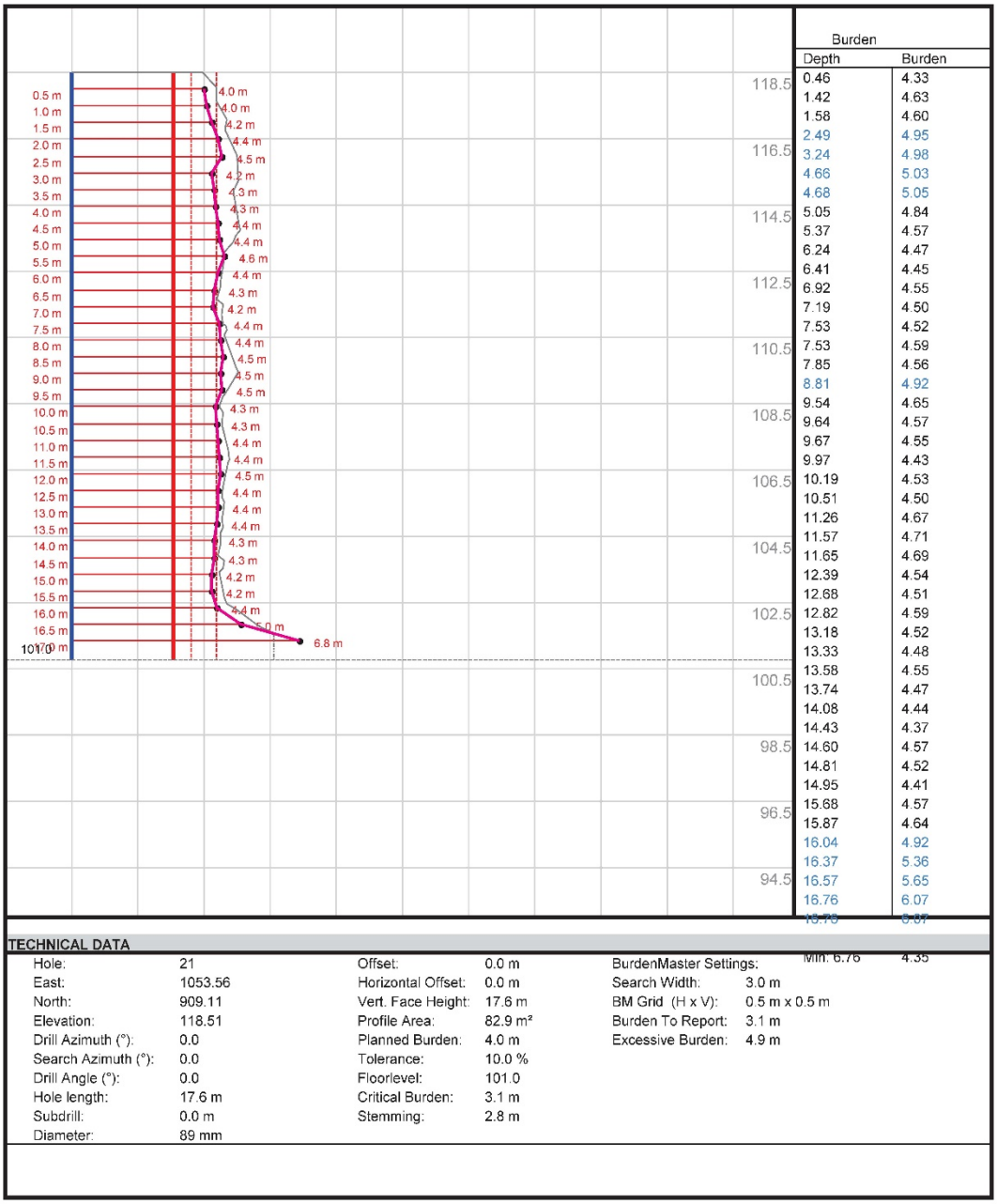

Burden	
Depth	Burden
0.46	4.33
1.42	4.63
1.58	4.60
2.49	4.95
3.24	4.98
4.66	5.03
4.68	5.05
5.05	4.84
5.37	4.57
6.24	4.47
6.41	4.45
6.92	4.55
7.19	4.50
7.53	4.52
7.53	4.59
7.85	4.56
8.81	4.92
9.54	4.65
9.64	4.57
9.67	4.55
9.97	4.43
10.19	4.53
10.51	4.50
11.26	4.67
11.57	4.71
11.65	4.69
12.39	4.54
12.68	4.51
12.82	4.59
13.18	4.52
13.33	4.48
13.58	4.55
13.74	4.47
14.08	4.44
14.43	4.37
14.60	4.57
14.81	4.52
14.95	4.41
15.68	4.57
15.87	4.64
16.04	4.92
16.37	5.36
16.57	5.65
16.76	6.07
[illegible]	[illegible]
Min: 6.76	4.35

TECHNICAL DATA

Hole:	21	Offset:	0.0 m	BurdenMaster Settings:	
East:	1053.56	Horizontal Offset:	0.0 m	Search Width:	3.0 m
North:	909.11	Vert. Face Height:	17.6 m	BM Grid (H x V):	0.5 m x 0.5 m
Elevation:	118.51	Profile Area:	82.9 m²	Burden To Report:	3.1 m
Drill Azimuth (°):	0.0	Planned Burden:	4.0 m	Excessive Burden:	4.9 m
Search Azimuth (°):	0.0	Tolerance:	10.0 %		
Drill Angle (°):	0.0	Floorlevel:	101.0		
Hole length:	17.6 m	Critical Burden:	3.1 m		
Subdrill:	0.0 m	Stemming:	2.8 m		
Diameter:	89 mm				

QuarryX

Blasting Engineer: Paul P. Kuznik, P. Eng.
Client: CRH Ogden Point
Site:CRH Ogden Point
Hole 23 of 25

Project: CRH Ogden Point P3 2018-01
Filename: OPC P3.qxd
Printed at: 2018-04-24 14:30:53
Scale: 1:150

DYNO Dyno Nobel

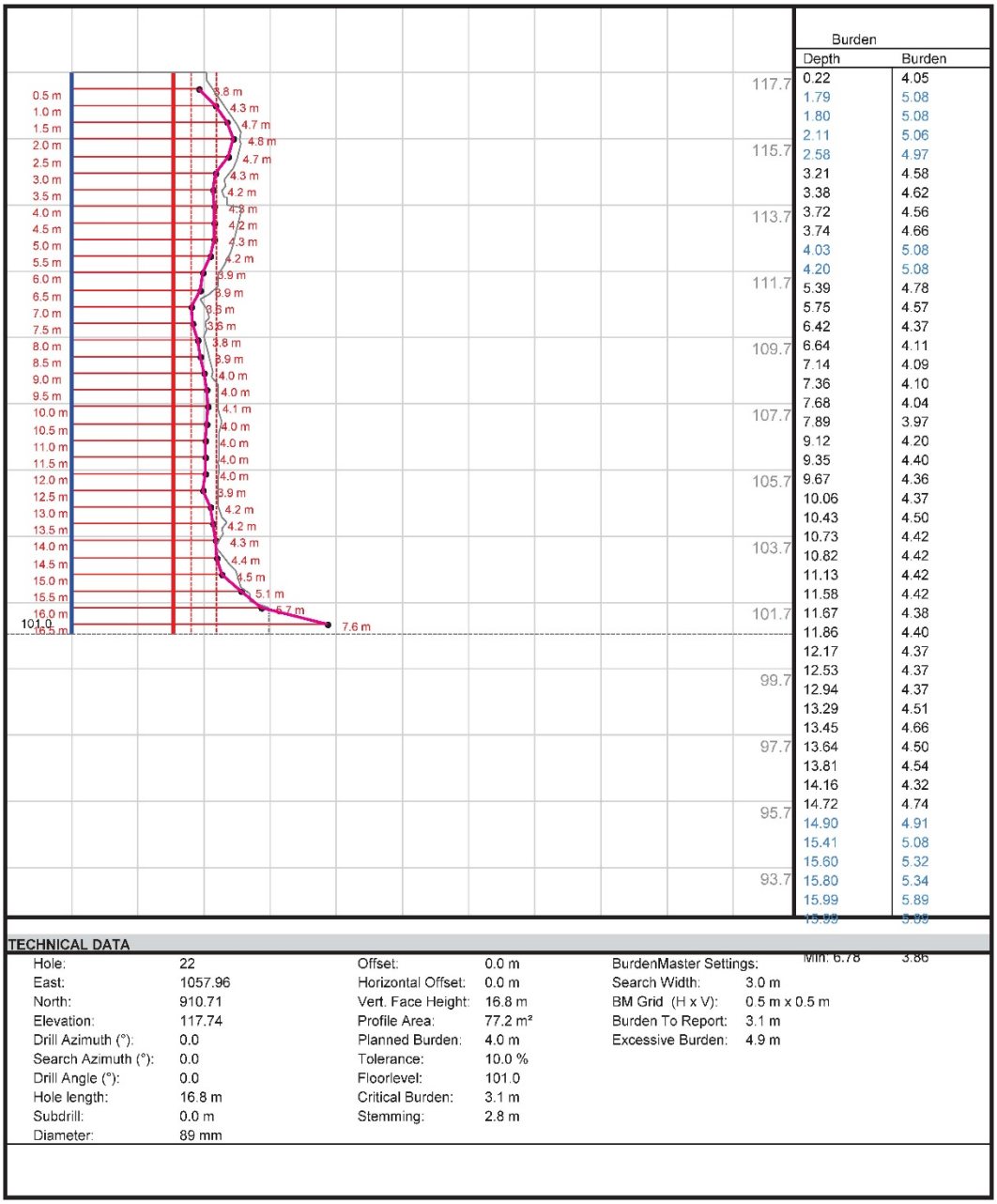

Burden	
Depth	Burden
0.22	4.05
1.79	5.08
1.80	5.08
2.11	5.06
2.58	4.97
3.21	4.58
3.38	4.62
3.72	4.56
3.74	4.66
4.03	5.08
4.20	5.08
5.39	4.78
5.75	4.57
6.42	4.37
6.64	4.11
7.14	4.09
7.36	4.10
7.68	4.04
7.89	3.97
9.12	4.20
9.35	4.40
9.67	4.36
10.06	4.37
10.43	4.50
10.73	4.42
10.82	4.42
11.13	4.42
11.58	4.42
11.67	4.38
11.86	4.40
12.17	4.37
12.53	4.37
12.94	4.37
13.29	4.51
13.45	4.66
13.64	4.50
13.81	4.54
14.16	4.32
14.72	4.74
14.90	4.91
15.41	5.08
15.60	5.32
15.80	5.34
15.99	5.89
[illegible]	[illegible]
Min: 6.78	3.86

TECHNICAL DATA

Hole:	22	Offset:	0.0 m	BurdenMaster Settings:	
East:	1057.96	Horizontal Offset:	0.0 m	Search Width:	3.0 m
North:	910.71	Vert. Face Height:	16.8 m	BM Grid (H x V):	0.5 m x 0.5 m
Elevation:	117.74	Profile Area:	77.2 m²	Burden To Report:	3.1 m
Drill Azimuth (°):	0.0	Planned Burden:	4.0 m	Excessive Burden:	4.9 m
Search Azimuth (°):	0.0	Tolerance:	10.0 %		
Drill Angle (°):	0.0	Floorlevel:	101.0		
Hole length:	16.8 m	Critical Burden:	3.1 m		
Subdrill:	0.0 m	Stemming:	2.8 m		
Diameter:	89 mm				

QuarryX

Blasting Engineer: Paul P. Kuznik, P. Eng.
Client: CRH Ogden Point
Site:CRH Ogden Point
Hole 24 of 25

Project: CRH Ogden Point P3 2018-01
Filename: OPC P3.qxd
Printed at: 2018-04-24 14:30:54
Scale: 1:150

DYNO Dyno Nobel

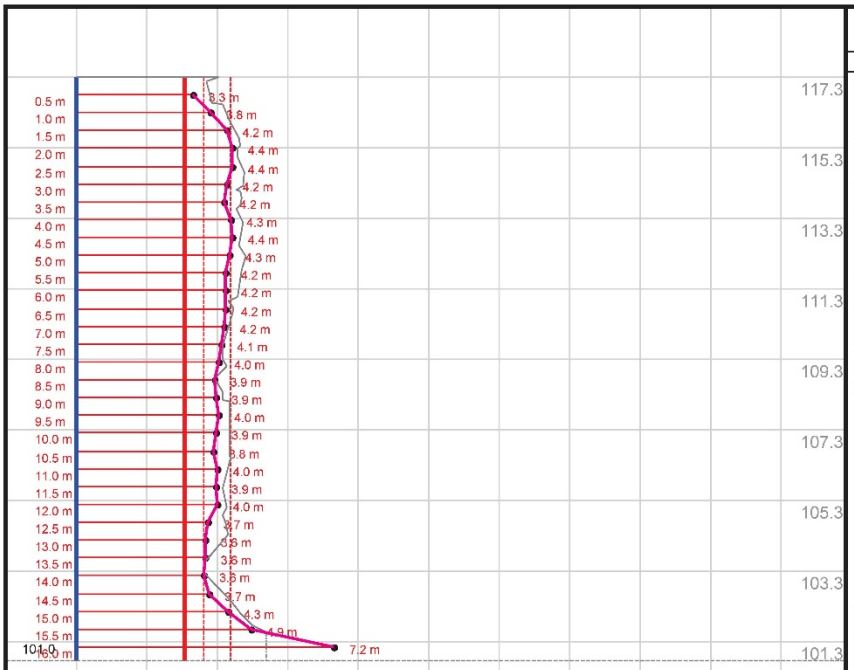

Burden	
Depth	Burden
0.13	3.67
0.76	4.12
1.22	4.29
1.94	4.61
1.99	4.54
2.67	4.71
3.04	4.70
3.19	4.60
3.40	4.66
3.60	4.62
3.70	4.51
4.06	4.68
4.71	4.59
5.04	4.77
5.40	4.66
6.16	4.55
6.30	4.28
6.48	4.42
6.66	4.38
7.54	4.12
7.92	4.12
8.13	4.22
8.46	3.90
8.86	4.10
9.06	4.10
9.11	4.29
9.19	4.31
9.28	4.29
9.83	4.29
10.14	4.31
10.63	4.29
10.67	4.34
11.56	4.10
12.09	4.22
12.30	4.10
12.51	4.18
12.67	4.23
12.85	4.26
13.59	3.63
13.92	3.58
14.69	4.34
15.06	4.62
15.40	4.95
15.60	5.33
[illegible]	[illegible]
Min: 13.92	3.58

TECHNICAL DATA

Hole:	23	Offset:	0.0 m	BurdenMaster Settings:	
East:	1062.41	Horizontal Offset:	0.0 m	Search Width:	3.0 m
North:	912.31	Vert. Face Height:	16.4 m	BM Grid (H x V):	0.5 m x 0.5 m
Elevation:	117.35	Profile Area:	71.4 m²	Burden To Report:	3.1 m
Drill Azimuth (°):	0.0	Planned Burden:	4.0 m	Excessive Burden:	4.9 m
Search Azimuth (°):	0.0	Tolerance:	10.0 %		
Drill Angle (°):	0.0	Floorlevel:	101.0		
Hole length:	16.4 m	Critical Burden:	3.1 m		
Subdrill:	0.0 m	Stemming:	2.8 m		
Diameter:	89 mm				

QuarryX

Blasting Engineer: Paul P. Kuznik, P. Eng.
Client: CRH Ogden Point
Site:CRH Ogden Point
Hole 25 of 25

Project: CRH Ogden Point P3 2018-01
Filename: OPC P3.qxd
Printed at: 2018-04-24 14:30:54
Scale: 1:150

DYNO Dyno Nobel

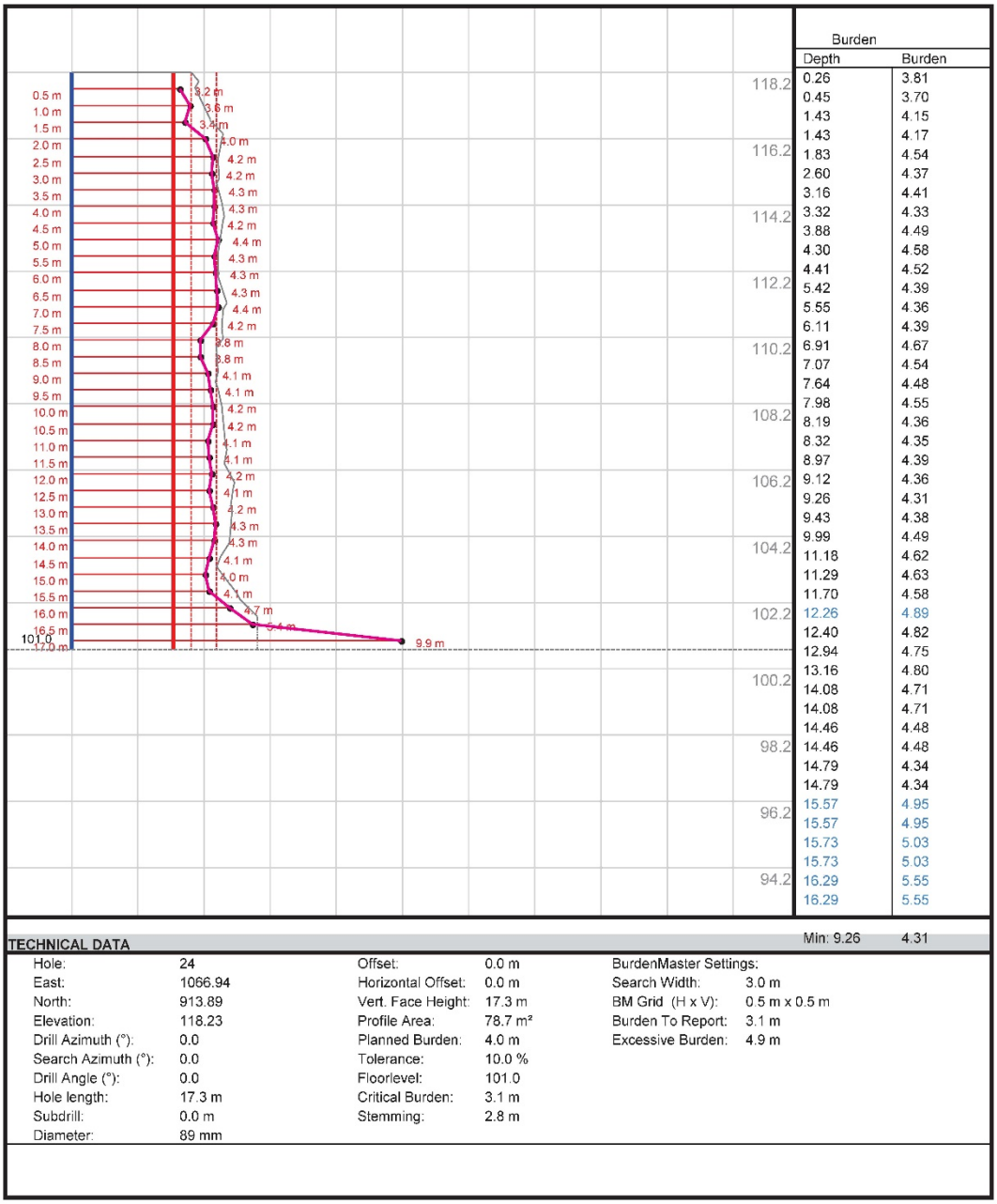

Burden	
Depth	Burden
0.26	3.81
0.45	3.70
1.43	4.15
1.43	4.17
1.83	4.54
2.60	4.37
3.16	4.41
3.32	4.33
3.88	4.49
4.30	4.58
4.41	4.52
5.42	4.39
5.55	4.36
6.11	4.39
6.91	4.67
7.07	4.54
7.64	4.48
7.98	4.55
8.19	4.36
8.32	4.35
8.97	4.39
9.12	4.36
9.26	4.31
9.43	4.38
9.99	4.49
11.18	4.62
11.29	4.63
11.70	4.58
12.26	4.89
12.40	4.82
12.94	4.75
13.16	4.80
14.08	4.71
14.08	4.71
14.46	4.48
14.46	4.48
14.79	4.34
14.79	4.34
15.57	4.95
15.57	4.95
15.73	5.03
15.73	5.03
16.29	5.55
16.29	5.55
Min: 9.26	4.31

TECHNICAL DATA

Hole:	24	Offset:	0.0 m	BurdenMaster Settings:	
East:	1066.94	Horizontal Offset:	0.0 m	Search Width:	3.0 m
North:	913.89	Vert. Face Height:	17.3 m	BM Grid (H x V):	0.5 m x 0.5 m
Elevation:	118.23	Profile Area:	78.7 m²	Burden To Report:	3.1 m
Drill Azimuth (°):	0.0	Planned Burden:	4.0 m	Excessive Burden:	4.9 m
Search Azimuth (°):	0.0	Tolerance:	10.0 %		
Drill Angle (°):	0.0	Floorlevel:	101.0		
Hole length:	17.3 m	Critical Burden:	3.1 m		
Subdrill:	0.0 m	Stemming:	2.8 m		
Diameter:	89 mm				

QuarryX

Blasting Engineer: Paul P. Kuznik, P. Eng.
Client: CRH Ogden Point
Site:CRH Ogden Point
Hole 26 of 25

Project: CRH Ogden Point P3 2018-01
Filename: OPC P3.qxd
Printed at: 2018-04-24 14:30:55
Scale: 1:150

DYNO Dyno Nobel

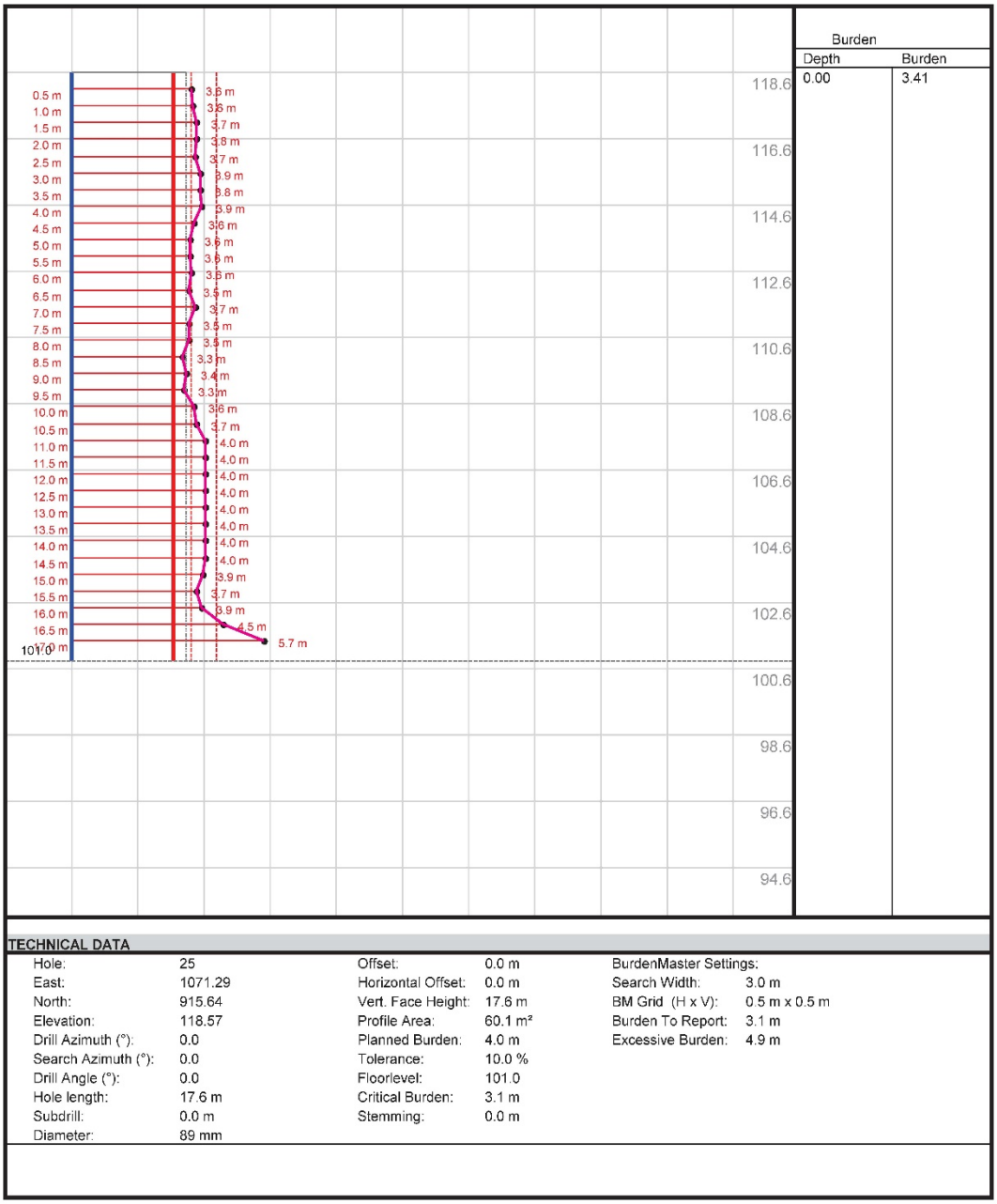

Burden

Depth	Burden
0.00	3.41

TECHNICAL DATA

Hole:	25	Offset:	0.0 m	BurdenMaster Settings:	
East:	1071.29	Horizontal Offset:	0.0 m	Search Width:	3.0 m
North:	915.64	Vert. Face Height:	17.6 m	BM Grid (H x V):	0.5 m x 0.5 m
Elevation:	118.57	Profile Area:	60.1 m²	Burden To Report:	3.1 m
Drill Azimuth (°):	0.0	Planned Burden:	4.0 m	Excessive Burden:	4.9 m
Search Azimuth (°):	0.0	Tolerance:	10.0 %		
Drill Angle (°):	0.0	Floorlevel:	101.0		
Hole length:	17.6 m	Critical Burden:	3.1 m		
Subdrill:	0.0 m	Stemming:	0.0 m		
Diameter:	89 mm				

Borehole Report

CRH Ogden Point 2018 01

CRH Ogden Point

26-04-18 7:40 PM

RENISHAW
apply innovation™

Project Information

Operator Name: Brad Asselstine

Site Name: CRH Ogden Point

Grid Magnetic Angle: 0.00(°)

Project Notes

Site Notes

Contents

1 Face 1

1.1 Hole Collar Report

Hole ID	X (m)	Y (m)	Z (m)
R1H1	750752.598	4875298.679	56.990
R1H2	750747.846	4875298.283	56.921
R1H3	750743.129	4875298.006	56.882
R1H4	750738.450	4875297.769	56.838
R1H5	750733.837	4875297.519	56.786
R1H6	750729.032	4875296.972	56.730
R1H7	750724.214	4875296.632	56.763
R1H8	750719.576	4875296.255	56.655
R1H9	750714.704	4875296.029	56.606
R1H10	750709.993	4875295.762	56.587
R1H11	750705.316	4875295.314	56.556
R1H12	750700.518	4875294.995	56.491
R1H13	750695.760	4875294.618	56.347
R1H14	750691.004	4875294.380	56.272
R1H15	750686.293	4875294.128	56.302
R1H16	750681.662	4875293.646	56.270
R1H17	750676.864	4875293.366	56.303
R1H18	750672.162	4875293.082	56.304
R1H19	750667.632	4875292.689	56.287
R1H20	750663.068	4875292.455	56.182
R1H21	750658.010	4875292.103	56.114
R1H22	750653.337	4875291.724	56.135
R1H23	750648.614	4875291.527	56.152
R1H24	750643.737	4875291.092	56.171
R1H25	750639.045	4875290.799	56.258
R1H26	750634.387	4875290.359	56.241

*Note: Boretrak Viewer will generate default X,Y,Z collar positions starting at 1000,1000,100 if no values have been entered by the user.

1.2 Plan View Report

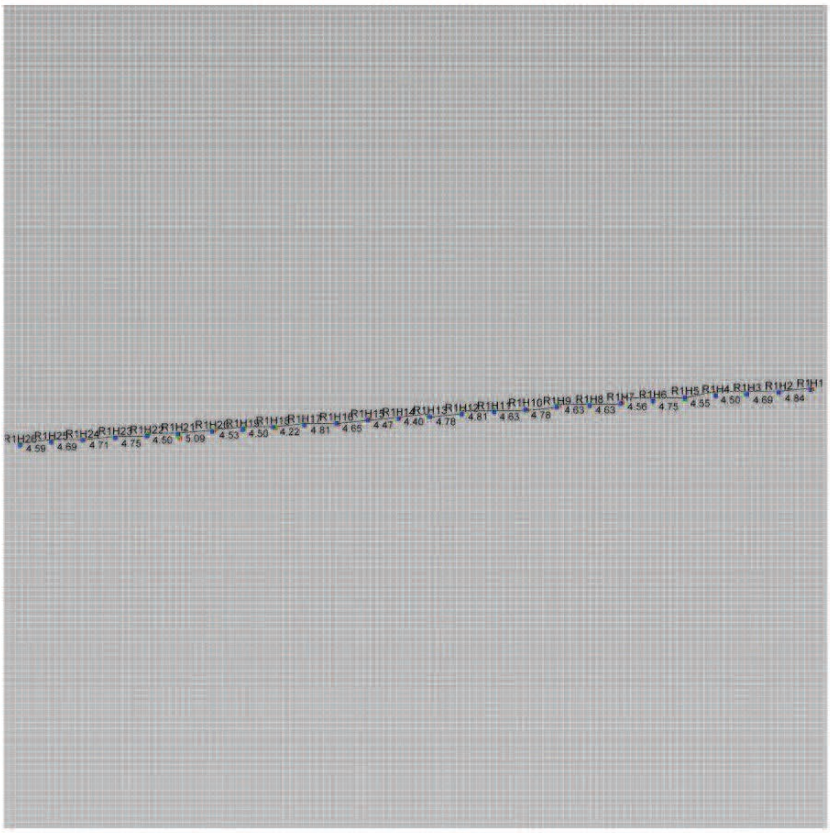

1.3.1 R1H1

Survey Data 1

Face : Face 1 Hole : R1H1 Survey Date : 22-01-18 Dep (m) : 18.00
Average Azimuth (°) : 79.45 Average Inclination (°) : 1.46
Designed Azimuth (°) : 0.00 Designed Inclination (°) : 0.00 Designed Depth (m) : 0.00

Plan View

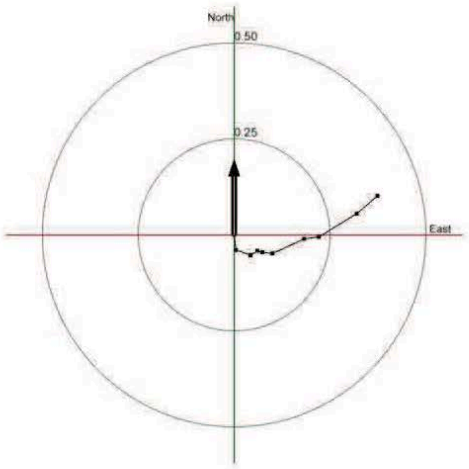

Front View

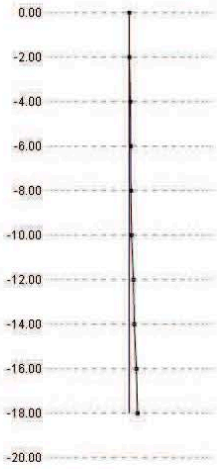

Side View

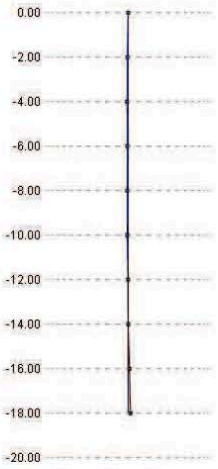

Face : 3 Hole : 1 Rod Increment : 2.00(m) Offset : 0.00(m) Dep : 18.00(m) Grid Magnetic Angle : 0.00(°)

Dep(m)	Heading(°)	Inclination(°)	Dev(m)
2.00	173.60	1.13	0.00
4.00	109.65	1.17	0.00
6.00	57.41	0.61	0.00
8.00	105.76	0.38	0.00
10.00	97.24	0.77	0.00
12.00	65.22	2.60	0.00
14.00	82.29	1.11	0.00
16.00	58.44	3.32	0.00
18.00	49.33	2.04	0.00

1.3.2 R1H2

Survey Data 1

Face : Face 1 Hole : R1H2 Survey Date : 22-01-18 Dep (m) : 18.00
Average Azimuth (°) : 207.62 Average Inclination (°) : 1.12
Designed Azimuth (°) : 0.00 Designed Inclination (°) : 0.00 Designed Depth (m) : 0.00

Plan View

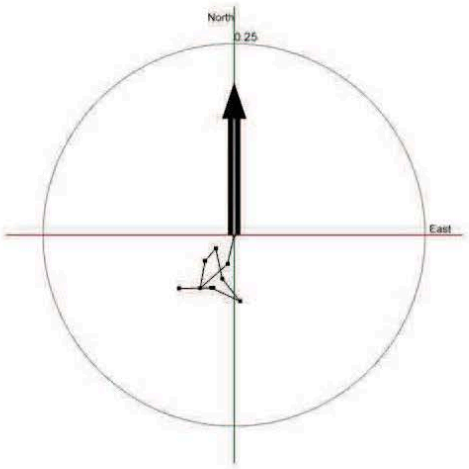

Front View

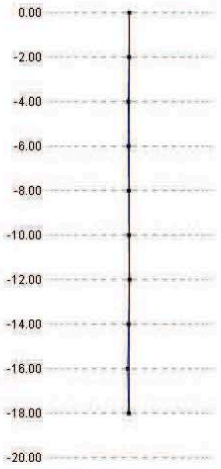

Side View

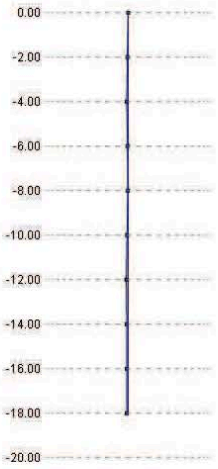

Face : 3 Hole : 2 Rod Increment : 2.00(m) Offset : 0.00(m) Dep : 18.00(m) Grid Magnetic Angle : 0.00(°)

Dep(m)	Heading(°)	Inclination(°)	Dev(m)
2.00	192.70	1.11	0.00
4.00	228.42	1.37	0.00
6.00	9.77	1.03	0.00
8.00	40.94	0.61	0.00
10.00	167.96	1.16	0.00
12.00	141.48	1.07	0.00
14.00	294.76	1.19	0.00
16.00	269.01	1.20	0.00
18.00	89.18	1.29	0.00

1.3.3 R1H3

Survey Data 1

Face : Face 1 Hole : R1H3 Survey Date : 22-01-18 Dep (m) : 18.00
Average Azimuth (°) : 261.20 Average Inclination (°) : 1.34
Designed Azimuth (°) : 0.00 Designed Inclination (°) : 0.00 Designed Depth (m) : 0.00

Plan View

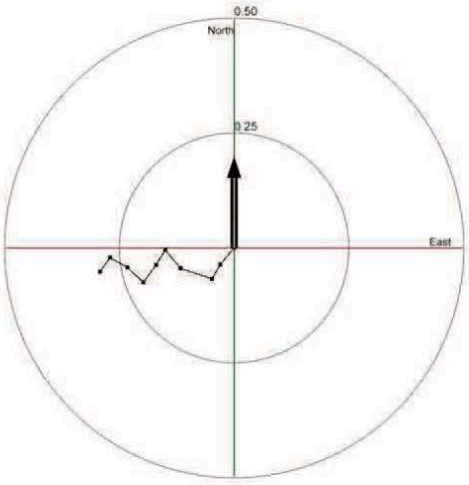

Front View

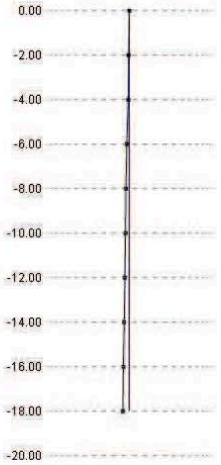

Side View

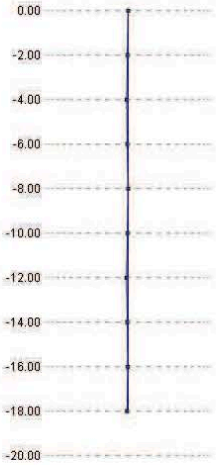

Face : 3 Hole : 3 Rod Increment : 2.00(m) Offset : 0.00(m) Dep : 18.00(m) Grid Magnetic Angle : 0.00(°)

Dep(m)	Heading(°)	Inclination(°)	Dev(m)
2.00	219.78	1.34	0.00
4.00	210.55	1.04	0.00
6.00	288.61	2.06	0.00
8.00	319.84	1.49	0.00
10.00	211.46	1.10	0.00
12.00	216.32	1.33	0.00
14.00	313.35	1.36	0.00
16.00	299.14	1.25	0.00
18.00	215.79	1.07	0.00

1.3.4 R1H4

Survey Data 1

Face : Face 1 Hole : R1H4 Survey Date : 22-01-18 Dep (m) : 18.00
Average Azimuth (°) : 324.71 Average Inclination (°) : 1.23
Designed Azimuth (°) : 0.00 Designed Inclination (°) : 0.00 Designed Depth (m) : 0.00

Plan View

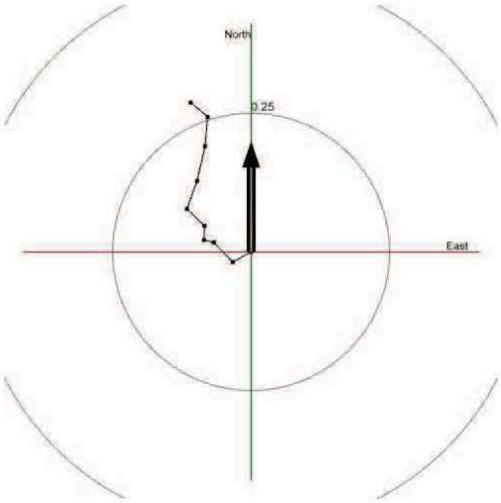

Front View

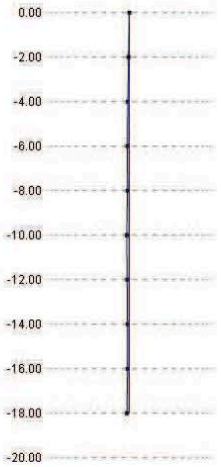

Side View

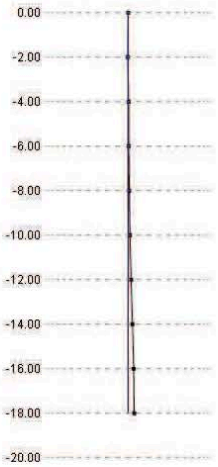

Face : 3 Hole : 4 Rod Increment : 2.00(m) Offset : 0.00(m) Dep : 18.00(m) Grid Magnetic Angle : 0.00(°)

Dep(m)	Heading(°)	Inclination(°)	Dev(m)
2.00	241.33	1.09	0.00
4.00	316.17	1.39	0.00
6.00	283.83	0.53	0.00
8.00	1.92	0.73	0.00
10.00	314.28	1.27	0.00
12.00	20.01	1.53	0.00
14.00	12.99	1.85	0.00
16.00	5.12	1.51	0.00
18.00	310.43	1.15	0.00

1.3.5 R1H5

Survey Data 1

Face : Face 1 Hole : R1H5 Survey Date : 22-01-18 Dep (m) : 18.00
Average Azimuth (°) : 165.68 Average Inclination (°) : 1.52
Designed Azimuth (°) : 0.00 Designed Inclination (°) : 0.00 Designed Depth (m) : 0.00

Plan View

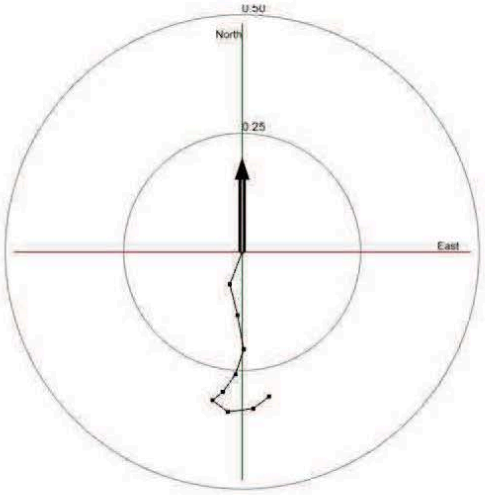

Front View

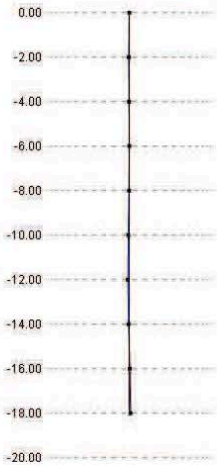

Side View

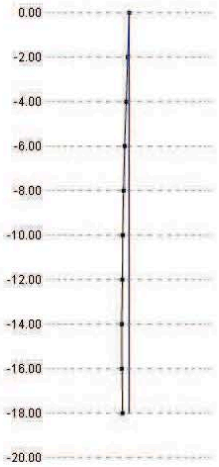

Face : 3 Hole : 5 Rod Increment : 2.00(m) Offset : 0.00(m) Dep : 18.00(m) Grid Magnetic Angle : 0.00(°)

Dep(m)	Heading(°)	Inclination(°)	Dev(m)
2.00	200.78	2.09	0.00
4.00	166.08	1.93	0.00
6.00	169.64	2.10	0.00
8.00	198.48	1.60	0.00
10.00	215.86	1.29	0.00
12.00	231.31	0.80	0.00
14.00	127.33	1.16	0.00
16.00	82.61	1.55	0.00
18.00	52.94	1.20	0.00

1.3.6 R1H6

Survey Data 1

Face : Face 1 Hole : R1H6 Survey Date : 22-01-18 Dep (m) : 18.00
Average Azimuth (°) : 133.96 Average Inclination (°) : 1.10
Designed Azimuth (°) : 0.00 Designed Inclination (°) : 0.00 Designed Depth (m) : 0.00

Plan View

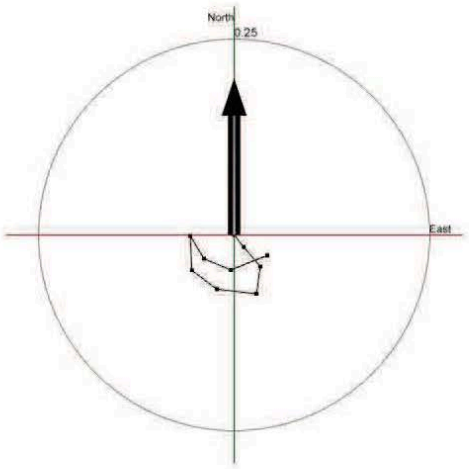

Front View

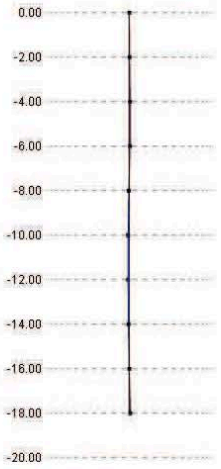

Side View

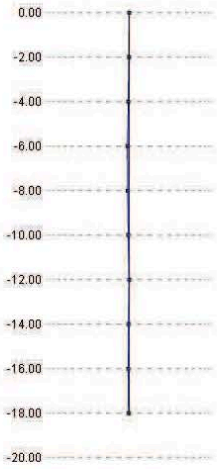

Face : 3 Hole : 6 Rod Increment : 2.00(m) Offset : 0.00(m) Dep : 18.00(m) Grid Magnetic Angle : 0.00(°)

Dep(m)	Heading(°)	Inclination(°)	Dev(m)
2.00	141.70	0.57	0.00
4.00	139.48	0.93	0.00
6.00	187.91	1.01	0.00
8.00	276.83	1.46	0.00
10.00	306.87	1.15	0.00
12.00	357.31	1.26	0.00
14.00	149.11	0.98	0.00
16.00	112.65	1.07	0.00
18.00	68.20	1.43	0.00

1.3.7 R1H7

Survey Data 1

Face : Face 1 Hole : R1H7 Survey Date : 22-01-18 Dep (m) : 18.00
Average Azimuth (°) : 59.47 Average Inclination (°) : 1.50
Designed Azimuth (°) : 0.00 Designed Inclination (°) : 0.00 Designed Depth (m) : 0.00

Plan View

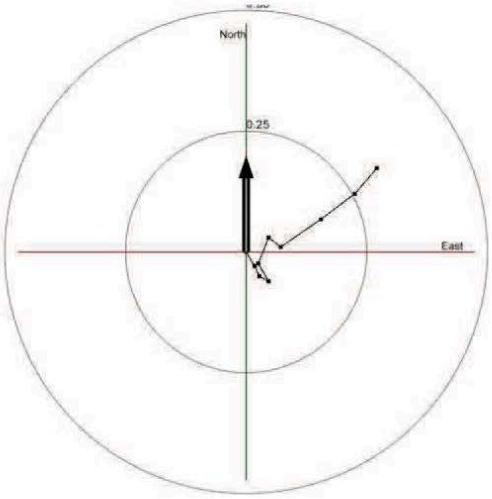

Front View

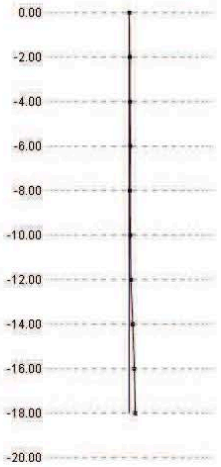

Side View

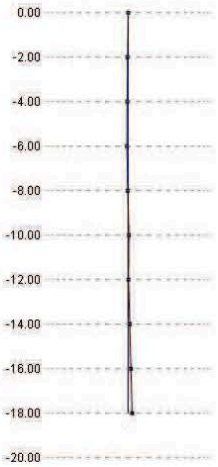

Face : 3 Hole : 7 Rod Increment : 2.00(m) Offset : 0.00(m) Dep : 18.00(m) Grid Magnetic Angle : 0.00(°)

Dep(m)	Heading(°)	Inclination(°)	Dev(m)
2.00	149.70	0.97	0.00
4.00	154.13	0.66	0.00
6.00	119.57	0.64	0.00
8.00	329.89	1.23	0.00
10.00	22.22	1.65	0.00
12.00	127.86	0.90	0.00
14.00	55.48	2.90	0.00
16.00	53.12	2.52	0.00
18.00	40.75	2.00	0.00

1.3.8 R1H8

Survey Data 1

Face : Face 1 Hole : R1H8 Survey Date : 22-01-18 Dep (m) : 18.00
Average Azimuth (°) : 23.69 Average Inclination (°) : 1.03
Designed Azimuth (°) : 0.00 Designed Inclination (°) : 0.00 Designed Depth (m) : 0.00

Plan View

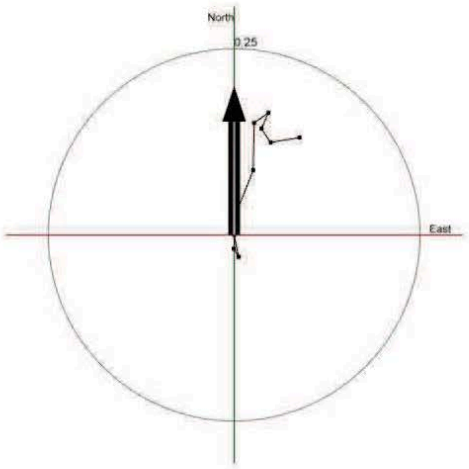

Front View

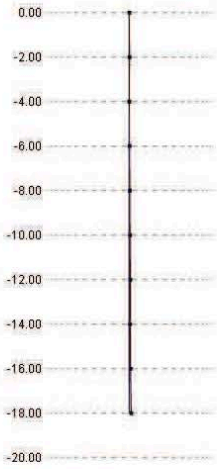

Side View

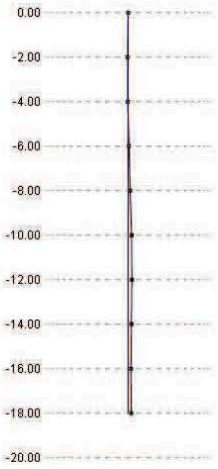

Face : 3 Hole : 8 Rod Increment : 2.00(m) Offset : 0.00(m) Dep : 18.00(m) Grid Magnetic Angle : 0.00(°)

Dep(m)	Heading(°)	Inclination(°)	Dev(m)
2.00	168.39	0.86	0.00
4.00	328.66	0.36	0.00
6.00	5.77	1.52	0.00
8.00	21.50	1.63	0.00
10.00	1.15	1.82	0.00
12.00	54.70	0.67	0.00
14.00	203.65	0.67	0.00
16.00	145.98	0.64	0.00
18.00	80.39	1.13	0.00

1.3.9 R1H9

Survey Data 1

Face : Face 1 Hole : R1H9 Survey Date : 22-01-18 Dep (m) : 18.00
Average Azimuth (°) : 46.66 Average Inclination (°) : 1.76
Designed Azimuth (°) : 0.00 Designed Inclination (°) : 0.00 Designed Depth (m) : 0.00

Plan View

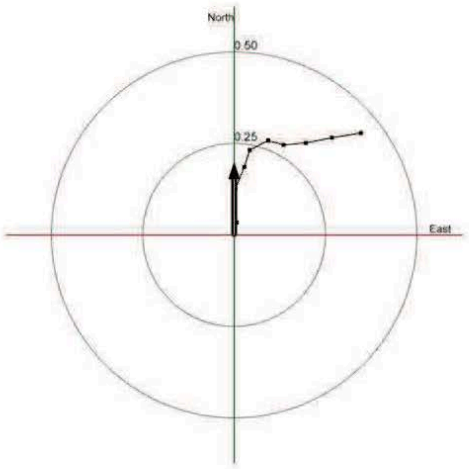

Front View

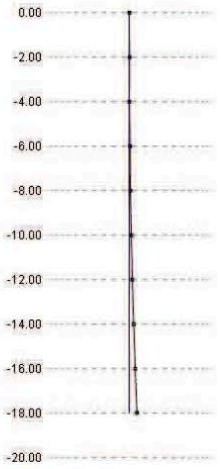

Side View

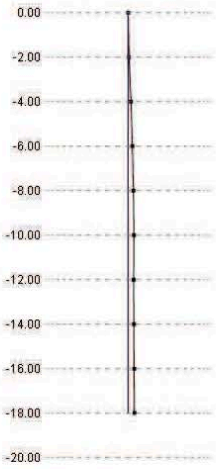

Face : 3 Hole : 9 Rod Increment : 2.00(m) Offset : 0.00(m) Dep : 18.00(m) Grid Magnetic Angle : 0.00(°)

Dep(m)	Heading(°)	Inclination(°)	Dev(m)
2.00	11.41	0.99	0.00
4.00	357.95	2.62	0.00
6.00	21.53	1.86	0.00
8.00	18.55	1.39	0.00
10.00	62.53	1.62	0.00
12.00	106.14	1.26	0.00
14.00	84.47	1.74	0.00
16.00	79.03	2.10	0.00
18.00	80.49	2.28	0.00

1.3.10 R1H10

Survey Data 1

Face : Face 1 Hole : R1H10 Survey Date : 22-01-18 Dep (m) : 18.00
Average Azimuth (°) : 126.38 Average Inclination (°) : 1.61
Designed Azimuth (°) : 0.00 Designed Inclination (°) : 0.00 Designed Depth (m) : 0.00

Plan View

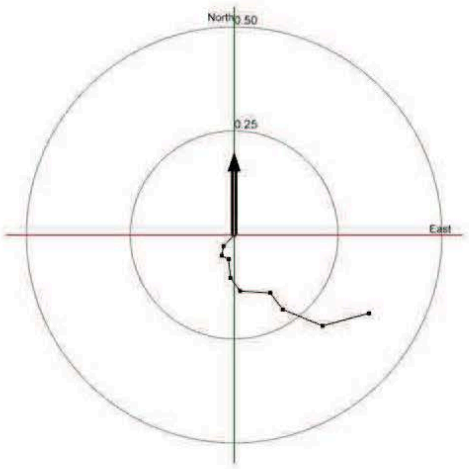

Front View

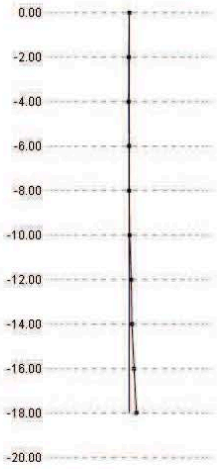

Side View

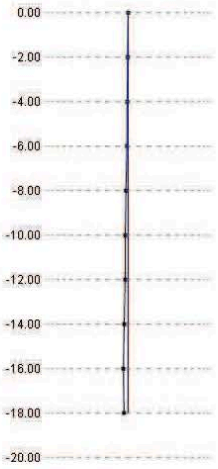

Face : 3 Hole : 10 Rod Increment : 2.00(m) Offset : 0.00(m) Dep : 18.00(m) Grid Magnetic Angle : 0.00(°)

Dep(m)	Heading(°)	Inclination(°)	Dev(m)
2.00	223.30	1.05	0.00
4.00	191.03	0.68	0.00
6.00	116.84	0.53	0.00
8.00	174.42	1.29	0.00
10.00	143.69	1.12	0.00
12.00	93.40	2.08	0.00
14.00	142.90	1.43	0.00
16.00	112.30	2.96	0.00
18.00	74.91	3.31	0.00

1.3.11 R1H11

Survey Data 1

Face : Face 1 Hole : R1H11 Survey Date : 22-01-18 Dep (m) : 18.00
Average Azimuth (°) : 2.42 Average Inclination (°) : 1.44
Designed Azimuth (°) : 0.00 Designed Inclination (°) : 0.00 Designed Depth (m) : 0.00

Plan View

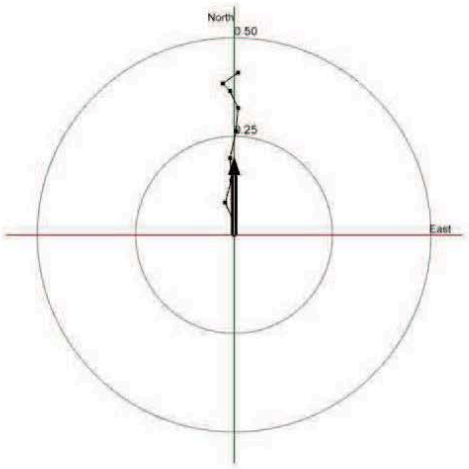

Front View

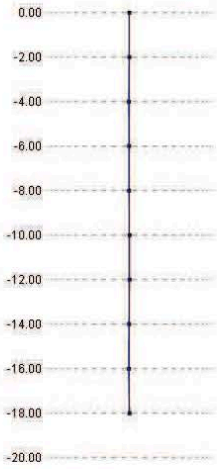

Side View

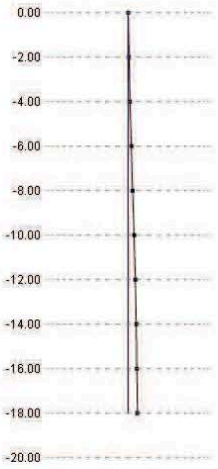

Face : 3 Hole : 11 Rod Increment : 2.00(m) Offset : 0.00(m) Dep : 18.00(m) Grid Magnetic Angle : 0.00(°)

Dep(m)	Heading(°)	Inclination(°)	Dev(m)
2.00	356.39	1.04	0.00
4.00	335.80	1.44	0.00
6.00	15.68	1.69	0.00
8.00	356.61	1.60	0.00
10.00	12.33	2.01	0.00
12.00	5.09	1.68	0.00
14.00	335.00	1.37	0.00
16.00	315.60	0.75	0.00
18.00	54.02	1.36	0.00

1.3.12 R1H12

Survey Data 1

Face : Face 1 Hole : R1H12 Survey Date : 22-01-18 Dep (m) : 18.00
Average Azimuth (°) : 334.89 Average Inclination (°) : 1.29
Designed Azimuth (°) : 0.00 Designed Inclination (°) : 0.00 Designed Depth (m) : 0.00

Plan View

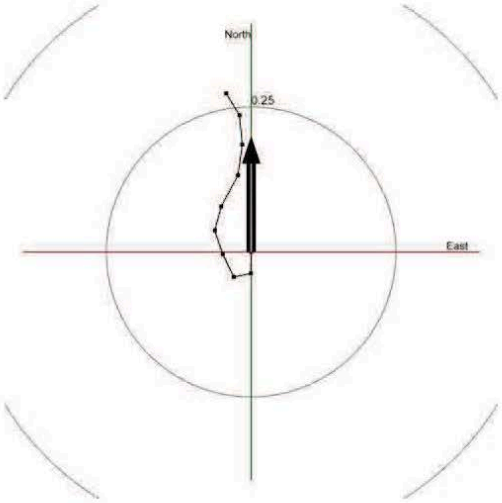

Front View

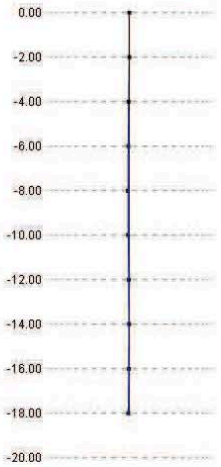

Side View

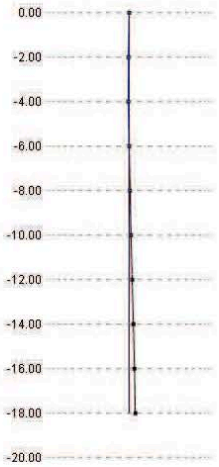

Face : 3 Hole : 12 Rod Increment : 2.00(m) Offset : 0.00(m) Dep : 18.00(m) Grid Magnetic Angle : 0.00(°)

Dep(m)	Heading(°)	Inclination(°)	Dev(m)
2.00	180.60	1.06	0.00
4.00	258.39	0.86	0.00
6.00	334.09	1.26	0.00
8.00	341.55	1.23	0.00
10.00	15.05	1.23	0.00
12.00	28.40	1.74	0.00
14.00	7.76	1.53	0.00
16.00	354.68	1.45	0.00
18.00	328.66	1.27	0.00

1.3.13 R1H13

Survey Data 1

Face : Face 1 Hole : R1H13 Survey Date : 22-01-18 Dep (m) : 18.00
Average Azimuth (°) : 288.95 Average Inclination (°) : 1.18
Designed Azimuth (°) : 0.00 Designed Inclination (°) : 0.00 Designed Depth (m) : 0.00

Plan View

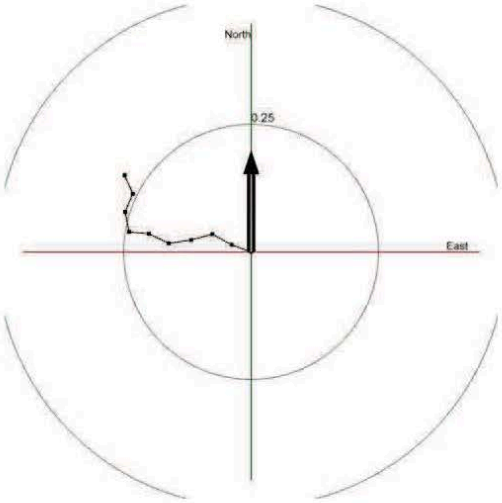

Front View

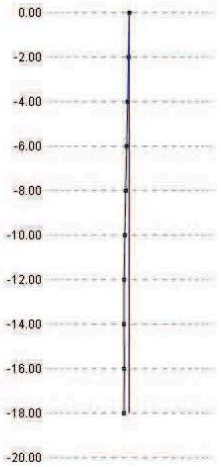

Side View

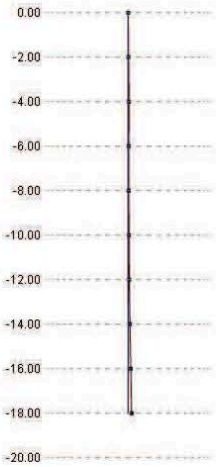

Face : 3 Hole : 13 Rod Increment : 2.00(m) Offset : 0.00(m) Dep : 18.00(m) Grid Magnetic Angle : 0.00(°)

Dep(m)	Heading(°)	Inclination(°)	Dev(m)
2.00	290.00	1.16	0.00
4.00	298.87	1.24	0.00
6.00	254.69	1.25	0.00
8.00	261.87	1.27	0.00
10.00	295.61	1.23	0.00
12.00	275.25	1.11	0.00
14.00	348.55	1.15	0.00
16.00	23.28	1.11	0.00
18.00	335.51	1.13	0.00

1.3.14 R1H14

Survey Data 1

Face : Face 1 Hole : R1H14 Survey Date : 22-01-18 Dep (m) : 18.00
Average Azimuth (°) : 77.11 Average Inclination (°) : 1.42
Designed Azimuth (°) : 0.00 Designed Inclination (°) : 0.00 Designed Depth (m) : 0.00

Plan View

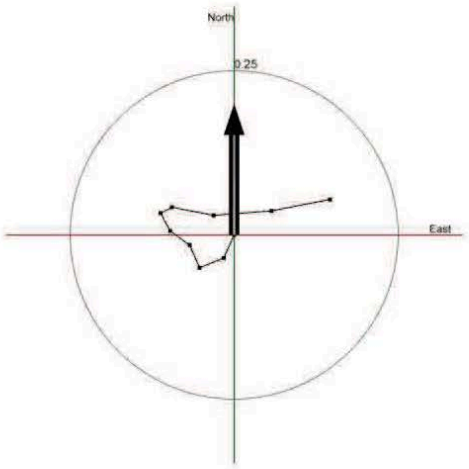

Front View

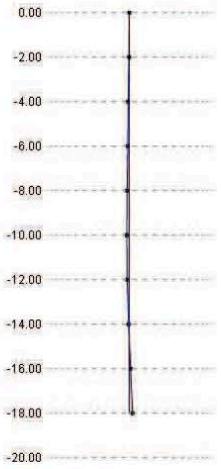

Side View

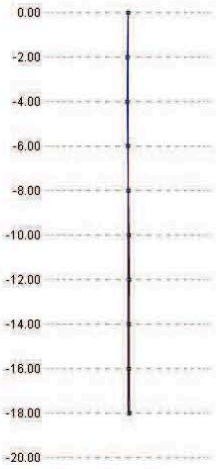

Face : 3 Hole : 14 Rod Increment : 2.00(m) Offset : 0.00(m) Dep : 18.00(m) Grid Magnetic Angle : 0.00(°)

Dep(m)	Heading(°)	Inclination(°)	Dev(m)
2.00	204.40	1.11	0.00
4.00	248.04	1.13	0.00
6.00	336.06	1.08	0.00
8.00	306.00	1.05	0.00
10.00	331.75	0.88	0.00
12.00	62.95	0.56	0.00
14.00	101.00	1.85	0.00
16.00	85.57	2.53	0.00
18.00	78.97	2.61	0.00

1.3.15 R1H15

Survey Data 1

Face : Face 1 Hole : R1H15 Survey Date : 22-01-18 Dep (m) : 18.00
Average Azimuth (°) : 65.82 Average Inclination (°) : 1.55
Designed Azimuth (°) : 0.00 Designed Inclination (°) : 0.00 Designed Depth (m) : 0.00

Plan View

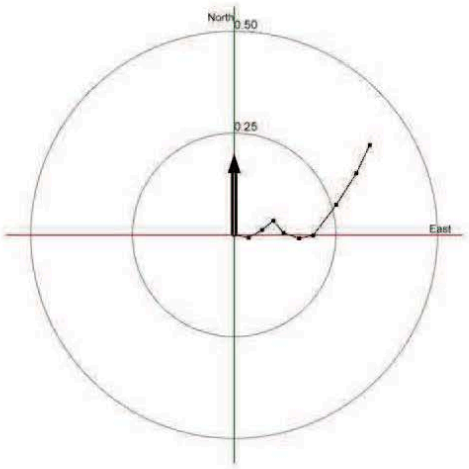

Front View

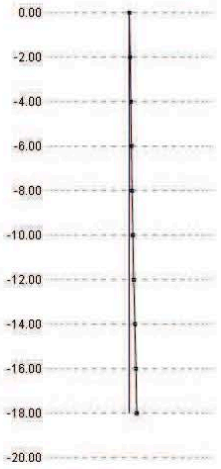

Side View

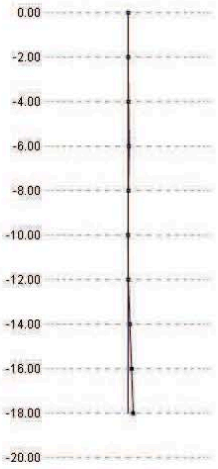

Face : 3 Hole : 15 Rod Increment : 2.00(m) Offset : 0.00(m) Dep : 18.00(m) Grid Magnetic Angle : 0.00(°)

Dep(m)	Heading(°)	Inclination(°)	Dev(m)
2.00	100.22	1.04	0.00
4.00	60.76	1.08	0.00
6.00	50.83	1.02	0.00
8.00	139.34	1.11	0.00
10.00	110.00	1.16	0.00
12.00	77.41	1.02	0.00
14.00	37.02	2.68	0.00
16.00	32.59	2.63	0.00
18.00	25.17	2.20	0.00

1.3.16 R1H16

Survey Data 1

Face : Face 1 Hole : R1H16 Survey Date : 22-01-18 Dep (m) : 18.00
Average Azimuth (°) : 113.39 Average Inclination (°) : 1.20
Designed Azimuth (°) : 0.00 Designed Inclination (°) : 0.00 Designed Depth (m) : 0.00

Plan View

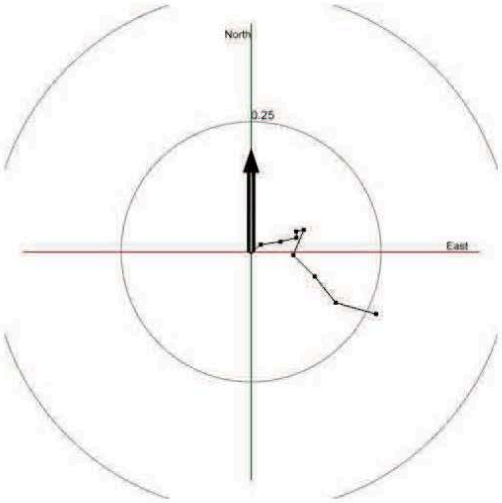

Front View

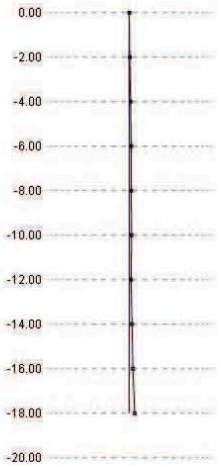

Side View

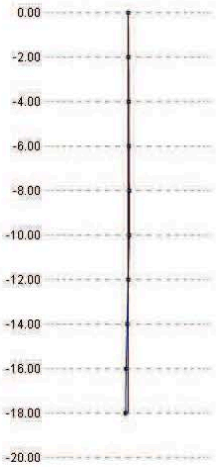

Face : 3 Hole : 16 Rod Increment : 2.00(m) Offset : 0.00(m) Dep : 18.00(m) Grid Magnetic Angle : 0.00(°)

Dep(m)	Heading(°)	Inclination(°)	Dev(m)
2.00	52.85	0.66	0.00
4.00	81.45	1.09	0.00
6.00	76.56	0.90	0.00
8.00	359.44	0.36	0.00
10.00	80.02	0.42	0.00
12.00	202.71	1.50	0.00
14.00	134.93	1.66	0.00
16.00	141.26	1.85	0.00
18.00	105.78	2.31	0.00

1.3.17 R1H17

Survey Data 1

Face : Face 1 Hole : R1H17 Survey Date : 22-01-18 Dep (m) : 18.00
Average Azimuth (°) : 333.13 Average Inclination (°) : 1.22
Designed Azimuth (°) : 0.00 Designed Inclination (°) : 0.00 Designed Depth (m) : 0.00

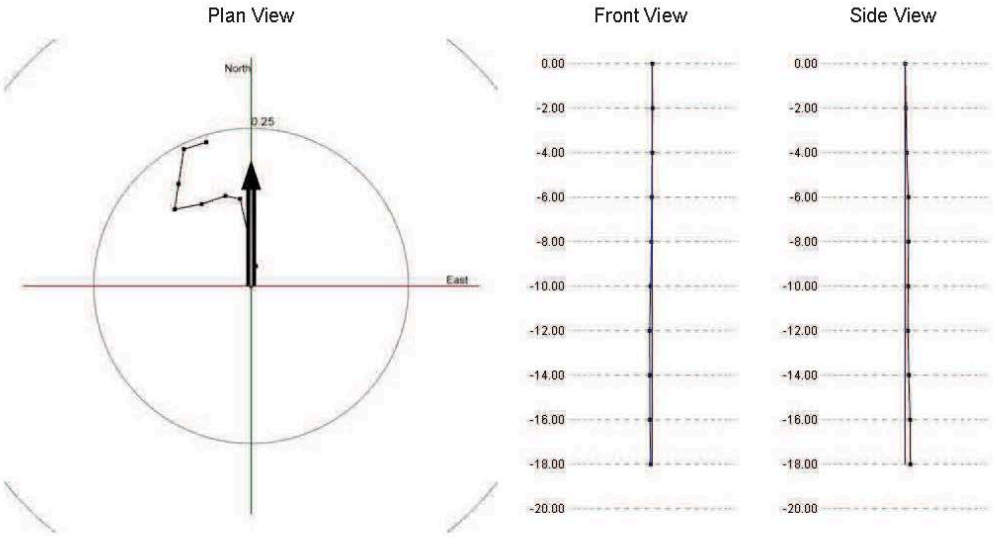

Face : 3 Hole : 17 Rod Increment : 2.00(m) Offset : 0.00(m) Dep : 18.00(m) Grid Magnetic Angle : 0.00(°)

Dep(m)	Heading(°)	Inclination(°)	Dev(m)
2.00	13.37	0.92	0.00
4.00	346.11	1.14	0.00
6.00	347.10	2.00	0.00
8.00	281.53	0.67	0.00
10.00	251.01	1.15	0.00
12.00	258.92	1.25	0.00
14.00	8.42	1.16	0.00
16.00	8.79	1.60	0.00
18.00	72.59	1.06	0.00

1.3.18 R1H18

Survey Data 1

Face : Face 1 Hole : R1H18 Survey Date : 22-01-18 Dep (m) : 18.00
Average Azimuth (°) : 103.36 Average Inclination (°) : 1.68
Designed Azimuth (°) : 0.00 Designed Inclination (°) : 0.00 Designed Depth (m) : 0.00

Plan View

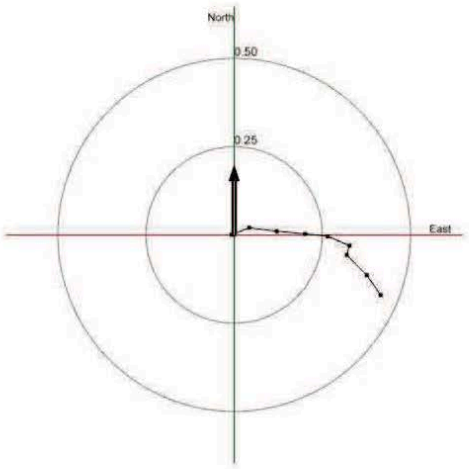

Front View

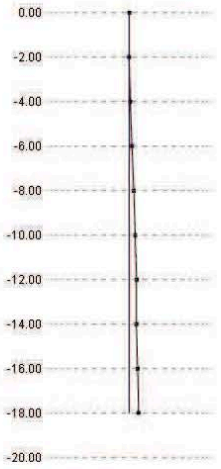

Side View

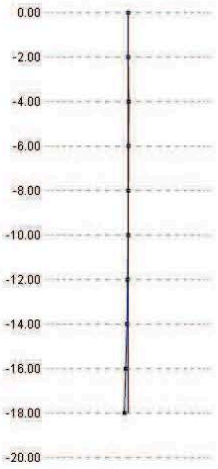

Face : 3 Hole : 18 Rod Increment : 2.00(m) Offset : 0.00(m) Dep : 18.00(m) Grid Magnetic Angle : 0.00(°)

Dep(m)	Heading(°)	Inclination(°)	Dev(m)
2.00	272.76	0.21	0.00
4.00	68.34	1.54	0.00
6.00	97.05	2.24	0.00
8.00	95.32	2.32	0.00
10.00	96.22	1.87	0.00
12.00	113.38	1.91	0.00
14.00	196.39	0.79	0.00
16.00	135.22	2.31	0.00
18.00	145.01	1.96	0.00

1.3.19 R1H19

Survey Data 1

Face : Face 1 Hole : R1H19 Survey Date : 22-01-18 Dep (m) : 18.00
Average Azimuth (°) : 67.31 Average Inclination (°) : 1.23
Designed Azimuth (°) : 0.00 Designed Inclination (°) : 0.00 Designed Depth (m) : 0.00

Plan View

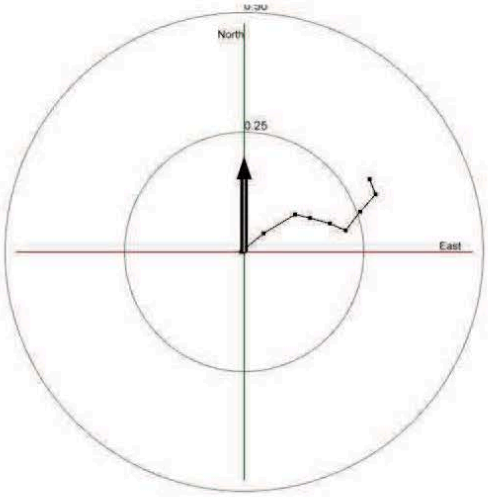

Front View

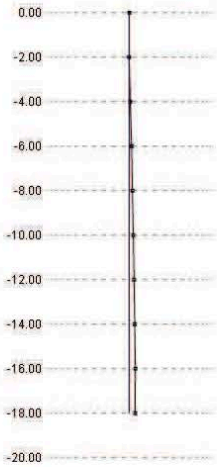

Side View

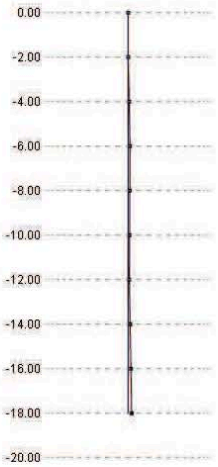

Face : 3 Hole : 19 Rod Increment : 2.00(m) Offset : 0.00(m) Dep : 18.00(m) Grid Magnetic Angle : 0.00(°)

Dep(m)	Heading(°)	Inclination(°)	Dev(m)
2.00	268.96	0.20	0.00
4.00	50.81	1.75	0.00
6.00	59.01	2.20	0.00
8.00	103.47	0.93	0.00
10.00	105.34	1.22	0.00
12.00	113.55	1.03	0.00
14.00	38.26	1.42	0.00
16.00	41.21	1.39	0.00
18.00	338.58	0.96	0.00

1.3.20 R1H20

Survey Data 1

Face : Face 1 Hole : R1H20 Survey Date : 22-01-18 Dep (m) : 18.00
Average Azimuth (°) : 71.74 Average Inclination (°) : 1.60
Designed Azimuth (°) : 0.00 Designed Inclination (°) : 0.00 Designed Depth (m) : 0.00

Plan View

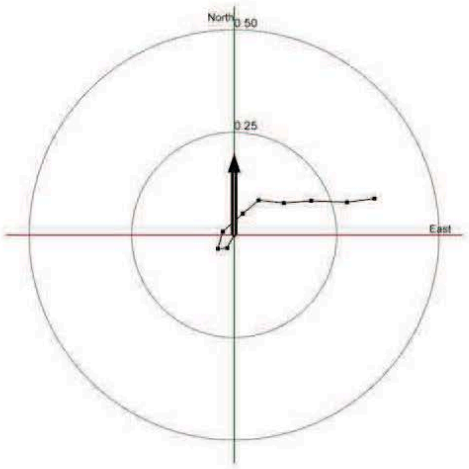

Front View

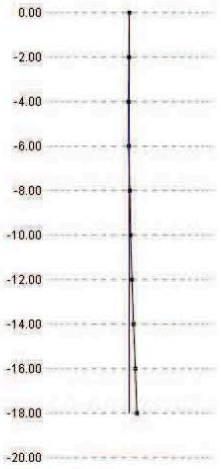

Side View

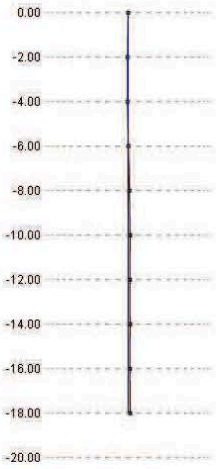

Face : 3 Hole : 20 Rod Increment : 2.00(m) Offset : 0.00(m) Dep : 18.00(m) Grid Magnetic Angle : 0.00(°)

Dep(m)	Heading(°)	Inclination(°)	Dev(m)
2.00	208.24	1.04	0.00
4.00	264.83	0.65	0.00
6.00	16.10	1.25	0.00
8.00	47.93	1.87	0.00
10.00	49.92	1.46	0.00
12.00	96.35	1.77	0.00
14.00	85.51	1.91	0.00
16.00	92.06	2.50	0.00
18.00	82.68	1.94	0.00

1.3.21 R1H21

Survey Data 1

Face : Face 1 Hole : R1H21 Survey Date : 22-01-18 Dep (m) : 18.00
Average Azimuth (°) : 158.86 Average Inclination (°) : 2.58
Designed Azimuth (°) : 0.00 Designed Inclination (°) : 0.00 Designed Depth (m) : 0.00

Plan View

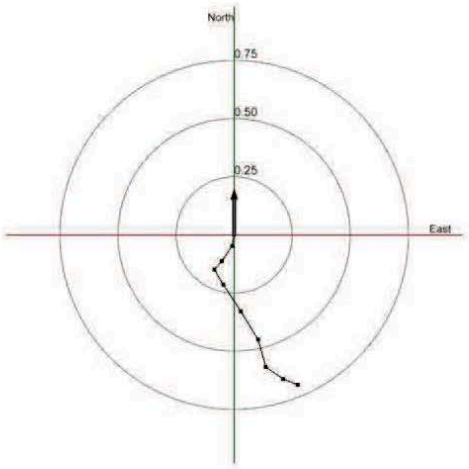

Front View

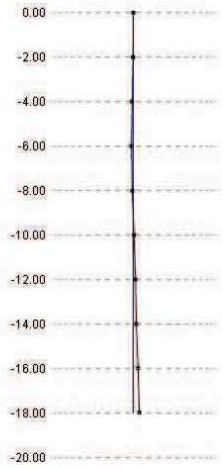

Side View

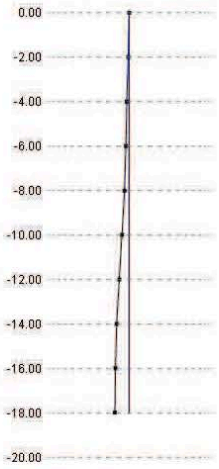

Face : 3 Hole : 21 Rod Increment : 2.00(m) Offset : 0.00(m) Dep : 18.00(m) Grid Magnetic Angle : 0.00(°)

Dep(m)	Heading(°)	Inclination(°)	Dev(m)
2.00	190.64	1.39	0.00
4.00	214.35	2.26	0.00
6.00	221.21	1.39	0.00
8.00	149.13	2.15	0.00
10.00	146.68	3.94	0.00
12.00	148.48	4.06	0.00
14.00	164.12	3.53	0.00
16.00	124.48	2.60	0.00
18.00	111.91	1.90	0.00

1.3.22 R1H22

Survey Data 1

Face : Face 1 Hole : R1H22 Survey Date : 22-01-18 Dep (m) : 18.00
Average Azimuth (°) : 35.98 Average Inclination (°) : 1.76
Designed Azimuth (°) : 0.00 Designed Inclination (°) : 0.00 Designed Depth (m) : 0.00

Plan View

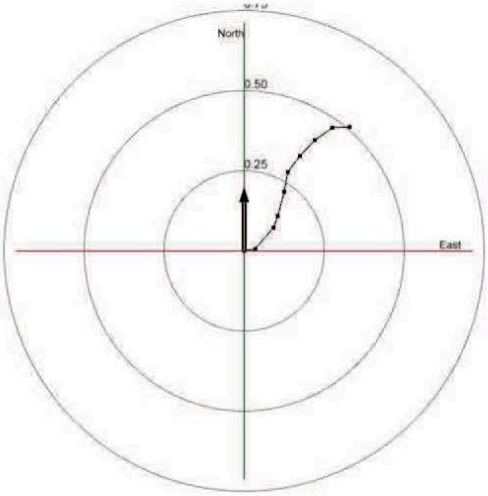

Front View

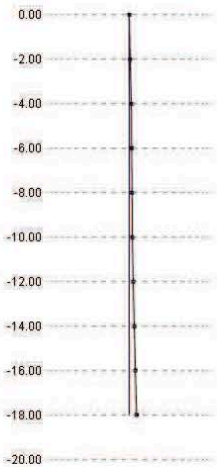

Side View

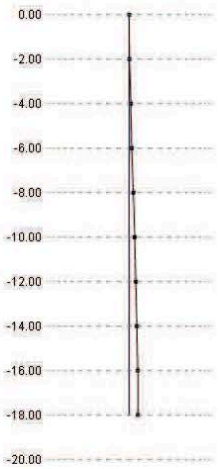

Face : 3 Hole : 22 Rod Increment : 2.00(m) Offset : 0.00(m) Dep : 18.00(m) Grid Magnetic Angle : 0.00(°)

Dep(m)	Heading(°)	Inclination(°)	Dev(m)
2.00	79.45	1.00	0.00
4.00	41.00	2.51	0.00
6.00	20.37	1.11	0.00
8.00	14.59	2.24	0.00
10.00	10.66	1.78	0.00
12.00	36.60	1.81	0.00
14.00	43.48	1.93	0.00
16.00	54.57	1.93	0.00
18.00	87.90	1.54	0.00

1.3.23 R1H23

Survey Data 1

Face : Face 1 Hole : R1H23 Survey Date : 22-01-18 Dep (m) : 18.00
Average Azimuth (°) : 250.94 Average Inclination (°) : 1.02
Designed Azimuth (°) : 0.00 Designed Inclination (°) : 0.00 Designed Depth (m) : 0.00

Plan View

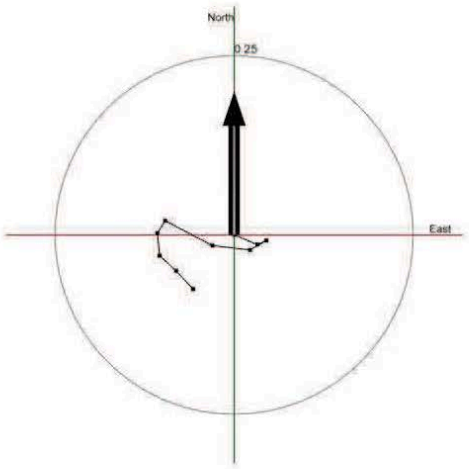

Front View

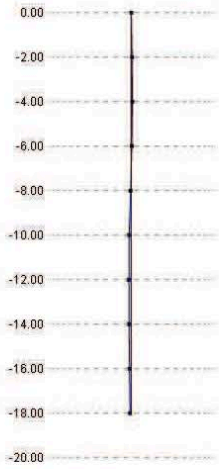

Side View

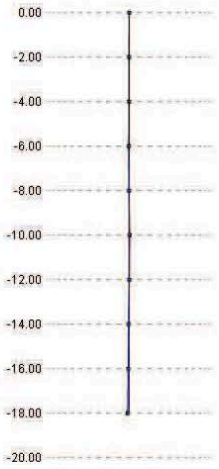

Face : 3 Hole : 23 Rod Increment : 2.00(m) Offset : 0.00(m) Dep : 18.00(m) Grid Magnetic Angle : 0.00(°)

Dep(m)	Heading(°)	Inclination(°)	Dev(m)
2.00	112.42	1.00	0.00
4.00	66.47	0.39	0.00
6.00	240.43	0.75	0.00
8.00	276.48	1.51	0.00
10.00	297.80	2.13	0.00
12.00	211.85	0.59	0.00
14.00	174.44	0.90	0.00
16.00	132.72	0.90	0.00
18.00	136.93	1.00	0.00

1.3.24 R1H24

Survey Data 1

Face : Face 1 Hole : R1H24 Survey Date : 22-01-18 Dep (m) : 18.00
Average Azimuth (°) : 36.23 Average Inclination (°) : 1.04
Designed Azimuth (°) : 0.00 Designed Inclination (°) : 0.00 Designed Depth (m) : 0.00

Plan View

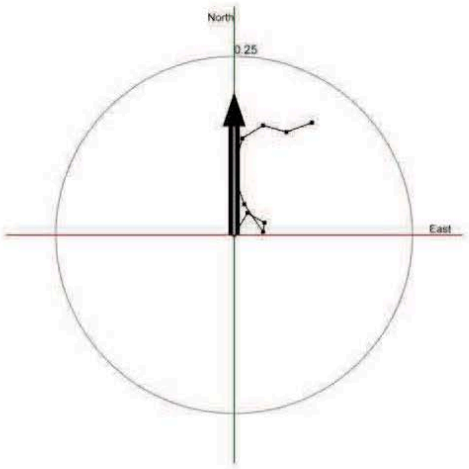

Front View

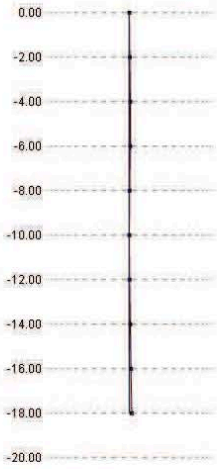

Side View

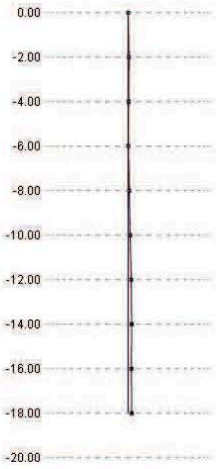

Face : 3 Hole : 24 Rod Increment : 2.00(m) Offset : 0.00(m) Dep : 18.00(m) Grid Magnetic Angle : 0.00(°)

Dep(m)	Heading(°)	Inclination(°)	Dev(m)
2.00	31.47	1.03	0.00
4.00	120.30	0.79	0.00
6.00	189.99	0.37	0.00
8.00	325.96	1.34	0.00
10.00	340.19	1.33	0.00
12.00	14.66	1.44	0.00
14.00	58.02	0.99	0.00
16.00	105.85	0.98	0.00
18.00	69.76	1.08	0.00

1.3.25 R1H25

Survey Data 1

Face : Face 1 Hole : R1H25 Survey Date : 22-01-18 Dep (m) : 18.00
Average Azimuth (°) : 27.28 Average Inclination (°) : 1.06
Designed Azimuth (°) : 0.00 Designed Inclination (°) : 0.00 Designed Depth (m) : 0.00

Plan View

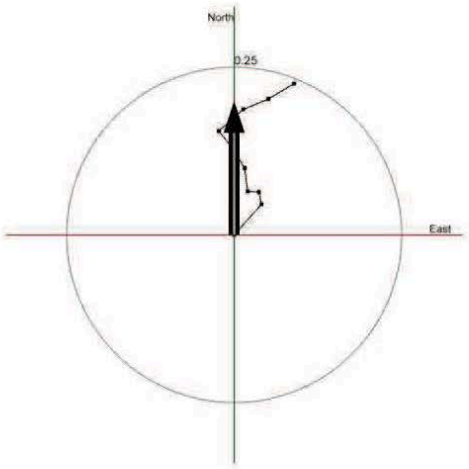

Front View

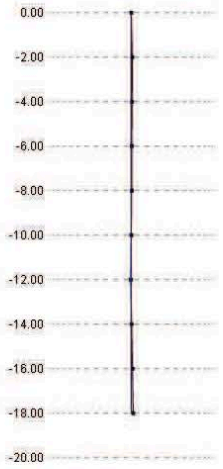

Side View

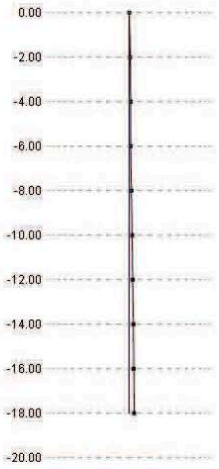

Face : 3 Hole : 25 Rod Increment : 2.00(m) Offset : 0.00(m) Dep : 18.00(m) Grid Magnetic Angle : 0.00(°)

Dep(m)	Heading(°)	Inclination(°)	Dev(m)
2.00	41.81	1.75	0.00
4.00	347.99	0.53	0.00
6.00	273.71	0.48	0.00
8.00	352.53	1.00	0.00
10.00	328.66	1.00	0.00
12.00	321.55	0.95	0.00
14.00	48.78	1.40	0.00
16.00	67.47	1.16	0.00
18.00	59.16	1.28	0.00

1.3.26 R1H26

Survey Data 1

Face : Face 1 Hole : R1H26 Survey Date : 22-01-18 Dep (m) : 18.00
Average Azimuth (°) : 20.70 Average Inclination (°) : 1.28
Designed Azimuth (°) : 0.00 Designed Inclination (°) : 0.00 Designed Depth (m) : 0.00

Plan View

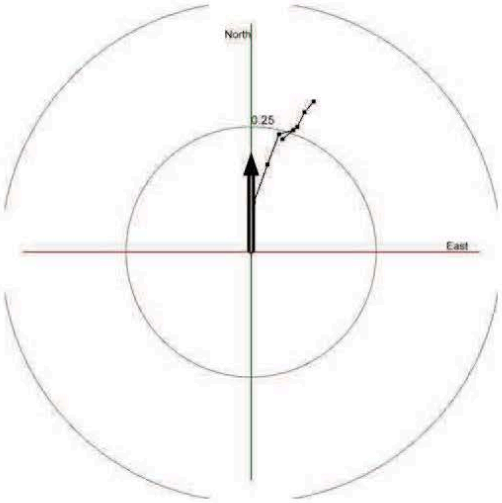

Front View

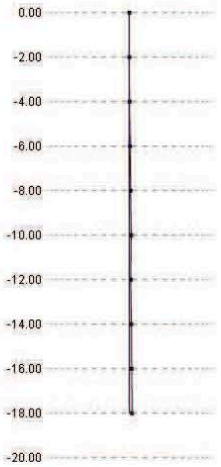

Side View

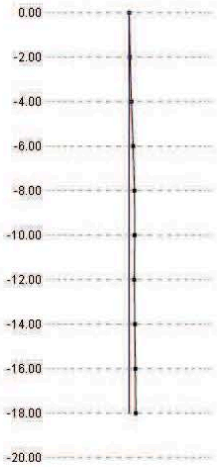

Face : 3 Hole : 26 Rod Increment : 2.00(m) Offset : 0.00(m) Dep : 18.00(m) Grid Magnetic Angle : 0.00(°)

Dep(m)	Heading(°)	Inclination(°)	Dev(m)
2.00	4.11	1.01	0.00
4.00	2.28	1.81	0.00
6.00	20.01	2.32	0.00
8.00	20.66	1.86	0.00
10.00	73.69	0.86	0.00
12.00	229.93	0.81	0.00
14.00	50.71	1.09	0.00
16.00	26.06	0.94	0.00
18.00	40.38	0.79	0.00

1.4 Hole Separation Report

Date : 26-04-18 Time : 7:41 PM Search Interval : 1.00(m) Minimum Found : 0.00(m) At Level of : 0.0(m)

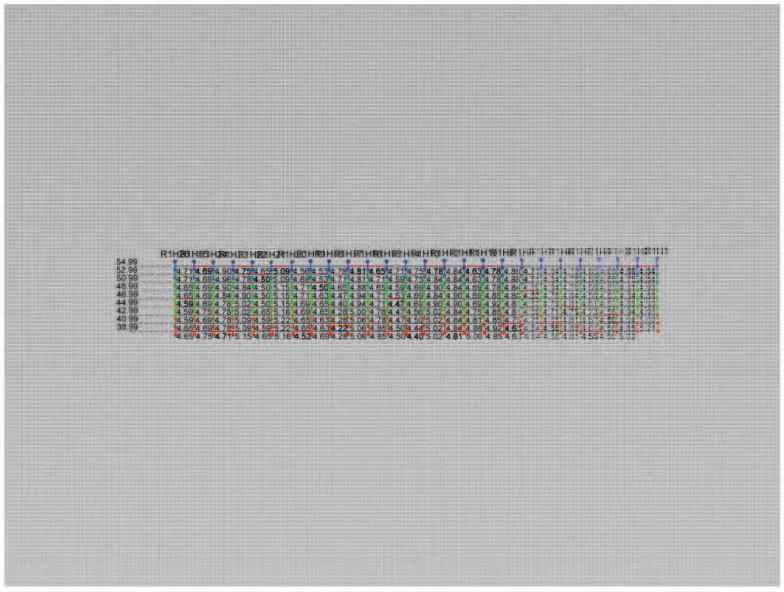

Dyno Nobel North America — BLAST REPORT

DYNO Dyno Nobel

SERVICE SITE LOCATION: Gamebridge ORDER NO.: 1114904

BLAST NUMBER: 2018-05 BLAST TIME: 3:29 pm BLAST DATE: 05/23/2018

CUSTOMER: CRH CANADA GROUP INC. MINE: OGDEN POINT QUARRY ADDRESS: Colborne, ON

ROCK TYPE: Limestone ROCK SPECIFIC GRAVITY: 2.65 EXPECTED VIBRATION: 0.000 MMS

LOCATION OF BLAST

LOCATION OF BLAST IN MINE: North BENCH: Level 3

BLAST GPS POINTS: N 043.98810 & W -077.87425

WEATHER

WEATHER: Clear CEILING: Unlimited TEMPERATURE: 23 C WIND DIRECTION & SPEED: Southwest 13 KPH

NEAREST NON-OWNED STRUCTURE

NAME: OGDEN POINT QUARRY GPS Points: N 043.99667 & W -077.87667

DISTANCE: 0 (KM) DIRECTION: 348°

SEISMOGRAPH DATA

	LOCATION	DISTANCE	GPS POINTS	CALIBRATION DATE
1	OGDEN POINT QUARRY	0 (KM)	N 043.99667 & W -077.87667	03/02/2018

	L	(F)	T	(F)	V	(F)	AIR (db)	SEISMOGRAPH	SERIAL	OPERATOR
1	2.770	51	3.090	34	2.500	30	127.1	MicroMate	UM13456	

BLAST DATA

		EXPLOSIVES SIZE, TYPE & WEIGHT		
NUMBER OF HOLES (EA)	88	SIZE	TYPE	WEIGHT
HOLE DIAMETER (CM)	10.14	BULK	TITAN XL 1000 G	14,061
HOLE DEPTH (M)	18.28	0.34 KG	SPARTAN 350	60
FACE HEIGHT (M)	18.28			
SUB DRILLING (M)	0			
AVG. STEM FACE HOLES (M)	2.13			
STEM OTHER HOLES (M)	2.13			
BURDEN FRONT ROW (M)	4.41			
BURDEN OTHER ROWS (M)	3.96			
SPACING FRONT ROW (M)	4.72			
SPACING OTHER ROWS (M)	4.72		TOTAL WEIGHT (KG):	14,121

DETONATORS USED IN BLAST: Electronic MATS USED: No STEM TYPE: CLEAN CRUSHED STONE TOTAL DRILL DEPTH: 1,609 (M

TYPE	MFG	DATE CODE	USED	TYPE	MFG	DATE CODE	USED
DIGISHOT 20FT	Dyno Nobel Global	NA	87	DIGISHOT 80FT	Dyno Nobel Global	NA	89
DIGISHOT SURFACE WIRE	Dyno Nobel Global		2	SPARTAN 350	Dyno Nobel Global	NA	176

M3 IN SHOT: 31,155 SCALED DISTANCE FACTOR: 0 % OF ANFO: 0

TONNES IN SHOT: 82,560 HOLES/DELAY : 1 FUEL OIL % (BULK): 0

MAX KGS/DELAY: 0 MAXIMUM KGS/HOLE: 161

POWDER FACTOR (KGS/MT): 0.17 POWDER FACTOR (KGS/M3): 0.45

BLASTER'S NAME: Porco, Domenic BLASTER'S NUMBER & STATE: NA

BLASTER'S SIGNATURE: SITE SAFETY INSPECTION PERFORMED: Yes

NUMBER OF PERSONNEL ON SITE: 4

REMARKS : Bench was flat and dry. Floor in front of the blast was dry and clear of muck. Hole size and timing for the blast was provided by Respec. All of the holes were full of water but loaded well. No seams or voids. Stemming material had fines in it. Wind picked up during the blast, very gusty. Very good fragmentation in the muck pile. Good seismograph readings.

START TIME	END TIME	TOTAL TIME	TRUCK NUMBERS
7:00 AM	2:00 PM	07:00	HT-0954

Dyno Nobel North America

CUSTOMER NAME: OGDEN POINT QUARRY
BENCH: Level 3
BLASTER'S NAME: Porco, Domenic

DIAGRAM

BLAST DATE: 05/23/2018
BLAST NUMBER: 2018-05

DYNO
Dyno Nobel

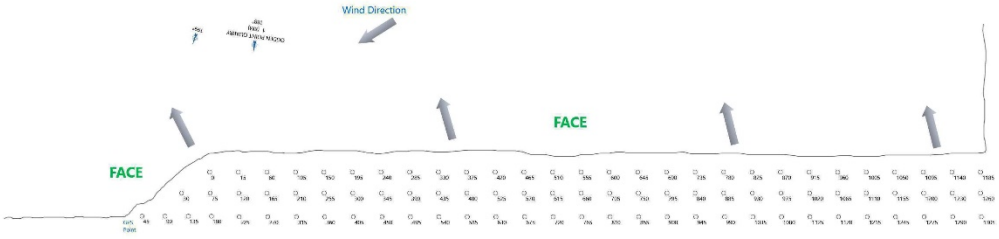

Dyno Nobel North America

CUSTOMER NAME: OGDEN POINT QUARRY

BLAST NUMBER: 2018-05

BLAST DATE: 05/23/2018

BENCH: Level 3

BLASTER'S NAME: Porco, Domenic

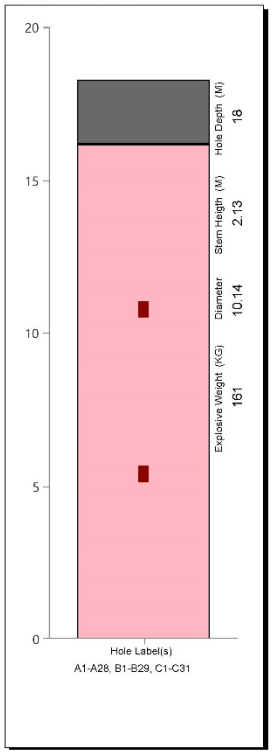

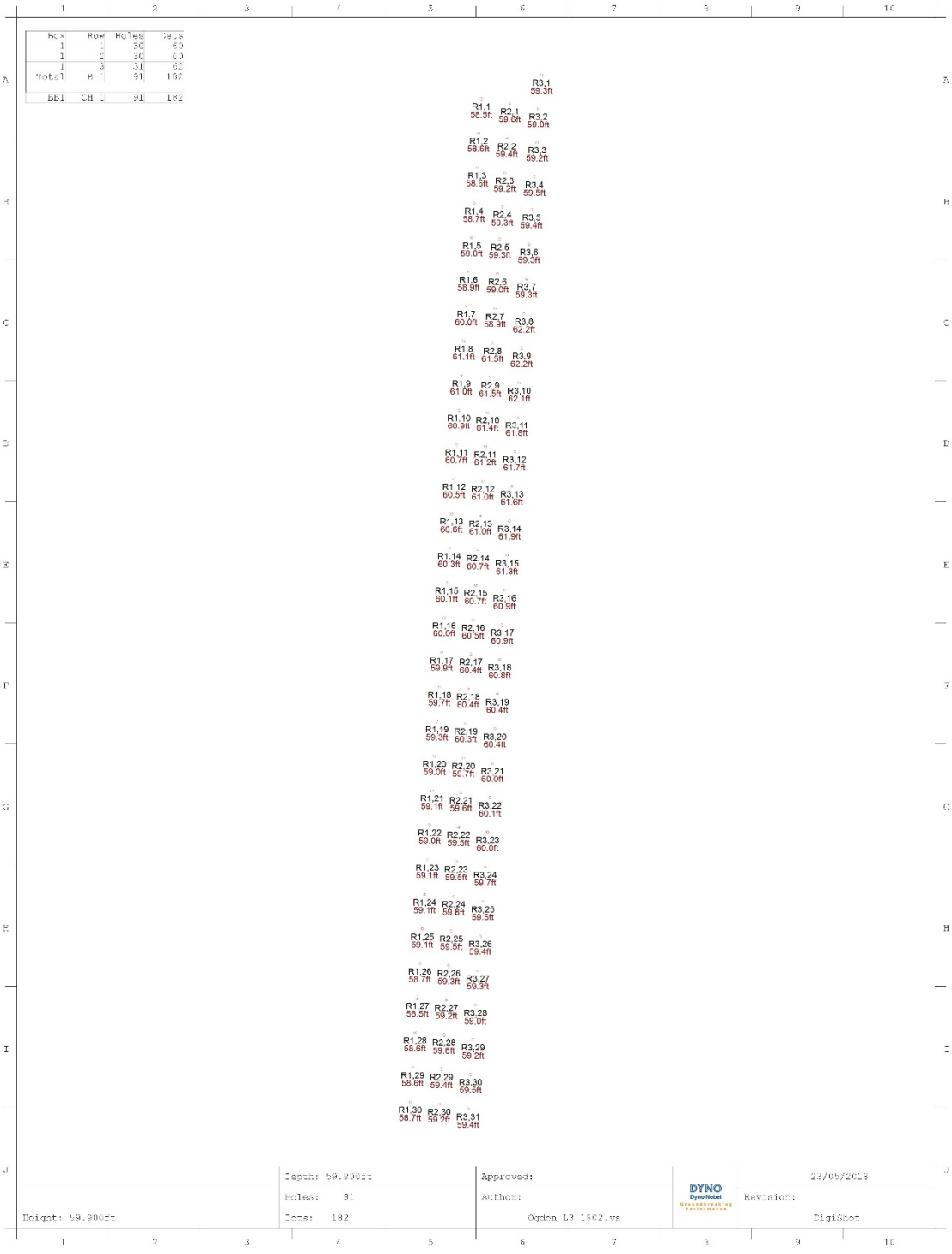
Box Row Holes Dets
1 1 30 60
1 2 30 60
1 3 31 62
Total 3 91 182
BB1 CH 1 91 182
R3,1 59.3ft
R1,1 58.5ft R2,1 59.6ft R3,2 59.0ft
R1,2 58.6ft R2,2 59.4ft R3,3 59.2ft
R1,3 58.6ft R2,3 59.2ft R3,4 59.5ft
R1,4 58.7ft R2,4 59.3ft R3,5 59.4ft
R1,5 59.0ft R2,5 59.3ft R3,6 59.3ft
R1,6 58.9ft R2,6 59.0ft R3,7 59.3ft
R1,7 60.0ft R2,7 58.9ft R3,8 62.2ft
R1,8 61.1ft R2,8 61.5ft R3,9 62.2ft
R1,9 61.0ft R2,9 61.5ft R3,10 62.1ft
R1,10 60.9ft R2,10 61.4ft R3,11 61.8ft
R1,11 60.7ft R2,11 61.2ft R3,12 61.7ft
R1,12 60.5ft R2,12 61.0ft R3,13 61.6ft
R1,13 60.6ft R2,13 61.0ft R3,14 61.9ft
R1,14 60.3ft R2,14 60.7ft R3,15 61.3ft
R1,15 60.1ft R2,15 60.7ft R3,16 60.9ft
R1,16 60.0ft R2,16 60.5ft R3,17 60.9ft
R1,17 59.9ft R2,17 60.4ft R3,18 60.8ft
R1,18 59.7ft R2,18 60.4ft R3,19 60.4ft
R1,19 59.3ft R2,19 60.3ft R3,20 60.4ft
R1,20 59.0ft R2,20 59.7ft R3,21 60.0ft
R1,21 59.1ft R2,21 59.6ft R3,22 60.1ft
R1,22 59.0ft R2,22 59.5ft R3,23 60.0ft
R1,23 59.1ft R2,23 59.5ft R3,24 59.7ft
R1,24 59.1ft R2,24 59.6ft R3,25 59.5ft
R1,25 59.1ft R2,25 59.5ft R3,26 59.4ft
R1,26 58.7ft R2,26 59.3ft R3,27 59.3ft
R1,27 58.5ft R2,27 59.2ft R3,28 59.0ft
R1,28 58.6ft R2,28 59.6ft R3,29 59.2ft
R1,29 58.6ft R2,29 59.4ft R3,30 59.5ft
R1,30 58.7ft R2,30 59.2ft R3,31 59.4ft
Depth: 59.900ft
Holes: 91
Dets: 182
Approved:
Author: Ogden L3 1502.vs
23/05/2018
Revision:
Height: 59.900ft
DigiShot

DynoConsult

Drill log

DYNO Dyno Nobel

Reference		**Date:**	April 26, 2018
Client:	CRH Group Canada inc.	**Blast no.:**	Level 3 2018-02
Site:	Ogden Point Quarry, Colborne ON		

BLAST PARAMETERS				
Pattern	1st row	14' x 15.5'	other rows	13' x 15.5'
Number of holes	91			
Hole diameter	4 in			
Notes				

DRILLING INFORMATION

Row ID	Hole ID	Design angle	Design depth (ft)	Measured depth (ft)	Comments
1	1	0	58.5		
1	2	0	58.6		
1	3	0	58.6		
1	4	0	58.7		
1	5	0	59.0		
1	6	0	58.9		
1	7	0	60.0		
1	8	0	61.1		
1	9	0	61.0		
1	10	0	60.9		
1	11	0	60.7		
1	12	0	60.5		
1	13	0	60.6		
1	14	0	60.3		
1	15	0	60.1		
1	16	0	60.0		
1	17	0	59.9		
1	18	0	59.7		
1	19	0	59.3		
1	20	0	59.0		
1	21	0	59.1		
1	22	0	59.0		
1	23	0	59.1		
1	24	0	59.1		
1	25	0	59.1		
1	26	0	58.7		
1	27	0	58.5		
1	28	0	58.6		
1	29	0	58.6		

SIGNATURES			
Driller		Date	
Blaster		Date	
Supervisor		Date	

DynoConsult

Drill log

DYNO Dyno Nobel

Reference		**Date:**	April 26, 2018
Client:	CRH Group Canada inc.	**Blast no.:**	Level 3 2018-02
Site:	Ogden Point Quarry, Colborne ON		

BLAST PARAMETERS				
Pattern	1st row	14' x 15.5'	other rows	13' x 15.5'
Number of holes	91			
Hole diameter	4 in			
Notes				

DRILLING INFORMATION					
Row ID	**Hole ID**	**Design angle**	**Design depth (ft)**	**Measured depth (ft)**	**Comments**
1	30	0	58.7		
2	1	0	59.6		
2	2	0	59.4		
2	3	0	59.2		
2	4	0	59.3		
2	5	0	59.3		
2	6	0	59.0		
2	7	0	58.9		
2	8	0	61.5		
2	9	0	61.5		
2	10	0	61.4		
2	11	0	61.2		
2	12	0	61.0		
2	13	0	61.0		
2	14	0	60.7		
2	15	0	60.7		
2	16	0	60.5		
2	17	0	60.4		
2	18	0	60.4		
2	19	0	60.3		
2	20	0	59.7		
2	21	0	59.6		
2	22	0	59.5		
2	23	0	59.5		
2	24	0	59.8		
2	25	0	59.5		
2	26	0	59.3		
2	27	0	59.2		
2	28	0	59.6		

SIGNATURES			
Driller		Date	
Blaster		Date	
Supervisor		Date	

DynoConsult

Drill log

DYNO Dyno Nobel

Reference		**Date:**	April 26, 2018
Client:	CRH Group Canada inc.	**Blast no.:**	Level 3 2018-02
Site:	Ogden Point Quarry, Colborne ON		

BLAST PARAMETERS				
Pattern	1st row	14' x 15.5'	other rows	13' x 15.5'
Number of holes	91			
Hole diameter	4 in			
Notes				

DRILLING INFORMATION

Row ID	Hole ID	Design angle	Design depth (ft)	Measured depth (ft)	Comments
2	29	0	59.4		
2	30	0	59.2		
3	1	0	59.3		
3	2	0	59.0		
3	3	0	59.2		
3	4	0	59.5		
3	5	0	59.4		
3	6	0	59.3		
3	7	0	59.3		
3	8	0	62.2		
3	9	0	62.2		
3	10	0	62.1		
3	11	0	61.8		
3	12	0	61.7		
3	13	0	61.6		
3	14	0	61.9		
3	15	0	61.3		
3	16	0	60.9		
3	17	0	60.9		
3	18	0	60.8		
3	19	0	60.4		
3	20	0	60.4		
3	21	0	60.0		
3	22	0	60.1		
3	23	0	60.0		
3	24	0	59.7		
3	25	0	59.5		
3	26	0	59.4		
3	27	0	59.3		

SIGNATURES			
Driller		Date	
Blaster		Date	
Supervisor		Date	

DynoConsult

Drill log

DYNO Dyno Nobel

Reference		**Date:**	April 26, 2018
Client:	CRH Group Canada inc.	**Blast no.:**	Level 3 2018-02
Site:	Ogden Point Quarry, Colborne ON		

BLAST PARAMETERS				
Pattern	1st row	14' x 15.5'	other rows	13' x 15.5'
Number of holes	91			
Hole diameter	4 in			
Notes				

DRILLING INFORMATION					
Row ID	**Hole ID**	**Design angle**	**Design depth (ft)**	**Measured depth (ft)**	**Comments**
3	28	0	59.0		
3	29	0	59.2		
3	30	0	59.5		
3	31	0	59.4		

SIGNATURES			
Driller		Date	
Blaster		Date	
Supervisor		Date	

Overview

Site Name:
Bench Name:
Blast Name:
Recording Date: 2018-05-21 11:30:54 PM
Rock Density: 2500 kg/m³
3D image: Final.jm3
Blast Site: Final.smb
Notes:

Blast Site Geometry

Minimal Bench Height:	16.94 m
Mean Bench Height:	17.20 m
Maximum Bench Height:	17.69 m
Front Plane Dipping:	89.56 °
Front Plane Dip Direction:	175.45 °
Lateral Distance between Delimiters:	142.56 m
Lateral Distance between Delimiting Planes:	142.56 m
Number of Boreholes:	30
Total Drilling Length:	515.22 m
Total Blasting Volume:	-
Total Blasting Mass:	-

Design Parameters

Burden:	4.27 m
Rows:	1
Row Shift:	0.0 m
Side Spacing:	3.0 m
Inclination:	0.01 °

It is noted that the blast site planned with BlastMetriX3D bases exclusively on the contact-free measured information of the bench face. The blast site planned with BlastMetriX3D has to be checked in any case for completeness and correctness by a responsible blaster. It is presumed that all legally binding laws, regulations and guidelines applicable in your country are met. By using BlastMetriX3D you agree to implement the result on your responsibility and free 3GSM from any possible claims.

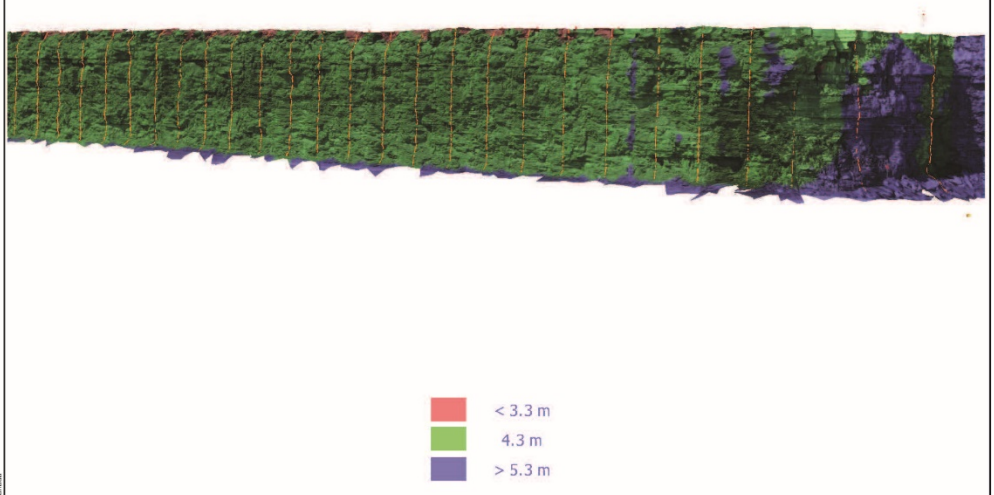

-

Scale 1:1200

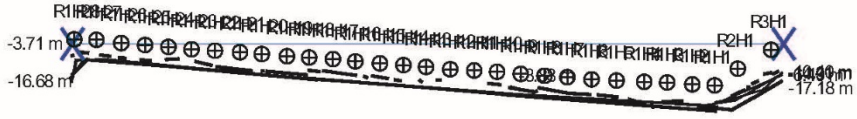

Delimiter
Reference line
Row
Borehole position
Borehole
All dimensions in [m]

Licensed: Dyno Nobel Canada

Date: 2018-05-21 11:41:34 PM
BlastMetrix3D 4.0.2

Ogden 2018-02 Level 3 Profile.pdf

Page: 2/37

Borehole details

Name	u [m]	v [m]	E [m]	N [m]	H [m]	Alpha [deg]	Inclination [deg]	Length [m]	Diameter [mm]
R3H1	140.05	-1.20	750658.78	4875300.19	55.29	120.00	0.01	17.46	100.00
R2H1	133.37	-4.97	750652.69	4875295.54	55.24	105.00	0.01	17.39	100.00
R1H1	128.73	-8.32	750648.54	4875291.59	55.23	86.71	0.01	17.36	100.00
R1H2	124.24	-8.10	750644.07	4875291.19	55.21	86.71	0.01	17.32	100.00
R1H3	119.19	-7.74	750639.02	4875290.86	55.22	86.71	0.01	17.31	100.00
R1H4	114.60	-7.60	750634.45	4875290.37	55.24	86.71	0.01	17.32	100.00
R1H5	109.07	-7.34	750628.93	4875289.87	55.28	86.71	0.01	17.35	100.00
R1H6	104.06	-7.12	750623.94	4875289.41	55.37	86.71	0.01	17.42	100.00
R1H7	99.20	-6.67	750619.07	4875289.19	55.38	86.71	0.01	17.40	100.00
R1H8	94.62	-6.39	750614.49	4875288.83	55.38	86.71	0.01	17.39	100.00
R1H9	89.86	-6.01	750609.73	4875288.56	55.40	86.71	0.01	17.39	100.00
R1H10	85.11	-5.59	750604.96	4875288.33	55.05	86.71	0.01	17.03	100.00
R1H11	80.52	-5.32	750600.38	4875287.96	55.00	86.71	0.01	16.96	100.00
R1H12	75.71	-5.08	750595.58	4875287.55	55.10	86.71	0.01	17.04	100.00
R1H13	70.86	-4.62	750590.72	4875287.34	55.09	86.71	0.01	17.02	100.00
R1H14	66.34	-4.25	750586.19	4875287.09	55.15	86.71	0.01	17.06	100.00
R1H15	61.63	-3.90	750581.47	4875286.79	55.16	86.71	0.01	17.06	100.00
R1H16	56.71	-3.51	750576.54	4875286.50	55.23	86.71	0.01	17.11	100.00
R1H17	52.22	-3.04	750572.03	4875286.35	55.20	86.71	0.01	17.06	100.00
R1H18	47.43	-2.73	750567.24	4875286.01	55.29	86.71	0.01	17.13	100.00
R1H19	43.00	-2.47	750562.82	4875285.66	55.31	86.71	0.01	17.13	100.00
R1H20	37.95	-2.04	750557.76	4875285.40	55.37	86.71	0.01	17.18	100.00
R1H21	33.58	-1.66	750553.38	4875285.17	55.36	86.71	0.01	17.15	100.00
R1H22	28.56	-1.36	750548.37	4875284.78	55.42	86.71	0.01	17.20	100.00
R1H23	23.87	-1.09	750543.68	4875284.41	55.44	86.71	0.01	17.19	100.00
R1H24	19.24	-0.61	750539.03	4875284.26	55.33	86.71	0.01	17.07	100.00
R1H25	14.56	-0.23	750534.34	4875283.99	55.32	86.71	0.01	17.04	100.00
R1H26	9.78	0.15	750529.55	4875283.72	55.28	86.71	0.01	16.99	100.00
R1H27	4.80	0.81	750524.53	4875283.69	55.16	86.71	0.01	16.85	100.00
R1H28	0.36	0.91	750520.12	4875283.18	55.18	95.00	0.01	16.85	100.00

-

R3H1 (Scale 1:150) Profile

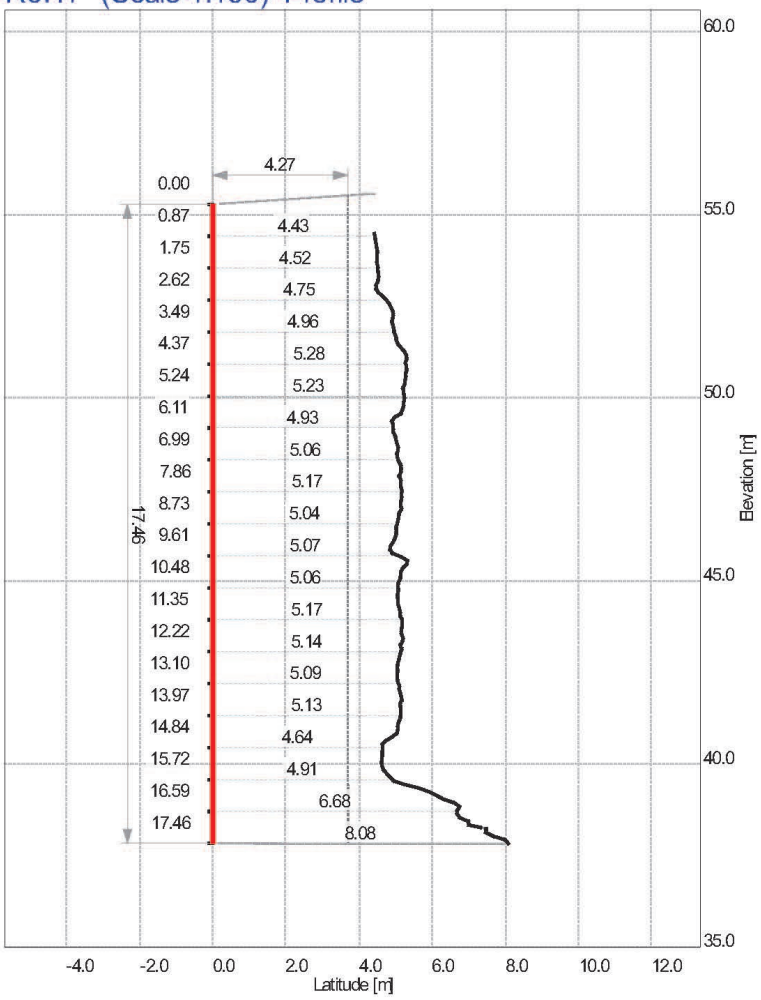

Inclination: 0.01 °
Length: 17.46 m
Diameter: 100.00 mm
Area: 90.4 m² (of profile)
Position: u: 140.05 m, v: -1.20 m
E: 750658.78 m, N: 4875300.19 m, H: 55.29 m
Subdrilling: 0 m

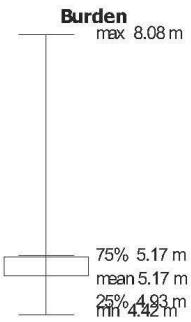

Depth	Profile
1.0	4.456
2.0	4.548
3.0	4.925
4.0	5.284
5.0	5.218
6.0	4.932
7.0	5.147
8.0	5.142
9.0	4.922
10.0	5.108
11.0	5.153
12.0	5.113
13.0	5.125
14.0	5.047
15.0	4.649
16.0	6.751
17.0	8.075

-

R2H1 (Scale 1:150) Profile

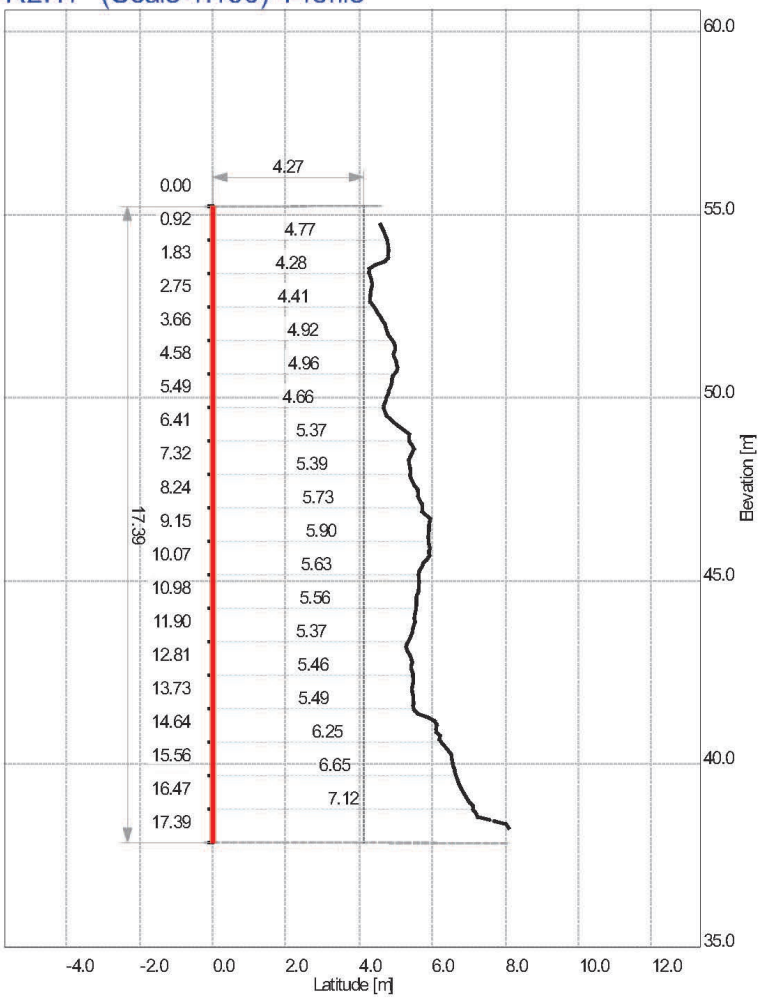

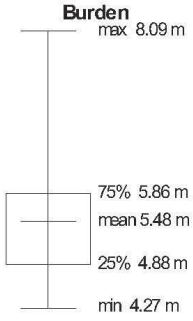

Inclination: 0.01 °
Length: 17.39 m
Diameter: 100.00 mm
Area: 95.8 m² (of profile)
Position: u: 133.37 m, v: -4.97 m
E: 750652.69 m, N: 4875295.54 m, H: 55.24 m
Subdrilling: 0 m

Depth	Profile
1.0	4.788
2.0	4.343
3.0	4.606
4.0	4.943
5.0	4.797
6.0	5.255
7.0	5.398
8.0	5.718
9.0	5.915
10.0	5.637
11.0	5.506
12.0	5.394
13.0	5.458
14.0	6.104
15.0	6.586
16.0	7.086
17.0	na

-

R1H1 (Scale 1:150) Profile

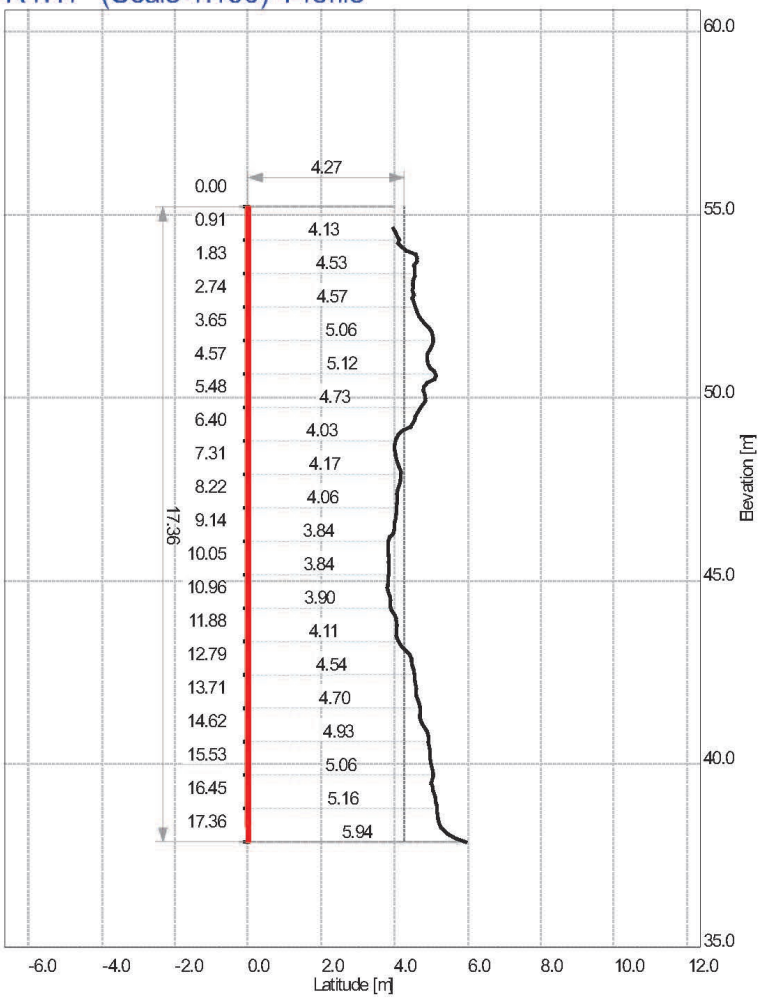

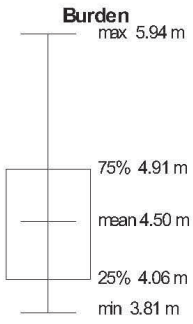

Inclination: 0.01 °
Length: 17.36 m
Diameter: 100.00 mm
Area: 77.8 m² (of profile)
Position: u: 128.73 m, v: -8.32 m
E: 750648.54 m, N: 4875291.59 m, H: 55.23 m
Subdrilling: 0 m

Depth	Profile
1.0	4.109
2.0	4.488
3.0	4.718
4.0	4.893
5.0	4.816
6.0	4.210
7.0	4.143
8.0	4.060
9.0	3.830
10.0	3.823
11.0	4.037
12.0	4.420
13.0	4.590
14.0	4.860
15.0	5.020
16.0	5.146
17.0	5.941

-

R1H2 (Scale 1:150) Profile

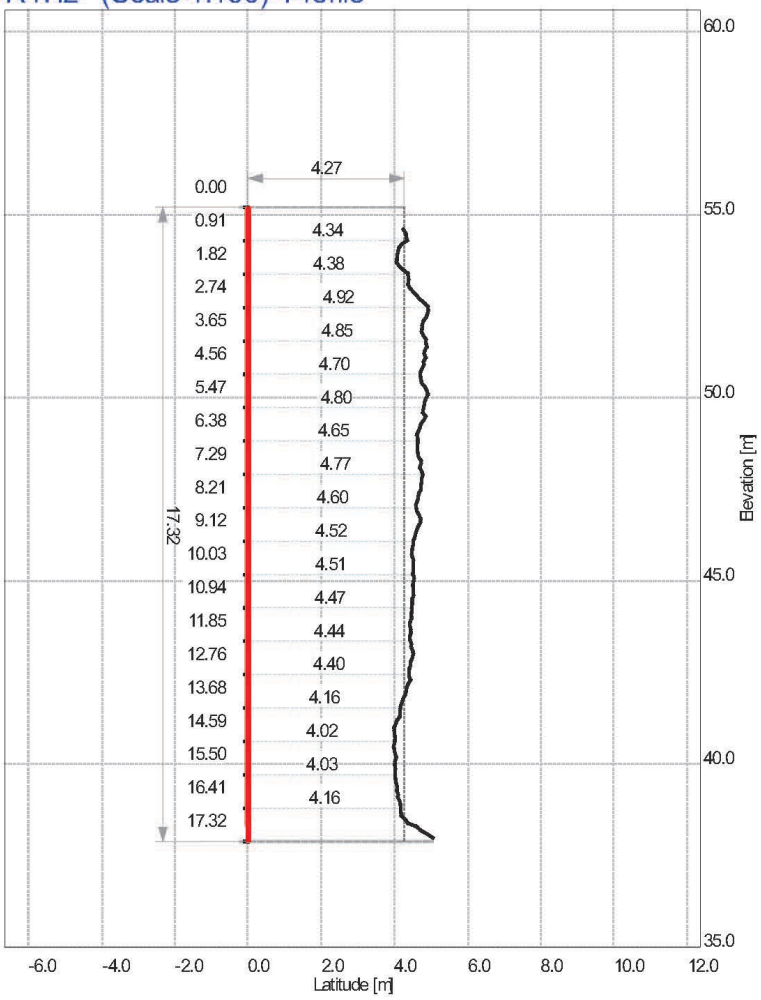

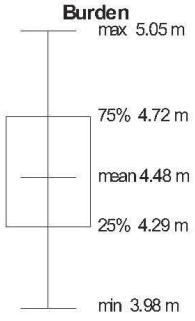

Inclination: 0.01 °
Length: 17.32 m
Diameter: 100.00 mm
Area: 77.5 m² (of profile)
Position: u: 124.24 m, v: -8.10 m
E: 750644.07 m, N: 4875291.19 m, H: 55.21 m
Subdrilling: 0 m

Depth	Profile
1.0	4.150
2.0	4.371
3.0	4.851
4.0	4.843
5.0	4.918
6.0	4.654
7.0	4.706
8.0	4.586
9.0	4.510
10.0	4.525
11.0	4.465
12.0	4.512
13.0	4.315
14.0	3.985
15.0	4.025
16.0	4.157
17.0	na

-

R1H3 (Scale 1:150) Profile

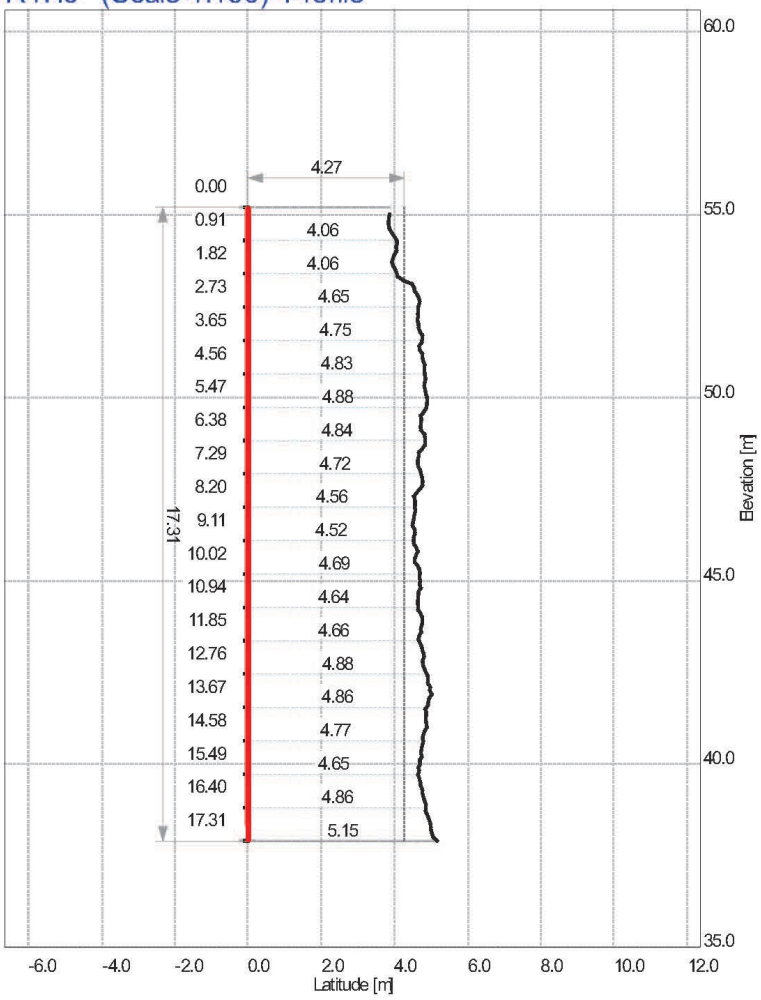

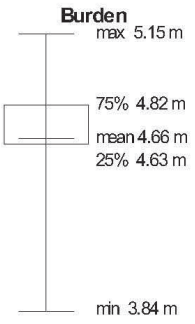

Inclination: 0.01 °
Length: 17.31 m
Diameter: 100.00 mm
Area: 80.5 m² (of profile)
Position: u: 119.19 m, v: -7.74 m
E: 750639.02 m, N: 4875290.86 m, H: 55.22 m
Subdrilling: 0 m

Depth	Profile
1.0	4.068
2.0	4.311
3.0	4.628
4.0	4.763
5.0	4.857
6.0	4.738
7.0	4.677
8.0	4.554
9.0	4.529
10.0	4.693
11.0	4.751
12.0	4.799
13.0	4.982
14.0	4.838
15.0	4.666
16.0	4.847
17.0	5.153

-

R1H4 (Scale 1:150) Profile

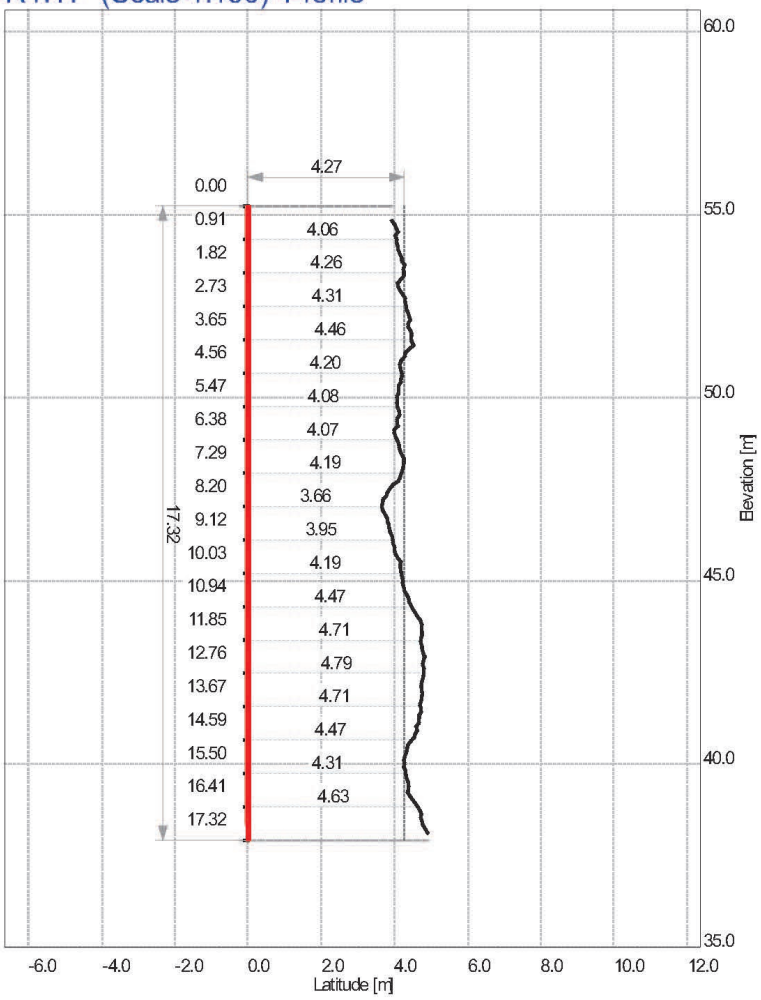

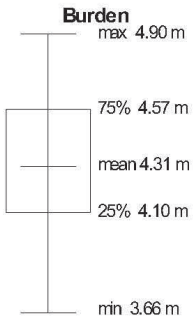

Inclination: 0.01 °
Length: 17.32 m
Diameter: 100.00 mm
Area: 74.5 m² (of profile)
Position: u: 114.60 m, v: -7.60 m
E: 750634.45 m, N: 4875290.37 m, H: 55.24 m
Subdrilling: 0 m

Depth	Profile
1.0	4.062
2.0	4.143
3.0	4.422
4.0	4.286
5.0	4.112
6.0	3.992
7.0	4.230
8.0	3.670
9.0	3.954
10.0	4.218
11.0	4.628
12.0	4.789
13.0	4.758
14.0	4.610
15.0	4.258
16.0	4.561
17.0	na

-

R1H5 (Scale 1:150) Profile

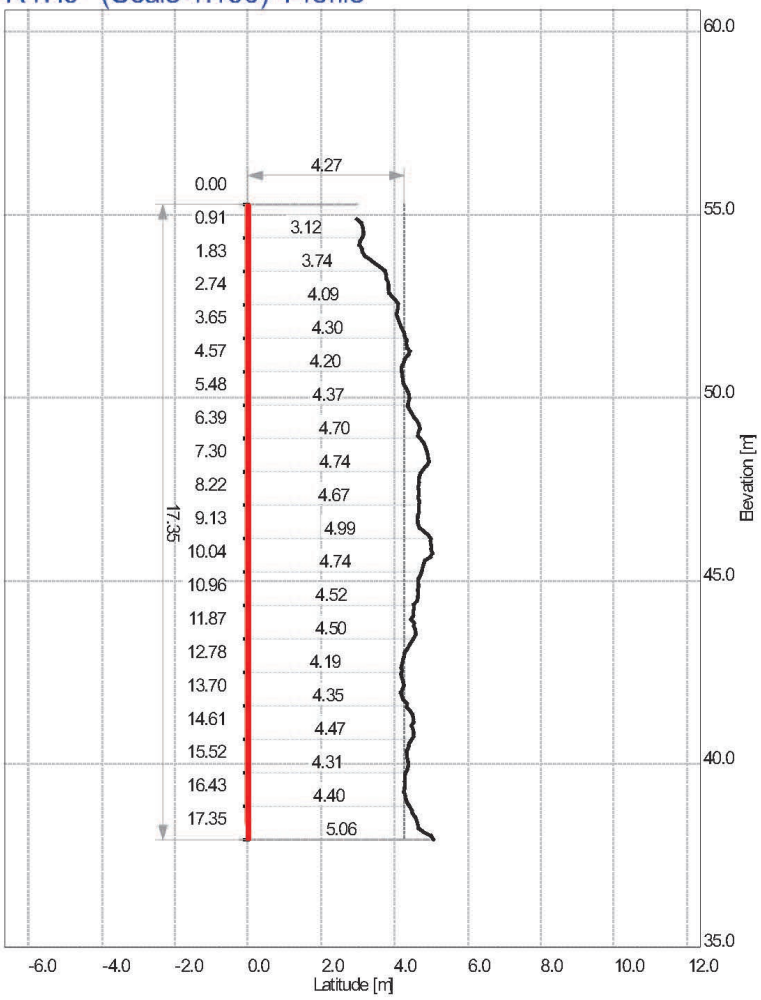

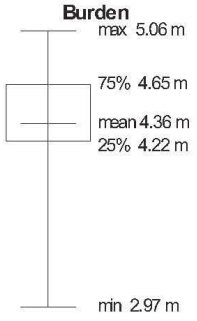

Inclination: 0.01 °
Length: 17.35 m
Diameter: 100.00 mm
Area: 75.0 m² (of profile)
Position: u: 109.07 m, v: -7.34 m
E: 750628.93 m, N: 4875289.87 m, H: 55.29 m
Subdrilling: 0 m

Depth	Profile
1.0	3.050
2.0	3.791
3.0	4.077
4.0	4.401
5.0	4.365
6.0	4.686
7.0	4.872
8.0	4.675
9.0	4.996
10.0	4.666
11.0	4.512
12.0	4.277
13.0	4.206
14.0	4.476
15.0	4.382
16.0	4.334
17.0	5.060

-

R1H6 (Scale 1:150) Profile

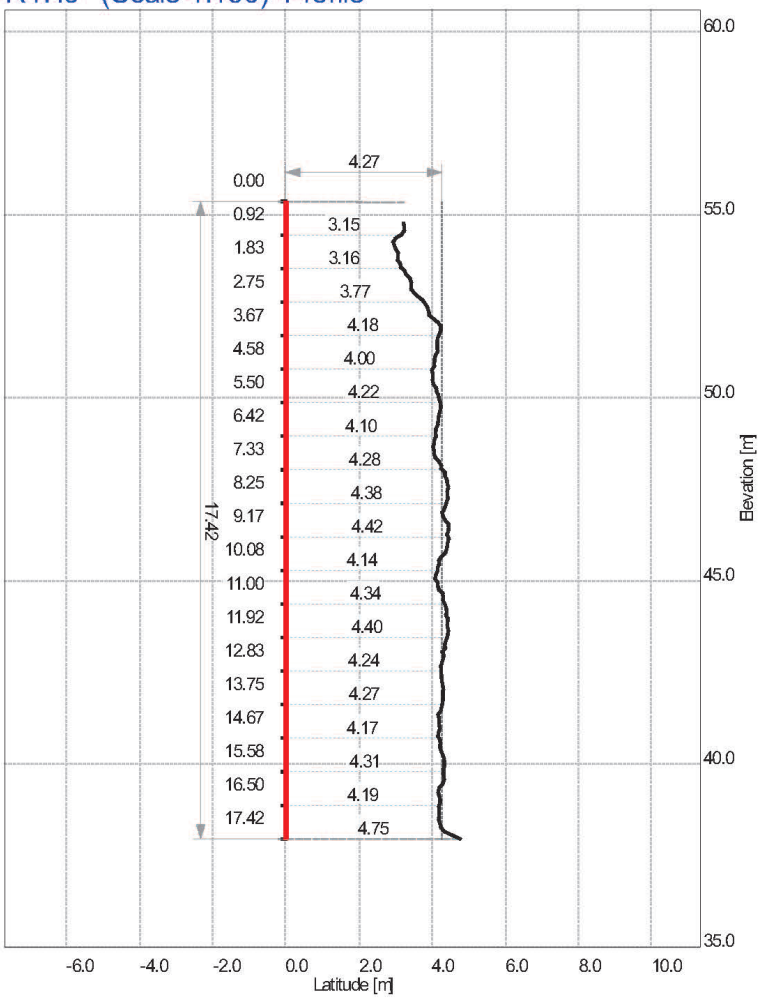

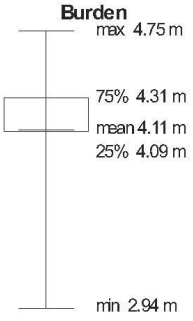

Inclination: 0.01 °
Length: 17.42 m
Diameter: 100.00 mm
Area: 70.9 m² (of profile)
Position: u: 104.06 m, v: -7.12 m
E: 750623.94 m, N: 4875289.41 m, H: 55.37 m
Subdrilling: 0 m

Depth	Profile
1.0	2.968
2.0	3.337
3.0	3.916
4.0	4.147
5.0	4.115
6.0	4.132
7.0	4.228
8.0	4.398
9.0	4.459
10.0	4.087
11.0	4.367
12.0	4.280
13.0	4.301
14.0	4.197
15.0	4.329
16.0	4.221
17.0	4.753

-

R1H7 (Scale 1:150) Profile

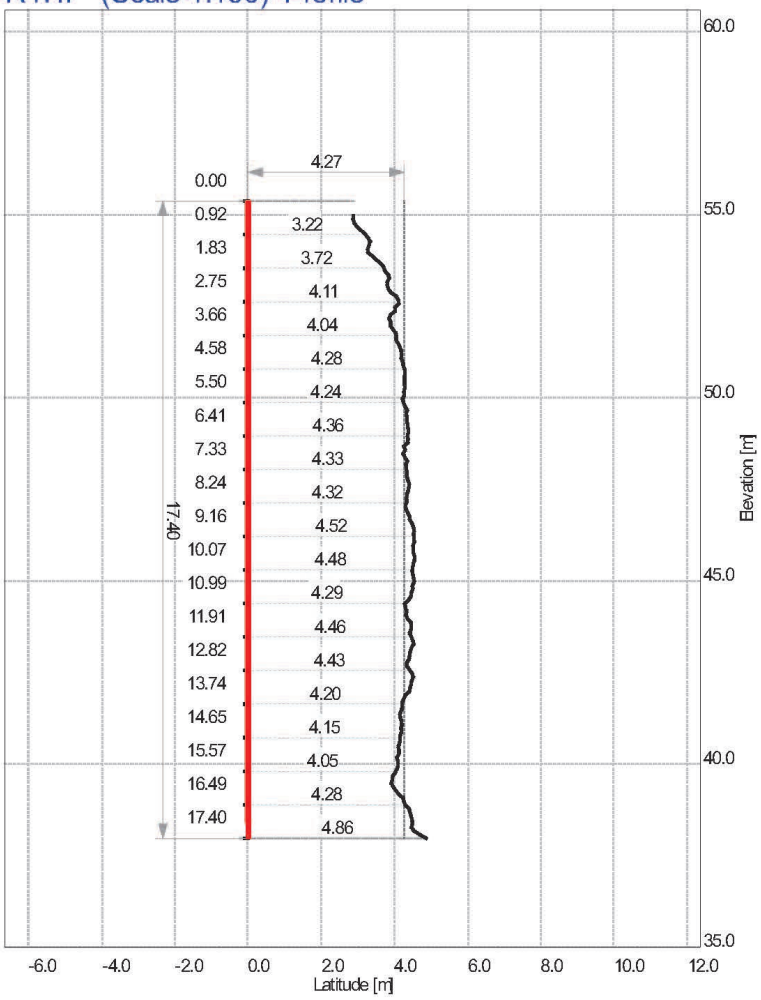

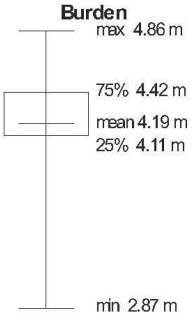

Inclination: 0.01 °
Length: 17.40 m
Diameter: 100.00 mm
Area: 72.4 m² (of profile)
Position: u: 99.20 m, v: -6.67 m
E: 750619.07 m, N: 4875289.19 m, H: 55.38 m
Subdrilling: 0 m

Depth	Profile
1.0	3.290
2.0	3.851
3.0	3.939
4.0	4.181
5.0	4.273
6.0	4.364
7.0	4.317
8.0	4.335
9.0	4.527
10.0	4.508
11.0	4.321
12.0	4.439
13.0	4.424
14.0	4.190
15.0	4.102
16.0	4.253
17.0	4.858

-

R1H8 (Scale 1:150) Profile

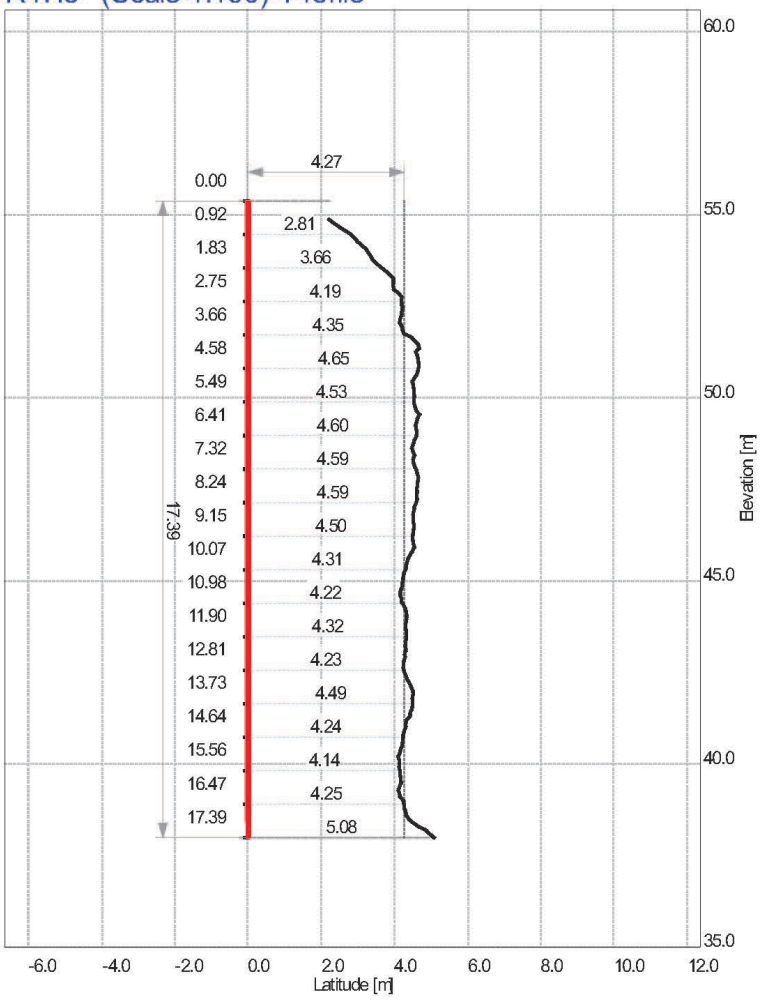

Depth	Profile
1.0	2.920
2.0	3.903
3.0	4.196
4.0	4.589
5.0	4.525
6.0	4.585
7.0	4.522
8.0	4.608
9.0	4.499
10.0	4.247
11.0	4.322
12.0	4.303
13.0	4.465
14.0	4.303
15.0	4.153
16.0	4.231
17.0	5.078

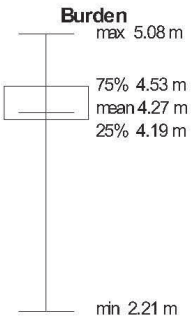

Inclination: 0.01 °
Length: 17.39 m
Diameter: 100.00 mm
Area: 73.3 m² (of profile)
Position: u: 94.62 m, v: -6.39 m
E: 750614.49 m, N: 4875288.83 m, H: 55.38 m
Subdrilling: 0 m

-

R1H9 (Scale 1:150) Profile

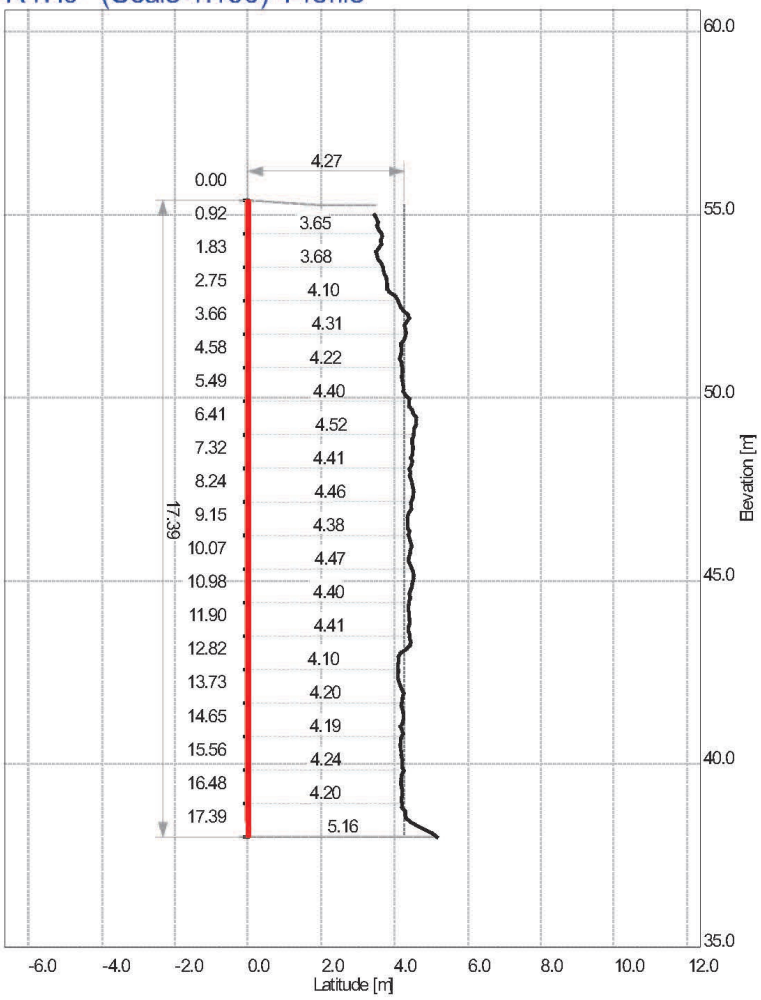

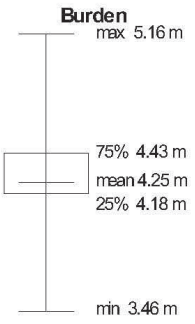

Inclination: 0.01 °
Length: 17.39 m
Diameter: 100.00 mm
Area: 73.2 m² (of profile)
Position: u: 89.86 m, v: -6.01 m
E: 750609.73 m, N: 4875288.56 m, H: 55.40 m
Subdrilling: 0 m

Depth	Profile
1.0	3.651
2.0	3.746
3.0	4.311
4.0	4.186
5.0	4.253
6.0	4.584
7.0	4.486
8.0	4.475
9.0	4.399
10.0	4.528
11.0	4.392
12.0	4.292
13.0	4.185
14.0	4.183
15.0	4.208
16.0	4.189
17.0	5.157

-

R1H10 (Scale 1:150) Profile

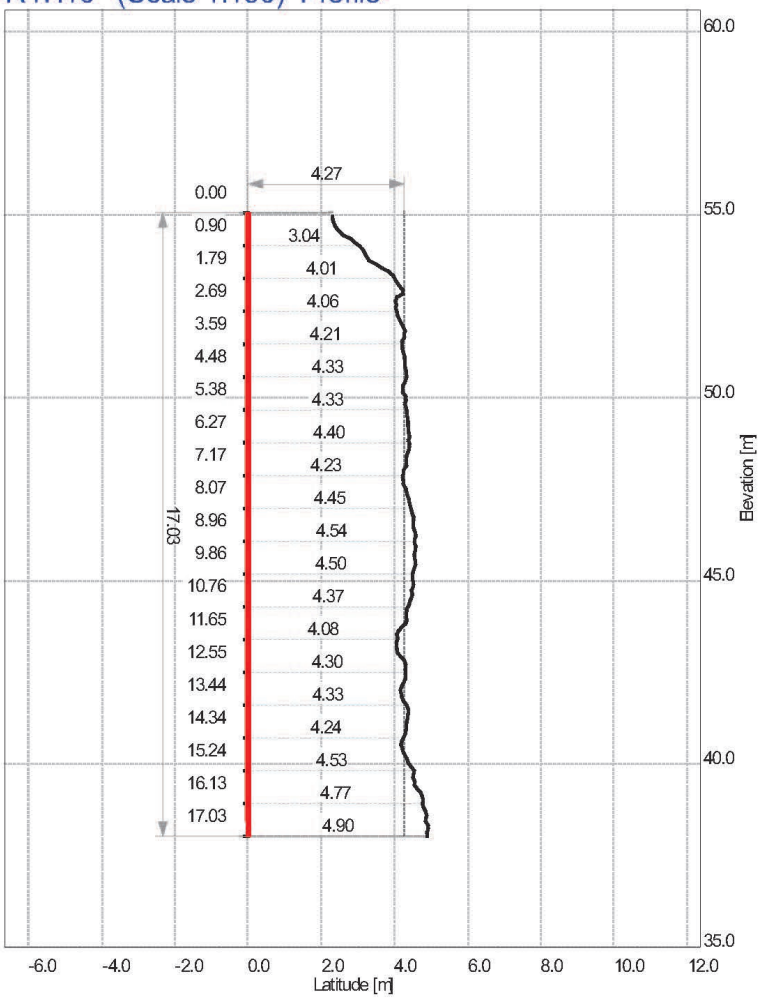

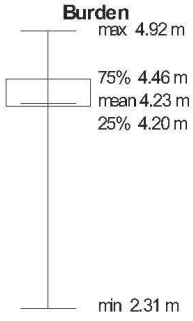

Inclination: 0.01 °
Length: 17.03 m
Diameter: 100.00 mm
Area: 71.9 m² (of profile)
Position: u: 85.11 m, v: -5.59 m
E: 750604.96 m, N: 4875288.33 m, H: 55.05 m
Subdrilling: 0 m

Depth	Profile
1.0	3.137
2.0	4.147
3.0	4.183
4.0	4.278
5.0	4.303
6.0	4.390
7.0	4.257
8.0	4.434
9.0	4.550
10.0	4.498
11.0	4.322
12.0	4.087
13.0	4.167
14.0	4.319
15.0	4.380
16.0	4.776
17.0	4.897

-

R1H11 (Scale 1:150) Profile

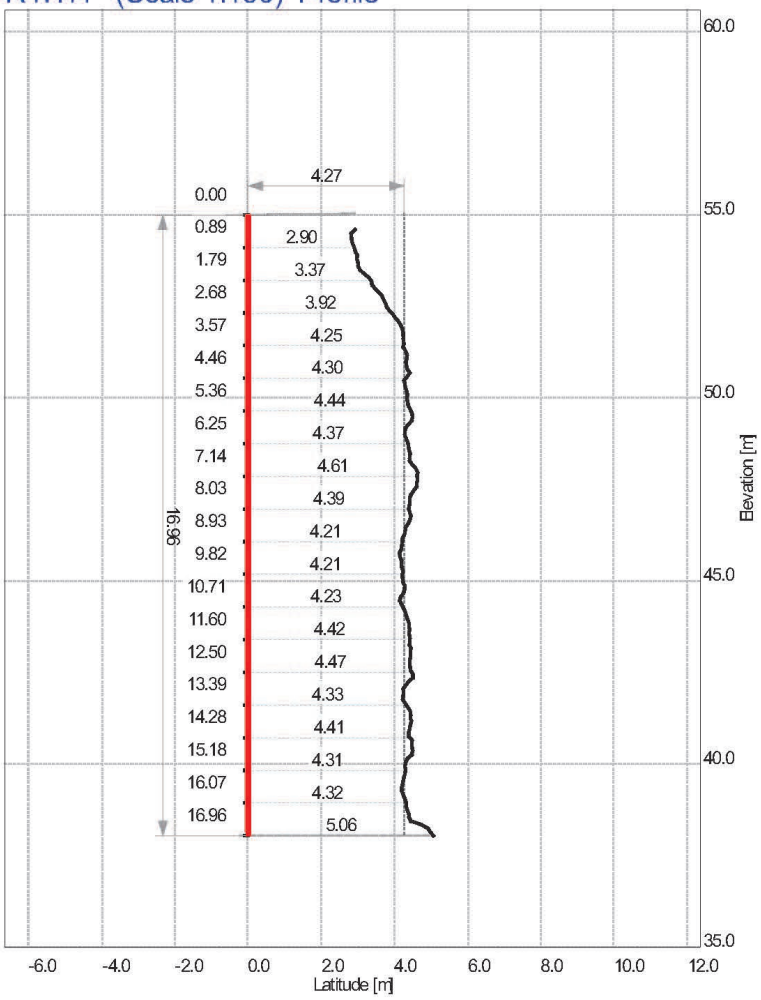

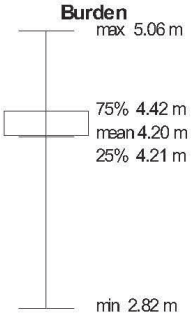

Inclination: 0.01 °
Length: 16.96 m
Diameter: 100.00 mm
Area: 70.8 m² (of profile)
Position: u: 80.52 m, v: -5.32 m
E: 750600.38 m, N: 4875287.96 m, H: 55.00 m
Subdrilling: 0 m

Depth	Profile
1.0	2.967
2.0	3.575
3.0	4.232
4.0	4.369
5.0	4.425
6.0	4.383
7.0	4.604
8.0	4.335
9.0	4.192
10.0	4.165
11.0	4.411
12.0	4.416
13.0	4.446
14.0	4.355
15.0	4.260
16.0	5.060

-

R1H12 (Scale 1:150) Profile

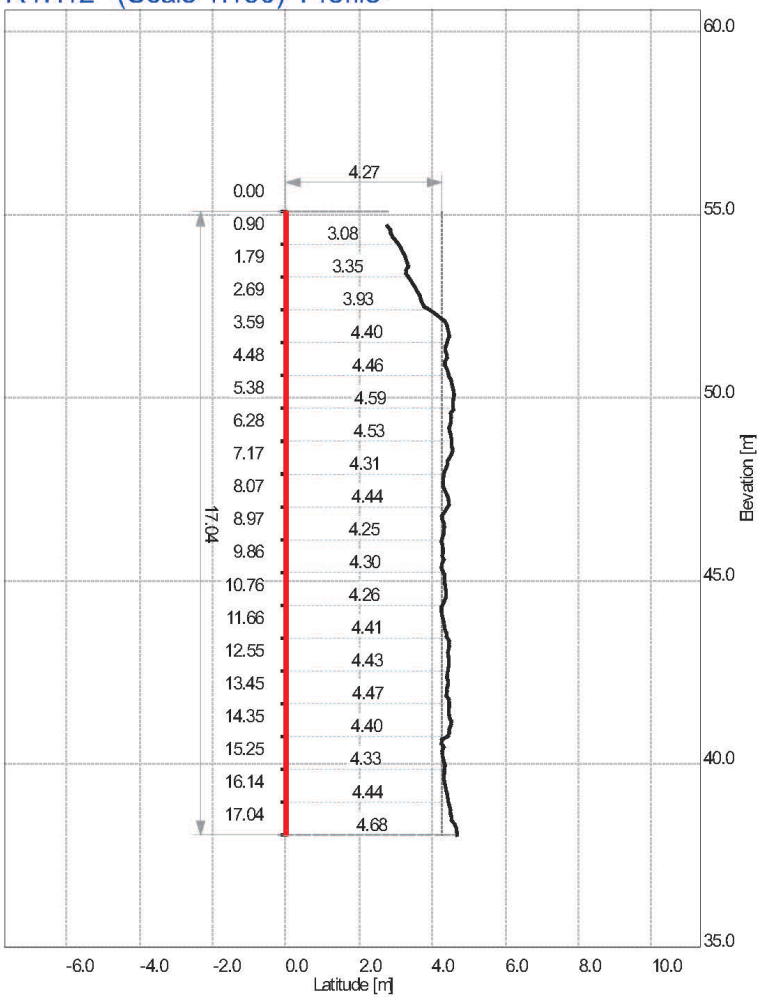

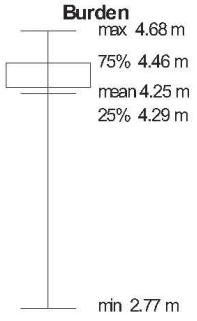

Inclination: 0.01 °
Length: 17.04 m
Diameter: 100.00 mm
Area: 71.8 m² (of profile)
Position: u: 75.71 m, v: -5.08 m
E: 750595.58 m, N: 4875287.55 m, H: 55.10 m
Subdrilling: 0 m

Depth	Profile
1.0	3.144
2.0	3.489
3.0	4.350
4.0	4.401
5.0	4.599
6.0	4.480
7.0	4.377
8.0	4.454
9.0	4.254
10.0	4.339
11.0	4.267
12.0	4.431
13.0	4.402
14.0	4.512
15.0	4.317
16.0	4.423
17.0	4.681

-

R1H13 (Scale 1:150) Profile

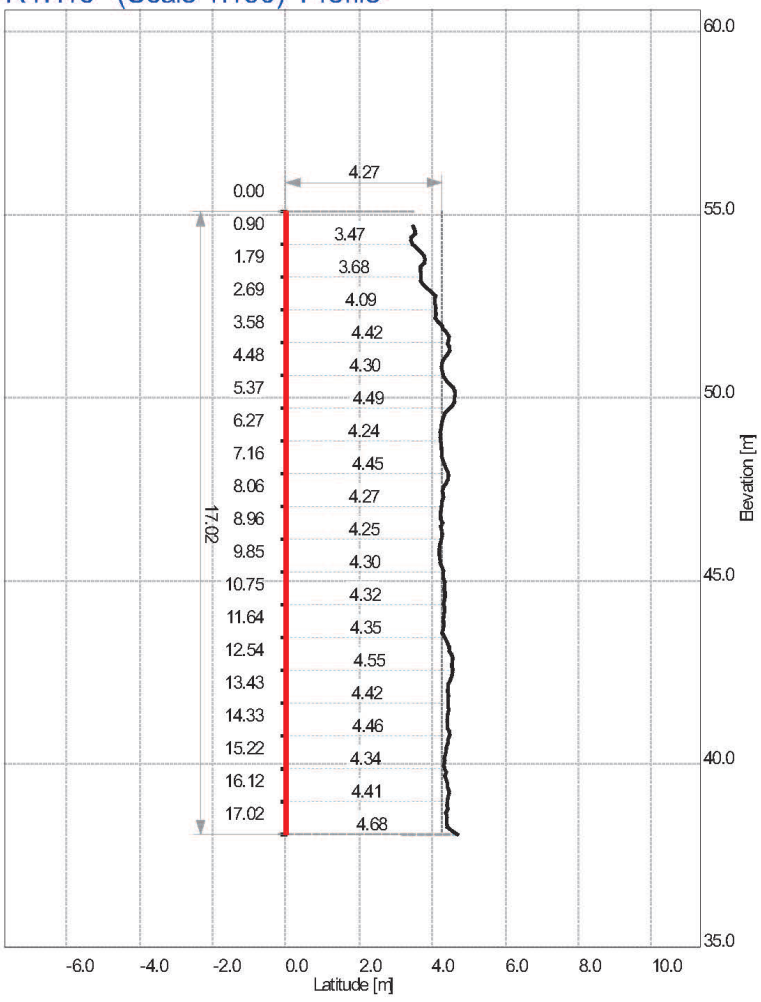

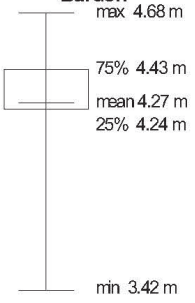

Inclination: 0.01 °
Length: 17.02 m
Diameter: 100.00 mm
Area: 72.5 m² (of profile)
Position: u: 70.86 m, v: -4.62 m
E: 750590.72 m, N: 4875287.34 m, H: 55.09 m
Subdrilling: 0 m

Depth	Profile
1.0	3.585
2.0	3.762
3.0	4.149
4.0	4.336
5.0	4.619
6.0	4.219
7.0	4.373
8.0	4.260
9.0	4.236
10.0	4.304
11.0	4.321
12.0	4.466
13.0	4.428
14.0	4.414
15.0	4.339
16.0	4.426
17.0	4.682

-

R1H14 (Scale 1:150) Profile

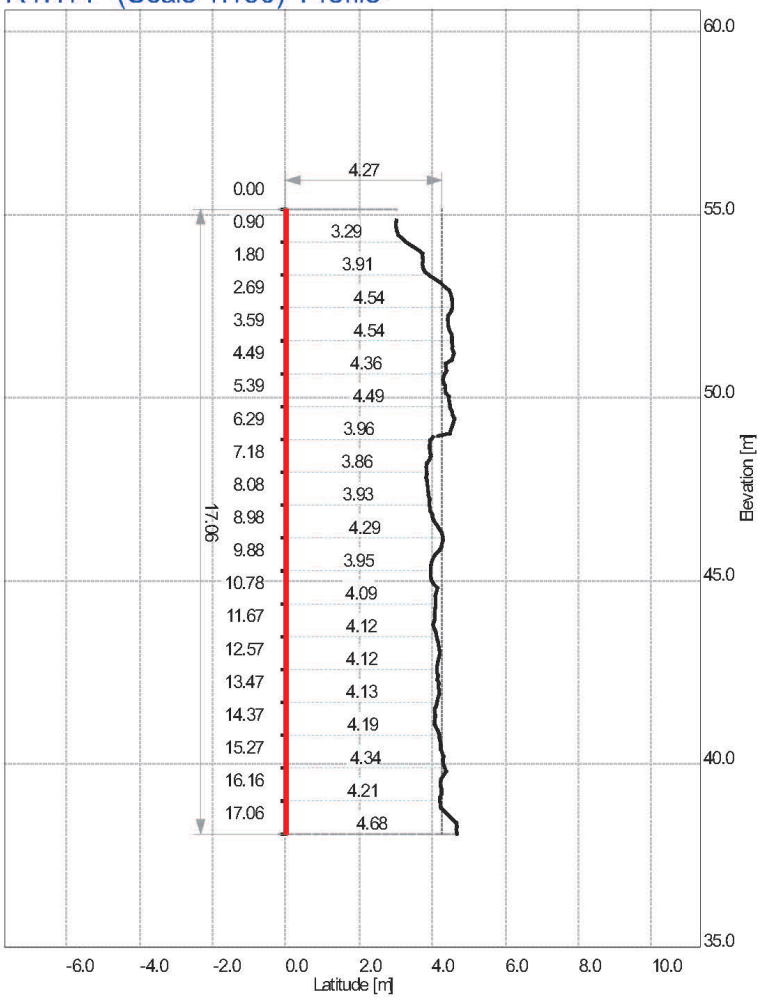

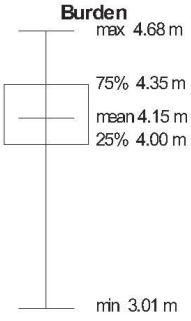

Inclination: 0.01 °
Length: 17.06 m
Diameter: 100.00 mm
Area: 70.5 m² (of profile)
Position: u: 66.34 m, v: -4.25 m
E: 750586.19 m, N: 4875287.09 m, H: 55.15 m
Subdrilling: 0 m

Depth	Profile
1.0	3.450
2.0	4.232
3.0	4.423
4.0	4.571
5.0	4.370
6.0	4.510
7.0	3.839
8.0	3.918
9.0	4.290
10.0	3.958
11.0	4.066
12.0	4.195
13.0	4.167
14.0	4.061
15.0	4.289
16.0	4.214
17.0	4.676

-

R1H15 (Scale 1:150) Profile

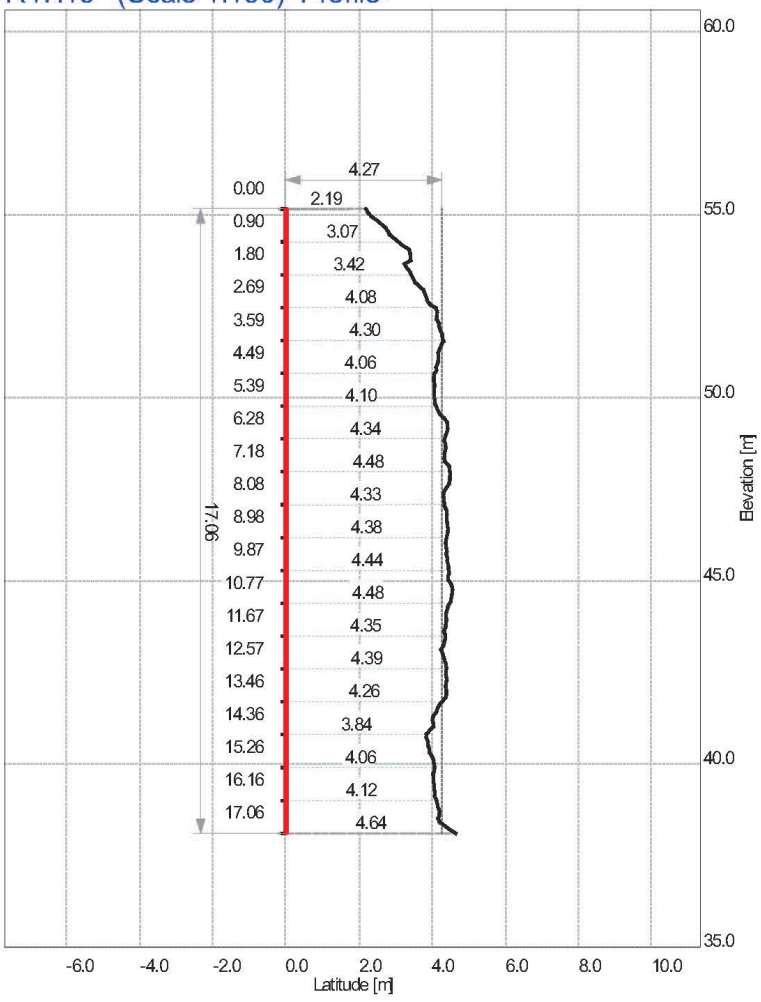

Inclination: 0.01 °
Length: 17.06 m
Diameter: 100.00 mm
Area: 69.9 m² (of profile)
Position: u: 61.63 m, v: -3.90 m
E: 750581.47 m, N: 4875286.79 m, H: 55.16 m
Subdrilling: 0 m

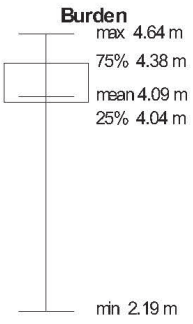

Depth	Profile
1.0	3.203
2.0	3.534
3.0	4.121
4.0	4.167
5.0	4.050
6.0	4.420
7.0	4.456
8.0	4.328
9.0	4.382
10.0	4.438
11.0	4.384
12.0	4.240
13.0	4.368
14.0	4.024
15.0	4.033
16.0	4.066
17.0	4.638

-

R1H16 (Scale 1:150) Profile

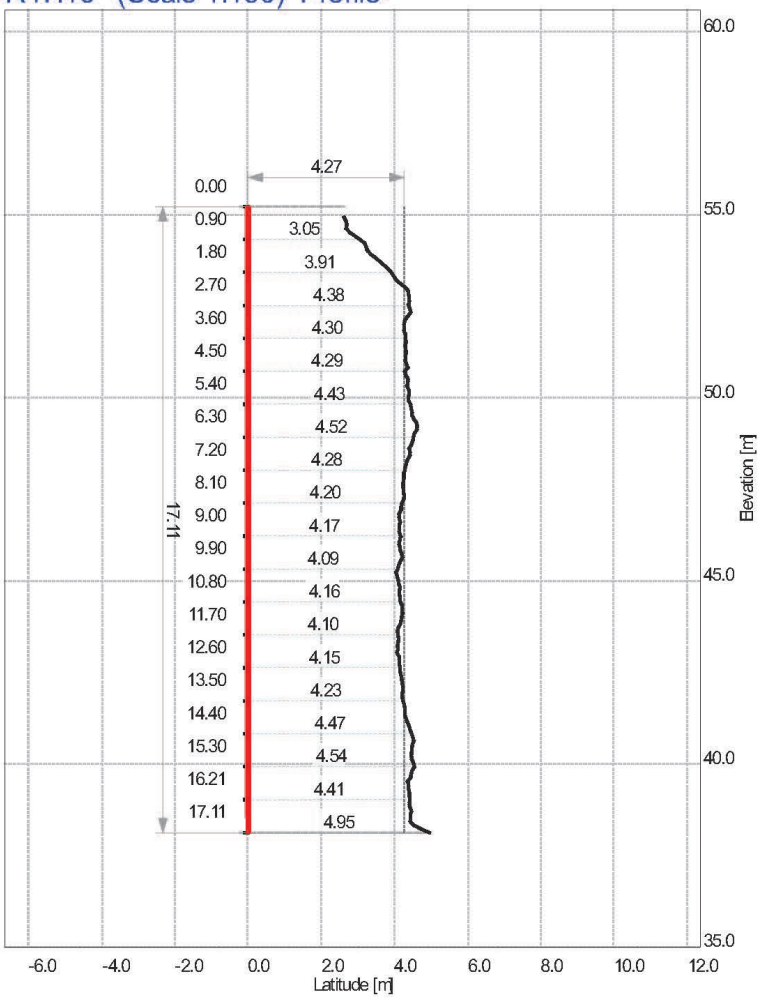

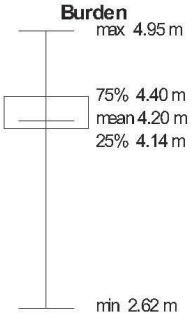

Inclination: 0.01 °
Length: 17.11 m
Diameter: 100.00 mm
Area: 71.3 m² (of profile)
Position: u: 56.71 m, v: -3.51 m
E: 750576.54 m, N: 4875286.50 m, H: 55.23 m
Subdrilling: 0 m

Depth	Profile
1.0	3.190
2.0	4.052
3.0	4.340
4.0	4.310
5.0	4.398
6.0	4.620
7.0	4.334
8.0	4.220
9.0	4.162
10.0	4.061
11.0	4.201
12.0	4.091
13.0	4.219
14.0	4.357
15.0	4.470
16.0	4.406
17.0	4.950

-

R1H17 (Scale 1:150) Profile

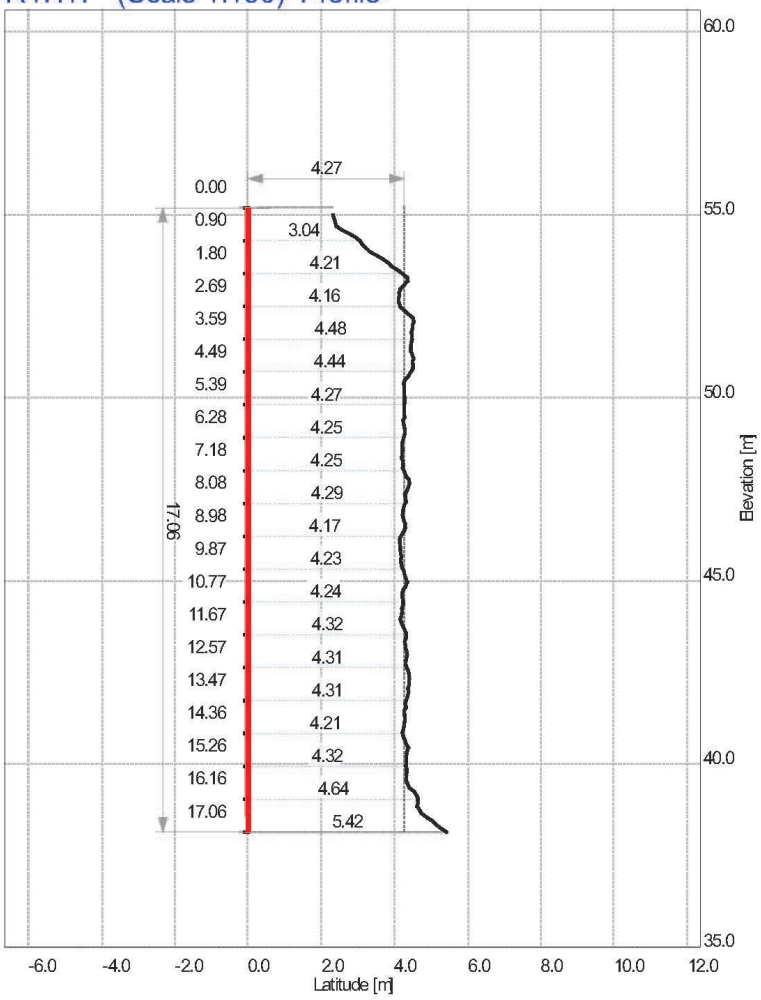

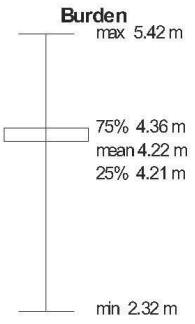

Inclination: 0.01 °
Length: 17.06 m
Diameter: 100.00 mm
Area: 71.7 m² (of profile)
Position: u: 52.22 m, v: -3.04 m
E: 750572.03 m, N: 4875286.35 m, H: 55.20 m
Subdrilling: 0 m

Depth	Profile
1.0	3.126
2.0	4.357
3.0	4.501
4.0	4.482
5.0	4.268
6.0	4.274
7.0	4.240
8.0	4.313
9.0	4.151
10.0	4.278
11.0	4.208
12.0	4.304
13.0	4.396
14.0	4.274
15.0	4.321
16.0	4.600
17.0	5.416

-

R1H18 (Scale 1:150) Profile

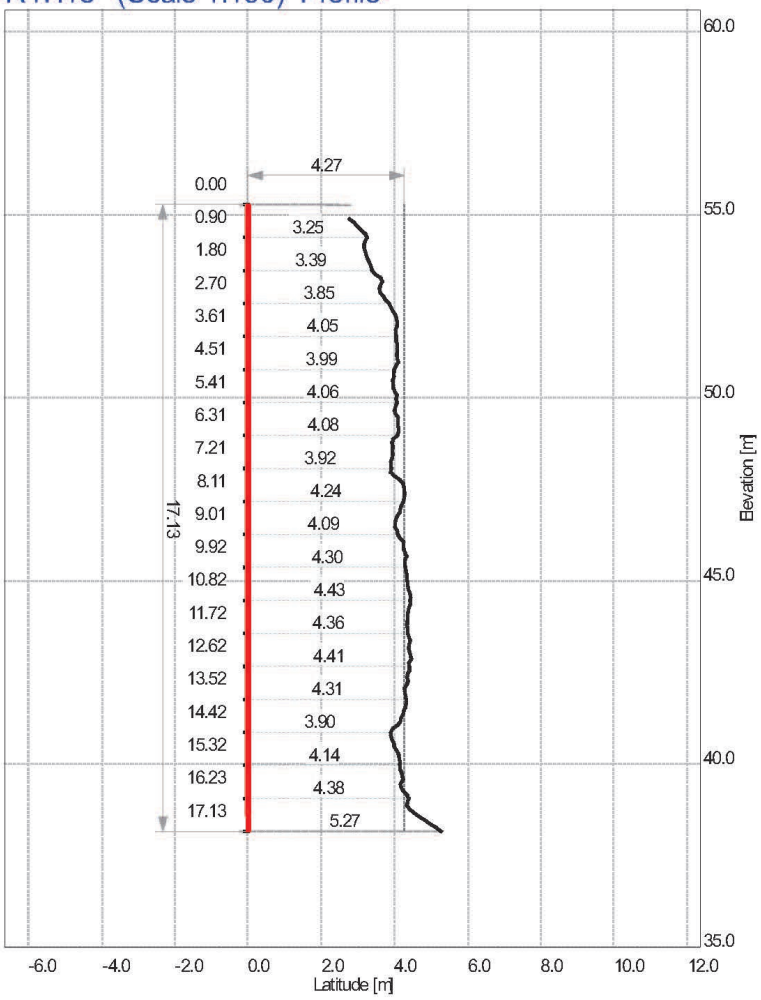

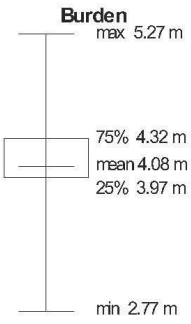

Inclination: 0.01 °
Length: 17.13 m
Diameter: 100.00 mm
Area: 69.4 m² (of profile)
Position: u: 47.43 m, v: -2.73 m
E: 750567.24 m, N: 4875286.01 m, H: 55.29 m
Subdrilling: 0 m

Depth	Profile
1.0	3.194
2.0	3.625
3.0	4.021
4.0	4.070
5.0	3.970
6.0	4.099
7.0	3.897
8.0	4.269
9.0	4.110
10.0	4.326
11.0	4.380
12.0	4.389
13.0	4.341
14.0	4.168
15.0	4.123
16.0	4.330
17.0	5.268

-

R1H19 (Scale 1:150) Profile

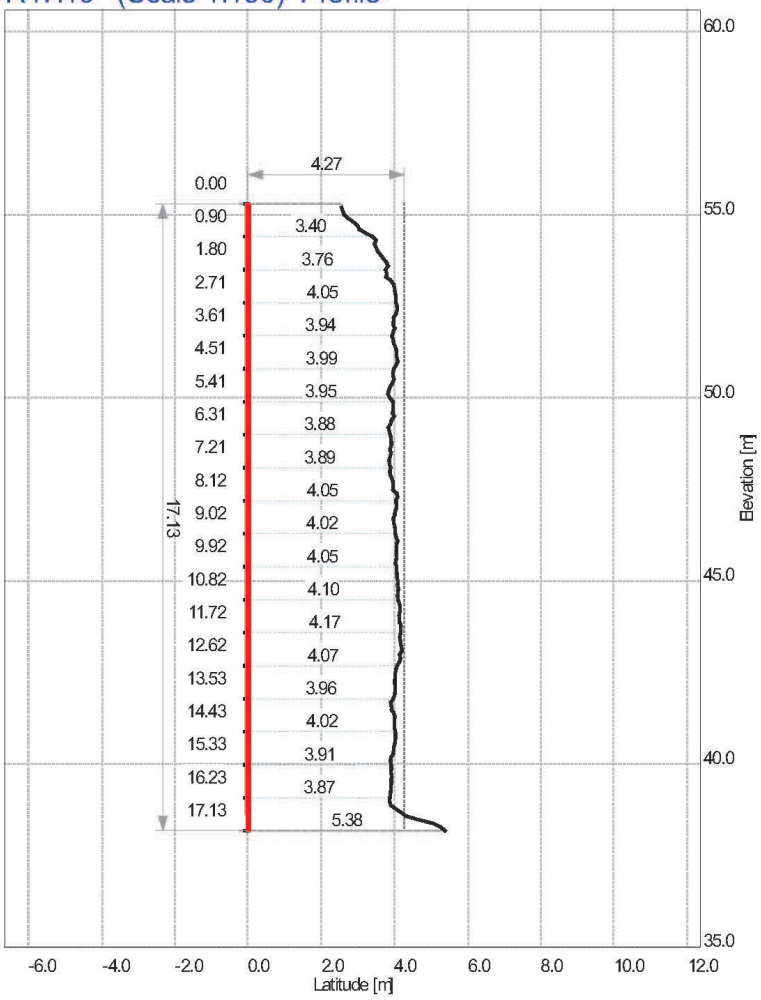

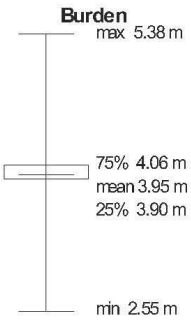

Inclination: 0.01 °
Length: 17.13 m
Diameter: 100.00 mm
Area: 67.5 m² (of profile)
Position: u: 43.00 m, v: -2.47 m
E: 750562.82 m, N: 4875285.66 m, H: 55.31 m
Subdrilling: 0 m

Depth	Profile
1.0	3.492
2.0	3.778
3.0	4.028
4.0	4.051
5.0	3.870
6.0	3.842
7.0	3.843
8.0	4.079
9.0	4.034
10.0	4.061
11.0	4.159
12.0	4.181
13.0	4.007
14.0	4.003
15.0	3.917
16.0	3.889
17.0	5.380

-

R1H20 (Scale 1:150) Profile

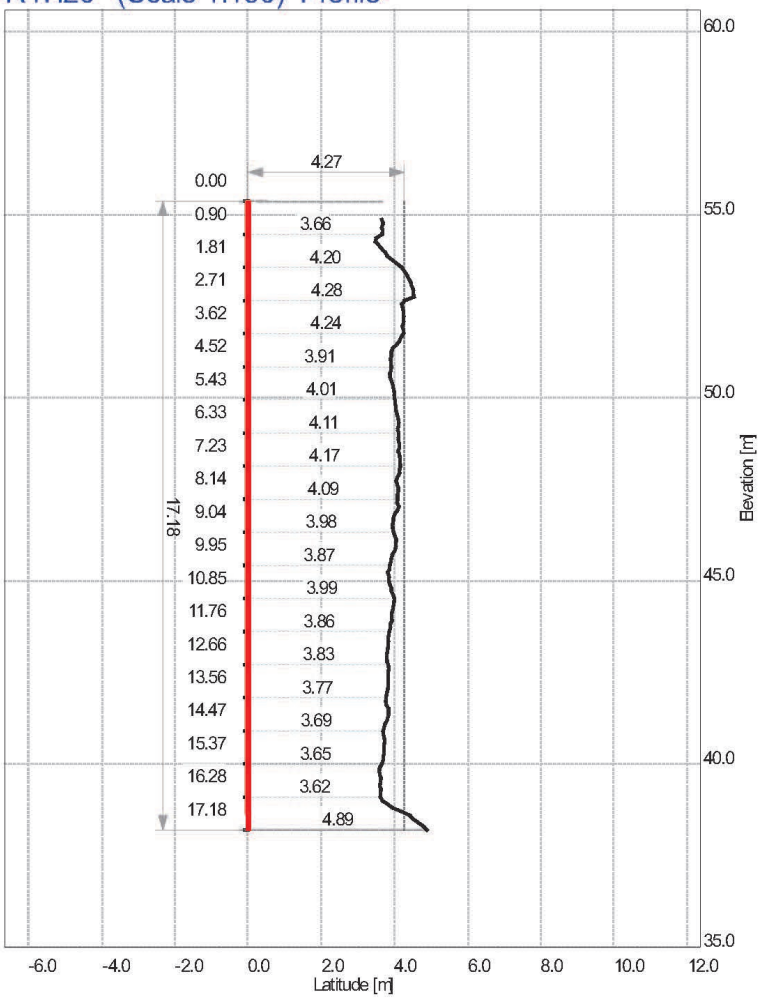

Inclination: 0.01 °
Length: 17.18 m
Diameter: 100.00 mm
Area: 67.9 m² (of profile)
Position: u: 37.95 m, v: -2.04 m
E: 750557.76 m, N: 4875285.40 m, H: 55.37 m
Subdrilling: 0 m

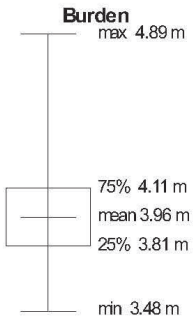

Depth	Profile
1.0	3.504
2.0	4.343
3.0	4.247
4.0	3.924
5.0	3.957
6.0	4.115
7.0	4.142
8.0	4.086
9.0	3.992
10.0	3.860
11.0	3.962
12.0	3.825
13.0	3.830
14.0	3.808
15.0	3.696
16.0	3.616
17.0	4.888

-

R1H21 (Scale 1:150) Profile

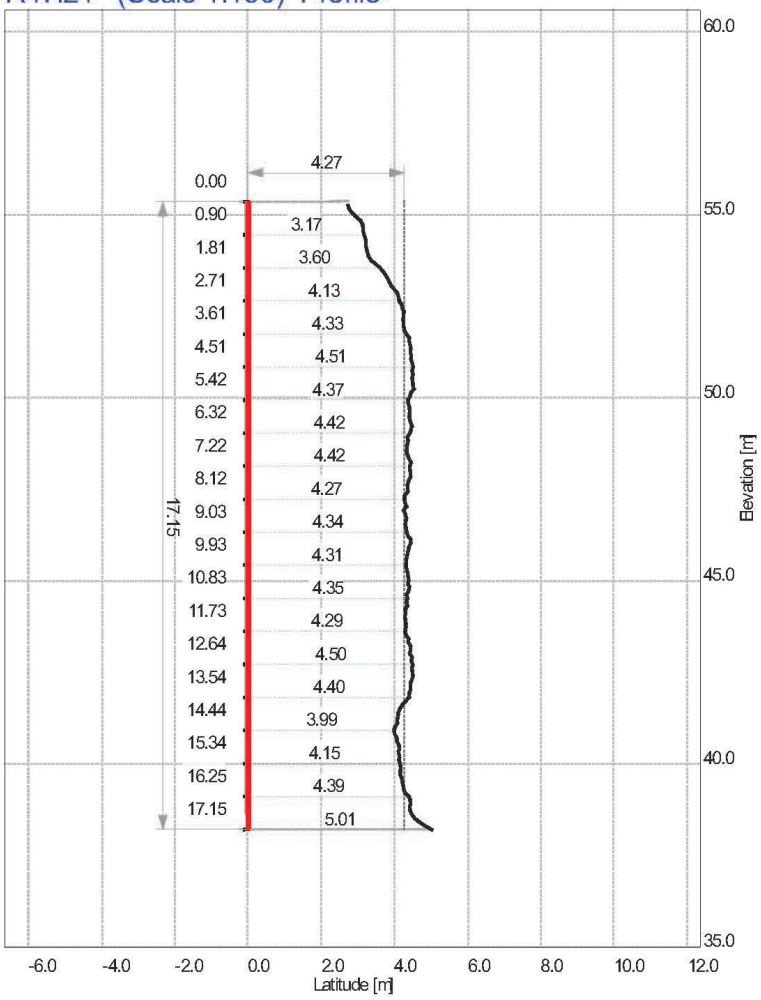

Depth	Profile
1.0	3.207
2.0	3.770
3.0	4.262
4.0	4.447
5.0	4.507
6.0	4.451
7.0	4.441
8.0	4.274
9.0	4.340
10.0	4.348
11.0	4.315
12.0	4.415
13.0	4.446
14.0	4.076
15.0	4.133
16.0	4.284
17.0	5.014

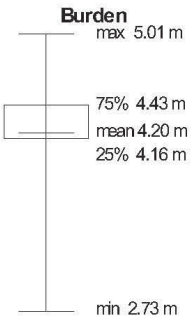

Inclination: 0.01 °
Length: 17.15 m
Diameter: 100.00 mm
Area: 72.0 m² (of profile)
Position: u: 33.58 m, v: -1.66 m
E: 750553.38 m, N: 4875285.17 m, H: 55.36 m
Subdrilling: 0 m

-

R1H22 (Scale 1:150) Profile

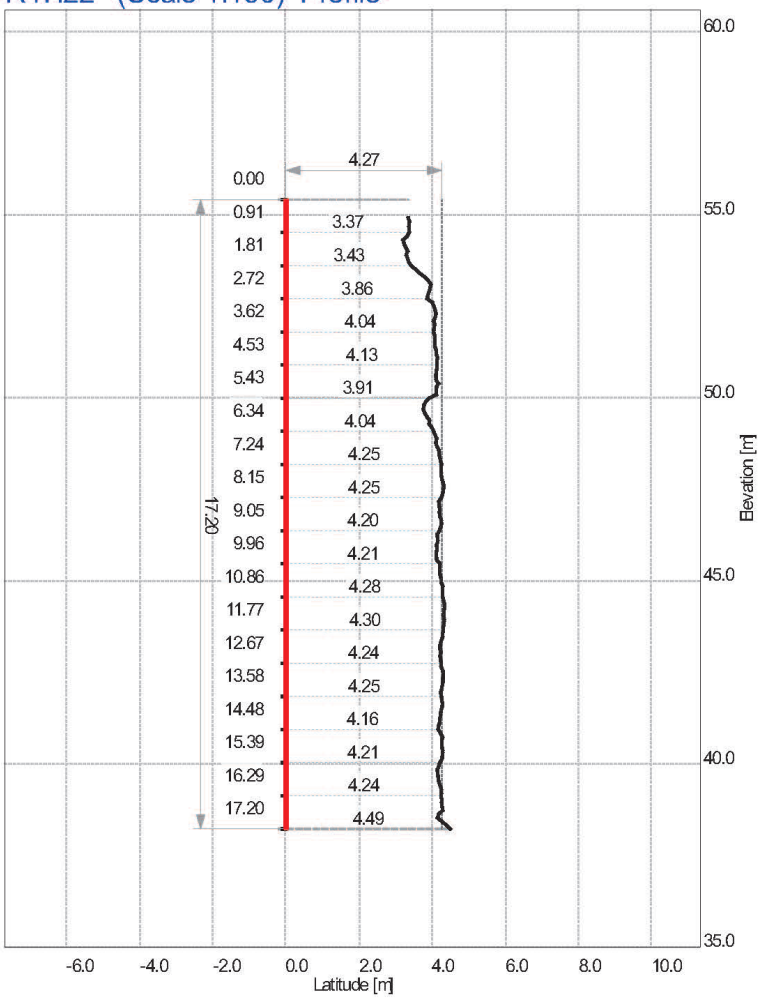

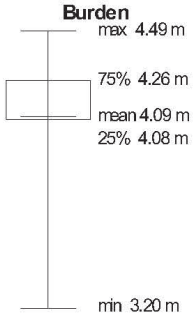

Inclination: 0.01 °
Length: 17.20 m
Diameter: 100.00 mm
Area: 70.0 m² (of profile)
Position: u: 28.56 m, v: -1.36 m
E: 750548.37 m, N: 4875284.78 m, H: 55.42 m
Subdrilling: 0 m

Depth	Profile
1.0	3.312
2.0	3.668
3.0	4.085
4.0	4.078
5.0	4.152
6.0	3.925
7.0	4.216
8.0	4.276
9.0	4.156
10.0	4.196
11.0	4.324
12.0	4.223
13.0	4.284
14.0	4.209
15.0	4.276
16.0	4.250
17.0	4.486

-

R1H23 (Scale 1:150) Profile

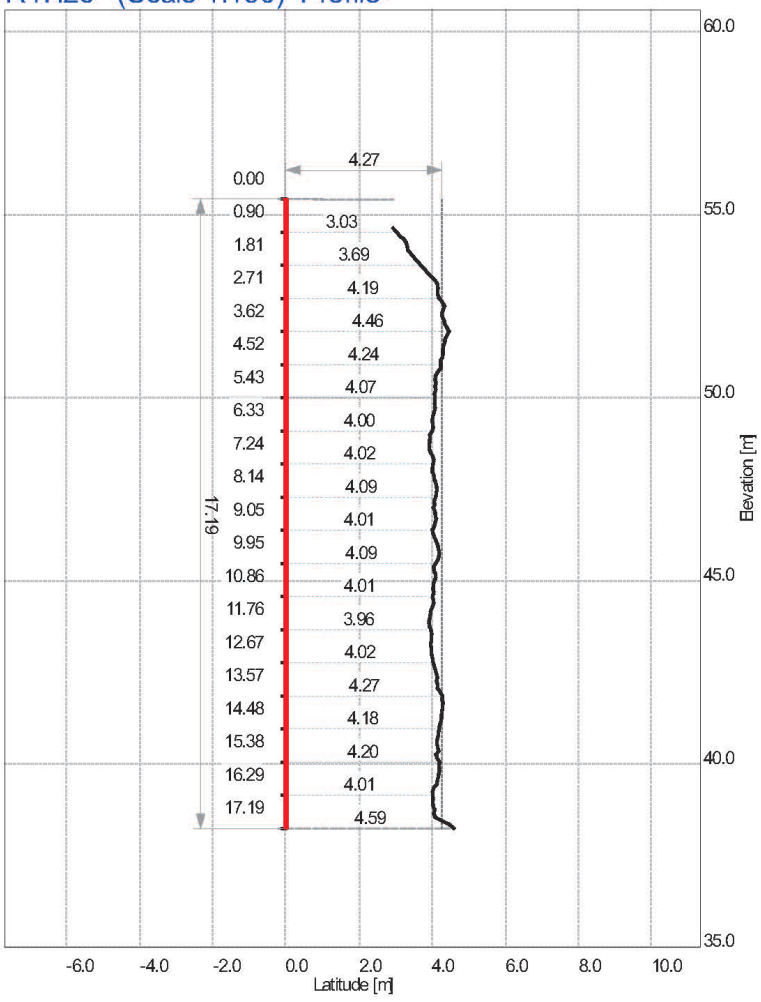

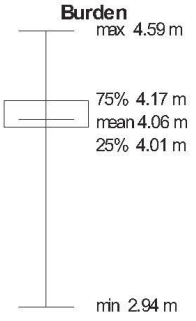

Inclination: 0.01 °
Length: 17.19 m
Diameter: 100.00 mm
Area: 68.9 m² (of profile)
Position: u: 23.87 m, v: -1.09 m
E: 750543.68 m, N: 4875284.41 m, H: 55.44 m
Subdrilling: 0 m

Depth	Profile
1.0	3.104
2.0	3.878
3.0	4.302
4.0	4.306
5.0	4.089
6.0	4.005
7.0	4.030
8.0	4.103
9.0	4.013
10.0	4.044
11.0	4.016
12.0	3.960
13.0	4.102
14.0	4.242
15.0	4.115
16.0	4.010
17.0	4.586

-

R1H24 (Scale 1:150) Profile

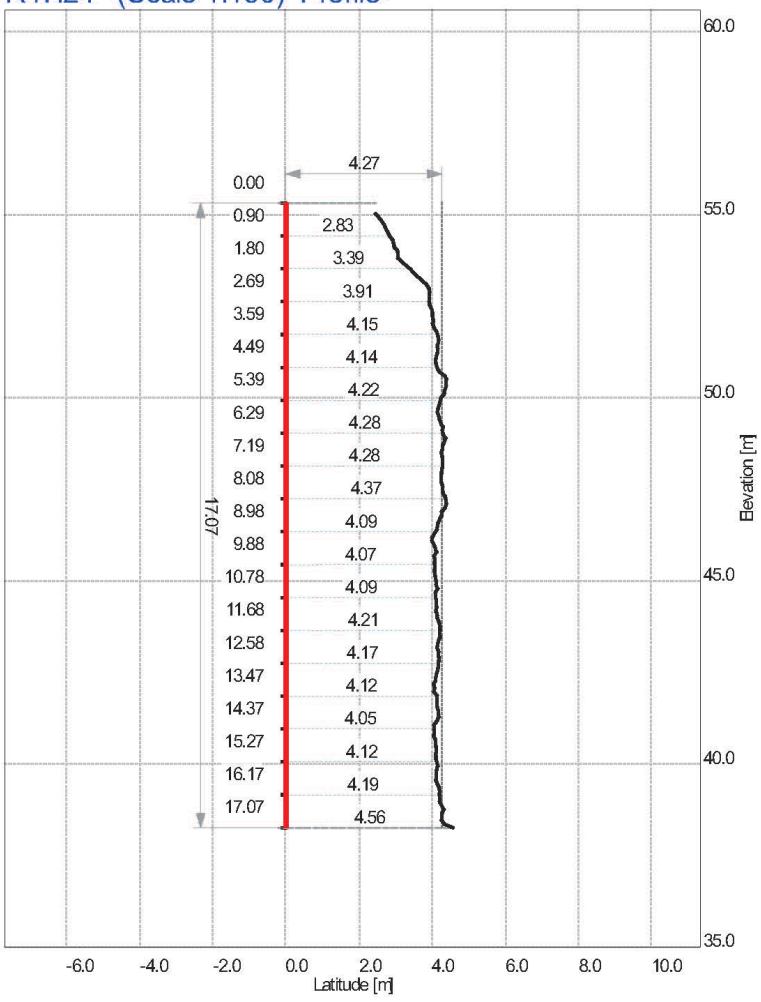

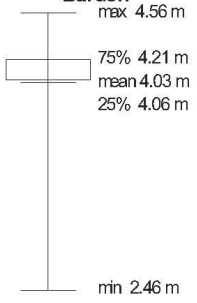

Inclination: 0.01 °
Length: 17.07 m
Diameter: 100.00 mm
Area: 68.4 m² (of profile)
Position: u: 19.24 m, v: -0.61 m
E: 750539.03 m, N: 4875284.26 m, H: 55.33 m
Subdrilling: 0 m

Depth	Profile
1.0	2.913
2.0	3.598
3.0	4.005
4.0	4.152
5.0	4.377
6.0	4.239
7.0	4.278
8.0	4.354
9.0	4.058
10.0	4.064
11.0	4.117
12.0	4.149
13.0	4.084
14.0	4.170
15.0	4.097
16.0	4.201
17.0	4.560

-

R1H25 (Scale 1:150) Profile

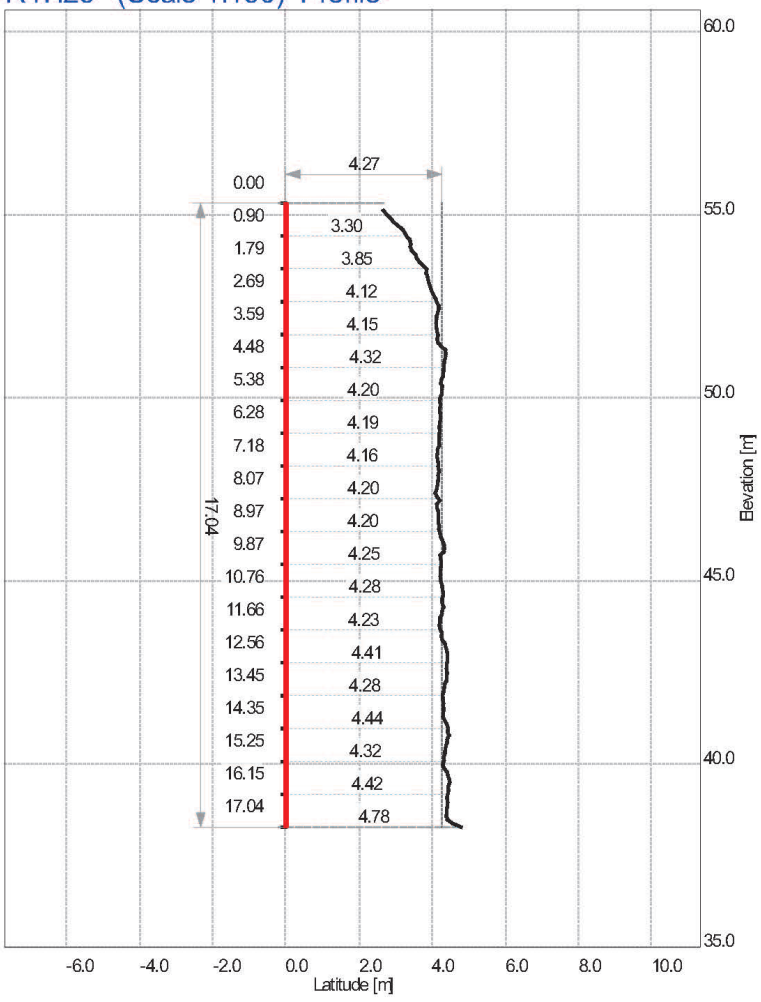

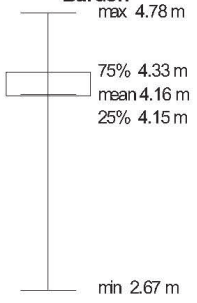

Inclination: 0.01 °
Length: 17.04 m
Diameter: 100.00 mm
Area: 70.7 m² (of profile)
Position: u: 14.56 m, v: -0.23 m
E: 750534.34 m, N: 4875283.99 m, H: 55.32 m
Subdrilling: 0 m

Depth	Profile
1.0	3.386
2.0	3.870
3.0	4.147
4.0	4.355
5.0	4.270
6.0	4.205
7.0	4.149
8.0	4.132
9.0	4.213
10.0	4.224
11.0	4.307
12.0	4.341
13.0	4.390
14.0	4.296
15.0	4.343
16.0	4.440
17.0	4.785

-

R1H26 (Scale 1:150) Profile

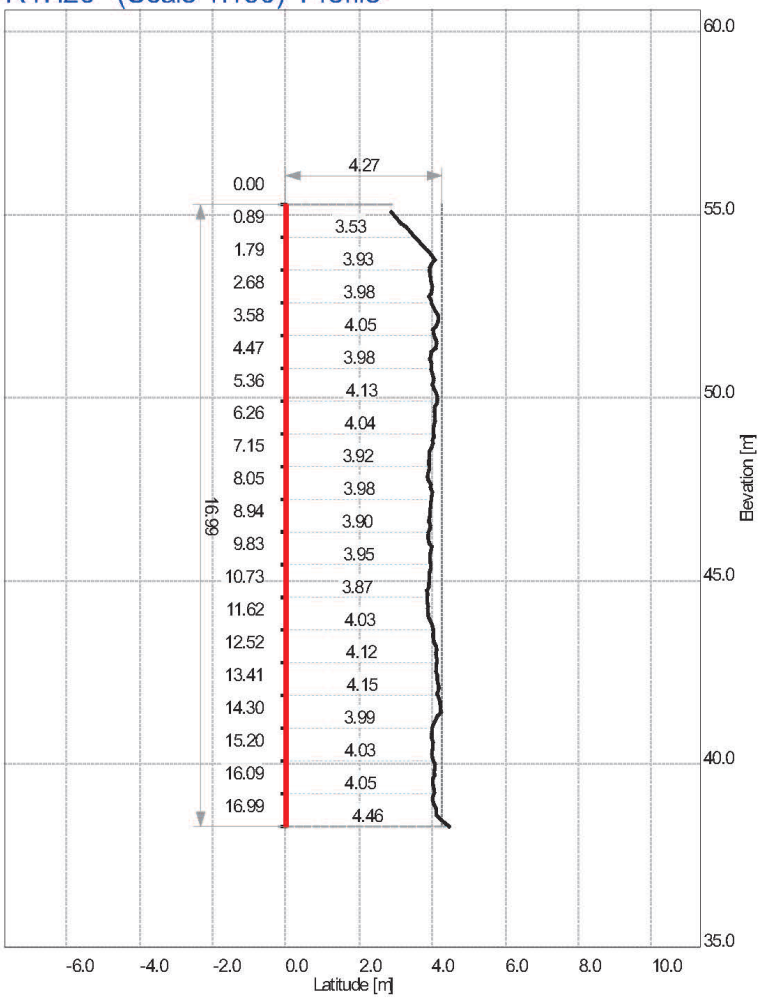

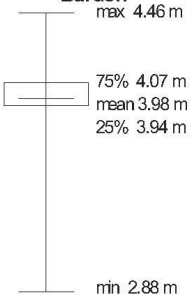

Inclination: 0.01 °
Length: 16.99 m
Diameter: 100.00 mm
Area: 67.4 m² (of profile)
Position: u: 9.78 m, v: 0.15 m
E: 750529.55 m, N: 4875283.72 m, H: 55.28 m
Subdrilling: 0 m

Depth	Profile
1.0	3.689
2.0	3.970
3.0	4.156
4.0	3.953
5.0	4.134
6.0	4.048
7.0	3.871
8.0	3.937
9.0	3.942
10.0	3.862
11.0	4.034
12.0	4.100
13.0	4.237
14.0	4.005
15.0	4.040
16.0	4.459

-

R1H27 (Scale 1:150) Profile

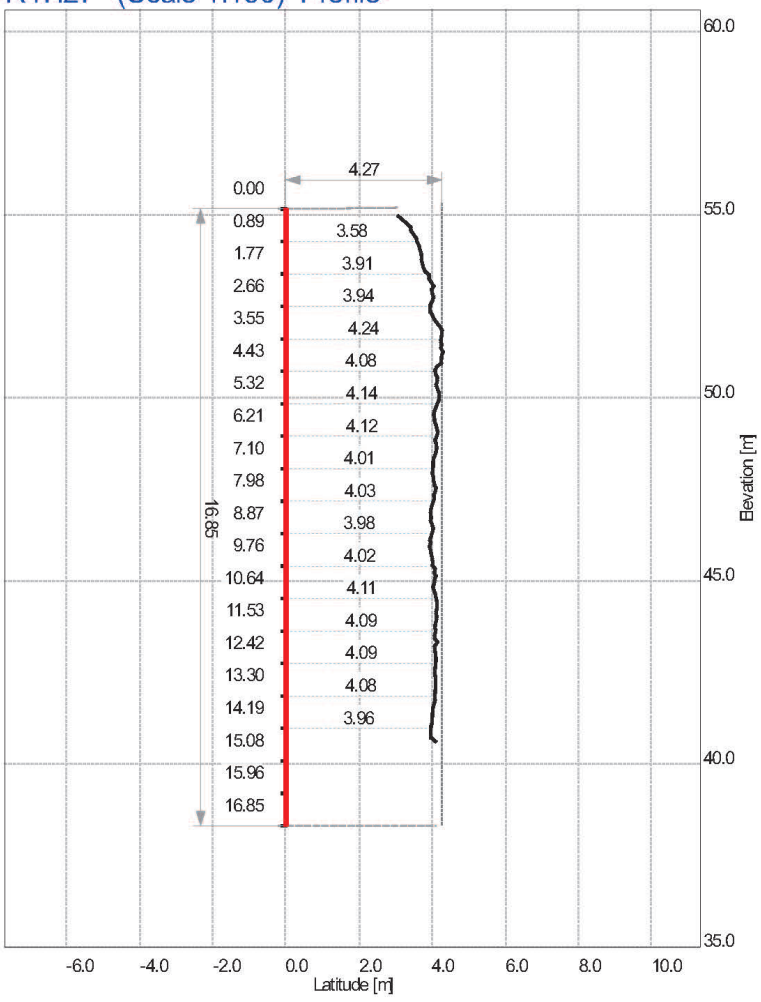

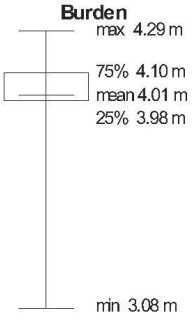

Inclination: 0.01 °
Length: 16.85 m
Diameter: 100.00 mm
Area: 69.2 m² (of profile)
Position: u: 4.80 m, v: 0.81 m
E: 750524.53 m, N: 4875283.69 m, H: 55.16 m
Subdrilling: 0 m

Depth	Profile
1.0	3.654
2.0	4.037
3.0	4.166
4.0	4.241
5.0	4.162
6.0	4.082
7.0	4.050
8.0	3.966
9.0	3.983
10.0	4.085
11.0	4.084
12.0	4.075
13.0	4.010
14.0	na
15.0	na
16.0	na

-

R1H28 (Scale 1:150) Profile

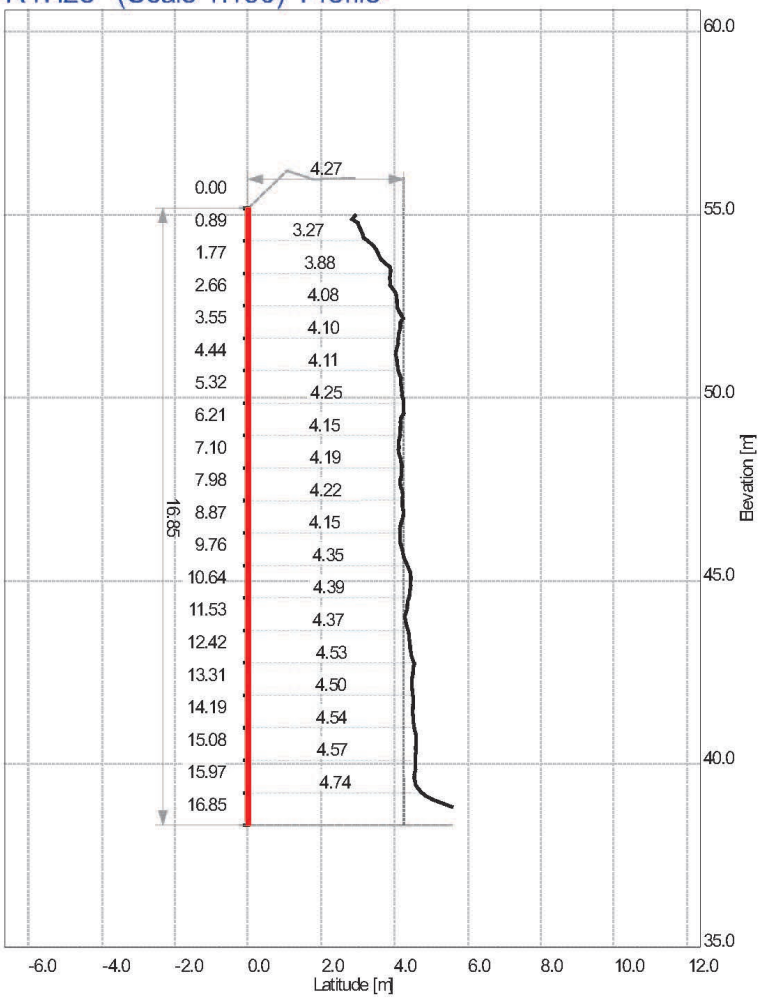

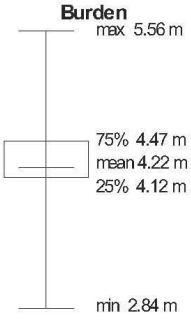

Inclination: 0.01 °
Length: 16.85 m
Diameter: 100.00 mm
Area: 73.6 m² (of profile)
Position: u: 0.36 m, v: 0.91 m
E: 750520.12 m, N: 4875283.18 m, H: 55.18 m
Subdrilling: 0 m

Depth	Profile
1.0	3.450
2.0	3.891
3.0	4.166
4.0	4.072
5.0	4.244
6.0	4.126
7.0	4.173
8.0	4.234
9.0	4.239
10.0	4.415
11.0	4.380
12.0	4.506
13.0	4.493
14.0	4.580
15.0	4.601
16.0	na

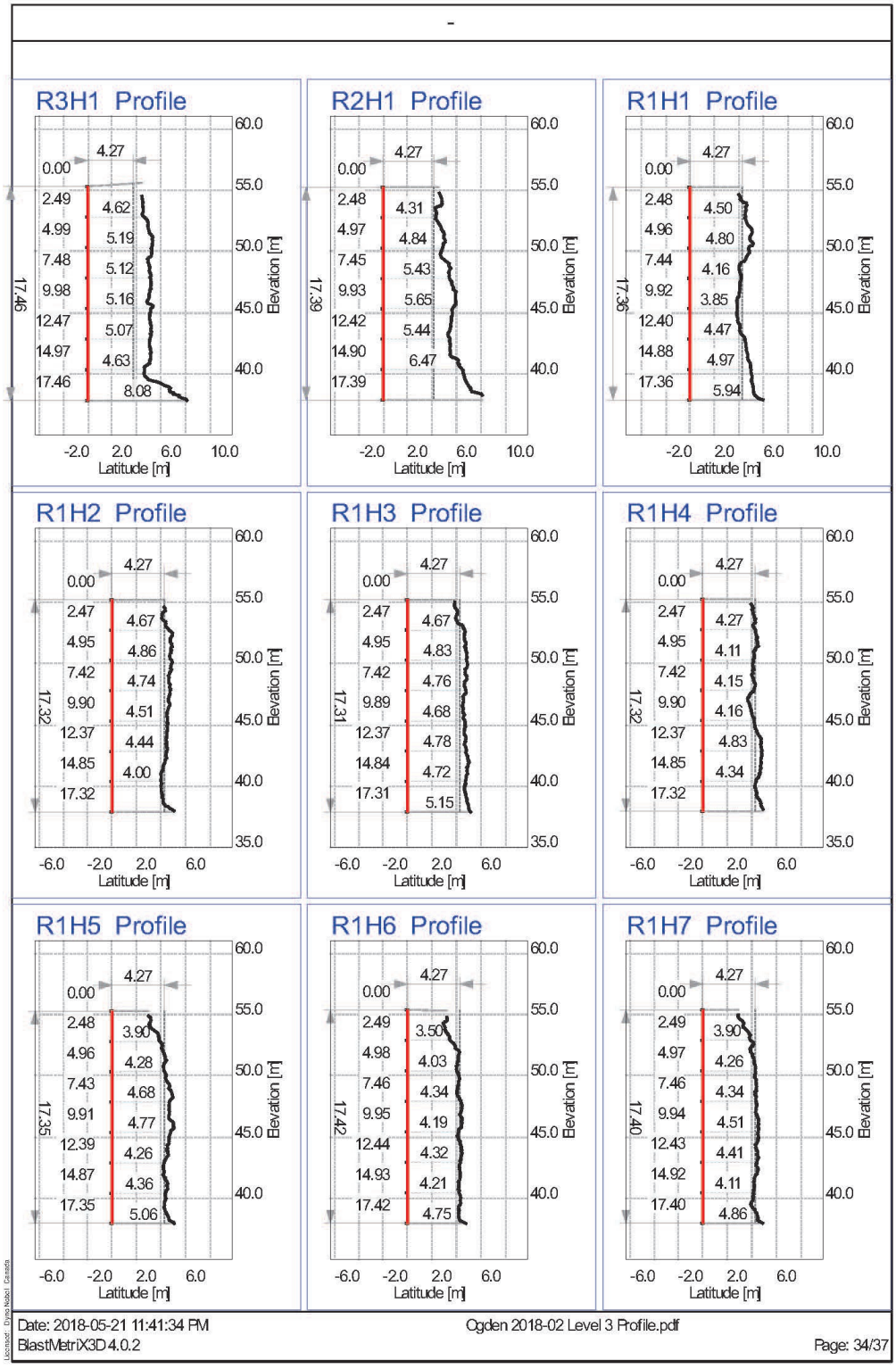
-
R3H1 Profile
0.00
2.49
4.99
7.48
9.98
12.47
14.97
17.46
4.27
4.62
5.19
5.12
5.16
5.07
4.63
8.08
17.46
R2H1 Profile
0.00
2.48
4.97
7.45
9.93
12.42
14.90
17.39
4.27
4.31
4.84
5.43
5.65
5.44
6.47
17.39
R1H1 Profile
0.00
2.48
4.96
7.44
9.92
12.40
14.88
17.36
4.27
4.50
4.80
4.16
3.85
4.47
4.97
5.94
17.36
R1H2 Profile
0.00
2.47
4.95
7.42
9.90
12.37
14.85
17.32
4.27
4.67
4.86
4.74
4.51
4.44
4.00
17.32
R1H3 Profile
0.00
2.47
4.95
7.42
9.89
12.37
14.84
17.31
4.27
4.67
4.83
4.76
4.68
4.78
4.72
5.15
17.31
R1H4 Profile
0.00
2.47
4.95
7.42
9.90
12.37
14.85
17.32
4.27
4.27
4.11
4.15
4.16
4.83
4.34
17.32
R1H5 Profile
0.00
2.48
4.96
7.43
9.91
12.39
14.87
17.35
4.27
3.90
4.28
4.68
4.77
4.26
4.36
5.06
17.35
R1H6 Profile
0.00
2.49
4.98
7.46
9.95
12.44
14.93
17.42
4.27
3.50
4.03
4.34
4.19
4.32
4.21
4.75
17.42
R1H7 Profile
0.00
2.49
4.97
7.46
9.94
12.43
14.92
17.40
4.27
3.90
4.26
4.34
4.51
4.41
4.11
4.86
17.40
60.0
55.0
50.0
45.0
40.0
35.0
Elevation [m]
-6.0
-2.0
2.0
6.0
10.0
Latitude [m]
Licensed: Dyno Nobel Canada
Date: 2018-05-21 11:41:34 PM
BlastMetrix3D 4.0.2
Ogden 2018-02 Level 3 Profile.pdf
Page: 34/37

-

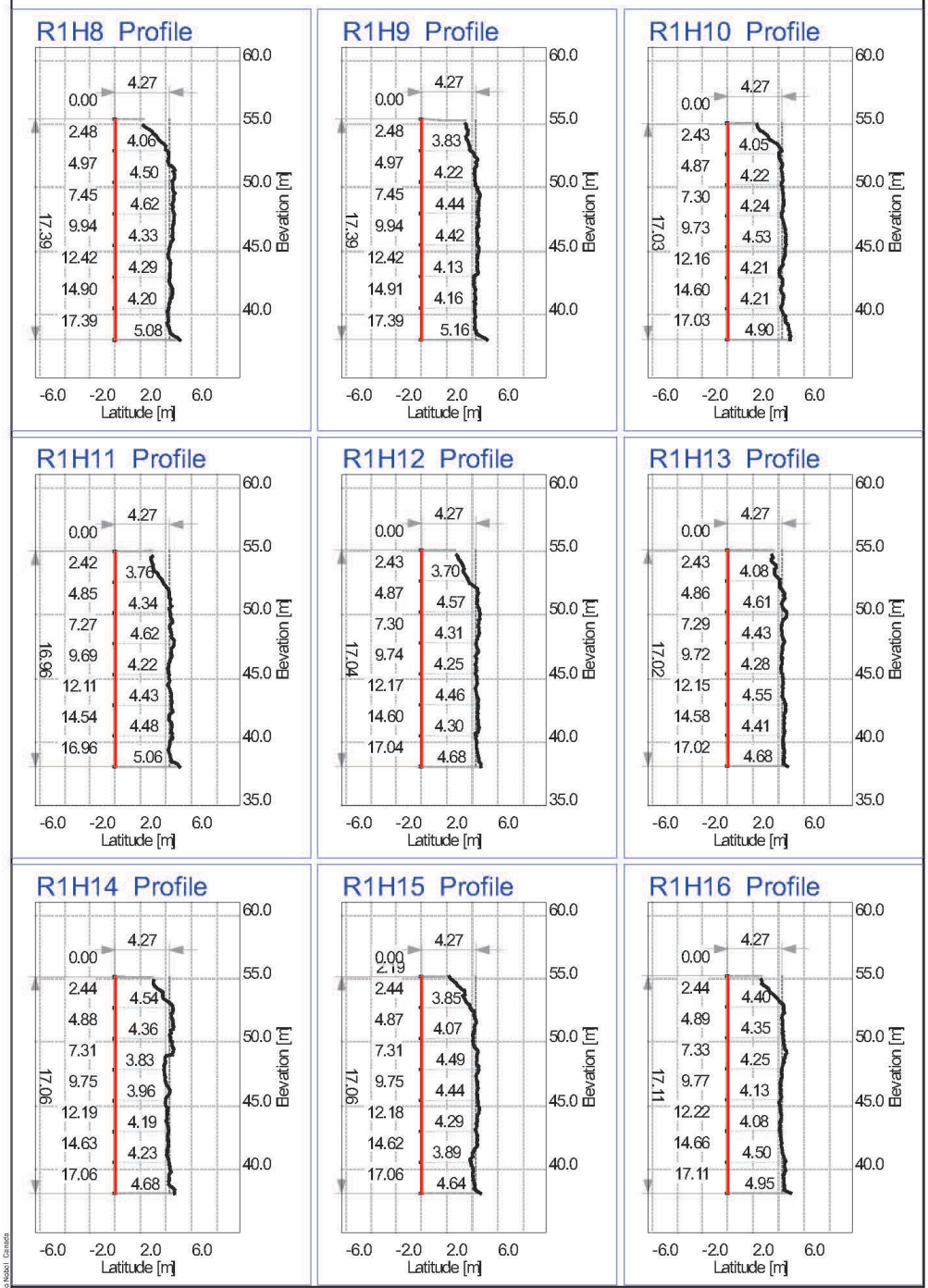

Licensed: Dyno Nobel Canada

Date: 2018-05-21 11:41:34 PM
BlastMetrix3D 4.0.2

Ogden 2018-02 Level 3 Profile.pdf

Page: 35/37

-

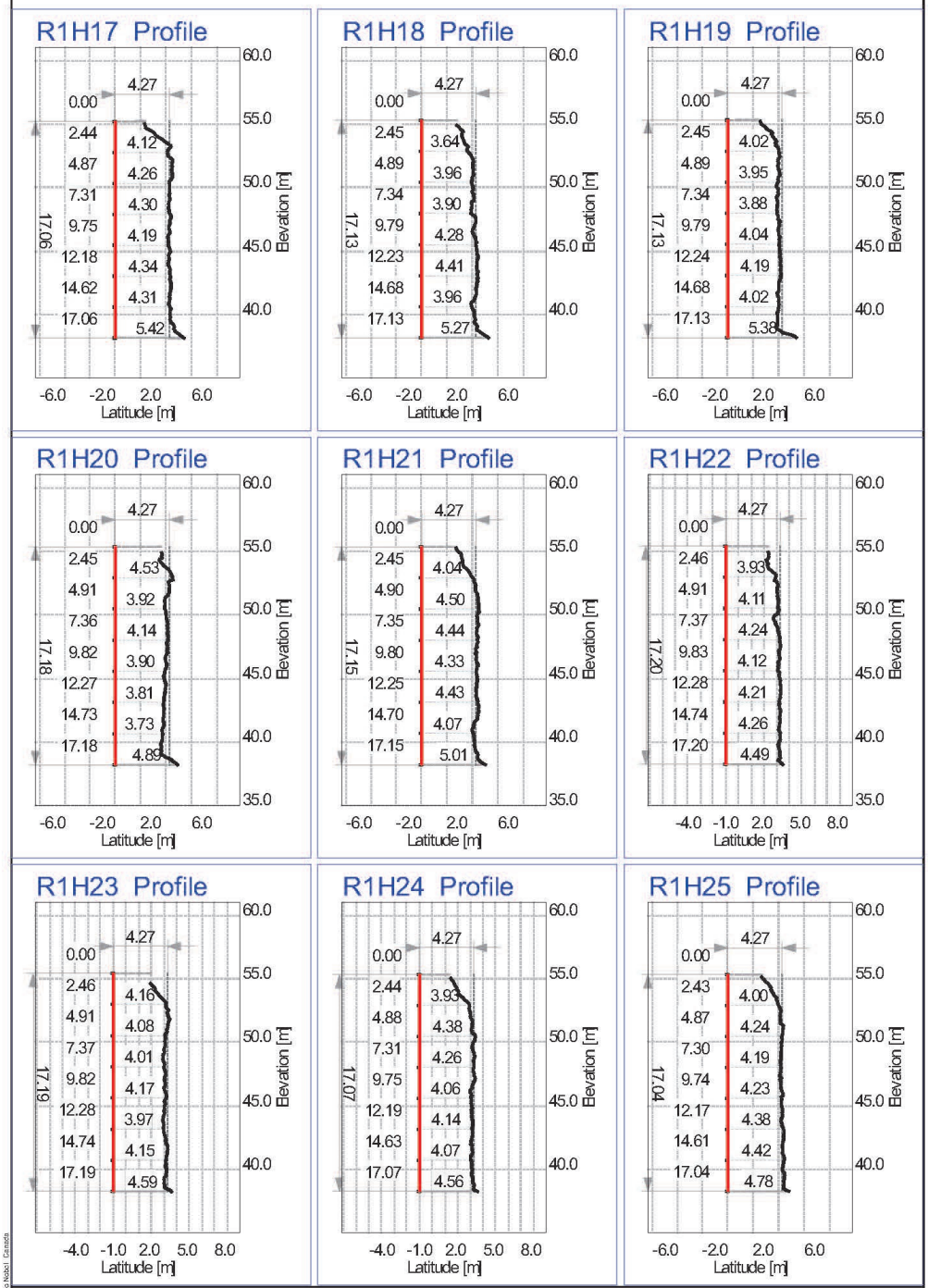

-

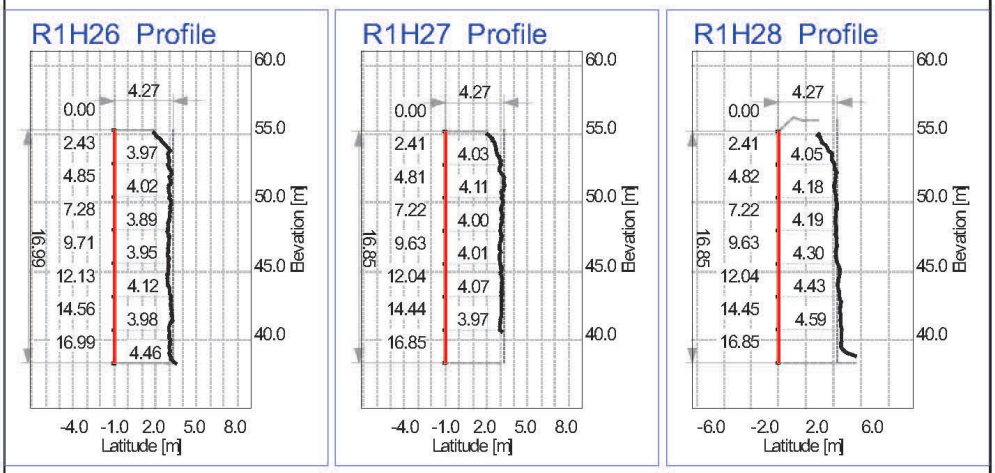

Borehole Report

2018 02 Level 3
CRH Ogden Point

21-05-18 10:39 PM

RENISHAW
apply innovation™

Project Information

Operator Name: Brad Asselstine

Site Name: CRH Ogden Point

Grid Magnetic Angle: 0.00(°)

Project Notes

Site Notes

Contents

1.3.29 - R1H27
1.3.30 - R1H28
1.4 - Hole Separation Report

1 OP

1.1 Hole Collar Report

Hole ID	X (m)	Y (m)	Z (m)
R3H1	750658.783	4875300.190	55.293
R2H1	750652.686	4875295.544	55.237
R1H1	750648.540	4875291.588	55.228
R1H2	750644.067	4875291.188	55.206
R1H3	750639.017	4875290.862	55.216
R1H4	750634.454	4875290.368	55.239
R1H5	750628.934	4875289.871	55.285
R1H6	750623.940	4875289.407	55.371
R1H7	750619.066	4875289.188	55.375
R1H8	750614.493	4875288.834	55.378
R1H9	750609.728	4875288.557	55.399
R1H10	750604.959	4875288.328	55.053
R1H11	750600.382	4875287.964	55.001
R1H12	750595.579	4875287.548	55.096
R1H13	750590.716	4875287.343	55.090
R1H14	750586.188	4875287.091	55.154
R1H15	750581.470	4875286.791	55.163
R1H16	750576.539	4875286.504	55.231
R1H17	750572.031	4875286.353	55.198
R1H18	750567.242	4875286.011	55.286
R1H19	750562.818	4875285.662	55.307
R1H20	750557.761	4875285.401	55.374
R1H21	750553.380	4875285.171	55.359
R1H22	750548.366	4875284.784	55.424
R1H23	750543.678	4875284.412	55.435
R1H24	750539.030	4875284.259	55.327
R1H25	750534.336	4875283.994	55.320
R1H26	750529.554	4875283.716	55.281
R1H27	750524.533	4875283.692	55.163
R1H28	750520.123	4875283.176	55.182

*Note: Boretrak Viewer will generate default X,Y,Z collar positions starting at 1000,1000,100 if no values have been entered by the user.

1.2 Plan View Report

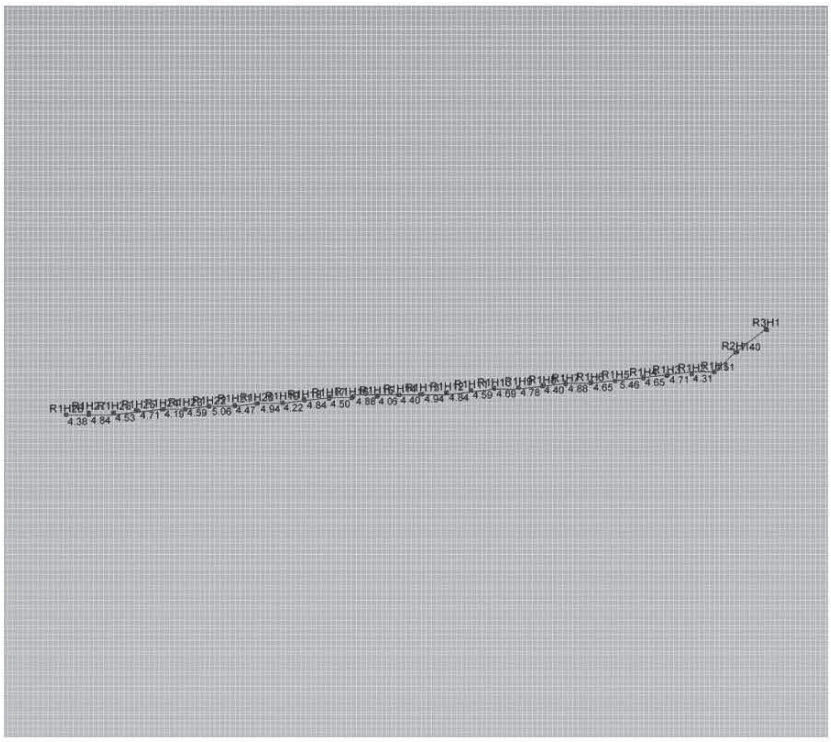

1.3.1 R3H1

Survey Data 1

Face : OP Hole : R3H1 Survey Date : 22-01-18 Dep (m) : 18.00
Average Azimuth (°) : 142.18 Average Inclination (°) : 2.43
Designed Azimuth (°) : 0.00 Designed Inclination (°) : 0.00 Designed Depth (m) : 0.00

Plan View

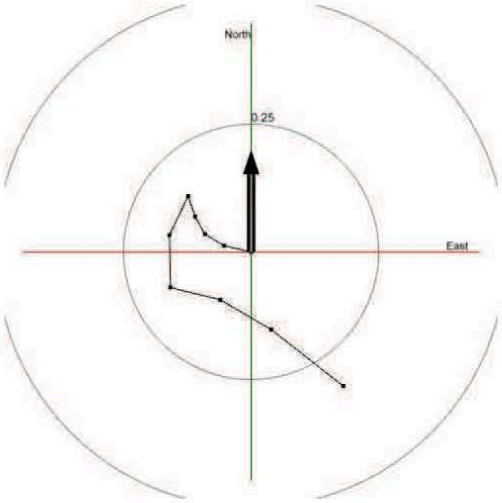

Front View

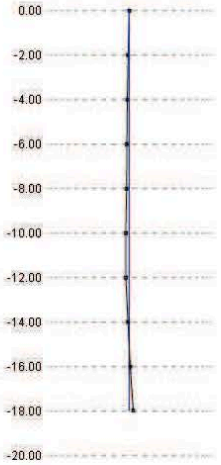

Side View

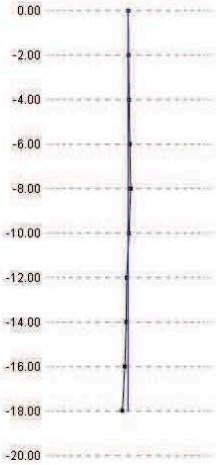

Face : 1 Hole : 1 Rod Increment : 2.00(m) Offset : 0.00(m) Dep : 18.00(m) Grid Magnetic Angle : 0.00(°)

Dep(m)	Heading(°)	Inclination(°)	Dev(m)
2.00	282.79	1.56	0.00
4.00	301.31	1.26	0.00
6.00	330.92	1.13	0.00
8.00	341.01	1.21	0.00
10.00	205.54	2.42	0.00
12.00	179.01	2.95	0.00
14.00	103.77	2.88	0.00
16.00	120.36	3.31	0.00
18.00	128.05	5.14	0.00

1.3.2 R2H1

Survey Data 1

Face : OP Hole : R2H1 Survey Date : 22-01-18 Dep (m) : 18.00
Average Azimuth (°) : 63.16 Average Inclination (°) : 1.85
Designed Azimuth (°) : 0.00 Designed Inclination (°) : 0.00 Designed Depth (m) : 0.00

Plan View

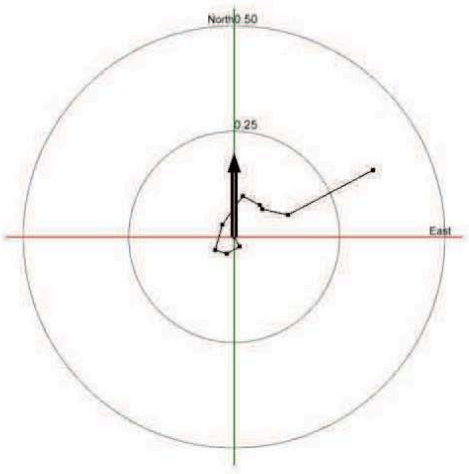

Front View

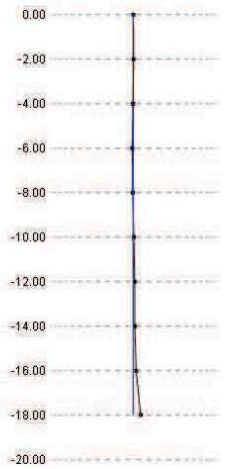

Side View

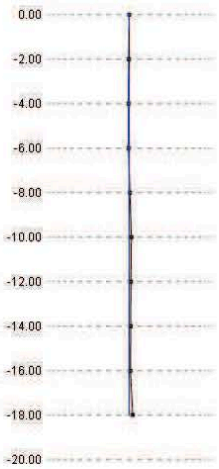

Face : 1 Hole : 2 Rod Increment : 2.00(m) Offset : 0.00(m) Dep : 18.00(m) Grid Magnetic Angle : 0.00(°)

Dep(m)	Heading(°)	Inclination(°)	Dev(m)
2.00	150.67	0.74	0.00
4.00	240.33	1.00	0.00
6.00	287.81	0.82	0.00
8.00	15.72	1.79	0.00
10.00	35.76	2.38	0.00
12.00	117.83	1.30	0.00
14.00	147.97	0.33	0.00
16.00	102.47	1.80	0.00
18.00	62.24	6.54	0.00

1.3.3 R1H1

Survey Data 1

Face : OP Hole : R1H1 Survey Date : 22-01-18 Dep (m) : 18.00
Average Azimuth (°) : 325.41 Average Inclination (°) : 1.34
Designed Azimuth (°) : 0.00 Designed Inclination (°) : 0.00 Designed Depth (m) : 0.00

Plan View

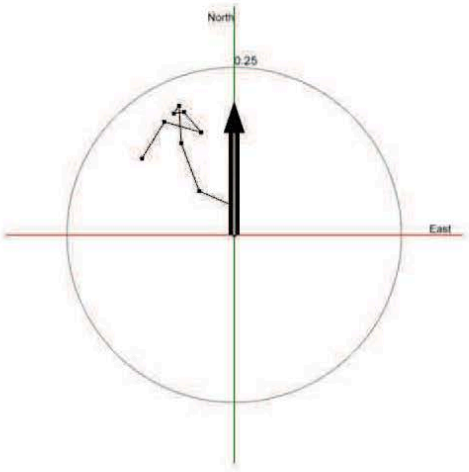

Front View

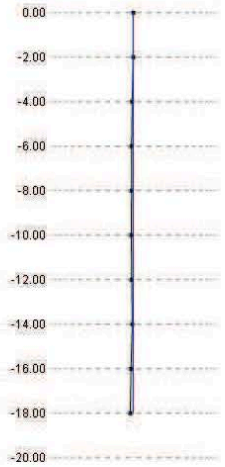

Side View

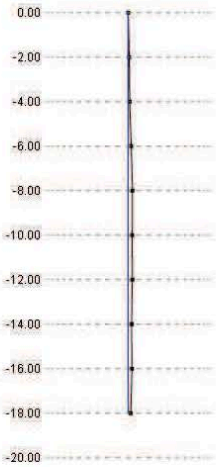

Face : 1 Hole : 3 Rod Increment : 2.00(m) Offset : 0.00(m) Dep : 18.00(m) Grid Magnetic Angle : 0.00(°)

Dep(m)	Heading(°)	Inclination(°)	Dev(m)
2.00	358.31	1.25	0.00
4.00	293.35	1.59	0.00
6.00	339.32	2.19	0.00
8.00	356.83	1.60	0.00
10.00	214.57	0.40	0.00
12.00	82.05	0.44	0.00
14.00	139.42	1.13	0.00
16.00	285.73	1.63	0.00
18.00	211.49	1.83	0.00

1.3.4 R1H2

Survey Data 1

Face : OP Hole : R1H2 Survey Date : 22-01-18 Dep (m) : 18.00
Average Azimuth (°) : 335.76 Average Inclination (°) : 1.41
Designed Azimuth (°) : 0.00 Designed Inclination (°) : 0.00 Designed Depth (m) : 0.00

Plan View

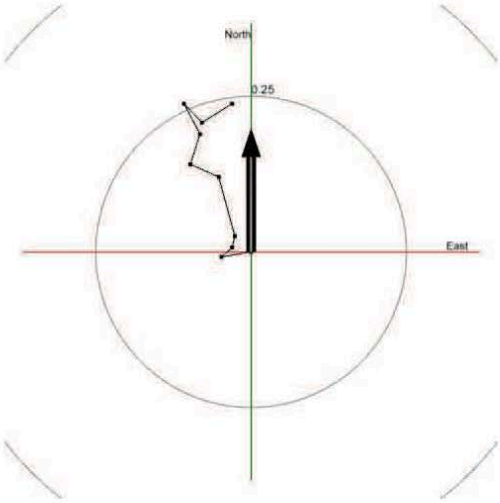

Front View

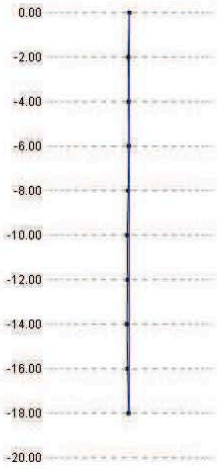

Side View

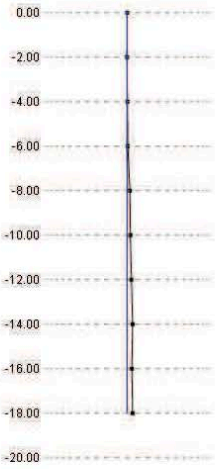

Face : 1 Hole : 4 Rod Increment : 2.00(m) Offset : 0.00(m) Dep : 18.00(m) Grid Magnetic Angle : 0.00(°)

Dep(m)	Heading(°)	Inclination(°)	Dev(m)
2.00	260.35	1.39	0.00
4.00	48.70	0.66	0.00
6.00	12.24	0.54	0.00
8.00	344.79	2.82	0.00
10.00	293.89	1.42	0.00
12.00	17.46	1.46	0.00
14.00	332.29	1.58	0.00
16.00	136.21	1.20	0.00
18.00	57.98	1.63	0.00

1.3.5 R1H3

Survey Data 1

Face : OP Hole : R1H3 Survey Date : 22-01-18 Dep (m) : 17.50
Average Azimuth (°) : 35.87 Average Inclination (°) : 1.80
Designed Azimuth (°) : 0.00 Designed Inclination (°) : 0.00 Designed Depth (m) : 0.00

Plan View

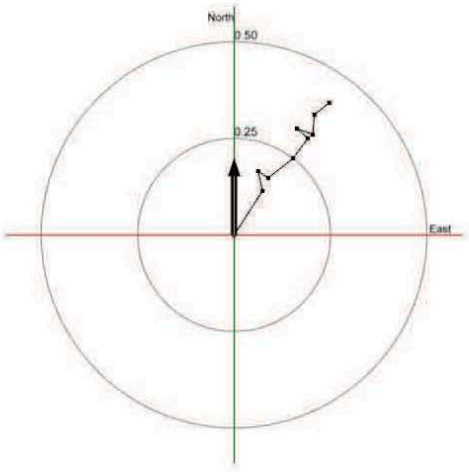

Front View

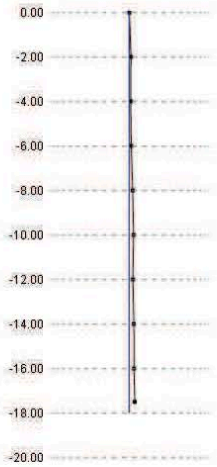

Side View

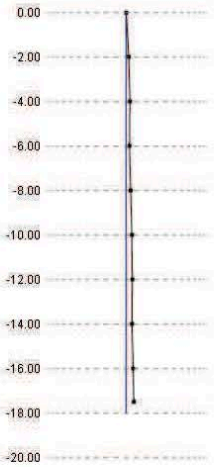

Face : 1 Hole : 5 Rod Increment : 2.00(m) Offset : 0.50(m) Dep : 17.50(m) Grid Magnetic Angle : 0.00(°)

Dep(m)	Heading(°)	Inclination(°)	Dev(m)
2.00	32.81	3.89	0.00
4.00	347.62	1.49	0.00
6.00	123.71	0.90	0.00
8.00	51.81	2.36	0.00
10.00	36.24	1.84	0.00
12.00	311.83	1.10	0.00
14.00	110.82	1.26	0.00
16.00	4.91	1.48	0.00
17.50	51.71	1.87	0.00

1.3.6 R1H4

Survey Data 1

Face : OP Hole : R1H4 Survey Date : 22-01-18 Dep (m) : 18.00
Average Azimuth (°) : 352.95 Average Inclination (°) : 1.68
Designed Azimuth (°) : 0.00 Designed Inclination (°) : 0.00 Designed Depth (m) : 0.00

Plan View

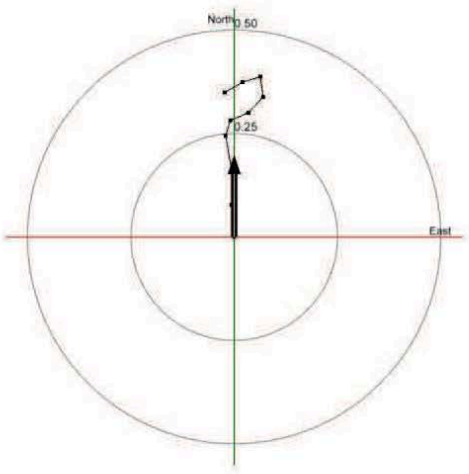

Front View

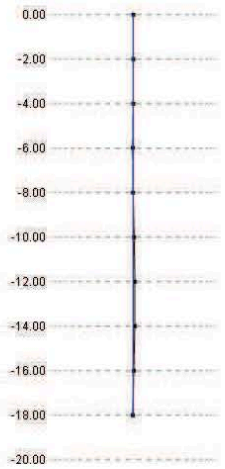

Side View

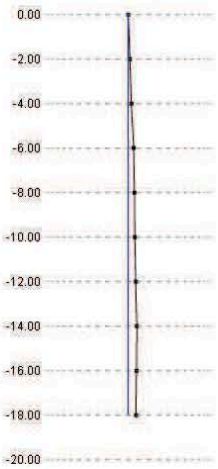

Face : 1 Hole : 6 Rod Increment : 2.00(m) Offset : 0.00(m) Dep : 18.00(m) Grid Magnetic Angle : 0.00(°)

Dep(m)	Heading(°)	Inclination(°)	Dev(m)
2.00	355.33	2.23	0.00
4.00	3.53	1.80	0.00
6.00	350.15	3.04	0.00
8.00	17.38	1.10	0.00
10.00	66.90	1.35	0.00
12.00	43.18	1.49	0.00
14.00	352.39	1.41	0.00
16.00	253.41	1.30	0.00
18.00	239.85	1.42	0.00

1.3.7 R1H5

Survey Data 1

Face : OP Hole : R1H5 Survey Date : 22-01-18 Dep (m) : 19.00
Average Azimuth (°) : 302.09 Average Inclination (°) : 1.06
Designed Azimuth (°) : 0.00 Designed Inclination (°) : 0.00 Designed Depth (m) : 0.00

Plan View

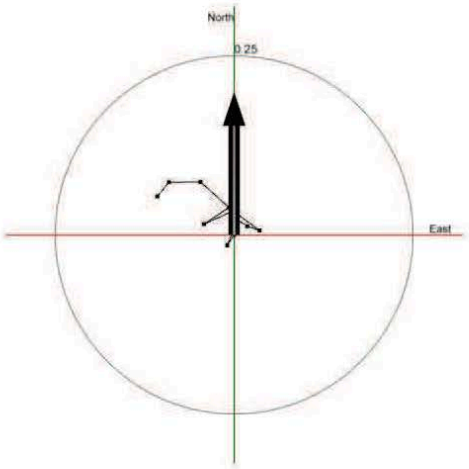

Front View

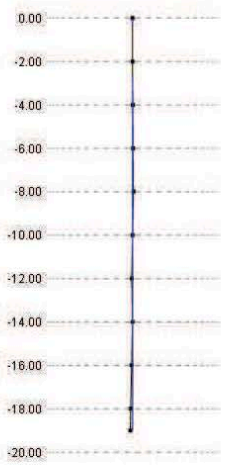

Side View

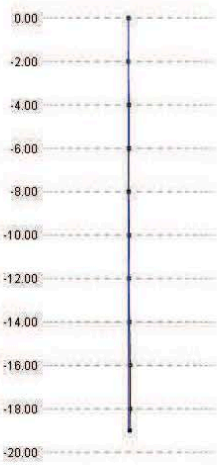

Face : 1 Hole : 7 Rod Increment : 2.00(m) Offset : 1.00(m) Dep : 19.00(m) Grid Magnetic Angle : 0.00(°)

Dep(m)	Heading(°)	Inclination(°)	Dev(m)
2.00	214.05	0.50	0.00
4.00	23.44	1.09	0.00
6.00	122.23	0.44	0.00
8.00	109.09	0.52	0.00
10.00	306.12	1.32	0.00
12.00	245.57	1.27	0.00
14.00	56.05	1.20	0.00
16.00	311.79	1.53	0.00
18.00	269.36	1.26	0.00
19.00	219.30	1.46	0.00

1.3.8 R1H6

Survey Data 1

Face : OP Hole : R1H6 Survey Date : 22-01-18 Dep (m) : 18.00
Average Azimuth (°) : 38.85 Average Inclination (°) : 1.58
Designed Azimuth (°) : 0.00 Designed Inclination (°) : 0.00 Designed Depth (m) : 0.00

Plan View

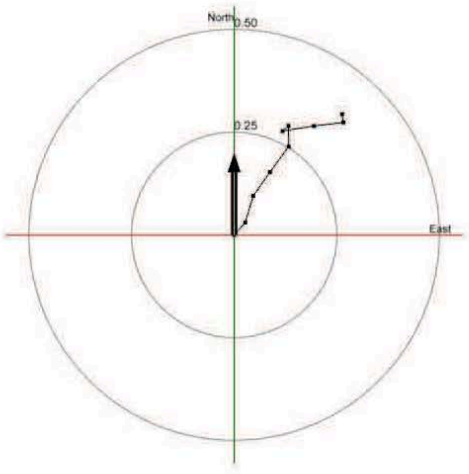

Front View

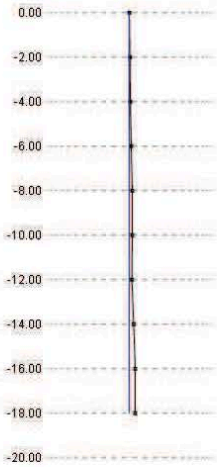

Side View

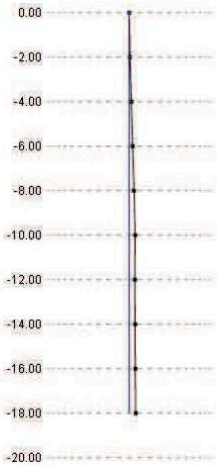

Face : 1 Hole : 8 Rod Increment : 2.00(m) Offset : 0.00(m) Dep : 18.00(m) Grid Magnetic Angle : 0.00(°)

Dep(m)	Heading(°)	Inclination(°)	Dev(m)
2.00	41.69	1.15	0.00
4.00	16.84	1.95	0.00
6.00	35.21	2.01	0.00
8.00	36.54	2.22	0.00
10.00	358.80	1.44	0.00
12.00	229.29	0.55	0.00
14.00	81.04	2.23	0.00
16.00	83.09	2.06	0.00
18.00	350.82	0.58	0.00

1.3.9 R1H7

Survey Data 1

Face : OP Hole : R1H7 Survey Date : 22-01-18 Dep (m) : 18.00
Average Azimuth (°) : 4.78 Average Inclination (°) : 1.83
Designed Azimuth (°) : 0.00 Designed Inclination (°) : 0.00 Designed Depth (m) : 0.00

Plan View

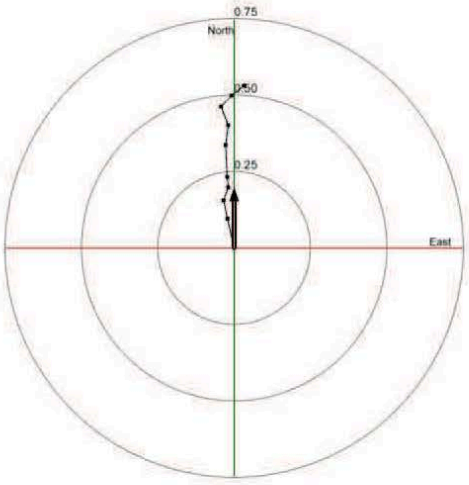

Front View

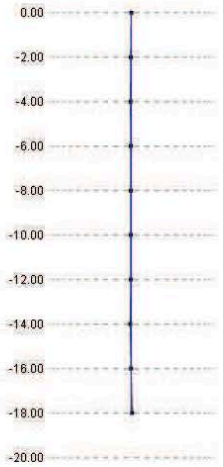

Side View

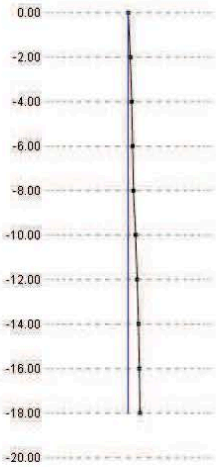

Face : 1 Hole : 9 Rod Increment : 2.00(m) Offset : 0.00(m) Dep : 18.00(m) Grid Magnetic Angle : 0.00(°)

Dep(m)	Heading(°)	Inclination(°)	Dev(m)
2.00	347.03	2.79	0.00
4.00	348.12	1.77	0.00
6.00	19.57	1.30	0.00
8.00	354.39	0.98	0.00
10.00	357.06	3.00	0.00
12.00	8.00	1.85	0.00
14.00	339.12	1.88	0.00
16.00	43.26	1.42	0.00
18.00	51.63	1.48	0.00

1.3.10 R1H8

Survey Data 1

Face : OP Hole : R1H8 Survey Date : 22-01-18 Dep (m) : 18.00
Average Azimuth (°) : 34.78 Average Inclination (°) : 1.79
Designed Azimuth (°) : 0.00 Designed Inclination (°) : 0.00 Designed Depth (m) : 0.00

Plan View

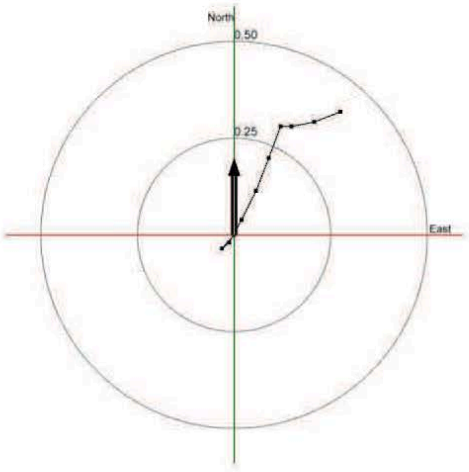

Front View

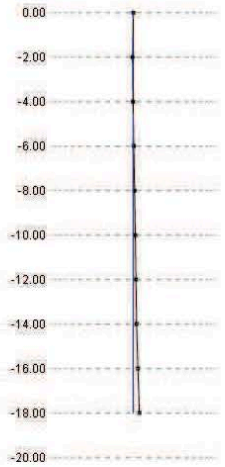

Side View

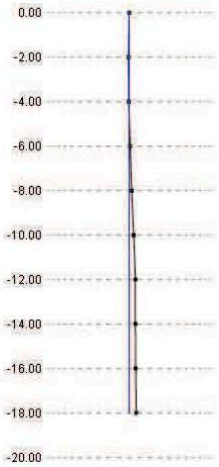

Face : 1 Hole : 10 Rod Increment : 2.00(m) Offset : 0.00(m) Dep : 18.00(m) Grid Magnetic Angle : 0.00(°)

Dep(m)	Heading(°)	Inclination(°)	Dev(m)
2.00	221.58	1.36	0.00
4.00	50.66	0.69	0.00
6.00	28.32	1.93	0.00
8.00	26.59	2.38	0.00
10.00	21.30	2.61	0.00
12.00	20.48	2.50	0.00
14.00	90.07	0.80	0.00
16.00	79.04	1.72	0.00
18.00	68.74	2.09	0.00

1.3.11 R1H9

Survey Data 1

Face : OP Hole : R1H9 Survey Date : 22-01-18 Dep (m) : 18.00
Average Azimuth (°) : 323.83 Average Inclination (°) : 1.28
Designed Azimuth (°) : 0.00 Designed Inclination (°) : 0.00 Designed Depth (m) : 0.00

Plan View

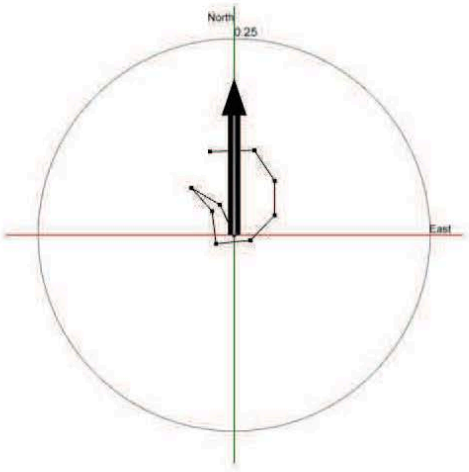

Front View

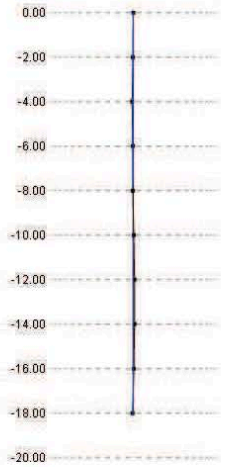

Side View

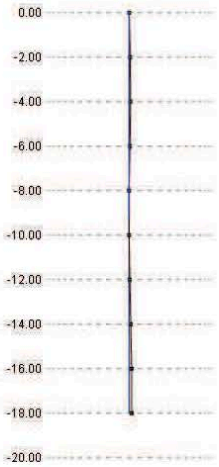

Face : 1 Hole : 11 Rod Increment : 2.00(m) Offset : 0.00(m) Dep : 18.00(m) Grid Magnetic Angle : 0.00(°)

Dep(m)	Heading(°)	Inclination(°)	Dev(m)
2.00	334.70	1.22	0.00
4.00	300.51	1.20	0.00
6.00	138.32	1.13	0.00
8.00	173.04	1.20	0.00
10.00	84.30	1.27	0.00
12.00	44.33	1.27	0.00
14.00	359.81	1.26	0.00
16.00	326.33	1.34	0.00
18.00	268.42	1.62	0.00

1.3.12 R1H10

Survey Data 1

Face : OP Hole : R1H10 Survey Date : 22-01-18 Dep (m) : 18.00
Average Azimuth (°) : 336.87 Average Inclination (°) : 1.24
Designed Azimuth (°) : 0.00 Designed Inclination (°) : 0.00 Designed Depth (m) : 0.00

Plan View

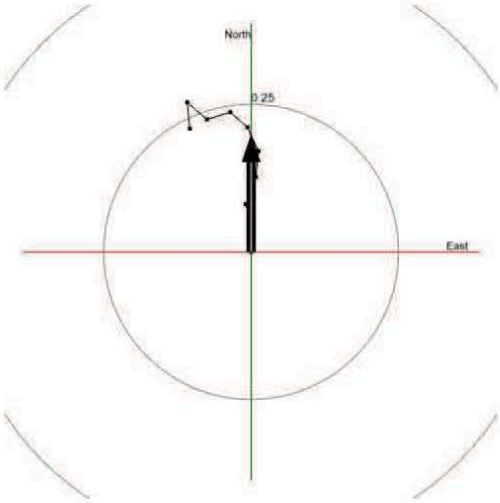

Front View

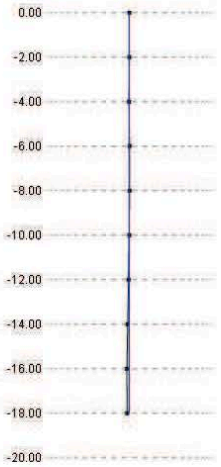

Side View

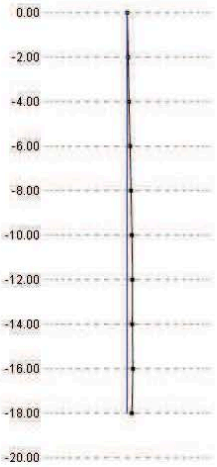

Face : 1 Hole : 12 Rod Increment : 2.00(m) Offset : 0.00(m) Dep : 18.00(m) Grid Magnetic Angle : 0.00(°)

Dep(m)	Heading(°)	Inclination(°)	Dev(m)
2.00	1.29	1.20	0.00
4.00	345.46	1.15	0.00
6.00	20.27	1.41	0.00
8.00	5.75	1.27	0.00
10.00	334.94	1.26	0.00
12.00	311.54	1.10	0.00
14.00	253.16	1.19	0.00
16.00	310.43	1.27	0.00
18.00	173.96	1.28	0.00

1.3.13 R1H11

Survey Data 1

Face : OP Hole : R1H11 Survey Date : 22-01-18 Dep (m) : 18.00
Average Azimuth (°) : 311.41 Average Inclination (°) : 1.07
Designed Azimuth (°) : 0.00 Designed Inclination (°) : 0.00 Designed Depth (m) : 0.00

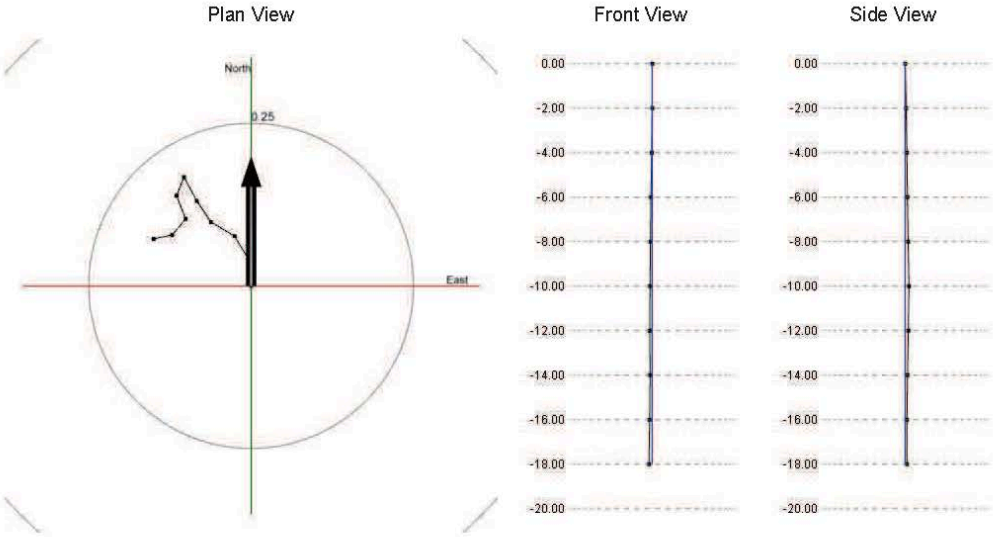

Face : 1 Hole : 13 Rod Increment : 2.00(m) Offset : 0.00(m) Dep : 18.00(m) Grid Magnetic Angle : 0.00(°)

Dep(m)	Heading(°)	Inclination(°)	Dev(m)
2.00	356.08	1.11	0.00
4.00	328.77	1.27	0.00
6.00	300.76	1.21	0.00
8.00	326.28	1.11	0.00
10.00	331.51	1.19	0.00
12.00	201.88	0.88	0.00
14.00	158.64	1.10	0.00
16.00	220.14	0.92	0.00
18.00	257.84	0.84	0.00

1.3.14 R1H12

Survey Data 1

Face : OP Hole : R1H12 Survey Date : 22-01-18 Dep (m) : 18.00
Average Azimuth (°) : 303.70 Average Inclination (°) : 1.17
Designed Azimuth (°) : 0.00 Designed Inclination (°) : 0.00 Designed Depth (m) : 0.00

Plan View

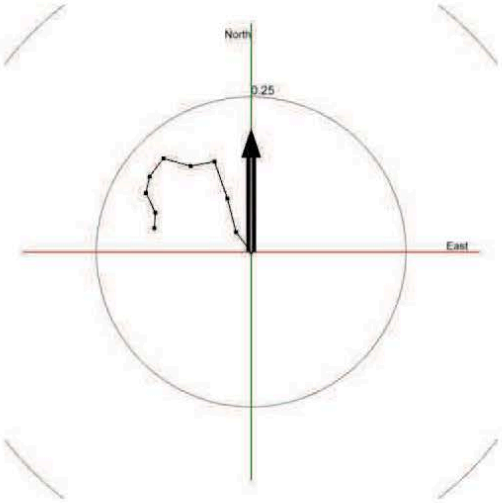

Front View

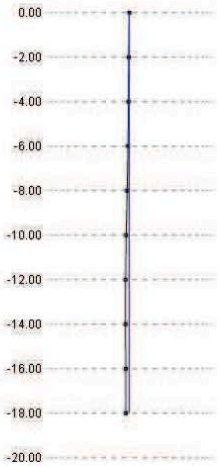

Side View

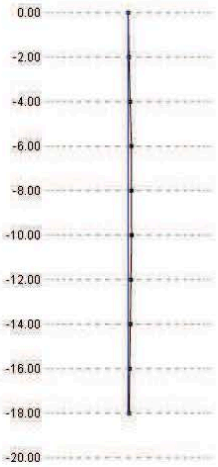

Face : 1 Hole : 14 Rod Increment : 2.00(m) Offset : 0.00(m) Dep : 18.00(m) Grid Magnetic Angle : 0.00(°)

Dep(m)	Heading(°)	Inclination(°)	Dev(m)
2.00	322.65	1.15	0.00
4.00	345.60	1.60	0.00
6.00	340.72	1.81	0.00
8.00	259.41	1.13	0.00
10.00	285.51	1.30	0.00
12.00	217.48	1.06	0.00
14.00	192.46	0.77	0.00
16.00	154.31	1.01	0.00
18.00	184.03	0.72	0.00

1.3.15 R1H13

Survey Data 1

Face : OP Hole : R1H13 Survey Date : 22-01-18 Dep (m) : 18.00
Average Azimuth (°) : 251.98 Average Inclination (°) : 1.71
Designed Azimuth (°) : 0.00 Designed Inclination (°) : 0.00 Designed Depth (m) : 0.00

Plan View

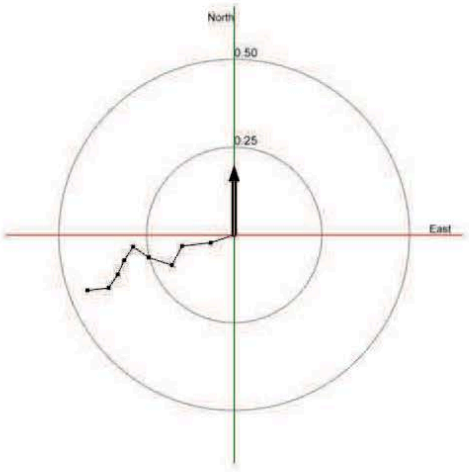

Front View

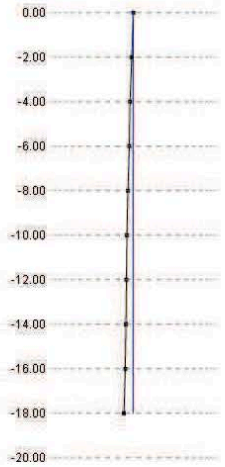

Side View

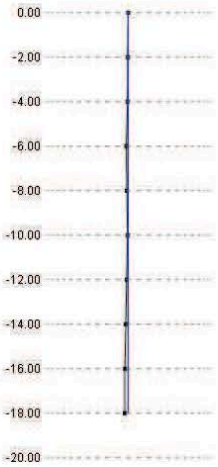

Face : 1 Hole : 15 Rod Increment : 2.00(m) Offset : 0.00(m) Dep : 18.00(m) Grid Magnetic Angle : 0.00(°)

Dep(m)	Heading(°)	Inclination(°)	Dev(m)
2.00	251.57	2.02	0.00
4.00	263.44	2.35	0.00
6.00	208.18	1.77	0.00
8.00	288.07	2.00	0.00
10.00	304.89	1.55	0.00
12.00	213.02	1.32	0.00
14.00	204.57	1.26	0.00
16.00	213.80	1.33	0.00
18.00	263.41	1.75	0.00

1.3.16 R1H14

Survey Data 1

Face : OP Hole : R1H14 Survey Date : 22-01-18 Dep (m) : 18.00
Average Azimuth (°) : 290.90 Average Inclination (°) : 1.41
Designed Azimuth (°) : 0.00 Designed Inclination (°) : 0.00 Designed Depth (m) : 0.00

Plan View

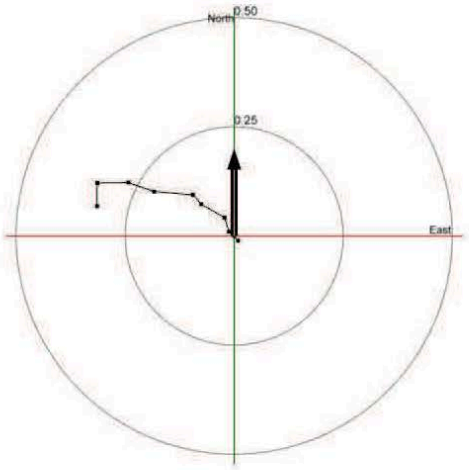

Front View

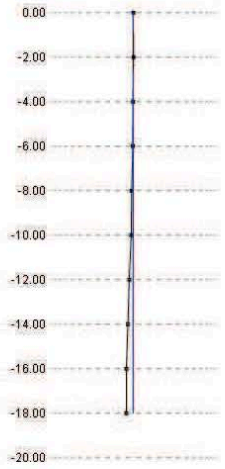

Side View

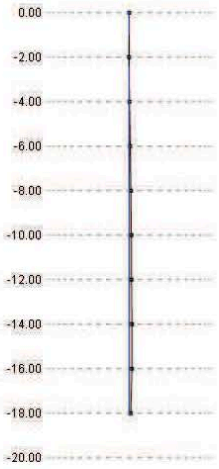

Face : 1 Hole : 16 Rod Increment : 2.00(m) Offset : 0.00(m) Dep : 18.00(m) Grid Magnetic Angle : 0.00(°)

Dep(m)	Heading(°)	Inclination(°)	Dev(m)
2.00	139.99	0.40	0.00
4.00	314.33	0.84	0.00
6.00	342.77	0.96	0.00
8.00	299.74	1.75	0.00
10.00	318.60	0.83	0.00
12.00	274.87	2.56	0.00
14.00	289.24	1.79	0.00
16.00	269.28	2.04	0.00
18.00	180.50	1.53	0.00

1.3.17 R1H15

Survey Data 1

Face : OP Hole : R1H15 Survey Date : 22-01-18 Dep (m) : 18.00
Average Azimuth (°) : 53.72 Average Inclination (°) : 1.54
Designed Azimuth (°) : 0.00 Designed Inclination (°) : 0.00 Designed Depth (m) : 0.00

Plan View

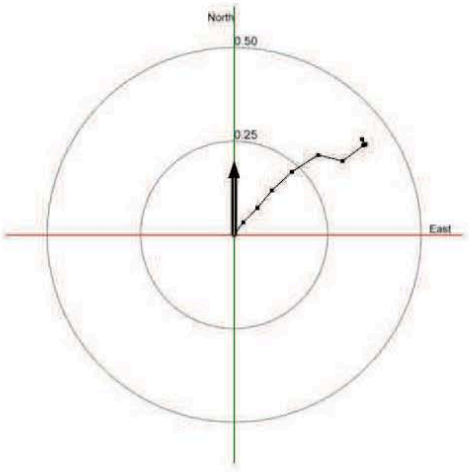

Front View

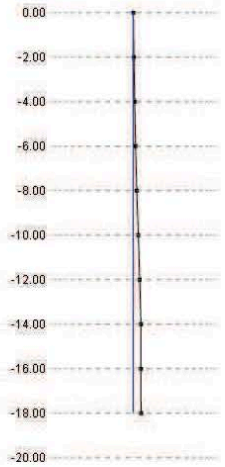

Side View

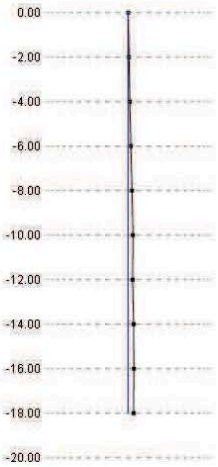

Face : 1 Hole : 17 Rod Increment : 2.00(m) Offset : 0.00(m) Dep : 18.00(m) Grid Magnetic Angle : 0.00(°)

Dep(m)	Heading(°)	Inclination(°)	Dev(m)
2.00	35.85	1.20	0.00
4.00	44.80	1.54	0.00
6.00	39.87	1.74	0.00
8.00	46.80	2.09	0.00
10.00	57.28	2.38	0.00
12.00	103.91	1.94	0.00
14.00	53.21	1.99	0.00
16.00	349.20	0.50	0.00
18.00	147.27	0.48	0.00

1.3.18 R1H16

Survey Data 1

Face : OP Hole : R1H16 Survey Date : 22-01-18 Dep (m) : 18.00
Average Azimuth (°) : 43.20 Average Inclination (°) : 1.91
Designed Azimuth (°) : 0.00 Designed Inclination (°) : 0.00 Designed Depth (m) : 0.00

Plan View

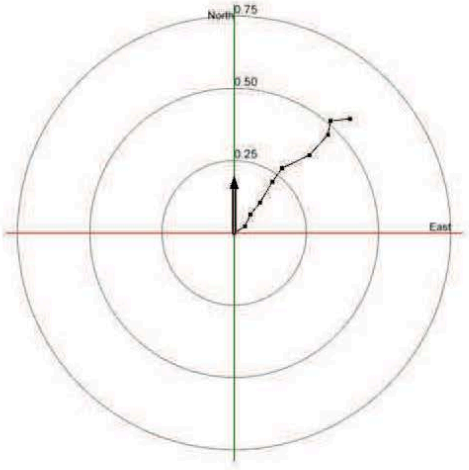

Front View

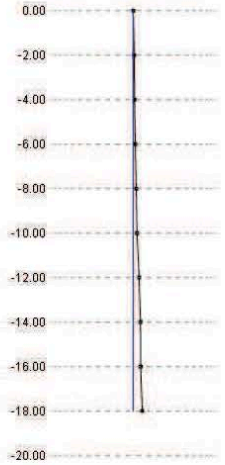

Side View

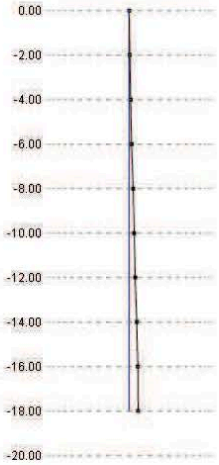

Face : 1 Hole : 18 Rod Increment : 2.00(m) Offset : 0.00(m) Dep : 18.00(m) Grid Magnetic Angle : 0.00(°)

Dep(m)	Heading(°)	Inclination(°)	Dev(m)
2.00	58.78	1.27	0.00
4.00	24.62	1.29	0.00
6.00	38.97	1.52	0.00
8.00	30.61	2.39	0.00
10.00	35.50	1.65	0.00
12.00	64.65	3.02	0.00
14.00	41.99	2.74	0.00
16.00	10.88	1.39	0.00
18.00	83.97	1.94	0.00

1.3.19 R1H17

Survey Data 1

Face : OP Hole : R1H17 Survey Date : 22-01-18 Dep (m) : 18.00
Average Azimuth (°) : 24.16 Average Inclination (°) : 1.77
Designed Azimuth (°) : 0.00 Designed Inclination (°) : 0.00 Designed Depth (m) : 0.00

Plan View

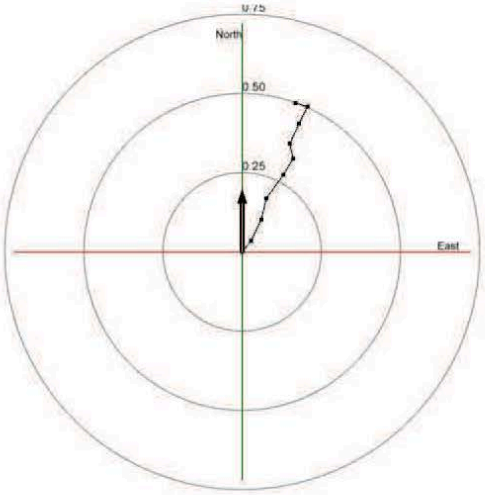

Front View

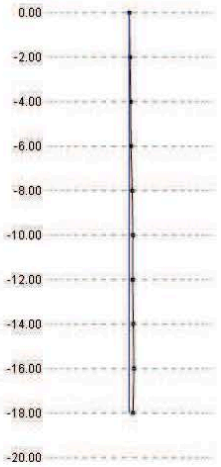

Side View

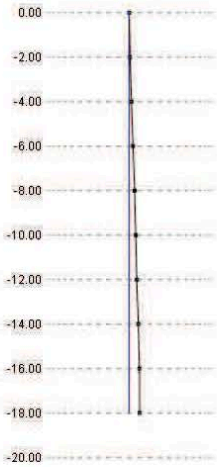

Face : 1 Hole : 19 Rod Increment : 2.00(m) Offset : 0.00(m) Dep : 18.00(m) Grid Magnetic Angle : 0.00(°)

Dep(m)	Heading(°)	Inclination(°)	Dev(m)
2.00	38.74	1.29	0.00
4.00	25.84	2.12	0.00
6.00	13.25	1.97	0.00
8.00	36.03	2.64	0.00
10.00	30.98	1.72	0.00
12.00	347.20	1.38	0.00
14.00	24.54	2.00	0.00
16.00	26.76	1.71	0.00
18.00	287.13	1.13	0.00

1.3.20 R1H18

Survey Data 1

Face : OP Hole : R1H18 Survey Date : 22-01-18 Dep (m) : 18.00
Average Azimuth (°) : 333.12 Average Inclination (°) : 1.47
Designed Azimuth (°) : 0.00 Designed Inclination (°) : 0.00 Designed Depth (m) : 0.00

Plan View

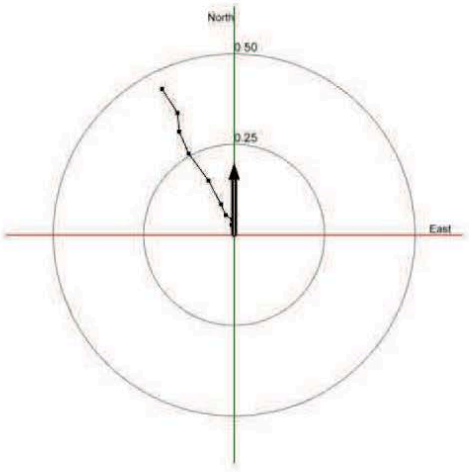

Front View

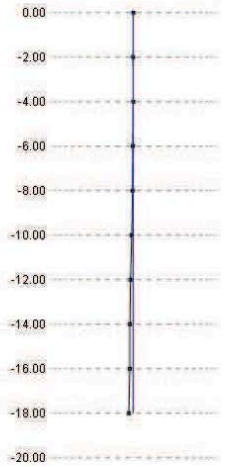

Side View

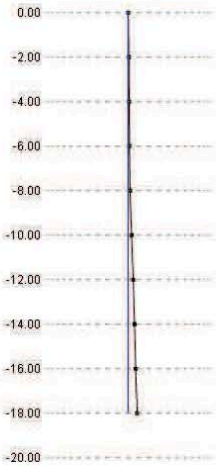

Face : 1 Hole : 20 Rod Increment : 2.00(m) Offset : 0.00(m) Dep : 18.00(m) Grid Magnetic Angle : 0.00(°)

Dep(m)	Heading(°)	Inclination(°)	Dev(m)
2.00	346.07	0.83	0.00
4.00	6.57	0.40	0.00
6.00	305.80	0.62	0.00
8.00	335.67	0.93	0.00
10.00	332.36	2.13	0.00
12.00	323.60	2.64	0.00
14.00	336.72	1.91	0.00
16.00	355.00	1.47	0.00
18.00	326.95	2.25	0.00

1.3.21 R1H19

Survey Data 1

Face : OP Hole : R1H19 Survey Date : 22-01-18 Dep (m) : 17.50
Average Azimuth (°) : 124.57 Average Inclination (°) : 0.94
Designed Azimuth (°) : 0.00 Designed Inclination (°) : 0.00 Designed Depth (m) : 0.00

Plan View

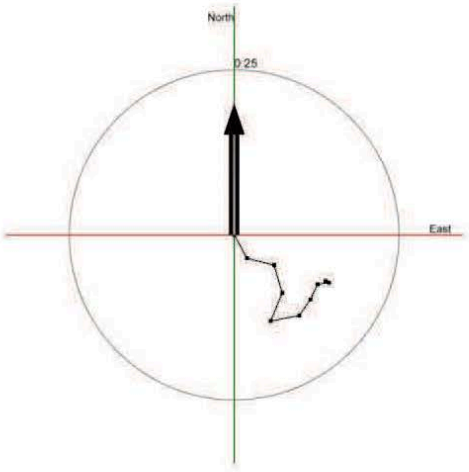

Front View

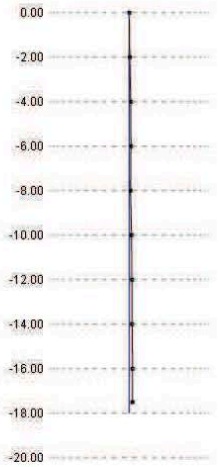

Side View

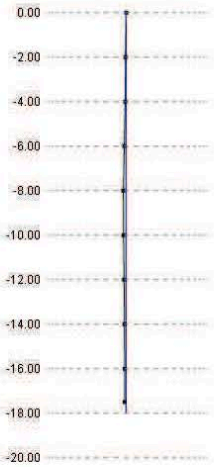

Face : 1 Hole : 21 Rod Increment : 2.00(m) Offset : 0.50(m) Dep : 17.50(m) Grid Magnetic Angle : 0.00(°)

Dep(m)	Heading(°)	Inclination(°)	Dev(m)
2.00	151.13	1.15	0.00
4.00	104.60	1.22	0.00
6.00	163.67	1.26	0.00
8.00	202.57	1.31	0.00
10.00	79.14	1.27	0.00
12.00	34.57	0.85	0.00
14.00	25.68	0.72	0.00
16.00	81.74	0.50	0.00
17.50	293.95	0.22	0.00

1.3.22 R1H20

Survey Data 1

Face : OP Hole : R1H20 Survey Date : 22-01-18 Dep (m) : 18.00
Average Azimuth (°) : 69.33 Average Inclination (°) : 1.09
Designed Azimuth (°) : 0.00 Designed Inclination (°) : 0.00 Designed Depth (m) : 0.00

Plan View

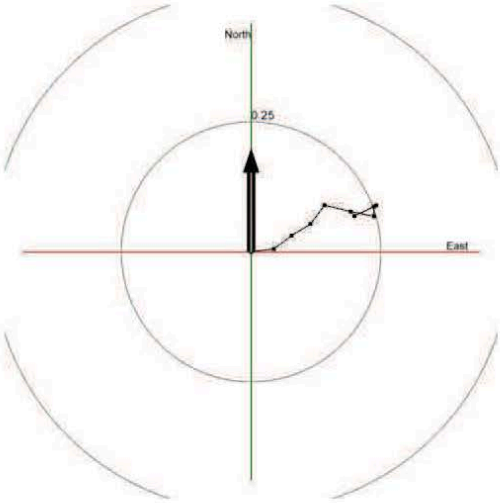

Front View

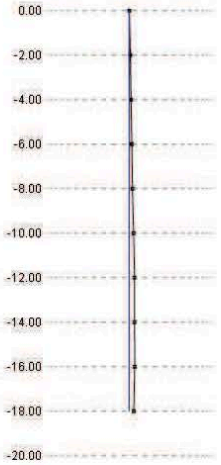

Side View

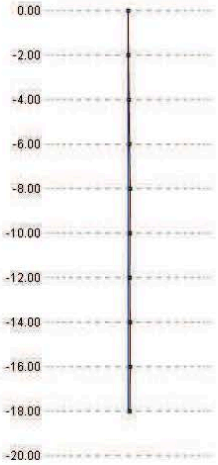

Face : 1 Hole : 22 Rod Increment : 2.00(m) Offset : 0.00(m) Dep : 18.00(m) Grid Magnetic Angle : 0.00(°)

Dep(m)	Heading(°)	Inclination(°)	Dev(m)
2.00	82.43	1.27	0.00
4.00	53.33	1.22	0.00
6.00	58.32	1.22	0.00
8.00	36.75	1.29	0.00
10.00	103.40	1.49	0.00
12.00	101.93	1.31	0.00
14.00	357.31	0.54	0.00
16.00	63.30	0.16	0.00
18.00	243.96	1.34	0.00

1.3.23 R1H21

Survey Data 1

Face : OP Hole : R1H21 Survey Date : 22-01-18 Dep (m) : 18.00
Average Azimuth (°) : 162.09 Average Inclination (°) : 1.35
Designed Azimuth (°) : 0.00 Designed Inclination (°) : 0.00 Designed Depth (m) : 0.00

Plan View

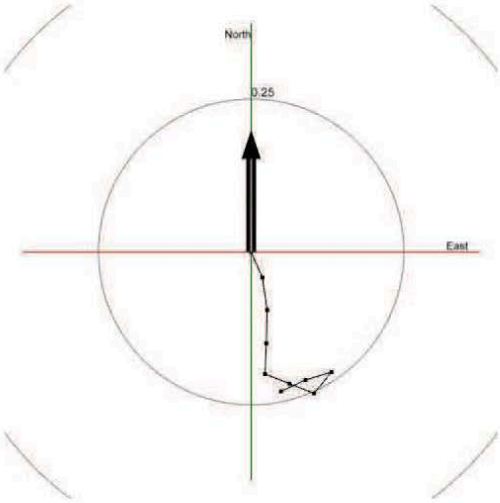

Front View

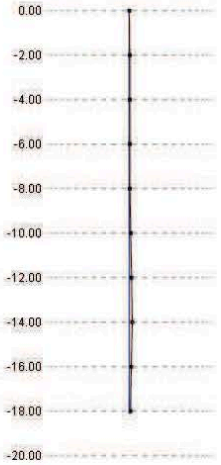

Side View

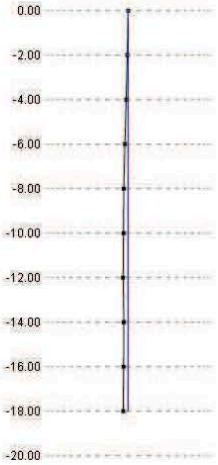

Face : 1 Hole : 23 Rod Increment : 2.00(m) Offset : 0.00(m) Dep : 18.00(m) Grid Magnetic Angle : 0.00(°)

Dep(m)	Heading(°)	Inclination(°)	Dev(m)
2.00	156.36	1.32	0.00
4.00	171.69	1.53	0.00
6.00	181.38	1.56	0.00
8.00	182.41	1.44	0.00
10.00	111.69	1.22	0.00
12.00	111.48	1.24	0.00
14.00	39.35	1.29	0.00
16.00	253.26	1.27	0.00
18.00	244.94	1.26	0.00

1.3.24 R1H22

Survey Data 1

Face : OP Hole : R1H22 Survey Date : 22-01-18 Dep (m) : 18.00
Average Azimuth (°) : 340.63 Average Inclination (°) : 1.33
Designed Azimuth (°) : 0.00 Designed Inclination (°) : 0.00 Designed Depth (m) : 0.00

Plan View

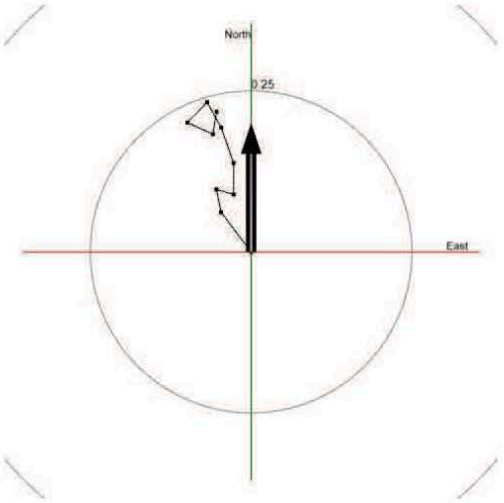

Front View

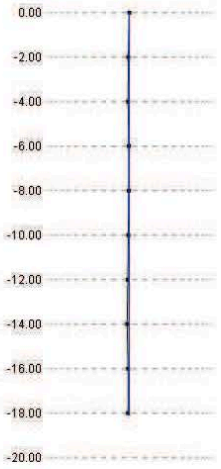

Side View

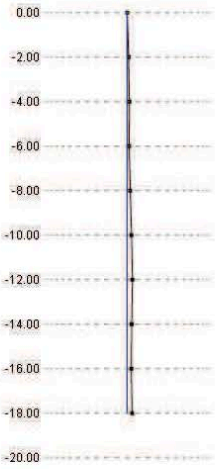

Face : 1 Hole : 24 Rod Increment : 2.00(m) Offset : 0.00(m) Dep : 18.00(m) Grid Magnetic Angle : 0.00(°)

Dep(m)	Heading(°)	Inclination(°)	Dev(m)
2.00	322.81	2.21	0.00
4.00	348.35	1.04	0.00
6.00	106.64	0.80	0.00
8.00	0.16	1.39	0.00
10.00	340.67	1.68	0.00
12.00	330.86	1.29	0.00
14.00	223.96	1.26	0.00
16.00	114.39	1.24	0.00
18.00	9.70	1.01	0.00

1.3.25 R1H23

Survey Data 1

Face : OP Hole : R1H23 Survey Date : 22-01-18 Dep (m) : 18.50
Average Azimuth (°) : 242.65 Average Inclination (°) : 1.25
Designed Azimuth (°) : 0.00 Designed Inclination (°) : 0.00 Designed Depth (m) : 0.00

Plan View

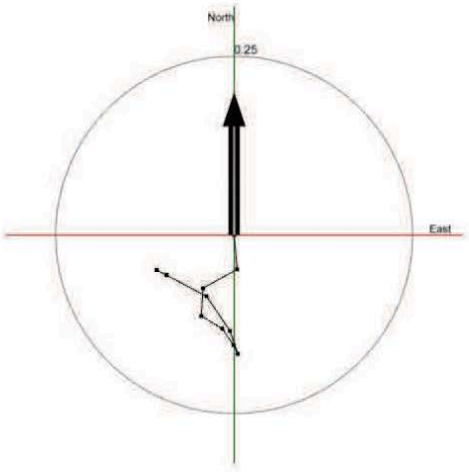

Front View

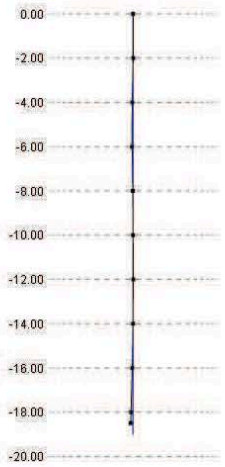

Side View

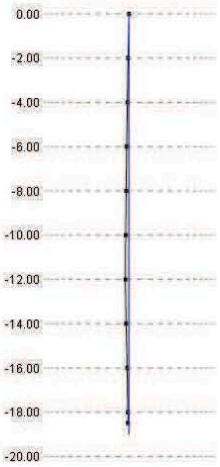

Face : 1 Hole : 25 Rod Increment : 2.00(m) Offset : 1.50(m) Dep : 18.50(m) Grid Magnetic Angle : 0.00(°)

Dep(m)	Heading(°)	Inclination(°)	Dev(m)
2.00	175.07	1.39	0.00
4.00	241.06	1.56	0.00
6.00	183.36	1.11	0.00
8.00	121.43	0.98	0.00
10.00	145.58	0.79	0.00
12.00	153.12	0.40	0.00
14.00	341.17	0.97	0.00
16.00	325.65	1.68	0.00
18.00	297.92	1.82	0.00
18.50	296.84	1.76	0.00

1.3.26 R1H24

Survey Data 1

Face : OP Hole : R1H24 Survey Date : 22-01-18 Dep (m) : 18.00
Average Azimuth (°) : 76.01 Average Inclination (°) : 1.58
Designed Azimuth (°) : 0.00 Designed Inclination (°) : 0.00 Designed Depth (m) : 0.00

Plan View

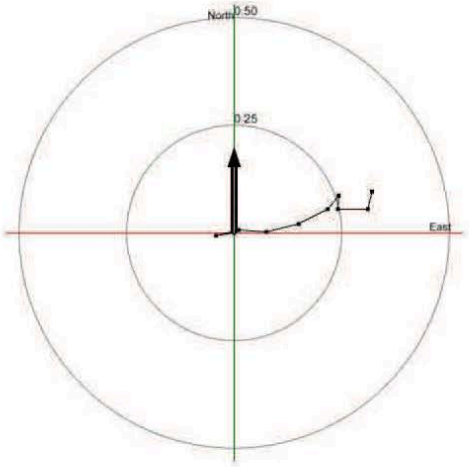

Front View

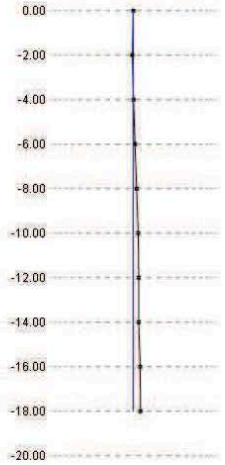

Side View

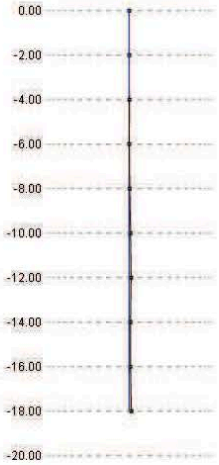

Face : 1 Hole : 26 Rod Increment : 2.00(m) Offset : 0.00(m) Dep : 18.00(m) Grid Magnetic Angle : 0.00(°)

Dep(m)	Heading(°)	Inclination(°)	Dev(m)
2.00	261.67	1.21	0.00
4.00	76.13	1.53	0.00
6.00	93.70	1.87	0.00
8.00	76.11	2.20	0.00
10.00	63.45	2.19	0.00
12.00	39.05	1.14	0.00
14.00	182.86	0.89	0.00
16.00	89.87	1.98	0.00
18.00	13.71	1.21	0.00

1.3.27 R1H25

Survey Data 1

Face : OP Hole : R1H25 Survey Date : 22-01-18 Dep (m) : 18.00
Average Azimuth (°) : 288.97 Average Inclination (°) : 2.03
Designed Azimuth (°) : 0.00 Designed Inclination (°) : 0.00 Designed Depth (m) : 0.00

Plan View

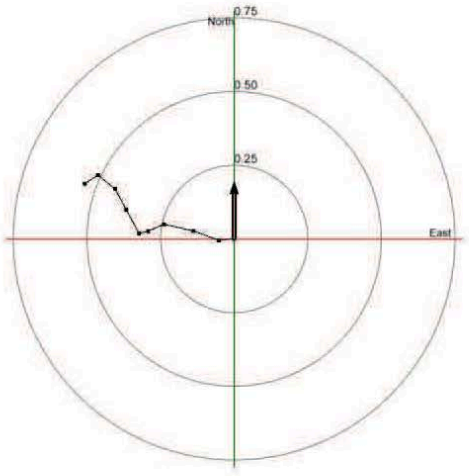

Front View

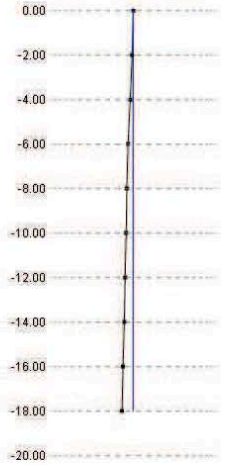

Side View

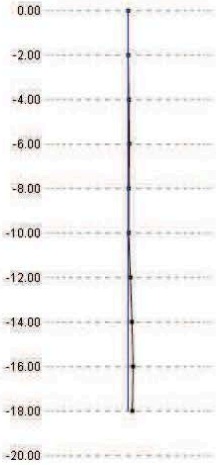

Face : 1 Hole : 27 Rod Increment : 2.00(m) Offset : 0.00(m) Dep : 18.00(m) Grid Magnetic Angle : 0.00(°)

Dep(m)	Heading(°)	Inclination(°)	Dev(m)
2.00	264.81	1.49	0.00
4.00	290.19	2.65	0.00
6.00	282.69	2.93	0.00
8.00	246.40	1.68	0.00
10.00	255.38	0.91	0.00
12.00	331.64	2.63	0.00
14.00	331.76	2.32	0.00
16.00	308.68	2.12	0.00
18.00	237.20	1.55	0.00

1.3.28 R1H26

Survey Data 1

Face : OP Hole : R1H26 Survey Date : 22-01-18 Dep (m) : 18.50
Average Azimuth (°) : 235.25 Average Inclination (°) : 1.52
Designed Azimuth (°) : 0.00 Designed Inclination (°) : 0.00 Designed Depth (m) : 0.00

Plan View

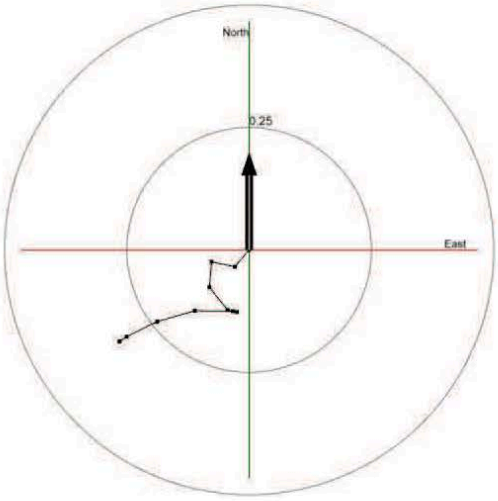

Front View

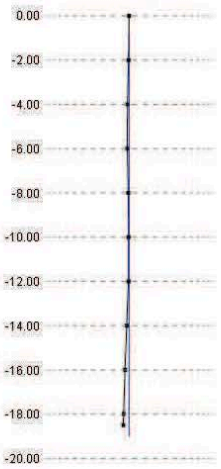

Side View

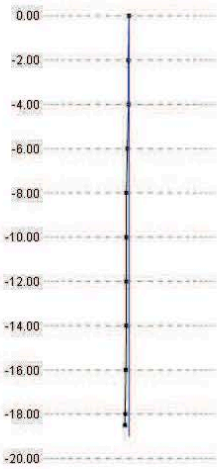

Face : 1 Hole : 28 Rod Increment : 2.00(m) Offset : 1.50(m) Dep : 18.50(m) Grid Magnetic Angle : 0.00(°)

Dep(m)	Heading(°)	Inclination(°)	Dev(m)
2.00	220.34	1.29	0.00
4.00	281.70	1.39	0.00
6.00	184.93	1.49	0.00
8.00	141.10	1.71	0.00
10.00	101.07	0.56	0.00
12.00	280.29	0.25	0.00
14.00	270.53	2.23	0.00
16.00	254.12	2.30	0.00
18.00	243.60	2.00	0.00
18.50	236.82	2.02	0.00

1.3.29 R1H27

Survey Data 1

Face : OP Hole : R1H27 Survey Date : 22-01-18 Dep (m) : 18.00
Average Azimuth (°) : 180.91 Average Inclination (°) : 1.97
Designed Azimuth (°) : 0.00 Designed Inclination (°) : 0.00 Designed Depth (m) : 0.00

Plan View

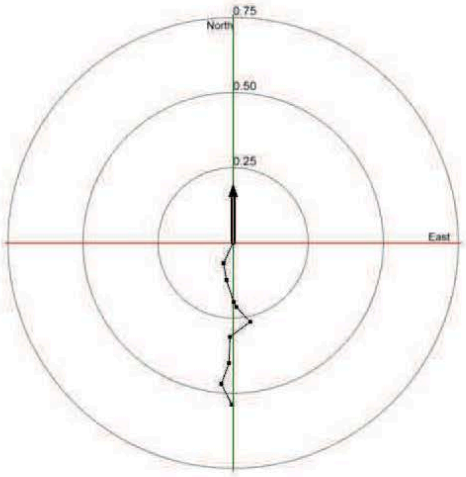

Front View

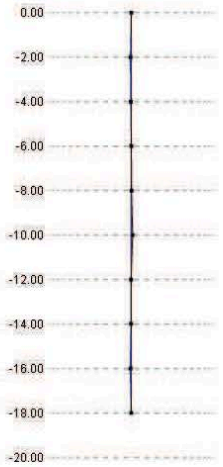

Side View

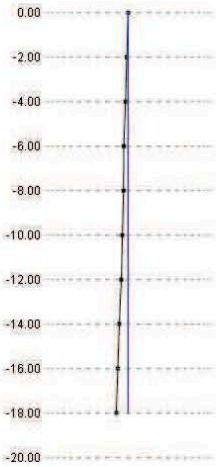

Face : 1 Hole : 29 Rod Increment : 2.00(m) Offset : 0.00(m) Dep : 18.00(m) Grid Magnetic Angle : 0.00(°)

Dep(m)	Heading(°)	Inclination(°)	Dev(m)
2.00	205.60	2.15	0.00
4.00	169.56	1.61	0.00
6.00	162.01	2.21	0.00
8.00	151.97	0.54	0.00
10.00	136.93	1.94	0.00
12.00	233.69	2.39	0.00
14.00	182.31	2.52	0.00
16.00	200.38	2.10	0.00
18.00	153.02	2.23	0.00

1.3.30 R1H28

Survey Data 1

Face : OP Hole : R1H28 Survey Date : 22-01-18 Dep (m) : 18.00
Average Azimuth (°) : 337.33 Average Inclination (°) : 1.34
Designed Azimuth (°) : 0.00 Designed Inclination (°) : 0.00 Designed Depth (m) : 0.00

Plan View

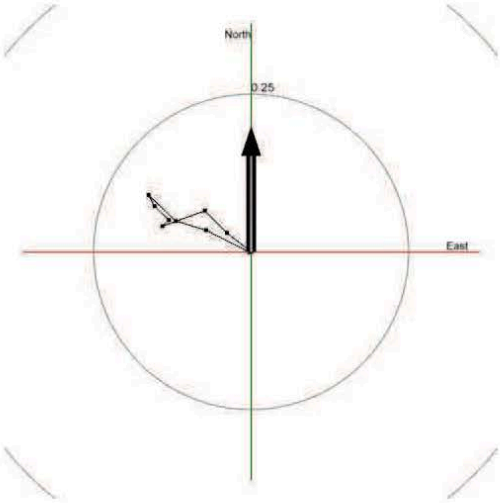

Front View

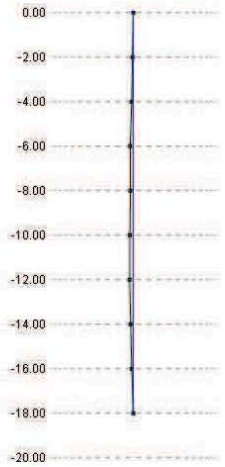

Side View

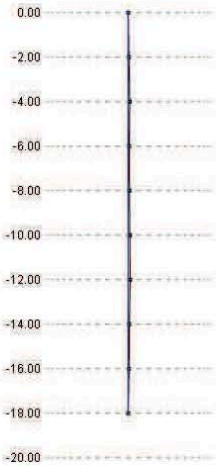

Face : 1 Hole : 30 Rod Increment : 2.00(m) Offset : 0.00(m) Dep : 18.00(m) Grid Magnetic Angle : 0.00(°)

Dep(m)	Heading(°)	Inclination(°)	Dev(m)
2.00	308.05	1.40	0.00
4.00	315.27	1.42	0.00
6.00	250.07	2.05	0.00
8.00	46.88	0.40	0.00
10.00	313.61	0.91	0.00
12.00	332.12	0.58	0.00
14.00	133.73	1.71	0.00
16.00	106.74	1.45	0.00
18.00	116.92	2.19	0.00

1.4 Hole Separation Report

Date : 21-05-18 Time : 10:40 PM Search Interval : 1.00(m) Minimum Found : 0.00(m) At Level of : 810048561943089000000000000

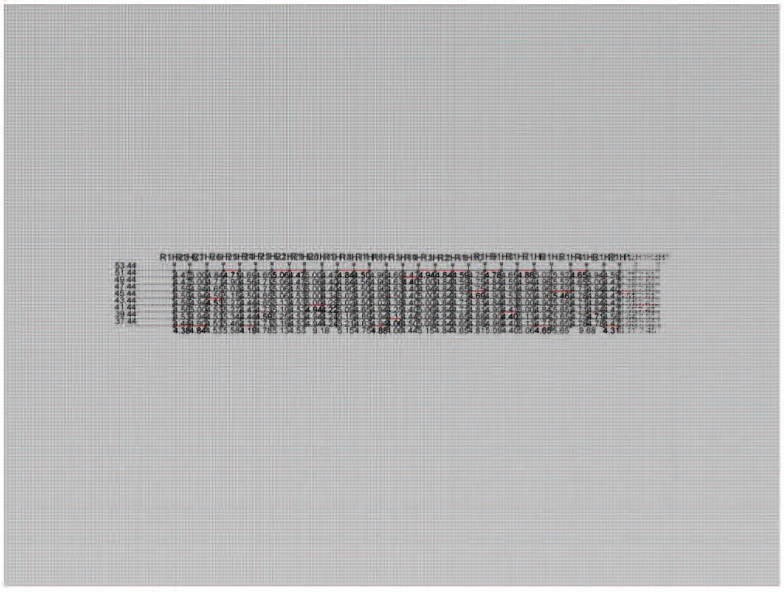

BULK REPORT

RESPONSIBLE PARTY INFORMATION

Date: MAY 23/18 Time In: 7:00

Location: OGDEN Point Time Out: 1:00

Customer: CRM Blaster In Charge: D Ponco

EXPLOSIVE LOADING

Type of Powder Delivered: Titan 1000 65" EM Temperature: 26°C

Pump Rate: 1201 Water Rate: 1.9

Average Density: 1.01 Acid Delivered: 58

Prill Delivered: 6 Sodium Delivered: 53

Fuel Delivered: / % of Fuel in Anfo: /

% of Anfo in Blend: / Average Depth: 60'

Hole Diameter: 4" Computer Total: 11453

Total Eulsion: 11,115

DENSITY CUPS

Density Cup #	Time	Density	Density Cup #	Time	Density
1	8:00	.94	5		
2	8:30	.98	6		
3	9:00	.96	7		
4			8		

BLAST AREA/ACCESS

Access Road Condition: OK Stemming Out/ In Place: OK

Remarks:

Operator: TOM DUCHARME (sign) Tom Duch

Blaster In Charge D Ponco (sign)

Scale In: 11453 KS Scale Out:

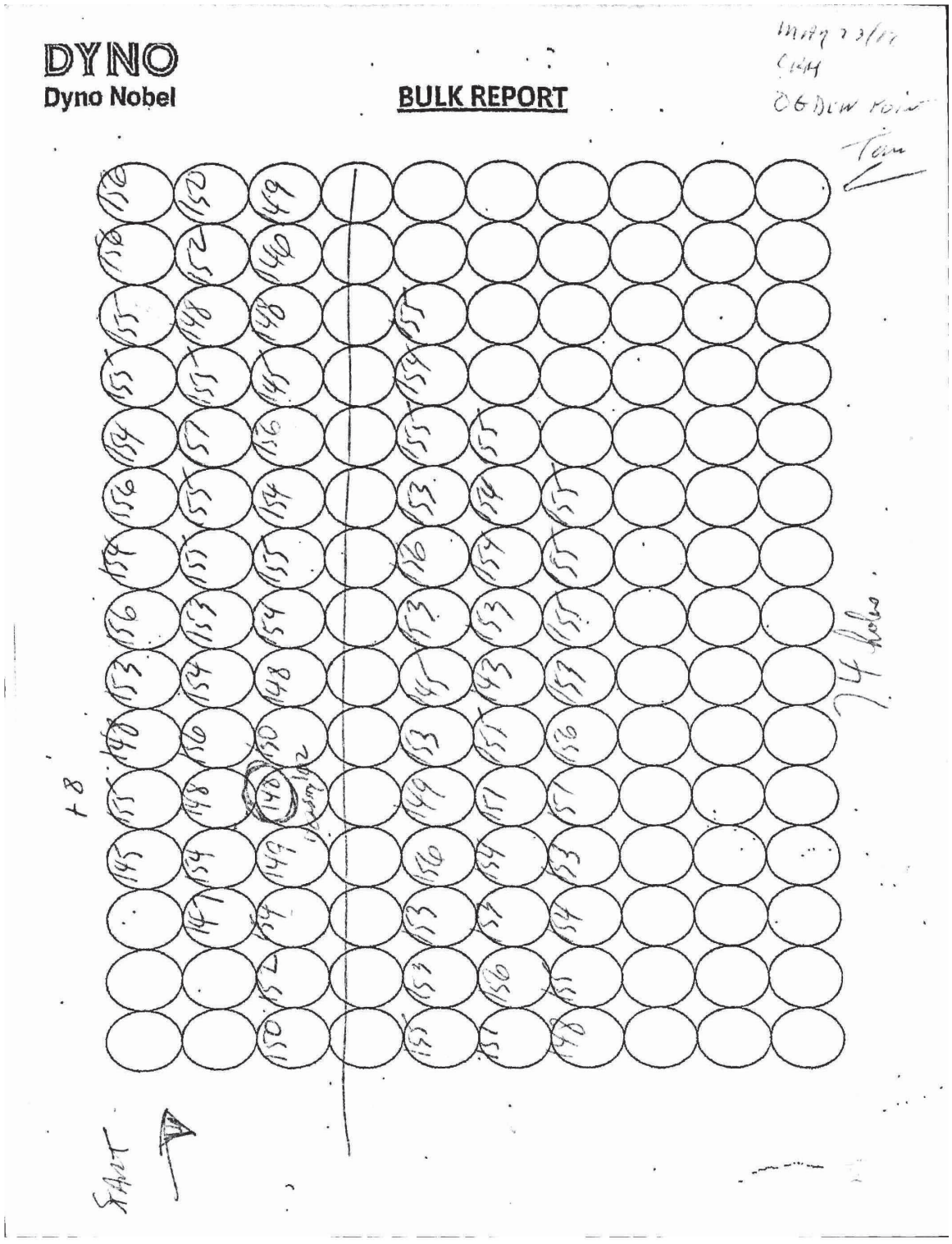
DYNO
Dyno Nobel
BULK REPORT
74 holes
+8
START

BULK REPORT

RESPONSIBLE PARTY INFORMATION

Date: May 23/18 Time In: 12:30

Location: Ogden Rt. Time Out: 2:40

Customer: CRH Blaster In Charge: Dominic Porco

EXPLOSIVE LOADING

Type of Powder Delivered: Titan 1000 EM Temperature: 28.4°

Pump Rate: 720/800 Water Rate: 2.10

Average Density: .98 Acid Delivered: 11

Prill Delivered: — Sodium Delivered: 15

Fuel Delivered: — % of Fuel in Anfo: —

% of Anfo in Blend: — Average Depth: 60'

Hole Diameter: 4.5" Computer Total: 2603

Total Eulsion: 2530

DENSITY CUPS

Density Cup #	Time	Density	Density Cup #	Time	Density
1	1:50	.98	5		
2			6		
3			7		
4			8		

BLAST AREA/ACCESS

Access Road Condition: ✓ Stemming Out/ In Place: ✓

Remarks:

Operator: P Grentile (sign) P Grentile

Blaster in Charge Dominic Porco (sign)

Scale In: Scale Out:

DYNO
Dyno Nobel

BULK REPORT

May 23/18
CRH
Ogden Pt

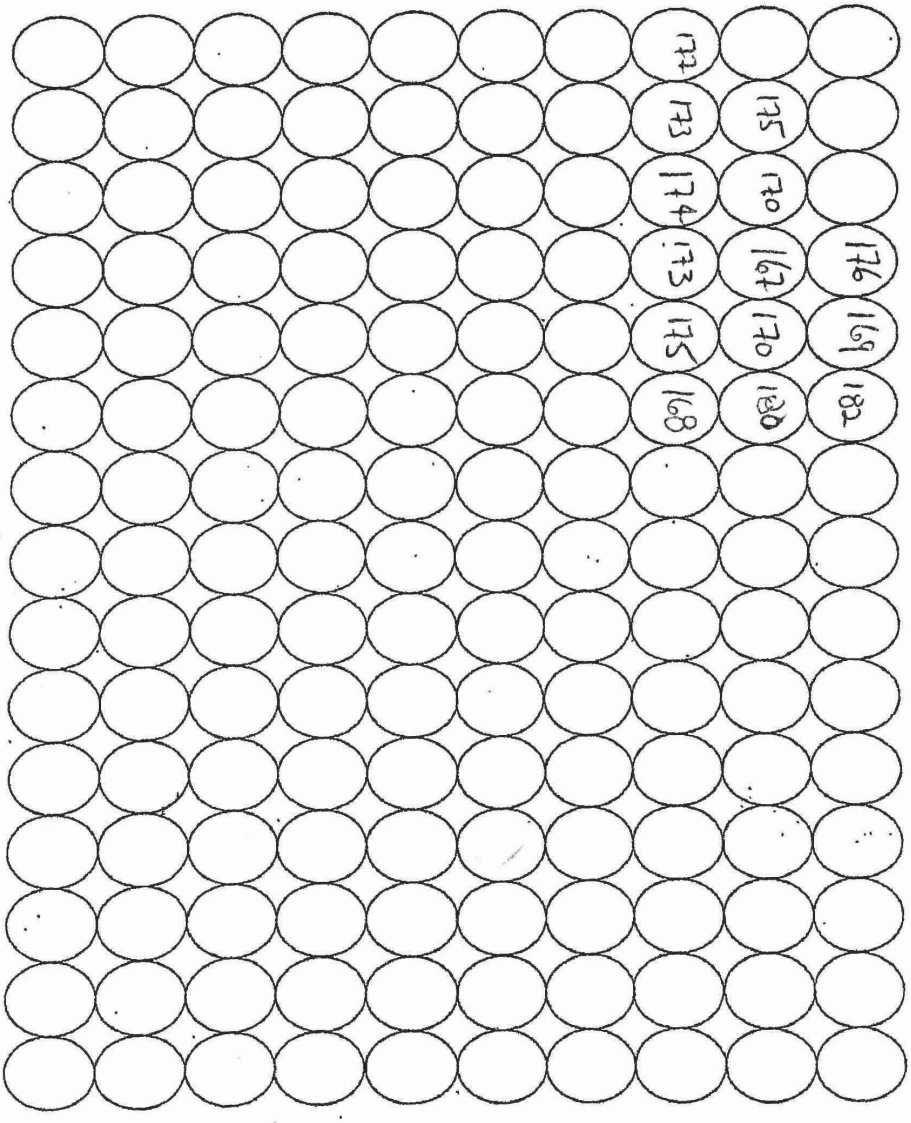

Dyno Nobel North America BLAST REPORT

PO NUMBER: 4500966390

SERVICE SITE LOCATION: Gamebridge ORDER NO.: 0082484709

DYNO Dyno Nobel

BLAST NUMBER: 2018-05 L3 BLAST TIME: 3:18 pm BLAST DATE: 05/24/2018

CUSTOMER: CRH CANADA GROUP INC. MINE: OGDEN POINT QUARRY ADDRESS: Colborne, ON

ROCK TYPE: Limestone ROCK SPECIFIC GRAVITY: 2.65 EXPECTED VIBRATION: 8.000 MMS

LOCATION OF BLAST

LOCATION OF BLAST IN MINE: Northeast BENCH: Level 3

BLAST GPS POINTS: N 043.99361 & W -077.87306

WEATHER

WEATHER: Partly Cloudy CEILING: Unlimited TEMPERATURE: 19 C WIND DIRECTION & SPEED: Southwest 14 KPH

NEAREST NON-OWNED STRUCTURE

NAME: OGDEN POINT QUARRY GPS Points: N 043.98417 & W -077.86917

DISTANCE: 1 (KM) DIRECTION: 163°

SEISMOGRAPH DATA

	LOCATION	DISTANCE	GPS POINTS	CALIBRATION DATE
1	OGDEN POINT QUARRY	1 (KM)	N 043.98417 & W -077.86917	03/02/2018

	L	(F)	T	(F)	V	(F)	AIR (db)	SEISMOGRAPH	SERIAL	OPERATOR
1	6.400	51	4.800	57	2.900	43	124.7	MicroMate	UM13456	Asselstine, John

BLAST DATA

		EXPLOSIVES SIZE, TYPE & WEIGHT		
NUMBER OF HOLES (EA)	57	SIZE	TYPE	WEIGHT
HOLE DIAMETER (CM)	10	BULK	TITAN XL 1000 G	8,997
HOLE DEPTH (M)	18.2	0.34 KG	SPARTAN 350	39
FACE HEIGHT (M)				
SUB DRILLING (M)	0			
AVG. STEM FACE HOLES (M)				
STEM OTHER HOLES (M)	2.1			
BURDEN FRONT ROW (M)				
BURDEN OTHER ROWS (M)	3.96 - 4.3			
SPACING FRONT ROW (M)				
SPACING OTHER ROWS (M)	4.72		TOTAL WEIGHT (KG):	9,036

DETONATORS USED IN BLAST: Electronic MATS USED: No STEM TYPE: CLEAN CRUSHED STONE TOTAL DRILL DEPTH: 1,037 (M)

TYPE	MFG	DATE CODE	USED	TYPE	MFG	DATE CODE	USED
DIGISHOT 20FT	Dyno Nobel Global	NA	40	DIGISHOT 30 FT	Dyno Nobel Global	NA	62
DIGISHOT 80FT	Dyno Nobel Global	NA	57	DIGISHOT SURFACE WIRE	Dyno Nobel Global		2
SPARTAN 350	Dyno Nobel Global	NA	159				

M3 IN SHOT: 19,645 SCALED DISTANCE FACTOR: 0 % OF ANFO: 0

TONNES IN SHOT: 52,060 HOLES/DELAY : 0 FUEL OIL % (BULK): 0

MAX KGS/DELAY: 0 MAXIMUM KGS/HOLE: 159

POWDER FACTOR (KGS/MT): 0.17 POWDER FACTOR (KGS/M3): 0.46

BLASTER'S NAME: Asselstine, John BLASTER'S NUMBER & STATE: License 123

BLASTER'S SIGNATURE: SITE SAFETY INSPECTION PERFORMED: Yes

NUMBER OF PERSONNEL ON SITE: 0

REMARKS : BLASTING TOE HOLE DIRECTLY BELOW THE PRODUCTION BLAST ON LEVEL 3 . TOE CONSISTED OF 39 DRILLED HOLES AT 3.5 INCH DIAMETER AND 6 FEET IN DEPTH. BLAST WAS DETONATED 1000 MS AFTER TOE HOLE DETONATED. BLAST DESIGN AND TIMING WAS PROVIDED BY RESPEC CONSULTING. - POST BLAST - BLAST HAD VERY GOOD FRAGMENTATION. NO STEMMING EJECTIONS AND NO FACE VENTING. TOE AREA WAS DEFINITELY TAKEN CARE OF.

START TIME	END TIME	TOTAL TIME	TRUCK NUMBERS
8:30 AM	2:00 PM	05:30	HT0953

Dyno Nobel North America
CUSTOMER NAME: OGDEN POINT QUARRY
BENCH: Level 3
BLASTER'S NAME: Asselstine, John

DIAGRAM
BLAST DATE: 05/24/2018
BLAST NUMBER: 2018-05 L3

DYNO
Dyno Nobel

Shot: 2018-05 L3

Bench: Level 3

Customer: CRH CANADA GROUP INC.

Site: Gamebridge

Load Sheet Report

DYNO
Dyno Nobel

Mine:	OGDEN POINT QUARRY	Shot:	2018-05 L3	Date:	5/24/2018	Time:	3:18PM
Blaster:	Asselstine, John	License:	License 123	Material:	Limestone	Holes:	57
Diameter:	10 (CM)	Burden:	4 (M)	Spacing:	5 (M)	Primers:	114
Exp. Vibration:	8.00 MMS	Fr. Burden:	(M)	Fr. Spacing:	(M)	Total Exp.:	9,036 (KG)
Fuel:	0 (KG)	AN:	0 (KG)	ANFO:	0 (KG)	Emulsion:	8,997 (KG)
Depth:	18.2 (M)	M3:	19,645	Tonnes:	52,060	Kgs/mT:	0.17
Liters of Fuel:	0						
Max KG/Delay:	0 (KG)	Holes / 8ms:	0	Location:	N 043.99361	&	W -077.87306
Temperature:	19° C	Wind Dir:	Southwest	Wind Speed:	14 KPH	Ceiling:	Unlimited
Conditions:	Partly Cloudy			Method of Detonation:	Electronic		
Pre-Blast Inspection Performed:	Yes / No			Initiation:	Electronic		
Load Started:	8:30 AM	Load Ended:	2:00 PM	Total Load Time:	05:30		

Comments: BLASTING TOE HOLE DIRECTLY BELOW THE PRODUCTION BLAST ON LEVEL 3 . TOE CONSISTED OF 39 DRILLED HOLES AT 3.5 INCH DIAMETER AND 6 FEET IN DEPTH. BLAST WAS DETONATED 1000 MS AFTER TOE HOLE DETONATED. BLAST DESIGN AND TIMING WAS PROVIDED BY RESPEC CONSULTING. - POST BLAST - BLAST HAD VERY GOOD FRAGMENTATION. NO STEMMING EJECTIONS AND NO FACE VENTING. TOE AREA WAS DEFINITELY TAKEN CARE OF.

Crew

Name	Hours	Name	Hours

Trucks Used: HT0953

Inventory

Description	Date Code	Out	Description	Date Code	Out
DIGISHOT SURFACE WIRE		2	SPARTAN 350	NA	159
DIGISHOT 20FT	NA	40	DIGISHOT 30 FT	NA	62
DIGISHOT 80FT	NA	57			

Services

Service	Quantity	Service	Quantity

Product Totals

Product	Total (KG)
SPARTAN 350	38.782
TITAN XL 1000 G	8,997.000

Row	Col	Depth	Rise	Stem	Wet?	Product	Hole Total (KG)
A	1	18.2	16.1	2.1	No	SPARTAN 350	0.680
A	1	18.2	16.1	2.1	No	TITAN XL 1000 G	157.842
A	2	18.2	16.1	2.1	No	SPARTAN 350	0.680
A	2	18.2	16.1	2.1	No	TITAN XL 1000 G	157.842
A	3	18.2	16.1	2.1	No	SPARTAN 350	0.680
A	3	18.2	16.1	2.1	No	TITAN XL 1000 G	157.842
A	4	18.2	16.1	2.1	No	SPARTAN 350	0.680
A	4	18.2	16.1	2.1	No	TITAN XL 1000 G	157.842
A	5	18.2	16.1	2.1	No	SPARTAN 350	0.680
A	5	18.2	16.1	2.1	No	TITAN XL 1000 G	157.842
A	6	18.2	16.1	2.1	No	SPARTAN 350	0.680
A	6	18.2	16.1	2.1	No	TITAN XL 1000 G	157.842
A	7	18.2	16.1	2.1	No	SPARTAN 350	0.680
A	7	18.2	16.1	2.1	No	TITAN XL 1000 G	157.842
A	8	18.2	16.1	2.1	No	SPARTAN 350	0.680
A	8	18.2	16.1	2.1	No	TITAN XL 1000 G	157.842
A	9	18.2	16.1	2.1	No	SPARTAN 350	0.680
A	9	18.2	16.1	2.1	No	TITAN XL 1000 G	157.842
A	10	18.2	16.1	2.1	No	SPARTAN 350	0.680
A	10	18.2	16.1	2.1	No	TITAN XL 1000 G	157.842
A	11	18.2	16.1	2.1	No	SPARTAN 350	0.680
A	11	18.2	16.1	2.1	No	TITAN XL 1000 G	157.842
A	12	18.2	16.1	2.1	No	SPARTAN 350	0.680
A	12	18.2	16.1	2.1	No	TITAN XL 1000 G	157.842
A	13	18.2	16.1	2.1	No	SPARTAN 350	0.680
A	13	18.2	16.1	2.1	No	TITAN XL 1000 G	157.842
A	14	18.2	16.1	2.1	No	SPARTAN 350	0.680
A	14	18.2	16.1	2.1	No	TITAN XL 1000 G	157.842
A	15	18.2	16.1	2.1	No	SPARTAN 350	0.680
A	15	18.2	16.1	2.1	No	TITAN XL 1000 G	157.842
A	16	18.2	16.1	2.1	No	SPARTAN 350	0.680
A	16	18.2	16.1	2.1	No	TITAN XL 1000 G	157.842
A	17	18.2	16.1	2.1	No	SPARTAN 350	0.680
A	17	18.2	16.1	2.1	No	TITAN XL 1000 G	157.842
A	18	18.2	16.1	2.1	No	SPARTAN 350	0.680
A	18	18.2	16.1	2.1	No	TITAN XL 1000 G	157.842
A	19	18.2	16.1	2.1	No	SPARTAN 350	0.680
A	19	18.2	16.1	2.1	No	TITAN XL 1000 G	157.842
A	20	18.2	16.1	2.1	No	SPARTAN 350	0.680
A	20	18.2	16.1	2.1	No	TITAN XL 1000 G	157.842
B	1	18.2	16.1	2.1	No	SPARTAN 350	0.680

B	1	18.2	16.1	2.1	No	TITAN XL 1000 G	157.842
B	2	18.2	16.1	2.1	No	SPARTAN 350	0.680
B	2	18.2	16.1	2.1	No	TITAN XL 1000 G	157.842
B	3	18.2	16.1	2.1	No	SPARTAN 350	0.680
B	3	18.2	16.1	2.1	No	TITAN XL 1000 G	157.842
B	4	18.2	16.1	2.1	No	SPARTAN 350	0.680
B	4	18.2	16.1	2.1	No	TITAN XL 1000 G	157.842
B	5	18.2	16.1	2.1	No	SPARTAN 350	0.680
B	5	18.2	16.1	2.1	No	TITAN XL 1000 G	157.842
B	6	18.2	16.1	2.1	No	SPARTAN 350	0.680
B	6	18.2	16.1	2.1	No	TITAN XL 1000 G	157.842
B	7	18.2	16.1	2.1	No	SPARTAN 350	0.680
B	7	18.2	16.1	2.1	No	TITAN XL 1000 G	157.842
B	8	18.2	16.1	2.1	No	SPARTAN 350	0.680
B	8	18.2	16.1	2.1	No	TITAN XL 1000 G	157.842
B	9	18.2	16.1	2.1	No	SPARTAN 350	0.680
B	9	18.2	16.1	2.1	No	TITAN XL 1000 G	157.842
B	10	18.2	16.1	2.1	No	SPARTAN 350	0.680
B	10	18.2	16.1	2.1	No	TITAN XL 1000 G	157.842
B	11	18.2	16.1	2.1	No	SPARTAN 350	0.680
B	11	18.2	16.1	2.1	No	TITAN XL 1000 G	157.842
B	12	18.2	16.1	2.1	No	SPARTAN 350	0.680
B	12	18.2	16.1	2.1	No	TITAN XL 1000 G	157.842
B	13	18.2	16.1	2.1	No	SPARTAN 350	0.680
B	13	18.2	16.1	2.1	No	TITAN XL 1000 G	157.842
B	14	18.2	16.1	2.1	No	SPARTAN 350	0.680
B	14	18.2	16.1	2.1	No	TITAN XL 1000 G	157.842
B	15	18.2	16.1	2.1	No	SPARTAN 350	0.680
B	15	18.2	16.1	2.1	No	TITAN XL 1000 G	157.842
B	16	18.2	16.1	2.1	No	SPARTAN 350	0.680
B	16	18.2	16.1	2.1	No	TITAN XL 1000 G	157.842
B	17	18.2	16.1	2.1	No	SPARTAN 350	0.680
B	17	18.2	16.1	2.1	No	TITAN XL 1000 G	157.842
B	18	18.2	16.1	2.1	No	SPARTAN 350	0.680
B	18	18.2	16.1	2.1	No	TITAN XL 1000 G	157.842
B	19	18.2	16.1	2.1	No	SPARTAN 350	0.680
B	19	18.2	16.1	2.1	No	TITAN XL 1000 G	157.842
C	1	18.2	16.1	2.1	No	SPARTAN 350	0.680
C	1	18.2	16.1	2.1	No	TITAN XL 1000 G	157.842
C	2	18.2	16.1	2.1	No	SPARTAN 350	0.680
C	2	18.2	16.1	2.1	No	TITAN XL 1000 G	157.842
C	3	18.2	16.1	2.1	No	SPARTAN 350	0.680
C	3	18.2	16.1	2.1	No	TITAN XL 1000 G	157.842

C	4	18.2	16.1	2.1	No	SPARTAN 350	0.680
C	4	18.2	16.1	2.1	No	TITAN XL 1000 G	157.842
C	5	18.2	16.1	2.1	No	SPARTAN 350	0.680
C	5	18.2	16.1	2.1	No	TITAN XL 1000 G	157.842
C	6	18.2	16.1	2.1	No	SPARTAN 350	0.680
C	6	18.2	16.1	2.1	No	TITAN XL 1000 G	157.842
C	7	18.2	16.1	2.1	No	SPARTAN 350	0.680
C	7	18.2	16.1	2.1	No	TITAN XL 1000 G	157.842
C	8	18.2	16.1	2.1	No	SPARTAN 350	0.680
C	8	18.2	16.1	2.1	No	TITAN XL 1000 G	157.842
C	9	18.2	16.1	2.1	No	SPARTAN 350	0.680
C	9	18.2	16.1	2.1	No	TITAN XL 1000 G	157.842
C	10	18.2	16.1	2.1	No	SPARTAN 350	0.680
C	10	18.2	16.1	2.1	No	TITAN XL 1000 G	157.842
C	11	18.2	16.1	2.1	No	SPARTAN 350	0.680
C	11	18.2	16.1	2.1	No	TITAN XL 1000 G	157.842
C	12	18.2	16.1	2.1	No	SPARTAN 350	0.680
C	12	18.2	16.1	2.1	No	TITAN XL 1000 G	157.842
C	13	18.2	16.1	2.1	No	SPARTAN 350	0.680
C	13	18.2	16.1	2.1	No	TITAN XL 1000 G	157.842
C	14	18.2	16.1	2.1	No	SPARTAN 350	0.680
C	14	18.2	16.1	2.1	No	TITAN XL 1000 G	157.842
C	15	18.2	16.1	2.1	No	SPARTAN 350	0.680
C	15	18.2	16.1	2.1	No	TITAN XL 1000 G	157.842
C	16	18.2	16.1	2.1	No	SPARTAN 350	0.680
C	16	18.2	16.1	2.1	No	TITAN XL 1000 G	157.842
C	17	18.2	16.1	2.1	No	SPARTAN 350	0.680
C	17	18.2	16.1	2.1	No	TITAN XL 1000 G	157.842
C	18	18.2	16.1	2.1	No	SPARTAN 350	0.680
C	18	18.2	16.1	2.1	No	TITAN XL 1000 G	157.842

Blaster's Pre/Post-Blast Checklist

DYNO Dyno Nobel

Customer: CRH CANADA GROUP INC. **Shot Number:** 2018-05 L3

Mine: OGDEN POINT QUARRY **Location:** Level 3

Blaster: Asselstine, John **Date:** 5/24/2018 3:18PM

1. Pre-Blast Checks	
1. Performed a pre-use inspection of all equipment and vehicles?	Yes
2. Sign in and notify the mine management that we are on site and ready to load shot?	Yes
3. Reviewed drilling log?	Yes
4. Reviewed seismic report from previous blast in this area?	Yes
5. Confirmed seismic monitoring and instrument placement for this shot?	Yes
6. Inspected the blast area for personnel or equipment working, broken down or other items that need to be addressed before loading?	Yes
7. Established blast site security and high wall safety zone by use of cones, markers, tape blasting signs or yellow blasting men?	Yes
8. Inspected the face for cracks, caves, overhangs or light burden area?	Yes
9. Inspected the blast site surface for cracks, slippery conditions and highwall hazards?	Yes
10. Checked for stray current, if applicable?	Yes
11. Placed stemming next to holes?	Yes
12. Checked actual layout versus diagram and measured burden and spacing at various points within the shot?	Yes
13. Held a tailgate meeting with the crew to assign duties and discuss the specifics of the shot?	Yes
14. Tape and check holes for proper depth, blockage and water?	Yes
15. Profile front row of holes for burden?	Yes
16. Calculated expected vibration at nearest non-company owned structure?	Yes
17. Expected Vibration IPS:	8
18. Structure or Seismograph:	Gate

2. Loading Checks	
1. Adjusted front row loading to prevent excessive face movement?	Yes
2. Cleared blast site of unnecessary personnel and equipment?	Yes
3. Completed final inspection of blast to check for proper initiation sequence?	Yes
4. Each connection physically checked by Blaster in charge and helper?	Yes
5. Blaster:	John Asselstine
6. Helper:	Erin Osbourne
7. Established setback markers and noted distance?	Yes
8. Set blast time, cleared safety zone, posted guards and established communication with them?	Yes
9. Protection provided for blaster and observers?	Yes

3. Post-Blast Checks	
1. Waited for fumes to clear and checked for misfire?	Yes
2. Given "All Clear" signal?	Yes
3. Reviewed seismic data and compared the expected versus actual?	Yes
4. Reviewed video of shot?	Yes
5. Completed blast report?	Yes
6. Back break distance:	0

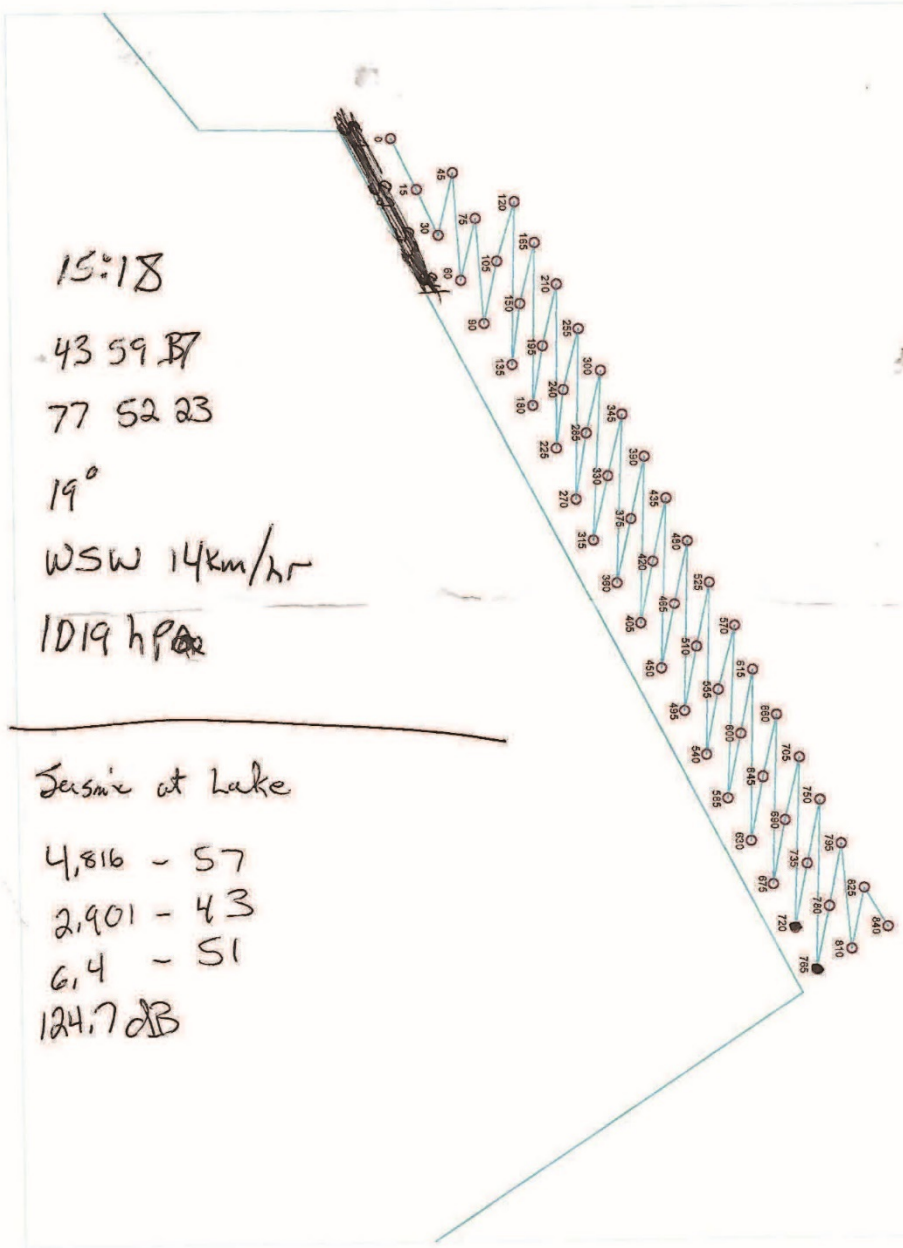
15:18
43 59 B7
77 52 23
19°
WSW 14km/hr
1019 hPa
Seismic at Lake
4,816 - 57
2,901 - 43
6,4 - 51
124.7 dB

BULK REPORT

RESPONSIBLE PARTY INFORMATION

Date: May 24/18 Time In: 7:15

Location: OGDEN Point Quarry Time Out: 1-15

Customer: CRM Blaster In Charge: JOHN ASSELSTINE

EXPLOSIVE LOADING

Type of Powder Delivered: TITAN 1000(G) EM Temperature: 33°C

Pump Rate: 120 Water Rate: 1.9

Average Density: .97 Acid Delivered: 29

Prill Delivered: / Sodium Delivered: 43

Fuel Delivered: / % of Fuel in Anfo: /

% of Anfo in Blend: / Average Depth: 60

Hole Diameter: 4 11 Computer Total: 8997

Total Eulsion: 8748

DENSITY CUPS

Density Cup #	Time	Density	Density Cup #	Time	Density
1	8:30	1.00	5		
2	9:00	.97	6		
3	9:20	98.5	7		
4			8		

BLAST AREA/ACCESS

Access Road Condition: OK Stemming Out/ In Place: OK

Remarks: _____

Operator: Tom DESROCHERS (sign) _____

Blaster in Charge JOHN ASSELSTINE (sign) _____

Scale In: _____ 8997 Kg Scale Out: _____

DYNO
Dyno Nobel

BULK REPORT

OGDEN Point
MAY 24/18
CRM

Tom

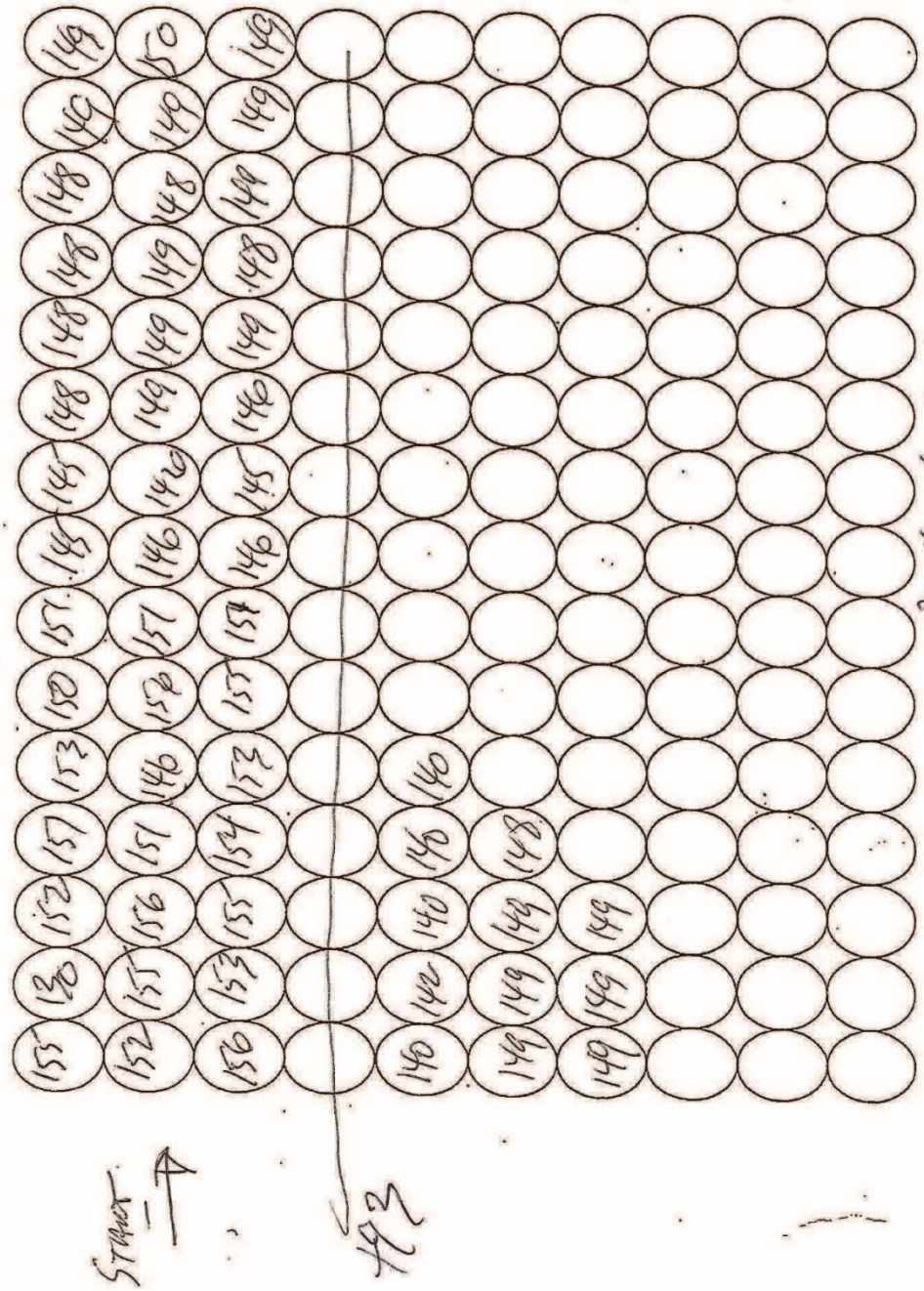

Survey report
Hole deviation

DYNO Dyno Nobel

SURVEY PARAMETERS

CUSTOMER	CRH Dufferin
LOCATION	Colborne, ON
OPERATOR	Brad Asselstine

SURVEY ID	R1H1
SURVEY NAME	Ogden Point Deviation
SURVEY RUN ON	May 23, 2018

TOOL	PeeWee, Devico
SERIAL NUMBER	8297

Mag.Decl.	0
Northing	0.00
Easting	0.00
Elevation	0.00

HOLE DEVIATION PLOT

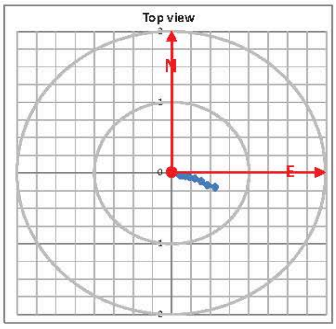

RECORDED DATA

Depth (m)	North. (m)	East. (m)	Elev. (m)	Temp. (°C)
0	0	0	21.3	21.3
1.8	-0.03	0.1	21.1	21.1
3.7	-0.03	0.12	21.1	21.1
5.5	-0.03	0.14	21.3	21.3
7.3	-0.04	0.18	21.1	21.1
9.1	-0.06	0.23	20.6	20.6
11	-0.08	0.3	20.2	20.2
12.8	-0.12	0.38	19	19
14.6	-0.17	0.46	17.3	17.3
16.5	-0.2	0.56	15.9	15.9

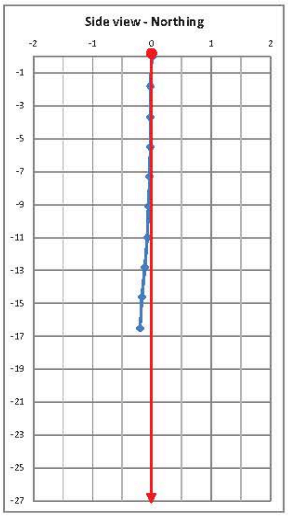

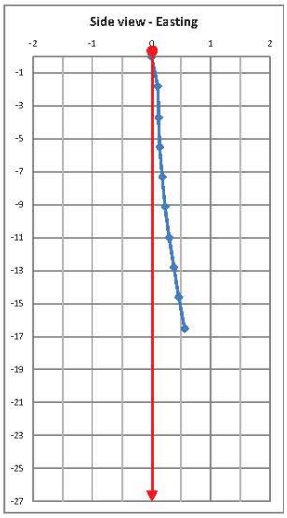

NOTES

BLAST LAYOUT

Not to scale

Survey report
Hole deviation

DYNO Dyno Nobel

SURVEY PARAMETERS

CUSTOMER	CRH Dufferin
LOCATION	Colborne, ON
OPERATOR	Brad Asselstine

SURVEY ID	R1H2
SURVEY NAME	Ogden Point Deviation
SURVEY RUN ON	May 23, 2018

TOOL	PeeWee, Devico
SERIAL NUMBER	8297

Mag.Decl.	0
Northing	0.00
Easting	0.00
Elevation	0.00

HOLE DEVIATION PLOT

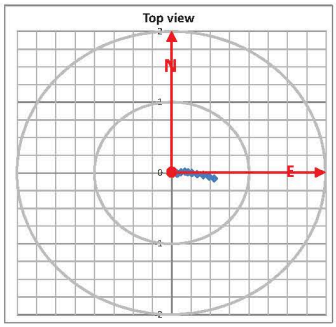

RECORDED DATA

Depth (m)	North. (m)	East. (m)	Elev. (m)	Temp. (°C)
0	0	0	0	12.9
2	-0.01	0.07	-1.83	13.1
4	0.01	0.12	-3.65	13.1
6	0.02	0.17	-5.48	12.7
7	0.01	0.21	-7.31	12.4
9	0	0.26	-9.14	12
11	-0.02	0.33	-10.97	11.7
13	-0.03	0.41	-12.79	11.7
15	-0.05	0.48	-14.62	11.7
17	-0.08	0.55	-16.45	11.5

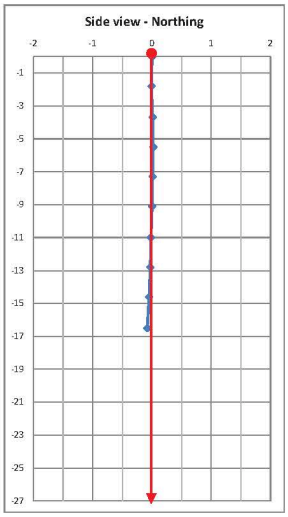

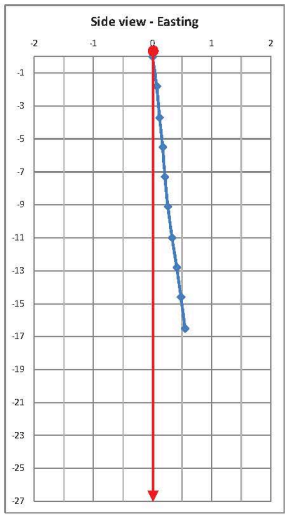

NOTES

BLAST LAYOUT

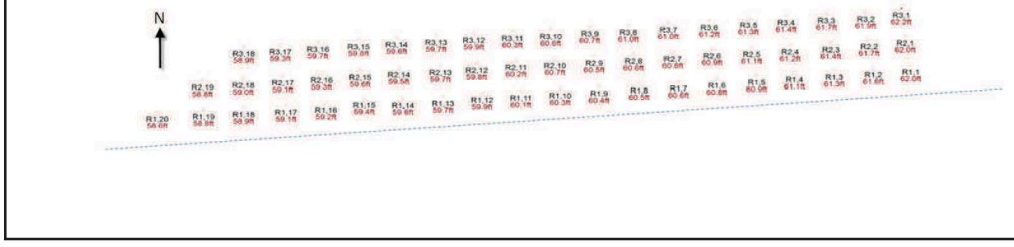

Survey report
Hole deviation

DYNO Dyno Nobel

SURVEY PARAMETERS

CUSTOMER	CRH Dufferin
LOCATION	Colborne, ON
OPERATOR	Brad Asselstine

SURVEY ID	R1H3
SURVEY NAME	Ogden Point Deviation
SURVEY RUN ON	May 23, 2018

TOOL	PeeWee, Devico
SERIAL NUMBER	8297

Mag.Decl.	0
Northing	0.00
Easting	0.00
Elevation	0.00

HOLE DEVIATION PLOT

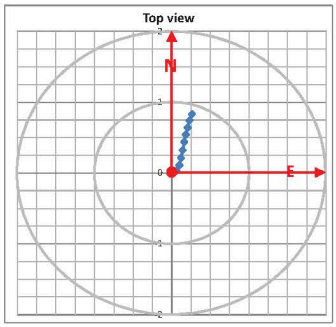

RECORDED DATA

Depth (m)	North. (m)	East. (m)	Elev. (m)	Temp. (°C)
0	0	0	0	11.3
2	0.03	0.06	-1.83	11.3
4	0.11	0.1	-3.65	11.5
6	0.21	0.12	-5.48	11.5
7	0.32	0.14	-7.3	11.5
9	0.44	0.16	-9.13	11.5
11	0.54	0.18	-10.96	11.3
13	0.64	0.21	-12.78	11.3
15	0.74	0.23	-14.61	11.5
17	0.83	0.26	-16.43	11.5

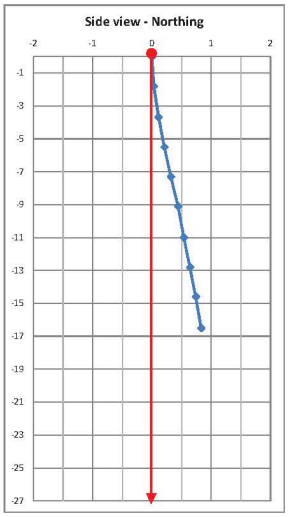

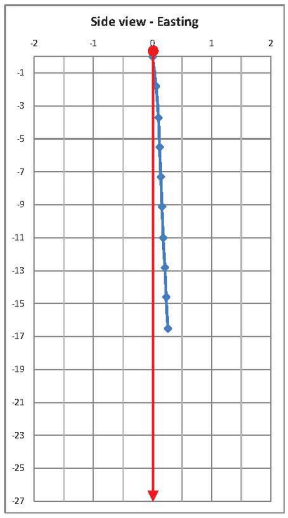

NOTES

BLAST LAYOUT

Not to scale

Survey report
Hole deviation

DYNO Dyno Nobel

SURVEY PARAMETERS

CUSTOMER	CRH Dufferin
LOCATION	Colborne, ON
OPERATOR	Brad Asselstine

SURVEY ID	R1H4
SURVEY NAME	Ogden Point Deviation
SURVEY RUN ON	May 23, 2018

TOOL	PeeWee, Devico
SERIAL NUMBER	8297

Mag.Decl.	0
Northing	0.00
Easting	0.00
Elevation	0.00

HOLE DEVIATION PLOT

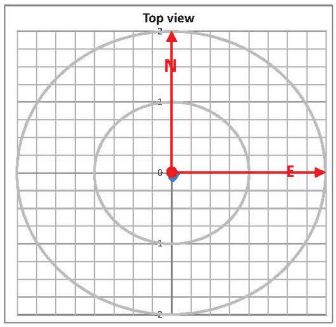

RECORDED DATA

Depth (m)	North. (m)	East. (m)	Elev. (m)	Temp. (°C)
0	0	0	0	11.5
2	-0.02	0.05	-1.83	11.5
4	-0.01	0.05	-3.66	11.7
6	-0.02	0.05	-5.48	11.7
7	-0.03	0.04	-7.31	11.7
9	-0.05	0.03	-9.14	11.5
11	-0.07	0.02	-10.97	11.5
13	-0.07	0.01	-12.8	11.5
15	-0.07	0.01	-14.63	11.5
17	-0.07	0.01	-16.46	11.3

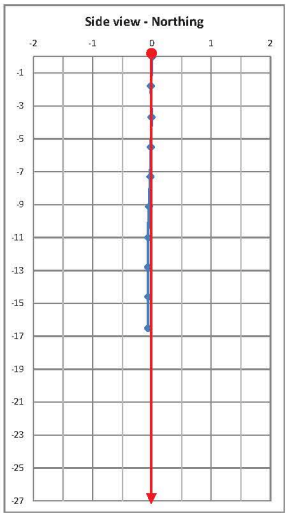

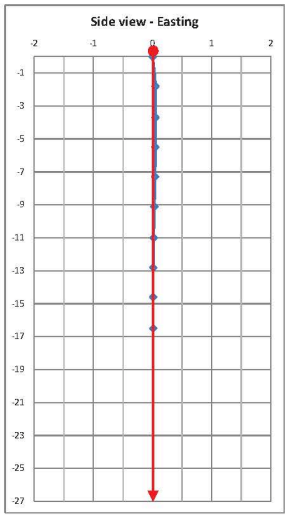

NOTES

BLAST LAYOUT

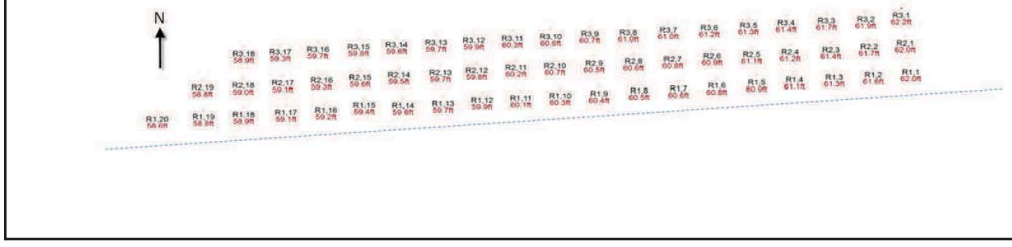

Survey report
Hole deviation

DYNO Dyno Nobel

SURVEY PARAMETERS

CUSTOMER	CRH Dufferin
LOCATION	Colborne, ON
OPERATOR	Brad Asselstine

SURVEY ID	R1H5
SURVEY NAME	Ogden Point Deviation
SURVEY RUN ON	May 23, 2018

TOOL	PeeWee, Devico
SERIAL NUMBER	8297

Mag.Decl.	0
Northing	0.00
Easting	0.00
Elevation	0.00

HOLE DEVIATION PLOT

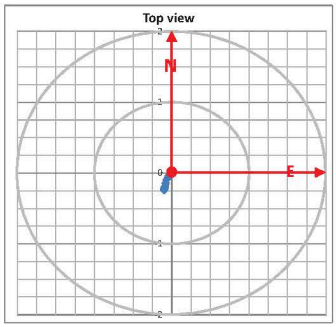

RECORDED DATA

Depth (m)	North. (m)	East. (m)	Elev. (m)	Temp. (°C)
0	0	0	0	11
2	-0.04	-0.04	-1.83	11.3
4	-0.07	-0.05	-3.66	11.3
6	-0.1	-0.07	-5.48	11.5
7	-0.15	-0.08	-7.31	11.3
9	-0.19	-0.09	-9.14	11.5
11	-0.2	-0.09	-10.97	11.3
13	-0.21	-0.09	-12.8	11.3
15	-0.22	-0.1	-14.63	11.5
17	-0.24	-0.1	-16.46	11.3

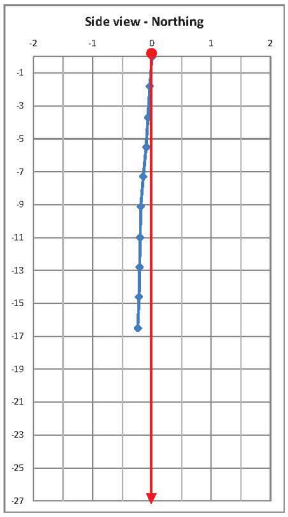

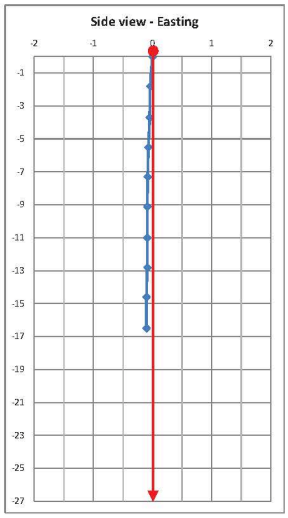

NOTES

BLAST LAYOUT

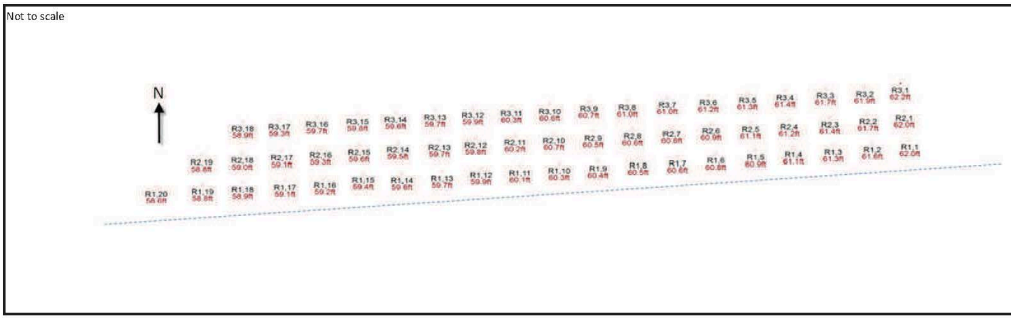

Survey report
Hole deviation

DYNO Dyno Nobel

SURVEY PARAMETERS

CUSTOMER	CRH Dufferin
LOCATION	Colborne, ON
OPERATOR	Brad Asselstine

SURVEY ID	R1H6
SURVEY NAME	Ogden Point Deviation
SURVEY RUN ON	May 23, 2018

TOOL	PeeWee, Devico
SERIAL NUMBER	8297

Mag.Decl.	0
Northing	0.00
Easting	0.00
Elevation	0.00

HOLE DEVIATION PLOT

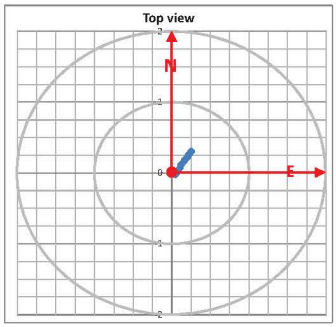

RECORDED DATA

Depth (m)	North. (m)	East. (m)	Elev. (m)	Temp. (°C)
0	0	0	0	19.2
2	-0.02	0.05	-1.83	19.2
4	0.02	0.07	-3.66	19
6	0.06	0.1	-5.48	18.7
7	0.11	0.12	-7.31	17.1
9	0.15	0.15	-9.14	16.6
11	0.19	0.17	-10.97	15.7
13	0.22	0.2	-12.8	14.8
15	0.26	0.22	-14.62	14.3
17	0.3	0.25	-16.45	13.8

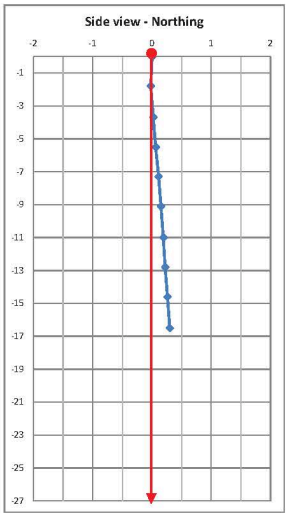

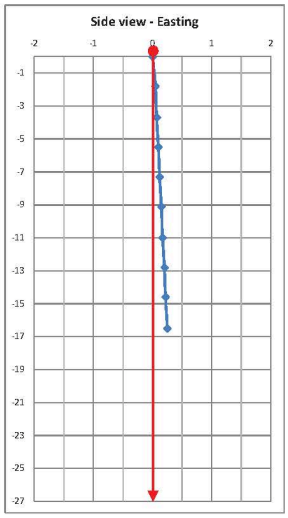

NOTES

BLAST LAYOUT

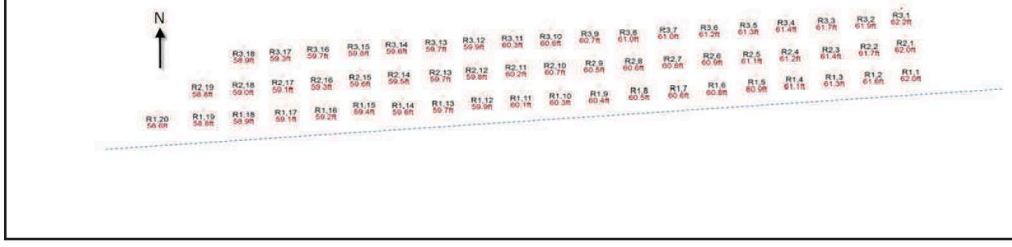

Survey report
Hole deviation

DYNO Dyno Nobel

SURVEY PARAMETERS

CUSTOMER	CRH Dufferin
LOCATION	Colborne, ON
OPERATOR	Brad Asselstine

SURVEY ID	R1H7
SURVEY NAME	Ogden Point Deviation
SURVEY RUN ON	May 23, 2018

TOOL	PeeWee, Devico
SERIAL NUMBER	8297

Mag.Decl.	0
Northing	0.00
Easting	0.00
Elevation	0.00

HOLE DEVIATION PLOT

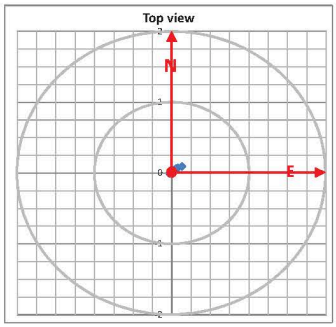

RECORDED DATA

Depth (m)	North. (m)	East. (m)	Elev. (m)	Temp. (°C)
0	0	0	0	11.3
2	-0.01	-0.03	-1.83	11.5
4	0	-0.03	-3.66	11.5
6	0.02	-0.02	-5.49	11.5
7	0.03	-0.01	-7.31	11.3
9	0.04	0.01	-9.14	11
11	0.05	0.03	-10.97	10.8
13	0.06	0.06	-12.8	11
15	0.07	0.08	-14.63	10.8
17	0.09	0.13	-16.46	10.8

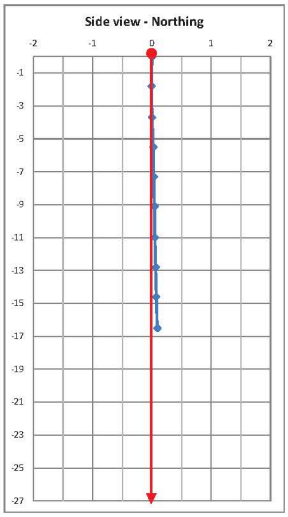

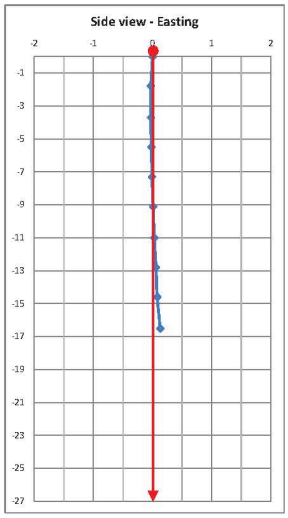

NOTES

BLAST LAYOUT

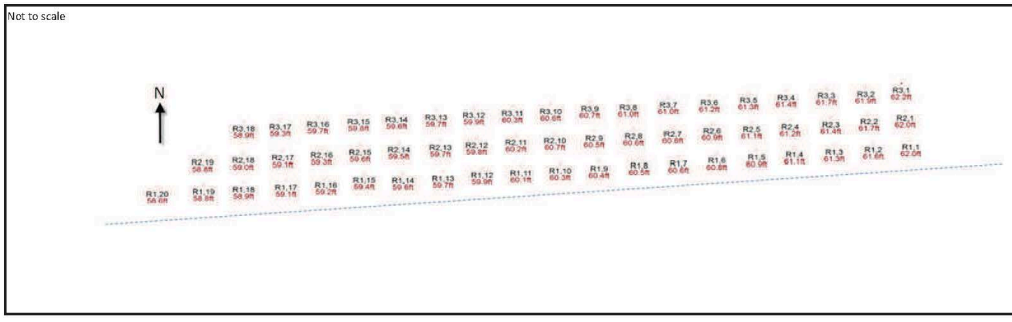

Survey report
Hole deviation

DYNO Dyno Nobel

SURVEY PARAMETERS

CUSTOMER	CRH Dufferin
LOCATION	Colborne, ON
OPERATOR	Brad Asselstine

SURVEY ID	R1H8
SURVEY NAME	Ogden Point Deviation
SURVEY RUN ON	May 23, 2018

TOOL	PeeWee, Devico
SERIAL NUMBER	8297

Mag.Decl.	0
Northing	0.00
Easting	0.00
Elevation	0.00

HOLE DEVIATION PLOT

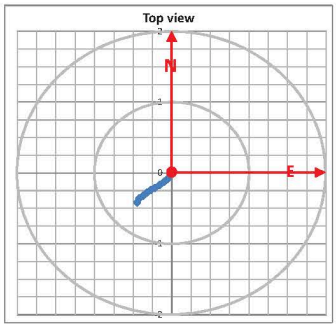

RECORDED DATA

Depth (m)	North. (m)	East. (m)	Elev. (m)	Temp. (°C)	
0	0	0	0	10.5	#
2	-0.09	-0.06	-1.82	10.8	#
4	-0.13	-0.1	-3.65	10.8	#
6	-0.17	-0.16	-5.48	10.8	#
7	-0.21	-0.22	-7.31	10.8	#
9	-0.24	-0.27	-9.13	10.8	#
11	-0.28	-0.32	-10.96	10.8	#
13	-0.32	-0.37	-12.79	10.8	#
15	-0.36	-0.42	-14.62	10.8	#
17	-0.42	-0.45	-16.45	10.8	#

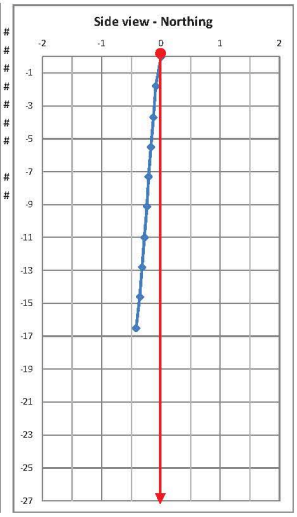

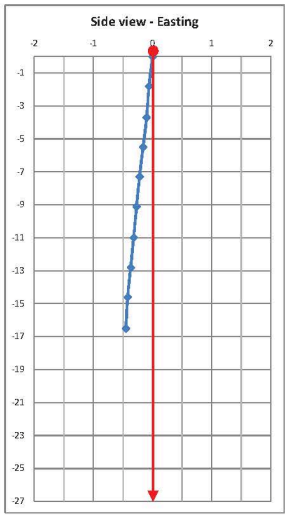

NOTES

BLAST LAYOUT

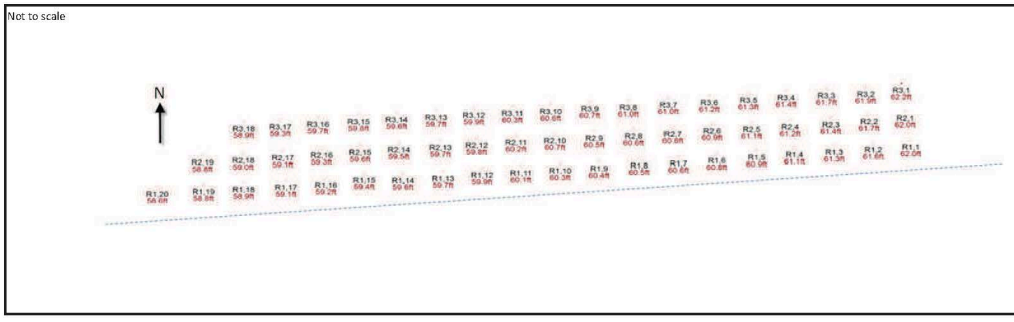

Survey report
Hole deviation

DYNO Dyno Nobel

SURVEY PARAMETERS

CUSTOMER	CRH Dufferin
LOCATION	Colborne, ON
OPERATOR	Brad Asselstine

SURVEY ID	R1H9
SURVEY NAME	Ogden Point Deviation
SURVEY RUN ON	May 23, 2018

TOOL	PeeWee, Devico
SERIAL NUMBER	8297

Mag.Decl.	0
Northing	0.00
Easting	0.00
Elevation	0.00

HOLE DEVIATION PLOT

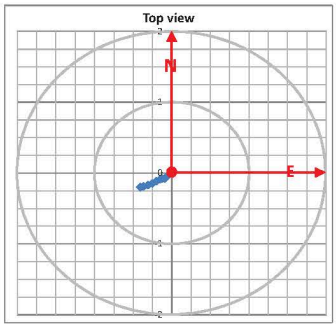

RECORDED DATA

Depth (m)	North. (m)	East. (m)	Elev. (m)	Temp. (°C)	
0	0	0	0	11.3	#
2	-0.06	-0.07	-1.83	11.3	#
4	-0.08	-0.09	-3.65	11.3	#
6	-0.08	-0.12	-5.48	11.5	#
7	-0.09	-0.15	-7.31	11.3	#
9	-0.12	-0.2	-9.14	11.3	#
11	-0.15	-0.25	-10.97	11.5	#
13	-0.17	-0.31	-12.79	11.3	#
15	-0.19	-0.37	-14.62	11.5	#
17	-0.2	-0.41	-16.45	11.5	#

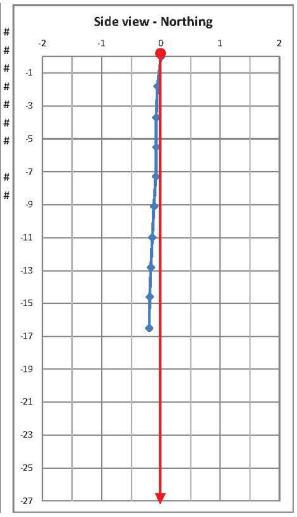

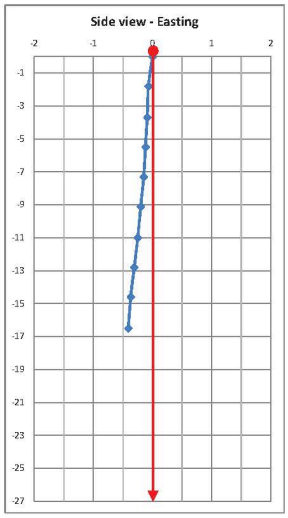

NOTES

BLAST LAYOUT

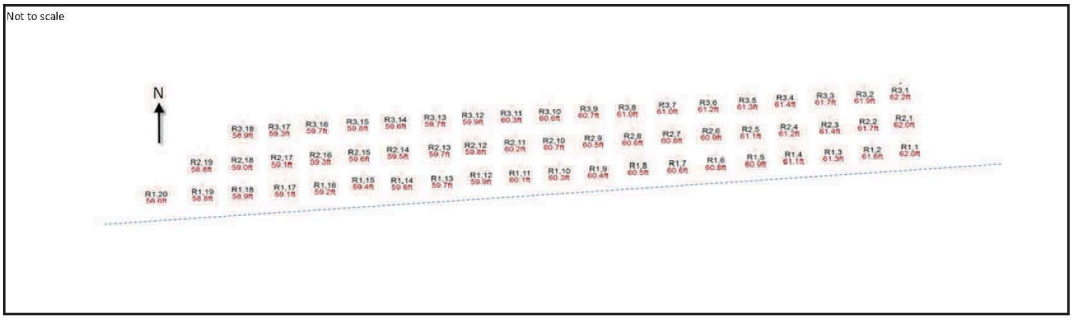

Survey report
Hole deviation

DYNO Dyno Nobel

SURVEY PARAMETERS

CUSTOMER	CRH Dufferin
LOCATION	Colborne, ON
OPERATOR	Brad Asselstine

SURVEY ID	R1H10
SURVEY NAME	Ogden Point Deviation
SURVEY RUN ON	May 23, 2018

TOOL	PeeWee, Devico
SERIAL NUMBER	8297

Mag.Decl.	0
Northing	0.00
Easting	0.00
Elevation	0.00

HOLE DEVIATION PLOT

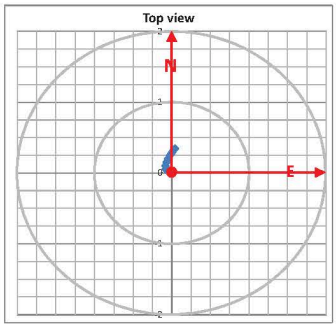

RECORDED DATA

Depth (m)	North. (m)	East. (m)	Elev. (m)	Temp. (°C)
0	0	0	0	11.5
2	0.05	-0.08	-1.82	11.7
4	0.1	-0.08	-3.65	12
6	0.15	-0.07	-5.48	11.7
7	0.2	-0.05	-7.31	12
9	0.24	-0.03	-9.14	11.7
11	0.27	-0.01	-10.96	12
13	0.3	0.01	-12.79	12
15	0.32	0.02	-14.62	12
17	0.34	0.04	-16.45	11.7

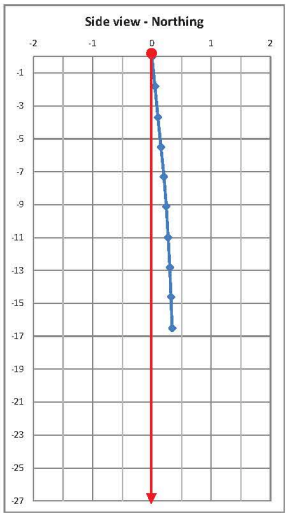

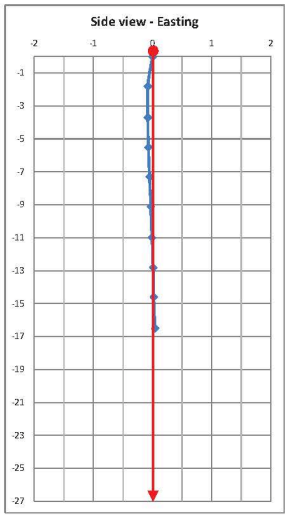

NOTES

BLAST LAYOUT

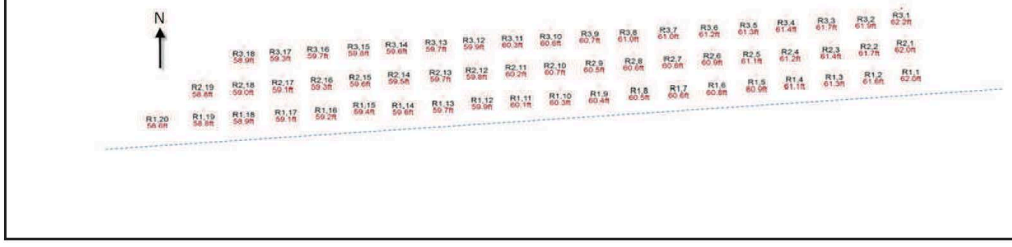

Survey report
Hole deviation

DYNO Dyno Nobel

SURVEY PARAMETERS

CUSTOMER	CRH Dufferin
LOCATION	Colborne, ON
OPERATOR	Brad Asselstine

SURVEY ID	R1H11
SURVEY NAME	Ogden Point Deviation
SURVEY RUN ON	May 23, 2018

TOOL	PeeWee, Devico
SERIAL NUMBER	8297

Mag.Decl.	0
Northing	0.00
Easting	0.00
Elevation	0.00

HOLE DEVIATION PLOT

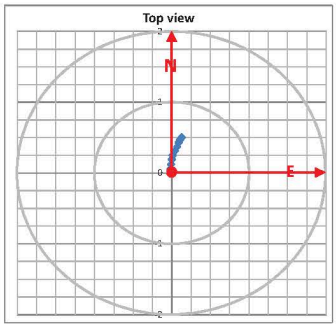

RECORDED DATA

Depth (m)	North. (m)	East. (m)	Elev. (m)	Temp. (°C)
0	0	0	0	12.2
2	0.05	-0.02	-1.83	12.4
4	0.12	-0.01	-3.65	12.2
6	0.19	0	-5.48	12.4
7	0.25	0.01	-7.31	12.2
9	0.31	0.04	-9.14	12.2
11	0.37	0.07	-10.97	12.4
13	0.43	0.09	-12.79	12.4
15	0.47	0.11	-14.62	12.2
17	0.5	0.13	-16.45	12.2

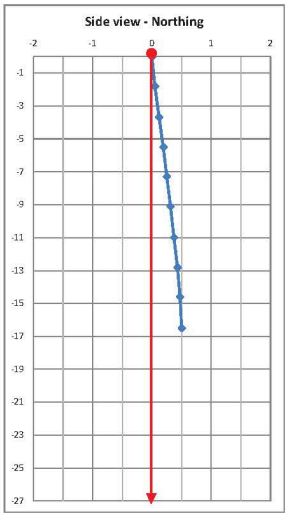

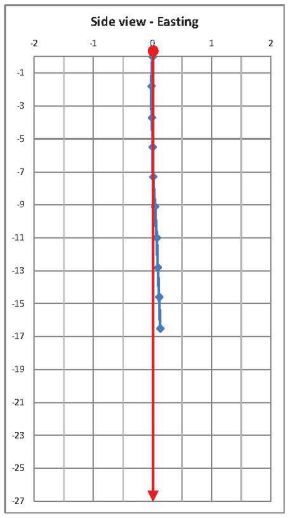

NOTES

BLAST LAYOUT

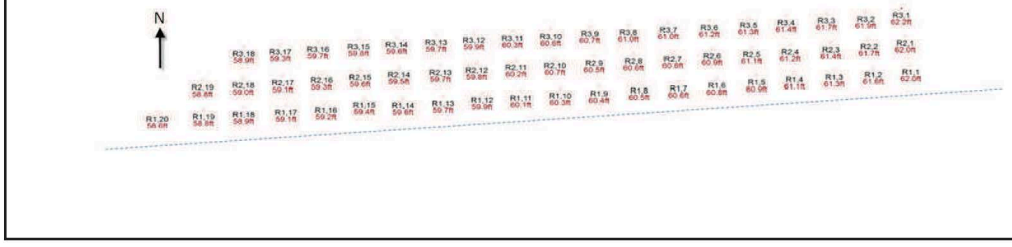

Survey report
Hole deviation

DYNO Dyno Nobel

SURVEY PARAMETERS

CUSTOMER	CRH Dufferin
LOCATION	Colborne, ON
OPERATOR	Brad Asselstine

SURVEY ID	R1H12
SURVEY NAME	Ogden Point Deviation
SURVEY RUN ON	May 23, 2018

TOOL	PeeWee, Devico
SERIAL NUMBER	8297

Mag.Decl.	0
Northing	0.00
Easting	0.00
Elevation	0.00

RECORDED DATA

Depth (m)	North. (m)	East. (m)	Elev. (m)	Temp. (°C)
0	0	0	0	12.7
2	-0.11	0	-1.82	12.7
4	-0.15	0	-3.65	12.7
6	-0.21	0	-5.48	12.7
7	-0.27	-0.01	-7.31	12.7
9	-0.34	-0.01	-9.14	12.9
11	-0.39	0	-10.96	12.7
13	-0.44	0	-12.79	12.7
15	-0.47	0.02	-14.62	12.7
17	-0.51	0.04	-16.45	12.7

HOLE DEVIATION PLOT

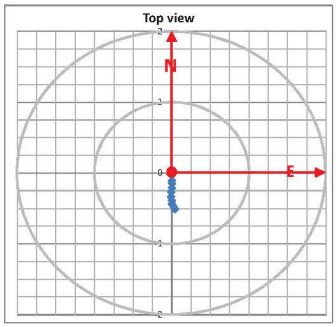

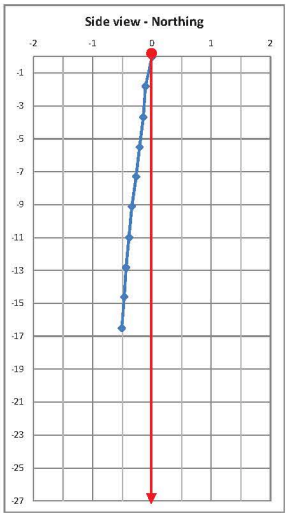

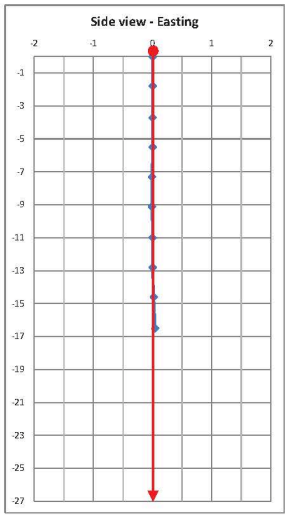

NOTES

BLAST LAYOUT

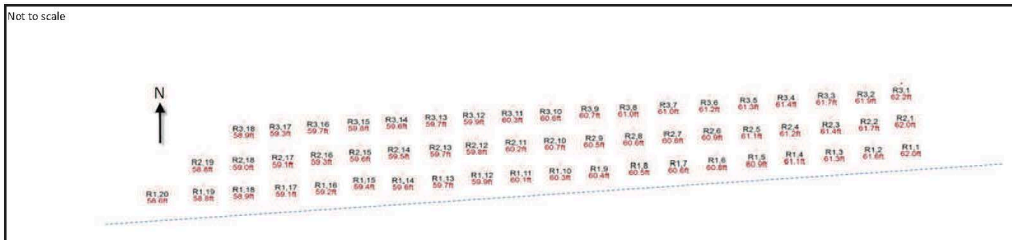

Survey report
Hole deviation

DYNO Dyno Nobel

SURVEY PARAMETERS

CUSTOMER	CRH Dufferin
LOCATION	Colborne, ON
OPERATOR	Brad Asselstine

SURVEY ID	R1H13
SURVEY NAME	Ogden Point Deviation
SURVEY RUN ON	May 23, 2018

TOOL	PeeWee, Devico
SERIAL NUMBER	8297

Mag.Decl.	0
Northing	0.00
Easting	0.00
Elevation	0.00

HOLE DEVIATION PLOT

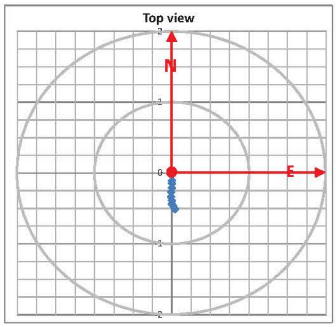

RECORDED DATA

Depth (m)	North. (m)	East. (m)	Elev. (m)	Temp. (°C)
0	0	0	0	12.7
2	-0.11	0	-1.82	12.7
4	-0.15	0	-3.65	12.7
6	-0.21	0	-5.48	12.7
7	-0.27	-0.01	-7.31	12.7
9	-0.34	-0.01	-9.14	12.9
11	-0.39	0	-10.96	12.7
13	-0.44	0	-12.79	12.7
15	-0.47	0.02	-14.62	12.7
17	-0.51	0.04	-16.45	12.7

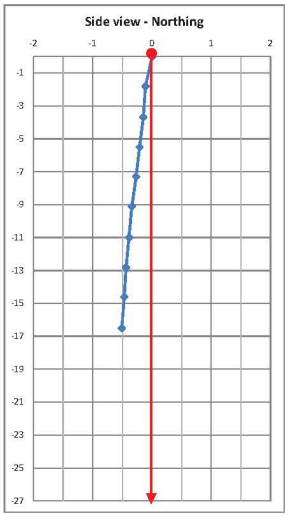

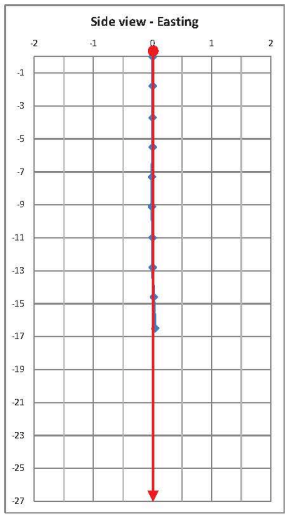

NOTES

BLAST LAYOUT

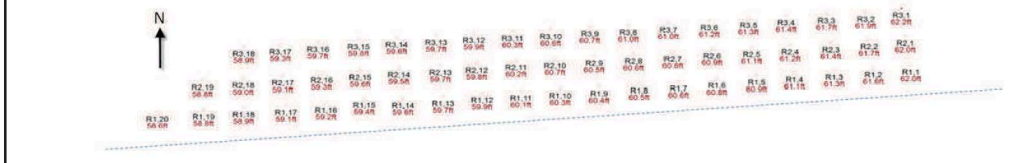

Survey report
Hole deviation

DYNO Dyno Nobel

SURVEY PARAMETERS

CUSTOMER	CRH Dufferin
LOCATION	Colborne, ON
OPERATOR	Brad Asselstine

SURVEY ID	R1H14
SURVEY NAME	Ogden Point Deviation
SURVEY RUN ON	May 23, 2018

TOOL	PeeWee, Devico
SERIAL NUMBER	8297

Mag.Decl.	0
Northing	0.00
Easting	0.00
Elevation	0.00

HOLE DEVIATION PLOT

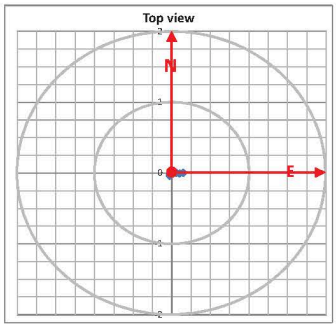

RECORDED DATA

Depth (m)	North. (m)	East. (m)	Elev. (m)	Temp. (°C)
0	0	0	0	12.4
2	-0.04	-0.03	-1.83	12.7
4	-0.04	-0.03	-3.66	12.7
6	-0.02	-0.03	-5.48	12.9
7	-0.01	-0.01	-7.31	12.7
9	0.01	0.01	-9.14	12.7
11	0.02	0.03	-10.97	12.9
13	0	0.06	-12.8	12.7
15	-0.01	0.1	-14.63	12.7
17	0	0.15	-16.46	12.7

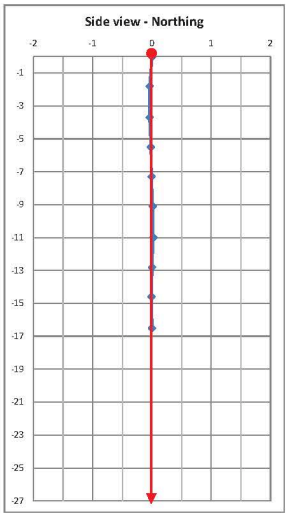

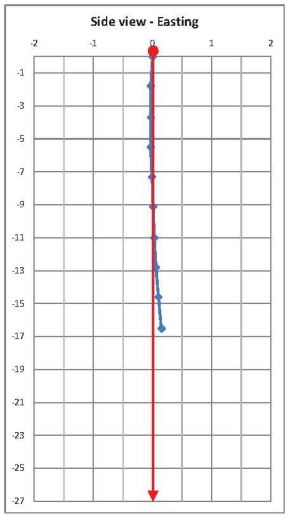

NOTES

BLAST LAYOUT

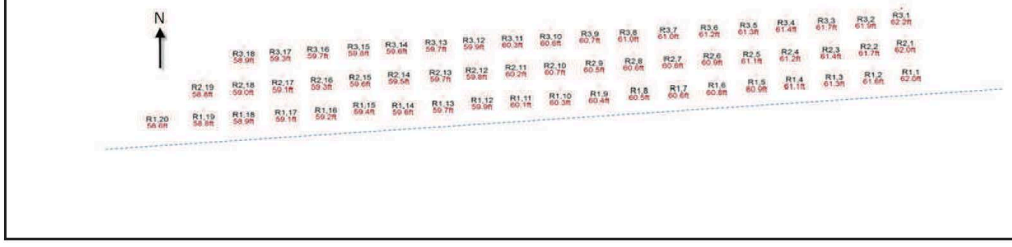

Survey report
Hole deviation

DYNO Dyno Nobel

SURVEY PARAMETERS

CUSTOMER	CRH Dufferin
LOCATION	Colborne, ON
OPERATOR	Brad Asselstine

SURVEY ID	R1H15
SURVEY NAME	Ogden Point Deviation
SURVEY RUN ON	May 23, 2018

TOOL	PeeWee, Devico
SERIAL NUMBER	8297

Mag.Decl.	0
Northing	0.00
Easting	0.00
Elevation	0.00

HOLE DEVIATION PLOT

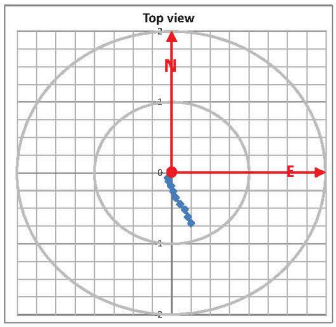

RECORDED DATA

Depth (m)	North. (m)	East. (m)	Elev. (m)	Temp. (°C)
0	0	0	0	12.9
2	-0.07	-0.05	-1.83	12.7
4	-0.12	-0.04	-3.65	12.9
6	-0.18	-0.01	-5.48	12.7
7	-0.26	0.02	-7.31	12.7
9	-0.35	0.05	-9.13	12.9
11	-0.44	0.11	-10.96	12.7
13	-0.52	0.17	-12.79	12.7
15	-0.62	0.21	-14.61	12.7
17	-0.71	0.25	-16.44	12.7

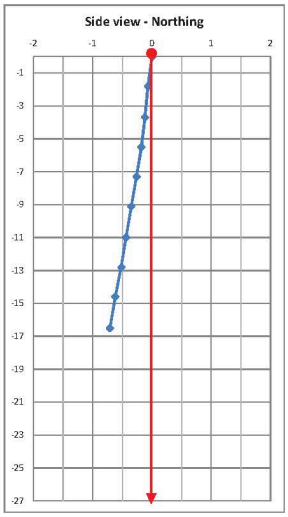

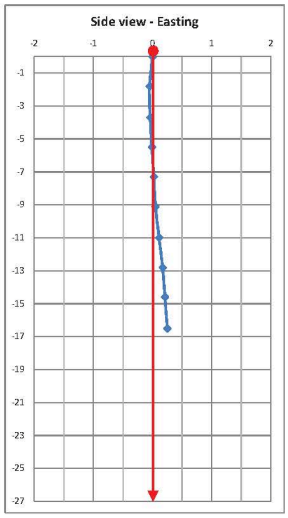

NOTES

BLAST LAYOUT

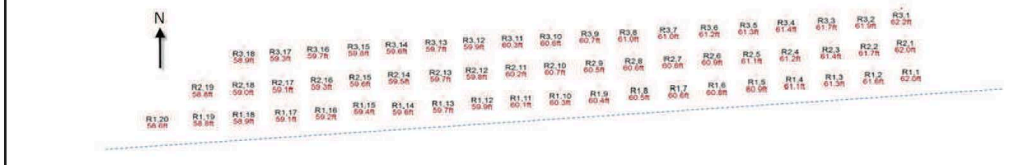

Survey report
Hole deviation

DYNO Dyno Nobel

SURVEY PARAMETERS

CUSTOMER	CRH Dufferin
LOCATION	Colborne, ON
OPERATOR	Brad Asselstine

SURVEY ID	R1H16
SURVEY NAME	Ogden Point Deviation
SURVEY RUN ON	May 23, 2018

TOOL	PeeWee, Devico
SERIAL NUMBER	8297

Mag.Decl.	0
Northing	0.00
Easting	0.00
Elevation	0.00

HOLE DEVIATION PLOT

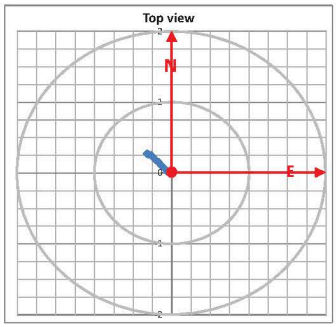

RECORDED DATA

Depth (m)	North. (m)	East. (m)	Elev. (m)	Temp. (°C)
0	0	0	0	18.3
2	0.02	-0.06	-1.83	18.3
4	0.07	-0.1	-3.66	18.5
6	0.11	-0.14	-5.48	18.3
7	0.15	-0.17	-7.31	18.5
9	0.18	-0.21	-9.14	18.3
11	0.22	-0.24	-10.97	18.3
13	0.25	-0.27	-12.8	18.3
15	0.26	-0.3	-14.62	18.3
17	0.27	-0.32	-16.45	18.3

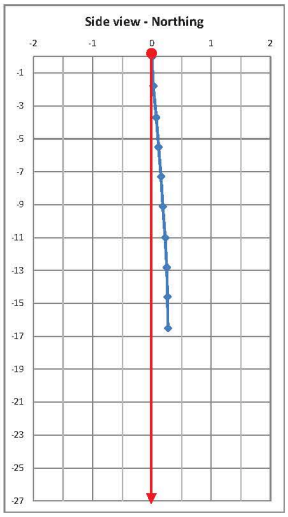

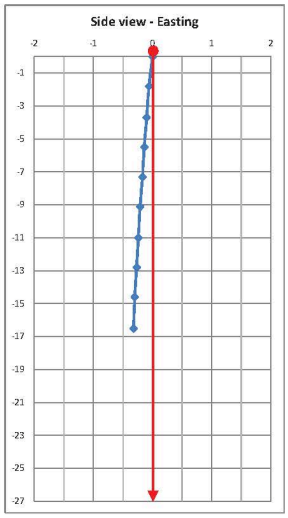

NOTES

BLAST LAYOUT

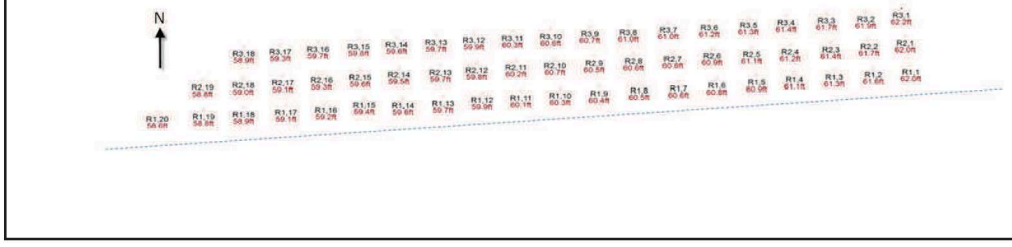

Survey report
Hole deviation

DYNO Dyno Nobel

SURVEY PARAMETERS

CUSTOMER	CRH Dufferin
LOCATION	Colborne, ON
OPERATOR	Brad Asselstine

SURVEY ID	R1H17
SURVEY NAME	Ogden Point Deviation
SURVEY RUN ON	May 23, 2018

TOOL	PeeWee, Devico
SERIAL NUMBER	8297

Mag.Decl.	0
Northing	0.00
Easting	0.00
Elevation	0.00

HOLE DEVIATION PLOT

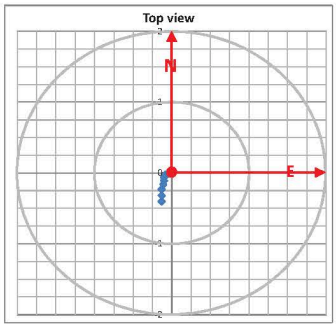

RECORDED DATA

Depth (m)	North. (m)	East. (m)	Elev. (m)	Temp. (°C)
0	0	0	0	18.3
2	-0.03	-0.07	-1.83	18.3
4	-0.03	-0.08	-3.66	18.3
6	-0.03	-0.09	-5.48	18.3
7	-0.06	-0.1	-7.31	18.3
9	-0.11	-0.1	-9.14	18.3
11	-0.16	-0.11	-10.97	18.3
13	-0.23	-0.13	-12.8	18.5
15	-0.32	-0.13	-14.62	18.3
17	-0.4	-0.13	-16.45	18.3

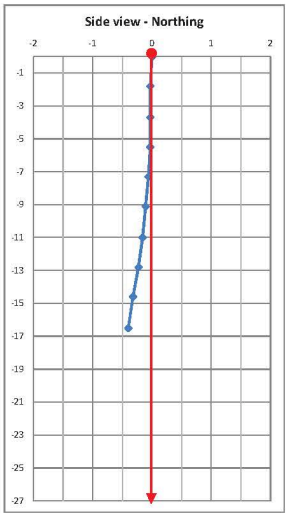

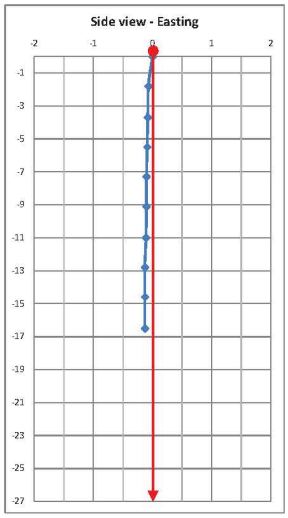

NOTES

BLAST LAYOUT

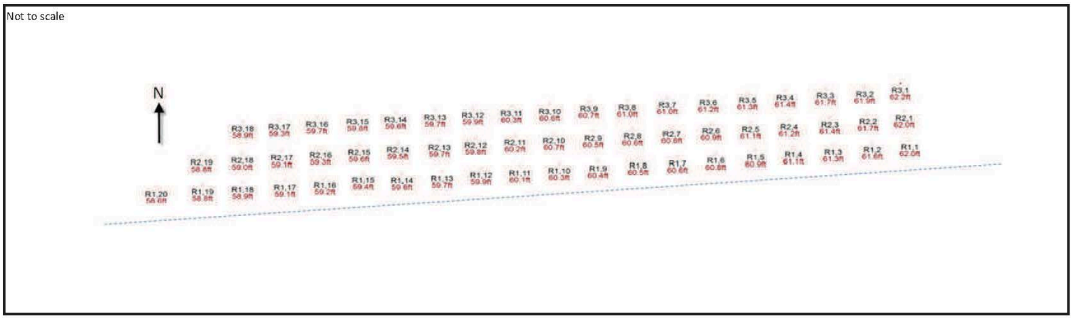

Survey report
Hole deviation

DYNO Dyno Nobel

SURVEY PARAMETERS

CUSTOMER	CRH Dufferin
LOCATION	Colborne, ON
OPERATOR	Brad Asselstine

SURVEY ID	R1H18
SURVEY NAME	Ogden Point Deviation
SURVEY RUN ON	May 23, 2018

TOOL	PeeWee, Devico
SERIAL NUMBER	8297

Mag.Decl.	0
Northing	0.00
Easting	0.00
Elevation	0.00

HOLE DEVIATION PLOT

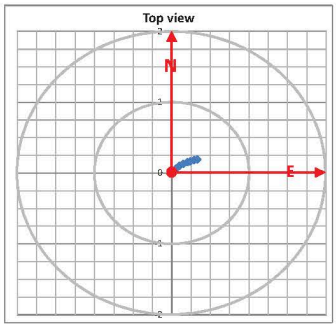

RECORDED DATA

Depth (m)	North. (m)	East. (m)	Elev. (m)	Temp. (°C)
0	0	0	0	18.3
2	0	-0.01	-1.83	18.3
4	0.03	0.02	-3.66	18.3
6	0.06	0.06	-5.48	18.3
7	0.1	0.1	-7.31	18.3
9	0.13	0.15	-9.14	18.3
11	0.15	0.2	-10.97	18.3
13	0.16	0.24	-12.8	18
15	0.18	0.29	-14.63	18
17	0.19	0.33	-16.45	18

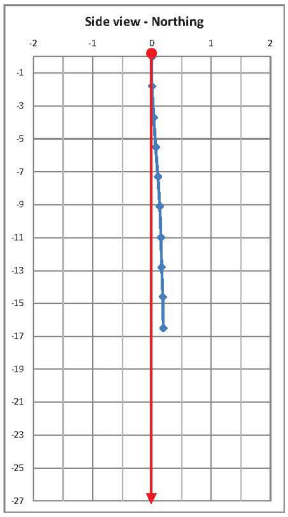

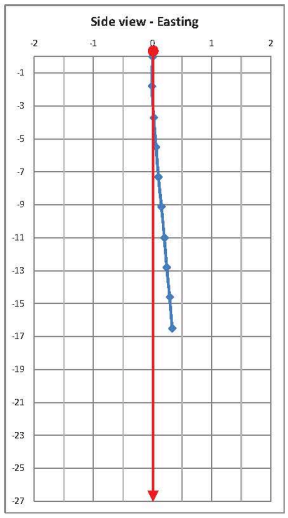

NOTES

BLAST LAYOUT

Not to scale

Survey report
Hole deviation

DYNO Dyno Nobel

SURVEY PARAMETERS

CUSTOMER	CRH Dufferin
LOCATION	Colborne, ON
OPERATOR	Brad Asselstine

SURVEY ID	R1H19
SURVEY NAME	Ogden Point Deviation
SURVEY RUN ON	May 23, 2018

TOOL	PeeWee, Devico
SERIAL NUMBER	8297

Mag.Decl.	0
Northing	0.00
Easting	0.00
Elevation	0.00

HOLE DEVIATION PLOT

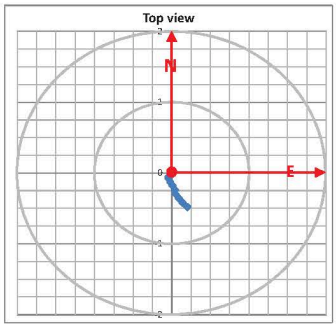

RECORDED DATA

Depth (m)	North. (m)	East. (m)	Elev. (m)	Temp. (°C)
0	0	0	0	17.3
2	-0.05	-0.04	-1.83	17.3
4	-0.08	-0.04	-3.66	17.3
6	-0.13	-0.02	-5.48	17.3
7	-0.18	0.01	-7.31	17.3
9	-0.24	0.04	-9.14	17.3
11	-0.3	0.05	-10.97	17.3
13	-0.36	0.09	-12.79	17.3
15	-0.42	0.14	-14.62	17.1
17	-0.48	0.2	-16.45	17.1

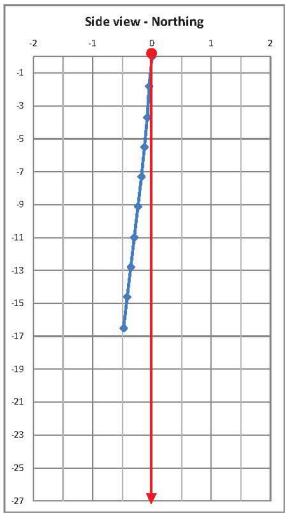

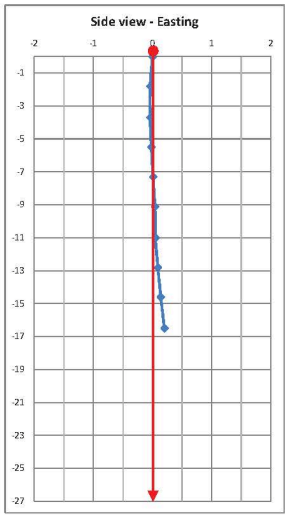

NOTES

BLAST LAYOUT

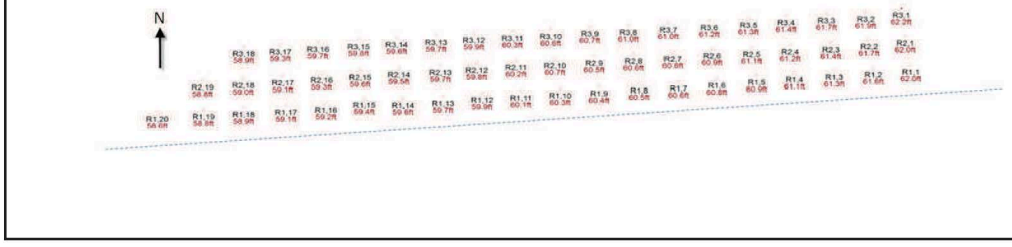

Survey report
Hole deviation

DYNO Dyno Nobel

SURVEY PARAMETERS

CUSTOMER	CRH Dufferin
LOCATION	Colborne, ON
OPERATOR	Brad Asselstine

SURVEY ID	R1H20
SURVEY NAME	Ogden Point Deviation
SURVEY RUN ON	May 23, 2018

TOOL	PeeWee, Devico
SERIAL NUMBER	8297

Mag.Decl.	0
Northing	0.00
Easting	0.00
Elevation	0.00

HOLE DEVIATION PLOT

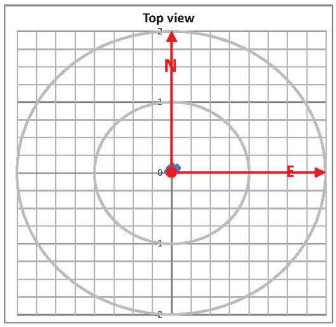

RECORDED DATA

Depth (m)	North. (m)	East. (m)	Elev. (m)	Temp. (°C)
0	0	0	0	17.3
2	0	-0.04	-1.83	17.3
4	0.01	-0.05	-3.66	17.6
6	0.03	-0.04	-5.49	17.3
7	0.06	-0.03	-7.31	17.3
9	0.07	-0.01	-9.14	17.3
11	0.08	0	-10.97	17.3
13	0.08	0.01	-12.8	17.6
15	0.08	0.02	-14.63	17.3
17	0.07	0.07	-16.46	17.3

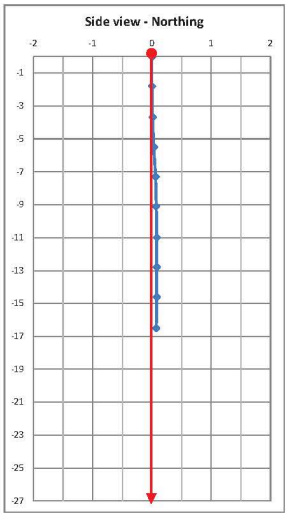

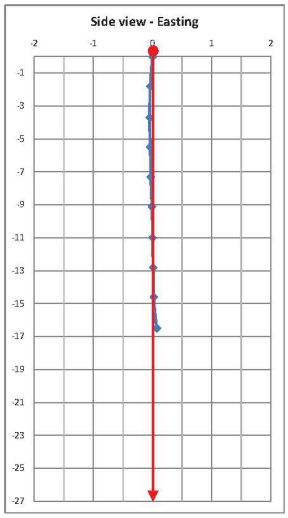

NOTES

BLAST LAYOUT

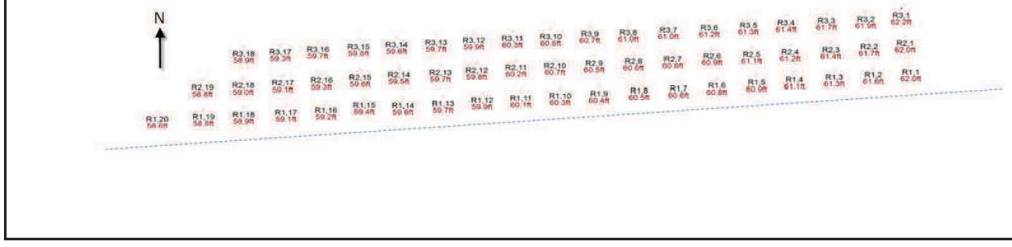

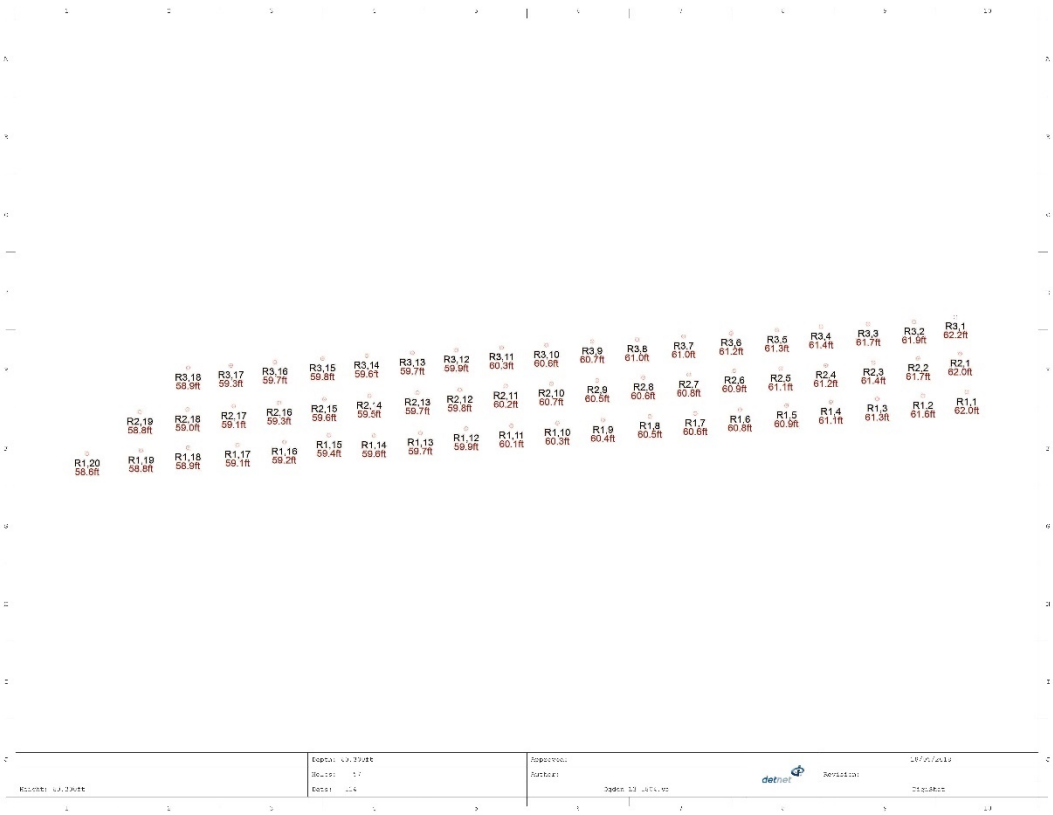
R3.18 58.9ft
R3.17 59.3ft
R3.16 59.7ft
R3.15 59.8ft
R3.14 59.6ft
R3.13 59.7ft
R3.12 59.9ft
R3.11 60.3ft
R3.10 60.6ft
R3.9 60.7ft
R3.8 61.0ft
R3.7 61.0ft
R3.6 61.2ft
R3.5 61.3ft
R3.4 61.4ft
R3.3 61.7ft
R3.2 61.9ft
R3.1 62.2ft
R2.19 58.8ft
R2.18 59.0ft
R2.17 59.1ft
R2.16 59.3ft
R2.15 59.6ft
R2.14 59.5ft
R2.13 59.7ft
R2.12 59.8ft
R2.11 60.2ft
R2.10 60.7ft
R2.9 60.5ft
R2.8 60.6ft
R2.7 60.8ft
R2.6 60.9ft
R2.5 61.1ft
R2.4 61.2ft
R2.3 61.4ft
R2.2 61.7ft
R2.1 62.0ft
R1.20 58.6ft
R1.19 58.8ft
R1.18 58.9ft
R1.17 59.1ft
R1.16 59.2ft
R1.15 59.4ft
R1.14 59.6ft
R1.13 59.7ft
R1.12 59.9ft
R1.11 60.1ft
R1.10 60.3ft
R1.9 60.4ft
R1.8 60.5ft
R1.7 60.6ft
R1.6 60.8ft
R1.5 60.9ft
R1.4 61.1ft
R1.3 61.3ft
R1.2 61.6ft
R1.1 62.0ft
detnet

DynoConsult

Drill log

DYNO Dyno Nobel

Reference		**Date:**	May 14, 2018
Client:	CRH Group Canada inc.	**Blast no.:**	Level 3 2018-04
Site:	Ogden Point Quarry, Colborne ON		

BLAST PARAMETERS				
Pattern	1st row	14' x 15.5'	other rows	13' x 15.5'
Number of holes	57			
Hole diameter	4 in			
Notes				

DRILLING INFORMATION					
Row ID	**Hole ID**	**Design angle**	**Design depth (ft)**	**Measured depth (ft)**	**Comments**
1	1	0	62.0		
1	2	0	61.6		
1	3	0	61.3		
1	4	0	61.1		
1	5	0	60.9		
1	6	0	60.8		
1	7	0	60.6		
1	8	0	60.5		
1	9	0	60.4		
1	10	0	60.3		
1	11	0	60.1		
1	12	0	59.9		
1	13	0	59.7		
1	14	0	59.6		
1	15	0	59.4		
1	16	0	59.2		
1	17	0	59.1		
1	18	0	58.9		
1	19	0	58.8		
1	20	0	58.6		
2	1	0	62.0		
2	2	0	61.7		
2	3	0	61.4		
2	4	0	61.2		
2	5	0	61.1		
2	6	0	60.9		
2	7	0	60.8		
2	8	0	60.6		
2	9	0	60.5		

SIGNATURES			
Driller		Date	
Blaster		Date	
Supervisor		Date	

DynoConsult

Drill log

DYNO Dyno Nobel

Reference		**Date:**	May 14, 2018
Client:	CRH Group Canada inc.	**Blast no.:**	Level 3 2018-04
Site:	Ogden Point Quarry, Colborne ON		

BLAST PARAMETERS				
Pattern	1st row	14' x 15.5'	other rows	13' x 15.5'
Number of holes	57			
Hole diameter	4 in			
Notes				

DRILLING INFORMATION

Row ID	Hole ID	Design angle	Design depth (ft)	Measured depth (ft)	Comments
2	10	0	60.7		
2	11	0	60.2		
2	12	0	59.8		
2	13	0	59.7		
2	14	0	59.5		
2	15	0	59.6		
2	16	0	59.3		
2	17	0	59.1		
2	18	0	59.0		
2	19	0	58.8		
3	1	0	62.2		
3	2	0	61.9		
3	3	0	61.7		
3	4	0	61.4		
3	5	0	61.3		
3	6	0	61.2		
3	7	0	61.0		
3	8	0	61.0		
3	9	0	60.7		
3	10	0	60.6		
3	11	0	60.3		
3	12	0	59.9		
3	13	0	59.7		
3	14	0	59.6		
3	15	0	59.8		
3	16	0	59.7		
3	17	0	59.3		
3	18	0	58.9		

SIGNATURES			
Driller		Date	
Blaster		Date	
Supervisor		Date	

-

Overview

Site Name:
Bench Name:
Blast Name:
Recording Date: 2018-05-23 8:36:29 PM
Rock Density: 2500 kg/m³
3D image: Ms12.jm3
Blast Site: Ms12.smb
Notes:

Blast Site Geometry

Minimal Bench Height:	17.34 m
Mean Bench Height:	17.53 m
Maximum Bench Height:	18.64 m
Front Plane Dipping:	89.55 °
Front Plane Dip Direction:	176.50 °
Lateral Distance between Delimiters:	98.58 m
Lateral Distance between Delimiting Planes:	98.58 m
Number of Boreholes:	20
Total Drilling Length:	349.83 m
Total Blasting Volume:	-
Total Blasting Mass:	-

Design Parameters

Burden:	4.27 m
Rows:	1
Row Shift:	0.0 m
Side Spacing:	3.0 m
Inclination:	0.01 °

It is noted that the blast site planned with BlastMetriX3D bases exclusively on the contact-free measured information of the bench face. The blast site planned with BlastMetriX3D has to be checked in any case for completeness and correctness by a responsible blaster. It is presumed that all legally binding laws, regulations and guidelines applicable in your country are met. By using BlastMetriX3D you agree to implement the result on your responsibility and free 3GSM from any possible claims.

< 3.3 m
4.3 m
> 5.3 m

-

Scale 1:750

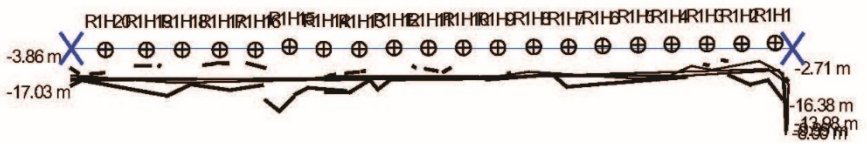

Delimiter
Reference line
Row
Borehole position
Borehole

All dimensions in [m]

-

Borehole details

Name	u [m]	v [m]	E [m]	N [m]	H [m]	Alpha [deg]	Inclination [deg]	Length [m]	Diameter [mm]
R1H1	96.17	0.75	750762.83	4875311.44	56.50	90.10	0.01	17.75	100.00
R1H2	91.61	0.64	750758.28	4875311.06	56.38	90.10	0.01	17.66	100.00
R1H3	86.86	0.60	750753.55	4875310.74	56.30	90.10	0.01	17.61	100.00
R1H4	82.04	0.56	750748.74	4875310.42	56.23	90.10	0.01	17.58	100.00
R1H5	77.44	0.47	750744.14	4875310.05	56.17	90.10	0.01	17.55	100.00
R1H6	72.60	0.34	750739.32	4875309.64	56.14	90.10	0.01	17.55	100.00
R1H7	67.94	0.23	750734.68	4875309.25	56.08	90.10	0.01	17.52	100.00
R1H8	63.18	0.22	750729.92	4875308.96	56.05	90.10	0.01	17.52	100.00
R1H9	58.29	0.11	750725.05	4875308.56	56.03	90.10	0.01	17.53	100.00
R1H10	53.57	0.10	750720.34	4875308.26	55.99	90.10	0.01	17.53	100.00
R1H11	48.80	0.08	750715.58	4875307.96	55.93	90.10	0.01	17.50	100.00
R1H12	44.09	0.08	750710.88	4875307.69	55.87	90.10	0.01	17.47	100.00
R1H13	39.34	-0.10	750706.15	4875307.22	55.79	90.10	0.01	17.42	100.00
R1H14	34.48	-0.08	750701.30	4875306.96	55.77	90.10	0.01	17.44	100.00
R1H15	29.81	0.24	750696.62	4875307.00	55.72	90.10	0.01	17.41	100.00
R1H16	25.14	-0.18	750691.98	4875306.30	55.66	90.10	0.01	17.39	100.00
R1H17	20.28	-0.19	750687.13	4875306.00	55.63	90.10	0.01	17.39	100.00
R1H18	15.13	-0.18	750681.99	4875305.71	55.56	90.10	0.01	17.35	100.00
R1H19	10.26	-0.19	750677.12	4875305.41	55.53	90.10	0.01	17.35	100.00
R1H20	4.66	-0.19	750671.54	4875305.08	55.47	90.10	0.01	17.33	100.00

-

R1H1 (Scale 1:150) Profile

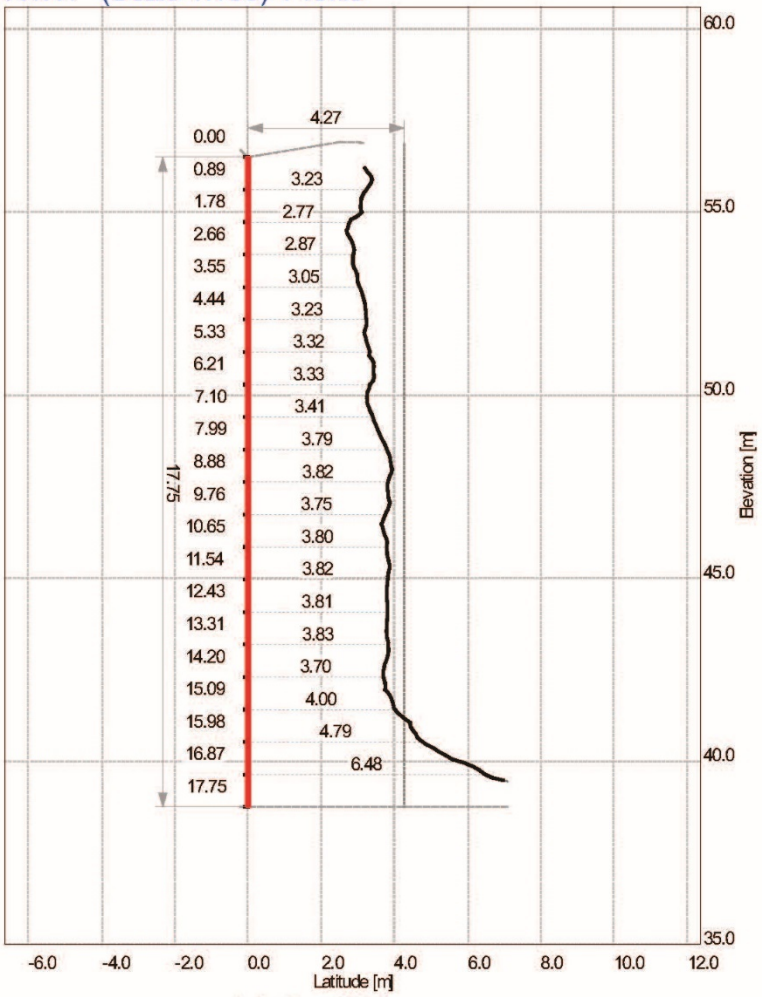

Depth	Profile
1.0	3.118
2.0	2.714
3.0	2.954
4.0	3.211
5.0	3.300
6.0	3.320
7.0	3.489
8.0	3.899
9.0	3.859
10.0	3.784
11.0	3.817
12.0	3.804
13.0	3.828
14.0	3.804
15.0	4.515
16.0	6.270
17.0	na

Inclination: 0.01 °
Length: 17.75 m
Diameter: 100.00 mm
Area: 68.2 m² (of profile)
Position: u: 96.17 m, v: 0.75 m
E: 750762.83 m, N: 4875311.44 m, H: 56.50 m
Subdrilling: 0 m

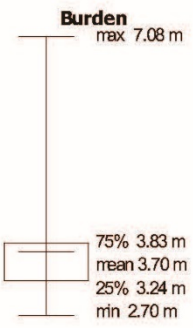

-

R1H2 (Scale 1:150) Profile

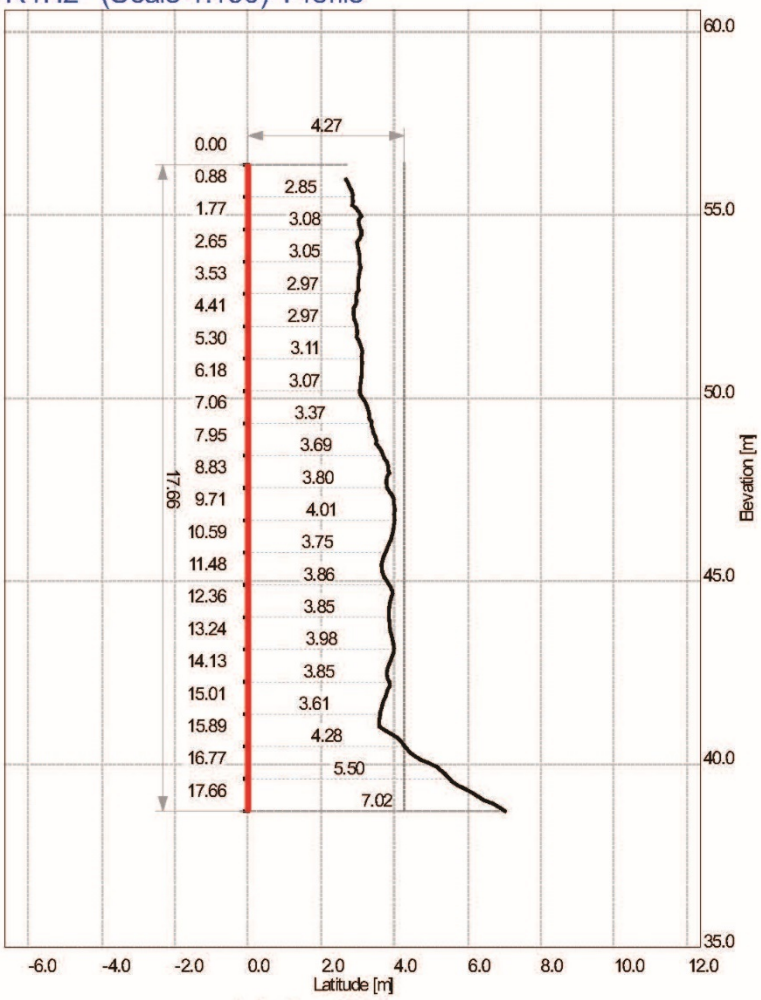

Depth	Profile
1.0	2.866
2.0	3.010
3.0	3.018
4.0	2.894
5.0	3.103
6.0	3.052
7.0	3.413
8.0	3.821
9.0	3.999
10.0	3.835
11.0	3.824
12.0	3.857
13.0	3.913
14.0	3.749
15.0	3.964
16.0	5.342
17.0	7.016

Inclination: 0.01 °
Length: 17.66 m
Diameter: 100.00 mm
Area: 64.7 m² (of profile)
Position: u: 91.61 m, v: 0.64 m
E: 750758.28 m, N: 4875311.06 m, H: 56.38 m
Subdrilling: 0 m

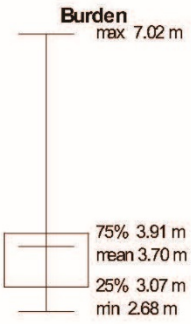

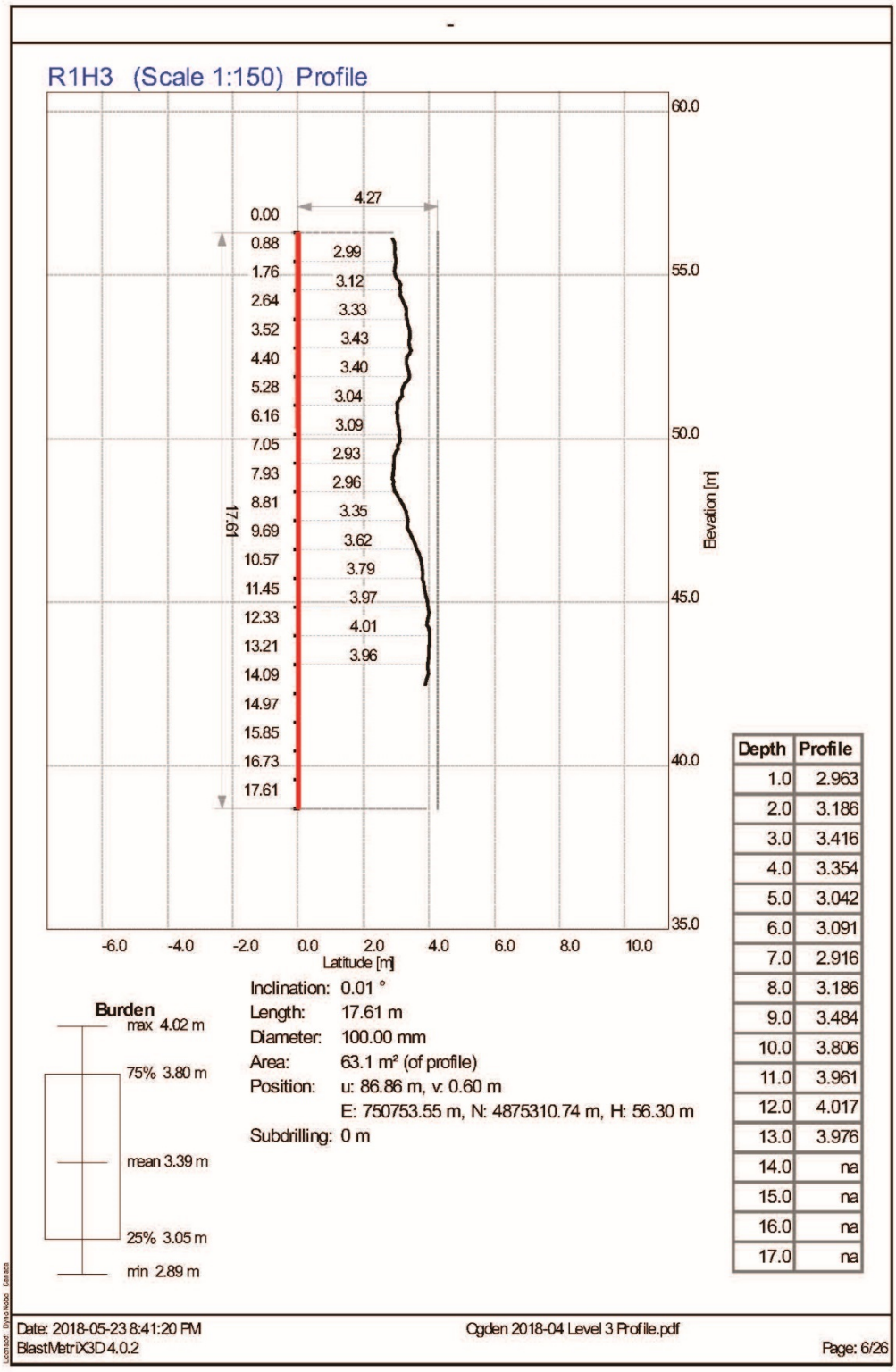
-
R1H3 (Scale 1:150) Profile
4.27
0.00
0.88
1.76
2.64
3.52
4.40
5.28
6.16
7.05
7.93
8.81
9.69
10.57
11.45
12.33
13.21
14.09
14.97
15.85
16.73
17.61
17.61
2.99
3.12
3.33
3.43
3.40
3.04
3.09
2.93
2.96
3.35
3.62
3.79
3.97
4.01
3.96
60.0
55.0
50.0
45.0
40.0
35.0
Elevation [m]
-6.0
-4.0
-2.0
0.0
2.0
4.0
6.0
8.0
10.0
Latitude [m]
Inclination: 0.01 °
Length: 17.61 m
Diameter: 100.00 mm
Area: 63.1 m² (of profile)
Position: u: 86.86 m, v: 0.60 m
E: 750753.55 m, N: 4875310.74 m, H: 56.30 m
Subdrilling: 0 m
Burden
max 4.02 m
75% 3.80 m
mean 3.39 m
25% 3.05 m
min 2.89 m
Depth | Profile
1.0 | 2.963
2.0 | 3.186
3.0 | 3.416
4.0 | 3.354
5.0 | 3.042
6.0 | 3.091
7.0 | 2.916
8.0 | 3.186
9.0 | 3.484
10.0 | 3.806
11.0 | 3.961
12.0 | 4.017
13.0 | 3.976
14.0 | na
15.0 | na
16.0 | na
17.0 | na
Date: 2018-05-23 8:41:20 PM
BlastMetriX3D 4.0.2
Ogden 2018-04 Level 3 Profile.pdf
Page: 6/26

-

R1H4 (Scale 1:150) Profile

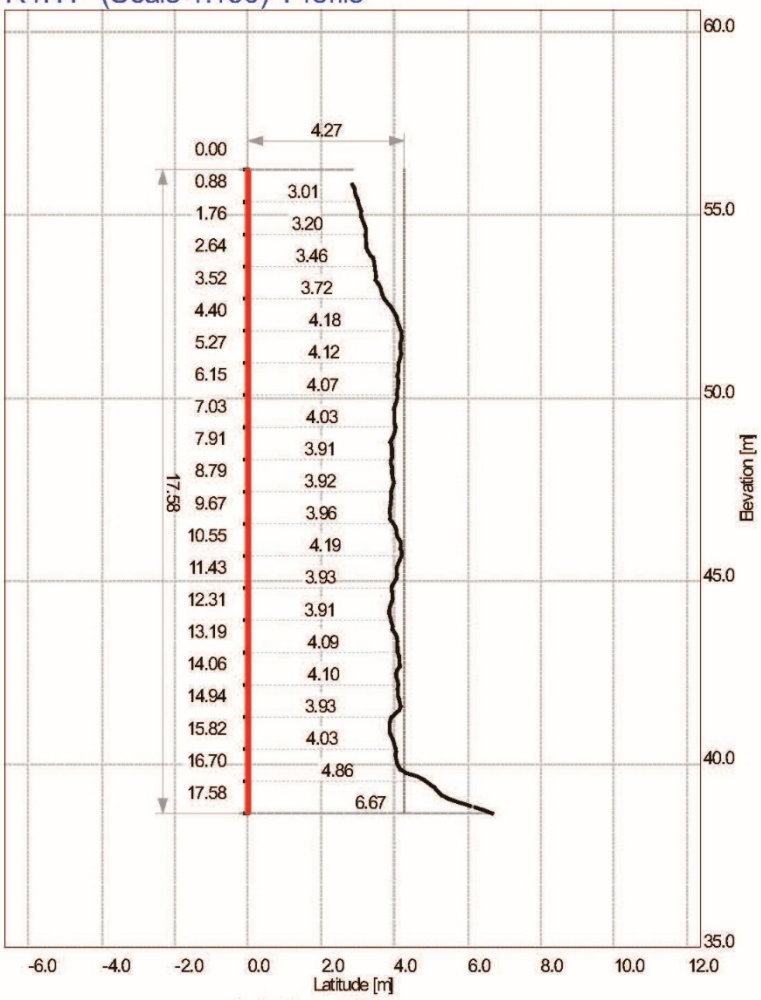

Inclination: 0.01 °
Length: 17.58 m
Diameter: 100.00 mm
Area: 69.4 m² (of profile)
Position: u: 82.04 m, v: 0.56 m
E: 750748.74 m, N: 4875310.42 m, H: 56.24 m
Subdrilling: 0 m

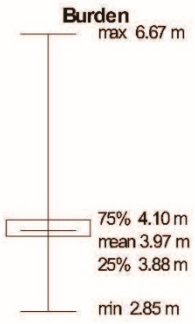

Depth	Profile
1.0	3.057
2.0	3.242
3.0	3.553
4.0	4.088
5.0	4.157
6.0	4.077
7.0	3.983
8.0	3.935
9.0	3.879
10.0	4.165
11.0	3.937
12.0	3.938
13.0	4.133
14.0	4.129
15.0	3.932
16.0	4.500
17.0	6.667

-

R1H5 (Scale 1:150) Profile

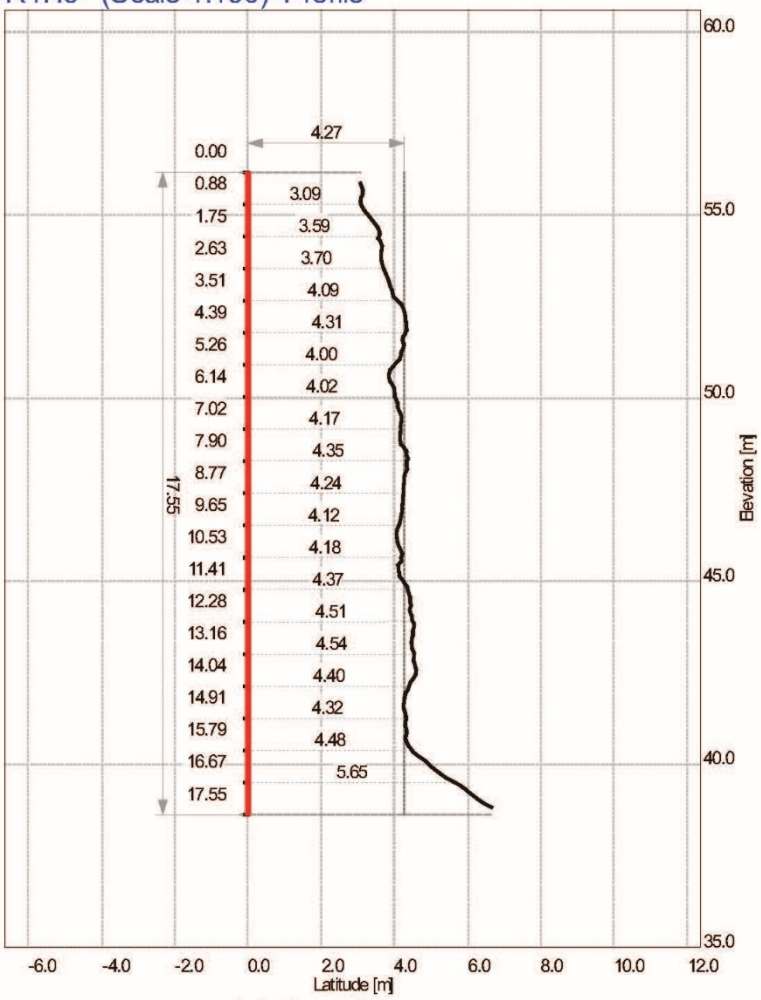

Inclination: 0.01 °
Length: 17.55 m
Diameter: 100.00 mm
Area: 74.3 m² (of profile)
Position: u: 77.44 m, v: 0.47 m
E: 750744.14 m, N: 4875310.05 m, H: 56.17 m
Subdrilling: 0 m

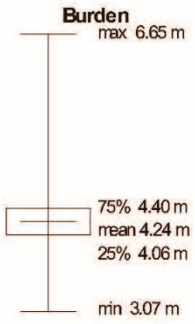

Depth	Profile
1.0	3.176
2.0	3.655
3.0	3.877
4.0	4.320
5.0	4.094
6.0	4.039
7.0	4.158
8.0	4.281
9.0	4.200
10.0	4.171
11.0	4.347
12.0	4.528
13.0	4.553
14.0	4.264
15.0	4.302
16.0	5.366
17.0	na

-

R1H6 (Scale 1:150) Profile

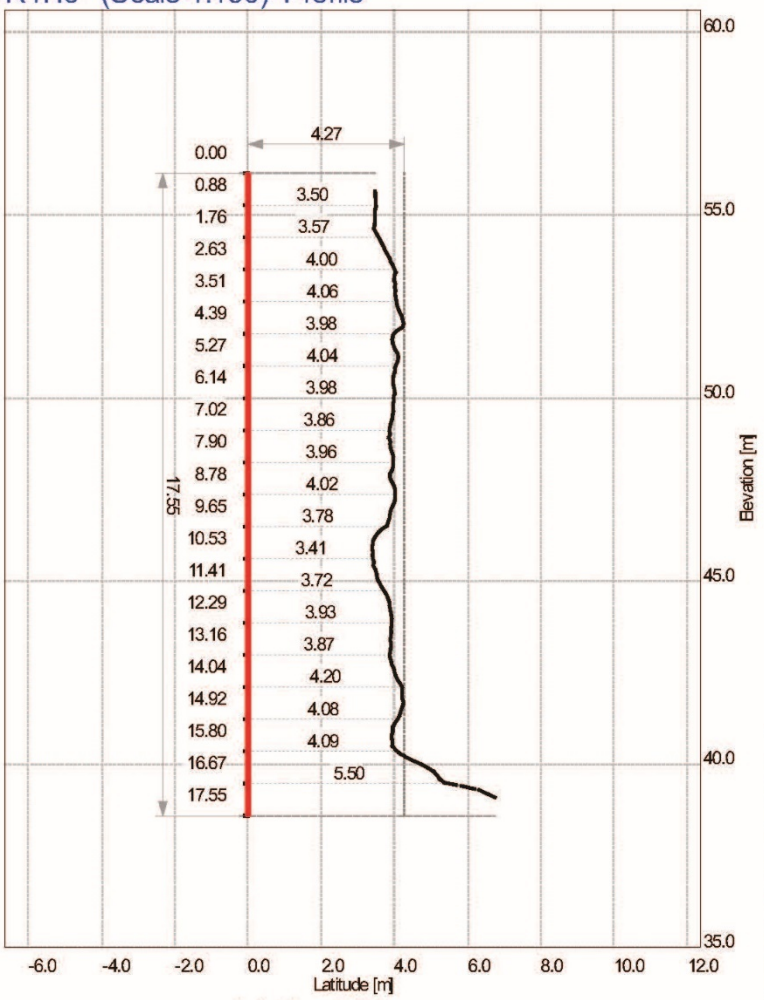

Inclination: 0.01 °
Length: 17.55 m
Diameter: 100.00 mm
Area: 70.4 m² (of profile)
Position: u: 72.60 m, v: 0.34 m
E: 750739.32 m, N: 4875309.64 m, H: 56.14 m
Subdrilling: 0 m

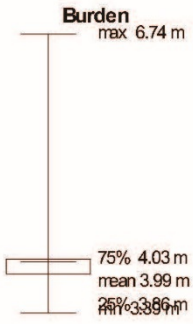

Depth	Profile
1.0	3.470
2.0	3.728
3.0	4.015
4.0	4.252
5.0	4.076
6.0	3.978
7.0	3.848
8.0	3.872
9.0	3.882
10.0	3.402
11.0	3.685
12.0	3.918
13.0	3.930
14.0	4.245
15.0	3.935
16.0	5.216
17.0	na

-

R1H7 (Scale 1:150) Profile

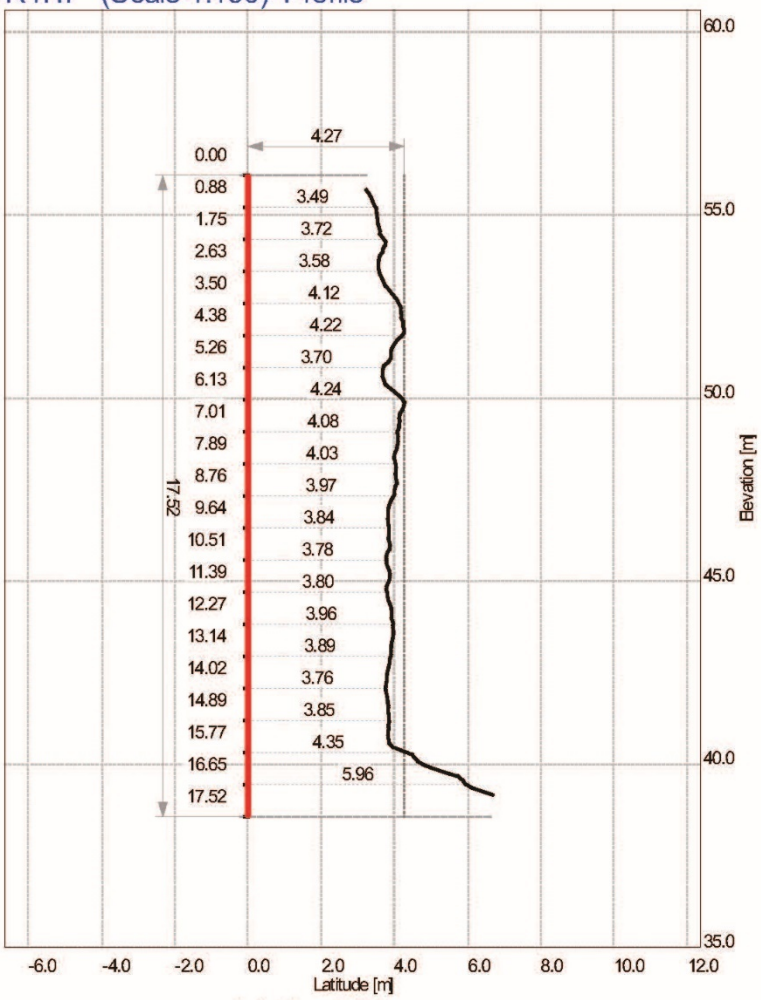

Inclination: 0.01 °
Length: 17.52 m
Diameter: 100.00 mm
Area: 70.4 m² (of profile)
Position: u: 67.94 m, v: 0.23 m
E: 750734.68 m, N: 4875309.25 m, H: 56.08 m
Subdrilling: 0 m

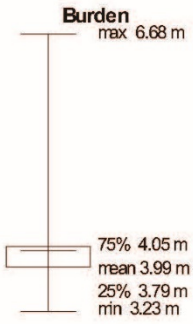

Depth	Profile
1.0	3.518
2.0	3.682
3.0	3.824
4.0	4.235
5.0	3.766
6.0	4.264
7.0	4.097
8.0	4.038
9.0	3.822
10.0	3.810
11.0	3.782
12.0	3.961
13.0	3.843
14.0	3.818
15.0	3.850
16.0	5.865
17.0	na

-

R1H8 (Scale 1:150) Profile

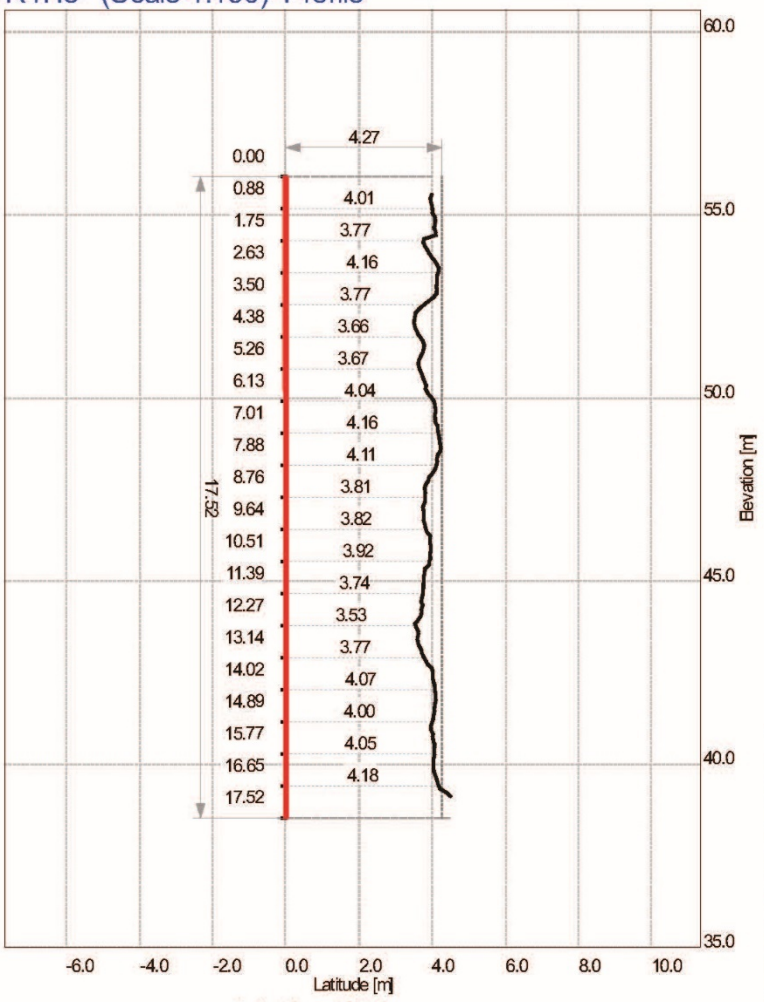

Depth	Profile
1.0	4.029
2.0	3.900
3.0	4.128
4.0	3.535
5.0	3.620
6.0	4.060
7.0	4.203
8.0	3.902
9.0	3.765
10.0	3.945
11.0	3.749
12.0	3.585
13.0	3.957
14.0	4.074
15.0	4.045
16.0	4.132
17.0	na

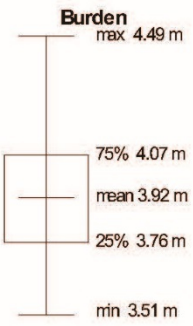

Inclination: 0.01 °
Length: 17.52 m
Diameter: 100.00 mm
Area: 69.0 m² (of profile)
Position: u: 63.18 m, v: 0.22 m
E: 750729.92 m, N: 4875308.96 m, H: 56.05 m
Subdrilling: 0 m

-

R1H9 (Scale 1:150) Profile

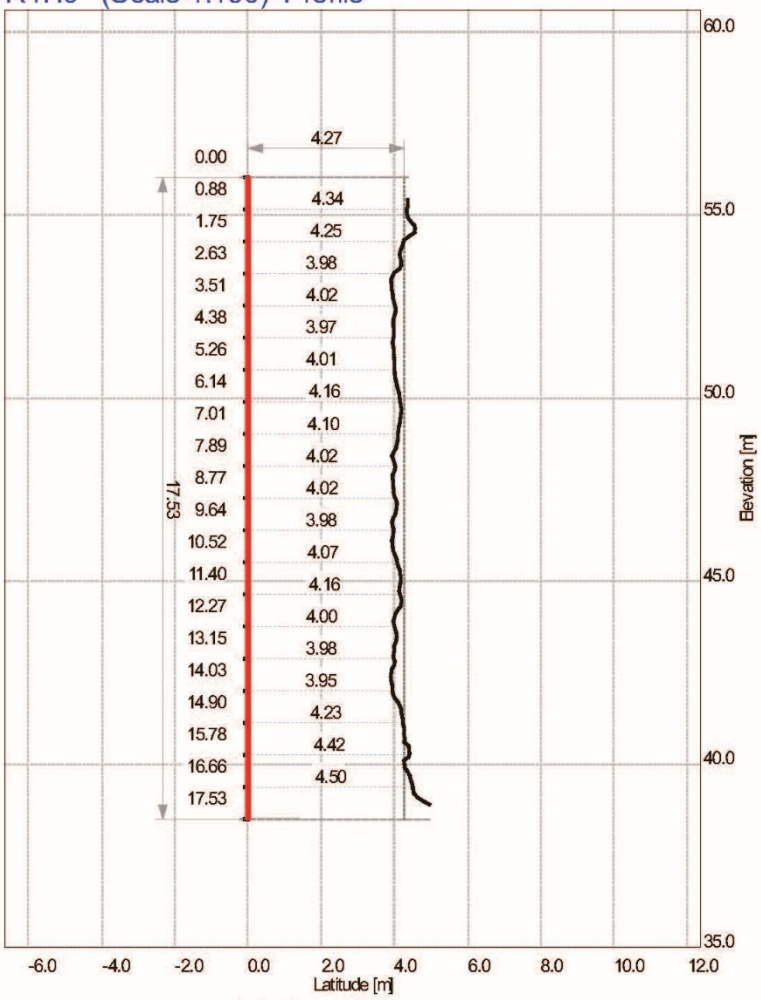

Inclination: 0.01 °
Length: 17.53 m
Diameter: 100.00 mm
Area: 72.5 m² (of profile)
Position: u: 58.29 m, v: 0.11 m
E: 750725.05 m, N: 4875308.56 m, H: 56.03 m
Subdrilling: 0 m

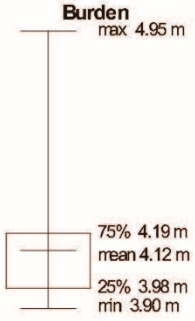

Depth	Profile
1.0	4.352
2.0	4.138
3.0	3.934
4.0	3.975
5.0	4.008
6.0	4.166
7.0	4.083
8.0	3.954
9.0	3.978
10.0	4.014
11.0	4.140
12.0	4.030
13.0	3.940
14.0	4.148
15.0	4.297
16.0	4.459
17.0	na

-

R1H10 (Scale 1:150) Profile

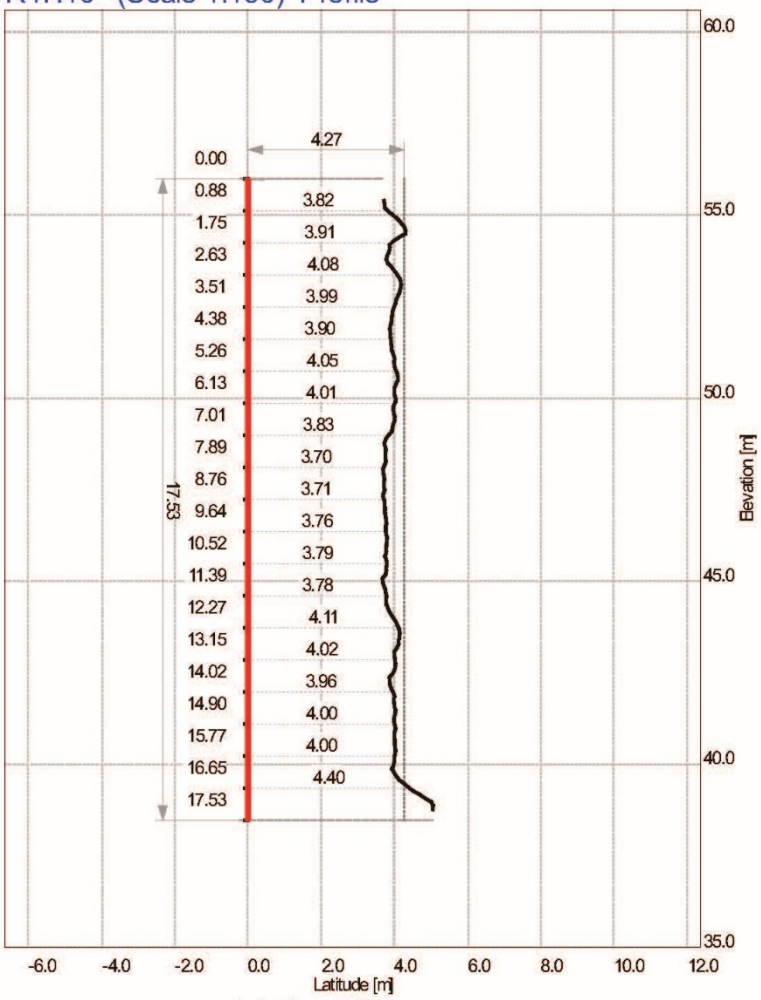

Depth	Profile
1.0	4.008
2.0	3.817
3.0	4.139
4.0	3.883
5.0	4.011
6.0	3.989
7.0	3.730
8.0	3.717
9.0	3.763
10.0	3.742
11.0	3.765
12.0	4.142
13.0	4.005
14.0	4.006
15.0	4.010
16.0	4.230
17.0	na

Inclination: 0.01 °
Length: 17.53 m
Diameter: 100.00 mm
Area: 69.4 m² (of profile)
Position: u: 53.57 m, v: 0.10 m
E: 750720.34 m, N: 4875308.26 m, H: 55.99 m
Subdrilling: 0 m

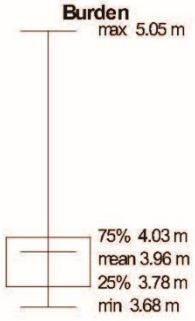

-

R1H11 (Scale 1:150) Profile

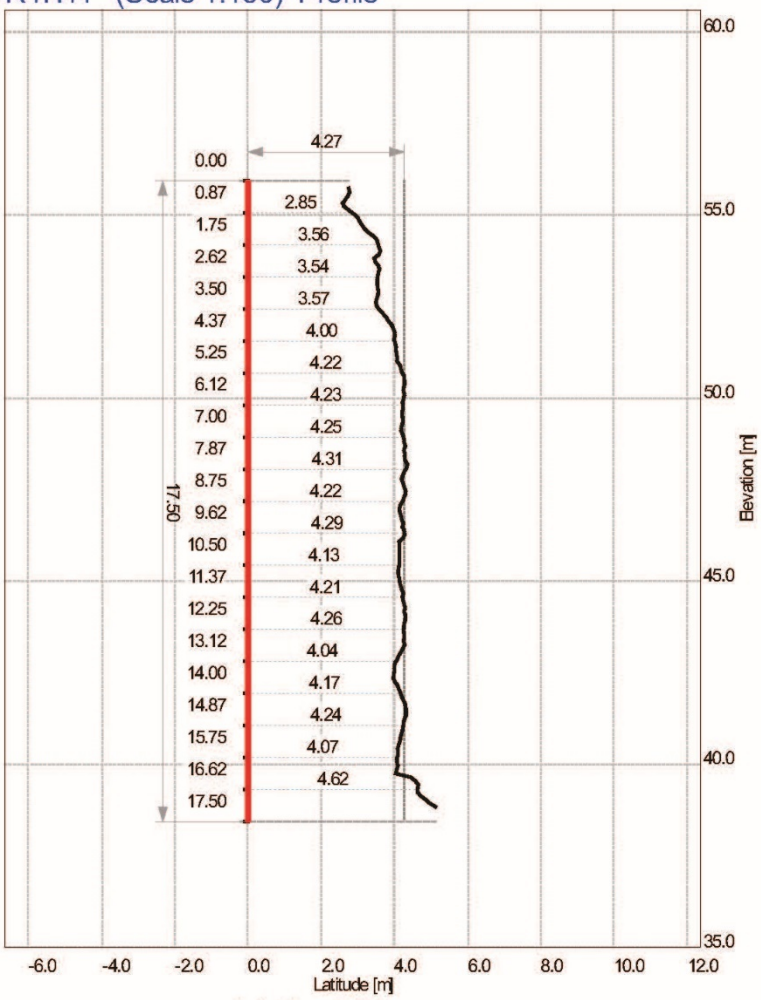

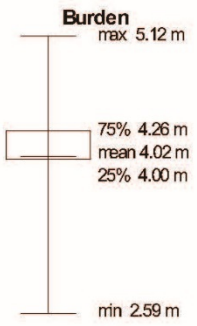

Inclination: 0.01 °
Length: 17.50 m
Diameter: 100.00 mm
Area: 70.4 m² (of profile)
Position: u: 48.80 m, v: 0.08 m
E: 750715.58 m, N: 4875307.97 m, H: 55.93 m
Subdrilling: 0 m

Depth	Profile
1.0	3.010
2.0	3.490
3.0	3.549
4.0	4.001
5.0	4.182
6.0	4.228
7.0	4.289
8.0	4.222
9.0	4.203
10.0	4.132
11.0	4.241
12.0	4.257
13.0	3.995
14.0	4.305
15.0	4.105
16.0	4.622
17.0	na

-

R1H12 (Scale 1:150) Profile

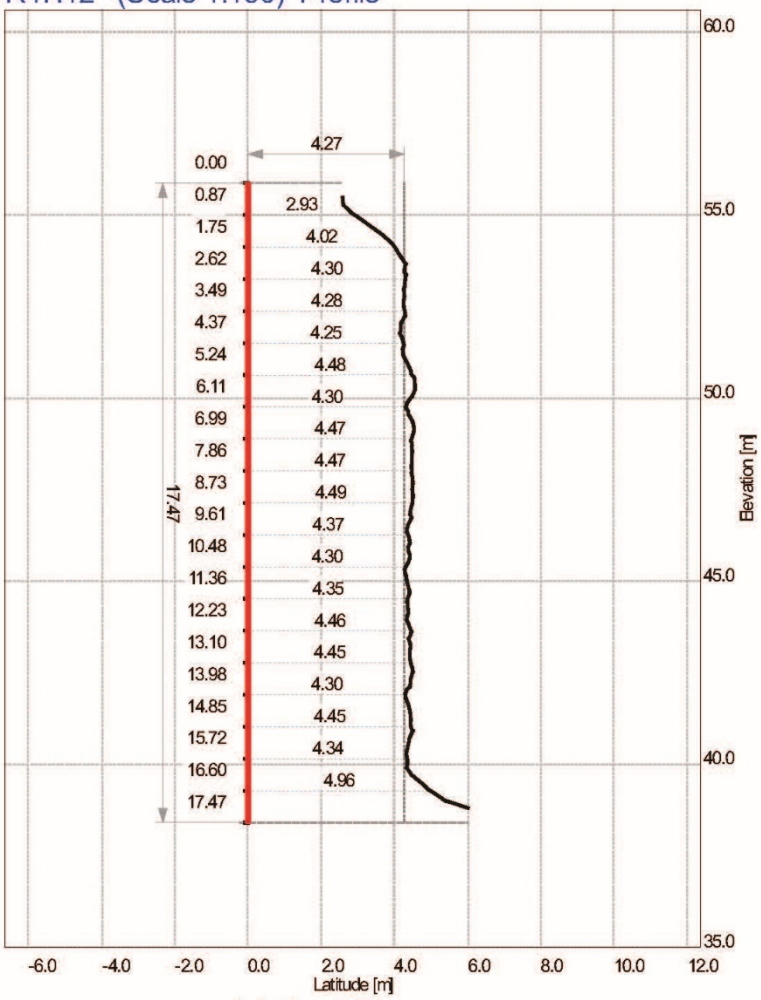

Depth	Profile
1.0	3.141
2.0	4.208
3.0	4.272
4.0	4.155
5.0	4.449
6.0	4.341
7.0	4.465
8.0	4.500
9.0	4.412
10.0	4.403
11.0	4.378
12.0	4.439
13.0	4.497
14.0	4.419
15.0	4.362
16.0	4.789
17.0	na

Inclination: 0.01 °
Length: 17.47 m
Diameter: 100.00 mm
Area: 75.2 m² (of profile)
Position: u: 44.09 m, v: 0.08 m
E: 750710.88 m, N: 4875307.69 m, H: 55.87 m
Subdrilling: 0 m

-

R1H13 (Scale 1:150) Profile

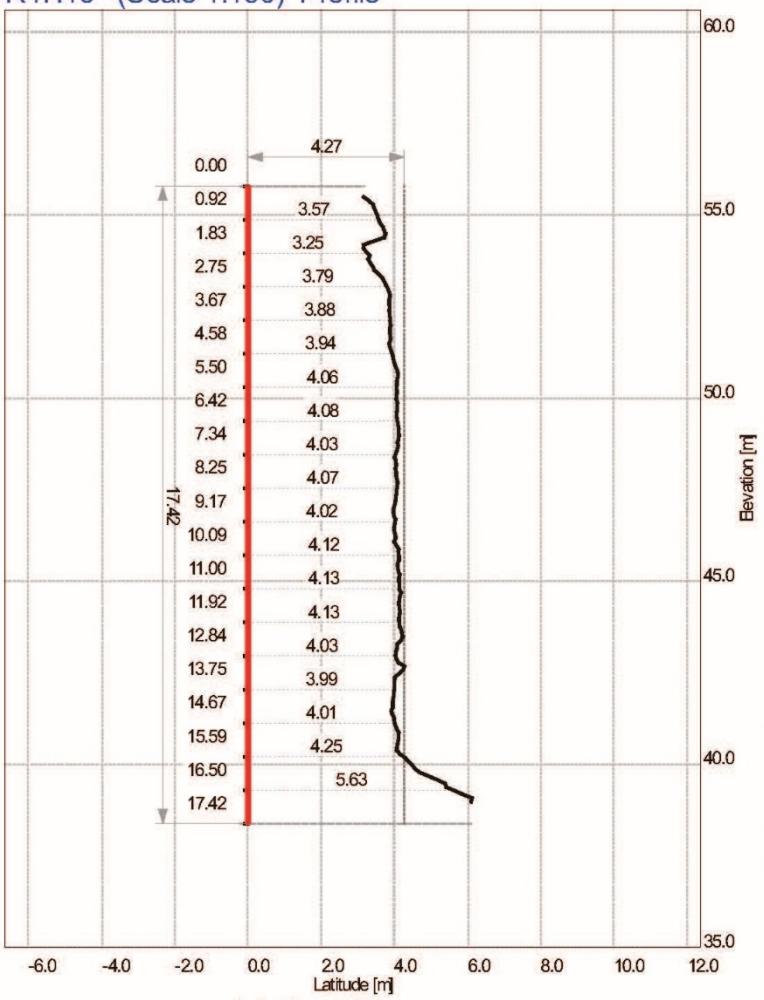

Depth	Profile
1.0	3.625
2.0	3.303
3.0	3.864
4.0	3.892
5.0	4.102
6.0	4.063
7.0	4.085
8.0	4.078
9.0	4.011
10.0	4.124
11.0	4.121
12.0	4.230
13.0	4.121
14.0	3.920
15.0	4.054
16.0	5.408
17.0	na

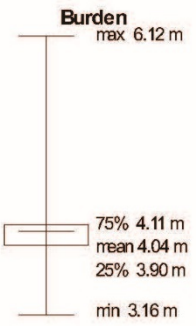

Inclination: 0.01 °
Length: 17.42 m
Diameter: 100.00 mm
Area: 70.7 m² (of profile)
Position: u: 39.34 m, v: -0.10 m
E: 750706.15 m, N: 4875307.22 m, H: 55.79 m
Subdrilling: 0 m

-

R1H14 (Scale 1:150) Profile

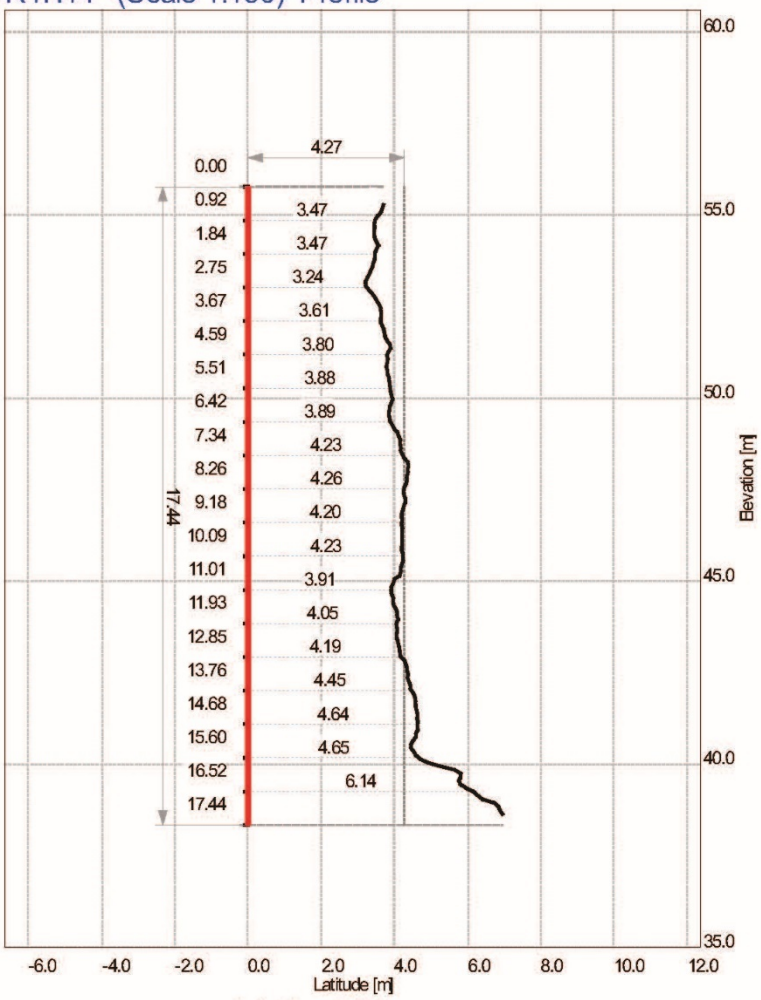

Depth	Profile
1.0	3.451
2.0	3.454
3.0	3.501
4.0	3.750
5.0	3.822
6.0	3.852
7.0	4.176
8.0	4.274
9.0	4.195
10.0	4.223
11.0	3.969
12.0	4.059
13.0	4.372
14.0	4.617
15.0	4.512
16.0	5.930
17.0	na

Inclination: 0.01 °
Length: 17.44 m
Diameter: 100.00 mm
Area: 73.3 m² (of profile)
Position: u: 34.48 m, v: -0.08 m
E: 750701.30 m, N: 4875306.96 m, H: 55.77 m
Subdrilling: 0 m

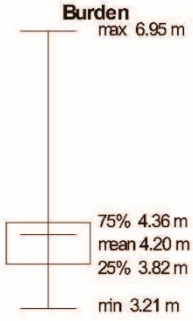

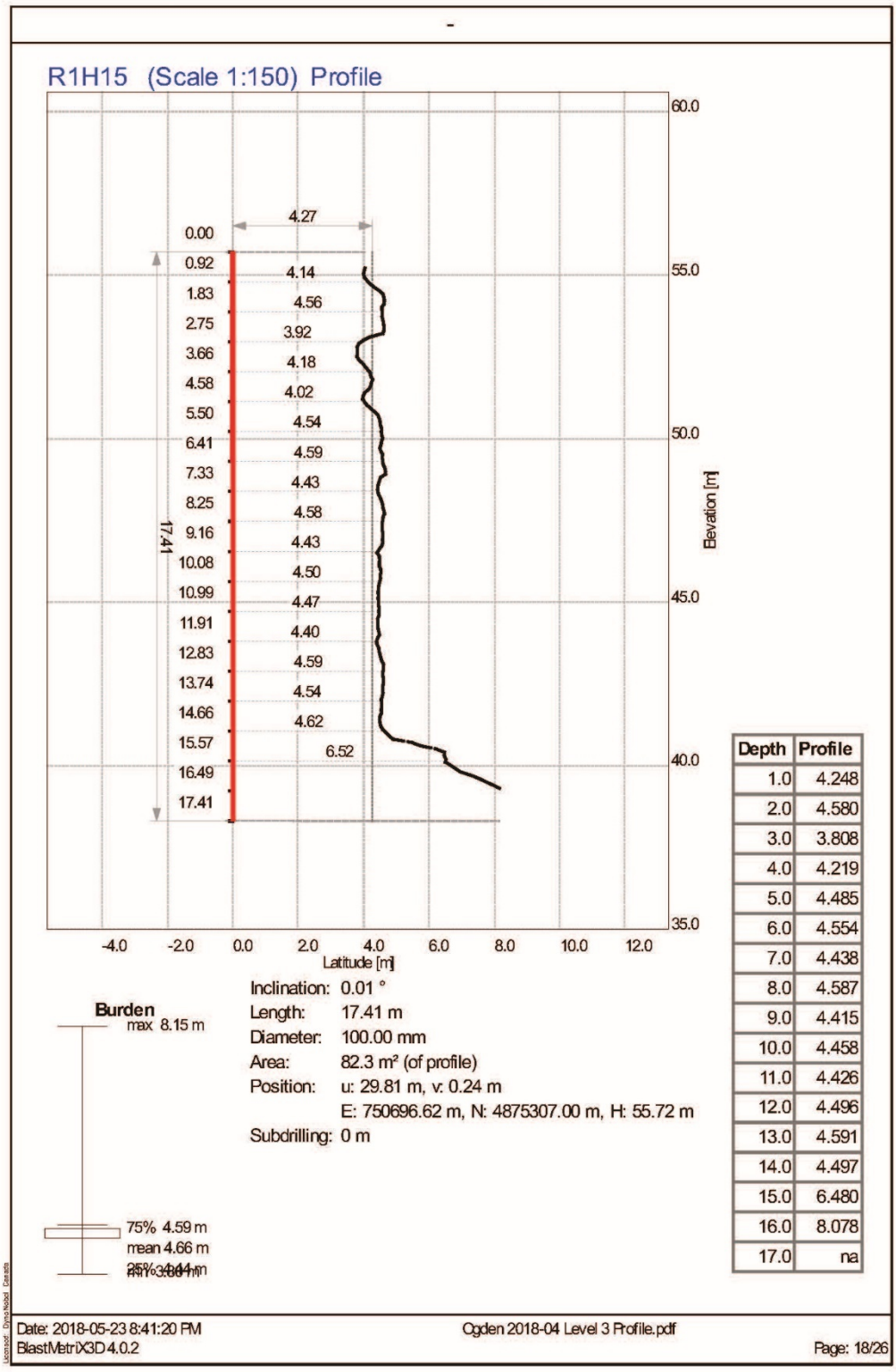
-
R1H15 (Scale 1:150) Profile
4.27
0.00
0.92
1.83
2.75
3.66
4.58
5.50
6.41
7.33
8.25
9.16
10.08
10.99
11.91
12.83
13.74
14.66
15.57
16.49
17.41
17.41
4.14
4.56
3.92
4.18
4.02
4.54
4.59
4.43
4.58
4.43
4.50
4.47
4.40
4.59
4.54
4.62
6.52
60.0
55.0
50.0
45.0
40.0
35.0
Elevation [m]
-4.0
-2.0
0.0
2.0
4.0
6.0
8.0
10.0
12.0
Latitude [m]
Inclination: 0.01 °
Length: 17.41 m
Diameter: 100.00 mm
Area: 82.3 m² (of profile)
Position: u: 29.81 m, v: 0.24 m
E: 750696.62 m, N: 4875307.00 m, H: 55.72 m
Subdrilling: 0 m
Burden
max 8.15 m
75% 4.59 m
mean 4.66 m
25% 3.44 m
min 3.66 m
Depth | Profile
1.0 | 4.248
2.0 | 4.580
3.0 | 3.808
4.0 | 4.219
5.0 | 4.485
6.0 | 4.554
7.0 | 4.438
8.0 | 4.587
9.0 | 4.415
10.0 | 4.458
11.0 | 4.426
12.0 | 4.496
13.0 | 4.591
14.0 | 4.497
15.0 | 6.480
16.0 | 8.078
17.0 | na
Date: 2018-05-23 8:41:20 PM
BlastMetriX3D 4.0.2
Ogden 2018-04 Level 3 Profile.pdf
Page: 18/26
Licensed: Dyno Nobel Canada

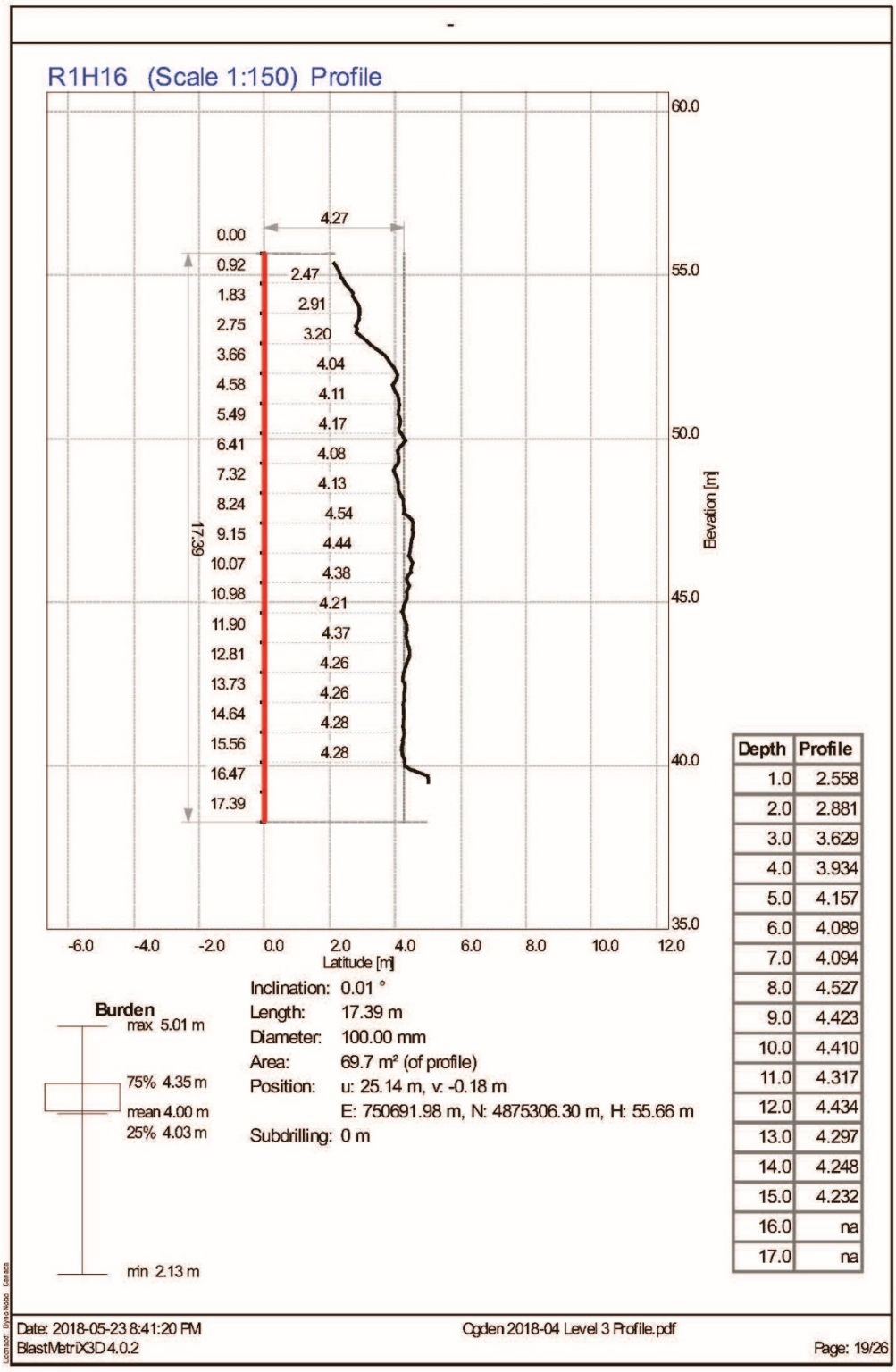
-
R1H16 (Scale 1:150) Profile
4.27
0.00
0.92
1.83
2.75
3.66
4.58
5.49
6.41
7.32
8.24
9.15
10.07
10.98
11.90
12.81
13.73
14.64
15.56
16.47
17.39
17.39
2.47
2.91
3.20
4.04
4.11
4.17
4.08
4.13
4.54
4.44
4.38
4.21
4.37
4.26
4.26
4.28
4.28
60.0
55.0
50.0
45.0
40.0
35.0
Elevation [m]
-6.0
-4.0
-2.0
0.0
2.0
4.0
6.0
8.0
10.0
12.0
Latitude [m]
Inclination: 0.01 °
Length: 17.39 m
Diameter: 100.00 mm
Area: 69.7 m² (of profile)
Position: u: 25.14 m, v: -0.18 m
E: 750691.98 m, N: 4875306.30 m, H: 55.66 m
Subdrilling: 0 m
Burden
max 5.01 m
75% 4.35 m
mean 4.00 m
25% 4.03 m
min 2.13 m
Depth | Profile
1.0 | 2.558
2.0 | 2.881
3.0 | 3.629
4.0 | 3.934
5.0 | 4.157
6.0 | 4.089
7.0 | 4.094
8.0 | 4.527
9.0 | 4.423
10.0 | 4.410
11.0 | 4.317
12.0 | 4.434
13.0 | 4.297
14.0 | 4.248
15.0 | 4.232
16.0 | na
17.0 | na
Date: 2018-05-23 8:41:20 PM
BlastMetrix3D 4.0.2
Ogden 2018-04 Level 3 Profile.pdf
Page: 19/26
Licensed: Dyno Nobel Canada

-

R1H17 (Scale 1:150) Profile

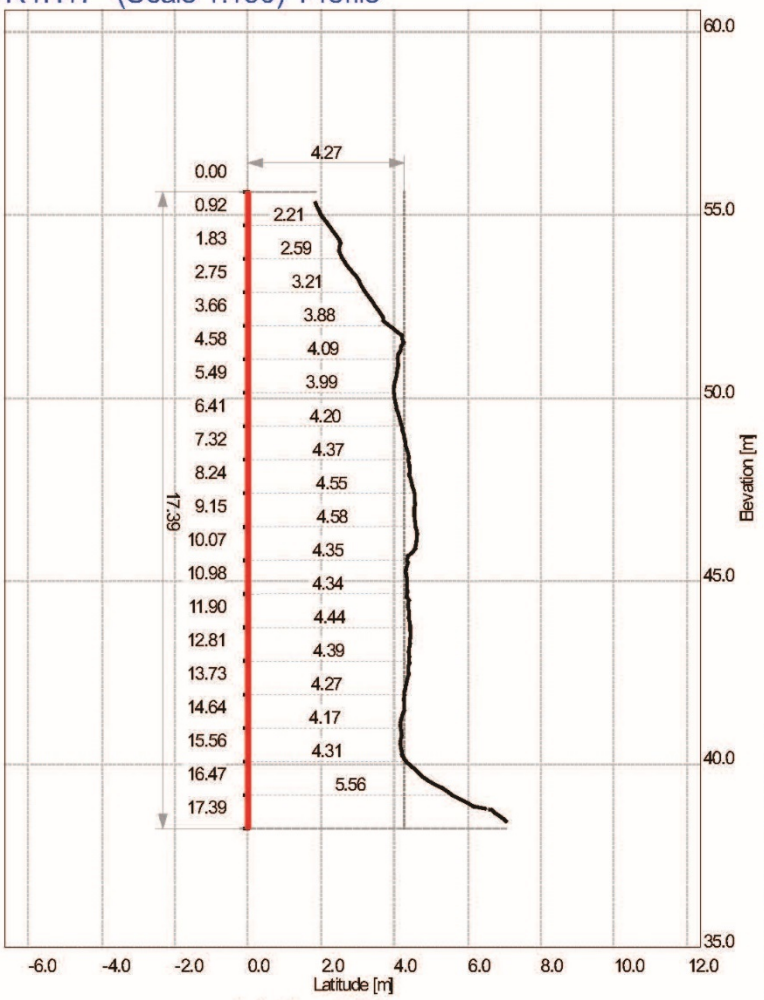

Depth	Profile
1.0	2.288
2.0	2.733
3.0	3.444
4.0	4.247
5.0	4.035
6.0	4.126
7.0	4.380
8.0	4.538
9.0	4.596
10.0	4.341
11.0	4.376
12.0	4.424
13.0	4.350
14.0	4.211
15.0	4.207
16.0	5.427
17.0	na

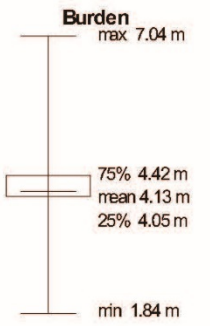

Inclination: 0.01 °
Length: 17.39 m
Diameter: 100.00 mm
Area: 71.3 m² (of profile)
Position: u: 20.28 m, v: -0.19 m
E: 750687.13 m, N: 4875306.00 m, H: 55.63 m
Subdrilling: 0 m

-

R1H18 (Scale 1:150) Profile

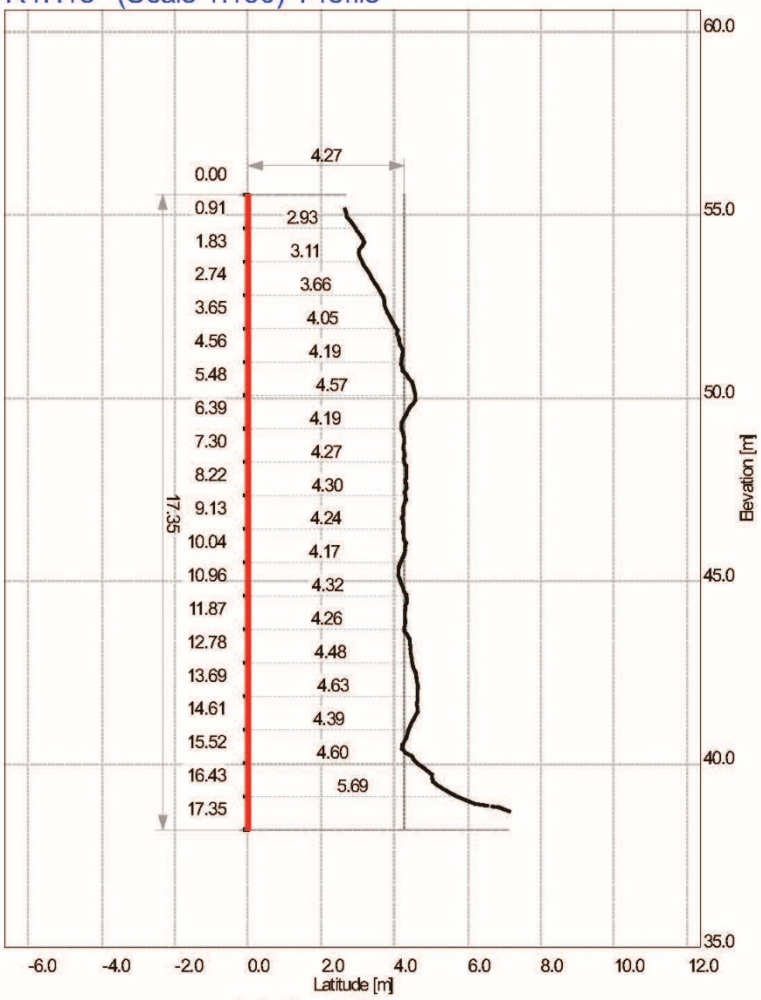

Depth	Profile
1.0	3.003
2.0	3.240
3.0	3.747
4.0	4.136
5.0	4.472
6.0	4.251
7.0	4.274
8.0	4.295
9.0	4.238
10.0	4.118
11.0	4.301
12.0	4.419
13.0	4.607
14.0	4.544
15.0	4.410
16.0	5.487
17.0	na

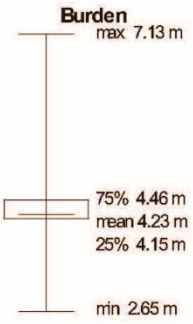

Inclination: 0.01 °
Length: 17.35 m
Diameter: 100.00 mm
Area: 73.4 m² (of profile)
Position: u: 15.13 m, v: -0.18 m
E: 750681.99 m, N: 4875305.71 m, H: 55.56 m
Subdrilling: 0 m

-

R1H19 (Scale 1:150) Profile

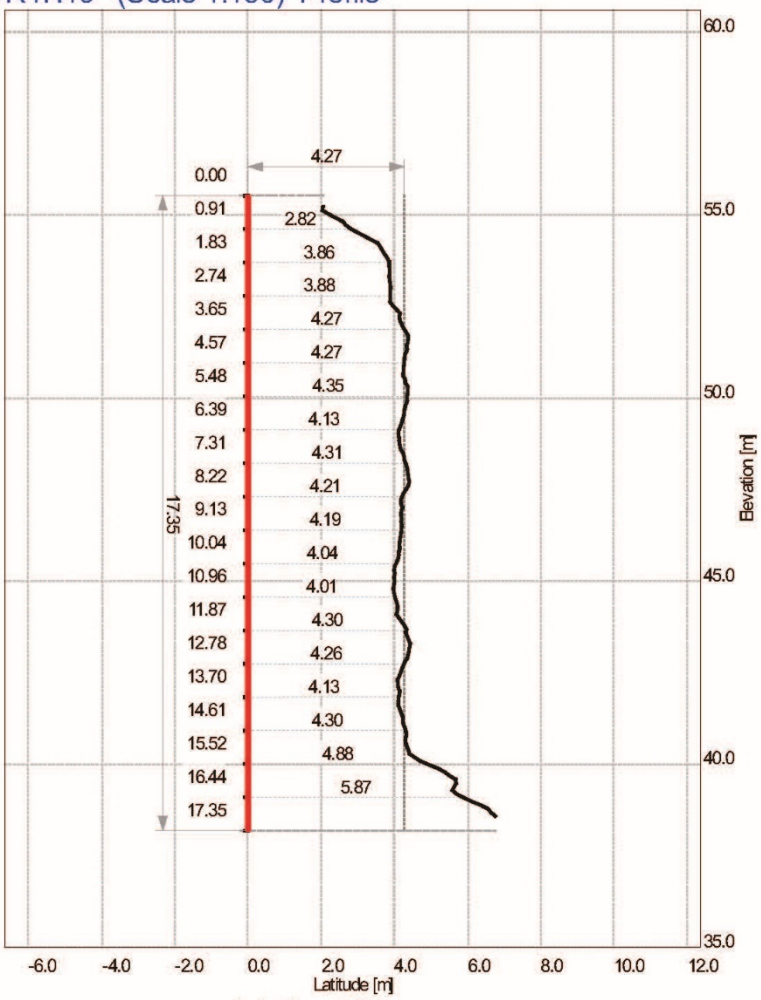

Depth	Profile
1.0	3.025
2.0	3.870
3.0	4.009
4.0	4.330
5.0	4.302
6.0	4.220
7.0	4.266
8.0	4.226
9.0	4.178
10.0	3.982
11.0	4.086
12.0	4.424
13.0	4.086
14.0	4.231
15.0	4.491
16.0	5.671
17.0	na

Inclination: 0.01 °
Length: 17.35 m
Diameter: 100.00 mm
Area: 73.2 m² (of profile)
Position: u: 10.26 m, v: -0.19 m
E: 750677.12 m, N: 4875305.41 m, H: 55.53 m
Subdrilling: 0 m

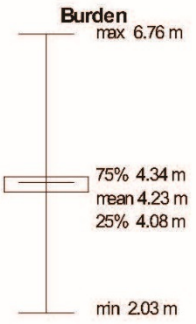

-

R1H20 (Scale 1:150) Profile

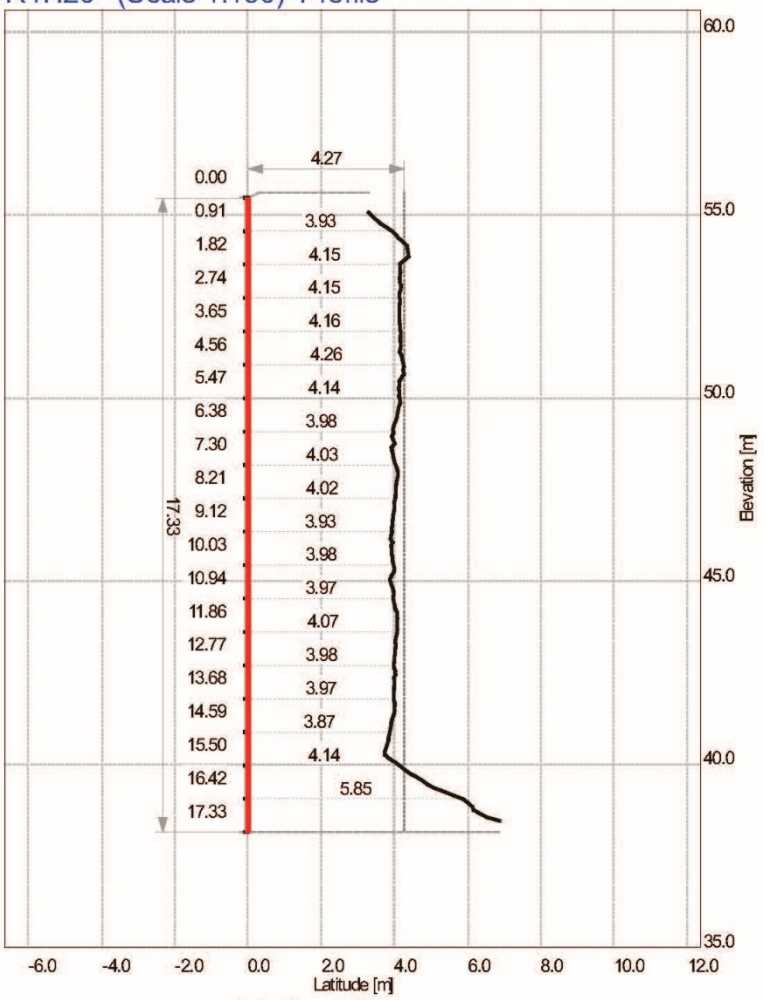

Depth	Profile
1.0	4.046
2.0	4.164
3.0	4.137
4.0	4.166
5.0	4.132
6.0	4.026
7.0	3.980
8.0	4.026
9.0	3.917
10.0	4.000
11.0	4.021
12.0	4.036
13.0	3.996
14.0	3.929
15.0	3.831
16.0	5.568
17.0	na

Inclination: 0.01 °
Length: 17.33 m
Diameter: 100.00 mm
Area: 72.5 m² (of profile)
Position: u: 4.66 m, v: -0.19 m
E: 750671.54 m, N: 4875305.08 m, H: 55.47 m
Subdrilling: 0 m

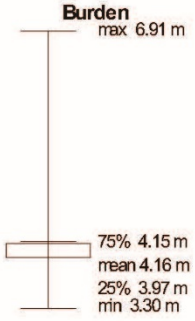

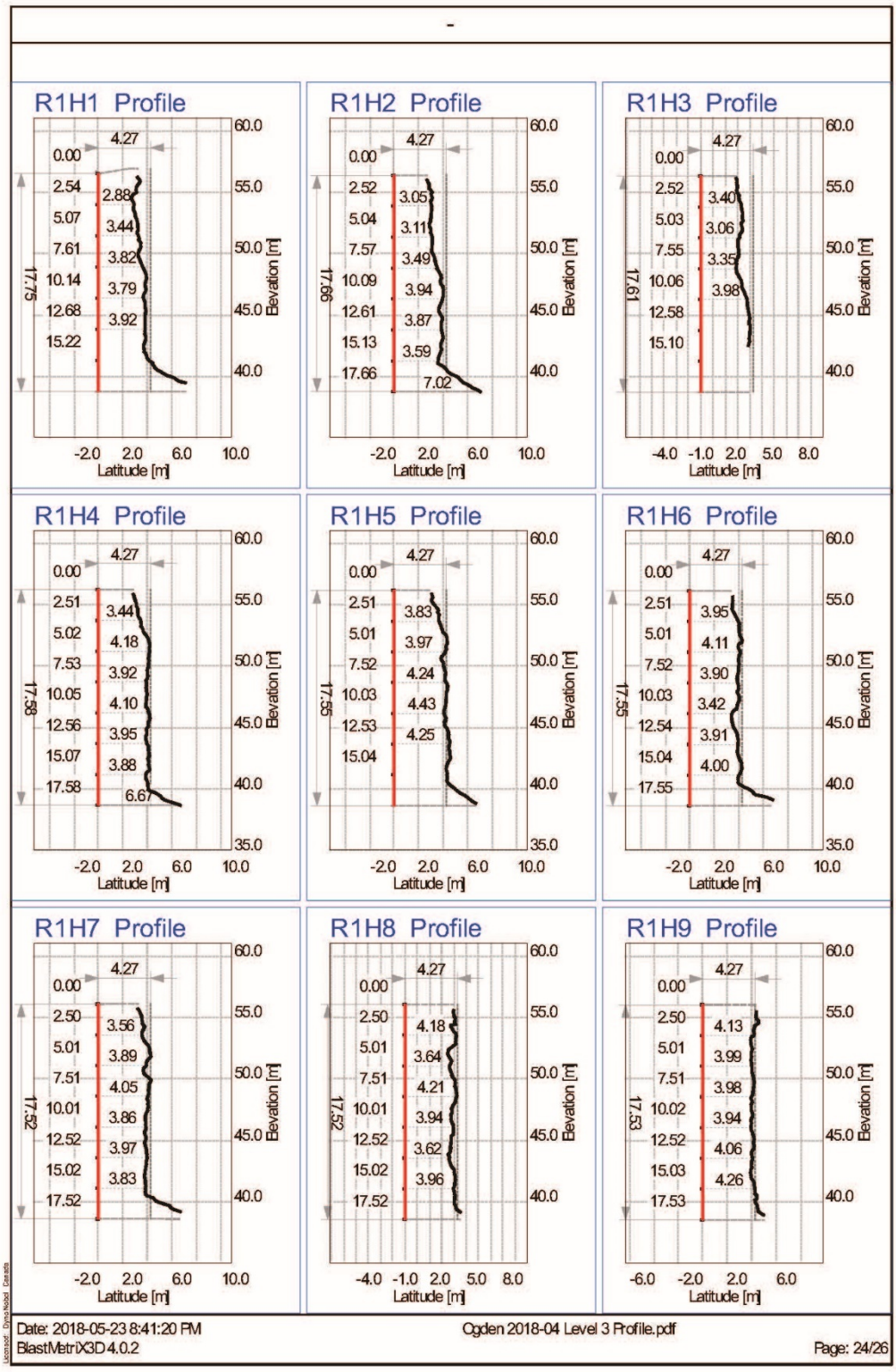
-
R1H1 Profile
4.27
0.00
2.54
5.07
7.61
10.14
12.68
15.22
2.88
3.44
3.82
3.79
3.92
17.75
60.0
55.0
50.0
45.0
40.0
Elevation [m]
-2.0 2.0 6.0 10.0
Latitude [m]
R1H2 Profile
4.27
0.00
2.52
5.04
7.57
10.09
12.61
15.13
17.66
3.05
3.11
3.49
3.94
3.87
3.59
7.02
17.66
60.0
55.0
50.0
45.0
40.0
Elevation [m]
-2.0 2.0 6.0 10.0
Latitude [m]
R1H3 Profile
4.27
0.00
2.52
5.03
7.55
10.06
12.58
15.10
3.40
3.06
3.35
3.98
17.61
60.0
55.0
50.0
45.0
40.0
Elevation [m]
-4.0 -1.0 2.0 5.0 8.0
Latitude [m]
R1H4 Profile
4.27
0.00
2.51
5.02
7.53
10.05
12.56
15.07
17.58
3.44
4.18
3.92
4.10
3.95
3.88
6.67
17.58
60.0
55.0
50.0
45.0
40.0
35.0
Elevation [m]
-2.0 2.0 6.0 10.0
Latitude [m]
R1H5 Profile
4.27
0.00
2.51
5.01
7.52
10.03
12.53
15.04
3.83
3.97
4.24
4.43
4.25
17.55
60.0
55.0
50.0
45.0
40.0
35.0
Elevation [m]
-2.0 2.0 6.0 10.0
Latitude [m]
R1H6 Profile
4.27
0.00
2.51
5.01
7.52
10.03
12.54
15.04
17.55
3.95
4.11
3.90
3.42
3.91
4.00
17.55
60.0
55.0
50.0
45.0
40.0
35.0
Elevation [m]
-2.0 2.0 6.0 10.0
Latitude [m]
R1H7 Profile
4.27
0.00
2.50
5.01
7.51
10.01
12.52
15.02
17.52
3.56
3.89
4.05
3.86
3.97
3.83
17.52
60.0
55.0
50.0
45.0
40.0
Elevation [m]
-2.0 2.0 6.0 10.0
Latitude [m]
R1H8 Profile
4.27
0.00
2.50
5.01
7.51
10.01
12.52
15.02
17.52
4.18
3.64
4.21
3.94
3.62
3.96
17.52
60.0
55.0
50.0
45.0
40.0
Elevation [m]
-4.0 -1.0 2.0 5.0 8.0
Latitude [m]
R1H9 Profile
4.27
0.00
2.50
5.01
7.51
10.02
12.52
15.03
17.53
4.13
3.99
3.98
3.94
4.06
4.26
17.53
60.0
55.0
50.0
45.0
40.0
Elevation [m]
-6.0 -2.0 2.0 6.0
Latitude [m]
Date: 2018-05-23 8:41:20 PM
BlastMetrix3D 4.0.2
Ogden 2018-04 Level 3 Profile.pdf
Page: 24/26
Licensed: Dyno Nobel Canada

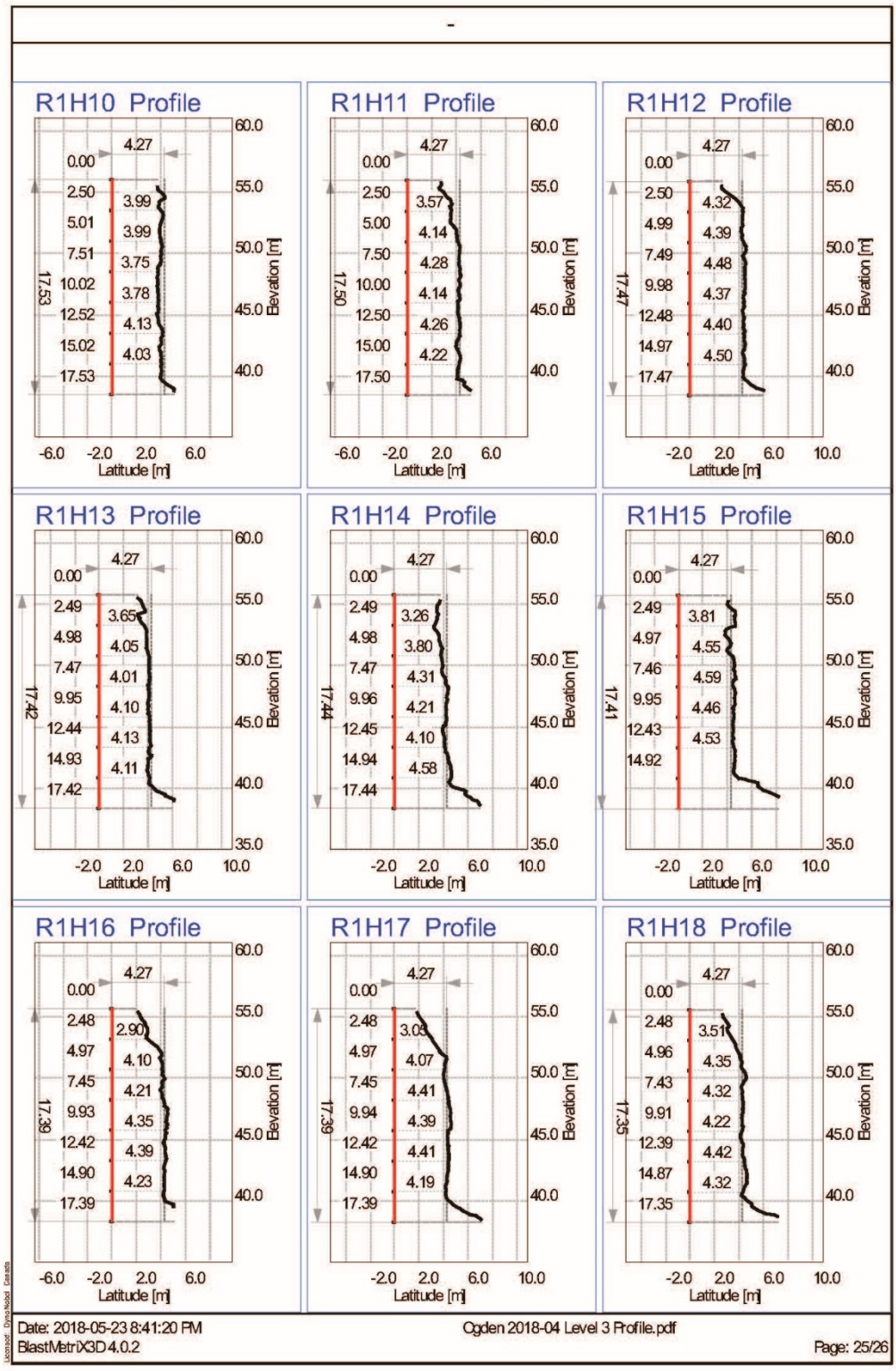
R1H10 Profile
4.27
0.00
2.50
5.01
7.51
10.02
12.52
15.02
17.53
17.53
3.99
3.99
3.75
3.78
4.13
4.03
60.0
55.0
50.0
45.0
40.0
Elevation [m]
-6.0 -2.0 2.0 6.0
Latitude [m]
R1H11 Profile
4.27
0.00
2.50
5.00
7.50
10.00
12.50
15.00
17.50
17.50
3.57
4.14
4.28
4.14
4.26
4.22
60.0
55.0
50.0
45.0
40.0
Elevation [m]
-6.0 -2.0 2.0 6.0
Latitude [m]
R1H12 Profile
4.27
0.00
2.50
4.99
7.49
9.98
12.48
14.97
17.47
17.47
4.32
4.39
4.48
4.37
4.40
4.50
60.0
55.0
50.0
45.0
40.0
Elevation [m]
-2.0 2.0 6.0 10.0
Latitude [m]
R1H13 Profile
4.27
0.00
2.49
4.98
7.47
9.95
12.44
14.93
17.42
17.42
3.65
4.05
4.01
4.10
4.13
4.11
60.0
55.0
50.0
45.0
40.0
35.0
Elevation [m]
-2.0 2.0 6.0 10.0
Latitude [m]
R1H14 Profile
4.27
0.00
2.49
4.98
7.47
9.96
12.45
14.94
17.44
17.44
3.26
3.80
4.31
4.21
4.10
4.58
60.0
55.0
50.0
45.0
40.0
35.0
Elevation [m]
-2.0 2.0 6.0 10.0
Latitude [m]
R1H15 Profile
4.27
0.00
2.49
4.97
7.46
9.95
12.43
14.92
17.41
3.81
4.55
4.59
4.46
4.53
60.0
55.0
50.0
45.0
40.0
35.0
Elevation [m]
-2.0 2.0 6.0 10.0
Latitude [m]
R1H16 Profile
4.27
0.00
2.48
4.97
7.45
9.93
12.42
14.90
17.39
17.39
2.90
4.10
4.21
4.35
4.39
4.23
60.0
55.0
50.0
45.0
40.0
Elevation [m]
-6.0 -2.0 2.0 6.0
Latitude [m]
R1H17 Profile
4.27
0.00
2.48
4.97
7.45
9.94
12.42
14.90
17.39
17.39
3.05
4.07
4.41
4.39
4.41
4.19
60.0
55.0
50.0
45.0
40.0
Elevation [m]
-2.0 2.0 6.0 10.0
Latitude [m]
R1H18 Profile
4.27
0.00
2.48
4.96
7.43
9.91
12.39
14.87
17.35
17.35
3.51
4.35
4.32
4.22
4.42
4.32
60.0
55.0
50.0
45.0
40.0
Elevation [m]
-2.0 2.0 6.0 10.0
Latitude [m]
Date: 2018-05-23 8:41:20 PM
BlastMetriX3D 4.0.2
Ogden 2018-04 Level 3 Profile.pdf
Page: 25/26

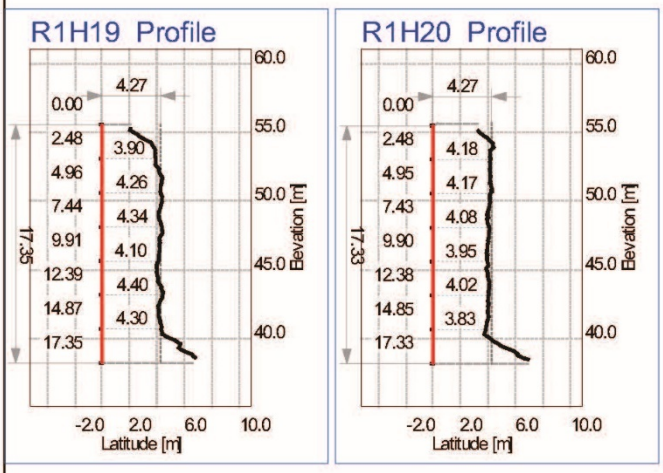

BIBLIOGRAPHY

Ash, R. (1968). The Design of Blasting Rounds. *The American Institute of Mining, Metallurgical, and Petroleum Engineers* (pp. 373-397). USA: AIME.

Bennett, J. (1936). Broken Coal. *Journal of the Institute of Fuel*(10), 22-39.

Bergmann, O., Wu, F., & Edl, J. (1974). Model Rock Blasting Measures Effect of Delays and Hole Pattern on Rock Fragmentation. *E/MJ Mining Guidebook: System for Emerging Technology*, 124-127.

Chiappetta, F. (2011, 11 24). *redForms*. Retrieved from IQPC: http://www.iqpc.com/redForms.

Chung, S., & Katsabanis, P. (2000). Fragmentation Prediction Using Improved Engineering Formulae. *Fragblast: International Journal for Blasting and Fragmentation*, 198-207.

Cunningham, C. (1983). The Kuz-Ram Model for Prediction of Fragmentation from Blasting. *International Symposium on Rock Fragmentation by Blasting* (pp. 439-53). Sweden: Lulea University of Technology.

Cunningham, C. (1987). Fragmentation Estimations and the Kuz-Ram model - Four Years On. *2nd International Symposium on Rock Fragmentation by Blasting* (pp. 475-87). Keystone: Colorado School of Mines.

Cunningham, C. (2005). The Kuz-Ram Fragmentation Model - 20 Years On. *3rd European Federation of Explosives Engineers* (pp. 201-10). EU: EFEE.

Djordjevic, N. (1999). Two-component Model of Blast Fragmentation. *6th International Symposium on Rock Fragmentation by Blasting* (pp. 213-9). Johannesburg: SAIMM.

DynoNobel. (1999). *Advanced Open Pit Blasting Manual.* Salt Lake City: Dyno Nobel.

Eloranta, J. (1997). Efficiency of Blasting verses Crushing and Grinding. *Annual Conference on Explosives and Blasting Technique.* Las Vegas: International Society of Explosives Engineers.

Esen, S., Onederra, I., & Bilgin, H. (2003). Modelling the size of the Crushed Zone Around a Blasthole. *International Journal of Rock Mechanics and Mining Sciences, 40*(4), 485-95.

Fleetwood, K., Villaescusa, E., & Li, J. (2009). Limitations of Using PPV Damage Models To Predict rock Mass Damage. *Blasting and Fragmentation Journal*, *1*, pp. 1-15.

Gates, O. (1915). Kick Vs. Rittinger: an Experimental Investigation in Rock Crushing, Performed at Purdue University. *Transactions of the American Institute of Mining, Metallurgical, and Petroleum Engineers*(52), 875-909.

Gaudin, A. (1926). An Investigation of Crushing Phenomena. *Transactions of the American Institute of Mining, Metallurgical, and Petroleum Engineers*(73), 253-316.

Gaudin, A., & Meloy, T. (1962). Model and Comminution Distribution Equation for Single Fracture. *Transactions of the American Institute of Mining, Metallurgical, and Petroleum Engineers, 223*, 43-50.

Gilvarry, J. (1961). Fracture of Brittle Solids - I Distribution Function for Fragment Size in Single Fracture (Theoretical). *Journal of Applied Physics, 32*(3), 391-9.

Gilvarry, J., & Bergstrom, B. (1961). Fracture of Brittle Solids - II Distribution Function for Fragment Size in Single Fracture (Experimental). *Journal of Applied Physics, 32*(3), 400-10.

Gkikizas, N. (2016, December 1). *Queen's Graduate Theses and Dissertations.* Retrieved from QSPACE: http://hdl.handle.net/1974/15321

Grady, D. (1990). Particle Size Statistics in Dynamic Fragmentation. *Journal of Applied Physics, 68*(12), 6099-105.

Grady, D., & Kipp, M. (1985). Geometric Statistics and Dynamic Fragmentation. *Journal of Applied Physics, 58*(3), 1210-22.

Grady, D., & Kipp, M. (1987). Dynamic Rock Fragmentation. *Fracture Mechanics of Rock* (pp. 429-75). London: Academic Press.

Hettinger, M. R. (2015). *The Effects of Short Delay Times on rock Fragmentation in Bench Blasts.* Rolla: Missouri S&T.

Holmberg, R. (1981). *Optimum Blasting in Bedded and Jointed Oil Shale Formations Technical Report PL 92216.* 1981: Colorado School of Mines.

Hunsaker, D. (2019). *Titan Bulk Emulsion Guide.* Salt Lake City: Dyno Nobel.

Hustrulid, W. (1999). *Blasting Principles of Open Pit Mining, Vol.1 - General Design Concepts and Vol. 2 - theorectical Foundations.* Rotterdam: A.A. Balkema.

ISEE. (2011). *ISEE Blasters' Handbook 18th Edition.* Cleveland: International Society of Explosives Engineers.

Jaeger, J., & Cook, N. (1979). *Fundamentals of Rock Mechanics 3rd edition.* London: Chapman and Hall.

Johansson, D., & Ouchterlony, F. (2013). Shock Wave Interactions in Rock Blasting: the Use of Short Delays to Improve Fragmentation in Model-Scale. *Rock Mech Rock Eng, 46*, 1-18.

Kanchibotla, S., Valery, W., & Morell, s. (1999). Modelling Fines in Blasting Fragmentation and its Impact on Crushing and Grinding. *Explo 1999* (pp. 137-44). Carlton: AusIMM.

Katsabanis, P. D., & Omidi, O. (2015). The Effect of Delay on Fragmentation Distribution through Small- and Medium-scale Testing and Analysis. *11th International Symposium on Rock Fragmentation by Blasting* (pp. 715-720). Sydney: AusIMM.

Koshelev, E., Kuznetsov, V., Sofronov, S., & Chernikov, A. (1971). Statistics of the Fragments Forming with the Destruction of Solids by Explosion. *Journal of Applied Mechanics and Technical Physics, 12*(2), 244-56.

Kuznetsov, V. (1973). The Mean Diameter of the Fragments Formed by Blasting Rock. *Soviet Mining Science, 9*(2), 144-8.

Langefors, U., & Kihlstrom, B. (1963). *The Modern Technique of Rock Blasting.* Stockholm: Almqvist and Wiksell.

Larsson, B. (1974). Blasting of Low and High Benches, Fragmentation From Production Blasting. *Annual Meeting of Swedish Rock Blasting Commitee* (pp. 247-41). Sweden: Swedish Rock Blasting Committee.

Tyler, L. J., & Worsey, P. N. (1984). *United States of America Patent No. 4674047.*

Lilly, P. (1986). An Empirical Method of Assessing Rock Mass Blastability. *The Large Open Pit Mine Conference* (pp. 89-92). Carlton: AusIMM.

Lundborg, N. (1971). *Computer program for charge calculations in bench blasting. Technical Report DS 1971:18.* Stockholm: Swedish Detonic Research Foundation.

Lusk, B., Hoffman, J., & Wedding, W. C. (2011). Electronic Detonator and Modern Non-Electric Shocktube Detonator Accuracy. *Annual Conference on Explosives and Blasting Technique* (pp. 1-14). USA: ISEE.

Lusk, B., Hoffman, J., Mulligan, P., & Worsey, T. (2013). Shock Tube Detonator Shelf Life in Relation to Timing Accuracy. *Annual Conference on Explosives and Blasting Technique* (pp. 1-6). USA: ISEE.

Merriam-Webster. (n.d.). (2020, November 9). *Stochastic*. Retrieved from Merriam-Webster.com dictionary: https://www.merriam-webster.com/dictionary/stochastic

Moser, P. (2005). Less Fines in Aggregate and Industrial Minerals Production - Results of a European Research Project. *3rd EFEE World Conference on Explosives and Blasting* (pp. 567-74). EU: EFEE.

Nobel, D. (1999). *Advanced Open Pit Blasting Manual.* Salt Lake City: Dyno Nobel.

Olofsson, S. (1988). *Applied Explosives Technology for Construction and Mining.* Arla: APPLEX.

Otterness, R., Stagg, M., Rholl, S., & Smith, N. (1991). Correlation of Shot Design Parameters to Fragmentation. *7th Annual Symposium on Explosives and Blasting Technology* (pp. 179-90). USA: ISEE.

Ouchterlony, F. (2003). *'Bend it Like Beckham' or a Wide-range yet Simple Fragment Size Distribution for Blasted and Crushed Rock. Less Fines. Technical Report 78.* EU: EU Project GRD-2000-25224.

Ouchterlony, F. (2005). The Swebrec Function, Linking Fragmentation by Blasting and Crushing. *Mining Technology, 114*, 29-44.

Ouchterlony, F. (2005). What does the Fragment Size Distribution from Blasting Look Like? *3rd EFEE World Conference on Explosives and Blasting* (pp. 189-99). EU: EFEE.

Ouchterlony, F. (2015). The median versus the mean fragment size and other issues with the Kuz-Ram model. *11th International Symposium on Rock Fragmentation by Blasting* (pp. 109-19). Carlton: AusIMM.

Ouchterlony, F., & Moser, P. (2006). Die Swebrec Funktion: eine neue Korngrosenverteilungsfunktion und ihr praktischer Einsatz in der Sprengtechnik. *BHM Berg- und Huttenmannishce Monatshefte, 151*(10), 389-404.

Ouchterlony, F., & Sanchidrian, J. (2019). A Review of Development of Better Prediction Equations for Blast Fragmentation. *Journal of Rock Mechanics and Geotechnical Engineering*, 1-17.

Ouchterlony, F., Olsson, M., Nyberg, U., Andersson, P., & Gustavsson, L. (2006). Constructing the Fragment Size Distribution of a Bench Blast Round, Using the New Swebrec Function. *Fragblast 8* (pp. 332-344). Santiago: Polytechnic University of Madrid.

Ouchterlony, F., Sachidrian, J., & Moser, P. (2017). Percentile Fragment SizeFan Predictions for Blasted Rock and the Fragmentation - Energy. *Rock Mech Rock Eng, 50*, 751-779.

Perkins, T. K., & Krech, W. W. (1968). The Energy Balance Concept of Hydraulic Fracturing. *Journal of the Society of Petroleum Engineers, 8*, 1-12.

Persson, A., & Holmberg, R. (1994). *Rock Blasting and Explosives Engineering.* Boca Raton: CRC PRESS.

Protodyakonov, M. (1962). Mechanical Properties and Drillability of Rocks. *The Fifth US Symposium on Rock Mechanics* (pp. 103-18). Minneapolis: University of Minnesota.

Rosin, P., & Rammler E. (1933). *KorngroBen-probeme des Kohlenstaubes und ihre Bedeutung fur die Vermanhlung. Bericht C 52 des Reichskohlenrates.* Berlin: VDI-Verlag.

Rosin, P., & Rammler, E. (1933). The Laws Governing Fineness of Powdered Coal. *Journal of the Institute of Fuel*(7), 29-36.

Sanchidrian, J. (2015). Ranges of Validity of Some Distribution Functions for Blast-fragmented Rock. *11th International Symposium on Rock Fragmentation by Blasting* (pp. 741-747). Sydney: AusIMM.

Sanchidrian, J., & Ouchterlony, F. (2017). A Distribution-Free Description of Fragmentation by Blasting Based on Dimensional Analysis. *Rock Mech Rock Eng, 50*, 781-806.

Sanchidrian, J., Ouchterlony, F., Segarra, P., & Moser, P. (2014). Size Distribution Functions for Rock Fragments. *International Journal of Rock Mechanics and Mining Sciences, 71*, 381-94.

Schuhmann, R. (1940). Principles of Comminution, I. Size Distribution and Surface Calculation. *American Institute of Mining, Metallurgical, and Petroleum Engineers*(1189), 1-11.

Scott, A., & Onederra, I. (2015). Characterising Rock Mass Properties for Fragmentation Modeling. *11th International Symposium on Rock Ragmentation by Blasting* (pp. 149-160). Sydney: AUSIMM.

Silva-Castro, J. (2012). *Blast Vibrtion Modeling Using Improved Signature Hole Technique for Bench Blast.* Lexington: University of Kentucky.

Silva-Castro, J., Lusk, B., Lee, N., & Jenks, P. (2016). Concepts and Case Study for Regular Rhythmic Timing and Sequence. *Annual Conference on Explosives and Blasting Technique* (pp. 1-9). USA: ISEE.

Spathis, A. (2004). A Correction Relating to the Analysis of the Origional Kuz-Ram Model. *International Journal for Blasting and Fragmentataion, 8*(4), 201-5.

Stagg, M., & Nutting, M. (1987). *Influence of Blast Delay Time on Rock Fragmentation: One-tenth-scale Tests. In: Surface Mine Blasting IC 9135.* USA: USBM.

Stagg, M., Rholl, S., Otterness, R., & Smith, N. (1990). Influence of Shot Design Parameters on Fragmentation. *3rd International Symposium on Rock Fragmentation by Blasting* (pp. 311-7). Carlton: AusIMM.

Thornton, D., Kanchibotla, S., & Esterle, J. (2001). A Fragmentation Model to Estimate ROM Size Distribution of Sock Rock Types. *27th Annual Conference on Explosives and Blasting Technology* (pp. 41-53). USA: ISEE.

Vanbrabant, F., & Espinosa, A. (2006). Impact of Short Delays Sequence on Fragmentation by Means of Electronic Detonators. *8th International Symposium of Rock Fragmentation by Blasting* (pp. 326-331). Santiago: Editec SA.

Weibull, W. (1939). *A Statistical Theory of the Strength of Materials.* Stockholm: Generalstabens Litografiska Anstalts Forlag.

Weibull, W. (1951). A Statistical Distribution Function of Wide Applicability. *Journal of Applied Mechanics, 18*(3), 293-7.
Worsey, P. N. (1981). *Geotechnical Factors Affecting the Application of Pre-split Blasting to Rock Slopes.* Newcastle: University of Newcastle.
Worsey, P. N. (2020, October 10th). Elusive Emeritus Professor. (T. Worsey, Interviewer)
Worsey, T. (2019). *Haile Gold Mine Void Space Testing.* Kershaw: Not Published.
Zhang, Z.-X. (2016). *Rock Facture and Blasting Theory and Applications.* Cambridge: Elsevier Inc.

VITA

Tristan Worsey attended Missouri University of Science and Technology where he was awarded a Bachelor of Science Degree in Mining Engineering in 2010 and a Master of Science Degree in Explosives Engineering 2012. Tristan went on to work at Newmont as a drill and blast engineer from 2012 to 2014. In 2014 he enrolled in the doctoral degree program at the University of Kentucky. Since enrollment Tristan has worked full time for a consulting agency called REPSEC as a drill and blast specialist and is currently working for Dyno Nobel as a principal consultant. Tristan plans on graduating with a Doctor of Philosophy Degree in Mining Engineering from the University of Kentucky in May of 2020. Tristan currently has two refereed journal publications since starting at the University of Kentucky. The two refereed journal publication references can be seen below.

- Silva, J., Worsey, T., Lusk, B. (2018). Practical assessment of rock damage due to blasting. *International Journal of Mining Science and Technology*, 29(3), 379-385. https://doi.org/10.1016/j.ijmst.2018.11.003
- Hall, K., Worsey, T., Rouse, N. (2018). Methods to quantify drilling accuracy. *The Journal of Explosives Engineers*, 35(5), 6-15.